Sedimentation Ponds and their Operation in Stormwater Systems

Linda J. Cobiac
B.E. (Hons)

Thesis submitted for the degree of
Master of Engineering Science

Department of Civil and Environmental Engineering
Adelaide University
March 2001

Table of Contents

CHAPTER 3: CATCHMENT SITES

CHAPTER 4: SEDIMENTS AND HEAVY METALS

Table of Appendices

List of Figures

List of Tables

Abstract

Sedimentation ponds are widely utilised in the treatment of storm water. Although they are heavily relied upon in catchment management there is still a lack of understanding of the functional processes that occur in sedimentation ponds, and how these affect treatment performance. In this research, the efficacy of sedimentation ponds as a means of sediment and heavy metal remediation has been investigated, with particular regard to the physical and chemical conditions that may lead to remobilisation of metals from the sediments.

A series of sediment sampling stations were set up at 5 sites (including two sedimentation ponds) around the Patawalonga and Torrens catchments in Adelaide, South Australia to determine the characteristic behaviour of sediments and heavy metals in the catchments and to evaluate the performance of existing sedimentation ponds. Long-term temperature stratification monitoring and intensive short-term measurements were made of the physical and chemical conditions in sedimentation ponds that are conducive to remobilisation. In addition a model was developed using STELLA™ to simulate stratification behaviour of sedimentation ponds and was validated with data collected in the field.

Heavy metals analysis of sediments trapped at a number of locations in the Patawalonga and Torrens catchments, indicated that heavy metal contamination of the sediment is a problem at all times of year, highlighting the need for treatment facilities. It was found that while sedimentation ponds are generally effective as a means of water quality treatment, their management and design should be individually tailored to local conditions to prevent or minimise inefficiencies in capture and retention of sediments and heavy metals due to persistent pond stratification and remobilising conditions.

The remobilising conditions were common in spring and autumn when pond flow was intermittent. They developed when the weather was warm and relatively calm following a high flow event, which increased the organic loading on the pond. Organic loadings were generally high, and it is recommended that sedimentation ponds be regularly cleaned to remove organic matter and contaminated sediment to circumvent the metal remobilisation problem.

Persistent pond stratification developed in summer and early autumn, when salinity was very high. Simulations with the pond model indicated that sedimentation pond stratification behaviour is highly dependent on local meteorological conditions, pond dimensions and flow regime characteristics such as salinity. It is recommended that stratification modelling be carried out using local data to evaluate the stratification potential of a variety of pond design scenarios as part of the sedimentation pond design process.

Statement of Originality

This work contains no material that has been accepted for the award of any other degree or diploma in any university or other tertiary institution and, to the best of my knowledge and belief, contains no material previously published or written by another person, except where due reference has been made in the text. I give consent to this copy of my thesis, when deposited in the University Library, being available for loan and photocopying.

SIGNED: .

DATE: ...16/3/01.....

Acknowledgements

The author would like to acknowledge the assistance of Dr David Walker, who supervised the research. David provided invaluable guidance on the direction of the research, always had an open door whenever advice was asked for and gave encouragement when it was most needed. He also invested a great deal of time and energy in the field work, which is gratefully acknowledged.

Recognition is given to the Patawalonga and Torrens Catchment Water Management Boards. Without their funding, this research would never have been possible. Special thanks are extended to former Technical Manager Geoff Fisher for his assistance, particularly in the early stages of the study.

The author is grateful for the assistance provided by many of the staff in the Department of Civil and Environmental Engineering. The laboratory staff fabricated most of the equipment used in the study and happily lent a hand in the field whenever needed. Their suggestions in the equipment design phase and willingness to construct replacement samplers (often at short notice) is much appreciated. The assistance of Stan Woithe is also acknowledged. Stan put the temperature monitoring equipment together and taught the author everything that needed to be known about the mysterious world of electronics.

In the Department of Geology and Geophysics, the assistance of John Stanley in the X-Ray Laboratory is gratefully acknowledged. He provided many hours of instruction on the preparation of sediment samples for x-ray analysis.

The author would also like to acknowledge her fellow postgraduates for their friendship and support throughout the research, particularly John 'JV' Vitkovsky who knows just about everything there is to know about formatting, printing, binding and everything else that goes into the preparation and submission of a thesis.

Finally, the author would like to thank her family for their continual love and support, especially her parents who have worked hard to provide the opportunities for the author to achieve this academic goal.

CHAPTER 1

INTRODUCTION

1.1 Background

When the redevelopment of the Glenelg foreshore and Environs was proposed in 1996, an EIS was prepared to assess the environmental impact of the proposed redevelopment of the mouth of the Patawalonga for the construction of a marine harbour and alteration of the Patawalonga Basin to improve water quality by flushing or diverting polluted stormwater.

In preparation for responding to the EIS, the Patawalonga Catchment Water Management Board commissioned Willing & Partners in association with the CRC for Freshwater Ecology to undertake a technical review of the water quality management implications of the proposed redevelopment.

In the review it was suggested that the physical and chemical conditions in the existing Patawalonga Basin, as well as high organic loadings were exacerbating the pollution problem through remobilisation of pollutants from the sediments, transforming them into a more toxic and bioavailable form (Willing and Partners, 1996). This raised the question – "is there potential for water quality to be similarly affected by pollutant remobilisation in other water bodies in the Patawalonga and Torrens catchments?"

This was a particularly pertinent question, since the current trend has been to retain stormwater in various artificially constructed water bodies so that it can be treated and potentially reused, rather than viewing it as a nuisance that must be speedily flushed away from urban areas and out to sea. Hence detention of water, mainly through construction of artificial wetlands and sedimentation ponds, is a primary objective in catchment management planning.

At the time of publication of the Patawalonga Catchment Water Management Plan in 1997, one sedimentation pond or wetland had been constructed, and a further seven were either under construction or being investigated as potential sites (Patawalonga Catchment Water

Management Board, 1997). In the Torrens catchment, three facilities were under construction, one was under design, and four other sites were under investigation for sedimentation pond or wetland development (Torrens Catchment Water Management Board, 1997).

Given the substantial public investment in sedimentation pond and wetland facilities and an increasing reliance on them as a catchment management option in the Patawalonga and Torrens catchments, catchment authorities were not surprisingly concerned about the potential for water quality to be adversely affected by pollutant remobilisation. Three of the most critical concerns, which led to this study, were:

- do existing water quality treatment ponds in the Patawalonga and Torrens catchments function effectively;
- are ponds an appropriate tool for treating water quality in other parts of the catchments; and
- if pond conditions are leading to a reduction in water quality or inefficiencies in treatment, can the management of these ponds or design of future facilities be improved to minimise the potential for these problematic conditions to occur?

1.2 Objectives

The primary aim of this study was to investigate the efficacy of sedimentation ponds as a means of sediment and heavy metal remediation, with particular regard to the physical and chemical conditions that may lead to remobilisation of metals from the sediments. The primary objectives were to:

- characterise the treatment efficiency of two existing sedimentation ponds in the Patawalonga catchment;
- investigate the physical and chemical conditions in one sedimentation pond that can affect pond performance, namely:
  - chemical conditions of redox potential and pH that can lead to metal remobilisation;
  - chemical conditions of dissolved oxygen that can lead to a fall in redox potential; and
  - physical conditions of salinity, temperature and turbidity that can lead to density stratification, which inhibits mixing of dissolved oxygen; and
- to develop a numerical computer model of the physical conditions in sedimentation ponds that can lead to density stratification, in order to:

- evaluate the relative importance of meteorological conditions, pond conditions and certain aspects of pond design on the development of stratified conditions; and hence
- make recommendations concerning the design and management of sedimentation ponds.

A secondary aim of the study was to characterise the nature and behaviour of sediments and heavy metals in the Patawalonga and Torrens catchments, in order to observe pollution trends within the two catchments and assess the potential for sedimentation pond treatment. Specifically, the objectives were to:

- identify the characteristics of the sediments, including their size, composition and heavy metal content;
- estimate the sediment flux; and
- detect any seasonal trend in sediment and heavy metal loads.

1.3 Methodology

The study involved a combination of field work in the Patawalonga and Torrens catchments and numerical modelling. This work involved:

- installation of sediment sampling equipment at five sites in the Patawalonga and Torrens catchments, with fortnightly sample collection and analysis, in order to characterise the nature and behaviour of the sediments and their heavy metal content;
- installation of monitoring equipment in the Morphett Road Sedimentation Pond for continuous monitoring of the temperature behaviour in the pond;
- intensive sessions of depth profiling of chemical and physical conditions in the Morphett Road Sedimentation Pond, in order to record the pond conditions that were conducive to metal remobilisation; and
- development of a numerical computer model of sedimentation pond behaviour, calibrated using data collected in the field, to evaluate the meteorological and pond conditions and aspects of pond design that lead to sedimentation pond stratification.

1.4 Outline of Thesis

Chapter 2 presents introductory background information about sediments and heavy metals in the aquatic environment followed by a review of the literature concerning sedimentation ponds and the application of numerical models to describe pond behaviour.

Chapter 3 describes the process by which sites were selected for inclusion in the study. Maps and photographs help to illustrate each of the five sites that were chosen.

Chapter 4 details the study of sediments and heavy metals in the Patawalonga and Torrens catchments. In the first part of the chapter, the design and installation of sediment sampling equipment, and sediment and heavy metal analysis procedures are described. The remainder of the chapter is dedicated to presentation of the results of the analysis and discussion of the characteristics and behaviour of sediments and heavy metal contamination in the Patawalonga and Torrens catchments.

Chapter 5 reports on the study of physical and chemical conditions in the Morphett Road Sedimentation Pond. A description of the depth profiling equipment and field work is given, followed by a discussion of the physical and chemical conditions in the pond, including an analysis of the long-term observations of temperature stratification in the Morphett Road Sedimentation Pond.

Chapter 6 presents the sedimentation pond model. The chapter begins with a theoretical explanation of the heat and salt transfer processes within a sedimentation pond. A description of the model's execution in STELLA, and its validation with data collected in the field is then given. Finally, the results of the pond model simulations of the Morphett Road Sedimentation Pond are presented and the implications of the pond model simulations are discussed.

Chapter 7 summarises the results of the study, highlighting the major advances that were made and giving the recommendations that have arisen from the work. The chapter concludes with recommendations for future work in this field.

CHAPTER 2

LITERATURE REVIEW

2.1 Introduction

Reducing the sediment load of urban stormwater is considered to be an effective means of reducing pollutant loads in the aquatic environment (Dempsey *et al.*, 1993; Duncan, 1995). Water quality improvement through sediment removal is the primary function of sedimentation ponds, and sedimentation ponds are a key element of the treatment process in artificial wetlands.

There are two goals in designing sedimentation ponds for water quality treatment –the pollutant load must be captured and the pollutants must be prevented from leaving the pond (Loganathan *et al.*, 1994). However, the pond conditions that must be achieved in order to meet these two goals can conflict. Capture of pollutants is dependent on the detention time, which is largely a function of the pond volume and its catchment area. Allowing water time to lie quiescent is the crucial factor in achieving pollutant removal (Horner *et al.*, 1994). Unfortunately the quiescent conditions necessary for pollutant removal may also enhance pollutant export from the pond by allowing the pond to stratify, which can lead to changes in the chemical environment of the pond. These changes in the chemical conditions (e.g. redox potential) can lead to remobilisation of pollutants from the sediments. There is then little to prevent these remobilised pollutants from being flushed from the pond during the next flow event.

In order to appreciate the intricacies of sedimentation pond function, it is essential to have an understanding of the origin and toxicity of sediments and heavy metals and the nature of the sediment-metal association in aquatic systems. Hence the initial sections of this chapter focus on the background to sediment and heavy metal contamination. This is then followed by a review of the literature surrounding the use of sedimentation ponds as a means of water quality improvement, including the treatment performance of current pond designs and the need for modelling of the sedimentation pond environment.

2.2 Sediments and Metals in the Aquatic Environment

2.2.1 Sediment Characteristics

Sediments can cause considerable harm to waterways and the receiving marine environment, through sedimentation of natural or engineered watercourses, wetlands, weirs and dams, and high turbidity. High turbidity is unsightly and inhibits penetration of light required for photosynthesis, which can kill or retard the growth of aquatic plants and the aquatic fauna that feed or live upon them (ANZECC, 1999). Filter-feeders and organisms with gills, such as fish, are also affected by excessive turbidity.

In the aquatic environment the mineralogical origin of sediments is primarily dictated by the geological nature of the catchment. Weathering and erosion processes largely determine the eventual mineralogical composition of sediments, although sediments are also generated by human activity within the catchment.

In urban catchments, sediment is primarily introduced into the waterways via runoff from roads, industrial and commercial premises and areas of land disturbance, such as road or housing construction sites. Bank or bed erosion is also a significant source, particularly where waterways have been altered from their natural state by urban development or other human activity. In rural areas, sediment input to the waterways is chiefly the result of poor agricultural land practices.

Organic material including leaf matter, bark, branches etc. is contributed mainly by deciduous trees along streets and streamlines, particularly in autumn. Native trees, although evergreen, shed leaves, bark and other debris all year round.

Sediments are generally divided into size fractions according to their mean particle diameter. The broad categories range from boulder to cobble, pebble, gravel, sand, silt and clay, which is the smallest particle size. Sands, silts and clays are sometimes further divided into fine, medium and course fractions. Table 2-1 shows the particle size classification given by the ANZECC (1999) guidelines.

Table 2-1: Particle size classification for sediments (after ANZECC (1999))

CLASSIFICATION	PARTICLE SIZE RANGE (μm)
Clay – fine	< 0.06*
Clay – medium	0.06 – 0.63
Clay – course	0.63 – 2
Silt – fine	2 – 6.3
Silt – medium	6.3 – 20
Silt – course	20 – 63
Sand	> 63

* In sediment analysis, any material less than 0.45μm is often considered to be dissolved rather than in particulate form.

In the urban environment, the proportion of finer particle sizes tends to be high. Ball and Abustan (1995) found that 70% to 92% by mass of sediments in runoff from a suburban catchment in Sydney were less than 100μm in size, and the median particle size was between 39μm and 73μm. In an analysis of road runoff in south-east Queensland by Drapper *et al.* (2000) the median size of particles by number was less than 1μm.

Studies overseas have also revealed high proportions of fine grained particles. Randall *et al.* (1982) found that 80% of suspended sediments captured during a runoff event were less than 25μm in size. Walling and Kane (1984) found that more than 75% of particles were less than 10μm in a study of suspended sediment in the Exe Basin in the United Kingdom.

Locally, Walker *et al.* (1997) studied stormwater samples from a variety of different land use catchments in the Tea Tree Gully area of Adelaide. They found that 60% of the sediment by weight was less than 40μm and over 90% was less than 100μm. It is possible that similar sediment size trends exist in the nearby Patawalonga and Torrens catchments, which have a similar geological origin and land use pattern. However, to date no studies have been undertaken to assess the sizes of sediments in the Patawalonga and Torrens catchments.

2.2.2 Metals

Metals in the aquatic environment come from a variety of natural and anthropogenic sources. Metals that occur naturally are the result of weathering of minerals in the catchment (or volcanic fallout in volcanically active areas).

Anthropogenic sources of heavy metals in the aquatic environment are numerous. They are frequently divided into point and non-point sources. Industrial effluent and domestic effluent are common anthropogenic point sources. They are generally easy to identify and can usually be systematically dealt with. Non-point sources however are much harder to treat. Common non-point sources of heavy metals include surface runoff and atmospheric fallout.

Heavy metal contamination is a site-specific problem – the characteristic metal contamination in any one location is largely dependent on local conditions and activities in the catchment (Athayde *et al.*, 1984). Numerous studies have been conducted in the Patawalonga and Torrens catchments to assess the extent of heavy metal contamination. In the Patawalonga catchment, levels of chromium, copper, lead, nickel and zinc have all been found to exceed the ANZECC Guidelines for protection of freshwater ecosystems and/or secondary water contact (Patawalonga Catchment Water Management Board, 1997). In the Torrens catchment intermittently high concentrations of contaminants such as chromium and lead are of major concern (Torrens Catchment Water Management Board, 1997).

Table 2-2 outlines the common sources of these metal pollutants in catchment runoff. Many are found in vehicle components (e.g. tyres, fuel, bearings, brake linings, etc.) and would be contributed by road runoff in urban areas. Industrial, agricultural and even water treatment activities (e.g. application of copper sulfate as an algicide) also contribute metal pollutants to the waterways.

Trace concentrations of metals are required for the basic life-functions of many aquatic flora and fauna, but in excessive concentrations the same metals can be lethal or impede natural growth processes.

A common pathway of human exposure to heavy metals is through consumption of metal contaminated fish or shellfish. Metal contaminants can accumulate in shellfish, which are unable to regulate their metal uptake. Fish can often excrete essential metals, such as iron and zinc, but not non-essential metals, such as cadmium (Connell and Miller, 1984).

Known toxic effects of metals in humans include the replacement of lead for calcium in bones (particularly during childhood skeletal development), disruption of zinc processes by cadmium, gastrointestinal and cardiac symptoms from arsenic, and adverse respiratory and dermatological effects from chromium.

In aquatic organisms the toxic effects, if not lethal, can cause physiological problems (e.g. inhibited growth), morphological tissue derangements, biochemical disruption (e.g. of enzyme activity) or behavioural or reproductive changes (Connell and Miller, 1984).

Although aquatic organisms may ingest metals in particulate form, the primary pathway is via respiratory or surface absorption of the free metal ion, or its ingestion in water (Connell and

Miller, 1984). In the ionic form metals are more toxic since they are capable of penetrating cell membranes (USEPA, 1996).

Table 2-2: Source of metal contaminants (after pH environment (1995); CCREM (1996); ATSDR (1999))

METAL	POSSIBLE SOURCES
Zinc	Tyres, oil additive, grease, galvanising, roof runoff, roof cleaning
Lead	Vehicle exhausts (leaded petrol), tyres, lubricating oil and grease, bearing wear, old paint, plumbing, roof flashing
Barium	Dye, brick, rubber and tile manufacture, paints, insecticides, steel hardening, fuel and oil additive
Copper	Metal plating, brake linings, bearings and other moving engine parts, copper piping, fungicides, insecticides
Boron	Glass manufacture, fire retardants, tanning industry, pesticides, timber treatment
Chromium	Metal plating, moving parts, break linings, timber treatment, tanning industry
Vanadium	Steel making, manufacture of car parts and aircraft engines, rubbers, plastics and ceramics
Nickel	Manufacture of coins, jewellery, ceramics and batteries, nickel plating
Arsenic	Timber treatment, glass manufacture, semiconductors, pesticides, herbicides, tanning industry, paints
Cobalt	Vehicle exhausts, coal and oil combustion, enamelling

Many heavy metals can exist in aquatic systems in more than one species, and each species may have a different level of toxicity. Arsenic, for example, in a dissolved form commonly exists in aquatic systems as either As^{3+} or As^{5+}, with As^{3+} more likely to dominate in well oxygenated environments and As^{5+} in poorly oxygenated environments. As^{3+} is typically more toxic to phytoplankton and higher order organisms, while plants tend to more sensitive to As^{5+} (ANZECC, 1999).

The species in which a metal such as arsenic exists, depends on the chemical conditions of redox potential (ORP) and pH of the surrounding environment. Changes in these chemical conditions may lead to either an increase or decrease in the metal's toxicity.

2.2.3 Sediment Transport of Heavy Metals

Particulate matter plays a fundamental role in the transportation and ultimate fate of contaminants in aquatic systems (Ongley *et al.*, 1981; Walling and Kane, 1984; Pye, 1994; Ball and Abustan, 1995). In the dissolved phase, metals can exist as ion, un-ionised organic chelates or complexes. In insoluble colloidal or particulate form, the metals usually occur either as oxides, hydroxides, sulfides or silicates or adsorbed to silica, clay or organic material.

In general, although all metals exist in surface waters they are primarily in the colloidal or particulate form, rather than in the dissolved phase (Kennish, 1992). Table 2-3 shows the proportion of metal transport that is typically associated with sediment.

Table 2-3: Sediment-associated metal transport as a proportion of total metal transport (adapted from Passfield and Phillips (1996), after Förstner (1977); Gibbs (1977); Meybeck (1984))

METAL	%
Cadmium	30 – 45
Chromium	88 – 90
Cobalt	98
Copper	93 – 96
Iron	99 – 99.8
Lead	73 – 84
Magnesium	56
Manganese	98
Nickel	97
Strontium	32
Titanium	99.6
Zinc	37 – 45

Studies of heavy metal contaminants in the Patawalonga and Torrens catchments have largely been based on the results of water sampling and analysis. Few studies have focused on heavy metal contamination of sedimentary material in either the Patawalonga or Torrens catchment. Environmental consultants, pH environment (1995) did analyse the heavy metal contamination of sediments taken from drainage pipes and channels, however the study was confined to the Sturt River sub-catchment of the Patawalonga catchment. Furthermore, the

metals analysis was restricted to sediments deposited on the bottom of pipes and channels, and does not provide an indication of the contamination of the finer material that remains in transport.

The study by pH environment (1995) found high concentrations of lead, zinc, copper, chromium and cadmium, which are all typical urban contaminants. A relationship was also identified between concentrations of heavy metals and particles less than 75μm in size. Many other researchers have also reported an inverse relationship between metal concentrations and particle size (e.g. Förstner (1981), Vaithiyanathan *et al.* (1992)). The finer particles (e.g. silts and clays) typically have a higher chemical reactivity, which is commonly attributed to their proportionally higher surface area and surface chemistry.

The availability and composition of sediment (e.g. content of organic material, iron and manganese oxides and hydroxides and clay minerals, particle size, etc.) have a powerful influence on the degree of metal uptake and therefore the bioavailability or toxicity of metals.

Metals have a particularly strong affinity for organic material. Organic matter can exist as discrete particles, but often forms a coating on other inorganic sediments to which metals can adsorb. The organic coating can also be caused by microorganisms, such as bacteria, which produce a sticky mucus on particle surfaces (Eisma, 1992). Like organic matter, oxides and hydroxides of iron and manganese also tend to form a surface coating on other particles, to which metal ions can bind (Förstner, 1981).

Metals can also adsorb to clay minerals through cation exchange, where positively charged metal ions are sorbed by negatively charged sites on the clay mineral, with an associated release of an equivalent charge. Or adsorption of metals can occur through intermolecular hydrogen bonding or van der Waals forces (Förstner, 1981). However, in natural aquatic systems, surface coatings of iron or manganese oxides or hydroxides or organic matter may mask the reactivity of clay minerals (Wang and Chen, 2000).

The permanence of the sediment-metal bond is also controlled by physical and chemical conditions in the water column, such as pH, redox potential, dissolved oxygen, temperature, turbidity and salinity. Redox potential and pH are the 'master variables' affecting the solubility and mobility of metals (Förstner, 1990; Bourg and Loch, 1995). Even small changes in the pH or redox potential can have a direct effect on the bioavailability of some metals (e.g. arsenic) or affect the solubility of iron and manganese oxides and hydroxides, to which metals attach (Bourg and Loch, 1995).

The redox potential of the water column and sediments is closely related to the amount of dissolved oxygen (DO) that is present. Redox potential becomes negative with depletion of DO (Butler and Smith, 1985), a situation which can occur in aquatic systems with a high level of biological activity. Microorganisms reduce the redox potential through consumption of DO

and production of metabolic products (Seki, 1982). DO is normally replenished via surface re-aeration and mixing through the water column. However, under certain conditions of temperature and/or salinity, the density of the water column can become stratified (this is sometimes triggered by a decline in water clarity e.g. due to increased turbidity). The stratification inhibits mixing of DO from the surface leading to progressive depletion of DO in the sub-surface waters and sediments.

2.3 Sedimentation Ponds for Water Quality Improvement

2.3.1 Capture of Pollutants

The ponds are designed to encourage flow retardation and allow sediments (and any attached heavy metals) to settle out of the water column under the action of gravity – a process known as sedimentation. Sedimentation is best achieved in quiescent waters, hence pond capacity must be sufficient to cope with the volume of catchment runoff, and short-circuiting of flow through the pond should be avoided.

As well as being a function of pond hydrodynamics, the amount of sedimentation that can occur in a pond is also dependent on the particle settling velocity, which is loosely proportional to the particle size (although the particle shape and density are also influential). In natural aquatic systems, sedimentation of the finer particles can be poor since they tend to remain in suspension even at low flow. Larger particles will settle out more quickly and are likely to be transported only intermittently in higher flow events (Warren and Zimmermann, 1994). Particles less than 10μm in diameter with a specific gravity close to one are least likely to be removed by sedimentation (Nix *et al.*, 1989). Natural or chemically induced aggregation of these particles to form larger masses that settle more quickly, is the best method of removal for these very fine particles. Macrophytic filtration and adhesion can also be effective (Wrigley *et al.*, 1991), but are not always incorporated into sedimentation pond designs.

Due to the lower settling velocity of the fine particles, which are believed to carry higher concentrations of heavy metals (see Section 2.2.3) some studies have cast doubt on the effectiveness of sedimentation ponds.

For example, Walker *et al.* (1997) examined the properties of stormwater sediments from a number of Adelaide catchments of different land uses. They concluded that the majority of pollutants were in the finer (<40μm) particle size fraction, and stated that the existing

guidelines for the design of sedimentation ponds were inadequate in that the ponds would be ineffective in retention of the most polluted particles.

Similarly, in a study of sediments from the creeks and drains of the Sturt sub-catchment of the Patawalonga by pH environment (1995), the finer particle size fraction (<75μm) was found to be the most contaminated, but was considered the least likely to be trapped in sedimentation ponds.

No studies have comprehensively determined the metal contamination of the different sediment particle sizes in the other sub-catchments of the Patawalonga catchment or in the Torrens catchment. Hence it is not known if the finer particles are indeed more polluted in the two catchments or if the existing sedimentation ponds are failing to capture the finer particle sizes.

2.3.2 Retention of Pollutants

Little is known about the chemical environment of sedimentation ponds. The sediment-metal association is dependent on a number of factors including the nature of the metal, the mineralogical composition of the sediment, and the presence or absence of organic material and iron or manganese oxides or hydroxides, combined with the chemical conditions of the surrounding environment. Numerous studies have shown that a change in pH and redox potential, particularly a fall in redox potential, may transform pollutants into more toxic forms.

If metals are remobilised from the sediments with a fall in redox potential of the pond environment, the ability of a sedimentation pond to function as an effective long-term sink for heavy metal pollutants is brought into question. It is essential that the construction of a sedimentation pond does not exacerbate the metal pollution problem or endanger the health of the downstream environment.

These remobilising conditions have been shown to exist in the sedimentation pond of a gross pollutant trap on Sullivan's Creek in the ACT (Whytcross *et al.*, 1998). The deposited pond sediments had a low redox potential, which was associated with an increase in concentration of chemical parameters. (Metal pollution was not significant in the pond, hence the effect of the low redox potential on metal contaminants was not an issue in the study.)

The conditions of low redox potential in the Sullivan's Creek study particularly occurred during periods of low flow. When conditions are quiescent there is a potential for the water column to become thermally stratified. Stratification of sedimentation ponds is undesirable since it can lead to the conditions of low redox potential. Low redox potential is associated with a reduction in DO in the water column and/or sediments. DO is consumed by microorganisms

during decomposition of organic matter, and water column stratification inhibits mixing of surface oxygen down through the water column to replenish DO supplies.

In the Sullivan's Creek sedimentation pond there was significant microbial activity and decomposition of organic matter associated with the conditions of low redox potential. However no measurements of temperature were made to determine whether temperature stratification was contributing to the remobilising chemical conditions in the pond.

2.3.3 Sedimentation Pond Design

Historically, artificial ponds were constructed purely for the purpose of flood control, a consequence of increased urbanisation. Sedimentation of these ponds or basins was considered a nuisance since it reduced the water detention capacity. Today, however, sedimentation is a primary objective in pond design. These types of ponds can be constructed for treatment of water quantity and quality, or water quality alone, although the design of dual purpose ponds often involves a compromise of objectives – flood detention is best achieved by a pond which is initially empty, while better water quality treatment is accomplished in a pond with a permanent pool and a long detention time (Duncan, 1995).

Initially, the design of sedimentation ponds for water quality treatment was based on the traditional design of flood detention ponds, where volume is the primary design criterion, and efficiency was measured in terms of the mass of pollutants removed. The experience with these ponds has been variable.

Wu *et al.* (1989) monitored the removal efficiency of zinc and iron during five flow events in two ponds in the Piedmont region of North Carolina. In one of the ponds, removal efficiency for the metals varied between 69% and 100% over the five flow events. In the second pond, removal efficiency varied between –29% and 85% over the five events. In the latter pond there was a net loss of suspended sediment during one flow event, which led to a net export of zinc from the pond.

In a more recent comparison of two ponds in Bellevue, Washington, Comings *et al.* (2000) found that the ponds were capable of achieving significant water quality improvement, but the results were similarly variable. Their study included suspended sediment, phosphorus and four typical urban stormwater contaminants – cadmium, copper, lead and zinc. Removal rates for the metals ranged from 37% to 73% in one pond and 47% to 76% in the other pond. From the comparison of the ponds, Comings *et al.* (2000) theorised that pond volume was the most influential factor in treatment efficiency, although minimising short-circuiting of flow was also important.

Pond treatment efficiency is also dependent on the initial input load (Duncan, 1995; Bartone and Uchrin, 1999). Removal rates typically increase with increasing input loads, although the corresponding output load also increases (Grizzard *et al.*, 1986). This effect on treatment efficiency is thought to be partly due to the relationship between particle size and mass in the input load. Treatment efficiency is directly affected by the particle size distribution of the input load (Ferrara and Witkowski, 1983; Wu *et al.*, 1989). The removal rate improves as the mean particle size of the input load increases, due to the reduced settling time for larger particles in the pond.

However, the relationship between particle size and pond treatment efficiency suggested by Ferrara and Witkowski (1983) and Wu *et al.* (1989) is based only on the mass of sediment removed, and does not take account of the typically higher concentration of pollutants on the finer particles. There are many factors that influence the efficiency of sedimentation ponds in achieving water quality improvement. According to the recent guidelines by Lawrence and Breen (1998), the important issues in sedimentation pond design are:

- incoming pollutants and flow conditions;
- critical pollutants and reduction targets;
- integration of the pond into the treatment train;
- siting constraints and opportunities; and
- pollutant interception and remobilisation processes.

Many of these issues can conflict and compromises must be made. For example, in urban environments, land availability is often a limiting factor. If a sedimentation pond is too small, the capture of pollutants may be low since flow rates may not be slowed sufficiently to allow sedimentation of the finer particles to occur. The obvious solution to this problem is to increase the volumetric capacity by increasing pond depth, however this can adversely affect pollutant retention by increasing the potential for density stratification to occur.

With so many factors to be taken into account in the design of sedimentation ponds, it is a difficult task to determine the optimal pond design and predict the associated performance outcomes. The application of an appropriate simulation model could simplify the decision-making process for sedimentation pond designers by taking over the difficult task of unraveling the complex inter-relationships between the various pond design factors and elucidating basic causes and effects.

Through simulation of different scenarios, this type of model could enable visualisation of the impact on sedimentation pond performance of different management and development

decisions, and it would be equally valuable to researchers who wish to better understand the intricacies of sedimentation pond behaviour.

The use of such a model as an educational and/or decision-making tool contrasts with the more common application of many models as a means of forecasting particular events. Hence such a model would need to have the capacity to be fully interactive, and thus the selection of an appropriate modelling platform that provides for easy manipulation of input variables, rapid simulation times and visualisation of the model output, including step-by-step behaviour of model variables, would be crucial.

Development of a model that would simplify sedimentation pond design was a primary objective in this research.

2.3.4 Sedimentation Pond Modelling

There is potential for developing a model that incorporates all the relevant factors in the design of sedimentation ponds, including economic and social variables (e.g. land prices, public safety constraints on pond side slopes, etc.). This type of model would be an excellent decision-support tool, particularly if it was essentially process-based (i.e. developed from mathematical descriptors of physical, chemical and/or biological reactions rather than empirical relationships) to maximise its applicability and therefore its usefulness as a design tool.

Since development of this kind of model is a very large task, in this research it was decided to focus on just one aspect of the modelling – sedimentation pond stratification. The aim was that the model would be effective as a stand-alone model but have the potential to be incorporated into an integrated sedimentation pond performance model.

To date, the spreadsheet-based model of Lawrence and Breen (1998) is the most comprehensive model of this type to have been developed for simulating sedimentation pond performance. Their model is comprised of a series of sub-models that simulate the catchment runoff and pollutant balance, adsorption and sedimentation, pollutant remobilisation, algal growth and pond aeration (Lawrence and Breen, 1998). However the model of Lawrence and Breen (1998) does not fully incorporate the effects of pond stratification on the mixing of DO through the water column in the pond aeration sub-model. In the Design Guidelines (Lawrence and Breen, 1998) the daily rate of transfer of oxygen through the water column is given by Equation 2.1.

$$W = 0.8 + 0.3u^{1.64} + 4\left(\frac{v}{d}\right)^{0.5} \times \left(C_{sat} - C_{pd}\right) \qquad (2.1)$$

where:

W is the rate of O_2 transfer;

u is the diurnally averaged wind velocity;

v is the average flow velocity through the pond;

C_{sat} is the O_2 saturation concentration at the prevailing water temperature; and

C_{pd} is the O_2 concentration in the pond.

Equation 2.1 formulates the physical mixing of the water column as a function of wind conditions and advection caused by pond inflow. In reality, water column stratification is dependent on a multitude of factors, including meteorological conditions (e.g. solar radiation, air and dew point temperatures, and wind speed and direction), pond conditions (e.g. water clarity, temperature and salinity) and pond design factors (e.g. depth, orientation and construction materials). Temperature and salinity are the primary factors, because they directly affect the density and therefore influence the stability of a pond.

Lawrence and Breen (1998) advise limiting pond depth to 2.5 – 3.0m to minimise the potential for temperature stratification to occur. However Scanlon *et al.* (1998) have observed stratification of a small urban pond at Streeton Views Estate in Melbourne that had a maximum depth of 1.5m, and Van Buren *et al.* (2000) recorded stratification of 3.4°C in a stormwater detention pond in Ontario, Canada that had a depth of around 1m.

Concerned about thermal pollution of urban stormwater runoff, Van Buren *et al.* (2000) modelled the mean temperature of the stormwater detention basin, but had mixed success, with resultant discrepancies between measured and simulated values, which they partly attributed to thermal stratification.

Waters and Luketina (1998) also observed stratification in a small wetland pond of approximately 1m depth in Sydney. Long-term monitoring of the temperature showed that stratification of up to 10°C was occurring. Furthermore, the stratification was persistent over the summer months, in one case lasting for more than two weeks. Unusual temperature inversions (negative temperature stratification) also occurred, which Waters and Luketina (1998) theorised were caused by penetrative convection and influx of saline groundwater.

In freshwater ponds, thermal stratification is caused by differential heating of the water column due to solar radiation. It is thought to be more likely to occur in quiescent, turbid waters during the summer, when solar radiation is high and winds are light (Lawrence and Breen, 1998). Re-mixing of a stratified pond usually occurs when the surface cools at night and leads to convective mixing of the water column. However in saline waters, thermal

gradients may be maintained for longer periods due to the additional density effects of salinity – temperature gradients of as much as 0.5°C/cm may occur in saline ponds, while gradients of just 0.1°C/cm are rare in freshwater lakes (Cole, 1983). Rainfall, groundwater seepage or inflow of water that has a different salinity can all induce these salinity effects.

These thermohaline dynamics are fundamental to ocean mixing and have been intensively studied by oceanographers (Rudnick and Ferrari, 1999). Studies have also been made of saline pools in rivers (Western *et al.*, 1996) and saline lakes (Rawson and Moore, 1944). However it is believed that this unusual thermohaline behaviour has not previously been identified or investigated in sedimentation ponds.

2.3.5 Stratification Modelling of Sedimentation Ponds

Stratification is a common seasonal phenomenon in deep lakes and reservoirs, where it has been linked to remobilisation of metals and nutrients. However, little is known about the potential for stratification to develop in sedimentation ponds, that are comparatively small in volume and experience very different hydrodynamic conditions. Although the experiences of Waters and Luketina (1998) and others indicates that stratification of shallow ponds can occur, no models have been developed to simulate the phenomenon in sedimentation ponds.

Numerous models have been developed to simulate the temperature structure of lakes and reservoirs or the density structure of oceans (e.g. DYRESM, the dynamic reservoir simulation model by Imberger and Patterson (1981)), but neither type of model is entirely appropriate for sedimentation ponds. For example, models developed for large water bodies are generally designed for long-term simulations (e.g. using time steps in the order of one day) and have a limited ability to simulate the diel processes that are important in small water bodies, such as sedimentation ponds. Reservoir models, for example are frequently used to predict annual thermal stratification and re-mixing, which affects algal growth and water quality. Such models typically make use of meteorological observations of daily frequency or less, and they are not designed to contend with heat or mass balances computed on an hourly basis from short-term observations.

Furthermore, lakes and reservoirs are generally considered to be of freshwater, hence the impact of salinity on the temperature structure in lakes and reservoirs has generally been neglected or has not been considered a prime component in stratification simulations. These models are therefore inadequate for modelling sedimentation ponds where the density is affected by salinity as well as temperature.

The size of the water body also influences the turbulent dynamics. The strong currents that occur in large water bodies can lead to turbulent forces far in excess of those in small ponds.

Wind wave development in sedimentation ponds for example is strictly limited by the small fetch. In lakes, models are structured to deal with large currents caused by forces such as winds, atmospheric pressure variation and unequal heating, and in oceans the modelling is further complicated by gravitational forces. These complex three-dimensional computations were unnecessary for small pond simulation, where a simple one-dimensional model was able to suffice.

Despite contrasting hydrodynamics and other differences, the theoretical elements of thermal and salt dynamics in sedimentation ponds often paralleled those in lakes, reservoirs or oceans. Lake and reservoir model in particular were a useful guide in many aspects of sedimentation pond model development.

Modelling of the thermal behaviour of lakes and reservoirs has been approached in two different ways. The earliest work involved an eddy diffusivity approach to modelling the vertical temperature structure. In this approach, the whole water body is viewed as a finite difference grid in which it is conceptually divided into a series of horizontal layers that are assumed to be perfectly horizontal and uniformly mixed. The primary difficulty was in defining the value of the coefficient of eddy or turbulent diffusion of heat between the layers either empirically or analytically, as well as describing the radiative heating. Most of these models have been based on lakes and reservoirs in the northern hemisphere.

The second modelling approach is an energy budget or integral energy approach. In this type of modelling, the water body is considered in two parts – an upper surface epilimnion, which is assumed to be instantaneously mixed, overlying water in which a temperature gradient is generated by diffusion and radiative heating. The depth of the upper mixed layer and the sub-surface temperature distribution depend on the balance of thermal and mechanical energy. Models by Kraus and Turner (1967) and Stefan and Ford (1975) were two early models of this type. The popular reservoir simulation model DYRESM (Imberger and Patterson, 1981) is also an integral energy type of model.

The integral energy approach has generally been used to model the seasonal temperature stratification cycle, where mean daily output is appropriate, rather than for simulating temperature over shorter time and small depth steps, although it has been done (e.g. Spigel *et al.* (1986)). However in this study the eddy diffusivity approach was adopted for simulating the diurnal heat dynamics in sedimentation ponds due to the success of other models of this type in small pond simulations where small time and depth steps are required (e.g. Losordo and Piedrahita (1991), Culberson and Piedrahita (1996)).

Losodo and Piedrahita (1991) successfully developed an eddy diffusion type model for simulation of the thermal behaviour of aquaculture ponds. Like sedimentation ponds, aquaculture ponds are shallow in depth and generally undergo diel cycles of thermal stratification and re-mixing, although they tend to be earthen rather than constructed of

concrete. The Losordo and Piedrahita (1991) model was tested in five aquaculture ponds at three different sites in California. It performed well for three of the ponds in northern California, but less accurately for two ponds at a southern California site, which the authors attributed to the poor position of the station for meteorological data collection. It was able to accurately predict the onset of stratification and the return to well-mixed conditions, but was less precise in predicting the peak magnitude of the pond temperature stratification.

The Losordo and Piedrahita (1991) model was later redeveloped by Culberson and Piedrahita (1996) who updated and revised the original model into a predictive model to be used as a decision making tool for aquaculturalists. Culberson and Piedrahita tested their model in aquaculture ponds in Honduras, Rwanda and Thailand and found that their revised model was able to predict the peak magnitude of thermal stratification to within 1°C.

CHAPTER 3

CATCHMENT SITES

3.1 Introduction

Selection of suitable sites for field testing and monitoring was critical to the success of the study. This included selection of several sites (including sedimentation ponds) in the Patawalonga and Torrens catchments for sediment sampling and selection of a sedimentation pond for a detailed study of metal remobilisation and stratification. This chapter first describes the process by which the sites were selected, and continues with a detailed description, photographs and general observations that were made at each site during the course of the study.

3.2 Site Selection

In the initial phase of site selection, maps of both the Torrens and Patawalonga catchments were studied, as well as catchment management plans and any existing reports or studies that could provide information on the catchment waterways. Prospective sites were selected according to their relative position in the catchment and site history. Emphasis was placed on locating sites within the major sub-catchments to ensure that the results were representative of each catchment overall, and preference was given to those sites with a history of contamination, odours or other problems.

A field survey was then performed to assess flow conditions, and pool size and depth at each potential location. Low flow conditions were desirable to minimise turbulent effects on sediment sampling equipment, and to prevent equipment being washed away during high rainfall events. For this reason, natural pools or places where water pooled upstream of a weir were particularly suitable for inclusion in the study, due to the decrease in water velocity.

A range of sites in the Torrens and Patawalonga catchments was evaluated according to the selection criteria, and after consultation with the Torrens and Patawalonga Catchment Water Management Boards the best six sites were selected for inclusion in the study:

- Torrens Catchment
  - Weir 2 (Thebarton)
  - Lockleys Weir
- Patawalonga Catchment
  - Burbridge Road Sedimentation Basin
  - Morphett Road Sedimentation Basin
  - Laffers Triangle
  - Patawalonga Basin

Each of these sites is described in detail in the following sections.

3.3 The Torrens Catchment

The River Torrens is fundamental to Adelaide's heritage, and its catchment is important as a place of recreation and amenity and as a habitat for wildlife. The Torrens catchment is commonly divided into three regions – an upper reach of approximately 270km^2, a middle reach of approximately 130km^2 and a lower reach of approximately 100km^2 (Torrens Catchment Water Management Board, 1997).

Land use in the Torrens catchment is very diverse. The upper reaches of the catchment are largely rural, and there are considerable expanses of native vegetation. The middle reach of the catchment is a mixture of rural and urban landuse, and the lower reaches are predominantly urban, although horses are also allowed to graze adjacent to the river as it flows through the western suburbs of Adelaide.

Figure 3-1 shows the Torrens catchment and the location of the two sites that were selected for the study.

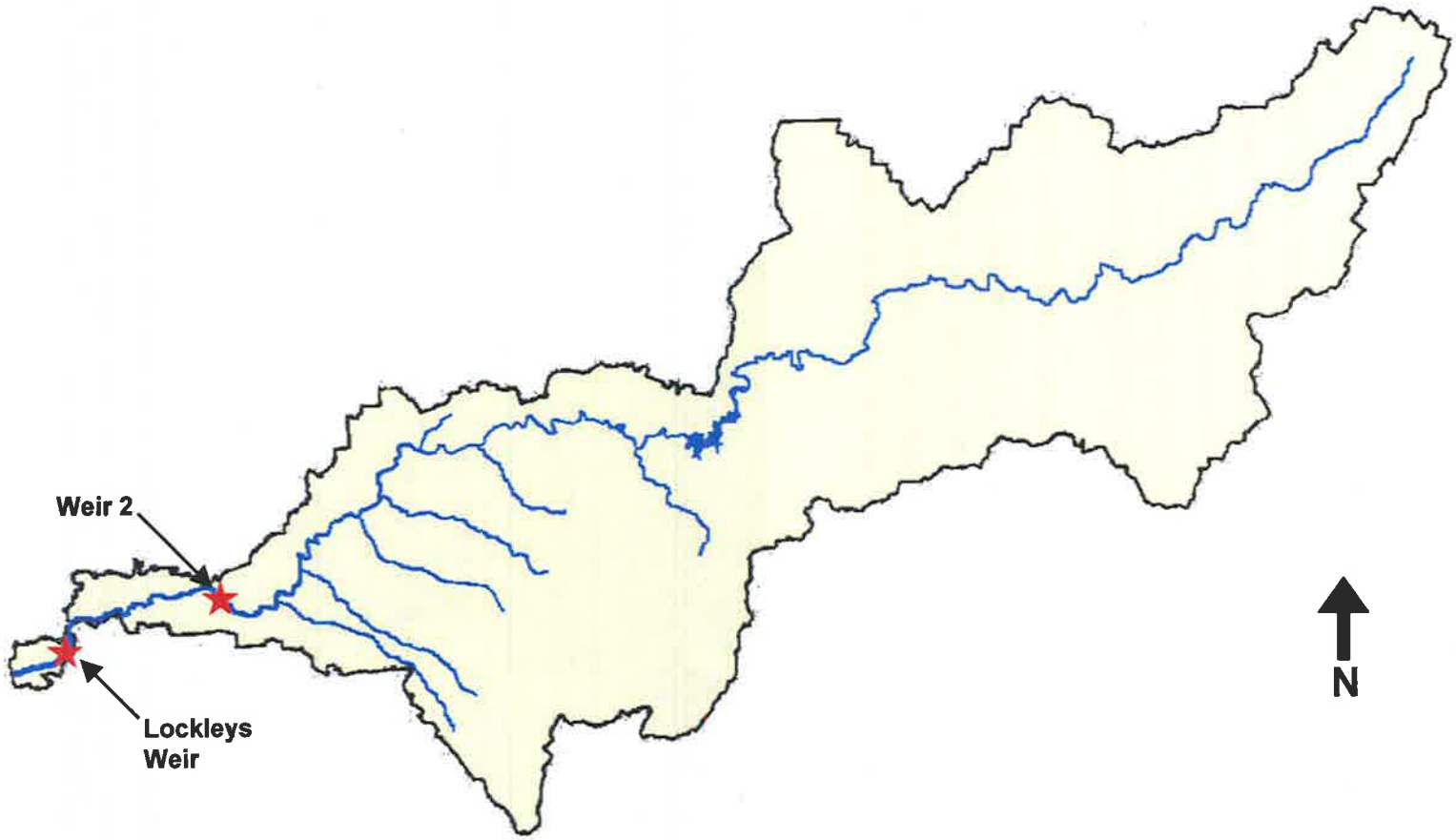

Figure 3-1: The Torrens catchment and study sites

3.3.1 Weir 2

Weir 2 is located in the north-west corner of the Adelaide Parklands at Thebarton. The runoff from the Adelaide Parklands area as well as the majority of runoff from the Adelaide CBD passes through this site.

The upstream Torrens Lake was rejected as a study site to avoid conflict with frequent boating and other recreational activities in the lake. Unfortunately, the Weir 2 lake also proved to be a popular place for water activities, which disrupted sediment sampling on several occasions. During the 18 months of field work at this site, equipment had to be replaced or repaired *in situ* a total of seven times, due to interference from other lake users or high flows.

Figure 3-2 shows the lake that is formed by Weir 2. The lake has a maximum depth of around 1.5m, and a boat was initially used to install equipment at the upstream end of the lake on 6 March 1998. The sampling site was later relocated closer to the weir, where deeper sediment provided a better base to hold the equipment in place, particularly during high flow events. The water in the new location was on average around 1m deep and equipment could be reached by wading.

Figure 3-2: Weir 2

3.3.2 Lockleys Weir

The second site selected in the Torrens catchment, was located further downstream in the River Torrens at Lockleys. In this section of river, horses are allowed to graze on the low-lying land either side of the river. Figure 3-3 shows the pool that is formed by the Lockleys weir and the adjoining horse paddocks.

Figure 3-3: Lockleys Weir

The 13 month study of Lockleys Weir pool began with the installation of sampling equipment in August 1998. Deep sediment at the bottom of the pool provided a secure foundation for the equipment, although sampling bottles were still lost on four occasions, due to high flow and corrosion of parts. A high rate of sedimentation during upstream construction of the Breakout Creek Demonstration Project, which began in January 1999, led to repeated burial of the sampling equipment.

The depth of the pool was highly variable due to sedimentation and flow variability, but the equipment was accessible by wading on all but one occasion. When equipment was first installed, the pool was approximately 1m deep, but it became shallower when flow in the River Torrens began to decrease in early November 1998. With low flows prevailing throughout the summer months and upstream flow disruption due to construction of the Breakout Creek Demonstration Project, the lower reach of the river was reduced to a series of pools. By the beginning of March 1999, the pool at Lockleys weir was only around 10cm

deep. However, as autumn continued the flow in the river increased and by mid-March 1999 the water level in the pool had again risen, although sedimentation had reduced the mean pool level by around 25%.

During the period of low flow, algal populations flourished in the Lockleys weir pool. By mid-November, the presence of iron sulfide (black mud) and the odour of hydrogen sulfide were indicative of anoxia and reducing conditions in the pool, and in late November, bubbles of odorous gas were being released when bottom sediments were disturbed. Although the dry conditions prevailed until autumn, by the end of January, very reducing conditions were no longer apparent in the Lockleys weir pool

3.4 The Patawalonga Catchment

The Patawalonga catchment is 208km^2 in area and encompasses much of the southern metropolitan region of Adelaide. It can be divided into five major sub-catchments – Airport Drain, Keswick Creek, Brownhill Creek, Sturt River, and the Local Patawalonga catchments.

Four sites were initially selected to ensure representation of the major sub-catchments in the study, but this was later reduced to three with the exclusion of the Laffers Triangle site. Figure 3-4 shows the Patawalonga catchment and the location of the selected sites.

3.4.1 Burbridge Road Sedimentation Pond

The Burbridge Road Sedimentation Pond is situated in the Airport Drain sub-catchment, one of the smallest sub-catchments, covering only 7% of the overall Patawalonga catchment area. Land use in the Airport Drain catchment is a blend of residential, commercial and industrial development. Much of the catchment is serviced by an underground drainage network, which flows into the concrete-lined airport drain. The Burbridge Road Sedimentation Pond, shown in Figure 3-5, is located part way along the airport drain, which runs along the northern side of Adelaide Airport, adjacent to Burbridge Road.

The pond is 56m long and 7.5m wide, concrete-lined and rectangular in cross-section. It is designed to retard the flow of water in the drain to allow the sediments and their attached pollutants to settle out. Trash racks are positioned at the downstream end of the pond to capture gross pollutants, such as litter, leaf matter and other debris. The depth of water is approximately 1m during low or no flow conditions, but during high flow events, the trash racks can become blocked creating a backwater effect that temporarily increases the water depth in the pond to very high levels.

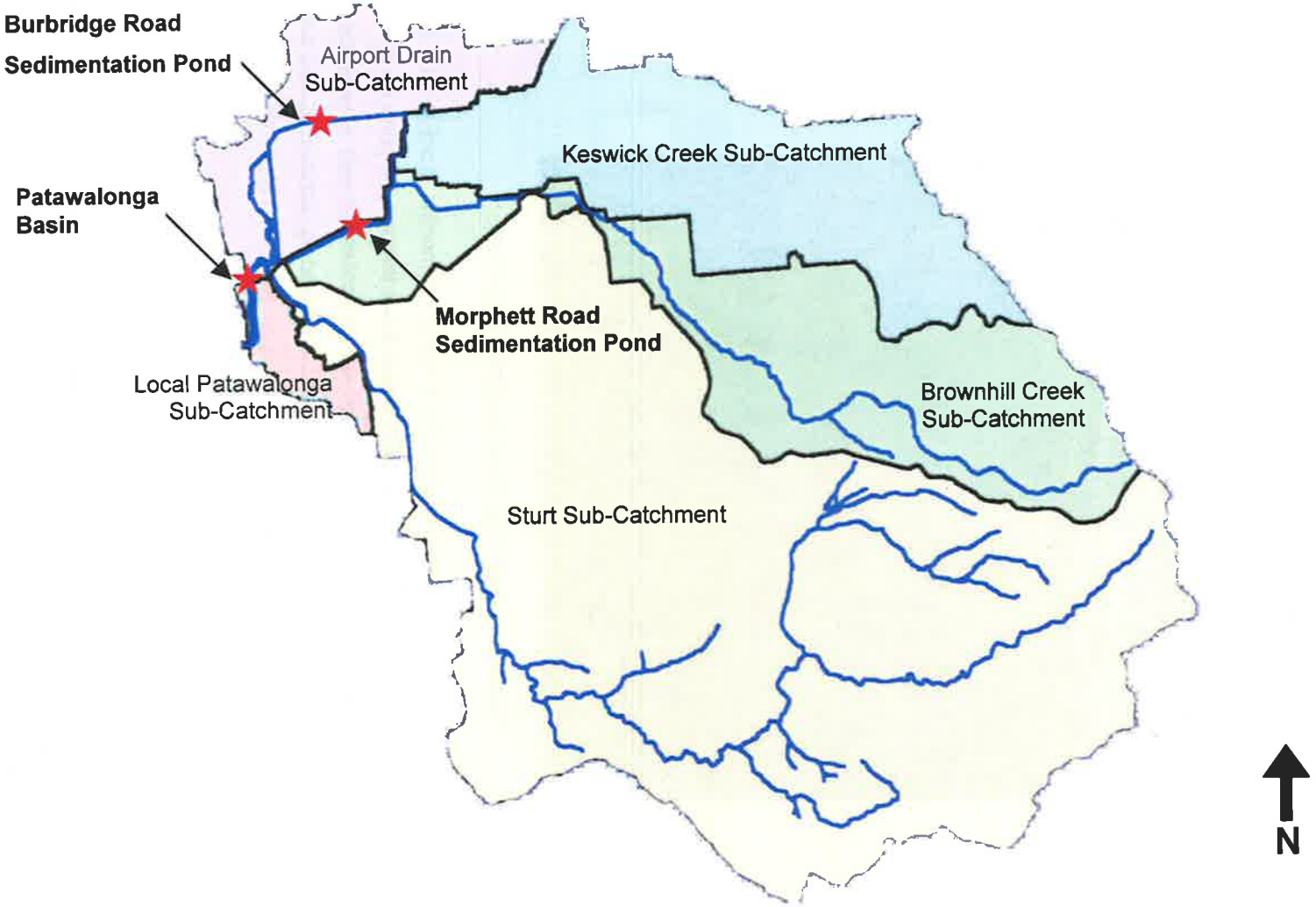

Figure 3-4: The Patawalonga catchment and study sites

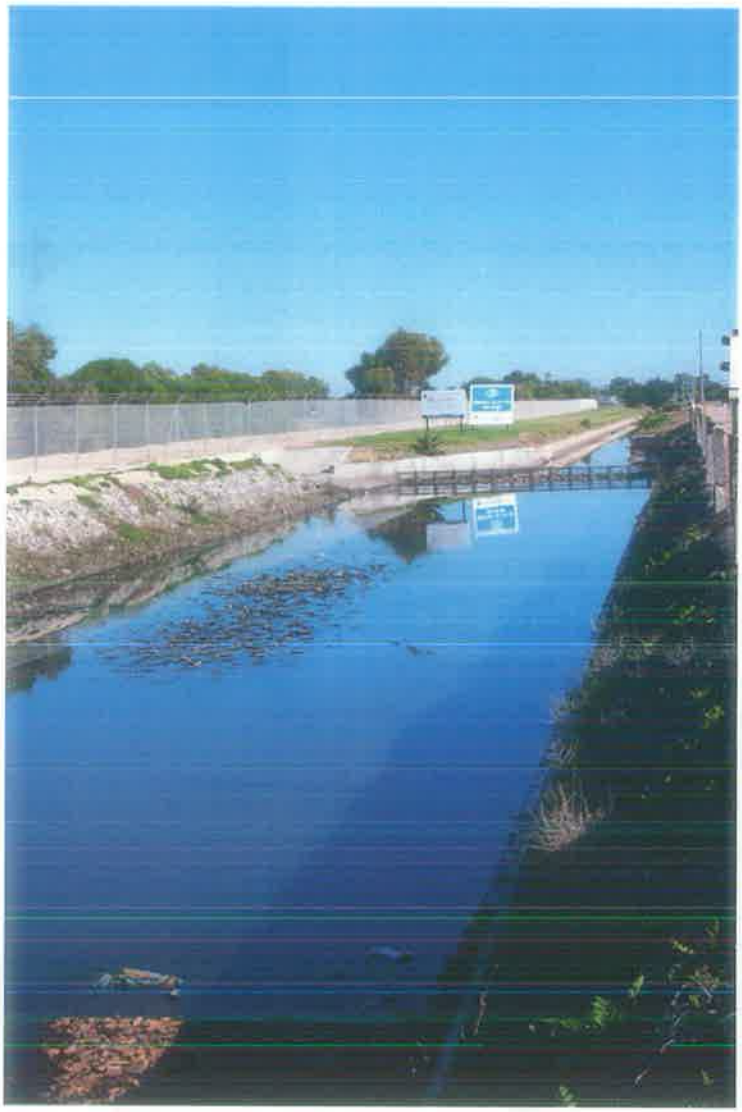

Figure 3-5: Burbridge Road Sedimentation Pond

The field study of Burbridge Road Sedimentation Pond lasted 13 months, from August 1998 until September 1999. Although there was evidence of high flows through the pond on several occasions, flow through the pond at the time of each sample collection was always low or non-existent. As a result, equipment was always accessible by wading, although it was made difficult by the accumulation of litter and organic matter such as leaves and tree branches, which was typically knee-deep.

Reducing conditions were evident in the Burbridge Road pond, from February 1999 until sampling ceased in September 1999. The reducing conditions generated ferrous sulfide, a very black mud, and odorous hydrogen sulfide gas. Flow events through the pond lessened but never eliminated the reducing conditions, and were instrumental in the appearance of algal blooms on two occasions – the first in July 1999 and the second in early September 1999.

3.4.2 Morphett Road Sedimentation Pond

The Morphett Road Sedimentation Pond, shown in Figure 3-6, is situated on the southern side of Adelaide Airport at the end of Morphett Road. Stormwater flowing through the pond comes from the Brownhill Creek and Keswick Creek catchments, where the land use is predominantly residential with some light industrial, commercial and rural areas.

Figure 3-6: Morphett Road Sedimentation Pond

The Morphett Road Sedimentation Pond is designed to remove pollutants, by slowing the flow of water and allowing sediments and their attached pollutants to settle out. The pond also has trash racks at the downstream end to capture gross pollutants. The channel upstream of the Morphett Road Sedimentation Pond is heavily vegetated, which helps to filter sediments from the water before it enters the pond. There may also be some uptake of dissolved pollutants by the vegetation upstream.

The pond is concrete-lined and trapezoidal in cross-section, with side slopes of approximately 1 in 2. It is 130m long and 20m wide, and has steeply sloping banks on either side. Mean depth in the pond is approximately 0.9m with low or no flow, but during high flow events water can rise as much as 2 to 3m above the mean water level due to the backwatering effect created when the trash racks become choked with debris.

Morphett Road Sedimentation Pond was studied more intensely than any other site. The three main reasons Morphett Road Sedimentation Pond was chosen for the study were that:

- there was plenty of surrounding space for easy access to the pond and for equipment installation;
- there was a meteorological station in close proximity; and
- it was in a relatively isolated position, which reduced the risk of equipment being vandalised.

The field study involved 16 months of sediment sampling and 15 months of temperature monitoring and depth profiling. Sediment sampling equipment was first installed in the Morphett Road sedimentation pond in August 1998. However, after the equipment was repeatedly pushed over during high flow events through the pond, a second, more stable sampler was installed three months later. Flow through the pond was generally low or non-existent at the time of sample collection, and on all but one occasion, immediately following a high rainfall event, the equipment was accessible by wading.

The temperature monitoring and depth profiling phase of the study began in January 1999, with the installation of a platform in the pond. The platform, which was used to support monitoring equipment and facilitate the depth profiling, was approximately $1m^2$ and could be accessed from the northern side of the pond via a narrow walkway. The platform and monitoring equipment are described in more detail in Chapter 5.

3.4.3 Laffers Triangle

The initial trials of the sediment sampling equipment were carried out at a site in the Sturt River at Laffers Triangle, near the junction of Sturt and Marion Roads. Figure 3-7 shows the small natural pool that provided an ideal site to sample sediment and water before the start of the concrete-lined drain, which channels the Sturt River all the way to the Patawalonga Basin. Land use in the catchment upstream of the site, is a blend of residential and commercial development, and open space.

Sediment sampling equipment was installed at Laffers Triangle in March 1998. The pool was no more than 0.5m deep, and equipment was easily accessible by wading. However the equipment disappeared during July 1998, due to either high flow or vandalism. Although replacement equipment was initially planned, with further disruption at the site due to earthworks and realignment of that section of river as part of the construction of the Warriparinga Wetlands, it was decided that Laffers Triangle would be excluded from the study.

Figure 3-7: The pond at Laffers Triangle

3.4.4 Patawalonga Basin

The Patawalonga Basin is currently the final collection point for water from the major sub-catchments of the Patawalonga catchment. The Sturt River, Brownhill Creek, Keswick Creek and Airport Drain catchments, as well as several local drains all flow into the Patawalonga Basin. Figure 3-8 shows the upstream end of the Patawalonga Basin where equipment was installed.

The field study in the Patawalonga Basin lasted 13 months, but sampling was continually disrupted due to high flow, high wind and waves, high salinity and interference from other activities in the Patawalonga Basin.

Sediment sampling equipment was first installed at the upstream end of the Patawalonga Basin in August 1998. However, the clamps holding the sample bottles corroded in the saline environment, and in less than three months, the sampler had to be replaced. A second sampler was installed in December 1998 and again in February 1999, after it had been removed to make way for other activities in the Basin. The second sampler then became encrusted with barnacles and a third sampler had to be installed in May 1999. The third sampler functioned successfully until the end of the field study in the Patawalonga Basin.

Figure 3-8: The Patawalonga Basin

The Patawalonga Basin was the deepest site to be included in the study. Equipment installation and initial sample collections were carried out using a boat. Later sample collections were carried out using a 1-person canoe, which was more manoeuverable in the water and easier to transport to the site. However, collecting samples in the canoe was more hazardous than wading, and it was necessary to abandon sample collection in the Patawalonga on three occasions, due to strong winds and wave action in the Basin.

Although the depth at the sampling site was generally between 1.2m and 1.5m, large fluctuations in the water level were observed. The depth ranged from less than 10cm in mid-July 1999, which allowed the sediment trap to be reached by wading, to approximately 1.9m less than 2 months later. When the Patawalonga Basin was at its deepest level, the sample bottles could not be retrieved at all because the equipment had been submerged by the high flow.

CHAPTER 4

SEDIMENTS AND HEAVY METALS

4.1 Introduction

Sedimentation ponds are an integral part of most urban stormwater management plans. However sedimentation ponds must be properly sited, designed, constructed and maintained, to fully achieve the desired water quality treatment targets. To determine the optimum siting and design of sedimentation ponds in the Patawalonga and Torrens catchments, it is necessary to first observe the behaviour of sediments and their metal contaminants in the two catchments, and to evaluate the performance of existing sedimentation pond facilities.

This chapter focuses on the investigation of sediments and heavy metals in the Patawalonga and Torrens catchments, and the efficacy of the existing sedimentation ponds (Burbridge Road Sedimentation Pond and Morphett Road Sedimentation Pond) in removing sediments and heavy metals.

Sediment samples were taken from the five sites in the Patawalonga and Torrens catchments that were described in Chapter 3. The first part of this chapter describes the selection and design of the sampling equipment, its installation at each site, and the sampling and analysis program that was undertaken. The second part of the chapter is dedicated to a discussion of sediment in the Patawalonga and Torrens catchment, including its composition, size, metal contamination and rate of accumulation, followed by an evaluation of the performance of the two sedimentation ponds.

4.2 Sediment Sampling

The sedimentary materials most commonly sampled include the bottom surface sediments, sub-surface sediments or suspended material in the water column. Interstitial water (the water contained within the pores of the bottom sediments) is also sometimes extracted due to its

importance in post-depositional reactions and diagenesis. Grab and core samplers are commonly used to sample the surface and sub-surface sediments. However, traditional techniques such as these are inappropriate for sampling the <62μm sediment size fraction, which is poorly represented in the bottom sediments (Ongley *et al.*, 1981).

Grab and core sampling are also of little use in determining time dependent variables, such as sediment flux on a short-term basis (e.g. over the course of a season or year). However time-integrating sediment trap samplers can be used to determine sedimentation rates and sample suspended sedimentary material (Förstner, 1981; Van Rijn, 1994).

A sediment trap generally consists of one or more bottles that are suspended in the water column for a period of time, to capture the sedimentary material that is settling or being resuspended. The bottles are supported in the water column by a bottle carrier, which is attached to a post or weighted cable. The bottle carrier can be raised or lowered at any time to exchange the bottles.

Sediment trap samplers are relatively simple in design and cheap to construct. Their major advantage however is their ability to measure sedimentation rates as already mentioned, and their ability to capture large quantities of material for analysis (Wangersky, 1994). For these reasons, sediment trapping was the sampling method chosen in this study.

4.2.1 Sediment Trap Design

Critical to the success of sediment trapping is the design of a sediment trap structure that causes the smallest possible disturbance to natural deposition and resuspension. The three main parts of the sediment trap, the post or cable, the bottle carrier and the sediment trap containers, must be carefully designed to minimise hydrodynamic disturbance, while allowing for easy removal and replacement of sediment samples.

Sediment traps are 100% efficient in still water, but in flowing water their efficiency decreases depending on turbulence generated within the trap, trap geometry and particle characteristics (Van Rijn, 1994). Of particular importance are the size and shape of the sediment trap containers, which govern the loss and accumulation of material in the trap.

In the 1980s numerous studies were made of sediment trap dynamics, specifically focussing on the influence of turbulence and flow on the efficiency of sediment trapping. Important work was done at this time by Gardner, who evaluated the performance of different sediment trap containers, first in the laboratory (Gardner, 1980b) and then in the field (Gardner, 1980a). Gardner found that the size and shape of a trap container and the internal eddies which are created inside it due to the surrounding hydrodynamics, critically affect the quantity of material that will be collected. After studying the trapping efficiency of cylinders, funnels, wide-

mouthed jars, and containers of different sizes, under different flow conditions, Gardner concluded that there was in fact no unique trap design that was superior under all conditions of velocity and turbulence. Instead, he suggested a series of guidelines for the use of different trap containers under different flow conditions.

In a review of Gardner's work, as well as of critical studies by Bloesch and Burns (1980) and Blomqvist and Håkanson (1981), Håkanson *et al.* (1989) concluded that cylindrical traps, with a diameter greater than 4 cm and an aspect ratio (height/diameter) greater than 3, were the best form of trap container, superior to funnels, which generally under-trap sediment, and narrow-necked bottles, which are likely to over-trap material. While there is no established protocol for the design of sediment traps Bloesch (1996), the criteria of Håkanson *et al.* (1989) are commonly used.

After evaluation of all the literature on sediment trap design, wide-mouth bottles with an aspect ratio of 3.7, a body diameter of 6cm and mouth diameter of 3.5cm were chosen. The bottles, made by Nalgene, were of low-density polyethylene, with a volume of 250mL and had a screw-top lid for easy transport of the samples. To ensure adequate sediment samples for analysis, each trap was designed to carry two sediment sample bottles.

Four different sediment trap structures were designed to cater for varying depths, pond or river-bed characteristics, and sampling objectives. The first sediment trap that was designed is shown in Figure 4-1 (a) and was a modified version of the trap used by Håkanson *et al.* (1989). It was designed to sample sediment at multiple positions through the water column. The bottle carrier was lowered up and down on a cable anchored to a heavy concrete weight at the base and a submerged buoy at the top. The buoy was submerged in order to hold the cable taut but minimise drag from wind and surface currents. A second buoy at the surface acted as a marker for the trap.

Numerous problems with the design became apparent after the sediment trap was tested in the Weir 2 lake. Of primary concern were the variable flow and depth conditions, which made it impossible to maintain a constant tension in the cable. Insufficient tension meant that the bottles were not in the necessary upright and stable position in the water column at all times. Furthermore, because the depth was less than 1.5m, it was possible that the trapping efficiency of bottles in the lower two positions might be hindered by an alteration in flow dynamics caused by the bottles above. The quantity of sediment that was captured in the bottles was also too small to enable analysis of the mineralogy or heavy metals for the separate depth fractions. After the trial of the multiple depth sediment trap it was replaced by a sediment trap of the design shown in Figure 4-2 (a), which is discussed below.

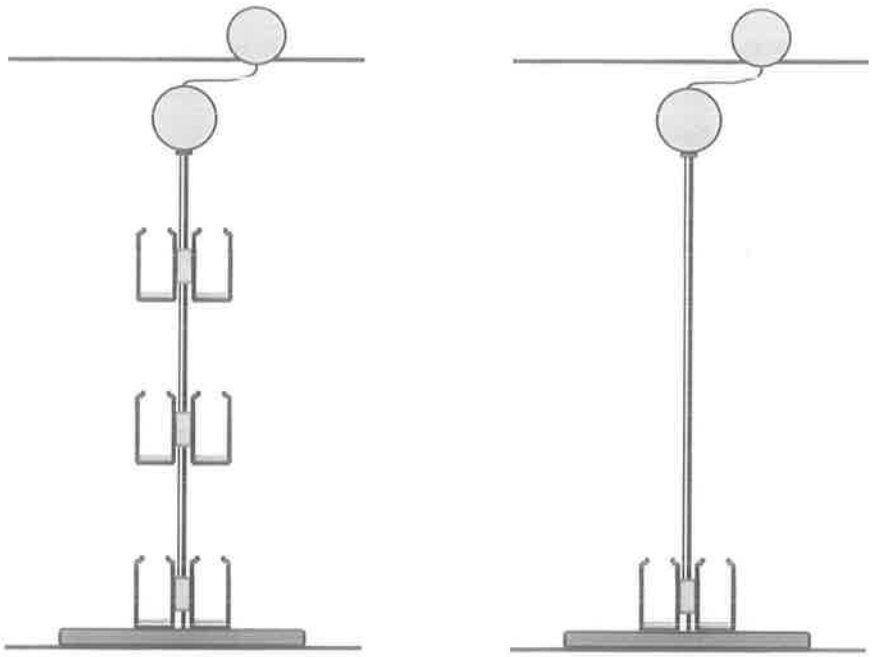

Figure 4-1: Sediment traps (a) for sampling at multiple depths (modified from Håkanson *et al.* (1989)); and (b) for a single water column sample in deep water

The sediment trap shown in Figure 4-1 (b) was similar in design to the trap constructed for multiple depth water column analysis. However, without bottles suspended at multiple depths there was less drag acting on the cable, and the bottles resting at the base of the cable were able to remain sufficiently upright. Although the trap functioned successfully, it had to be replaced after only three months due to corrosion of the bottle carrier. It was replaced by a trap of the style shown in Figure 4-2 (a) below, which had been found to be simpler to construct and install in the water.

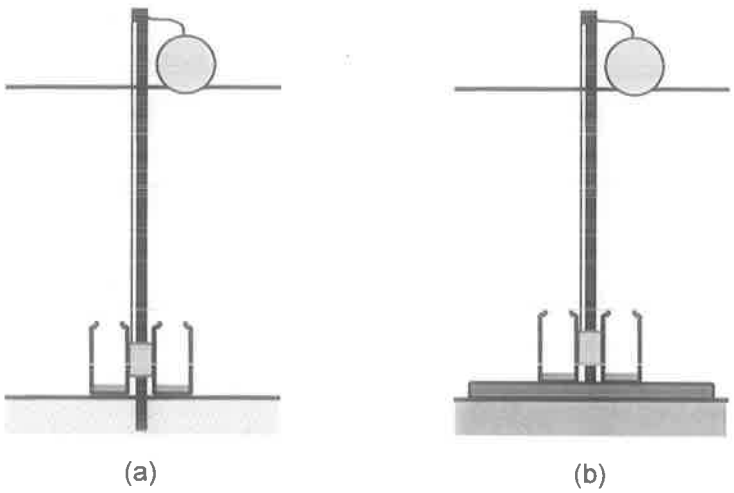

Figure 4-2: Sediment traps (a) for a sedimentary pond or river-bed; and (b) for a concrete-based sedimentation pond

The shallow water trap shown in Figure 4-2 (a) consisted of a post and a bottle carrier, which held the sediment trap bottles. The carrier was raised and lowered on the post using a fine wire cable, which was shackled to the top of the post. A buoy was attached as a marker at sites where boating or other water activities took place. The addition of a concrete base as in Figure 4-2 (b) enabled the traps to be used in the concrete-based sedimentation ponds, where a post could not be driven into sediments. Figure 4-3 shows a concrete-based sediment trap prior to installation in the Morphett Road Sedimentation Pond.

Figure 4-3: A sediment trap before installation in the Morphett Road Sedimentation Pond

4.2.2 Sediment Trap Construction and Installation

The sediment traps were constructed in the Department of Civil and Environmental Engineering workshop, according to the specified designs. At most sites, the water was shallow enough to wade out and either hammer the trap into the sediment, or lower the trap

into the water if it had a concrete base. Where the water was deeper, in the Patawalonga Basin and at the initial sampling location in the Weir 2 lake, a boat or canoe was used when installing the traps.

The traps were oriented in the water, so that the bottles were suspended perpendicular to the primary direction of flow, as shown in Figure 4-4. In this arrangement the bottles were most likely to be equally exposed to the settling and resuspended sediment. Where a star dropper style post was used, it was aligned so as to minimise disruption of the streamlines.

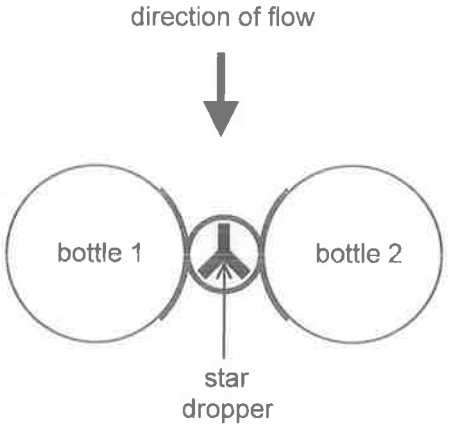

Figure 4-4: Top view of a sediment trap showing the correct orientation

Table 4-1 shows the dates of installation and removal of sediment traps at each location, and a reference to the illustration of the corresponding type of sediment trap. Where sediment traps were washed away or disappeared, no date of removal is shown in the table.

Appendix A contains details of the dates of trap installation, removal or disappearance and any repair work that was carried out. Whenever possible repairs to the sediment traps were done *in situ*. High flows, corrosion and suspected vandalism were the most common causes of sediment trap disturbance. Repairs mostly involved modification of the bottle carrier or righting and re-securing the trap, but when repair was not possible or the trap had disappeared, a replacement trap had to be constructed and was installed at the earliest opportunity.

The basic design of the sediment traps was continually improved and updated as each new trap was constructed. Modifications to the design ranged from minor changes, such as enlarging the size of the concrete base to improve stability in high flows, and changing to different sample bottles, to more major changes, such as a complete re-design of the bottle carrier.

Loss of sample bottles from the sediment traps was a problem at all of the sampling sites, and a number of samples were lost before a successful design was determined. Bottle carriers were initially designed with simple hose clamps that could be adjusted with a screwdriver.

However the sample bottles were pre-frozen and could not be tightly clamped into the traps because the diameter slowly decreased as they thawed. A gradual switch was made to bottles of a higher density polyethylene, which was stiffer and suffered less distortion when water expanded as it froze. Although the new bottles were slightly more successful, rust, sediment and algae gradually made it impossible to screw and unscrew the clamps, so bottles had to be additionally secured to the carrier with rubber bands.

Table 4-1: Sediment trap installation and removal

SITE	DATE OF INSTALLATION	DATE OF REMOVAL	TYPE OF SEDIMENT TRAP
Weir 2	6 May 1998	13 May 1998	Figure 4-1 (a)
	13 August 1998		Figure 4-2 (a)
	23 September 1998		Figure 4-2 (a)
	16 October 1998		Figure 4-2 (a)
	6 January 1999	30 September 1999	Figure 4-2 (a)
Lockleys	13 August 1998		Figure 4-2 (a)
	29 July 1999	16 September 1999	Figure 4-2 (a)
Burbridge Road Sedimentation Pond	20 August 1998	30 September 1999	Figure 4-2 (b)
Morphett Road Sedimentation Pond	27 August 1998	9 October 1998	Figure 4-2 (b)
	30 November 1998	2 December 1999	Figure 4-2 (b)
Patawalonga Basin	27 August 1998		Figure 4-1 (b)
	18 December 1998	3 March 1999	Figure 4-2 (a)
	15 April 1999	29 April 1999	Figure 4-2 (a)
	13 May 1999	30 September 1999	Figure 4-2 (a)

The most significant problem with the initial clamping arrangement was corrosion. In the Patawalonga Basin for example, the clamps had rusted into pieces after only 10 weeks. As a result, the bottle carriers were refashioned in stainless steel, with rubber O-rings to hold the bottles. The rubber O-rings maintained a tight hold on the sample bottles even as they thawed, and were easy to replace if they lost their elasticity. The new clamping arrangement proved successful, and was gradually phased in as the bottle carriers with the older style clamping needed replacing.

4.2.3 Sediment Sample Removal

Raising or lowering the bottles too quickly or roughly can disturb the bottom sediment layer, and may have a flushing effect on the bottle contents. Kirchner (1975) added brine to the trap bottles to establish a density gradient, to minimise disturbance of the bottom sediment layer during raising of the bottles. However, in a comparison of trapping with and without the addition of brine, Peterson and Dam (1990) found that the rate of capture of swimmers in the trap with added brine was 10 to 100 times greater. Since the additional source of both particulate and dissolved organic matter due to swimmers could bias sediment flux results, brine was not used in this study. Care was taken to minimise the disturbance of samples while raising the sediment bottles. Fortunately since the depths of bottle deployment were significantly shallower than in the majority of sediment trapping experiments that were reviewed, there was less potential for sediments to be disturbed while the sample bottles were being removed from the traps.

At the time of retrieval, bottles were slowly raised to the surface, where they were capped before being packed in ice for transport to the laboratory. Replacement bottles were filled with millipore water and frozen to prevent entry of sediment as the bottles were lowered into position, as was done by Fennessy *et al.* (1994).

4.2.4 Sediment Sampling Frequency

There appears to be no uniformly used or recommended time interval for retrieval of sediment trap samples. A review of the sediment trap methodology used in a variety of studies, revealed trapping intervals ranging from bi-weekly (Tamminga, 1992) to 120 days (Evans and Håkanson, 1992). The most common trapping interval was either weekly or monthly (Johnson, 1977; Weyhenmeyer *et al.*, 1995; Nõges *et al.*, 1999), while in another study (Weyhenmeyer, 1996) trap samples were retrieved on a weekly basis during summer and monthly during winter.

Extremely long trapping intervals are undesirable due to the potential for mineralisation of trapped material. The use of preservatives or poisons, such as mercuric chloride, formaldehyde and chloroform effectively inhibit microbial activity (Lee *et al.*, 1992), but their use is controversial due to the influence on swimmers in the traps. Swimmers compromise sediment trapping results due to their consumption of trapped material and contribution to trap material through fecal pellet production or death (Lee *et al.*, 1992; Wakeham *et al.*, 1993; Hansell and Newton, 1994). Poisons or preservatives may lead to an increased death rate among swimmers, which may alter the mass and composition of the trapped material.

Håkanson *et al.* (1989) opposed the use of preservatives, and recommended repeated weekly or bi-weekly sample retrieval. However, with the number of sites that were included in this study, a weekly or bi-weekly trapping interval would not have allowed sufficient time for collection and processing of all the samples. Instead, a fortnightly sample retrieval was decided upon, although due to time and weather constraints, the actual trapping interval ranged from 8 to 21 days. Although no preservative or other treatment agent was used, the traps were designed with replaceable sample bottles. By replacing the trap containers with clean bottles at the time of each retrieval, rather than decanting the sample from fixed trap containers, there was less potential for algal growth to establish on the walls of the trapping container, and influence the results.

The dates of sample collection at each of the study sites are summarised in Appendix A.

4.3 Sediment Analysis

Sediment samples, once collected and transported to the laboratory, were kept in darkness in a refrigerator below 4°C until undergoing analysis, in accordance with the standards set out in Standard Methods for the Examination of Water and Wastewater (APHA, 1995).

The laboratory analysis of the sediment samples was carried out in four stages. Table 4-2 outlines the objectives of each stage and the laboratory where the analysis was performed. While Figure 4-5 provides an overview of the laboratory procedures that were carried out in each stage of the sediment analysis to obtain the analytical objectives.

Table 4-2: The stages of sediment analysis

	ANALYTICAL OBJECTIVES	TESTING LOCATION
STAGE 1	Sediment flux. (Separation and drying for stages 2, 3 & 4)	Environmental Laboratory, Department of Civil and Environmental Engineering, The University of Adelaide
STAGE 2	Heavy metal contamination.	Gribbles Analytical Laboratories, Melbourne
STAGE 3	Particle size distribution.	Department of Chemical Engineering, The University of Adelaide
STAGE 4	Sediment composition (mineralogy, organic matter content and elemental nature).	Department of Geology and Geophysics, The University of Adelaide

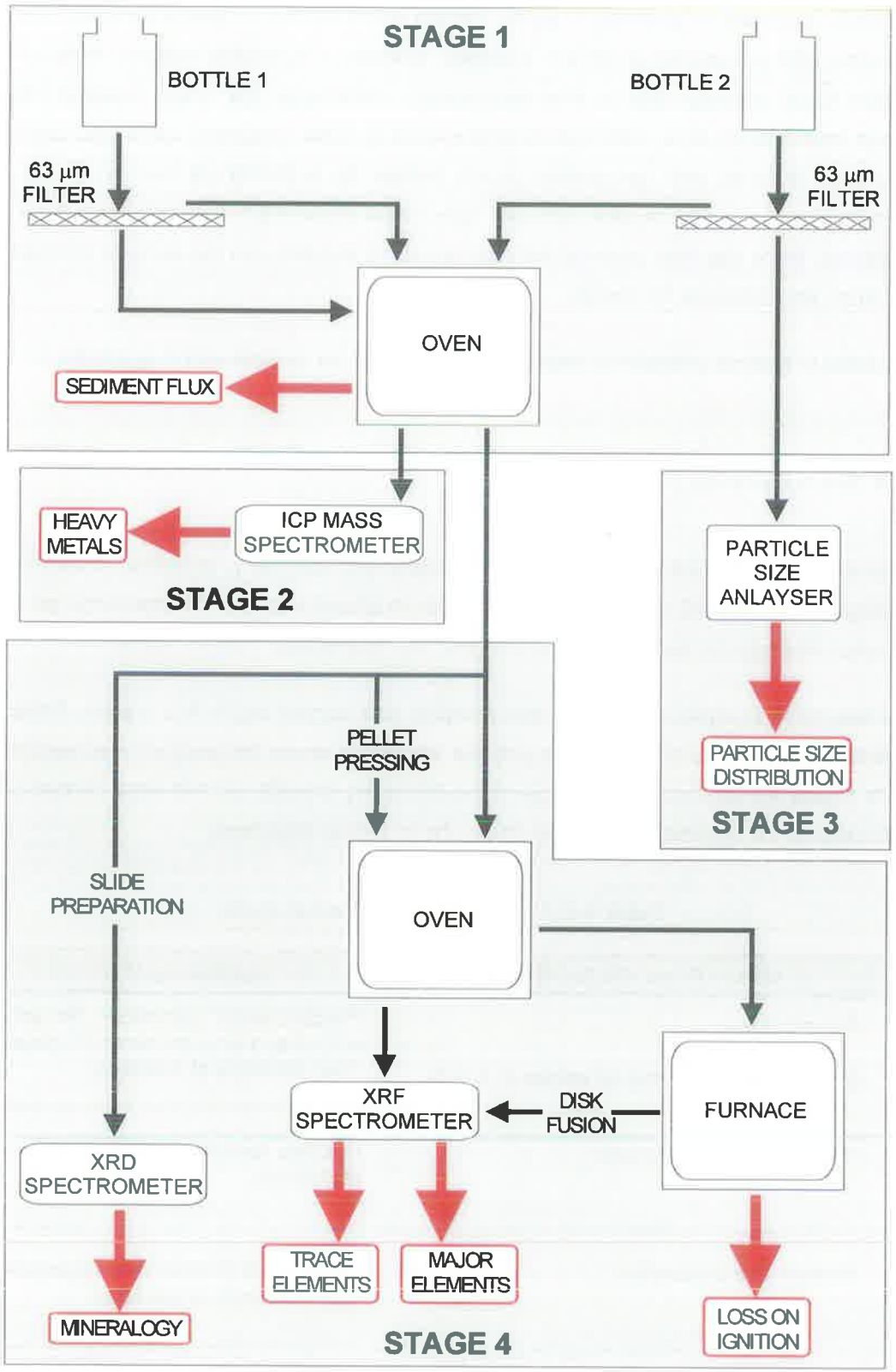

Figure 4-5: Overview of the sediment analysis procedures

4.3.1 Sediment Flux (Stage 1)

The sedimentation rates are not comparable between sites since the flow rate affects both the rate of deposition and resuspension, but they are still indicative of the nature of the material in transport.

The sediment flux or rate of sedimentation of both the <63μm and >63μm particle size fractions at each site was determined by drying and weighing the sediment trap samples. This was performed in Stage 1 of the analysis process.

For each sediment trap bottle (two for each site) the sample was first poured through pre-weighed 63μm filter mesh under vacuum filtration to separate the <63μm and >63μm particle size fractions. Millipore water was used to flush the sample through the filter and to rinse the sample bottle and each piece of equipment during removal of the separate particle size fractions from the filtration equipment to ensure no sediment was left behind. (All equipment was washed thoroughly with tap water then rinsed three times with Millipore water between each sample.)

Two sample bottles were filtered for each site. The filtrate (<63μm) from one bottle was decanted into pre-weighed evaporating dishes and the filtrate from the second bottle was stored in 1L sample bottles below 4°C in preparation for particle size analysis. The filter circles holding the sediment residue (>63μm) were placed on petri dishes and dried in an oven at 80°C for a minimum of 48 hours.

When dry, the evaporating dishes and filter circles were separately weighed, and the total sediment mass calculated for each sample using Equation 4.1 for the <63μm particle size fraction and Equation 4.2 for the >63μm particle size fraction.

$$M_{<63} = \Sigma\left(M_e - M_{e\,dw}\right) \tag{4.1}$$

$$M_{>63} = \Sigma\left(M_f - M_{f\,dw}\right) \tag{4.2}$$

where: $M_{<63}$ is the total mass of sediment <63μm in g;

$M_{>63}$ is the total mass of sediment >63μm in g;

M_e is the weight of the empty evaporating dish before the sample is added in g;

$M_{e\,dw}$ is the weight of the evaporating dish + dry weight of sample in g;

M_f is the weight of the unused filter circle before the sample is added in g; and

$M_{e\,dw}$ is the weight of the filter circle + dry weight of sample in g.

The average sediment flux or rate of sedimentation during each sampling period was then calculated for each particle size fraction using Equation 4.3.

$$\phi_{Sx} = \frac{M_x}{n} \times \frac{1}{A} \qquad (4.3)$$

$\phi_{S\,x}$ is the sediment flux for particle size fraction x in g/m^2/day;

M_x is the mass of particle size fraction x in g;

x is the particle size fraction (either <63μm or >63μm);

n is the number of days in the sampling period in days; and

A is the surface area of the mouth of the trap bottle in m^2.

In preparation for analysis in stages 2, 3 and 4, the sediment fractions were then extracted from the evaporating dishes or filter circles. Seasonal composite samples were prepared for all sites except the Patawalonga Basin, where samples from the finer fraction collected in summer and autumn were isolated for individual analysis.

Until required for further analysis, the composite and individual samples were sealed in glass vials and stored with sachets of silica gel, a desiccant, which minimised absorption of moisture by the dried samples.

4.3.2 Heavy Metal Contamination (Stage 2)

Water quality testing has been conducted in the Torrens catchment by the Engineering and Water Supply Department of South Australia (SA Water Corporation) and others since 1940 (Torrens Catchment Water Management Board, 1997). Heavy metals testing has included the metals aluminium, arsenic, barium, boron, cadmium, chromium, copper, iron, lead, manganese, mercury, nickel, selenium, silver and zinc, and has indicated levels of chromium, lead, nickel, aluminium, copper and zinc in excess of ANZECC Guidelines for protection of freshwater ecosystems, and chromium and nickel levels in excess of ANZECC Guideline levels for secondary contact (Torrens Catchment Water Management Board, 1997).

In the Patawalonga catchment, heavy metals tested have included arsenic, cadmium, chromium, cobalt, copper, lead, nickel and zinc, with levels of chromium, copper, lead, nickel and zinc found to be in excess of ANZECC Guidelines for protection of freshwater

ecosystems and/or secondary water contact (Patawalonga Catchment Water Management Board, 1997)

Based on the previous studies and in order to identify any unusual metal behaviour in the sediment samples, a large number of metals were selected for analysis. These included antimony, arsenic, barium, beryllium, boron, cadmium, chromium, cobalt, copper, lead, molybdenum, nickel, selenium, tin, vanadium and zinc.

For metal analysis, sediment samples are usually first digested (e.g. by nitric acid or microwave digestion) to decrease the organic matter content. The digestion process also converts the sample into the form required for analysis, which is generally performed by atomic absorption spectroscopy or inductively coupled plasma spectroscopy.

Other metal analysis techniques include the flame atomic adsorption method, electrothermal atomic adsorption spectrometry and the dithizone method. All techniques have possible complications such as chemical, physical or spectral interference or interference from other metals present. The choice of test largely depends on the particular metal being analysed and its likely range of concentration.

The sediment samples were sent to Gribbles Analytical Laboratories in Melbourne, which test for heavy metals using microwave digestion with the inductively coupled plasma and mass spectrometry technique.

From the sediment samples from each site, seasonal composite samples were prepared for both the <63μm and >63μm particle size fractions. Although due to the unique appearance and distinctive behaviour of sediments from the Patawalonga Basin, samples from the <63μm particle size fraction that were collected during summer and autumn, were analysed individually.

4.3.3 Particle Size Distribution (Stage 3)

The full particle size classification of sediments is shown in Table 2-1 in Chapter 2. The particles that were of interest in this study were those at the small end of the scale – silts and clays, which were less than 63μm in size. This sediment size fraction has sometimes been termed the 'geochemically active' fraction (Ongley *et al.*, 1981) due to the high chemical reactivity of particles in the <63μm size range. The high reactivity is commonly attributed to the proportionally higher surface area and surface chemistry of the finer particles.

Separation of the <63μm particle size fraction for analysis of metals is generally accepted as standard around the world (de Groot, 1995). In this study, sediment samples from the different sites were normalised by separation and analysis of this <63μm particle size fraction.

Particle separation techniques traditionally used in geotechnical analysis of particle sizes, such as dry sieving, are inappropriate for separation of very small particles. The smallest sieve sizes generally used in geotechnical investigations are commonly no smaller than 63μm in size. For analysis of particles below 63μm, alternative methods are required. The more common techniques include vacuum filtration, sedimentation, the Coulter Counter method and laser diffraction.

Vacuum filtration involves the use of a pump, a funnel and flask and a filter circle of paper or mesh of the required size. The pump is used to suck the sample though the pre-weighed filter circle at the bottom of the funnel into the flask below. Each filter circle is then dried and weighed to determine the mass of residue.

It is a simple and inexpensive method of particle size separation, but tedious for the analysis of many sizes or large sample volumes, which require multiple filter circle replacements. Each replacement of a filter circle reduces the accuracy of the technique, since the small sediment particles are invisible to the naked eye and may escape detection by adhering to the sides of the equipment despite flushing with millipore water. The accuracy of the technique also relies on the accuracy of the weighing scales and the precision of the woven mesh, which may be warped while filter circles are being measured and cut.

Particle size separation by sedimentation can be achieved a number of ways, all of which rely on the relationship between particle size and settling velocity. This relationship is represented by Stokes' Law (Equation 4.4).

$$v = \frac{2 g r^2}{9 \mu}(\rho_s - \rho) \qquad (4.4)$$

where: v is the fall velocity in m/s;

g is the gravitational acceleration in m/s^2;

r is the particle radius in m;

ρ_s is the density of the particle in kg/m^3;

ρ is the density of the water in kg/m^3; and

μ is the viscosity of the water in kg/m s.

The simplest of these methods involves the use of a settling column, from which known volumes of liquid are extracted at known time intervals, usually by pipette. The samples are dried and weighed to determine the change in concentration over time, from which the particle size may be determined according to Stokes' Law. An alternative method involves repeated

settling, decanting and mixing of the sample in a settling column over set time periods. Both methods produce similar particle size distributions (Fontaine *et al.*, 2000).

The hydrometer method operates on the same basic principles, but instead plots the change in depth of a hydrometer in a settling column over time. The depth of the hydrometer at any moment in time depends on the density of the particle suspension, and again Stokes' Law is used to determine the relevant particle size distribution.

The two main assumptions of Stokes' Law are that all the particles have the same density and all are perfectly spherical – neither of which will be truly accurate for sediment trap samples. For example, during the mineralogical analysis (see Section 4.4.2.1) the mineral muscovite was identified as a major constituent in samples from each site. In general, muscovite crystals tend to be monoclinic and the mineral has a perfect basal cleavage, making it flakey in appearance – far from the perfect spheroid.

Sedimentation is also influenced by variability in the sample temperature (which affects the viscosity and may produce convective currents (Metcalf and Eddy, 1991)) and particle aggregation. Warren and Zimmermann (1994) observed a shift in particle size distribution from finer clay-sized particles to silt-sized particles with increasing water temperature. They theorised that the warmer water temperatures were enhancing aggregation of the finer clay-sized particles, possibly through bacterial mediation.

Despite the possible inaccuracies of the sedimentation techniques, like vacuum filtration they are easy and inexpensive to perform. However sedimentation techniques are also very time consuming.

The Coulter Counter method of particle size analysis is quicker and easier than either vacuum filtration or sedimentation, but the initial expense for the equipment is high. It relies on the difference in electrical conductivity between the particles (which act as insulators) and the surrounding fluid (which is an electrolyte and a good conductor) (Van Rijn, 1994). As the particle suspension passes through a small aperture in the Coulter Counter, electrodes on either side record the fluctuation in electrical current, which is proportional to the volume of particles. The magnitude and frequency of the current fluctuations are used to determine the volumetric distribution of particles in the sample.

Unlike the sedimentation techniques, which assume that the particles are spherical in shape, the Coulter Counter method produces a volumetric distribution, which is completely independent of the particle shape. For analysis of suspended sediment type of samples, there has been both support for the technique and doubts about its effectiveness. Walling and Kane (1984) who have experimented with a number of particle size analysis techniques thought the Coulter Counter method to be an effective technique. Ward (1984) on the other hand,

expressed doubts about the accuracy of the Coulter Counter in measuring small clay-sized particles due to coagulation.

Like the Coulter Counter method of particle size analysis, laser diffraction equipment is initially expensive, but is a quick and easy technique to perform. It is based on the principle of light diffraction – when light is incident on a particle it will diffract the light, and the angle of diffraction will be dependant on the size of the particle. In general, the smaller the particle, the greater the diffraction angle. The diffraction pattern (known as a Fraunhofer diffraction pattern) is seen as a ring surrounding the central beam. A particle size distribution can be determined from the angular position and intensity of the diffraction pattern produced by the diffraction rings of many particles (Van Rijn, 1994).

An advantage of the laser diffraction method is that mechanical mixing and/or ultrasonic dispersion is often incorporated into the laser diffraction equipment to break up aggregates that commonly develop in sediment samples. A disadvantage of the laser diffraction technique is that the particles are assumed to be spherical. Some laser diffraction units incorporate a correction for non-spherical particles, but this can only be applied if the shape of the majority of particles is known.

In this study, due to the quantity of samples that required particle size analysis, the time-consuming vacuum filtration and sedimentation techniques were not feasible. The ease and rapidity of the Coulter Counter method and laser diffraction made them viable on a time basis. Unfortunately a Coulter Counter was not readily available to test its effectiveness in this study. However, there was a Malvern MasterSizer Series 2600 laser diffraction unit available in the Department of Chemical Engineering in The University of Adelaide.

The Malvern MasterSizer Series 2600 equipment consisted of a mixing bath, pumping unit, a flow-through cell, a laser transmitter, light receiving unit, lenses and computer to interpret the results. A choice of three lenses of different focal lengths was available – selection of the appropriate lens depended on the particle size range to be measured (63mm lens: 1.2 – 118mm; 100mm lens: 1.9 – 188mm; 300mm lens: 5.8 – 564mm). The 63mm lens was selected in this study, since all samples were pre-filtered through to remove particles larger than 63μm.

The particle size analysis was performed in stage 3 of the sediment analysis. Initially, the mixing bath was filled with Millipore water. The in-built pump established a continuous flow of the water sample from the mixing bath through the flow-through cell and back into the mixing bath. The laser light beam directed on the cell produced a diffraction pattern that was received by the light detector unit and was recorded by the software to establish a background reading.

A sample of the filtrate (prepared in stage 1 of the analysis) was then homogenised and a sample pipetted into the mixing bath with the mechanical cell stirrer and ultrasonic dispersion device in operation. The sample was diluted with Millipore water and pumped through the flow-through cell. Additional sample or Millipore water was added to the mixing bath until the Malvern indicated that the required concentration had been reached. The reading was then recorded by the computer software, which interpreted the diffraction pattern and produced a particle size distribution in graphical and tabular form.

Although obtaining a particle size analysis using the Malvern particle size analyser was simple and very quick, cleaning the equipment between samples and maintaining cleanliness of the tubing and flow-through cell window was much more time-consuming. The addition of DECON 90 to the wash solution helped to reduce the cleaning time between samples. Later versions of the Malvern particle size analysis equipment are self-cleaning.

4.3.4 Sediment Composition (Stage 4)

A 6g sample of sediment from each fraction was taken to the Department of Geology and Geophysics in The University of Adelaide for further laboratory preparation and x-ray diffraction (XRD), loss on ignition (LOI) and x-ray fluorescence (XRF) analyses, under the direction of Mr John Stanley. Appendix B can be consulted for a detailed description of the method used to prepare the samples and perform each test.

The aim of the XRD analysis was to determine the origin of the individual sediment components. A small quantity of each sample was used to prepare a series of slides. The slides were scanned using XRD to determine the dominant, minor and trace components of minerals including quartz, feldspar (orthocalse and plagioclase), halite, chlorite, mica, calcite, dolomite, siderite, muscovite, kaolinite, hematite, illite, corundum, gypsum and bassanite (hydrated gypsum).

LOI (given as a percentage of the dry weight) represents the organic matter, CO_2 and H_2O^+ content of a sediment sample. It may also include S, Cl and other volatiles, depending on the mineralogy of the sample. To determine the LOI value of the trapped sediments, a sample from each sediment fraction was dried in an oven at 110°C for a minimum of two hours to remove any moisture that may have re-absorbed during storage. The dried samples were then weighed and ignited overnight in a furnace at 960°C. After ignition the samples were re-weighed to determine the LOI value.

For the XRF analysis, a fused disk of the sample was scanned to determine the major elemental components (expressed as oxides), which included SiO_2, Al_2O_3, Fe_2O_3, MnO, MgO, CaO, Na_2O, K_2O, TiO_2, P_2O_5 and SO_3.

4.4 Sediments and Heavy Metals in the Patawalonga and Torrens Catchments

4.4.1 Sediment Accumulation

The sediment trapping enabled estimation of the rate of sedimentation at each location and observation of the seasonality of sediment movement. Material less than 63μm in size is easily suspended even at low flow, while transport of coarser material tends to be intermittent (Warren and Zimmermann, 1994), hence sediments were separated into fine (<63μm) and coarse (>63μm) particle size fractions for analysis of the rate of accumulation.

Sediment flux data for all sites are shown in Appendix C. Figure 4-6 and Figure 4-7 summarise the seasonal accumulation of sediment in each particle size fraction at the five sites.

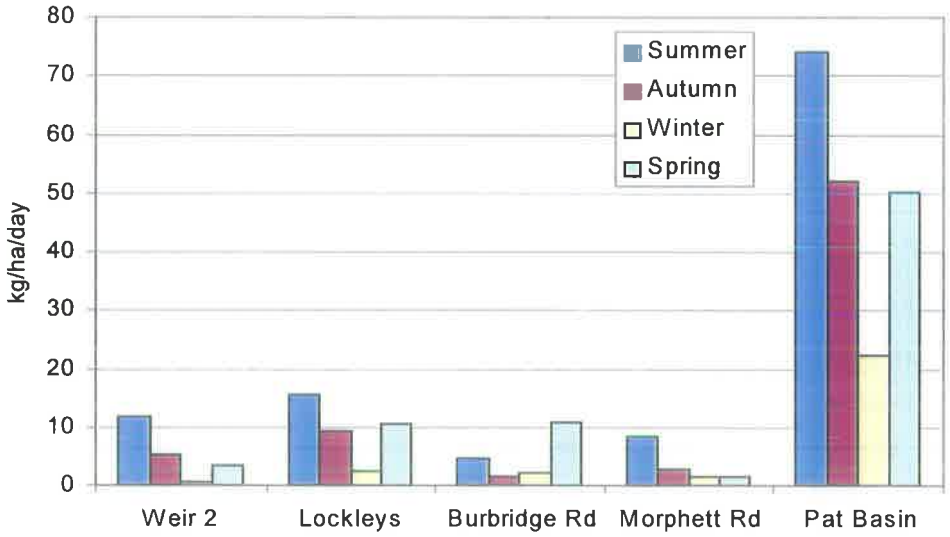

Figure 4-6: Accumulation rate of sediment less than 63μm

Overall accumulation of sediment was highest in autumn at Weir 2, the Morphett Road Sedimentation Pond and the Patawalonga Basin, and highest in spring at Lockleys and the Burbridge Road Sedimentation Pond.

The accumulation of fine material was typically highest in summer when there was little or no flow and lowest in winter when the flow was most rapid. The exception was in the Burbridge Road Sedimentation Pond, where fine particle accumulation was highest in spring and lowest in autumn.

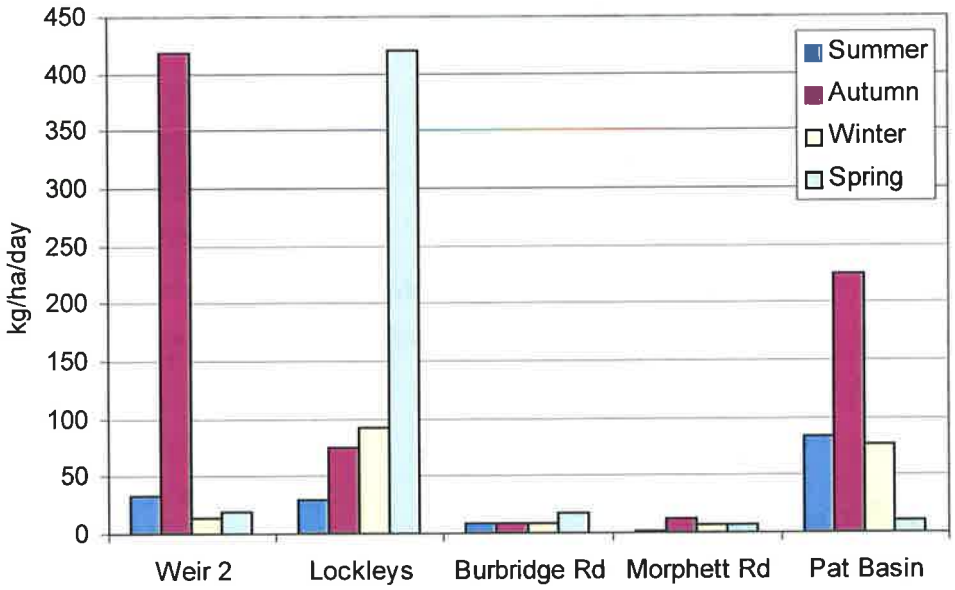

Figure 4-7: Accumulation rate of sediment greater than 63µm

The rate of accumulation of the finer sediment was highest in the Patawalonga Basin. However the weir just upstream of the sediment trap in the Patawalonga Basin would have prevented movement of sediment, particularly the coarser particle sizes, which may have contributed to the high proportion of fine material captured in the trap. The Patawalonga Basin trap was also located in deeper water than at other sampling locations in the two catchments, which may have allowed for greater settling of the finer sediments.

The total capture of coarse material was greater at Weir 2, Lockleys and in the Patawalonga Basin than in the two sedimentation ponds. It is likely that this was partly due to differences in flow regime and partly caused by movement of the river bed, which could not occur in the concrete-based sedimentation ponds. Significant changes in the river bed were observed at Weir 2 and Lockleys and the Patawalonga Basin, particularly after high flow events.

At Weir 2, 86% of the coarse sediment was captured in autumn, however the majority of this material was captured during one large event that caused significant shifting of the river bed. River bed movement during two large events was also responsible for the high rate of accumulation of coarse material at Lockleys in spring (68% of the total capture of coarse material). However, on several occasions during construction of the Breakout Creek wetland upstream of the Lockleys site, sedimentation exceeded the capacity of the sediment traps, hence the figures are not truly reflective of the high rate of sedimentation that occurred.

A net accumulation of around 25 – 30cm of sediment was observed in the Lockleys weir pool during the 13 months of sampling, and the majority of this sediment build up occurred during the construction phase of the Breakout Creek wetland project. This indicated that either the strategies that were employed to minimise sediment movement during construction (e.g.

barriers of hay bales) were inadequate or that the altered flow regime led to increased bed erosion along the intervening reach of river.

4.4.2 Sediment Composition

The >63μm particle size fraction was analysed to determine the sedimentary composition and organic matter content of sediment from each site. Table 4-3 shows the results of the mineralogical x-ray diffraction analysis and the LOI.

4.4.2.1 Mineralogy

Sediments from all five sites were mineralogically quite similar – predominantly quartz (SIO_2), with minor amounts of other silicates including muscovite ($KAl_2[AlSi_3O_{10}](OH)_2$), feldspar (orthoclase - $K[AlSi_3O_8]$ and plagioclase - $Na[AlSi_3O_8]$, $Ca[Al_2Si_2O_8]$), kaolinite ($Al_2Si_2O_5(OH)_4$) and chlorite ($Mg_3[Si_4O_{10}](OH)_2.Mg_3(OH)_6$), and minor amounts of carbonate minerals including calcite ($CaCO_3$) and dolomite ($CaMg(CO_3)_2$). These minerals are common to the Adelaide area.

Metals that are incorporated into crystalline minerals are frequently in inert positions within the crystal lattice (Förstner, 1981). The silicate minerals quartz and feldspar, which were present in high concentrations, tend to have a low metal content while clay minerals contain higher amounts.

Concentrations of clay minerals, such as kaolinite, chlorite and illite were mostly present at trace or trace/minor levels. However, clay minerals tend to be smaller in size and since only the coarser particle size fraction could be analysed, the clay minerals were not expected to be present in high concentrations.

The XRF analysis of the major and trace elements in the sediment samples supported the findings of the XRD analysis. The mean major elements of the >63μm particle size fraction are shown in Figure 4-8. All data, including all trace elements, are contained in Appendix D.

All sediment samples were predominantly silica. This was due to the high quartz content and the prevalence of other silicate minerals such as muscovite and feldspar. Other elements, including aluminium, magnesium, calcium, sodium and potassium were also present. These were constituents of the majority of minerals that were identified by XRD.

Table 4-3: Composition of sediment (>63µm)

	Season	Mineralogy, (% LOI)
WEIR 2	Summer	dQ, mM, mCH, mFP, mC, mD, O, (17.73)
	Autumn	dQ, mF, mC, tD, tK, tMI, t?, (4.08)
	Winter	dQ, mM, mPF, tK, tD, tSC, O, (12.96)
	Spring	dQ, mPF, mM, tK, tCH?, tC, tD, O, (13.47)
LOCKLEYS	Summer	dQ, mM. mCH, mPF, mC?, tG, O, (14.4)
	Autumn	dQ, sub-dFP, mCH, mM, (8.66)
	Winter	dQ, mPF, mM, tmCH?, tmK, (4.64)
	Spring	dQ, tmPF, tmC, tM, tK, (4.4)
BURBRIDGE RD	Summer	dQ, mD, mC, mOF, mM, tCH, O, (42.99)
	Autumn	dQ, mF, mC, mD, mM, tCH, tK, O, (38.57)
	Winter	dQ, mM, mPF, mD, tmC, tK, tCH?, O, (35.76)
	Spring	dQ, mM, mPF, mC, mD, tmK, tmCH?, tG, O, (36.22)
MORPHETT RD	Summer*	-
	Autumn	dQ, mPF, mM, mK,mC, mD, O, (16.83)
	Winter	dQ, mPF, mM, mK, tD, tH, O, (17.31)
	Spring	dQ, mM, mPF, mC, tmD, O, (23.13)
PAT BASIN	Summer	dQ, mF, mC, tI, tCO, tD, tH?, (5.26)
	Autumn	dQ, mFP, mC, tK, tD, tS?, (4.63)
	Winter	dQ, tmK, tmM, tmC, tPF, tCH?, (6.97)
	Spring	dQ, mM, mPF, tmK, tmC, tD, O, (22.34)

* insufficient sample for analysis

Mineral names:

Q=quartz, M=muscovite, MI=mica, PF=plagioclase feldspar, OF=orthoclase feldspar, CH=chlorite, C=calcite, CO=corundum, F=feldspar, D=dolomite, K=kaolinite, H=hematite, HA=halite, G=gypsum, I=Illite, S=siderite, SC=swelling clay, O=organic material

Concentration amounts:

d=dominant, m=major, tm=trace/minor, t-trace

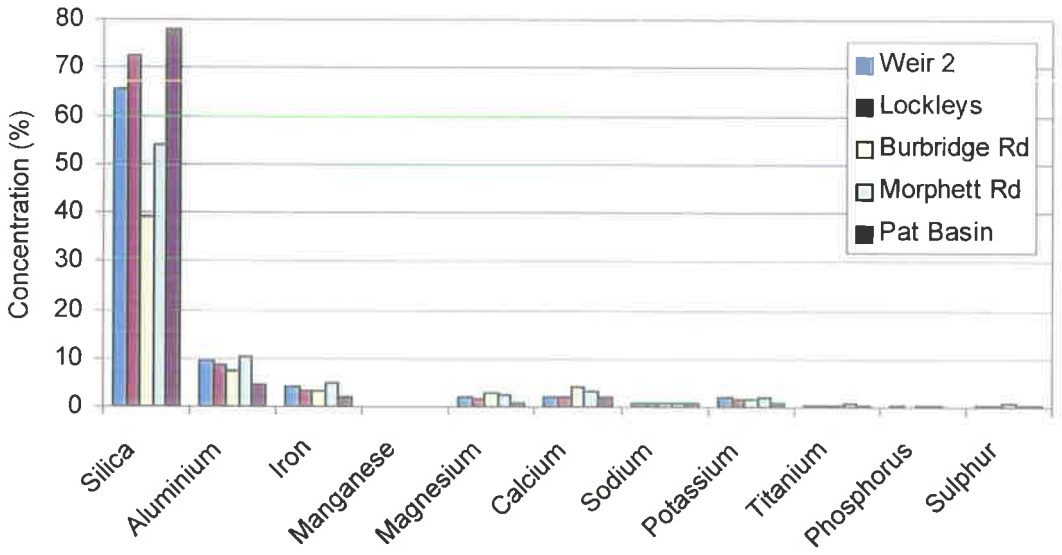

Figure 4-8: Mean concentrations of the major elements in sediments from each site

Iron was also identified in small concentrations. Iron can form small concentric nodules in the aquatic environment (Alloway and Ayres, 1997). However, the iron was not a constituent of the major characteristic minerals identified by XRD. Only a possible trace of siderite, ($FeCO_3$) was identified at one site (Patawalonga Basin).

The iron may have been originally present in the sediment samples as an hydroxide coating on some particles. In aquatic systems, metal contaminants have a strong affinity for iron hydroxide, but a fall in redox potential can lead to reduction of the iron and a release of the attached metals into the water column. Possible traces of the iron mineral siderite were identified in the Patawalonga Basin. Siderite can form in weakly reducing conditions, but forms primarily in strongly reducing conditions (Berner, 1981).

Manganese can also form a surface oxide layer on other particles, to which metal contaminants can attach. Manganese was not identified as a major element, but reduction of manganese oxide tends to occur before the reduction of iron hydroxide, hence the manganese may have been present in its dissolved form. The absence of manganese, but presence of iron, could indicate a mildly reducing environment in which all manganese and possibly some iron have been remobilised, but in which a proportion of iron still remains in an oxidised form.

Sulphur was present in only low concentrations, although the black iron sulfide mud was often observed in sediments from the Patawalonga Basin and Burbridge Road Sedimentation Pond. It should be remembered however, that in the main only the mineralogy of the >63μm particle size fraction was analysed. Other elements and other minerals may have been present in the <63μm particle size fraction. Due to the very small amounts of sediment in the <63μm particle size fraction there was insufficient sediment to perform both mineralogical and

metals analysis of the <63μm fraction. To meet the objectives of the study, priority was given to analysis of the metal contaminants in the <63μm particle size fraction.

However, samples of the <63μm particle size fraction were analysed for some samples trapped in the Patawalonga Basin and Morphett Road Sedimentation Pond when sufficient sediment was collected. The fine sediments of the Patawalonga Basin were predominantly halite, which is common salt. The high halite content was seen in all seasons and reflected the saline nature of the Patawalonga Basin throughout the year. Sea water intrusion was the likely source of halite in the Patawalonga Basin.

Halite was also dominant in fine sediments collected during summer from the Morphett Road Sedimentation Pond, which was too far inland for sea water to intrude. Dissolved salts in a water body can come from inflow of sea water or saline river water, groundwater intrusion or from the decomposition of sediments and organic matter (Imberger and Patterson, 1990). Intrusion of saline groundwater was not possible in the concrete-based sedimentation pond, and there was no inflow to the pond during the summer months when salinity was highest. It is likely that the high rate of evaporation during summer coupled with decomposition of sediments and organic matter that had been captured in the pond were the reasons for the high halite concentration. The high halite content accounted for the high salinity readings that were taken in the pond in January, February and March 2000 (see Chapter 5).

4.4.2.2 Organic Matter

Organic matter plays an important role in particle flocculation and metal solubility. Organic materials can form a surface coating on particles, which can enhance particle flocculation (see Section 4.4.3) and facilitate sediment adsorption of metal contaminants. Furthermore, if sediment-bound metals (e.g. metals bound to iron or manganese oxides or hydroxides) are released due to changes in redox conditions, they may complex with organic materials. These metal organic complexes are soluble and bioavailable, and may persist in the environment despite re-oxidation.

LOI was indicative of the organic matter content of each sediment sample. Figure 4-9 shows the seasonal change in LOI at each site in the two catchments. (LOI data are shown in Table 4-3.)

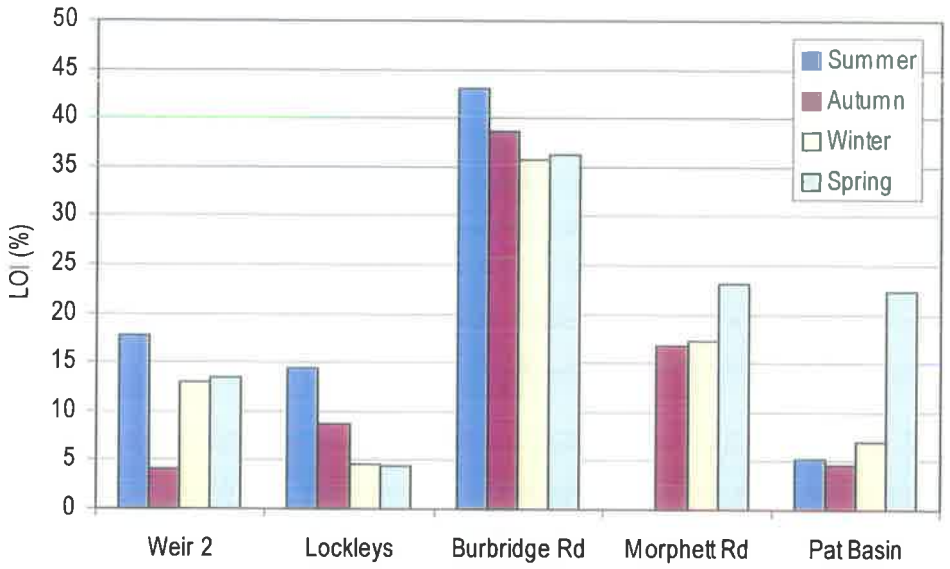

Figure 4-9: LOI for sediment >63μm in size

Organic matter was present in sediments from all five sites. LOI ranged from 4% in sediments sampled in autumn at Weir 2 to 43% in summer sediments from the Burbridge Road Sedimentation Pond. On average, it was lowest overall in sediments from Lockleys and highest in sediments captured in the Burbridge Road Sedimentation Pond.

No seasonal trend was identified in the LOI results. LOI was greater in summer for sediments from Weir 2, Lockleys and the Burbridge Road Sedimentation Pond, but greater in spring for sediments from the Patawalonga Basin. Unfortunately LOI could not be determined for sediments from Morphett Road Sedimentation Pond during summer, since little material of a large particle size was settling in the pond and there was insufficient material for analysis.

The organic matter content of the sedimentation ponds is discussed in more detail in Section 4.5.

4.4.3 Sediment Size

Graphs of the particle size distributions of samples from each site are shown in Appendix E. Figure 4-10 is a summary of the particle size distributions for sediment less than 63μm in size captured at each of the study sites. It shows the mean particle size distributions determined from separate analyses of samples collected between 10 September 1998 and 6 January 1999 at Lockleys, the Burbridge Road Sedimentation Pond and the Patawalonga Basin, from samples collected between 22 October 1998 and 2 December 1998 at Weir 2, and from samples collected between 18 December 1998 and 6 January 1999 at the Morphett Road Sedimentation Pond.

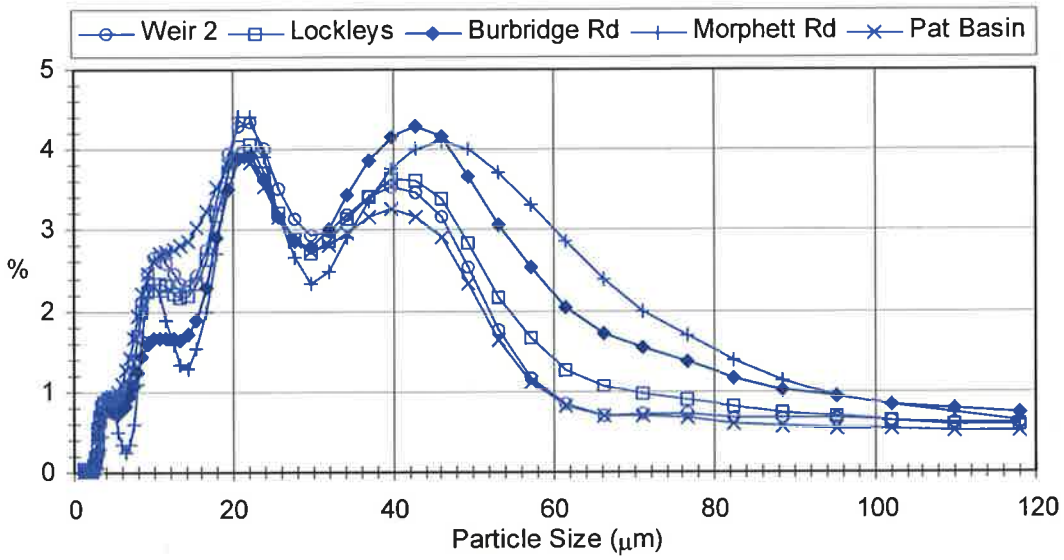

Figure 4-10: The mean particle size distribution of sediment (<63μm) captured at each site

The mean particle size distributions of all five sites were similar in appearance displaying peaks at approximately 20μm and 40μm and a local minimum at approximately 30μm. There was a complete absence of particles less than 2μm in size (clay-sized particles) at all sites, although these particles could have been present in proportions below 0.1%, which was the limit of accuracy of the instrument.

An absence of particles of a very small size was quite likely due to their lower settling velocity. Very slow settling particles were less likely to enter the sediment trap bottles, which were positioned at the bottom of the water column. However, doubts have also been raised about the accuracy of the Malvern particle size in measuring very small particles in natural sediment samples. Gee and Bauder (1986) found that with either a 63mm or 100mm lens, the Malvern particle sizer underestimated the proportion of particles below 1.9μm in samples with a clay content of more than 25%. McCave *et al.* (1986) also recommended caution in interpreting Malvern particle size analyses of samples with a clay content in this range. Clay particles, which are generally less than or equal to 2μm in size, have a stronger than normal tendency to coagulate due to their surface charge. Although the Malvern instrumentation could measure particles down to a size of 1.2μm with a 63mm lens, the accuracy of the instrument in measuring particles less than 2μm must be questioned since the exact clay content of the samples was unknown.

The reason for the relatively low proportion of particles of around 30μm in size in the mean particle size analysis at each site is not known – either the particles were not present in the samples or the 30μm particles aggregated, altering their apparent size.

A true absence of 30μm particles in nature is unlikely, but it is possible that the relatively low proportion of 30μm particles was caused by the sediment trap design. Particle settling velocity

is a function of particle size. Particles of a particular settling velocity might have been eliminated due to hydrodynamic effects generated by the trap bottles or supporting structure. Since settling velocity is a function of particle shape and density, as well as particle size, this theory would suggest that there was a common particle composition leading to a similar size and density pattern amongst the five sites.

Another possible explanation for the low proportion of 30μm particles is that the particles aggregated after sampling. Particle aggregation can be influenced by the salt concentration of the fluid suspension (McManus, 1988), which would have been affected by the addition of Millipore water during filtration and particle size analysis. Vacuum filtration can disrupt aggregates, while shaking may enhance aggregation if air bubbles are entrained (Wotton, 1994).

Common trapping, analysis and storage techniques would have produced similar settling conditions in the samples (e.g. agitation, temperature, oxygen exposure, etc.) that may have produced similar patterns of aggregation, leading to the strong similarities in particle size distribution between the five sampling sites.

Organic material plays an important role in aggregation, and samples from all sites were found to have a significant organic content, which was not removed prior to particle size analysis. Aggregated particles have been observed in studies of sediment samples under scanning electron microscopy (e.g. Mercier *et al.* (1995), Hurl (2000)).

Samples were filtered to remove the sediments larger than 63μm in size. However, an average of around 8% of the particles were still found to be in the coarser particle size range, which would indicate that finer particles had aggregated in the time between filtration and particle size analysis.

Due to the number of sites, travel time for sample collection, location of instrumentation, and pre-treatment requirements it was not possible to perform the particle size analysis immediately following sample collection. However samples were always analysed within two weeks of collection and agitation was used for up to 5 minutes before and during the analysis to encourage disaggregation.

Clearly however not all the aggregates were broken up by agitation using the mechanical stirrer and ultrasonic dispersion. Aggregation might have been reduced by removing organic material before analysis (e.g. by chemical oxidation), athough aggregation of clay particles could still have occurred. Alternatively, deployment of the ultrasonic equipment for a longer time period or addition of a chemical dispersing agent such as Calgon during the particle size analysis might have helped to break up the aggregates.

However, strong chemical dispersing agents can also break up naturally occurring aggregates. Within the natural river environment aggregation can affect both the size and density of particles, altering their transport and depositional behaviour (Walling, 1996). Laboratory particle size analysis may underestimate the *in situ* particle size distribution by an order of magnitude (Eisma, 1992; Pye, 1994).

Walling *et al.* (1996) performed Malvern particle size analyses on sediment samples from the River Culm both with and without chemical dispersal agents. They compared the particle size distribution determine shortly after sample collection with the particle size distribution of another sample from the same sample period that had been chemically dispersed, and found that the majority of finer clay-sized material were actually incorporated into larger sized aggregate particles.

Although the finer particle sizes have a greater capacity for adsorption due to the larger surface area, aggregation of the fine particles into larger sized structures may influence the overall adsorption capacity.

4.4.4 Metals

4.4.4.1 Metal Concentration

Seasonal composite samples of sediment were tested for 16 metals – antimony, arsenic, barium, beryllium, boron, cadmium, chromium, cobalt, copper, lead, molybdenum, nickel, selenium, tin, vanadium and zinc. Data from the ICP-MS metals analysis are shown in Appendix F.

Figure 4-11 summarises the mean concentrations of metals in the sediments from each site. Antimony, beryllium, cadmium, molybdenum, selenium and tin were either not detected or present in only very small quantities and have not been included in the graph.

Analysis of sediments from all sites in the Patawalonga and Torrens catchments showed that the majority of metals were in highest concentration in sediments from the Burbridge Road Sedimentation Pond and in lowest concentration in sediments from the Patawalonga Basin.

Zinc was the most highly concentrated metal at each of the five sites and the average concentrations were higher than the sediment quality guidelines of 200mg/kg recommended by ANZECC (1999) at all sites except the Patawalonga Basin. The ANZECC (1999) guideline level for lead was exceeded at all sites, and the guideline level for copper was exceeded at Weir 2 and in the Burbridge Road Sedimentation Pond. Concentrations of cadmium were also

exceeded in sediments from Burbridge Road Sedimentation Pond. Levels for chromium, nickel, arsenic and antimony were within recommended levels at all sites. No guidelines are provided by ANZECC (1999) for other metals that were detected, including barium, boron, vanadium, cobalt, beryllium, molybdenum, selenium and tin.

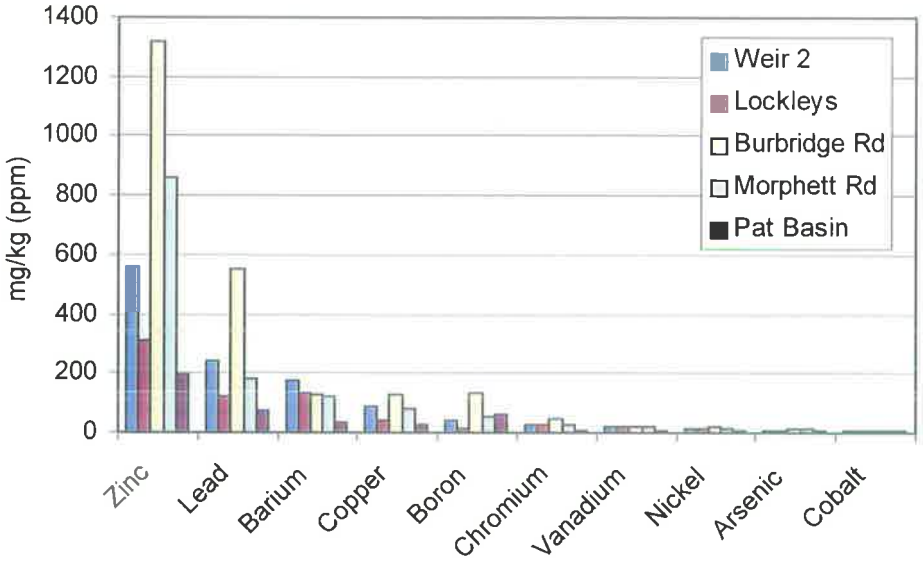

Figure 4-11: Mean metal concentrations by ICP-MS

These figures represent only the sediment contamination. It is possible that metals had been remobilised from the sediments into the more toxic and bioavailable soluble form (e.g. in the Patawalonga Basin where zinc contamination of the sediment was within ANZECC (1999) guideline levels).

Numerous studies have noted a relationship between metals and sediments in the finer particle size range (Ongley *et al.*, 1981; Slotton and Reuter, 1995; Characklis and Wiesner, 1997). The relationship is thought to be due to the proportionally higher particle surface area and higher proportion of reactive clay minerals in the finer particle size fraction.

In this study boron and tin were significantly more concentrated in the finer particle size fraction at all sites. Figure 4-12 and Figure 4-13 illustrate the larger concentrations of boron and tin in the <63μm particle size fractions. Graphs of concentration of all other metals are shown in Appendix G.

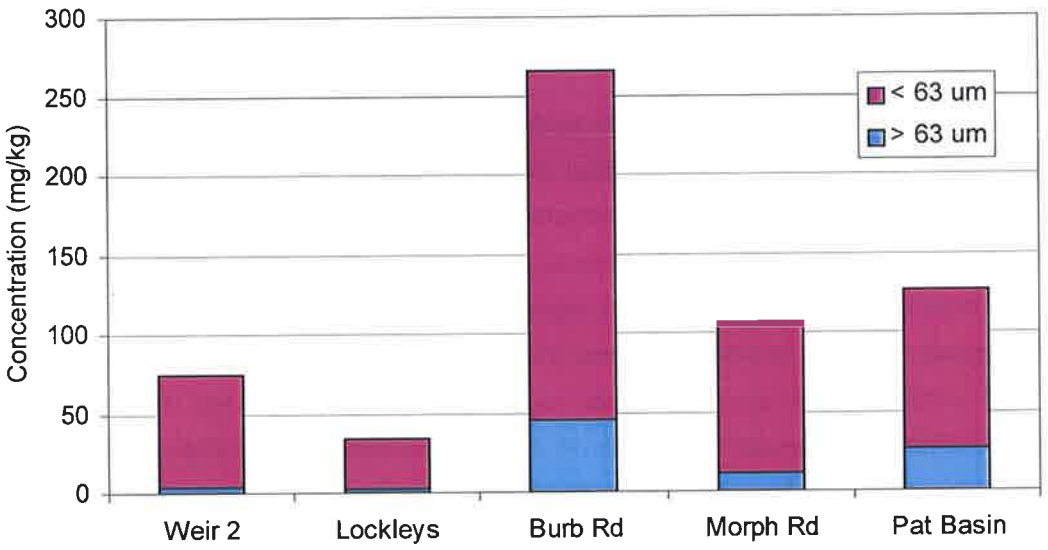

Figure 4-12: A comparison of the mean concentration of boron in the <63μm and >63μm particle size fractions from each site

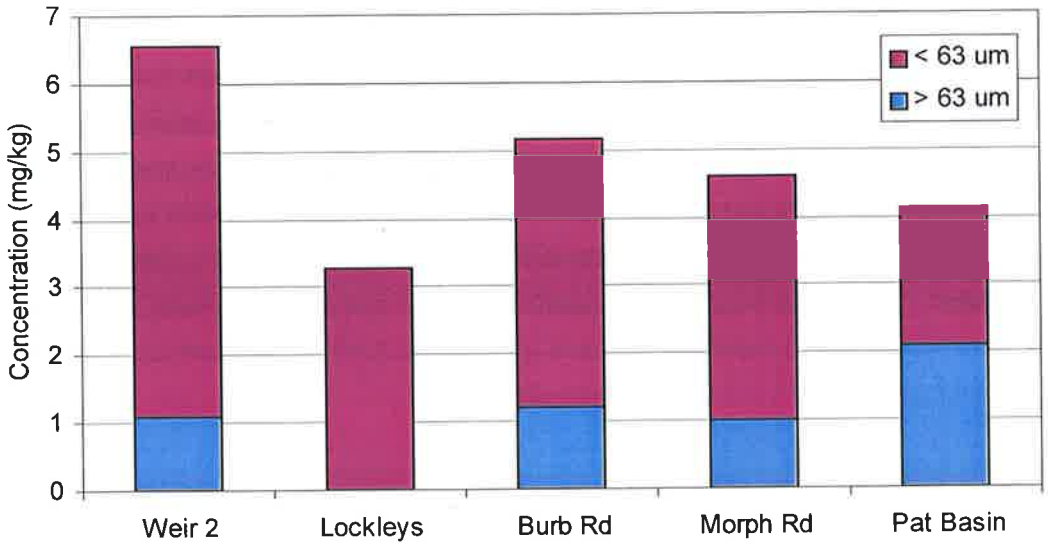

Figure 4-13: A comparison of the mean concentration of tin in the <63μm and >63μm particle size fractions from each site

In the Torrens catchment, the majority of all metals were slightly more concentrated in the finer particles. In the Patawalonga catchment however the majority of metals other than boron and tin were more concentrated in the coarser particle size fraction. This result was unexpected since particle size analysis indicated that the very fine particles (e.g. <10μm), which have a very low settling velocity were being captured in the sediment traps (see Section 4.4.3). There were a number of possible reasons for the lower concentration of

metals on the finer particle size fraction in the Patawalonga catchment, and three of these reasons have been detailed below.

1. The lower concentration of metals in the finer particle size fraction may have been due to aggregation of the finer particles either *in situ*, within the sediment trap bottles or during transport, storage, preparation or analysis of the sediment samples. Particle size analysis of the finer fraction suggested that some aggregation was occurring following filtration of the samples (see Section 4.4.3). Although sediment samples from all sites were subjected to similar conditions during transport, storage, preparation and analysis, the high proportion of organic matter in the sediments from the Burbridge Road Sedimentation Pond and Morphett Road Sedimentation Pond may have enhanced particle aggregation in samples from these sites.

2. The relatively low concentration of metals on the finer particle size fraction of sediments from the Patawalonga catchment sites may have been due to peculiarities in the sediment-metal bond, which depends on a number of factors, including the nature of the sediment, the identity of the metal and the presence of organic material and iron or manganese oxides or hydroxides. While there was no significant contrast in iron or manganese content or mineralogy of the coarse particle size fraction between sediments from the Torrens catchment and sediments from the Patawalonga catchment, the characteristics of the finer particles could not be determined at all sites due to insufficient sample. Thus there may have been differences in the nature of the finer material in the Patawalonga catchment, which lessened its adsorptive capacity. Of the fine sediments for which there was sufficient sample for mineralogical analysis, the content was found to be predominantly halite, to which metals do not adsorb. The high salt content, which was identified in samples from the Patawalonga Basin, and Morphett Road Sedimentation Pond in summer and autumn, may have reduced the apparent concentration of metals in the finer particle size fraction from these sites.

3. Redox and pH conditions in the Patawalonga Basin, Burbridge Road Sedimentation Pond and Morphett Road Sedimentation Pond may also have led to remobilisation of metals. This might have been relatively greater in the finer particle size fraction due to the nature of the finer material (e.g. higher proportion of clay minerals), leading to a lower concentration of metals in the finer particle size fraction. (Remobilising conditions were observed at the three Patawalonga catchment sites.)

It is most likely that a combination of these factors was responsible for the relatively higher concentration of metals on the coarser particle sizes in the Patawalonga catchment. Since the coarser particles will settle out of the water column more quickly, these metals would be expected to be less mobile in the Patawalonga catchment.

There was no strong seasonal pattern in metal concentration in the sediments. Average metal concentration was highest at Lockleys and the Morphett Road Sedimentation Pond in summer, at Burbridge Road Sedimentation Pond in autumn, at Weir 2 in winter and at the Patawalonga Basin in spring. The change in metal concentration at each site over the four seasons is shown in Figure 4-14.

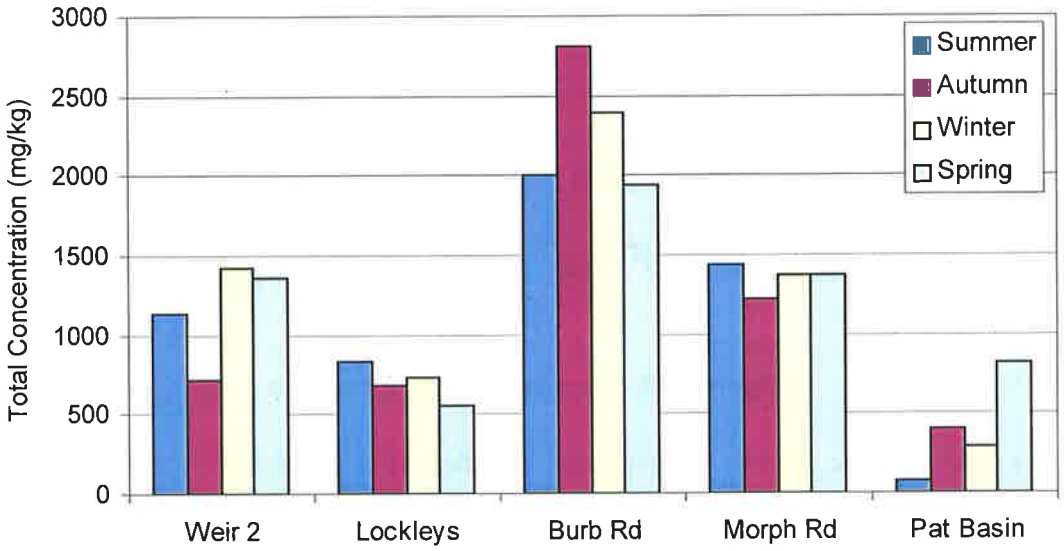

Figure 4-14: The seasonal change in total metal concentration at each site

4.4.4.2 Metal Load

The concentrations of metals in the sediments did not represent the degree of metal contamination at each site. The metal load captured at each site was dependent on the quantity of sediment that was collected, as well as the concentration of metal within the sediment. This is illustrated in Figure 4-15, which shows the mean metal loading rates for the five study sites.

Due to its high concentration in the sediments, zinc was the highest pollutant at all sites. Lead was also high, as was barium in the two Torrens catchment sites (Weir 2 and Lockleys). Lead and zinc are very common pollutants in urban areas due to road runoff. Both have already been recognised as pollutants of concern in the Torrens and Patawalonga catchments based on metals testing of water samples (Patawalonga Catchment Water Management Board, 1997; Torrens Catchment Water Management Board, 1997).

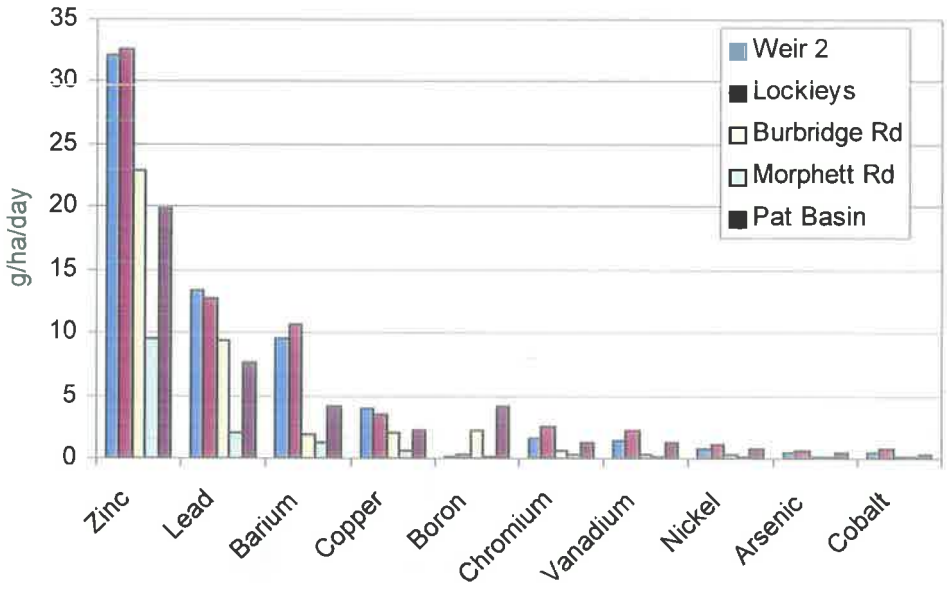

Figure 4-15: Mean metal loads at each site

Unlike lead and zinc, barium has not been identified as a significant metal contamination problem in the Torrens and Patawalonga catchments. Potential sources of barium include fuels and oils, insecticides and various manufacturing industries. It was present in sediment samples from all sites, but contamination was significantly higher in sediments from Weir 2 and Lockleys in the River Torrens.

Heavy metal loads were highest during autumn at Weir 2, the Morphett Road Sedimentation Pond and the Patawalonga Basin, but highest during spring at Lockleys and the Burbridge Road Sedimentation Pond. This is shown in Figure 4-16.

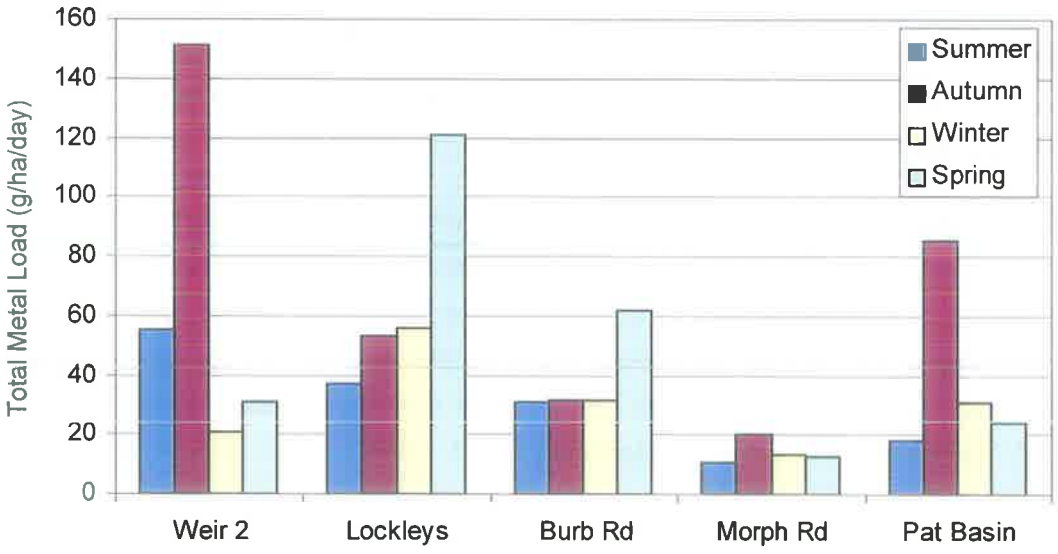

Figure 4-16: The seasonal change in total metal load at each site

The season during which the metal loading was highest, correlated with the season of highest sedimentation. It did not correlate in any way with the season of highest metal concentration (compare Figure 4-14 with Figure 4-16). At all sites, the sediment load was of more importance than the metal concentration in predicting the overall metal load.

The majority of the heavy metal load at each site was contributed by the coarser particles (>63μm). Table 4-4 shows the mean proportion of the total mass taken by each particle size fraction, and the particle size association of the mean heavy metal load.

Table 4-4: Mean sediment size and mean heavy metal load

(% by mass)	SEDIMENT MASS		HEAVY METAL LOAD	
	<63μm	>63μm	<63μm	>63μm
Weir 2	4	96	9	91
Lockleys	6	94	11	89
Burbridge Rd	31	69	16	84
Morphett Rd	34	66	19	81
Pat Basin	33	67	29	71

In the Torrens catchment, metals were slightly more concentrated in the finer (<63μm) particle size fraction, but a low proportion of the trapped material was of this size. Of the sediment that was trapped at Weir 2 and Lockleys in the Torrens catchment, 94% to 96% by mass was of the coarser (>63μm) particle size, and this contributed 89% to 91% of the overall metal load.

Although trapping of the finer (<63μm) particle sizes was proportionally higher in the Patawalonga catchment, the concentration of metals on particles of this size was proportionally lower. In the sediments captured in the sedimentation ponds and Patawalonga Basin, metals were slightly more concentrated in the coarser (>63μm) particle size fraction. The proportion by mass of coarse (>63μm) sediments was 66% to 69%, and the proportion of the metal load contributed by the coarser (>63μm) particle size fraction was still relatively high, between 71% and 84%.

4.5 Sedimentation Pond Performance

Concentrations of the majority of metals were higher in the Burbridge Road Sedimentation Pond than at other sites. The only exceptions, were vanadium and selenium, which were slightly higher in the Morphett Road Sedimentation Pond, and beryllium, which was not present in either pond. Overall, mean loads of all metals were higher in the Burbridge Road Sedimentation Pond than in the Morphett Road Sedimentation Pond, with the exception of cobalt, for which mean loading rates were approximately equal.

The results in Table 4-4 show that 66% to 69% of material captured in the two sedimentation ponds was of the coarser >63μm particle size. The coarser particles would have settled more quickly and therefore would be more likely to remain in the pond rather than be flushed downstream. Coarser particles are also more easily removed from the pond than the finer material, which will tend to resuspend during pond dredging.

Figure 4-17 shows the seasonal variation in the metal loads captured in the Burbridge Road Sedimentation Pond and Morphett Road Sedimentation Pond.

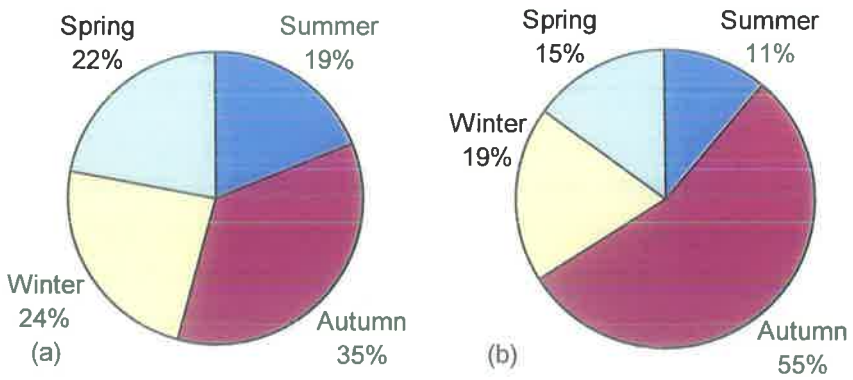

Figure 4-17: Seasonal total metal load in (a) Burbridge Road Sedimentation Pond, and (b) Morphett Road Sedimentation Pond

Due to the higher concentration of metals in the coarser material, approximately 81% to 84% of the sediment metal load would have been removed by getting rid of the coarser material in the sedimentation ponds. The majority of this metal load was captured during autumn in both the Burbridge Road Sedimentation Pond (35%) and the Morphett Road Sedimentation Pond (55%).

Based on LOI values (see Figure 4-9) the proportion of organic material in autumn, winter and spring samples was higher in sediments from the two sedimentation ponds than in sediments from any other site. The proportion of organic matter trapped in summer samples was highest in sediments from the Burbridge Road Sedimentation Pond site, but no summer data were available for the Morphett Road Sedimentation Pond due to insufficient sample for analysis.

From observations of the small amount of material that was trapped, the Morphett Road Sedimentation Pond sediments contained a high proportion of organic material by volume. Due to a low sedimentation rate however it is considered unlikely that the total organic loading was high during the summer. Of the two ponds, the LOI was significantly higher in sediments trapped in the Burbridge Road Sedimentation Pond in every season.

The LOI results concurred with basic field observations carried out fortnightly at each site (e.g. by wading, boating, etc.) during the sediment sampling period. On all occasions, there was a greater prevalence of organic gross pollutants (and also litter) in the Burbridge Road Sedimentation Pond than in the Morphett Road Sedimentation Pond or in the water at any other site. Figure 4-18 is a typical illustration of the organic material that clogged the Burbridge Road Sedimentation Pond.

Figure 4-18: Organic matter and litter in the Burbridge Road Sedimentation Pond

Microbial consumption of the organic material was believed to be the reason for an absence of oxygen and reducing redox conditions in the Burbridge Road Sedimentation Pond. Black iron sulfide mud and a strong odour of hydrogen sulfide gas were first apparent in February 1999 and remained present for the rest of the Burbridge Road Sedimentation Pond field study, which ended in September 1999. These chemical conditions were the result of sulfate reduction, which occurs when there is anoxia and strongly reducing redox conditions in the water and sediments of a pond. Although mineralogical analysis of sediments from Burbridge Road Sedimentation Pond did not reveal a high sulfur content (see Section 4.4.2.1), only the

coarser (>63μm) particle size fraction was analysed by XRF spectroscopy, hence sulfur may have been present in the finer (<63μm) particle size fraction.

High flow events from heavy autumn and winter rains lessened the problem in the Burbridge Road Sedimentation Pond but were not sufficient to re-oxygenate the sediments. Each high flow event refreshed the organic loading in the pond, which is believed to have led to increased microbial activity and a subsequent reduction in DO levels.

Algal blooms occurred on two occasions during the period of reducing redox conditions – in July 1999 and September 1999. Both blooms occurred during a spell of dry weather and no flow, which followed a high flow event through the pond.

Figure 4-19 shows the Burbridge Road sedimentation pond on 29 July 1999 during the first algal bloom. The algae gave a 'milky' appearance to the water in the pond, which contrasted with the trail of frothy black sediment that was caused by stirring of the black iron sulfide mud and release of trapped bubbles of hydrogen sulfide gas at the bottom of the pond.

Figure 4-19: The Burbridge Road Sedimentation Pond on 29 July 1999 during the first algal bloom

Observations of the Burbridge Road Sedimentation Pond indicate that the trash rack at the downstream end of the pond captures large quantities of gross organic pollutants and litter that have been washed through the sedimentation pond. However the trash rack is under-utilised to a certain extent because a proportion of the gross pollutants including litter, tree

branches, leaves and other organic refuse that would normally be captured in a trash rack device, are instead trapped in the sedimentation pond. Installation of a trash rack at the upstream end of the Burbridge Road Sedimentation Pond might prevent many of the pollutants from entering the pond and lessen the organic pollution problem, which was believed to be responsible for past anoxia and reducing redox conditions in the pond.

Whytcross *et al.* (1998) investigated the performance of a gross pollutant trap (GPT) on Sullivan's Creek in the ACT, where the trash rack was positioned at the upstream end of the sedimentation pond. Like the Burbridge Road Sedimentation Pond, the inlet to the GPT was a concrete lined channel. At the upstream end of the GPT were flow tranquilisers, followed by the trash rack and then the sedimentation pond. A submerged culvert outlet allowed for water level control.

On investigation of the GPT, 30% of pollutants retained by the GPT were captured upstream of the trash rack, with the remaining 70% captured in the sedimentation pond. An analysis of the pollutants showed that a large proportion of sediment was trapped by the trash rack rather than the sedimentation pond. Whytcross *et al.* (1998) therefore recommended that trash racks be placed at the downstream end of sedimentation ponds to ensure that trash racks were not over-utilised in a capacity for which they were not primarily designed and that the sedimentation ponds were made to operate at maximum capacity.

However in the Burbridge Road Sedimentation Pond, where the trash rack was placed at the downstream end of the pond, the sedimentation pond appeared to be over-loaded with gross pollutants that it was not designed to capture, while the trash rack was instead under-utilised.

What can be concluded from both these experiences is that there appear to be advantages and disadvantages associated with both sedimentation pond and trash rack combinations. The key issue in the design of these devices is really that it is essential to perform frequent cleaning of the trash rack and/or the sedimentation pond to remove build up of sediment and gross pollutants.

As well as recommending the installation of trash racks downstream, Whytcross *et al.* (1998) did recognise the need for regular cleaning and recommended it as part of a long term management strategy for the Sullivans Creek GPT. Other authors (e.g. Bartone and Uchrin (1999)) have also stressed the importance of frequent sediment removal to prevent sediment resuspension and hence improve water quality in ponds.

The Patawalonga Catchment Water Management Board is aware of the need for regular cleaning of trash racks (Patawalonga and Torrens Catchment Water Management Boards, 2000) however additional water quality improvements might be achieved by more frequent removal of pollutants from the sedimentation ponds. In the Burbridge Road Sedimentation

Pond this would reduce the organic loading in the pond, and may lead to fewer instances of algal blooming and strong odours and a reduced potential for metal remobilisation.

Interestingly the gross pollutant problem did not exist to the same extent in the Morphett Road Sedimentation Pond as it did in the Burbridge Road Sedimentation Pond. It is likely that there was a combination of reasons for the apparent contrast in gross pollutant contamination. These included:

1. that there were fewer gross pollutants entering the Morphett Road Sedimentation Pond due to pre-treatment upstream;

2. that there were fewer gross pollutants entering the pond due to differences in catchment size and land use activities;

3. that the pond was much larger in volume and in surface area, so the pollution problem was not as visible; or

4. that the pond was slightly shallower and had more sloping sides, which may have enabled gross pollutants to be flushed through the pond more effectively, although this is unlikely.

The contrasting pre-treatment of water entering the two sedimentation ponds can be seen by comparing the photographs of the inflowing channels at the upstream end of each pond in Figure 4-20.

The channel upstream of the Morphett Road Sedimentation Pond was heavily vegetated, which would have helped to filter the water of sediments. The shape and surface roughness of the channel would also have impeded channel flow, allowing more sediment and larger pollutants to settle out before the water reached the pond. In contrast, the channel upstream of the Burbridge Road Sedimentation Pond was concrete-lined and much of the catchment area was serviced by an underground drainage network. Hence, there was less opportunity for removal of either gross pollutants, sediments or metal contaminants from the water before it entered the pond.

4.6 Conclusions

By mass, the majority of sediment that was captured was of the coarser (>63μm) particle size, which settles more rapidly. Capture of the coarser (>63μm) material was significantly higher in the two Torrens catchment sites (Weir 2 and Lockleys), where there was significant movement of the river bed, particularly during a few large flow events.

(a) (b)

Figure 4-20: The channel upstream of (a) the Morphett Road Sedimentation Pond; and (b) the Burbridge Road Sedimentation Pond

Mineralogical composition of the coarser (>63μm) sediments was reasonably uniform across all sites in the two catchments – predominantly quartz, with a major proportion of other silicate minerals and some carbonates.

No general seasonal trend was identified in the rate of sedimentation of either particle size fraction, or in the nature of the material that was captured (e.g. mineralogy, metal concentration), probably due to contrasts in catchment activities and flow management between sites. For example, construction of the Breakout Creek wetland upstream of the Lockleys site led to a dramatic increase in the rate of sedimentation due to disruption of the flow regime and/or inadequate sediment management strategies. While wetlands and sedimentation pond have the potential to improve problems of water quality and quantity, extreme care must be taken to ensure that their construction does not lead to increased pollution of the downstream environment in the short-term.

This relationship was observed at all sites and in all seasons. For most metals, concentrations were not significantly higher in one particle size fraction than in the other, with the exception of boron and tin, which were more concentrated on the finer (<63μm) particles. On average, metals were slightly more concentrated on the finer particles in the Torrens catchment and slightly more concentrated on the coarser particles in the Patawalonga catchment.

Average lead and zinc contamination of the sediment exceeded ANZECC (1999) guidelines for the protection of freshwater aquatic ecosystems at all sites except the Patawalonga Basin, where average zinc concentrations in the sediments were below guideline levels. Average copper contamination of the sediment exceeded ANZECC (1999) guidelines at Weir 2 and in the Burbridge Road Sedimentation Pond, and average cadmium levels also exceeded ANZECC (1999) guidelines in the Burbridge Road Sedimentation Pond. However average concentrations of chromium, nickel, arsenic and antimony were within recommended limits at all sites. (Other metals were present, but as yet no safe levels have been determined by ANZECC.)

The sediment and heavy metals analysis indicated that sedimentation ponds have the potential to be effective as a means of sediment and metal removal from the waterways. On average, in the Patawalonga catchment there was a marginally higher concentration of heavy metals on the coarser (>63μm) particle sizes, which were most likely to settle in the pond due to their higher settling velocity. 66% to 69% of the material captured in the two sedimentation ponds was of the coarser (>63μm) particle size, and this contributed 81% to 84% of the metal load. The majority of this metal load was captured in autumn.

The proportion of organic material captured in both the sedimentation ponds was high, increasing the potential for metal remobilisation to occur. In the Burbridge Road Sedimentation Pond where there was a high organic matter content, anoxia and reducing redox conditions were observed, which led to algal blooms and strong odours. Regular

cleaning of the Burbridge Road Sedimentation Pond is recommended to remove the build-up of organic material and contaminated sediment, to reduce the pollution problem and to minimise the potential for metal remobilisation to occur.

The overall treatment capacity of each sedimentation pond was strongly influenced by the pond size and its position within the catchment, which affected sediment and heavy metal contamination of inflow to each pond. Capture of sediments and heavy metal concentrations was higher in the Burbridge Road Sedimentation Pond than in the Morphett Road Sedimentation Pond, where there was a well-vegetated channel upstream that could have filtered some of the contaminated sediment from the water before it entered the pond. This contrasted with the Burbridge Road Sedimentation Pond, which was largely serviced by an underground drainage network and open concrete channels that provided little opportunity for pre-treatment of stormwater before it entered the pond.

CHAPTER 5

METAL REMOBILISATION

5.1 Introduction

One of the primary objectives in this study was to investigate the physical and chemical conditions in a sedimentation pond that can affect pond performance. Temperature, DO, redox potential, pH, salinity and water clarity all directly or indirectly affect the remobilisation of metals from sediments. Of these physico-chemical conditions, redox potential and pH are the 'master variables' affecting the solubility and mobility of metals (Förstner, 1990), and even small changes in these variables can have an effect on metal bioavailability (Bourg and Loch, 1995).

This chapter describes how a platform was set up in the Morphett Road Sedimentation Pond with equipment to monitor the temperature stratification behaviour of the pond, and how profiles of DO, redox potential, pH and salinity, and measurements of water clarity were obtained during the peak stratification period of summer and early autumn. The results of these studies are then presented along with a discussion of the implications for sedimentation pond stratification and metal remobilisation.

5.2 Measurement of Physical and Chemical Conditions in the Morphett Road Sedimentation Pond

A platform was erected in the Morphett Road Sedimentation Pond on 21 January 1999 to facilitate the measurement of the physical and chemical parameters in the Morphett Road Sedimentation Pond. The platform is shown in Figure 5-1.

Figure 5-1: The platform in the Morphett Road Sedimentation Pond

The platform supported permanent temperature monitoring equipment in the pond, and was used as a base for profiling the redox potential, pH, DO salinity, turbidity and water clarity at different depths in the water column.

5.2.1 Depth Profiling Equipment

Initially, a pump operated water sampler was employed to determine redox potential, DO, pH and temperature at multiple depths through the water column. The pump-operated water sampler was constructed in the Department of Civil and Environmental Engineering workshop according to the design shown in Figure 5-2. A SHURflo diaphragm pump was used to pump water into a 1L perspex cell, where the water was tested using Hahn temperature, pH and ORP probes and a HACH DO probe, which were inserted into the cell. A secondary outlet valve allowed a sample of water to be extracted from the cell for salinity analysis.

The pump-operated water sampler was tested from the platform in Morphett Road Sedimentation Pond on 13 July 1999, 4 August 1999 and 1 December 2000. However the equipment became redundant before the monitoring program began, when a HYDROLAB MiniSonde that had been purchased for another project became available for use in the pond monitoring study in January 2000. The HYDROLAB consisted of a MiniSonde Water Quality Multiprobe, containing temperature, DO, pH, specific conductivity and turbidity probes and a depth sensor, and a Surveyor 4 Data Display unit. An ORP probe was not included in the

HYDROLAB MiniSonde, but a HAHN ORP probe was made waterproof and attached to the outside of the MiniSonde so that it could be lowered simultaneously.

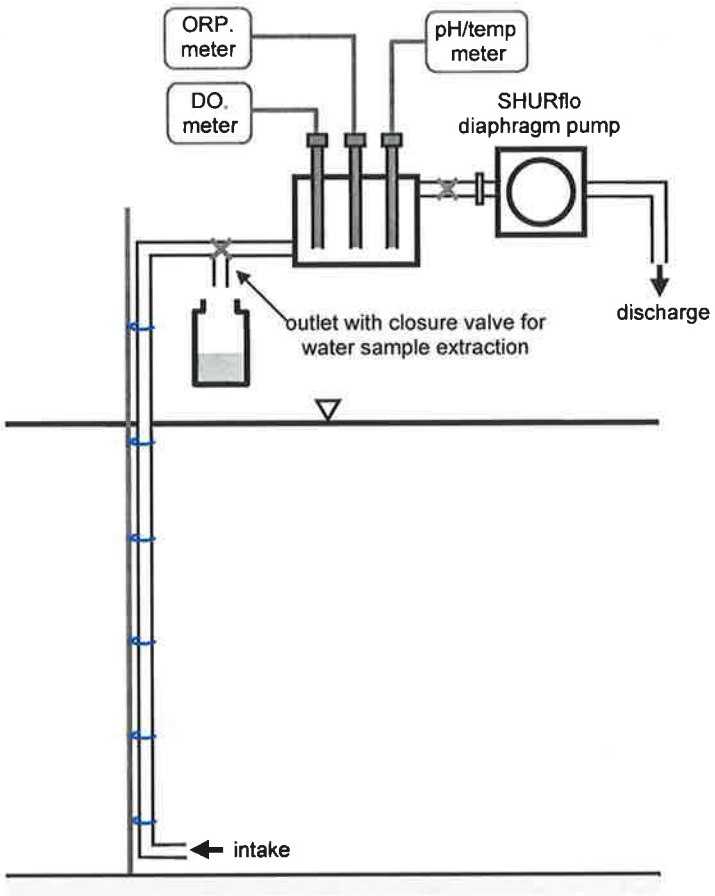

Figure 5-2: Pump-operated water sampler

The MiniSonde was weighted for submersion to depths of 30m. A cable linked the MiniSonde to a handheld 3 hour rechargeable Surveyor 4, which could take an instantaneous record of date, time, depth, and battery voltage, as well as temperature, DO, pH, specific conductivity and turbidity, in the operator's choice of units (e.g. % saturation or mg/L for DO). The Surveyor 4 could store up to 12 readings at a time.

The HYDROLAB MiniSonde was trialled in the Morphett Road Sedimentation Pond on 6 January 2000 and was found to be superior to the pump-operated water sampler in both efficiency and reliability of monitoring. Most importantly, the submersibility of the HYDROLAB MiniSonde negated the need to pump water to the surface for testing, a process that could potentially compromise DO and ORP readings by exposing sub-surface water to oxygen from the atmosphere.

5.2.2 Redox Potential

The work done in transferring an electron from a reduced substance to an oxidised substance can be measured electrically. The tendency for an oxidant or reductant to either gain or lose electrons is known as the 'redox potential' (Henderson-Sellers, 1984). Redox potential measurement is very important in assessing the speciation and mobility of metals (Grundl, 1995).

The hydrogen redox couple, consisting of hydrogen ion (H^+) as the oxidant and molecular hydrogen (H_2) as the reductant is used as a reference, and assigned a redox potential free energy level of zero. All other redox couples are assigned a potential difference Eh, which is the difference in the free energy of an electron, between its source and the hydrogen ion. An oxidant, which will tend to gain electrons, will have an Eh value greater than zero, while a reductant, which tends to lose electrons, will have an Eh value less than zero.

Redox potential is generally measured in mV in reference to a standard hydrogen electrode (Eh), but may be represented as the negative base 10 logarithm of electron activity (pE) (Grundl, 1995). pE is dimensionless and represents the availability of electrons in the same way that pH is a dimensionless characterisation of proton activity. A high pE indicates low electron activity and oxidising conditions, while a low pE is an indication of high electron activity and reducing conditions. The relationship between pE and Eh is represented by Equation 5.1 (Hostettler, 1984).

$$pE = \frac{F\,Eh}{2.303\,R\,T} \qquad (5.1)$$

where: Eh is the potential difference in V;

F is 96 485$Cmol^{-1}$;

R is the gas constant (8.314$JK^{-1}mol^{-1}$); and

T is the temperature in K.

Unfortunately however, due to the continual non-equilibrium of organism growth and decay processes, and due to the fact that redox reactions are kinetically slow anyway and rarely reach an equilibrium state, the difference between the measured redox potential and the actual value may be large (Grundl, 1995).

In every natural aquatic system, a number of redox couples are likely to be present, each couple in its own state of disequilibrium. The system will be dominated by just one redox couple (Grundl, 1995). The dominance of any one couple is influenced by the concentration of chemically active species in the system, and the redox potential of the dominant couple

controls the redox balance of other couples in the system (Lower, 1998). It is possible to measure the concentration of redox couple components to gauge the redox status of a system, but this requires knowledge of the chemical composition and redox couple dominance of the system. Measurement of the concentration of the components of just one redox couple (e.g. Fe^{2+}/Fe^{3+}) indicates the redox status of that couple but does not represent the redox status of the whole system, which would be a combination of potentials from a mixture of redox couples. Gauging the redox status of the system using an indicator couple such as Fe^{2+}/Fe^{3+} is further complicated by the likely disequilibrium of the couple.

Other techniques have been suggested for determining the redox capacity (e.g. total oxidative capacity – OXC), but since the capacity describes the potential of the system (i.e. if a state of equilibrium were reached) and is not representative of the actual state of the system, these techniques were not considered.

Two common techniques for measuring redox potential in natural aqueous systems are by measurement with an electrode or by employing a redox couple as an indicator of the system's potential for oxidation or reduction. Both techniques measure the redox intensity of the system rather than the redox capacity, and require a state of equilibrium either between the solution and the electrode or between the solution and the indicator, as well as equilibrium within the solution itself.

Speciation models such as MINTEQ and GEOCHEM, generally assume an equilibrium state and are therefore only useful as an indicator of potential metal toxicity. To model metal speciation without assuming equilibrium, assumptions must be made about rates of transformation for each redox couple, which is difficult due to the different kinetics in each system.

Standard Methods for the Examination of Water and Wastewater (APHA, 1995) recommend a platinum or gold indicator electrode with a calomel or silver/silver chloride (Ag/Ag^{+}) reference electrode for measurement of ORP in natural surface waters.

A HACH Combination ORP Electrode (Model 50230) was used to measure redox potential in the Morphett Road Sedimentation Pond. The electrode measures the intensity of the system, rather than the capacity of the system for oxidation and reduction. The HACH ORP Electrode used a silver/silver chloride redox couple as a reference rather than the standard hydrogen couple, which is fragile and impractical for use in the field (APHA, 1995). The redox potential reading was converted to a reading that was relative to a normal hydrogen electrode using Equation 5.2 from the HACH manual (Hach, 1996). Equation 5.2 incorporated a water temperature dependent conversion factor (C) that was determined using the graph in Figure 5-3.

$$Eh = E + C \qquad (5.2)$$

where: Eh is the potential of the sample relative to a normal hydrogen electrode in mV;

E is the potential reading of the HACH electrode; and

C is a temperature dependent conversion factor (see Figure 5-3).

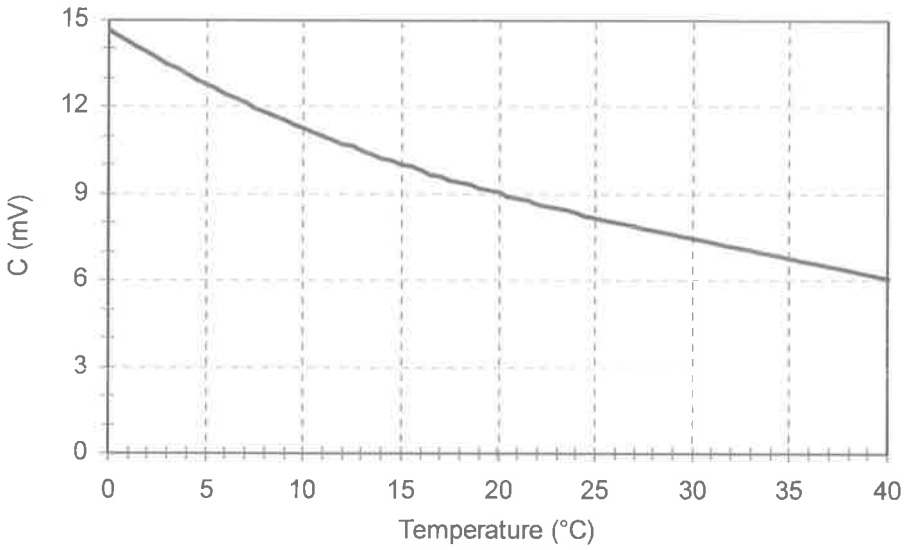

Figure 5-3: Conversion factor for electrode potential reading (after Hach (1996))

The central sensing element, which acted as the indicator electrode accepting or donating electrons as required, was made of platinum. Platinum is a noble metal and is relatively inert, but may react selectively with oxygen, forming a surface oxide layer, or can absorb a surface film from contact with organic matter or sulfide (Grundl, 1995). . There is no indicator electrode material that is perfectly inert and behaves ideally in all aqueous systems (APHA, 1995). To minimise the electrode error, the electrode surface was maintained in a clean condition and Light's standard solution was used to check for drift in the electrode performance.

Standard Methods for the Examination of Water and Wastewater (1995) advises that there should be minimal atmospheric contact and delay in analysis, hence redox potential measurements were made *in situ*.

5.2.3 pH

The pH probe consisted of a glass electrode filled with potassium chloride solution. The potassium chloride solution was saturated with silver chloride (the reference electrode), which provided a constant electrode potential.

The pH meter was calibrated using the two buffer method. A buffer of pH 7.0 was used to set the intercept of the electrode response curve so that the electrode potential was 0mV at pH 7 (the isopotential point). A second buffer of pH 10.0 was used to set the slope about the isopotential point.

When the pH electrode was immersed in solution, a layer of hydrogen ions built up at the surface of the glass electrode bulb through exchange with sodium ions, and negatively charged silicates at the surface of the bulb opposed anions in the solution. The hydrogen ion activity of the solution produced a potential, which defined the pH of the solution.

The pH meter had a range of 0 to 14 pH units and was accurate to ±0.2 units. Resolution of the pH readings was 0.01 units.

5.2.4 Dissolved Oxygen

Concentrations of DO are generally represented as either a concentration or as a percentage of saturation. Concentration in mg/L was chosen as the unit of measurement for DO in this study.

A popular method for measurement of DO concentration is the Winkler method. The Winkler method is a laboratory titration in which a combination of chemicals, usually manganous sulphate, potassium hydroxide and potassium iodide, are added to a sample of water to produce iodine, which is dark brown in colour. Sodium thiosulphate is used as an indicator to determine when the iodine colour vanishes. The DO saturation can be determined from the quantity of sodium thiosulphate that is required to eliminate the iodine.

Unfortunately the laboratory equipment and chemicals required to perform the Winkler test made it inappropriate for use in the field. An alternative was to transport water samples from the field to the laboratory for analysis, but this would have introduced potential sources of error due to the time delay and exposure to the atmosphere. Organic chemicals in the test sample may also interfere with the Winkler titration method (Hach, 1997).

Dissolved oxygen probes, which can measure concentration of DO *in situ*, are an alternative to the Winkler method. The DO probe method is a quicker and easier test to perform, particularly with field testing. The use of a fully submersible probe allows measurement of sub-surface water without having to bring a sample to the surface, where oxygen from the atmosphere can alter the DO concentration before the test is complete.

Initial trials in the Morphett Road Sedimentation Pond were performed using a HACH DO175 Dissolved Oxygen Meter in a flow-through cell, but later DO measurement were taken using the submersible HYDROLAB MiniSonde that could take measurements *in situ*. The

HYDROLAB MiniSonde DO probe consisted of an anode/cathode electrode system and potassium chloride (KCl) electrolyte that was separated from the sample by an oxygen-permeable membrane. The current caused by diffusion of molecular oxygen across the membrane was directly proportional to the concentration in the sample.

The DO probe was calibrated for the local barometric pressure, which was approximated using Equation 5.3. The Morphett Road Sedimentation Pond was at an altitude of approximately 1.5m above mean sea level.

$$BP = 760 - 2.5\left(\frac{0.3048\ A}{100}\right) \tag{5.3}$$

where: BP is the barometric pressure in mmHg; and

A is the altitude above mean sea level in m.

The HYDROLAB MiniSonde probe could take DO readings between 0 and 20mg/L to within ±0.2mg/L and with a resolution of 0.01mg/L.

5.2.5 Salinity

In order to determine the absolute salinity of natural water with reliability, a complete chemical analysis is required, but it is a time-consuming method that can be imprecise (APHA, 1998). It is easier to measure the physical properties of a solution to calculate salinity by using a relationship determined empirically from a standard solution. Physical properties that may be used to indirectly measure the salinity of a solution include density, conductivity, sound speed or refractive index. Standard Methods (1998) recommends the use of either density or conductivity methods for field work. Conductivity is most commonly used due to its good sensitivity and the simplicity of the technique (APHA, 1998), and is the method that was chosen for measurement of salinity in this study.

For an aqueous solution, electrical conductivity is a measure of the solution's capacity for carrying an electric current. Current carrying capacity depends on the concentration, mobility and valence of ions in the solution (APHA, 1998), and is also affected by temperature. The electrical conductivity increases by about 2% for each 1°C rise in temperature (Wetzel, 1975), hence it is common to standardise readings to 25°C (Equation 5.4). This is sometimes referred to as 'specific conductance'.

$$EC@25°C = EC \times f(T) \tag{5.4}$$

where: EC is the electrical conductivity in μS/cm;

EC@25°C is the electrical conductivity in μS/cm at 25°C; and

f(T) is a non-linear function of temperature in °C.

Electrical conductivity (EC@25°C) was measured using a conductivity sensor comprised of four graphite electrodes and temperature sensor, which were incorporated into the HYDROLAB MiniSonde. An in-built freshwater temperature compensation function was selected for conversion of EC to EC@25°C (Equation 5.5, (HYDROLAB, 1997)).

$$f(T) = c_1 T^5 + c_2 T^4 + c_3 T^3 + c_4 T^2 + c_5 T + c_6 \quad (5.5)$$

where: $c_1 = 1.4326 \times 10^{-9}$;

$c_2 = -6.0716 \times 10^{-8}$;

$c_3 = -1.0665 \times 10^{-5}$;

$c_4 = 1.0943 \times 10^{-3}$;

$c_5 = -5.3091 \times 10^{-2}$;

$c_6 = 1.8199$; and

T is the water temperature in °C.

The conductivity of a solution is a function of the electrode surface area and the distance between electrodes. Conductivity proportionality was determined by calibrating the instrument with de-ionised water and a standard KCl solution. Following calibration, the instrument could measure conductivity between 0 and 100 000μS/cm with 4-digit resolution and an accuracy of ±0.001μS/cm.

5.2.6 Turbidity and Water Clarity

Measurement of turbidity is not always an accurate indication of particulate concentration but it can still be a useful means of approximation (Wetzel and Likens, 1991). The two methods that are commonly used to measure the water turbidity are nephelometric turbidity techniques or the process of filtration, drying and weighing of suspended particulate matter (SPM) from a water sample. A third technique involves the use of a secchi disk although this is a measure of water clarity rather than turbidity.

Nephelometric turbidity measurements are more often used in the water quality industry (e.g. drinking water quality standards and guidelines) whereas the secchi disk depth technique is

more frequently applied in limnology. Both techniques were applied in the study of Morphett Road Sedimentation Pond. The SPM analysis technique was impractical for field measurement.

A turbidity sensor was incorporated into the HYDROLAB MiniSonde. The turbidity sensor consisted of an infrared emitter, which emitted infrared light with a wavelength of 880nm, and a photodiode, which detected light scattered at 90° from the emitter. The sensor was shuttered to prevent fouling of the optical lens, a common problem with turbidimeters. The turbidity sensor was calibrated using the calibration procedure outlined in the manual (HYDROLAB, 1997). After calibration, the sensor could measure turbidity in the range 0 – 1000NTU with an accuracy of 2.6%. It automatically adjusted to a resolution of 0.1NTU for readings under 100NTU and a resolution of 1NTU for readings between 100 and 1000NTU.

The HYDROLAB MiniSonde turbidity sensor was very sensitive to interference from floating weed, litter and other objects in the water, which led to a number of extreme and uncharacteristic turbidity readings. However a secchi disk was used concurrently as an additional indicator of water clarity. Turbidity is strongly related to water clarity (Smith *et al.*, 1997), however secchi disk measurements are not directly comparable to the turbidity sensor results since the sensor measures only scattering, while the secchi disk depth provides an indication of scattering and absorption, both of which are important in assessing water clarity (Effler, 1988). Smith *et al.* (1997) recommended secchi disk style measurement of clarity, due to the greater relevance of clarity in water resource management than measurements of turbidity alone.

The secchi disk is a very old and simple method of measuring transparency. The idea of using a disk to measure the transparency of the ocean was conceived by Captain Berard in the 18th century, but it did not become known as a 'secchi disk' until the Italian physicist Angelo Secchi conducted a series of experiments with the technique for the Papal Navy on board the SS L'Immacolata Concezione in the 19th century (Tyler, 1968). The secchi disk depth is the average of the depth at which the disk is no longer visible upon being lowered into the water and the depth at which it again becomes visible as it is raised to the surface. Light is reflected from the surface of the disk, hence dissolved matter and particulates and light absorption in the water affect its visibility.

There is currently no standard protocol for the design or use of the secchi disk. Most secchi disks are 20cm in diameter and weighted for lowering into deep water. Originally white in colour they are now often designed with alternate black and white quadrants.

Secchi disk depth measurements are dependent on the whiteness of the disk, refraction of its image, the solar altitude and any shadowing of the water by the platform or boat from which the reading is being made (Smith and Hoover, 1999). Readings are also affected by any currents, which may tilt the disk or put excessive drag on the rope, and will always be subject

to the operator's visual perception. Secchi recommended using the disk in shadow (Tyler, 1968) while Smith and Hoover (1999) recommend measurement in a sunny location, but with a viewer box to prevent water surface glare and glitter. Wetzel and Likens (1991) advocate Secchi's shaded measurement technique and further advise that it is best done near midday.

The secchi disk that was used in this study was a 20cm diameter weighted disk with alternate white and black quadrants. The disk was lowered into the water from the platform (see Figure 5-1) in the Morphett Road Sedimentation Pond. The platform was designed to cause minimum shading of the water, which could interfere with ongoing temperature monitoring, thus it was necessary to make all secchi disk readings in full sunlight. A secchi disk depth was determined in the Morphett Road Sedimentation Pond every 15 minutes during the first two sessions of monitoring and each hour during the last monitoring session.

The secchi disk was lowered into the pond until it disappeared and was then raised until it reappeared. The average of the two depths was recorded as the secchi disk depth (SDD). On occasions when the disk reached the bottom of the pond but still remained visible (i.e. there was very high water clarity), the depth of water in the pond was recorded as the SDD.

5.2.7 Temperature

Although a temperature sensor was incorporated into the HYDROLAB MiniSonde that was used during the three sessions of depth profiling, the HYDROLAB MiniSonde sensor was not required since temperature monitoring equipment was already in place in the pond to continuously record the temperature profile.

The monitoring equipment, which consisted of 8 temperature sensors, circuitry, a data logger and the associated computer software, was put together in the Department of Civil and Environmental Engineering instrumentation laboratory. Figure 5-4 shows the set up of equipment in the Morphett Road Sedimentation Pond. (The platform is pictured in Figure 5-1 earlier in the chapter.)

The temperature sensors protruded from a piece of stainless steel tubing, which was held vertically in the water column by two supporting arms that were clamped to the side of the platform. The wiring for the temperature sensors was threaded through the tubing and enclosed in a cable that led from the top of the sensor tube to a waterproof junction box containing a screw terminal, which was attached to the top of the platform. A second cable led from the junction box to a logger box containing an interface board and data logger, which was programmed using the assembly language program 'CEL3.asm'. The logger box was buried at the top of the bank, well above the highest water level.

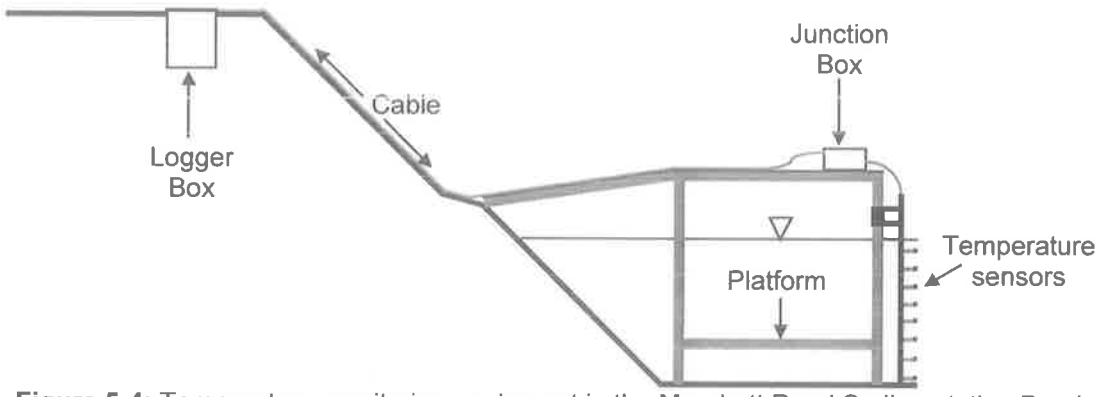

Figure 5-4: Temperature monitoring equipment in the Morphett Road Sedimentation Pond (not to scale)

The pond had a mean depth of approximately 0.9m. The eight temperature sensors were positioned at 12cm intervals through the water column, with the deepest sensor located 2.5cm from the pond bottom as shown in Figure 5-5. Due to fluctuations of the water level in the pond, the concrete base of the pond was used as a depth reference for the eight temperature sensors. For example, the top or shallowest temperature sensor in the pond had a 'depth' of 86.5cm, while the bottom or deepest temperature sensor had a 'depth' of 2.5cm.

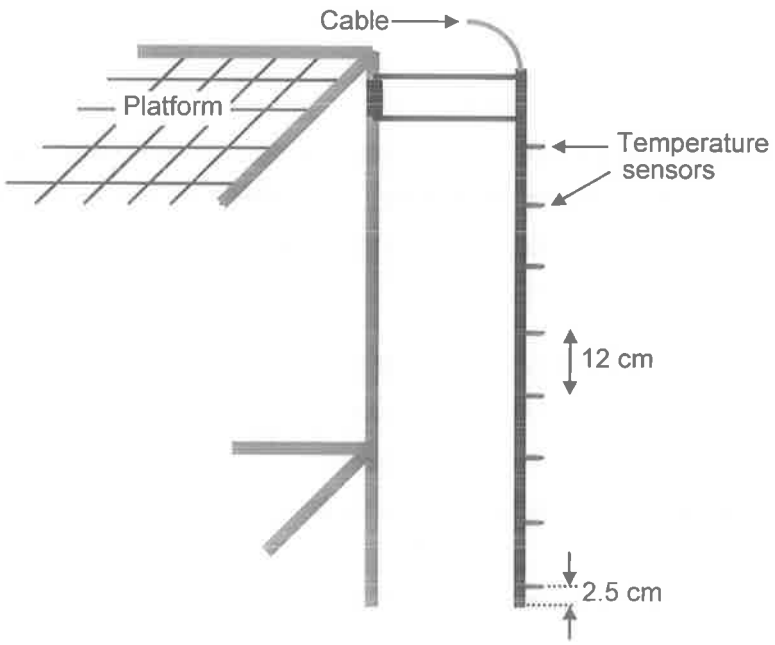

Figure 5-5: The arrangement of temperature sensors in the Morphett Road Sedimentation Pond (not to scale)

Each temperature sensor had a unique temperature-voltage relationship that was determined using the calibration procedure set out in Appendix H. Ten temperature sensors were calibrated, and the best eight were selected for use in the field. The eight sensors that were selected were accurate to 0.2°C after calibration.

The eight temperature sensors were monitored continuously from 12 March 1999 to 10 April 2000. The temperatures of the eight sensors were recorded by a data logger, which was powered by two rechargeable 12V batteries. Every two weeks (range: 4 – 50 days) the logger was stopped while the batteries were replaced and the temperature data was downloaded using the STERM (Serial Terminal) program in DOS, which was loaded onto a laptop computer. The logger was then re-started. Initially the logger was programmed to record temperatures at 5 minute intervals, but after observing data recorded during the first 3 weeks, the logging frequency was reduced to intervals of 10 minutes, which extended the life of the batteries, but still captured adequate detail of temperature fluctuations in the pond.

Figure 5-6 shows the temperatures recorded in the pond during March, the first month of operation of the temperature monitoring equipment.

The deepest temperature sensor in the pond was positioned only 2.5cm from the concrete bottom of the pond, where it would have been subjected to the effects of accumulation and movement of sedimentary and organic material on the pond bottom. Temperature fluctuations at the bottom of the pond were expected to be different to the fluctuations in the overlying water, due to the different thermal properties of the sediment, organic matter and underlying concrete in comparison to water. However, on the second day of operation in the pond, the temperature of the deepest temperature sensor dropped by approximately 15°C over a period of about 17 hours. After the initial drop in temperature, the temperature fluctuations recorded by the deepest temperature sensor mimicked the heating and cooling trends of the temperature sensors above, although well below the mean pond temperature. This trend continued until late April 1999, when the temperature of the bottom sensor rose above the mean temperature of the other seven sensors.

Although all parts were siliconed in place to make the structure water-tight, it is possible that a leak occurred in the bottom sensor. Water is highly conductive and may have increased the current, leading to a falsely low voltage, which would correspond to a lower than expected temperature reading. The effect would have been exagerated in saline water, which has a higher electrical conductivity than freshwater. Salinity was high during late summer and early autumn of 2000, and it is likely that similar pond conditions existed in the even drier weather that was experienced in 1999. The increase in rainfall and flow that were observed with the progression of autumn would have reduced the salinity of the water. A gradual decrease in salinity and corresponding decline in conductivity might explain why the temperature recorded by the bottom sensor gradually increased to mean pond level during autumn. Due to the unreliability of the deepest temperature sensor, data from that sensor was disregarded in the analysis of the pond temperature stratification.

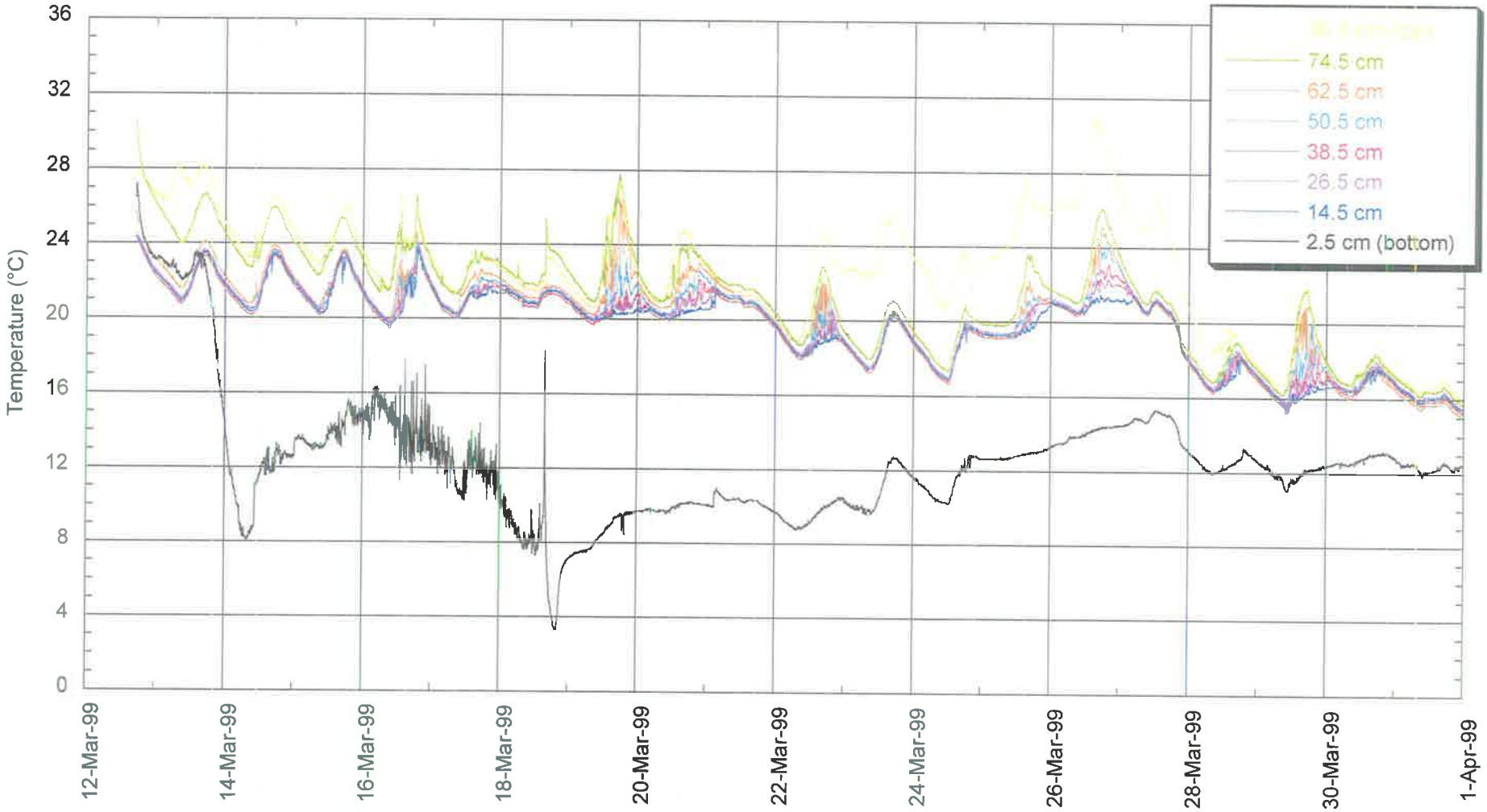

Figure 5-6: Temperature variation during the first month of monitoring in the Morphett Road Sedimentation Pond

Few other problems were experienced with the temperature monitoring equipment. On one occasion (22 March 1999 to 28 March 1999) the depth of water in the pond was so low that the top temperature sensor was above the water surface (see Figure 5-6). And on a second occasion (3 November 1999 to 18 November 1999), the top four temperature sensors recorded erroneous values, possibly due to moisture or a loose connection in the wiring, but the problem rectified itself when the batteries were changed.

5.3 Physical and Chemical Conditions in the Morphett Road Sedimentation Pond

The temperature sensors were operational in the pond between 12 March 1999 and 10 April 2000, continuously recording the temperature profile every 10 minutes (initially every 5 minutes but later changed).

The depth profiling of redox potential, DO, pH, specific conductivity, turbidity and pond clarity was carried out during three intensive sessions of monitoring from 18 January 2000 to 22 January 2000, 7 February 2000 to 11 February 2000 and from 29 February 2000 to 2 March 2000. Measurements were made at the surface middle and bottom of the pond every 15 minutes for between 7 and 9 hours each day.

Figure 5-7 shows the meteorological conditions, including air temperature, dew point temperature, wind speed and total daily solar radiation, at the Morphett Road Sedimentation Pond during the three monitoring sessions, and Table 5-1 gives the monthly average values. The meteorological data was obtained from the adjacent Adelaide Airport Bureau of Meteorology station. (The measurement techniques and quality of the data is discussed in more detail in Chapter 6.)

Table 5-1: The average values of total daily solar radiation, air and dew point temperatures and wind speed during January, February and March 2000

Month	Total Daily Solar Radiation	Air Temperature	Dew Point Temperature	Wind Speed
Jan-00	25.55	21.93	8.84	5.10
Feb-00	24.54	25.11	11.62	3.96
Mar-00	19.11	20.27	11.05	3.76

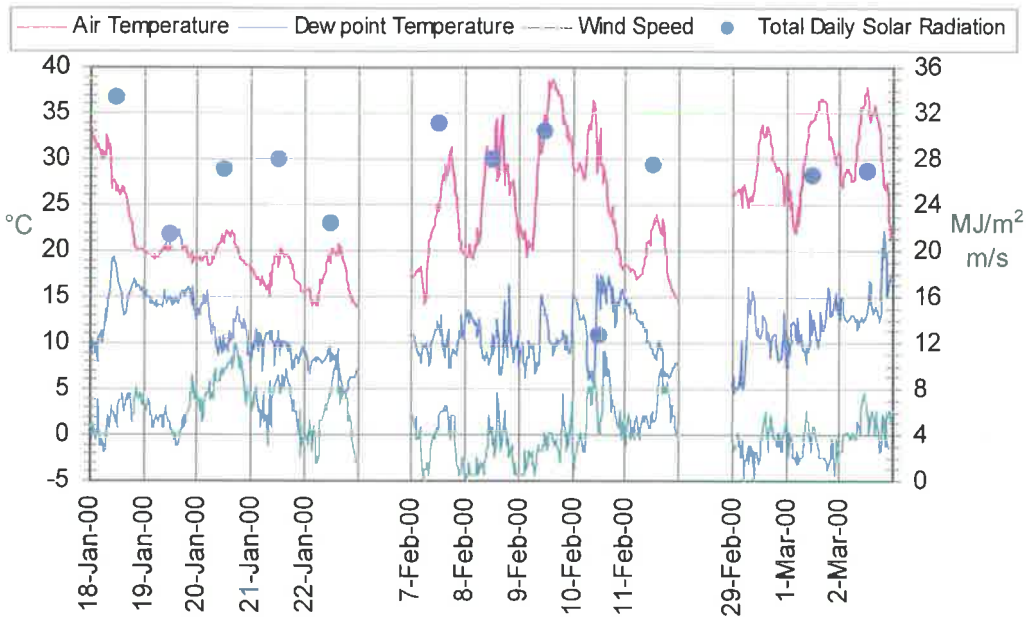

Figure 5-7: Meteorology at the Morphett Road Sedimentation Pond during the three sessions of monitoring

Average daily dew point temperature was above average on all the days of profiling. Air temperatures were also warmer than average on the final three days of profiling. Total daily solar radiation was high on two of these days, but no record is available for the other day (29 February 2000). None of the other meteorological parameters were remarkable in comparison to monthly average values.

5.3.1 Redox Potential

All living organisms obtain energy from the chemical energy released from chemical compounds during redox reactions (Seki, 1982). Carbon, nitrogen, oxygen, sulfur, iron and manganese are the major elements involved in redox reactions in natural waters, and the redox reactions involved in the cycling of these elements are an important source of energy for organisms in aquatic environments (Lower, 1998).

Oxidation-reduction reactions involve the transfer of electrons (e^-) in the same way that pH or acid-base reactions involve the transfer of protons (H^+). Unlike acid-base reactions however, which are generally very rapid, redox reactions in natural waters are often extremely slow and an equilibrium state is rarely reached, although the catalytic action of organisms helps to speed the reactions (Lower, 1998).

Redox reactions are also sometimes called oxidation-reduction reactions. They involve a transfer of electrons from a reduced substance to an oxidised substance, which acts as an

electron acceptor (i.e. oxidised substance + electron = reduced substance). They are frequently represented by two half-equations – one a reduction, which leads to the release of electrons, and the other an oxidation, in which the electrons are accepted.

Carbon compounds, which are generated by photosynthesis, are a major store of energy in the biosphere. Microbial oxidation of organic carbon typically controls the redox status of natural aqueous systems (Grundl, 1995). The important oxidation step in biological metabolism in aquatic ecosystems, is the oxidation of carbon compounds, principally carbohydrate molecules (CH_2O), to release the stored energy. This is represented by the following half-equation:

$$(CH_2O) + H_2O \rightarrow CO_2 + 4H^+ + 4e^- .$$

Carbohydrate oxidation is always accompanied by a reduction reaction. For the reduction reaction, organisms will utilise the substance that releases the most energy for metabolism. In aerobic or well-oxygenated environments oxygen is the most common electron acceptor (Seki, 1982). In these environments the half-equation accompanying carbohydrate oxidation will involve the reduction of oxygen, since it is the most energy productive compound. However, when oxygen consumption outpaces the rate of oxygen replenishment in the water column, an alternative electron acceptor must eventually be used (Spiro and Stigliani, 1996). Common electron acceptors of anaerobic metabolism, shown in order of metabolic preference, include nitrate (NO_3^-), manganese dioxide (MnO_2), ferric hydroxide ($Fe(OH)_3$), sulfate (SO_4^{2-}) and under very reducing conditions, carbon dioxide (CO_2). Half-equations for the reduction of each of these substance are given below.

1. Reduction of oxygen is represented by the following half-equation:

$$O_2 + 4H^+ + 4e^- \rightarrow 2H_2O .$$

2. In nitrate reduction, denitrifying bacteria reduce nitrate (NO_3^-) to nitrogen gas (N_2). The greenhouse gas nitrous oxide (N_2O) is also released in the denitrification process (Spiro and Stigliani, 1996). The half-equation for this process is represented by:

$$2NO_3^- + 10e^- + 12H^+ \rightarrow N_2 + 6H_2O .$$

3. The reduction of Mn^{4+} to Mn^{2+} occurs if manganese dioxide is present. The reduction of manganese is represented by the following half-equation:

$$MnO_2 + 2e^- + 4H^+ \rightarrow Mn^{2+} + 2H_2O .$$

4. The reduction of ferric iron (Fe^{3+}) to ferrous iron (Fe^{2+}) is almost entirely mediated by microorganisms (Baldwin *et al.*, 1997). However, in surface waters ferric iron can be

reduced to ferrous iron by the direct absorption of light by ferrous iron (i.e. it is not microbially mediated), even when oxygen is present (Lower, 1998). Ferric iron reduction is represented by the following half-equation:

$$Fe(OH)_3 + e^- + 3H^+ \rightarrow Fe^{2+} + 3H_2O.$$

5. Sulfate reducing bacteria reduce sulfate to hydrogen sulfide gas, which is extremely odorous and also toxic. The production of hydrogen sulfide can reduce the redox potential to -300 mV (Seki, 1982). Sulfides may bind to free heavy metals, forming insoluble metal sulfides, which are generally resistant to oxidation, although metal release can occur if, for example, anaerobic sediments are exposed to the atmosphere. The half-equation for sulfate reduction is:

$$H_2SO_4 + 8e^- + 8H^+ \rightarrow H_2S + 4H_2O.$$

6. The reduction of carbon dioxide occurs via a process known as methanogenesis, in which methanogens reduce carbon dioxide to methane. Production of methane is undesirable, it is odorous and it contributes to the greenhouse effect. This is represented by the following half-equation:

$$CO_2 + 8e^- + 8H^+ \rightarrow CH_4 + 2H_2O$$

Methane can also be produced anaerobically by the splitting of acetate (CH_3COOH), a product of cellulose, or when partially reduced carbon compounds (CH_2O) disproportionate (Spiro and Stigliani, 1996). These are represented by the following reactions:

$CH_3COOH \rightarrow CH_4 + CO_2$; and

$CH_2O + CH_2O \rightarrow CH_4 + CO_2$.

Of the redox reactions shown in the list above, oxygen and sulfur are the most important electron acceptors for redox reactions in natural aqueous systems (Grundl, 1995), although the choice of electron acceptor depends on the availability of nitrate, manganese, ferric iron, sulfate and carbon dioxide in each aquatic system. In the absence of an oxidant or reductant required for redox transformation, the reactions may be irreversible or extremely slow (Pardue and Patrick Jr., 1995).

Many of the redox reactions shown above also involve the transfer of hydrogen ions (H^+) hence they are also dependent on pH. Most reactions in the natural environment involve are dual reactions involving both redox and pH changes (Baas Becking *et al.*, 1960). This is further discussed in Section 5.3.2.

5.3.1.1 Redox Reactions and Metal Toxicity

Redox reactions affect the toxicity of metals and metalloids in aquatic systems by altering the speciation of metal or metalloid. The oxidant may be more toxic than the reductant for example, or vice versa, depending on which form is more soluble. These reactions however are not always perfectly reversible if the transformation from oxidant to reductant involves a different mechanism from the reverse transformation of reductant to oxidant.

Transformation of a metal or metalloid can occur either directly through a change in state of the metal or metalloid, or indirectly through a change in state of an organic or inorganic substance to which the metal or metalloid is attached. Metals or metalloids that are directly affected by change in redox potential, are those that have multiple valence states (Pardue and Patrick Jr., 1995).

Chromium transformation occurs both directly and indirectly, depending on whether it is an oxidation or reduction. In a study of chromium behaviour in the water and sediments of a flooded wetland by Masscheleyn *et al.* (1992), direct reduction of Cr^{6+} to Cr^{3+} was observed at a redox potential of 300mV. The reverse oxidation of Cr^{3+} to the more toxic Cr^{6+} however was controlled by manganese oxide.

Changes in redox potential can induce similar direct shifts between the four valence states of selenium and the two valence states of arsenic (Pardue and Patrick Jr., 1995). While selenium was found to have a higher solubility in aerobic conditions (Masscheleyn *et al.*, 1990), the solubility of arsenic was shown to be greater in anaerobic conditions (Masscheleyn *et al.*, 1991).

Other metals and metalloids, such as boron, cobalt, copper, molybdenum and zinc do not themselves undergo redox reactions, but solubility is affected indirectly. Concentrations of these metals are likely to increase with dissolution of iron and manganese oxides and hydroxides (Alloway and Ayres, 1997). Copper, manganese, molybdenum and vanadium absorb to iron oxides, cobalt, iron and lead absorb to manganese oxides, while nickel and zinc can absorb to both iron and manganese oxides (Alloway and Ayres, 1997).

Under oxic conditions, iron and manganese oxides and hydroxides form a coating on sediments to which metals can sorb (Förstner, 1981; Alloway and Ayres, 1997). Under conditions of low redox potential however, the iron and manganese oxides and hydroxides can be reduced to water-soluble forms, which instantaneously releases the attached metals. The metal ions may complex with organic molecules or precipitate as metal sulfides. Metal sulfides are highly insoluble, but metal organic complexes are soluble and will be resistant to oxidation into a less bioavailable form.

In reservoirs, iron is transformed from the ferric iron to ferrous iron during temperature stratification, and the transformation of manganese follows a similar pattern, generally slightly preceding the reduction of iron (Henderson-Sellers, 1984). Brookes *et al.* (2000) found a significant correlation between the annual maximum concentration of iron and manganese and the duration of the stratification.

Figure 5-8 shows the mean redox potential in the Morphett Road Sedimentation Pond during the three monitoring sessions while Figure 5-9 shows the difference in redox potential between the surface and the bottom of the pond.

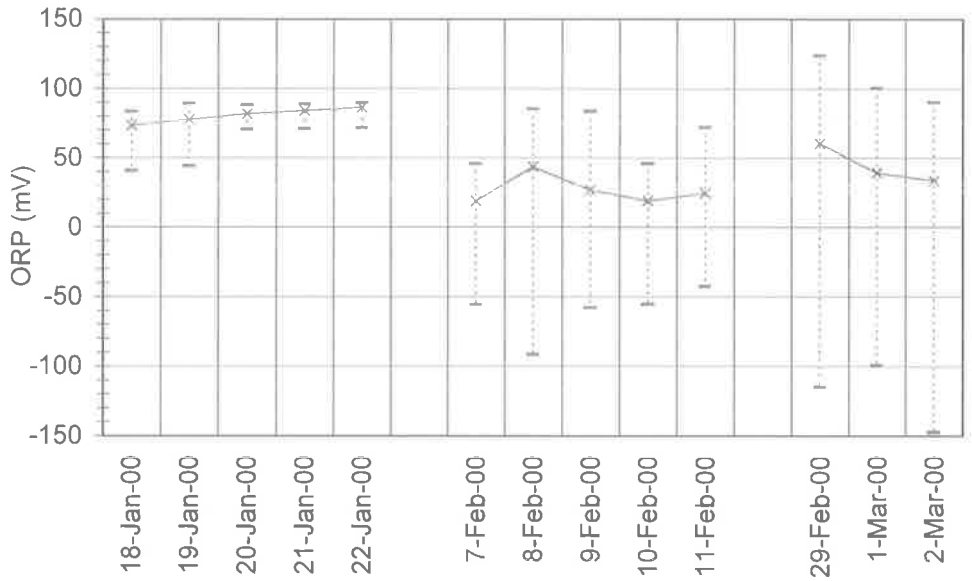

Figure 5-8: The mean redox potential (ORP) on each day of monitoring in the Morphett Road Sedimentation Pond (the dashed lines illustrate the range of values that was recorded)

The mean redox potential was highest and most stable during the first monitoring session (18 January 2000 – 22 January 2000). Hour by hour, there was an increase in redox potential at the surface and bottom of the pond during the monitoring, and there was a gradual increase in mean redox potential over the five days. During the first monitoring session, redox potential was consistently slightly higher at the bottom of the pond than at the surface.

Conversely during the second and third monitoring sessions (7 February 2000 – 11 February 2000 and 29 February 2000 – 2 March 2000) the mean redox potential was significantly higher at the middle and surface of the pond. The mean redox potential at the bottom of the pond was negative on 9 February 2000 and 10 February 2000 during the second monitoring session and 1 March 2000 and 2 March 2000 during the third session. Those days corresponded to when the surface to bottom redox potential difference was highest.

The surface to bottom redox potential difference was greatest on the final two days of monitoring (1 March 2000 and 2 March 2000) with the onset of temperature stratification. As

the temperature stratification progressed, the redox potential at the bottom of the pond became increasingly negative. Surface redox potential also fell, but the magnitude of the decrease was less significant. Redox potential readings in the Morphett Road Sedimentation Pond on 2 March 2000 are shown in Figure 5-10. Since the redox potential was not monitored through the night when the mean pond temperature and temperature stratification were increasing, it is not known whether the difference between redox potential at the surface and the bottom decreased with the temperature stratification towards dawn the following day as would have been expected.

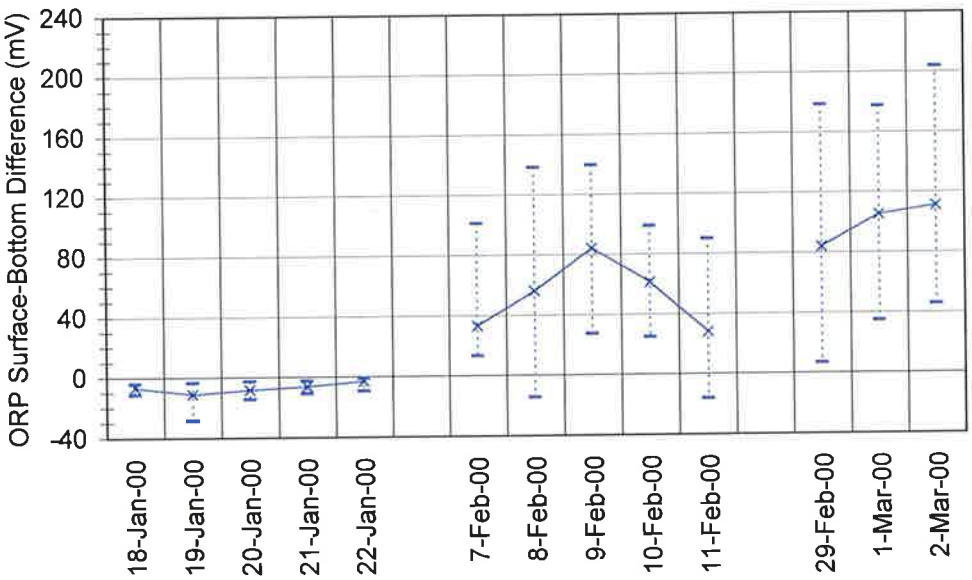

Figure 5-9: The mean difference in redox potential (ORP) between the surface and bottom of the Morphett Road Sedimentation Pond on each day of monitoring (the dashed lines illustrate the range of values that was recorded)

Redox potential readings were also much more variable during the last two monitoring sessions, as can be seen for 2 March 2000 in Figure 5-10. Variability was highest at the bottom of the pond, possibly due to disturbance of the sediments when the HYDROLAB MiniSonde struck the bottom, which may have released porewaters with a lower redox potential. Redox potential in the sediments typically decreases with increasing sediment depth, although sediment depth was limited in the Morphett Road Sedimentation Pond by the concrete pond base.

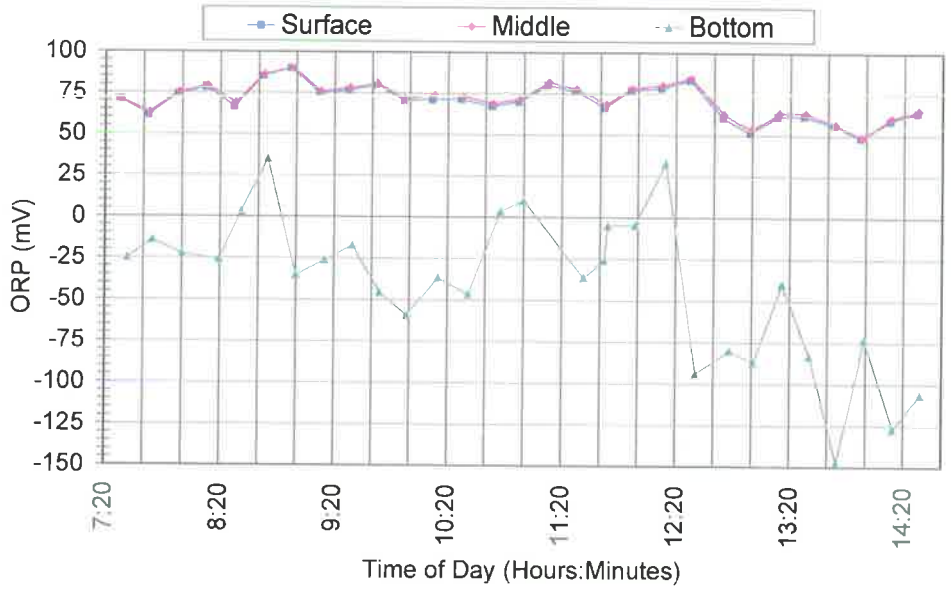

Figure 5-10: Redox potential (ORP) readings at the surface, middle and bottom of the Morphett Road Sedimentation Pond on 2 March 2000

5.3.2 pH

pH is a measure of hydrogen ion activity (Equation 5.6) and is an indication of the intensity of acidity of a solution.

$$pH = -\log a_{H^+} \qquad (5.6)$$

where: pH is dimensionless; and

a_{H+} is the hydrogen ion activity.

Natural aquatic environments generally have a pH of between 5 and 9, depending on the concentrations of cations, carbonate, bicarbonate and CO_2 (Seki, 1982). Microbial consumption and production can also influence pH levels.

The magnitude of fluctuations in pH levels depends on the buffering capacity of the aquatic system. The 'buffer capacity' of an aquatic system can be measured by determining the quantity of strong acid or strong base required to produce a pH change of 1 unit in 1L of water (APHA, 1998). Waters with a high buffering capacity are resistant to pH change, while water with a low buffering capacity can experience large changes in pH. Waters containing low quantities of dissolved matter tend to have a low buffer capacity (Seki, 1982).

The level of pH and the buffering capacity are very important in aquatic systems, since the species composition and solubility of heavy metals are a function of pH. With an increase or

decrease in pH of an aquatic system the solubility of each metal contaminant may be altered. This largely depends on whether a metal behaves like an anion or a cation, as shown in Figure 5-11.

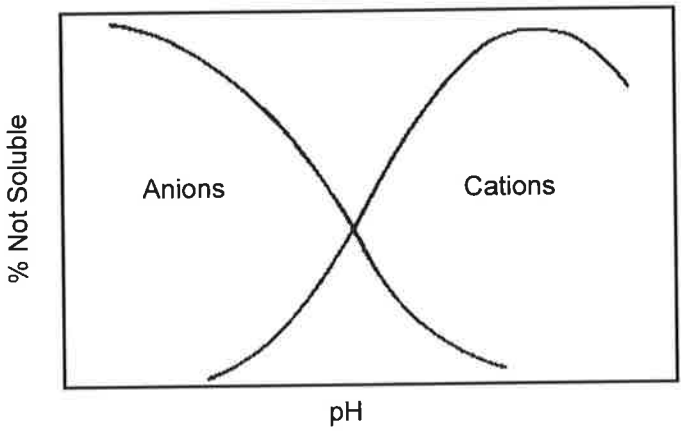

Figure 5-11: Heavy metal anion and cation solubility as a function of pH (Bourg and Loch, 1995)

In natural aquatic system, the behaviour of heavy metals (either like a cation or like an anion) depends on the type of metal, and relative concentration of metal, organic matter and inorganic solids (Bourg and Loch, 1995). Heavy metals adsorbed to inorganic solids tend to display cation-like behaviour (e.g. Pb, Cu), but when strongly complexed to dissolved organic matter heavy metals will instead display anion-like behaviour. Oxyanions of metalloids and transition metals also display anion-like behaviour.

The solubility of heavy metals is also dependent on redox potential (this was described in Section 5.3.1), and the products of redox reactions can affect pH levels. The products of redox reduction are generally less acidic than the oxidised substances so pH tends to increase with reduction processes. Although re-oxidation could bring the pH of the water back down, the loss of reduced products, such as nitrogen gas to the atmosphere, mean that it is not completely reversible, and the system may become progressively alkaline (Bourg and Loch, 1995).

Metal speciation under different combinations of redox and pH conditions is typically represented by pE-pH or Eh-pH diagrams (pE and Eh are different redox scales, which are related by Equation 5.1). The Eh-pH characteristics of natural aquatic systems are primarily determined by redox reactions involving iron and sulfur, along with photosynthesis and respiration (Baas Becking *et al.*, 1960). Figure 5-12 shows the Eh-pH characteristics that are typical of natural fresh water environments. The diagram is a summary of 347 sets of data, approximately 40% from Australian waters. The lower potentials were recorded in still water (e.g. lakes).

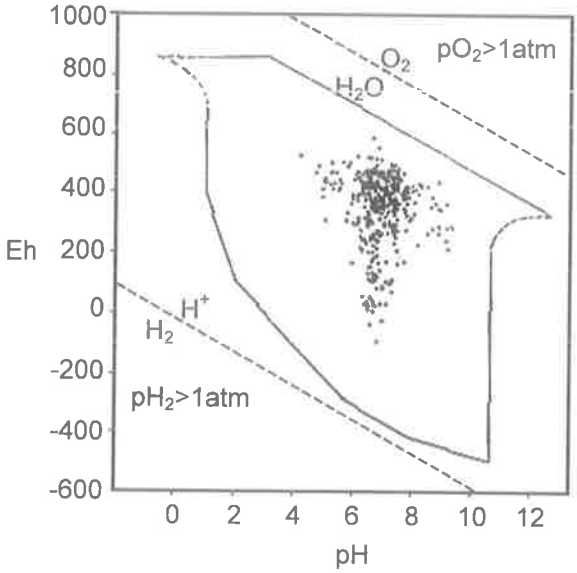

Figure 5-12: The distribution of Eh and pH measurements in fresh waters (after Baas Becking *et al.* (1960))

In general, the solubility of heavy metals is highest in acidic and oxidising environments (Spiro and Stigliani, 1996). Decreases in pH lead to dissolution of carbonates and hydroxides and increased desorption of metal cations (Förstner, 1981). Figure 5-13 shows the solubility trends of minerals and heavy metals as a function of pE and pH when organic matter is not present.

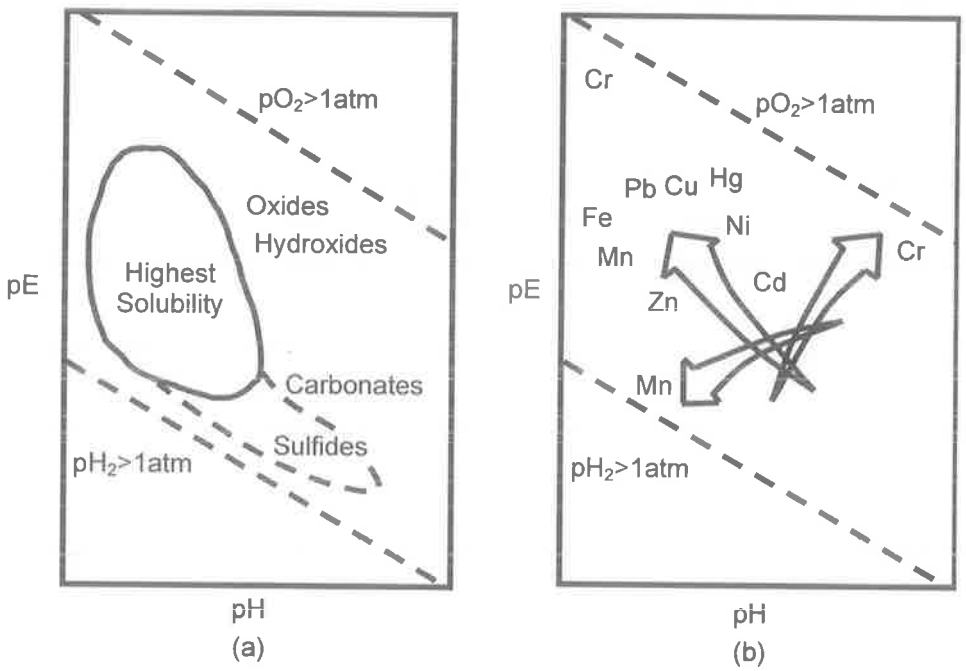

Figure 5-13: Solubility trends when organic matter is not present (a) for minerals; and (b) for heavy metals (after Bourg and Loch (1995))

Oxides and hydroxides of iron and manganese are of particular importance in aquatic systems for their ability to reduce metal toxicity by facilitating absorption of metals and metalloids from the water. As was seen in Figure 5-13, iron and manganese tend to be solubilised under acidic and oxidising conditions, which would lead to an undesirable release of toxic metal ions into the water. The typical solubility pattern of iron and manganese as a function of pE and pH are shown in Figure 5-14.

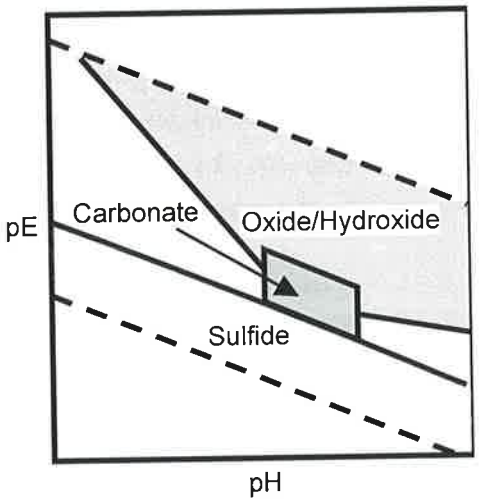

Figure 5-14: Speciation of Fe and Mn as a function of pE and pH assuming total dissolved activities of inorganic C and S of 10^{-3} (after Bourg and Loch (1995))

As oxides and hydroxides, iron and manganese are strong adsorbents for heavy metals, but under more reducing conditions and a slightly alkaline pH, iron and manganese will tend to form carbonates. Cabonates of iron and manganese are not as strongly adsorbing as oxides and hydroxides (Bourg and Loch, 1995). Under reducing conditions, the iron and manganese and the released heavy metal ions will form metal sulfides, which are highly insoluble. Although if the supply of sulfur is limited heavy metal bioavailability may increase under reducing conditions due to the absence of sulfidic binding sites.

Unfortunately, the use of relationships such as those shown in Figure 5-13 and Figure 5-14 to quantitatively describe metal solubility is limited to situations where organic matter is not present. Organic matter is present in varying concentrations in all natural aquatic systems.

Organic matter plays an important role in the bioavailability of metal and metalloid contaminants, since metal ions can directly complex with organic substances. Organic matter can also interfere with the absorptive properties of metal oxides and hydroxides (Honeyman and Santschi, 1988). Under certain conditions of pH for example, the adsorptive capacity of metal oxides may be masked by surface sorption of organic matter (Wang and Chen, 2000). There is still much to be learned about the relative importance of metal oxides and organic materials in controlling the adsorption of metals (Dong *et al.*, 2000).

Dong *et al.* (2000) investigated the adsorption behaviour of surface coating materials including metal oxides and organic matter for Pb and Cd, by analysing biofilms that developed on the surface of glass slides in the oxic waters of Cayuga Lake in New York. They found that Mn oxides were the most important factor controlling the adsorption of Pb, the action of Fe oxides and organic material was also significant. In the adsorption of Cd, Fe oxides were most important while Mn oxides and organic matter were of less significance.

Most natural aquatic environments have a pH of between 5 and 9 (Seki, 1982). During the monitoring of Morphett Road Sedimentation Pond in January, February and early March, the mean pH was 8.94 (Range: 7.04 – 9.57), which was slightly outside the ANZECC (1999) guidelines for freshwater lakes and reservoirs of 7.8 – 8.3. The mean and range of pH values recorded on each day of monitoring in the Morphett Road Sedimentation Pond, are shown in Figure 5-15.

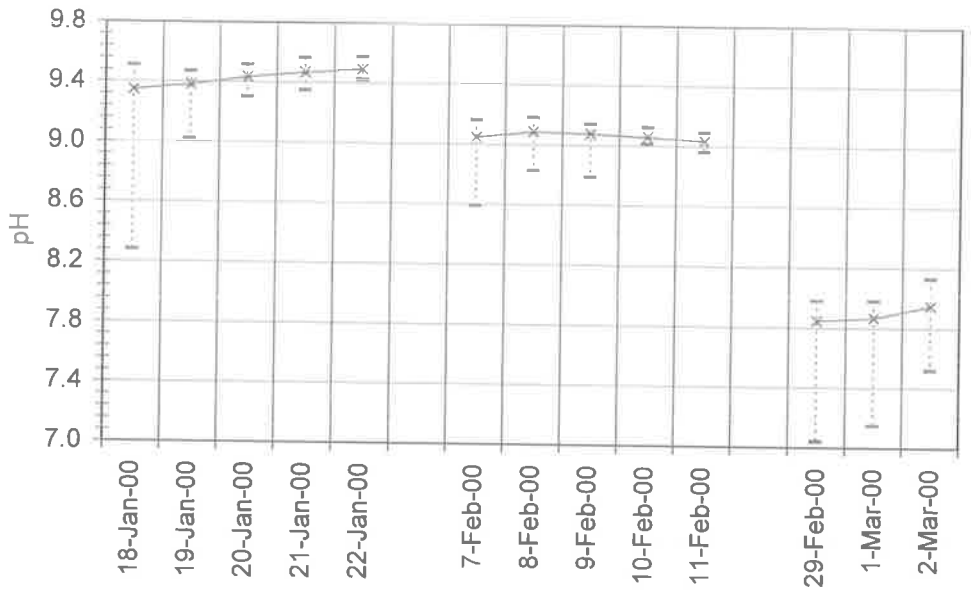

Figure 5-15: The mean pH on each day of monitoring in the Morphett Road Sedimentation Pond (the dashed lines illustrate the range of values that was recorded)

pH was expected to reach high levels in summer in the Morphett Road Sedimentation Pond primarily due to the Mediterranean climate of the region. In summer there is more sunlight for photosynthesis, which can drive pH to high levels during the day, and rainfall is low hence there is also a limited influx of water from rain or flow to neutralise the pH. The low flow, along with the typically lighter summer winds, also inhibits vertical mixing, which increases the depth of the euphotic zone (the depth to which photosynthesis can occur in the pond).

Mean pH in the Morphett Road Sedimentation Pond fell from 9.42 during the first monitoring session (18 January 2000 – 22 January 2000), to 9.06 during the second monitoring session (7 February 2000 – 11 February 2000) to 7.89 during the third monitoring session (29

February 2000 – 2 March 2000). The third session followed rain and a flow event through the pond, which helped to neutralise the high pH.

On all days of monitoring in the Morphett Road Sedimentation Pond, pH was lowest during early morning and increased during the day, probably due to photosynthetic consumption of carbon dioxide, that affects hydrogen ion concentration. Diurnal fluctuations were greatest in January and February (greater than 1 pH unit) and indicated that the pond waters had a poor capacity to buffer or resist changes in pH. Poorly buffered waters must rely on replenishment of carbon dioxide from the atmosphere, which may not keep pace with photosynthetic demand, leading to changes in the pH. The changes in pH were undesirable because they could potentially affect metal solubility.

The maximum daily fluctuation in pH was observed on the first day of profiling (18 January 2000) when there was a 1.23 unit rise in pH during the day. The increase in pH was most rapid between 8:30AM and 10:00AM. This is illustrated in Figure 5-16, which shows the change in pH in the Morphett Road Sedimentation Pond on 18 January 2000.

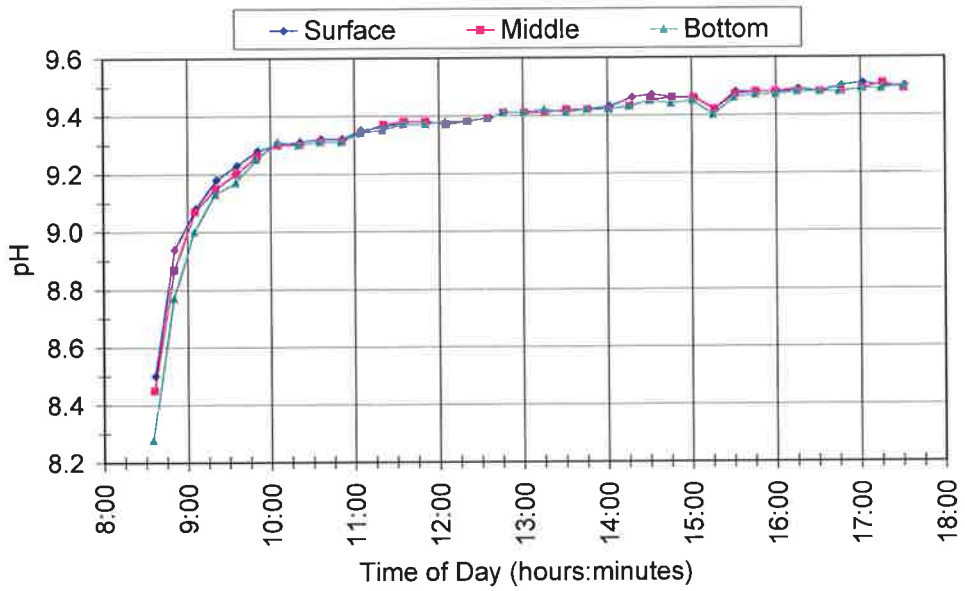

Figure 5-16: pH readings at the surface, middle and bottom of the Morphett Road Sedimentation Pond on 18 January 2000

Figure 5-17 shows the mean difference in pH between the surface and the bottom of the Morphett Road Sedimentation Pond. There was generally little or no variation in pH with increasing depth in the pond.

The difference in pH between water at the surface and water at the bottom was normally less than ±0.2 units, which was equivalent to the accuracy of the instrument. pH differences of less than -0.2 units were due to intermittent fluctuations in pH at the surface of the pond, as can be seen for 2 March 2000 in Figure 5-18.

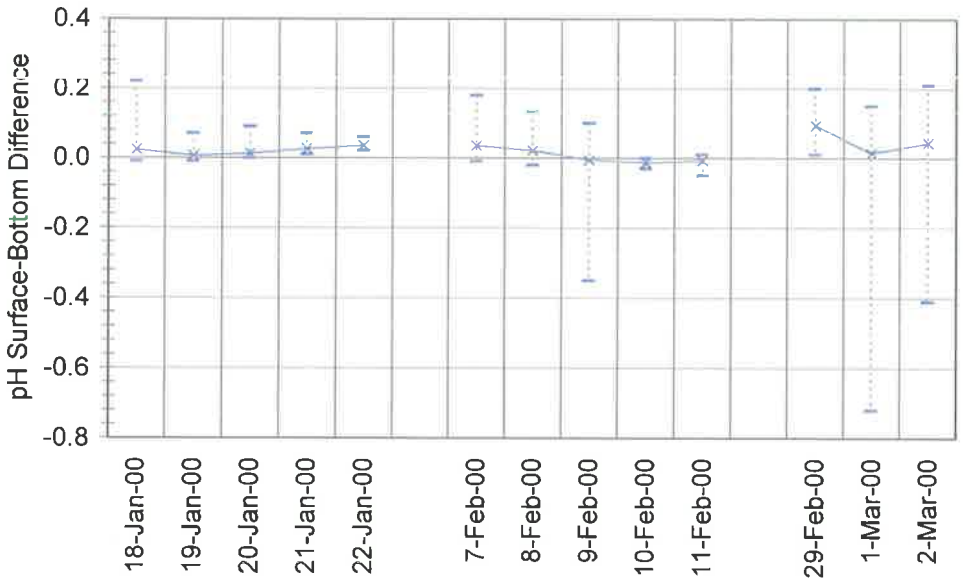

Figure 5-17: The mean difference in pH between the surface and bottom of the Morphett Road Sedimentation Pond on each day of monitoring (the dashed lines illustrate the range of values that was recorded)

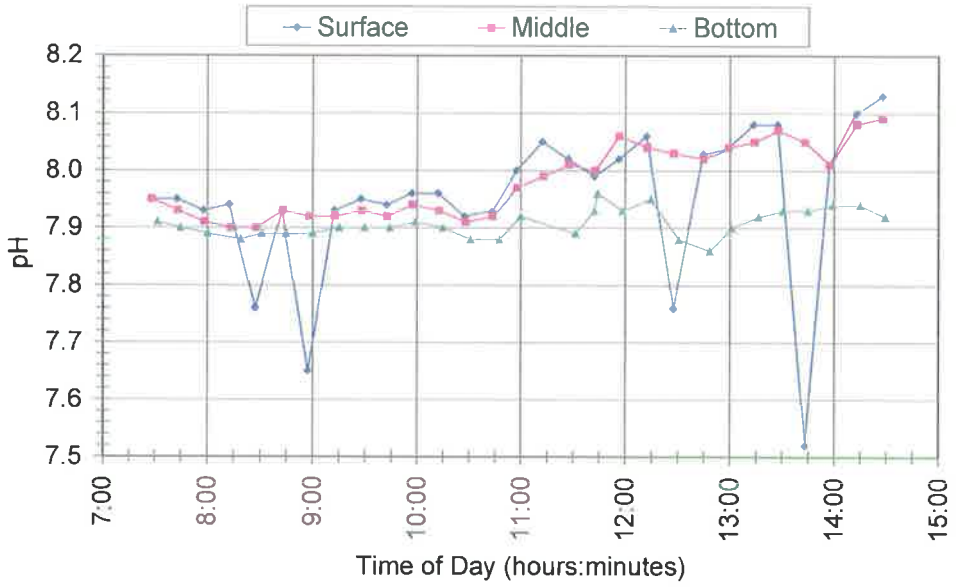

Figure 5-18: pH readings at the surface, middle and bottom of the Morphett Road Sedimentation Pond on 2 March 2000

pH differences of more than 0.2 units occurred on 18 January 2000 and on two days in the third monitoring session (29 February 2000 and 2 March 2000). On 18 January 2000, the pH difference was high early in the morning, but decreased to 0 by 10:00AM as the pH of the pond rose sharply (see Figure 5-16). During the third monitoring session, when the Morphett Road Sedimentation Pond became thermally stratified, pH at the surface of the pond increased while pH at the bottom remained relatively low (see Figure 5-18). The decrease in

water clarity that was observed on these days, which is believed to have triggered the thermal stratification, may also have restricted photosynthesis at the bottom of the pond.

5.3.3 Dissolved Oxygen

Microbial photosynthesis and respiration and atmospheric fluxes control the DO cycle in a pond (Ginot and Hervé, 1994). Atmospheric aeration and photosynthesis by algae and macrophytes (if present) are the major sources of DO in a pond, while the primary sinks include respiration, microbial and abiotic oxidation and atmospheric losses.

The atmosphere acts as both a source and a sink for DO, depending on oxygen tension in the water and conditions at the surface, such as waves. Turbulence, which is caused by waves and flow, enhances re-aeration, which is the major source of oxygen for pond ecosystems (ANZECC, 1999). Natural re-aeration is decreased by channelisation of natural watercourses, which reduces channel complexity that causes turbulence (USEPA, 1996).

Photosynthesis depends on sunlight hence it is limited to the euphotic zone of a pond, the depth of which is dependent on water clarity. Below the euphotic zone, the main source of oxygen is via diffusion from over-lying water and advection.

During daylight hours, macrophytes photosynthesise oxygen, which helps to re-aerate the sediments surrounding the macrophytic root zone. There is also photosynthetic production of oxygen by algae, which is represented by the chemical equation:

$$6CO_2 + 6H_2O \rightarrow C_6H_{12}O_6 + 6O_2 .$$

Glucose ($C_6H_{12}O_6$), the product of photosynthesis, is an essential source of energy and materials for cellular activities for the algae.

The rate of production of oxygen in a pond due to photosynthesis depends on the productivity of the algal species that are present. Intensity of photosynthetically active solar radiation (PAR), light attenuation in the water column, temperature, pH and concentration of nutrients will all affect algal productivity (Culberson and Piedrahita, 1996), hence the rate of oxygen production via photosynthesis will vary acording to depth in the pond and time of year. Population numbers will also be influenced by the predator/prey relationship between algae and higher order species, such as zooplankton and fish. Rates of growth and decay will be further influenced by nutrient availability.

Respiration is essentially the reverse of photosynthesis and is a primary sink for DO in a pond. All organisms other than anaerobic bacteria, including algae, zooplankton and fish, require oxygen for respiration. Respiration is represented by the chemical equation:

$$C_6H_{12}O_6 + 6O_2 \rightarrow 6CO_2 + 6H_2O + \text{Energy}$$

When an organism respires, the conversion of glucose, in the presence of oxygen, to carbon dioxide and water, releases energy that is used for growth, reproduction and synthesis of new materials. Respiration can occur in the absence of oxygen. When oxygen is not available as an electron acceptor, alternatives such as nitrates and carbonates may be used, although the energy yield is less and the reactions tend to proceed at a slower rate (Reddy and D'Angelo, 1994). These anaerobic respiration processes are fundamental to the remobilisation of heavy metals and were discussed in more detail in Section 5.3.1.

Organisms are frequently classified in terms of their ability to utilise oxygen. Organisms that require oxygen to grow and reproduce are classified as obligate aerobes, and their respiration follows the chemical equation that has been illustrated. In contrast, obligate anaerobes can only function under anoxia (i.e. when oxygen is not present). Facultative aerobes, which are also known as facultative anaerobes (Seki, 1982), can metabolise in either an oxic or an anoxic environment. One further class is the microaerophilic organisms, which require oxygen, but only at pressures lower than atmospheric pressure (Reysenbach, 1999).

Organic matter is comprised of carbon, which forms the basic building blocks of all cellular material. Decomposition of organic matter into cellular carbon is an important sink for DO in aquatic environments. The organic matter oxidation processes occur in both the water column and in the bottom sediments. Since the processes tend to be both temporally and spatially variable, they are very difficult to quantify (Henderson-Sellers, 1984).

Meteorological conditions, altitude, salinity, surface tension and the hydrostatic pressure of overlying water all influence the solubility of oxygen in water. The molecular processes that dictate the exchange of oxygen at the air-water interface can be described by numerical equations for a smooth surface at equilibrium. In a real pond however the water surface is rarely perfectly smooth, there is diffusion of oxygen downwards and a constant flux between the many oxygen sources and sinks, hence the true situation is one of dynamic equilibrium, which is more difficult to describe numerically.

The solubility of oxygen is inversely and non-linearly dependent on temperature. When the water temperature is higher, the concentration of DO at which the water is fully saturated will be lower. Similarly, as the salinity of water increases the solubility of oxygen decreases exponentially, due to the lowering effect of salt on the vapour pressure. This relationship is illustrated in Figure 5-19.

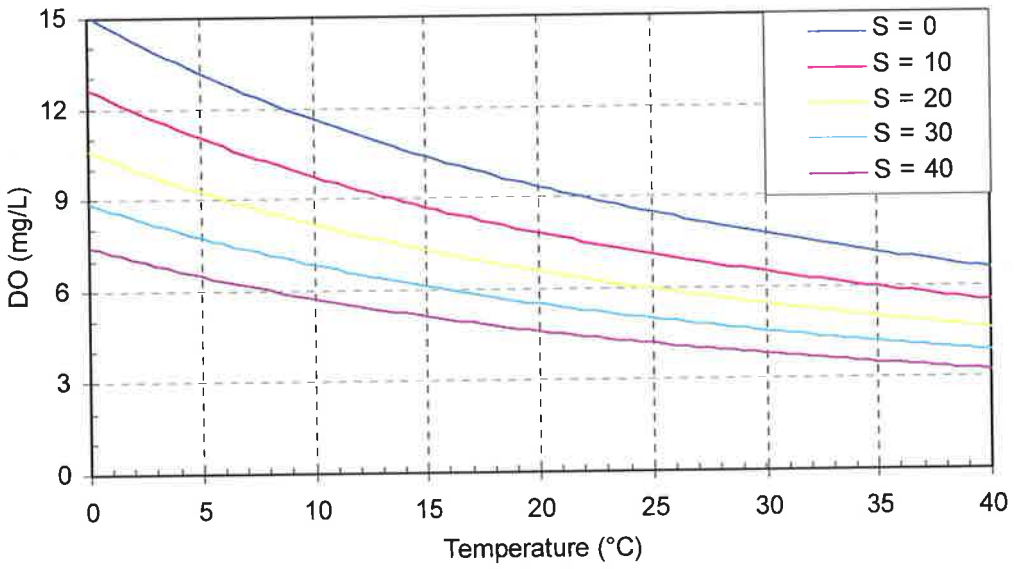

Figure 5-19: The variation in oxygen solubility with changing temperature and salinity (after APHA (1998))

Figure 5-19 is only for ponds at standard atmospheric pressure of 101.3kPa. At high altitudes, there is less oxygen by volume in the air and the partial pressure of oxygen is lower. The solubility of oxygen in water is governed by Henry's Law, which relates the concentration of DO to the partial pressure of oxygen by a proportionality factor, Henry's constant. The value of Henry's gas solubility constant is a function of the temperature and is different for every gas. (Air is a mixture of gases – mainly nitrogen with about 20.95% oxygen by volume (Wetzel, 1975), and a much smaller percentage of other gases like carbon dioxide and argon.) For ponds at high altitudes therefore, by Henry's Law the concentration of DO at the point of saturation will be lower, hence anoxia can occur more easily.

The concentration of DO in a pond is not uniformly distributed over the depth. The equation given above for the equilibrium concentration of DO relates to the pressure at the surface of the water. Below the surface however, there is an additional hydrostatic pressure exerted by the overlying water, which inhibits bubble formation and increases oxygen solubility.

The ANZECC Draft Guidelines for Fresh and Marine Water Quality (1999) advise of a possible risk of adverse affects on the health of aquatic ecosystems in freshwater lakes and reservoirs if DO concentrations fall below 90% saturation, which is approximately 6mg/L. Figure 5-20 shows the mean DO concentration and range of DO concentration readings that were recorded on each day of monitoring in the Morphett Road Sedimentation Pond.

Mean daily DO readings were always above guideline levels during the first monitoring session in the Morphett Road Sedimentation Pond, although DO was frequently below 6mg/L first thing in the morning. Throughout the second monitoring session however, the mean DO concentration at the bottom of the pond was at or below the ANZECC (1999) guideline level,

and mean surface DO also dropped below the ANZECC (1999) guideline level on the final day. By the third monitoring session, all DO readings in the Morphett Road Sedimentation Pond were well below 6mg/L, indicating that there was a possible risk of adverse effects on the health of aquatic ecosystems.

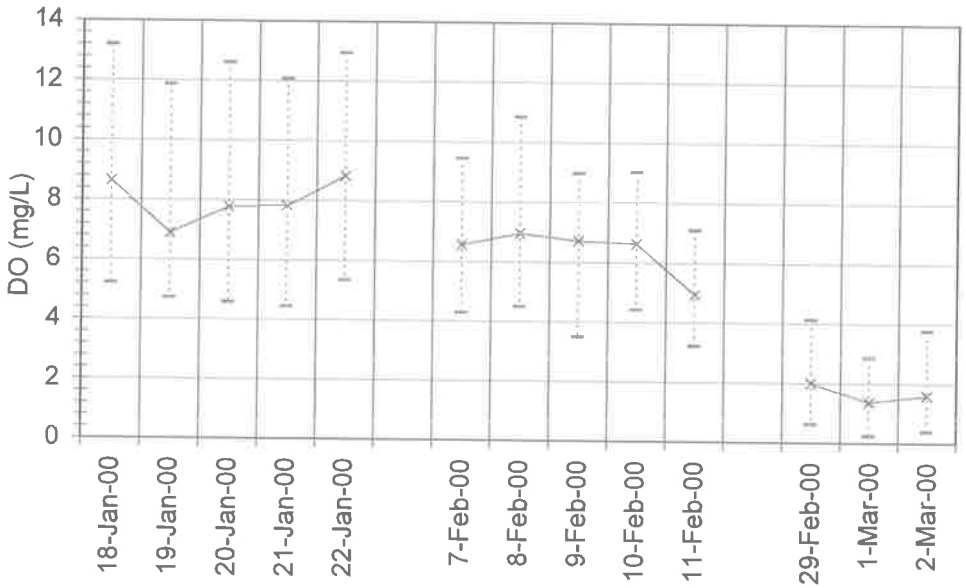

Figure 5-20: The mean DO on each day of monitoring in the Morphett Road Sedimentation Pond (the dashed lines illustrate the range of values that was recorded)

In general, when DO in the pond was high, there was little difference in DO between the surface, middle and bottom, and there was a high degree of DO variability over the day, indicating that there was good mixing between the surface and the bottom of the pond. When DO was low, there was a significant difference between DO at the surface and the bottom of the pond, and there was more stability in DO readings, indicating that the pond was stratified and little vertical mixing was occurring. This is illustrated by Figure 5-21, which shows the difference between the mean DO concentration at the surface and bottom of the Morphett Road Sedimentation Pond.

Mean DO was highest during the first monitoring session (18 January 2000 – 22 January 2000), ranging between 6.89mg/L on 19 January 2000 and 8.83mg/L on 22 January 2000. There were significant fluctuations in the DO readings (range: 4.45 – 13.2mg/L), primarily at the bottom of the pond, and only a small mean difference between the surface and bottom readings (mean range: -1.01 – 0.23mg/L), indicating that the pond was relatively well mixed. The surface-bottom DO difference was negative until the fifth day, indicating that DO was generally slightly higher at the bottom of the pond until the fifth day when the situation reversed and DO was marginally higher at the pond surface.

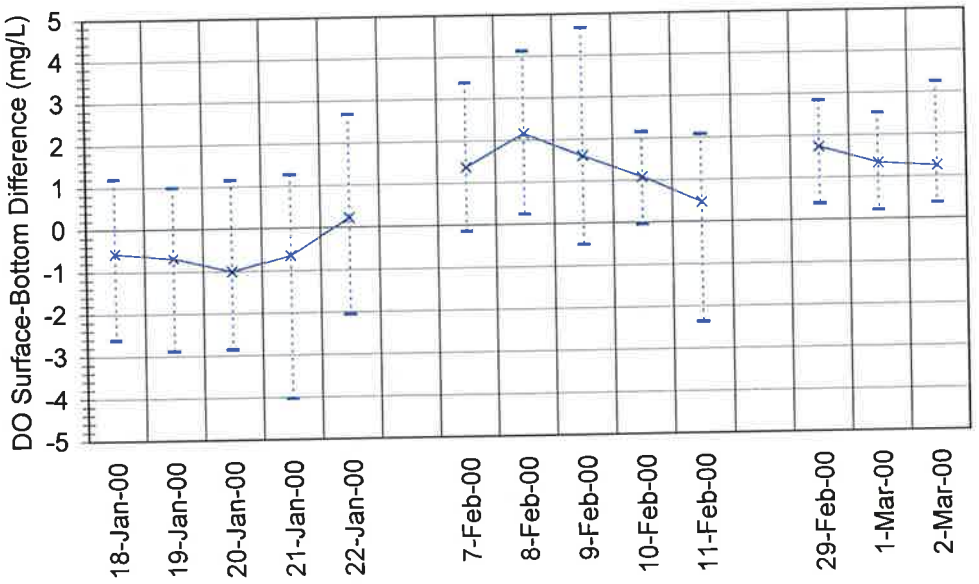

Figure 5-21: The mean difference in DO between the surface and bottom of the Morphett Road Sedimentation Pond on each day of monitoring (the dashed lines illustrate the range of values that was recorded)

During the second monitoring session (7 February 2000 – 11 February 2000), mean DO in the Morphett Road Sedimentation Pond was slightly lower. Mean DO was highest on 8 February 2000 with a mean DO of 6.95mg/L and lowest on 11 February 2000, when the mean DO was down to 4.94mg/L. There was slightly less fluctuation in the DO readings in the pond (range: 3.22 – 10.85mg/L) and the mean difference between DO at the surface and the bottom of the pond had increased (mean range: 0.47 – 2.16mg/L), with DO consistently lower at the pond bottom.

The third session of monitoring (29 February 2000 – 2 March 2000) followed a flow event through the pond, which increased the organic matter loading. Mean DO was substantially lower, decreasing from a mean of 1.73mg/L on 29 March 2000 to a mean of 1.25mg/L on 2 March 2000. This was despite a large decrease in salinity, which would have led to higher oxygen solubility in the water. There was also less variability in pond DO readings (range: 0.24 – 4.13mg/L) during the third monitoring session, and a significant difference between DO at the surface and the bottom of the pond (mean range: 1.25 – 1.73mg/L), with lower DO at the bottom.

Although 24 hour monitoring was not performed in the Morphett Road Sedimentation Pond, readings were taken every 15 minutes from about 7:45AM until 3:00PM (extended until 5:30PM on one day).

DO concentrations are generally highest during the day when photosynthesis occurs and lower at night, when aquatic organisms respire but there is no sunlight for photosynthesis. The USEPA (1996) states that the minimum daily concentration of DO typically occurs shortly

before dawn. Different diel DO trends do however occur. For example Butcher and Covington (Butcher and Covington, 1996) observed that the DO reached a minimum around 8:00PM rather than shortly before dawn, in a study of diel stream temperature and DO variability in the Santa Margarita River in southern California.

The DO readings taken in the Morphett Road Sedimentation Pond indicated that although there was typically an increase in mean DO concentration during the morning and afternoon, the time at which DO concentration was a minimum varied from day to day, sometimes occurring several hours after dawn. The temporal behaviour of DO in the pond was also highly dependent on the depth at which the readings were taken, with the DO behaviour at the bottom of the pond sometimes quite dissimilar to DO at the surface and middle of the pond. This DO behaviour is illustrated in Figure 5-22.

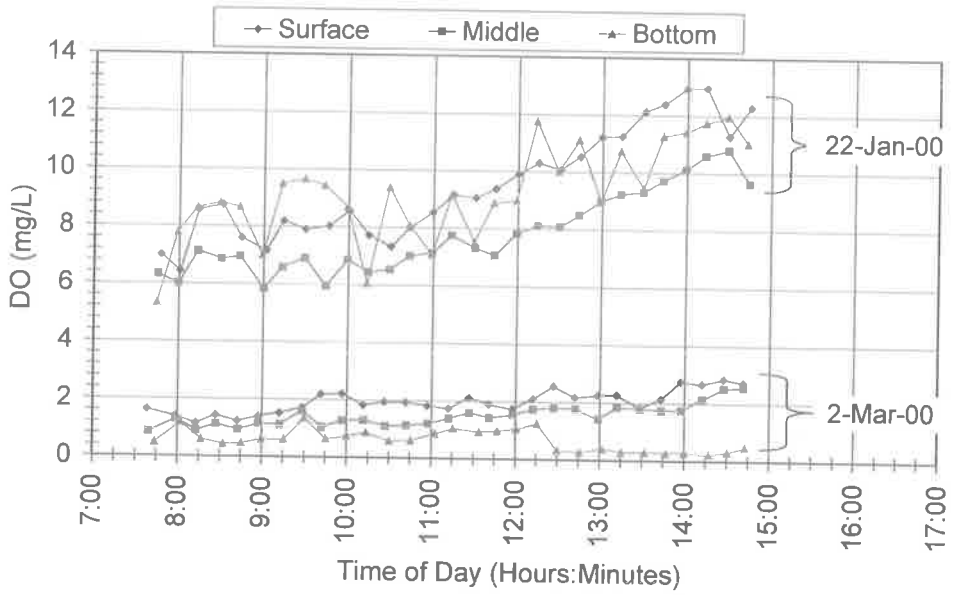

Figure 5-22: DO readings at the surface, middle and bottom of the Morphett Road Sedimentation Pond on 22 January 2000 and 2 March 2000

During the first two monitoring sessions, DO concentrations were typically low in the early morning and increased during the day. DO had not reached a peak by the time monitoring ended each day at around 3:00PM or by 5:30PM on one day. On a number of days (19 January 2000, 21 January 2000 – 22 January 2000, 10 February 2000) the DO concentration dipped slightly before rising, reaching a minimum concentration around 9:00AM to 9:30AM, before rising. On two days (8 February 2000 – 9 February 2000) the dip in DO concentration only occurred in water at the bottom of the pond.

During the third monitoring session, DO concentration at the surface and middle of the pond either increased or dipped slightly and then increased during the day. However, at the bottom of the pond, the DO concentration decreased as the concentrations at the surface and middle increased. The timing of the divergence of oxygen conditions at the surface and bottom of the

pond corresponded with the onset of temperature stratification, which would have inhibited mixing of DO downwards from the surface. Furthermore, since clarity in the pond was reduced at that time, decreased light at the bottom of the pond would have slowed photosynthetic production of oxygen.

5.3.4 Salinity

Salinity is the total concentration of inorganic ions in solution. The salt ions commonly found in inland waters are Na^+, Ca^{2+}, Mg^{2+}, K^+, Cl^-, CO_3^{2-} and SO_4^{2-} (Wetzel, 1975). The specific ionic composition is determined mainly by the mineralogy of the catchment.

The rate of concentration of salt ions in a pond or other water body is influenced by the inflow and outflow of water and salts, the ratio of volume to surface area as well as atmospheric precipitation and evaporation processes.

Salinity is commonly reported in parts per million (ppm), however alternative concentration terms may be used, such as 'total dissolved solids' or 'filterable residue', which have units of mg/L. The salinity units of mg/L are approximately equivalent to ppm. 'Electrical conductivity' (EC), which is measured in μS/cm, is also sometimes used as a measure of salinity. Equation 5.7 (ANZECC, 1992) shows the relationship that is generally used to convert electrical conductivity to the total dissolved solids concentration (or filterable residue).

$$TDS = EC \times 0.68 \qquad (5.7)$$

where: TDS is the total dissolved solids in mg/L; and

EC is the electrical conductivity in μS/cm.

Sea water has a salinity of around 32 000ppm or about 47 000EC (ANZECC, 1999). The average salinity of freshwater rivers and lakes around the world has been estimated to be around 100ppm or about 147EC (Seki, 1982).

The addition of salt ions to a solution decreases the free energy of water molecules hence increased salinity reduces water activity. This slows the speed of biochemical reactions (Seki, 1982) and physical processes such as evaporation (Rawson and Moore, 1944; Wetzel, 1975; Salhotra *et al.*, 1985; Yechieli *et al.*, 1998). The rate of evaporation decreases with increasing salinity because the decrease in water activity leads to a reduction in the saturation vapour pressure at the surface.

Excessive changes in salinity can have harmful physiological affects on aquatic organisms. Enzymes required for biochemical reactions are sensitive to the salt concentration, and the

modification of viscosity can affect reactions that rely on diffusion mechanisms. Some organisms are euryhaline - able to adapt to a broad range of salt concentrations. The majority of organisms however, are stenohaline - able to survive in only a narrow range of salt concentrations (ANZECC, 1999). Excessive changes in salinity may lead to growth inhibition or death of stenohalic organisms, and can completely alter the entire species composition of the ecosystem.

Salinity has a number of indirect effects on the remobilisation of metals. As the salinity of water increases, the solubility of oxygen decreases exponentially (see Figure 5-19), which can lead to a fall in the redox potential and increased metal availability. Salinity can also influence the composition of micro-organic species that mediate many of the important remobilisation reactions, and is a major factor in the formation of density stratification. Evaporation, precipitation or pond inflow or outflow of water of a contrasting salinity can lead to density stratified conditions, which can inhibit mixing of DO.

Figure 5-23 shows the mean conductivity at the surface and bottom of the Morphett Road Sedimentation Pond during the three sessions of monitoring. Freshwaters generally have an EC reading below 1000μS/cm (ANZECC, 1999), but the average of conductivity readings in the Morphett Road Sedimentation Pond was 5125μS/cm. Although zero readings were recorded at the surface during light rain and following a flow event through the pond, only centimetres below the surface the conductivity remained high. Subsurface conductivity exceeded 6000μS/cm in January and 7000μS/cm in February, and was still above 1300μS/cm in early March following a flow event through the pond.

From 18 January 2000 to 20 January 2000 and 10 February 2000 to 11 February 2000, conductivity in the pond was similar at all depths. The conductivity throughout the pond was relatively stable and increased during the day by between 6 and 14μS/cm during each hour of monitoring. The days when uniform conductivity was observed in the pond corresponded to the days when there was a mean difference in temperature between the surface and the bottom of less than 0.2°C (i.e. the pond was thermally mixed).

On the other days, when the temperature difference between the surface and the bottom was greater than 0.2°C (21 January 2000 – 22 January 2000, 7 February 2000 – 9 February 2000, 29 February 2000 – 2 March 2000), a conductivity gradient was also present in the pond. Conductivity in the lower layers was relatively stable and increased during the day by between 7 and 17μS/cm during each hour of monitoring. At the surface however, conductivity was lower due to rain or previous flow through the pond, and was much more variable. This is illustrated in Figure 5-24 for 21 January 2000, when light rain decreased conductivity at the surface of the pond. While the conductivity of the lower layers increased slowly and steadily during the day from around 6650μS/cm to 6730μS/cm, the conductivity readings at the surface fluctuated between 0μS/cm and 3880μS/cm.

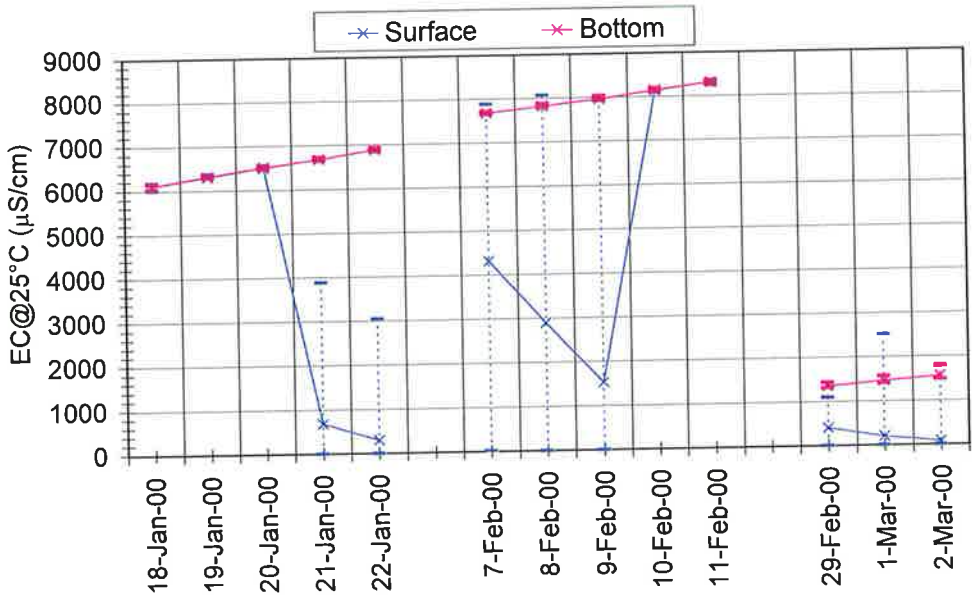

Figure 5-23: The mean conductivity at the surface and bottom of the Morphett Road Sedimentation Pond on each day of monitoring (the dashed lines illustrate the range of values that was recorded)

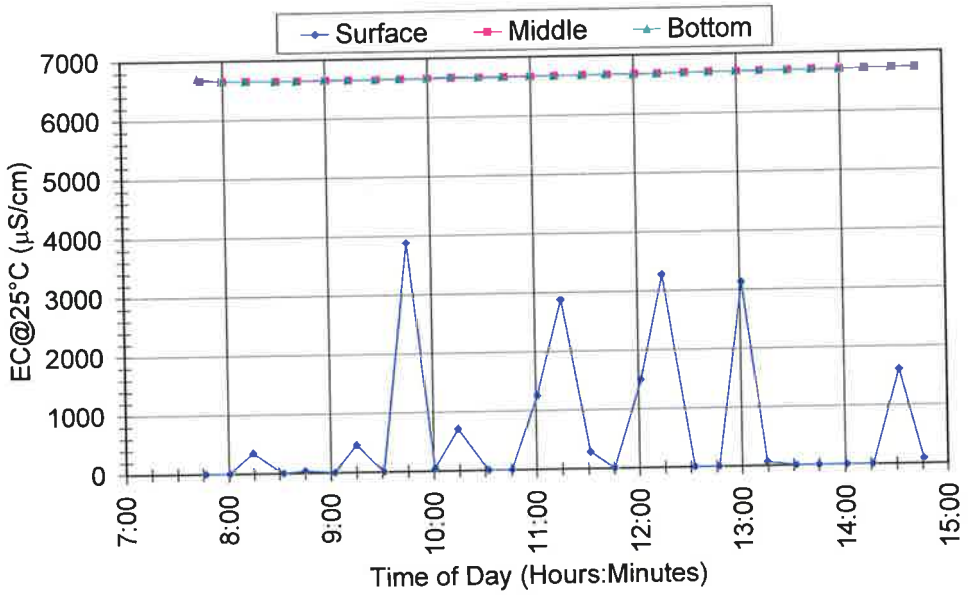

Figure 5-24: Conductivity readings at the surface, middle and bottom of the Morphett Road Sedimentation Pond on 21 January 2000

The ANZECC (1999) guidelines advise of a potential risk for adverse effects to freshwater aquatic ecosystems when there is an increase of more than 60µS/cm. Daily conductivity fluctuations were frequently greater than 60µS/cm (primarily in the surface layer) as shown in Table 5-2.

Table 5-2: The magnitude of conductivity flucutations at the surface, middle and bottom of the Morphett Road Sedimentation Pond during each day of monitoring (in μS/cm)

DAY	SURFACE	MIDDLE	BOTTOM
18-Jan-00	94*	90*	80*
19-Jan-00	33	25	22
20-Jan-00	49	36	38
21-Jan-00	676*	30	33
22-Jan-00	299*	40	34
7-Feb-00	4295*	42	33
8-Feb-00	2896*	33	35
9-Feb-00	1530*	33	37
10-Feb-00	42	43	38
11-Feb-00	47	39	64*
29-Feb-00	400*	12	42
1-Mar-00	198*	24	54
2-Mar-00	76*	28	68*

* Exceeds ANZECC (1999) guidelines of 60μS/cm.

Differences of up to 7980μS/cm between conductivity at the surface and the bottom of the pond were also observed on a number of days (21 January 2000 – 22 January 2000, 7 February 2000 – 9 February 2000, 29 February 2000 – 2 March 2000) as shown in Figure 5-25. There were no visible signs of aquatic life in the Morphett Road Sedimentation Pond during the first or second monitoring sessions. However, following a flow event through the pond in late February, which did reduce salinity, there was an abundance of aquatic life visible in the pond during the third monitoring session, despite large daily fluctuations in conductivity and high variability in conductivity through the depth of the pond.

5.3.5 Turbidity and Water Clarity

Water clarity in a pond or other water body is primarily a function of water column turbidity, although the optical characteristics of dissolved matter are also influential (e.g. the yellow colour imparted by some dissolved aquatic humus).

In turbid waters, suspended particulates scatter and adsorb the light that penetrates the surface, inhibiting transmission of the light energy to the deeper water. The particulates, both inorganic and organic, such as clays and silts, phytoplankton and detritus come primarily from soil and stream bank erosion, with lesser amounts from stormwater runoff, industrial effluent and sewage wastewaters. The turbidity is caused by tubulence, which is greatest during flow events or in high wind. Turbulent disturbances may also be caused by fish, such as the European carp, and other aquatic creatures that forage in the bottom sediments of rivers, ponds and other water bodies.

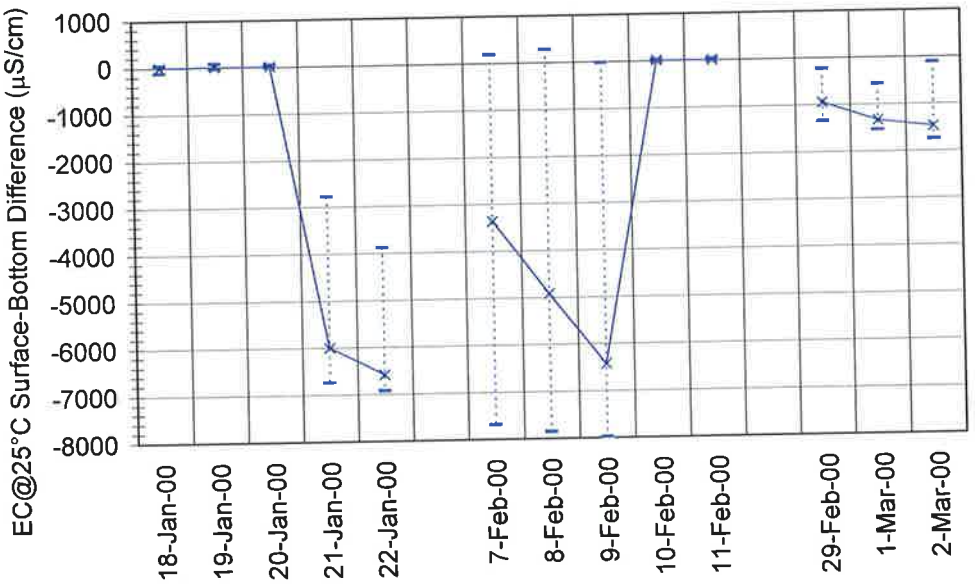

Figure 5-25: The mean difference in conductivity between the surface and bottom of the Morphett Road Sedimentation Pond on each day of monitoring (the dashed lines illustrate the range of values that was recorded)

Increased turbidity can have a direct effect on mortality and stress levels in fish and macroinvertebrate populations, but the main impact of increased turbidity is the effect on light penetration. The depth of the euphotic zone of zone of light penetration is often used as an indictor of ecosystem health. A decrease in the depth of the euphotic zone due to increased turbidity for example, leads to a reduction in photosynthetic activity of phytoplankton and aquatic macrophytes.

The depth of the euphotic zone should not be confused with the secchi disk depth that was mentioned earlier in Section 5.2.6. The euphotic zone is often about one half to one third of the secchi disk depth (Goldman and Horne, 1983), and it extends to the depth at which photosynthetically active radiation (PAR) is only about 1% of the surface PAR (ANZECC, 1999). PAR is important in assessing the health of an aquatic environment for flora and fauna, since it is the portion of the light spectrum that is utilised by photosynthetic organisms.

Decreased light penetration also has an important influence on pond temperatures. Without light, the deeper waters of a pond do not heat as quickly as the surface waters and the pond can become thermally stratified.

Figure 5-26 shows the mean turbidity in the Morphett Road Sedimentation Pond during the three sessions of monitoring. During the first two monitoring sessions (18 January 2000 – 22 January 2000 and 7 February 2000 – 11 February 2000), HYDROLAB MiniSonde turbidity readings were occasionally extreme due to floating masses of weed, litter and other objects, but were very low or zero the remainder of the time. During the final monitoring session (29 February 2000 – 2 March 2000) the extremely high readings did not occur since a flow event during the preceding week had flushed the debris to the downstream end of the pond. Since the extreme readings were included in the evaluation of mean turbidity shown in Figure 5-26, the mean turbidity appears to be higher than it actually was for the majority of the first two monitoring sessions. This was further illustrated by the large range of values recorded on most of these days.

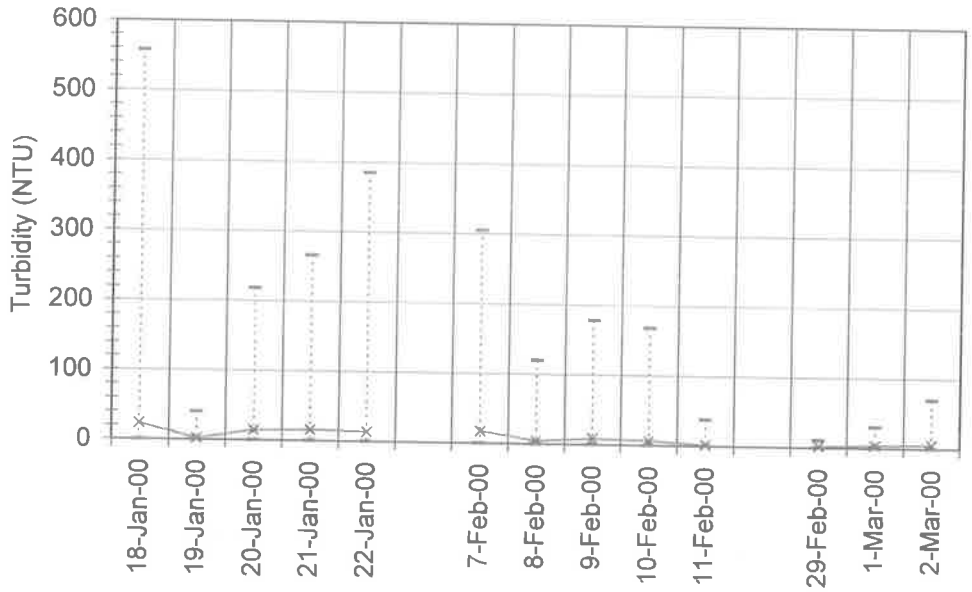

Figure 5-26: The mean turbidity on each day of monitoring in the Morphett Road Sedimentation Pond (the dashed lines illustrate the range of values that was recorded)

The SDD readings shown in Figure 5-28 and Figure 5-27 proved to be a much better indicator of the true clarity of water in the pond. Minor variability in SDD readings over the day, illustrated for 2 March 2000 in Figure 5-27, were due to wave action or seicheing in the pond, which caused temporary depth fluctuations at the measurement point, and evaporation, which gradually reduced the total pond volume (particularly on sunny days).

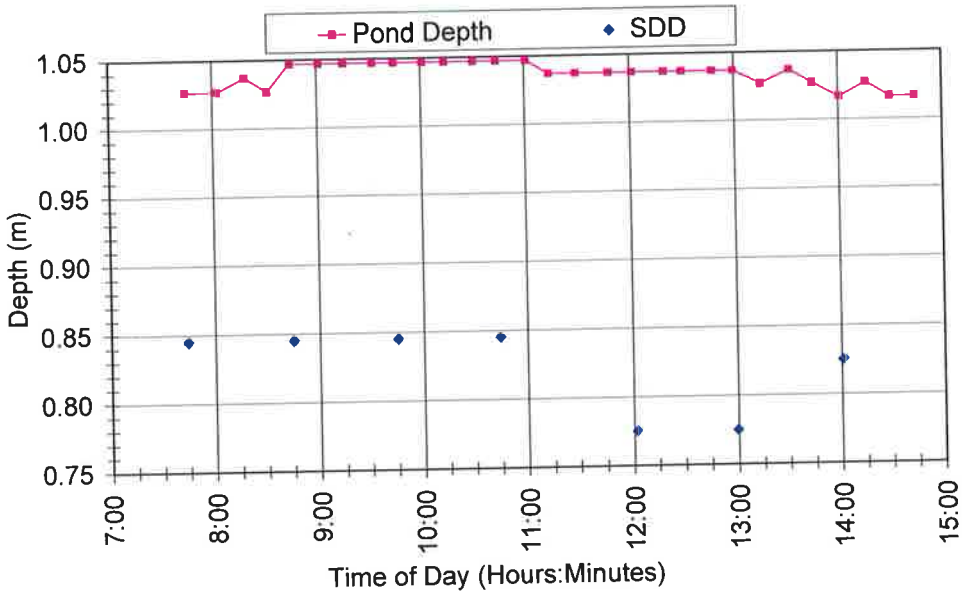

Figure 5-27: SDD and total depth of the Morphett Road Sedimentation Pond on 2 March 2000

Decreases in the mean SDD from day to day, which are shown in Figure 5-28, were due to evaporation, while increases in the mean SDD were due to rain. The rainfall was never high enough to cause flow into or out of the pond.

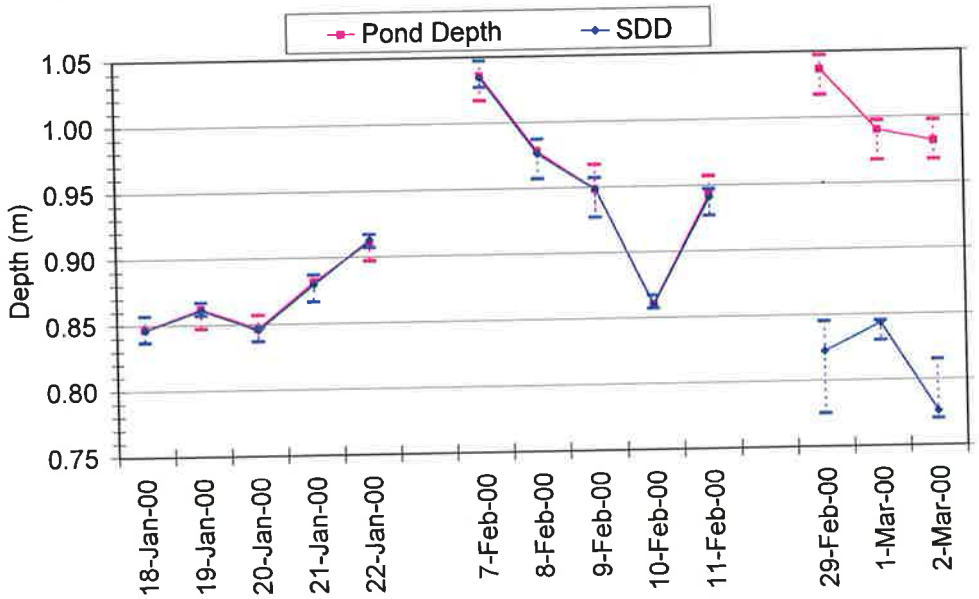

Figure 5-28: The mean SDD and total pond depth on each day of monitoring in the Morphett Road Sedimentation Pond (the dashed lines illustrate the range of values that was recorded)

During the first two monitoring sessions (18 January 2000 – 22 January 2000 and 7 February 2000 – 11 February 2000) SDD readings were consistently 100% of the total pond depth. However, during the final monitoring session (29 February 2000 – 2 March 2000) there was a slight decrease in water clarity with the mean SDD decreasing to around 94% of the total

pond depth (range: 86 – 100%). The decrease in water clarity followed a flow event through the Morphett Road Sedimentation Pond during the previous week, which may have brought more sediment into the pond and would have stirred sediments from the bottom.

5.3.6 Temperature

Like salinity, temperature is a major factor in the formation of density stratification in ponds and other water bodies, which can inhibit mixing of DO through the water column. Temperature also has a direct effect on oxygen solubility (see Figure 5-19).

The temperature of all aquatic environments varies between -1.9°C (the freezing point of seawater, depending on the exact salinity) and 40°C, but is generally less than 30°C (Seki, 1982). The majority of microorganisms in aquatic environments are sensitive to the temperature of their environment. Every organism has an optimum temperature range between minimum and maximum growth threshold temperatures. They are sometimes classified as 'psychrophilic' if the optimum growth temperature is 15°C or less and the minimum growth temperature is 0°C or less, 'mesophilic' if the temperature optimum is between 25°C and 40°C, or 'thermophilic' if the optimum temperature is above 45°C to 50°C (Seki, 1982). Organisms that can exist in more than one of the classified temperature ranges are termed 'facultative'. The greater adaptability of the facultative organisms better equips them for coping with temperature fluctuations.

Some fluctuations in temperature are natural. For example the diurnal and seasonal heating and cooling of the water. Thermal pollution however is not natural. Excessive heat from power station discharge or cold water release from reservoirs for example, can kill plants and animals or have a chronic long-term affect on their growth and survival.

Changes in the temperature regime can have both a direct impact on the life functions of organisms (e.g. growth rate, metabolism), and an indirect affect through other ecosystem changes (e.g. loss of habitat). Alteration of the temperature regime can occur quite subtly, for example through changes in the flow regime or removal of aquatic vegetation. Hence the effect of a change in temperature may incur gradual metabolic, growth rate, reproductive, mobility or migratory changes that are not immediately obvious. For example, a time lag of two months has been observed between seasonal change in temperature and the resulting change in growth rate of the dominant species of microflora in the Atlantic Ocean (Seki, 1982).

Changes in temperature can also alter the progression of chemical and physical processes. For example the toxicity of un-ionised ammonia increases with a rise in temperature (USEPA, 1996). It has been estimated that for every 10°C rise in temperature, there is an approximate

two-fold increase in the rate of chemical reactions (Kim and Chapra, 1997) and the physiological demands of organisms (ANZECC, 1999).

Figure 5-29 and Figure 5-30 illustrate the mean value and range of values of temperature and temperature stratification recorded on each day of monitoring in the Morphett Road Sedimentation Pond.

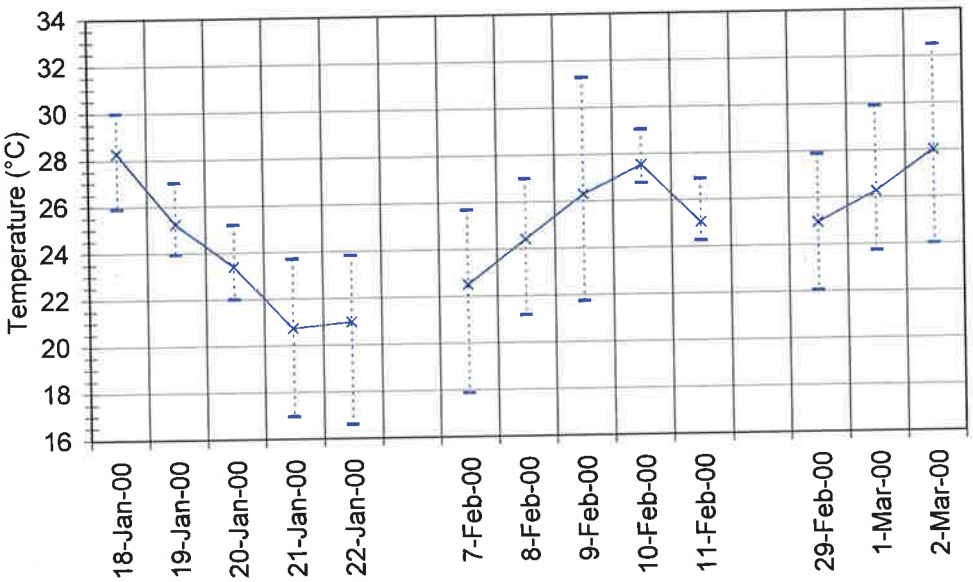

Figure 5-29: The mean temperature of the Morphett Road Sedimentation Pond on each day of monitoring (the dashed lines illustrate the range of values that was recorded)

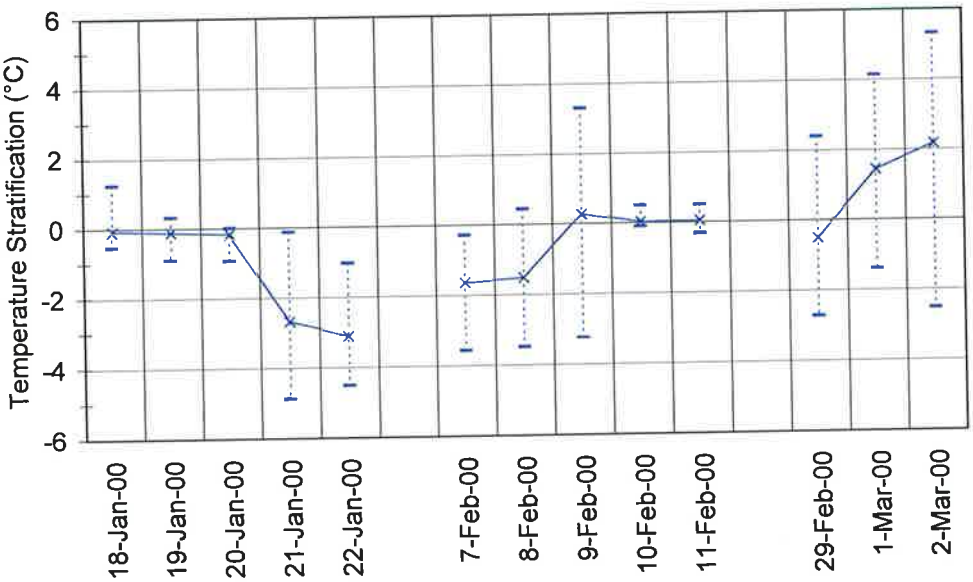

Figure 5-30: The mean temperature stratification of the Morphett Road Sedimentation Pond on each day of monitoring (the dashed lines illustrate the range of values that was recorded)

Table 5-3 summarises the temperature statistics for the Morphett Road Sedimentation Pond during the three monitoring sessions. No strong correlation was observed between the mean, maximum or minimum temperature and meteorological conditions (e.g. solar radiation, air temperature, dew point temperature or wind speed).

Table 5-3: Temperature statistics during the three sessions of depth profiling in the Morphett Road Sedimentation Pond

Maximum mean pond temperature	28.27°C	18 January 2000
Minimum mean pond temperature	20.73°C	21 January 2000
Maximum pond temperature	32.48°C	2 March 2000
Minimum pond temperature	16.60°C	22 January 2000

Mean pond temperatures and the minimum overall pond temperature were recorded on 21 January 2000 and 22 January 2000. On both these days, air temperature was relatively low and the mean wind speed relatively high, which led to a high rate of heat loss at the surface of the pond. Hence, mean temperature stratification in the Morphett Road Sedimentation Pond was strongly negative on both 21 January 2000 and 22 January 2000.

Both the minimum temperature (16.60°C recorded at 8:31AM) and maximum temperature (32.48°C recorded at 11:27AM) recorded in the pond were recorded at the surface. Temperature fluctuations were more significant at the surface where evaporation, convection, back radiation and other surface heat transfer processes would have been acting, than at the middle and bottom of the pond.

Temperature stratification was observed on the final two days of profiling – 1 March 2000 and 2 March 2000, following a flow event through the pond. Figure 5-31 shows the temperature recorded by the temperature sensors at seven positions in the water column on these two days.

The flow event through the Morphett Road Sedimentation Pond the previous week reduced water clarity (see Section 5.3.5) and led to a conductivity gradient. On the two days of temperature stratification the weather was also warm and calm. This combination of conditions was conducive to differential heating of the water column. The total daily solar radiation was high, but not extreme for the time of year, and no higher than on some other days of depth profiling in the pond.

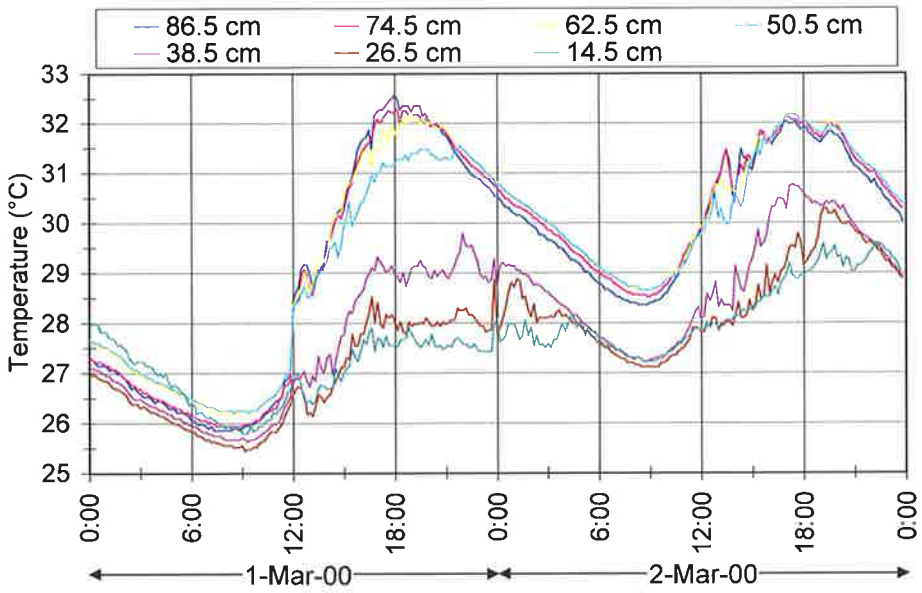

Figure 5-31: Temperature stratification on the last two days of depth profiling in the Morphett Road Sedimentation Pond (the top temperature sensor was at 86.5cm and the bottom temperature sensor was at 14.5cm)

Although similar weather conditions occurred on 29 February 2000, the first day of depth profiling following the flow event through the pond, temperature stratification was not significant. Although the wind speed on 29 February 2000 was also low, the air temperature was slightly cooler. Unfortunately solar radiation information was not available from the Bureau of Meteorology for that day so no comparison can be drawn, although overcast conditions were noted during the monitoring. It is believed that the successive days of warm, calm weather, combined with a reduction in water clarity triggered the temperature stratification on the final two days of profiling.

5.4 Stratification of the Morphett Road Sedimentation Pond

Graphs showing each month of temperature data recorded by the temperature sensors in the Morphett Road Sedimentation Pond are shown in Appendix I.

Minimum temperature in the pond was 8.4°C at 6:10AM on 14 June 1999 following a day of low solar radiation and a night of very strong winds. The maximum pond temperature of 35.3°C was recorded on 28 February 2000, following a day of high solar radiation and a low mean wind speed. The air temperature remained warm (above 25°C) throughout the night and the maximum pond temperature was recorded at the bottom of the pond at 11:40PM, which was long after sunset at 7:56PM.

Figure 5-32 illustrates a typical diurnal temperature stratification event in the Morphett Road Sedimentation Pond on 29 March 1999. The mean pond temperature typically reached a minimum shortly after dawn, since high banks on either side of the pond and a bridge at one end prevented the sun's rays from striking the surface in the early morning. The surface water (measured at 86.5cm) then began to warm quickly followed by the deeper layers of water. The temperature of the water at the deepest monitoring point (14.5cm) increased very slowly in comparison to the surface water, thus producing the temperature differential. On 29 March 1999, maximum stratification of 5.59°C occurred at around 3:40PM.

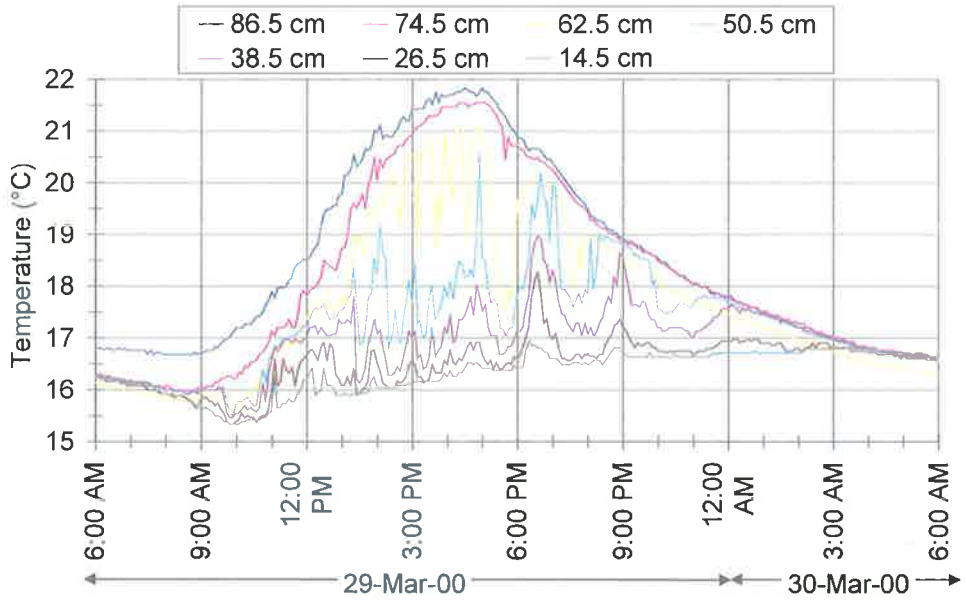

Figure 5-32: Diurnal stratification in the Morphett Road Sedimentation Pond on 29 March 1999 (the top temperature sensor was at 86.5cm and the bottom temperature sensor was at 14.5cm)

During the stratification event on 29 March 1999, large temperature fluctuations were observed at intermediate depths in the pond, while temperature fluctuations at the surface and bottom of the pond were minimal. These internal temperature fluctuations were visible to varying degrees during all diurnal stratification events that were observed in the Morphett Road Sedimentation Pond. They can also be identified in water temperature profiles recorded at various locations in the Torrens Lake (Australian Water Quality Centre, 2000).

The temperature fluctuations are believed to have been due to internal gravity waves, which propagate in density stratified waters under the influence of buoyancy forces. When there is a disturbance in a density stratified fluid (e.g. due to a mixing event), gravity forces act to restore the equilibrium thus producing horizontal or vertical waves (Hughes *et al.*, 1998). It is the same theory that is responsible for waves at the water's surface, which are generated by the difference in density between air and water, and the rippling cloud patterns that are sometimes observed in the atmosphere.

Figure 5-33 shows the percentage of time during the monitoring when stratification was greater than 2°C in the Morphett Road Sedimentation Pond.

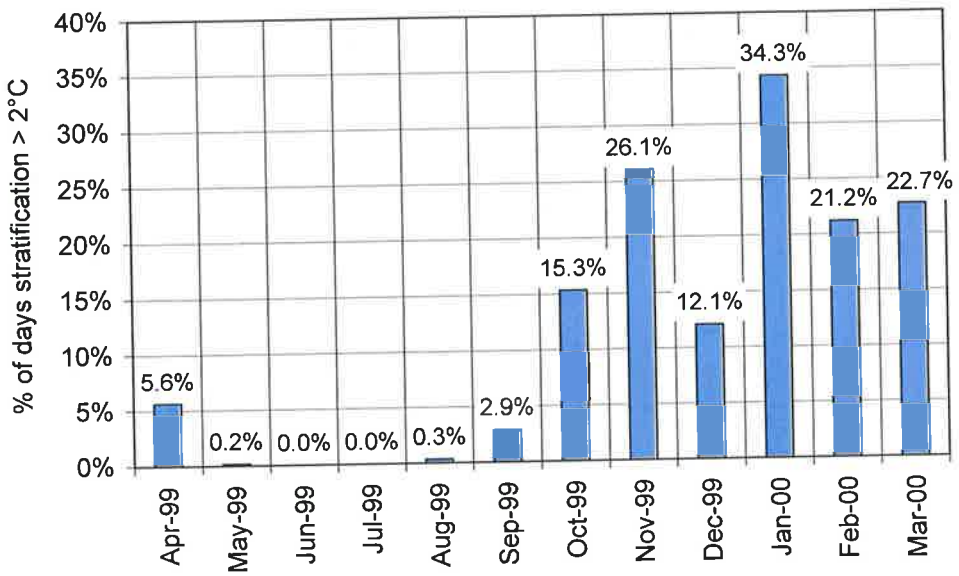

Figure 5-33: The percentage of time during which the stratification exceeded 2°C (Data from the first and last months of monitoring (March 1999 and April 2000) have been excluded due to incomplete data sets for those months.)

Although temperature stratification was observed during all seasons, it was least frequently observed during the winter months of June, July and August, when there was continuous flow through the pond that kept the waters well mixed. In winter, there were also fewer hours of daylight and the mean wind speed was higher, which aided mixing.

The percentage of time the pond was stratified increased during spring (mean of 12%), was high during summer (mean of 22%) and decreased during autumn (mean of 9.5%). Figure 5-34 shows the mean magnitude of pond temperature stratification in the Morphett Road Sedimentation Pond during these months.

Stratification was strong during spring and autumn, when flow through the pond was intermittent. It is likely that during these seasons, a flow event through the pond increased the turbidity, which inhibited heating of the lower layers of water. When this was followed by a day of calm winds and high solar radiation, the surface water heated more quickly than the bottom waters and the pond became stratified.

In summer and early autumn, temperature gradients in the Morphett Road Sedimentation Pond were frequently reversed, with the warmest waters at the bottom of the pond. Similar temperature inversions were observed by Waters and Luketina (1998) in a small wetland pond in Sydney, which were thought to be due to either penetrative convection or inflow of saline groundwater (see Section 2.3.4).

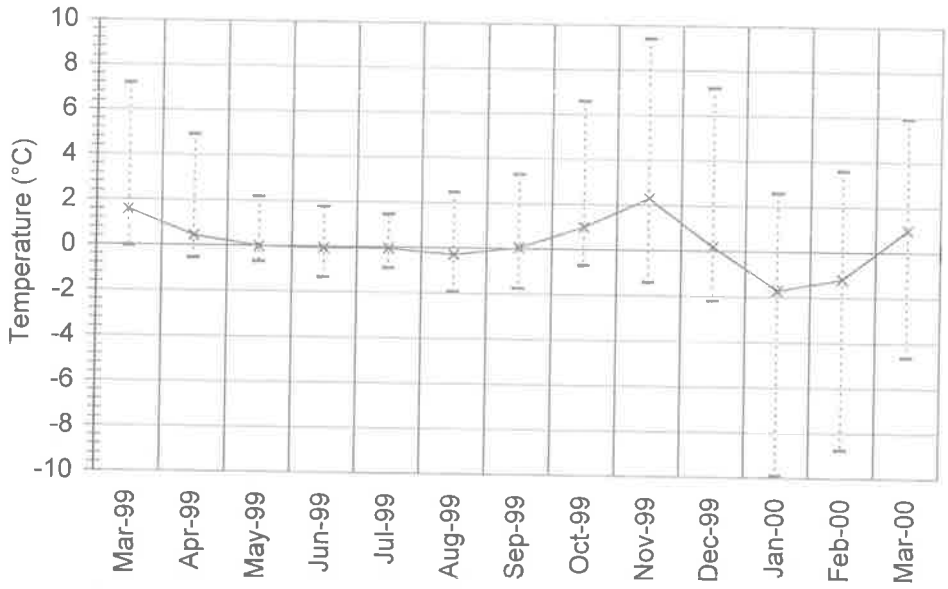

Figure 5-34: Mean monthly temperature stratification

From fortnightly observation of the Morphett Road Sedimentation Pond, pond clarity was seen to be generally low during summer, but additional density effects due to high salinity levels are believed to have inhibited pond mixing, allowing negative temperature gradients (i.e. temperature inversion) to persist, often for many days. This is illustrated in Figure 5-35.

Saline water has a higher density than freshwater hence rainfall may lead to a layer of less dense water at the surface. Similarly, fresh water inflow into the saline pond may flow across the surface with minimal impact on the pond waters below. Heat loss from the pond water occurs primarily at the surface, and the movement of heat upward from the bottom waters occurs through convective mixing. When the surface layers are cooled below the temperature of the bottom layers in a pond of uniform salinity, the resulting buoyancy imbalance causes convective mixing. If however, the surface waters are less saline due to rainfall or an influx of freshwater, the additional density effect may inhibit convective mixing, which prevents the movement of heat upwards to the surface.

Persistent positive temperature stratification also developed, where the top layers of water were warmer than the lower layers. This is illustrated in Figure 5-36, where diurnal warming and cooling of the upper layers and lower layers of water occurred independently, and the two halves of the pond remained separate and unmixed from about 1 March 2000 until about 17 March 2000. Initially the upper layers were consistently warmer than the lower layers, but on 11 March 2000 the lower layers peaked in temperature later in the day and were frequently warmer than the upper layers of water after this time.

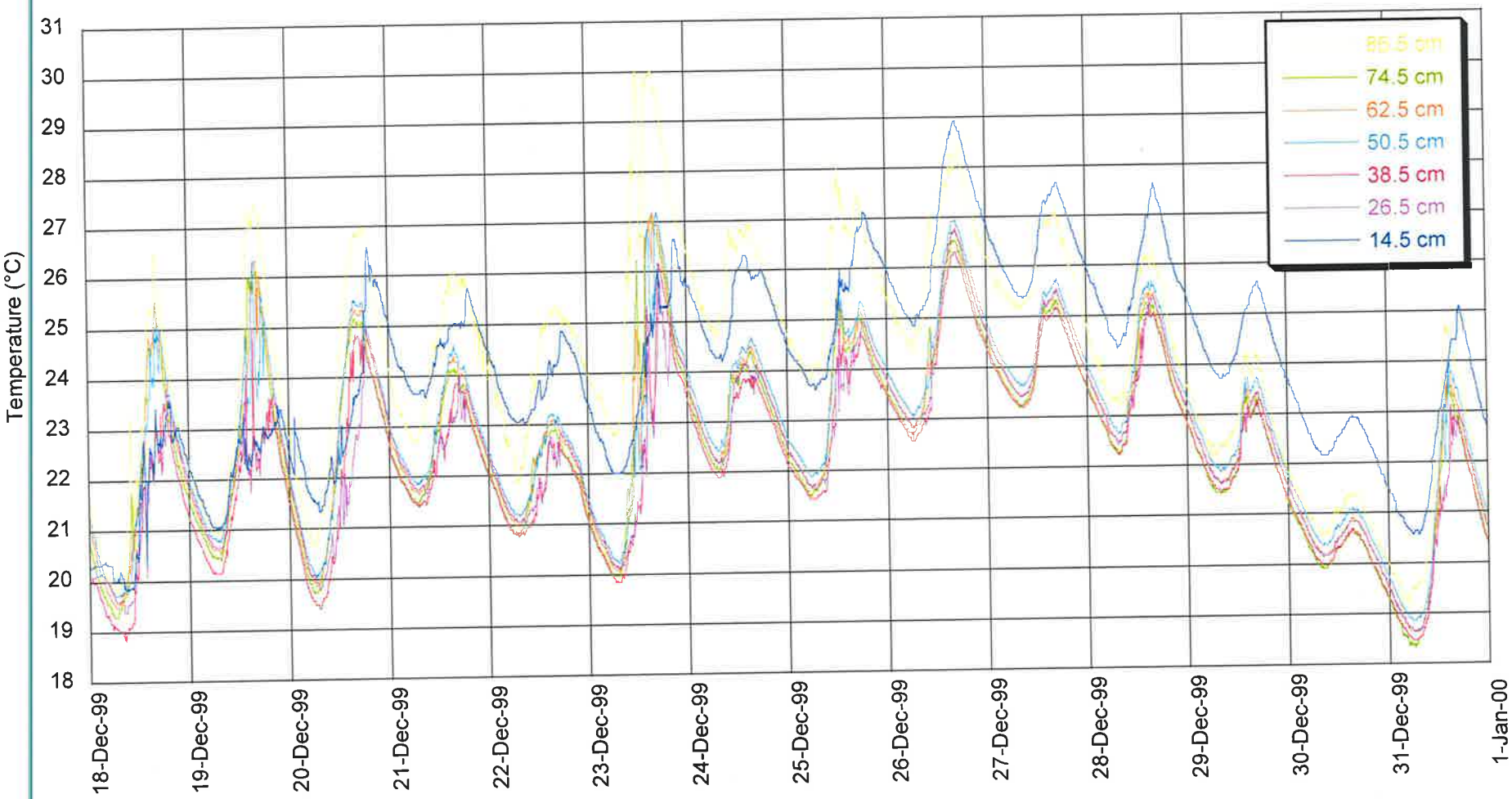

Figure 5-35: Temperature inversion observed in the Morphett Road Sedimentation Pond during late December 2000

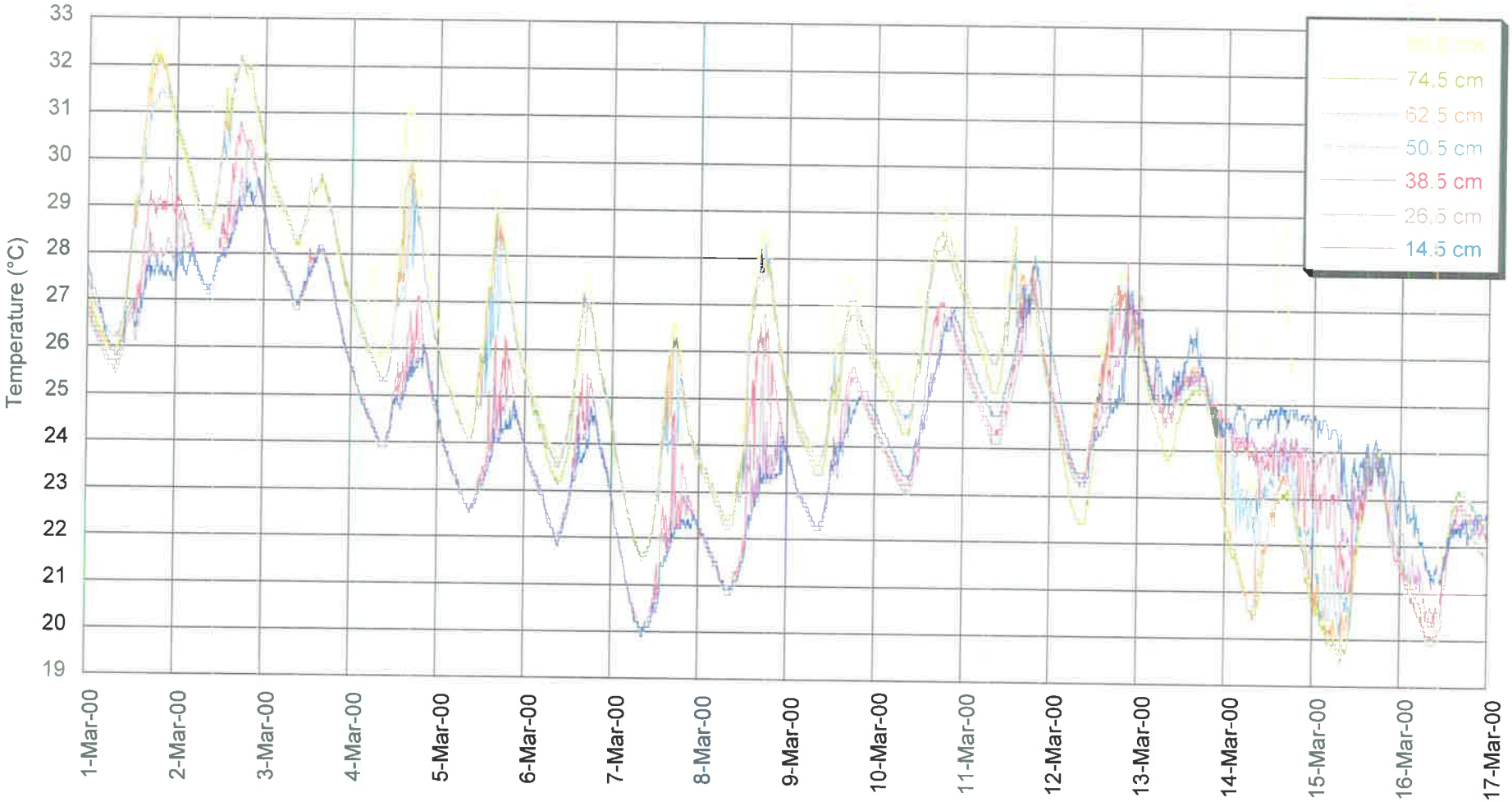

Figure 5-36: The independent behaviour of the upper and lower halves of the pond

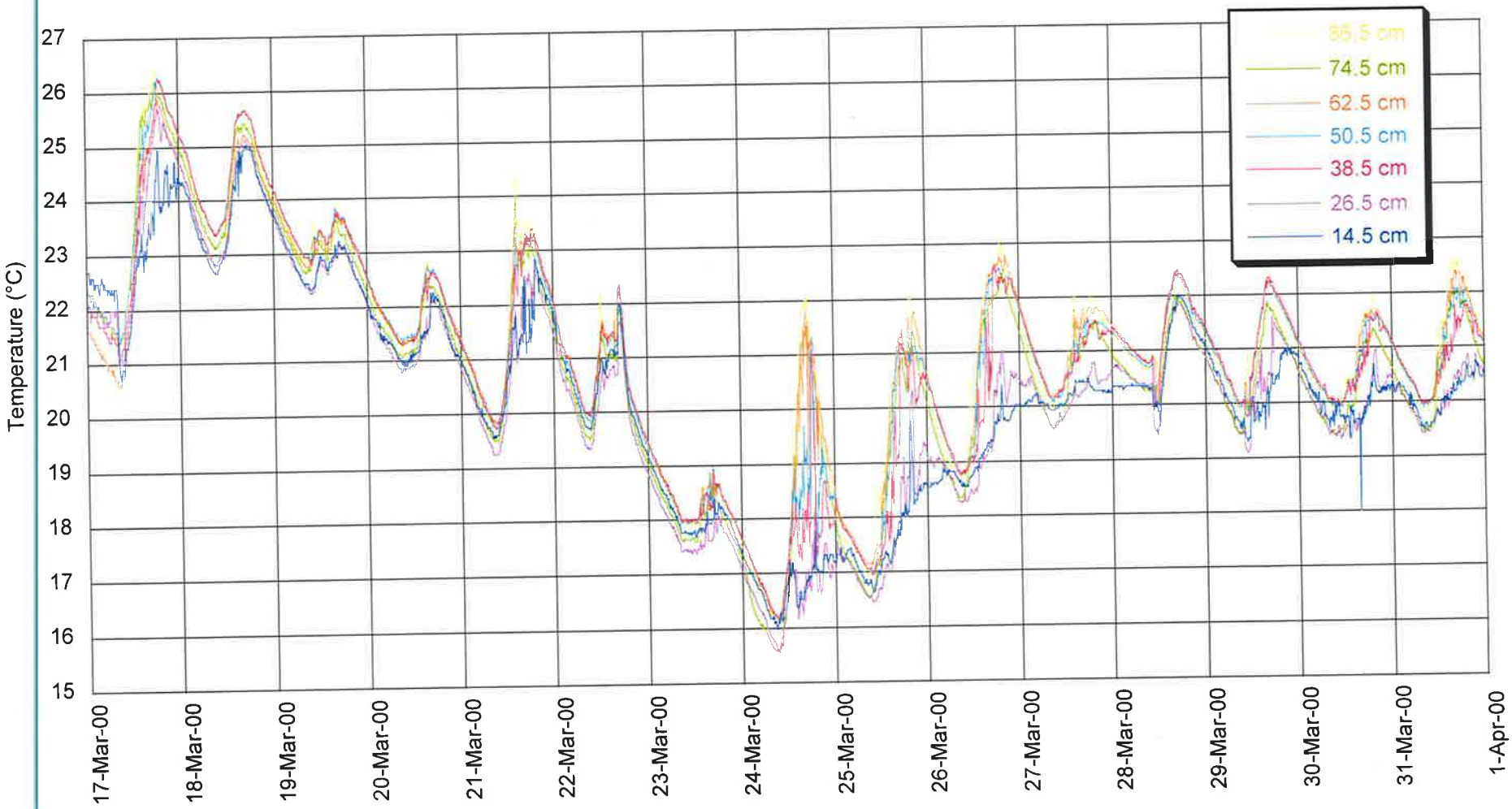

Figure 5-37: The pond was thermally mixed following a flow event in mid-March, but then stratified strongly on successive days late in the month

This type of stratification could effectively decrease the retention time for water passing through the pond by allowing it to short-circuit. Treatment in sedimentation ponds is reliant on the principal of sedimentation, whereby water is slowed sufficiently to enable sediment (and the attached metal contaminants) to settle out, allowing the water to flow on down through the catchment in a less polluted state. If water passes too rapidly through the pond, too little sediment, particularly the finer sediment will settle out of the water, effectively reducing its treatment capacity.

These persistent stratification effects occurred frequently between late October 1999 and mid-March 2000. Between early December 1999 and mid-March 2000, the Morphett Road Sedimentation Pond rarely became thermally uniform. This persistent stratification may have influenced the amount of sediment and metal removal that occurred in the pond during this time.

Following a flow event mid-March 2000, which helped to mix the pond, temperatures became relatively uniform through its depth. Over the next 6 days the pond did not stratify significantly and the mean pond temperature gradually fell. The pond then stratified on four successive days, from 24 March 2000 until 28 March 2000. This can be seen in Figure 5-37.

It is likely that the flow event in mid-March 2000 not only thermally mixed the pond but also broke up the salinity gradient that had been present and diluted the overall salinity. A reduction in water clarity due to the flow probably limited heating of the pond over subsequent days (causing the mean temperature to fall) while continued flow through the pond kept the waters well mixed. However, as flow through the pond declined and the weather stayed fine (air temperatures remained warm and wind speed relatively low) it is likely that there was differential heating of the water column, caused by poor clarity towards the bottom of the pond.

Since conductivity and water clarity were not monitored during late March 2000, this explanation of circumstances leading to the stratification from 24 March 2000 until 28 March 2000 is merely speculative. However, a similar sequence of events preceded the stratification events observed in the pond earlier the same month, on 1 March 2000 and 2 March 2000, when depth profiling of temperature, conductivity and water clarity was performed. These measurements concurred with the explanation of flow and stratification events that has been proposed.

A similar scenario is believed to have occurred in late March 1999. Although conductivity was not measured in the Morphett Road Sedimentation Pond at that time, the unusual behaviour of the eighth temperature sensor at the very bottom of the pond suggested a similar seasonal pattern in salinity. This was explained in Section 5.2.7.

During the stratification observed on 1 March 2000 and 2 March 2000 in the Morphett Road Sedimentation Pond, DO readings were well below ANZECC (1999) guideline levels at all depths in the pond. The fall in DO coincided with a fall in redox potential to reducing levels.

Despite the indication of a potential risk of adverse affects on ecosystem health due to very low DO levels, there was an abundance of aquatic life in the Morphett Road Sedimentation Pond – fish were spawning and a number of yabbies and tortoises could be spotted. Furthermore the increased ecosystem productivity was not just confined to life within the waters – there was also a noticeable rise in insect, bird and fox activity on or around the pond.

This contrasted with the complete absence of aquatic activity on previous days of monitoring, when DO levels were above guideline levels and excellent pond clarity facilitated observation of any creatures. However, the fall in DO during the final monitoring session, particularly at the bottom of the pond, may have forced some creatures to swim closer to the surface where more oxygen was available, making them easier to observe.

The increase in numbers of aquatic creatures may have been partly the result of the fall in salinity and pH levels, and due to an increase in the quantity of organic matter that followed the flow event through the pond. The rapid increase in aquatic populations was probably accompanied by an enormous increase in populations of microorganisms, which were too small to observe. The increase in demand for oxygen would have led to the fall in DO concentrations in the pond.

Thermal stratification is usually not considered to be an important issue in the construction of sedimentation or wetland ponds of less than 2.5 – 3m in depth. However the results of this study have shown that while seasonal thermal stratification like that seen in deep lakes and reservoirs does not occur in shallow ponds, diurnal stratification is not uncommon and more persistent stratification effects do occur due to the combined influence of temperature and salinity on the pond density.

The hot and dry summers, which are characteristic of Adelaide's Mediterranean climate are conducive to high evaporation and transient flow conditions, which enhance pond salinity. In general, salinity levels are rising in many of Australia's waterways largely due to poor land management practices of the past and present. The potential for salinity to impact upon the density stratification of sedimentation ponds should be recognised and accounted for in pond design and management.

5.5 Conclusions

Investigation of the physical and chemical conditions in the Morphett Road Sedimentation Pond indicated that there is reason to be concerned about the efficiency of sedimentation

ponds in capturing and retaining heavy metal pollutants, due to stratification and remobilising redox conditions. Measurements of redox potential in the Morphett Road Sedimentation Pond confirmed that remobilisation conditions were occurring, and that the conditions were exacerbated by the onset of thermal stratification.

In the Morphett Road Sedimentation Pond diurnal temperature stratification occurred frequently during spring and autumn when periods of high flow, which reduced water clarity, commonly alternated with periods of low flow and weather that was warm and relatively calm. Unusual persistent stratification was also observed during summer and early autumn when salinity levels were high. In fact complete thermal mixing was rare in the Morphett Road Sedimentation Pond between early December 1999 and mid-March 2000. This is believed to have been due to the combined effects of temperature and salinity on the density.

These persistent stratified conditions led to short-circuiting of low through the Morphett Road Sedimentation Pond during late summer and early autumn, which may have inhibited capture of sediments and heavy metals in the pond. Unfortunately, flow events at that time of year, which were most likely to be short-circuited, were also likely to be carrying above average pollutant loads due to the build-up of pollutants on the catchment during the preceding period of dry weather.

The combination of hot and dry conditions in summer, which is typical of Adelaide's Mediterranean climate is conducive to high salinity levels, and thus it is suspected that the increase in salinity (and therefore the reduction in capture efficiency due to flow short-circuiting) is an annual event in the Morphett Road Sedimentation Pond.

Fortunately, the long-term stratification did not automatically bring about reducing redox conditions, probably due to a low demand for DO caused by low summer organic loadings or pond conditions that were not conducive to microbial growth.

High salinity and the poor pH buffering capacity that were measured in the Morphett Road Sedimentation Pond during summer and low DO levels that were measured in later summer and early autumn did not comply with the ANZECC (1999) guidelines. This indicated a potential risk for adverse effects to the freshwater aquatic ecosystem of the Morphett Road Sedimentation Pond.

Accordingly, there was little observable aquatic life in the pond during summer (when salinity was extreme and large pH fluctuations occurred). However, aquatic life did return and remobilising conditions did occur when a flow event in late February reduced salinity and pH and increased the organic loading. This brought about the conditions of low DO.

Cleaning of the pond following the flow event in late February to reduce the supply of organic material and remove polluted sediments before metal contaminants could be remobilised,

might have restricted the development of the remobilising conditions and minimised the potential supply of metal contaminants.

CHAPTER 6

THE SEDIMENTATION POND MODEL

6.1 Introduction

Monitoring of pond temperature behaviour and redox potential in the Morphett Road Sedimentation Pond, as described in Chapter 5, showed that reducing redox conditions are affected by pond temperature stratification. Numerical modelling was thus carried out to investigate the causes of this pond temperature behaviour. The primary objectives of the sedimentation pond modelling were:

- to improve understanding of heat transfer and wind mixing processes, with particular regard to the stratification behaviour of sedimentation ponds and pond behaviour in the Mediterranean climate of Adelaide; and
- to explore different pond behaviour scenarios by altering the features of pond design (e.g. pond size, shape, orientation and base thickness), pond conditions (e.g. water clarity) and meteorological conditions.

Stratification is caused by density gradients in the water column. The density of the water at any one depth is a function of both the water temperature and water salinity. Hence the model that was developed in this study consisted of two parts – one to simulate the thermal stratification and the other to simulate the salinity stratification.

The thermal part of the sedimentation pond model was developed from the aquaculture pond model of Losordo and Piedrahita (1991) and Culberson and Piedrahita (1996). Their model was based on the eddy diffusion approach, and employed basic heat transfer equations originally developed by Munk and Anderson (1948), Sundaram and Rehm (1973), Octavio *et al.* (1977) and others.

This chapter describes the theoretical background to the Losordo and Piedrahita (1991) model and explains how it was re-worked to modify it for local climatic and geographic characteristics and data availability, and how it was extended to incorporate the unique

design characteristics of sedimentation ponds. It also describes the salinity part of the sedimentation pond model, which was derived from the basic principles of salt dynamics in the aquatic environment.

The chapter continues with an explanation of the testing and validation of the model using data collected from the Morphett Road Sedimentation Pond. The procedures used to validate the model, while essential in assessing the model's overall accuracy in timing and magnitude of stratification, provided valuable information about the nature of the processes underlying the development of stratified conditions in sedimentation ponds.

The description of the testing and validation of the model is then followed up with results of experimentation with the model in the Morphett Road Sedimentation Pond to assess the sensitivity of stratification to meteorological conditions, water characteristics and pond design parameters.

6.2 The Sedimentation Pond Model

The basic equation for heat transfer in the vertical (or depth) direction that is commonly used in temperature stratification models is given in Equation 6.1 (Henderson-Sellers, 1984). The equation is comprised of a temperature term, vertical advection term, a diffusion term and a boundary heat flux term. The most important boundary is the surface, although there can be considerable heat losses or gains at the bottom and edges of the pond.

$$A_z\left[\frac{\partial T}{\partial t}+w\frac{\partial T}{\partial z}\right]=\frac{\partial}{\partial z}\left[A_z\left(\alpha+K_z\right)\frac{\partial T}{\partial z}\right]+\frac{\partial}{\partial z}\left[\frac{\phi A_z}{\rho_w c_{pw}}\right] \qquad (6.1)$$

where: T is the water temperature;

A_z is the cross-sectional area at depth z;

w is the vertical velocity;

ρ_w is the density of the water;

c_{pw} is the heat capacity;

ϕ is the heat flux;

α is the coefficient of molecular diffusion; and

K_z is the coefficient of eddy diffusion.

Equation 6.1 has generally been applied to deep water bodies such as lakes and reservoirs, rather than shallow ponds, hence it was necessary to make three major modifications before it could be applied to sedimentation ponds. Two of the modifications involved simplifications of Equation 6.1. Firstly, the vertical velocity term (w) was neglected due to the relatively smooth concrete base of most sedimentation ponds that minimised vertical advection. The second simplification was because of the vertical or steeply sloping sides of most sedimentation ponds, which meant that there was negligible variability in the cross-sectional area of the pond with depth in comparison to a natural lake or reservoir.

The third modification concerned the flow of energy into and out of the sides and bottom of the pond, which was assumed to be negligible. The assumption of negligible heat flux at the bottom of the water body is reasonable for a large water body but not for sedimentation ponds, where the ratio of surface area to depth is typically high. In the sedimentation pond model the heat loss into and out of the sides of the pond was considered to be negligible, but the exchange with the pond bottom was taken into account.

The form of the heat transfer equation that was used in the sedimentation pond model is given by Equation 6.2, where ϕ is the sum of the relevant heat flux terms. The diffusion term from Equation 6.1 appears to have been eliminated, however it was actually incorporated as a heat flux term in Equation 6.2. The heat flux terms include the surface energy exchange (ϕ_{net}), the penetrating solar irradiance ($\phi_{sn,z}$), diffusive heat flux ($\phi_{d,z}$) and convective heat flux ($\phi_{conv,z}$) at depth z, and the concrete heat exchange (ϕ_{conc}). These are illustrated in Figure 6-1. In sedimentation ponds, dredging is performed periodically to remove sedimentary and organic material that accumulates at the bottom of the pond, hence the influence of this material on the thermal flux was assumed to be negligible.

$$\frac{\partial T}{\partial t} = \frac{\partial \phi}{\partial z} \frac{1}{\rho_w c_{pw}} \tag{6.2}$$

Figure 6-1 shows how a sedimentation pond was modelled, by dividing it into a series of volume elements for one-dimensional simulation of heat and salt transfer. To illustrate the concept, the pond has been divided into only 3 volume elements, although in the actual simulations a much larger number of volume elements were used.

The heat flux of each volume element was calculated using Equations 6.3 to 6.6, and Equation 6.7 was used to determine the mass flux of salt between all adjacent volume elements of the pond. Equations 6.8 and 6.9 were then used to determine the temperature and salt concentration of each volume element at each step in time.

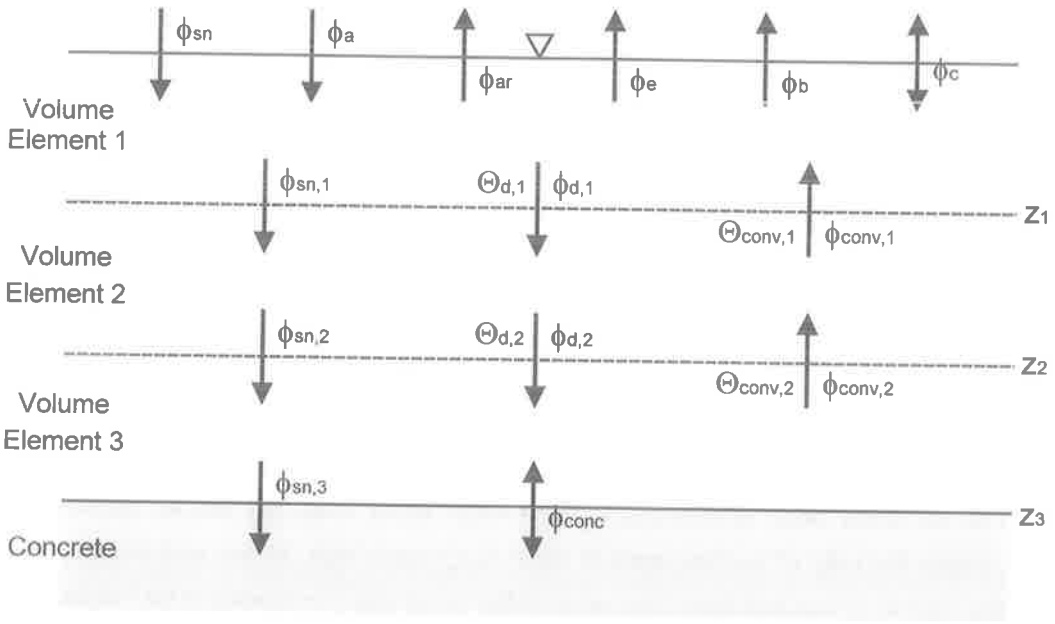

Figure 6-1: Heat (ϕ) and salt (Θ) transfer between the volume elements of a pond

$$\frac{dH_1}{dt} = (\phi_{net} - \phi_{sn,1} - \phi_{d,1})\,A \tag{6.3}$$

$$\frac{dH_2}{dt} = (\phi_{sn,1} - \phi_{sn,2} + \phi_{d,1} - \phi_{d,2})\,A \tag{6.4}$$

$$\frac{dH_3}{dt} = (\phi_{sn,2} - \phi_{sn,3} + \phi_{d,2} - \phi_{conc})\,A \tag{6.5}$$

$$\frac{dH_{conc}}{dt} = (\phi_{sn,3} + \phi_{conc} - \phi_{sed})\,A \tag{6.6}$$

$$\frac{dM}{dt} = \Theta\,A \tag{6.7}$$

where: H is the heat energy in kJ;

ϕ is the heat flux in kJ/m^2/h;

M is the mass of salt in kg;

Θ is the salt flux in kg/m^2/s;

t is the time in h; and

A is the cross-sectional area in m^2.

$$T_{z,t} = \left[H_{z,t-1} + \left(\frac{dH}{dt}\right)dt\right]\frac{1}{\rho_w c_{pw} V} \quad (6.8)$$

$$S_{z,t} = \left[M_{z,t-1} + \left(\frac{dM}{dt}\right)dt\right]\frac{1}{V} \quad (6.9)$$

where: $S_{z,t}$ is the salt concentration of the volume element at time t in kg/m^3;

$T_{z,t}$ is the temperature of the volume element at time t in °C; and

V is the volume of the volume element in m^3.

6.2.1 Surface Heat Transfer

The major exchanges of heat energy occur at the air-water interface of the pond. The surface heat flux processes are dependent on the water temperature at the surface of the pond and atmospheric meteorological variables, including solar radiation, wind speed, and air and dew point temperatures. Heat transfer due to precipitation is generally considered to be insignificant (Octavio *et al.*, 1977; Henderson-Sellers, 1984) and was not simulated in the pond model.

The net exchange of energy between the water at the surface of the pond and the atmosphere was represented by Equation 6.10 from Losordo and Piedrahita (1991). A negative net heat flux (ϕ_{net}) indicated a loss of heat from the pond surface to the atmosphere

while a positive heat flux indicated an addition of heat to the pond from the atmosphere.

$$\phi_{net} = \phi_{sn} + \phi_a - \phi_{ar} - \phi_e - \phi_b \pm \phi_c \quad (6.10)$$

where: ϕ_{net} is the net heat flux at the surface in kJ/m^2/h;

ϕ_{sn} is the penetrating solar irradiance in kJ/m^2/h;

ϕ_a is the atmospheric radiation in kJ/m^2/h;

ϕ_{ar} is the reflected atmospheric radiation in kJ/m^2/h;

ϕ_e is the evaporative heat flux in kJ/m^2/h;

ϕ_b is the water surface back radiation in kJ/m^2/h; and

ϕ_c is the convective heat flux in kJ/m^2/h.

The following sections of this chapter give a description of each flux term in Equation 6.10.

6.2.1.1 Net Short Wave Solar Radiation

Solar radiation is the driving force behind temperature fluctuations in most water bodies (the major exceptions being those water bodies affected by thermal pollution or geo-thermal activity). Not all of the radiation that is emitted from the sun reaches the surface of the earth directly, due to clouds, dust particles and gases. The solar radiation is reflected, scattered by air molecules and aerosols, and absorbed, mainly by water vapour, oxygen, carbon dioxide, ozone and aerosols. As a result, the solar radiation reaching the pond surface has two components – direct radiation from the sun and diffuse radiation due to atmospheric affects. While it can be highly variable, around 20% of total radiation has been estimated to be diffuse (Goldman and Horne, 1983).

The majority of the solar radiation that heats the water, is in the short wavelength range of 0.25 to 4.0μm (BOM, 1999b). This was the primary heat input in the pond model. It was simulated using Equation 6.11, which determines the amount of radiation traversing the air-water boundary of the pond after some has been reflected from the water surface.

$$\phi_{sn} = \phi_s (1 - R) \tag{6.11}$$

where: ϕ_{sn} is the penetrating solar irradiance in kJ/m^2/h;

ϕ_s is the direct solar irradiance in kJ/m^2/h; and

R is the reflectivity of the water surface (decimal fraction).

Maximum reflection occurs in calm conditions, when the water takes on a glassy or mirror-like appearance and is reduced by wind-driven waves. In the pond model, the value of the reflectivity was adjusted for the wind conditions using Equation 6.12 from Culberson and Piedrahita (1996).

$$R = R_s (1 - 0.08 W_2) \tag{6.12}$$

where: R is the reflectivity (decimal fraction);

R_s is the smooth reflectivity (Equation 6.13); and

W_2 is the wind speed 2 m above the water surface in m/s.

The degree of reflectivity of a smooth water surface depends on the angle of incidence of the sun's rays, the cloudiness of the sky and the wind speed. Reflection is higher at sunrise and sunset and during the winter months when the sun is lower in the sky. It was simulated in the pond model by Equation 6.13 from Losordo and Piedrahita (1991). The cloud parameters, A and B in Equation 6.13 were taken from Table 2-1.

$$R_s = A\left(180\,\frac{\lambda}{\pi}\right)^B \qquad (6.13)$$

where: R_s is the smooth reflectivity (decimal fraction);

A and B are empirical cloud parameters (see Table 2-1); and

λ is the solar altitude angle in radians.

Table 6-1: Values for cloud parameters A and B (after Fritz *et al.* (1980))

CLOUD COVER	A	B
Clear (0%)	1.18	-0.77
Scattered clouds (10 – 50%)	2.20	-0.97
Broken clouds (60 – 90%)	0.95	-0.75
Overcast (100%)	0.35	-1.45

The solar altitude angle required in determining the smooth reflectivity in Equation 6.13 is the angular distance of the sun above the horizon (see Figure 6-2). Due to the inclination and rotation of the earth, and its orbit around the sun, the position of the sun in the sky will change from one location to another, from one day to the next, and from one year to another. The solar altitude angle was simulated using Equation 6.14 from Hsieh (1986).

$$\sin\alpha = \sin L \sin\delta + \cos L \cos\delta \cos\omega \qquad (6.14)$$

where: α is the solar altitude angle in ° (see Figure 6-2);

L is the latitude of the pond in ° (negative in the southern hemisphere);

δ is the declination of the sun in °; and

ω is the hour angle in °.

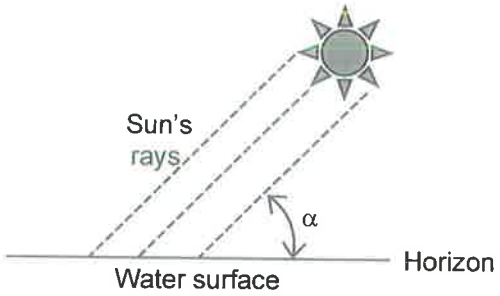

Figure 6-2: The solar altitude angle (α)

In astronomy the celestial co-ordinates of declination ('celestial latitude') and right ascension ('celestial longitude'), are used to pin-point the location of stars. Theoretically, the declination of the sun (a medium sized star) used in Equation 6.14 is the angular distance between a hypothetical line joining the centres of the sun and the earth, and the projection of that line on a plane passing through the equator (north declination is positive and south declination is negative). This is illustrated in Figure 6-3.

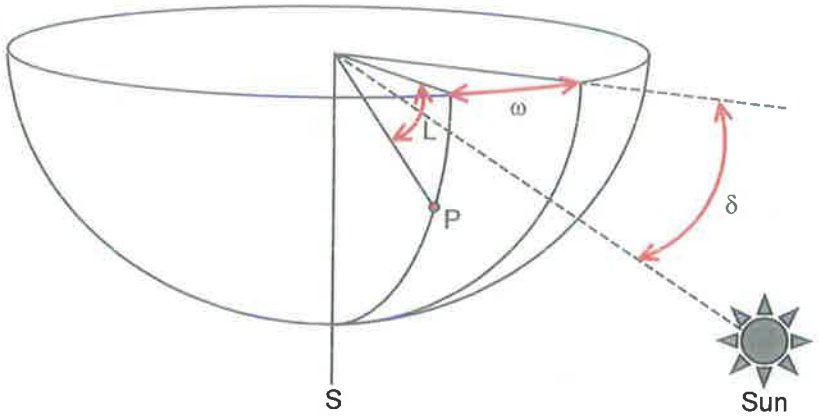

Figure 6-3: The latitude (L), declination of the sun (δ) and hour angle (ω) for a point P in the southern hemisphere

The sun's declination was simulated in the pond model using Equation 6.15 from Hsieh (1986), which is an approximation for the sun's declination based on the day of the year. The summer solstice falls when the sun's declination is maximum (23.5°) and the winter solstice falls when it is minimum (-23.5°). Although the declination of the sun will vary over the course of a day, the variation is small and is generally neglected in engineering calculations (Hsieh, 1986).

$$\delta = 23.45 \sin\left[\frac{360}{365}(284 + n)\right] \qquad (6.15)$$

where: δ is the declination of the sun in °; and

n is the number of the day in the year.

The hour angle (ω), illustrated in Figure 6-3 and used in Equation 6.14, is the angular distance between the hour circle and the meridian (the hour circle at noon). It was calculated using Equation 6.16.

$$\omega = \pm \frac{1}{15}(h) \tag{6.16}$$

where: ω is the hour angle in °; and

h is the number of hours from solar noon.

The hour angle is equal to 0 at solar noon, 15° at 1 o'clock, 30° at 2 o'clock, etc., but is negative for the hours before solar noon, for example - 15° at 11 o'clock. Solar noon is not equivalent to noon in the local time system hence time corrections were required to account for geographical and astronomical anomalies (e.g. longitudinal displacement from the centre of the timezone, daylight saving, planetary motion, etc.).

The equation of time was used to correct standard time for the seasonal variability in velocity of the earth due to its elliptical orbit about the sun, and the minor irregularities in the earth's rotation about its own axis. Numerous functions have been derived empirically for the equation of time (Figure 6-4). The difference between the functions of Stuart (1995), Hsieh (1986), The Astronomical Almanac (1999) and Spencer (1971) was minor (range: 6 – 88 seconds). The formulations from Hsieh and The Astronomical Almanac were both developed from northern hemisphere data. While the Spencer equation was developed at the CSIRO in Melbourne, and has been applied accurately in Perth and Sydney, the Stuart equation was found to be more accurate when used to predict the time of sunrise and sunset in a comparison by Sinnot (1995). Stuart's formulation, given by Equation 6.17, was the equation used to simulate the equation of time in the pond model.

$$E = 4 \times \frac{180}{\pi}\left[\operatorname{atan}\left(\tan\left(L_0 + 0.03342\sin\left(L_0 + 1.345\right)\right)\right) - \operatorname{atan}\left(0.9175\tan\left(L_0 + 0.03342\sin\left(L_0 + 1.345\right)\right)\right) - 0.03342\sin\left(L_0 + 1.345\right)\right] \tag{6.17}$$

where: E is the equation of time in minutes; and

L_0 is the sun's mean longitude in radians (Equation 6.18).

$$L_0 = 4.8771 + 0.0172\left(n + 0.5 - \frac{L}{360}\right) \tag{6.18}$$

where: n is the number of the day in the year; and

L is the longitude in °.

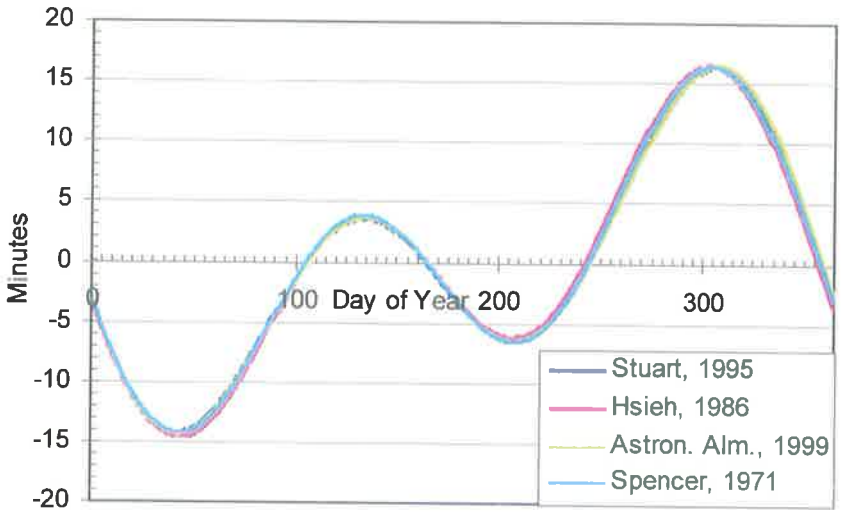

Figure 6-4: Empirical functions for the equation of time

A second time correction was required to account for the difference between the longitude of the pond and the longitude at the centre of the timezone in which the pond was located. A four minute time correction was applied for each 1° difference in longitude. The overall equation that was used in the pond model to adjust standard time to solar time is given by Equation 6.19 from Hsieh (1986).

$$T_s = T + \frac{1}{15}(L_{tz} - L) + \frac{1}{60}E \qquad (6.19)$$

where: T_s is the solar time in hours;

T is the standard time in hours;

L_{tz} is the standard longitude of the timezone in °;

L is the longitude of the pond in °; and

E is the equation of time in minutes.

6.2.1.2 Net Atmospheric Radiation (Long Wave)

Only a portion of the solar radiation emitted by the sun reaches the earth's surface, with the rest absorbed, scattered and reflected in the atmosphere. The solar radiation that is emitted by clouds, dust and atmospheric gases (e.g. carbon dioxide and ozone) has a spectral range

of 4 to 100μm, and is known as atmospheric or long-wave radiation. Atmospheric radiation is the primary heat input to a pond during the night or when the sky is cloudy.

Due to atmospheric thermal gradients and non-homogeneity, atmospheric radiation is difficult to quantify. Hence in the pond model, the atmospheric flux was computed using an empirical formula from Ocatvio *et al.* (1977), shown as Equation 6.20, which was applied successfully in the pond model of Culberson and Piedrahita (1996).

$$\phi_a = \varepsilon \sigma (T_a + 273)^4 \tag{6.20}$$

where: ϕ_a is the atmospheric radiation in $kJ/m^2/h$;

ε is the average atmospheric emissivity (dimensionless);

σ is the Stefan-Boltzmann constant ($\sigma = 2.04 \times 10\text{-}7 kJ/m^2/h/K^4$); and

T_a is the air temperature in °C.

A small portion of the incoming atmospheric radiation is reflected from the water surface. The degree of reflectance depends on the albedo of the water surface. Water behaves as a near black body, and a reflectance of 3% is commonly used (Octavio *et al.*, 1977). Equation 6.21 represents the atmospheric radiation reflected from the surface of a pond.

$$\phi_{ar} = r \phi_a \tag{6.21}$$

where: ϕ_{ar} is the reflected atmospheric radiation in $kJ/m^2/h$; and

r is the surface reflectance (0.03).

6.2.1.3 Evaporative Heat Transfer

Evaporative losses are generally the biggest cause of heat loss from ponds (Rafferty, 1986). Evaporation leads to a reduction of heat energy at the water surface due to a loss of latent heat as water molecules change from a liquid to a gaseous phase (water vapour). There is also an associated loss of heat due to the reduction in water volume, but it is so small that it has generally been neglected (Octavio *et al.*, 1977; Henderson-Sellers, 1984) and was omitted from the evaporative flux calculations in the pond model.

The loss of latent heat from the water surface is dependent on relative humidity, air and water temperatures and the wind speed. As water temperature rises or relative humidity decreases, the rate of evaporation increases, but as water evaporates, the relative humidity of the air

immediately above the water surface increases, which slows the rate of evaporation. In windy conditions however, the amount of evaporation will be higher since the air movement discourages build-up of the saturated boundary layer immediately above the water surface.

Numerous formulae have been devised for the evaporative heat flux, most of which are a function of the wind speed, the difference between the saturated vapour pressure at the water temperature and the actual vapour pressure at air temperature (e_s - e_a), and an empirical constant. The majority of empirical constants that are used in evaporative heat flux formulae have been derived from evaporation studies in the northern hemisphere.

Equation 6.22 is the formula that was applied by Losordo and Pierahita (1991) and Culberson and Piedrahita (1996) to simulate evaporative heat flux from the surface of aquaculture ponds. The formula was taken from Fritz *et al.* (1980) who used it in computations of the temperature of waste stabilisation ponds, and it is the evaporative heat flux equation that was employed in the sedimentation pond model. The empirical constant in Equation 6.22 (N = 5.0593kJ/m^2/km) has been derived from studies of Lake Hefner in the United States. However it has also been applied successfully by Webb (1960) to studies of evaporation from Lake Eucumbene in New South Wales

$$\phi_e = N W_2 (e_s - e_a) \tag{6.22}$$

where: ϕ_e is the evaporative heat flux in kJ/m^2/h;

N is a constant (N = 5.0593kJ/m^2/km);

W_2 is the wind speed 2m above the water surface in km/h;

e_s is the saturated vapour pressure at T_w in mmHg; and

e_a is the actual vapour pressure above the water surface in mmHg.

The vapour pressures that were required to simulate the evaporative heat flux in Equation 6.22 were modelled using Equation 6.23 from Culberson and Piedrahita (1996), and Equation 6.24 from Henderson-Sellers (1984). T_w was wrongly reported to be in degrees Celsius rather than Kelvin by Culberson and Piedrahita (1996).

$$e_s = 25.374 \exp\left(17.62 - \frac{5271}{T_w}\right) \tag{6.23}$$

$$e_a = 610.78 \exp\left[17.2694 \frac{T_d - 273.16}{T_d - 35.86}\right] \frac{760}{101.325} \frac{1}{1000} \tag{6.24}$$

where: T_w is the water surface temperature in degrees K; and

T_d is the dew point temperature in degrees K.

6.2.1.4 Convective Heat Transfer

The convective heat transfer (which is also sometimes known as conductive or sensible heat transfer) is related to the evaporative mass flux described above in Section 6.2.1.3. Unlike evaporation however, convection may involve either a gain or a loss of heat from the water surface. The heat is transferred between the water and the air by conduction, and convectively transported by air currents above the water surface. This heat loss/gain was approximated in the pond model using Equation 6.25 from Culberson and Piedrahita (1996).

$$\phi_c = 1.5701\, W_2\, (T_w - T_a) \tag{6.25}$$

where: ϕ_c is the convective heat flux in $kJ/m^2/h$;

W_2 is the wind speed at 2m above the pond surface in km/h;

T_w is the water surface temperature in °C; and

T_a is the air temperature in °C.

6.2.1.5 Back Radiation

Back radiation involves a loss of heat from the pond surface due to emission of longwave radiation. Any material at a temperature above absolute zero will radiate energy. A perfect black body would be the ideal radiator, and would be given an 'emissivity' value of 1. Water does not behave as a perfect black body due to reflection from the surface hence it has an emissivity of 0.97. The emission of longwave radiation from the water surface was approximated in the pond model using the fourth-power law of Stefan-Boltzman (Equation 6.26).

$$\phi_b = 0.97\, \sigma\, (T_w + 273)^4 \tag{6.26}$$

where: ϕ_b is the water surface back radiation in $kJ/m^2/h$;

σ is the Stefan-Boltzmann constant ($\sigma = 2.04 \times 10\text{-}7 kJ/m^2/h/K^4$); and

T_w is the water surface temperature in °C.

6.2.2 Internal Heat and Salt Transfer

Although the major input of heat into the pond occurs at the water surface, there is also an influx of heat energy to the subsurface waters through solar radiation absorption, and continual transfer of heat and/or salt between the volume elements by diffusion (molecular and turbulent) and convection. Molecular diffusion occurs whenever there is a temperature or salt gradient. Turbulent (or eddy) diffusion occurs when there is a temperature or salt gradient and turbulence, which comprises small-scale irregular movements of water (e.g. due to wind mixing). Diffusion leads to a transfer of heat or salt, with no net movement of water unlike convection, which involves large-scale regular movements of water (e.g. currents) that transport the heat or salt within the water.

In a freshwater pond there are essentially two internal mixing scenarios – when the pond is warming there is diffusion of heat downwards, and when the pond is cooling, there will be convective mixing taking heat upwards. However, in a saline pond, there are potentially four different density scenarios due to the complementary or opposing effects of heat and salt on the density. These are illustrated in Figure 6-5 for a simplified two-layer system.

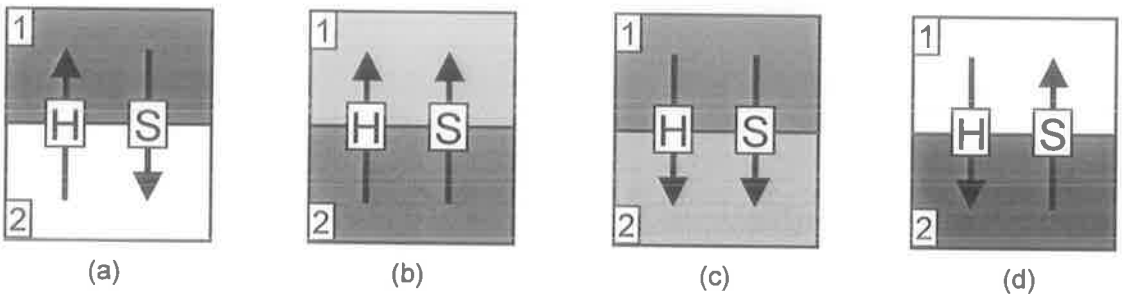

Figure 6-5: The four density scenarios (the striped regions represent the cooler of the two layers, the shaded regions represent the layer of higher salt concentration, and the arrows indicate the general direction of heat and salt movement)

In scenarios (a) and (d) in Figure 6-5, the mixing response of the two layers is relatively straightforward since density gradients due to both the salt concentration and the temperature complement one another. In scenario (a), cold salty water overlying warmer less salty water is buoyantly unstable and leads to convective mixing of heat upwards and salt downwards. The layers are reversed in scenario (d), where warm less salty water overlying colder saltier water leads to a stable density gradient and double diffusion of heat downwards and salt upwards.

In scenarios (b) and (c) the heat and salt have opposing effects on the density, which leads to combined diffusive and convective transfer. The resultant vertical mixing can be much greater than in a purely freshwater system where mixing is caused by either diffusion or convection alone (Turner, 1985). The type of mixing that occurs in scenarios (b) and (c) is affected by the relative diffusivities of heat and salt. Molecular diffusion of heat is around 100 times faster

than molecular diffusion of salt (Stewart, 1998). Therefore, in calm conditions (i.e. when there is little turbulence to cause diffusion) the difference between the rate of diffusion of heat and salt can lead to density instability at the interface. This phenomenon is sometimes referred to as 'convective diffusion' or 'thermohaline convection'.

In scenario (b), cold less salty water overlying warmer saltier water leads to double diffusion of heat and salt upwards. When turbulence is low, the difference between the rate of molecular diffusion of heat and salt can lead to interfacial density instability. The resulting convection that occurs separately in each layer keeps the two layers well-mixed and sharpens the density interface. If the calm conditions continue, the density difference between the two layers may actually increase.

In scenario (c) warm salty water overlying colder less salty water leads to double diffusion of heat and salt downwards. In quiescent waters the difference between the rate of molecular diffusion of heat and salt can lead to salt fingering, whereby a thin, cool, salty, intermediate layer develops, which then sinks (in a finger-like pattern) due to its greater density. The descending fingers increase in density through conduction of heat horizontally to adjacent ascending fingers, which correspondingly become less dense (horizontal transfer of salt also occurs, although more slowly than the heat transfer). Hence, although the density gradient of the whole system appears to be stable, the localised instability at the finger edges leads to convective mixing within the two layers.

Salt fingering and convective diffusion are most likely to occur in calm conditions when molecular rather than turbulent diffusion is dominant. Turbulence is primarily caused by wind, and an examination of wind speed data from the Morphett Road Sedimentation Pond (28 February 1999 to 27 April 2000), showed that the half hourly recorded wind speed was 0m/s less than 4% of the time. 85% of these records were recorded at night or when the pond was cooling, when convection rather than diffusion was likely to have been the primary means of heat transfer. Hence in the sedimentation pond model salt fingering and convective diffusion effects at the interface were assumed to be negligible.

In the sedimentation pond model, the mechanism of heat and salt transfer between layers was dictated by the density gradient across the interface – diffusion was assumed to occur when the density gradient was negative and convective mixing was assumed to occur when the density gradient was positive.

6.2.2.1 Solar Radiation Absorption

In a pond, the solar radiation that is not reflected penetrates the water surface and is attenuated with increasing depth. Below the surface, the light is scattered by water molecules

as well as dissolved and suspended particulate matter, and is transformed to heat energy through absorption. The attenuation of light below the surface is generally modelled using the Lambert-Beer Law given by Equation 6.27 (Farrow and Patterson, 1994).

$$I_z = I_0 \, e^{-\eta z} \tag{6.27}$$

where: I_z is the light intensity at a depth zm below the surface in W/m^2;

I_0 is the light intensity at the surface W/m^2; and

η is the light extinction coefficient.

Equation 6.28 from Culberson and Piedrahita (1996) is the heat flux formulation of the Lambert-Beer Law that was applied in the pond model. A surface absorption factor, β, is incorporated into Equation 6.28 to account for observed deviations in the penetrating solar irradiance from the Lambert-Beer Law predictions, close to the water surface. The deviations are due to long wave radiation, which is absorbed very near the surface and provides little heat to the water below. The surface absorption is related to the turbidity of the water, and was simulated in the pond model using Equation 6.29 from Henderson-Sellers (1984).

$$\phi_{sn,z} = \phi_{sn}(1-\beta)\exp(-\eta_e z) \tag{6.28}$$

$$\beta = 0.265\ln(\eta_e) + 0.614 \tag{6.29}$$

where: $\phi_{sn,z}$ is the penetrating solar irradiance at depth zm in $kJ/m^2/h$;

ϕ_{sn} is the penetrating solar irradiance at the surface in $kJ/m^2/h$;

β is the surface absorption factor (decimal fraction); and

η_e is the effective light extinction coefficient.

Light intensity decreases exponentially with depth (Goldman and Horne, 1983). The rate at which light is absorbed below the water surface, is represented by a light extinction coefficient (or diffuse attenuation coefficient). The light extinction coefficient (η) is highly dependent on the turbidity of the water, which was measured in this study using a secchi disk (see Section 5.2.6). In the pond model, the light extinction coefficient was calculated as a function of secchi disk depth, using Equation 6.30 from Henderson-Sellers (1984).

$$\eta = \frac{\kappa}{SDD} \tag{6.30}$$

where: η is the light extinction coefficient;

κ is a constant; and

SDD is the secchi disk depth in m.

The light extinction coefficient is also a function of the angle of incidence of the solar rays on the water surface, which is a function of the solar altitude angle (see Equation 6.32). Due to the difference in optical density of air and water, light is refracted as it penetrates the water surface. The amount of refraction is determined by the angle of incidence of the light as well as the refractive indices of air and water, which are proportional to the speed of the light waves through each medium. The angle of incidence and the angle of refraction, which are illustrated in Figure 6-6, are related by Snell's Law (Equation 6.31).

$$N_a \sin\theta_i = N_w \sin\theta_r \tag{6.31}$$

where: N_a is the refractive index of air (1.0003, Davidson and Abramowitz (2000));

N_w is the refractive index of water (1.33, Davidson and Abramowitz (2000));

θ_i is the angle of incidence of light in ° (see Equation 6.32); and

θ_r is the angle of refraction of light in °.

$$\theta_i = z = 90 - \alpha \tag{6.32}$$

where: z is the solar zenith angle in °; and

α is the solar altitude angle in ° (see Figure 6-2).

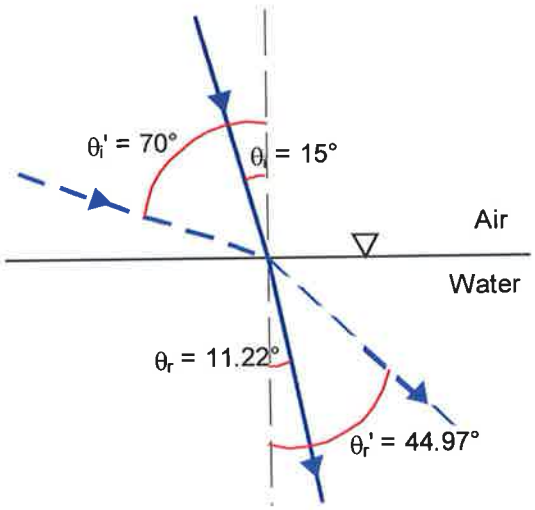

Figure 6-6: Angles of incidence (θ_i) and refraction (θ_r) of light at the air-water interface

As can be seen in Figure 6-6, the amount of refraction will be higher during early morning and late afternoon, when the sun is low in the sky and the angle of incidence is therefore greatest. At these times of the day, when refraction is high, the light must travel $1/\cos\theta_r$ further to reach a given depth. The light extinction coefficient was therefore adjusted by a factor of $1/\cos\theta_r$ as suggested by Rabl and Nielsen (1975) (Equation 6.33), and was then referred to as the *effective* light extinction coefficient.

$$\eta_e = \frac{\eta}{\cos\theta_r} \tag{6.33}$$

where: η is the light extinction coefficient;

η_e is the effective light extinction coefficient; and

θ_r is the angle of refraction.

The value of the constant κ in Equation 6.30 depended on the reflectance, water colour (i.e. due to dissolved material) and the spectral composition of the incident light. As shown in Figure 6-7, absorption of light is highest for light in the long wavelength infrared region of the spectrum and lowest for shorter wavelength light in the blue region, but slightly greater for the even shorter UV wavelengths. Hence the light attenuation coefficient was affected by variations in the spectral distribution of the incident light and colouring of the water by suspended particulates or dissolved materials.

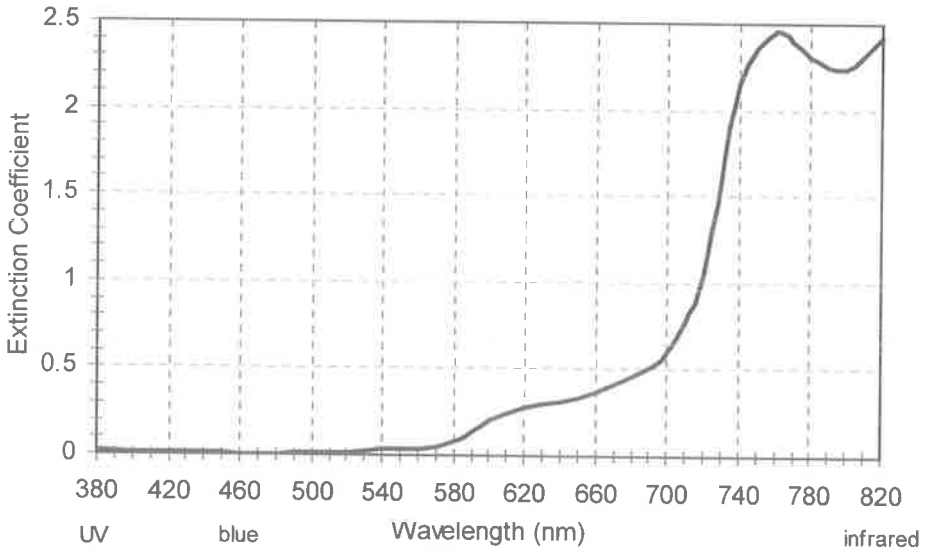

Figure 6-7: The extinction coefficient for light of different wavelengths in a 1m column of distilled water (after Wetzel (1975))

Although κ is unlikely to be a true constant, an average value has often been assumed (Effler, 1988), but in Equation 6.30 it has been given values ranging from 1.16 to 2.3 (Davies-Colley and Vant, 1988). In modelling shallow aquaculture ponds, Culberson and Piedrahita (1996) assigned to κ a value of 1.7, and this value was assumed in the pond model.

6.2.2.2 Diffusion

The diffusive transfer of salt was simulated by a basic Fickian diffusion equation (Equation 6.34). The transfer of heat by turbulent processes is analagous to the Fickian diffusion of a solute in an undisturbed liquid, and was represented by Equation 6.35. The coefficients of eddy conductivity of heat (the term 'coefficient of eddy diffusivity' or 'eddy diffusion coefficient' is more commonly used in heat transfer analysis rather than the term 'coefficient of eddy conductivity') and eddy diffusivity of mass are very similar. Many ocean models, which incorporate the effects of both temperature and salinity on the density, assume identical values for the coefficients (Gargett, 2000) and equivalence was assumed in the pond model.

$$\frac{dM}{dt} = A\,\Theta = A\,K_{zS}\,\frac{dS}{dz} \tag{6.34}$$

$$\frac{dH}{dt} = A\,\phi = A\,\rho_w\,c_{pw}\,(\alpha + K_z)\frac{dT}{dz} \tag{6.35}$$

where: M is the mass of salt in kg;

S is the concentration of salt in kg/m^3;

A is the cross-sectional area in m^2;

K_{zS} is the coefficient of eddy diffusivity of salt in m^2/h;

H is the heat in J;

ρ_w is the density of water in kg/m^3;

c_{pw} is the heat capacity of water in J/kg/°C;

α is the coefficient of molecular diffusion of heat in m^2/h;

K_z is the coefficient of eddy diffusion of heat in m^2/h; and

T is the water temperature in °C.

The transfer of heat in the vertical direction is principally via turbulent processes (Jassby and Powell, 1975). The molecular diffusion coefficient, α, is generally small in comparison to the eddy diffusion coefficient (Octavio *et al.*, 1977), and in some temperature models (e.g. Culberson and Piedrahita (1996)) it has been assumed to be negligible and not included in diffusion calculations. Although included in the sedimentation pond model, due to its small magnitude the molecular diffusion coefficient was expected to have little impact on model simulations other than in very calm conditions when turbulent diffusion would be minimal.

The true value of the molecular diffusion coefficient is dependent on temperature, but in those models that do include a molecular diffusion component, it is generally assumed to be a constant between $1.2 \times 10^{-7} m^2/s$ and $1.4 \times 10^{-7} m^2/s$ (Henderson-Sellers, 1984). A value of $1.2 \times 10^{-7} m^2/s$ was used for the molecular diffusion coefficient in the pond model, which was the value found by Jassby and Powell in diffusion measurements in Castle Lake in California (Jassby and Powell, 1975).

In early attempts at temperature modelling the eddy diffusion coefficient, like the molecular diffusion coefficient, was assumed to be a constant. However Henderson-Sellers *et al.* (1983) found that this assumption was invalid at other than low wind speeds and in deep lakes. In reality, the eddy diffusion coefficient is both spatially and temporally variable. In water bodies where there is no through flow, temperature simulations are highly sensitive to the value of the eddy diffusion coefficient (Octavio *et al.*, 1977).

Numerous equations have been derived empirically, semi-empirically or analytically for the eddy diffusion coefficient. In the sedimentation pond model, Equation 6.36 was used to determine the eddy diffusion coefficient. Originally derived by Rossby and Montgomery (1935), the equation incorporated a stability function to relate the eddy diffusion coefficient in stratified conditions to the eddy diffusion coefficient when stratification was not present (the neutral eddy diffusion coefficient).

The neutral value of the eddy diffusion coefficient was calculated using an exponential function given by Equation 6.37, from Henderson-Sellers (1984). Equations 6.36 and 6.37 were used by Losordo and Piedrahita (1991) and Culberson and Piedrahita (1996), who found that they performed satisfactorily in simulating temperature profiles in shallow aquaculture ponds.

$$K_z = K_{z0} \left(1 + \sigma Ri_z\right)^{-n} \qquad (6.36)$$

where: K_z is the eddy diffusion coefficient at depth zm;

K_{z0} is the neutral eddy diffusion coefficient at depth zm;

σ and n are empirical constants; and

Ri_z is the Richardson number at depth zm.

$$K_{z0} = \frac{(w^*)^2}{\mu_s k} \exp(-k z) \tag{6.37}$$

where: K_{z0} is the neutral eddy diffusion coefficient at depth zm;

w^* is the frictional velocity in m/s;

μ_s is the drift velocity in m/s; and

k is a decay coefficient in m^{-1}.

The drift velocity in Equation 6.37 is induced by wind drag on the water surface, hence it is a function of the frictional velocity. An empirical relationship given by Equation 6.38 from Culberson and Piedrahita (1996) was used to calculate the drift velocity in the pond model.

$$\mu_s = 30\, w^* \tag{6.38}$$

where: μ is the drift velocity in m/s; and

w^* is the frictional velocity in m/s.

The decay coefficient, k, in Equation 6.37 is related to Ekman's theory of an exponential decline in current speed with depth due to friction and turbulence losses. Ekman identified a depth of frictional resistance at which the current reverses direction and below which there is negligible flow (Equation 6.39, Smith (1979)). The value of k depends on the assumed ratio of the current speed at the depth of frictional resistance to the current speed at the surface (Equation 6.40).

$$D^* = \frac{30.47\,\tau_0}{u_0 \sin L} \tag{6.39}$$

$$\frac{u_{D^*}}{u_0} = \exp(-kD^*) \tag{6.40}$$

where: D^* is the depth of frictional resistance in m;

L is the latitude in °;

τ_0 is the shear stress at the surface in Pa;

u_0 is the current velocity at the surface in m/s;

u is the current velocity at depth D* in m/s; and

k is the decay coefficient in m^{-1}.

The depth of frictional resistance increases with increasing wind speed, hence the current speed decay coefficient, k, is related inversely to the wind speed. Equation 6.41 is an empirical relationship derived by Smith (1979) that has been frequently used to determine k from the wind speed.

$$k = \frac{6}{(W_{10})^{1.84}} \tag{6.41}$$

where: W_{10} is the wind speed at 10m above the surface in m/s.

The depth of frictional resistance in a pond decreases with increasing distance from the equator i.e. with increasing latitude. Equation 6.41 was derived from lake data at a latitude of 56°, a fact that was not cited in the pond models of Losordo and Piedrahita (1991) or Culberson and Piedrahita (1996), despite applying their models to ponds in Hawaii (approximately 56°N), California (approximately 33 – 42°N), Honduras (approximately 15°N), Rwanda (approximately 2°S) and Thailand (approximately 6 – 20°N).

Henderson-Sellers (1989) in his one-dimensional eddy diffusion model (EDD1) used a variation of the Smith (1979) equation (Equation 6.41) that incorporates the effect of latitude. This modified Smith equation, shown as Equation 6.42, was used to simulate the decay coefficient in the pond model, due to the significant difference in latitude of sedimentation ponds in Australia.

$$k = \frac{6.6\sqrt{\sin L}}{(W_{10})^{1.84}} \tag{6.42}$$

where: L is the latitude in °; and

W_{10} is the wind speed at 10m above the surface in m/s.

The adjustment of the neutral eddy diffusion coefficient for the degree of stability of the water column, shown in Equation 6.36, was dependent on the Richardson number and two empirical constants, σ and n. Numerous values have been suggested for σ and n. Munk and Anderson (1948) suggested a value of 10/3 for σ and 3/2 for n, while Sundaram and Rehm (1973) and Henderson-Sellers (1984) used 0.1 for σ and 1 for n. Losordo and Piedrahita (1991) used a value of 1 for n, but reduced σ to 0.05 during model calibration, when temperature simulations appeared to be over-estimating the pond stratification. Reducing σ

had the effect of increasing the effective diffusion coefficient, which resulted in greater pond mixing. The values $\sigma = 0.1$ and $n = 1$ were used in the sedimentation pond model.

The Richardson number was also required in Equation 6.36. It was originally introduced into meteorology by Richardson (1926) as a measure of stability of vertical turbulence in the atmosphere. It has since been applied to the analysis of water column stability, where it is formulated as a function of water density and current velocity. Equation 6.43 is the general form of the Richardson number. It is a function of the Brunt-Väisälä frequency (Equation 6.44), which is the frequency of the internal waves that develop due to a negative density gradient.

$$Ri_z = -\frac{N^2}{\left(\frac{\partial \mathbf{u}}{\partial z}\right)^2} \tag{6.43}$$

where: N is the Brunt-Väisälä frequency (Equation 6.44);

$\mathbf{u}$ is the current (u,v) in m/s; and

z is the depth in m.

$$N = \sqrt{-\frac{g}{\rho}\left(\frac{\partial \rho}{\partial z}\right)} \tag{6.44}$$

where: g is the acceleration due to gravity in m/s^2; and

ρ_w is the density of water in kg/m^3.

A positive Richardson number indicates stable stratification, a negative Richardson number indicates instability, while a Richardson number of 0 indicates neutral stratification, and the water column is homogeneous (Welch, 1980). In waters with a high Richardson number, the stability has a dampening effect on turbulence in the water column.

In the past, the horizontal velocity gradient required to determine the Richardson number was a difficult quantity to estimate or measure, hence there was relatively little data from which a functional relationship for its calculation could be deduced. An alternative often used is the assumption of Sundaram and Rehm (1973), where the current is replaced by the frictional velocity, which is due to the drag force exerted by the wind on the water surface (Equation 6.46). This modified formulation of the Richardson number, shown as Equation 6.45, was applied in the pond model.

$$Ri_z = -\frac{1}{\rho_w}\frac{\partial \rho_w}{\partial z}\frac{g z^2}{(w^*)^2} \tag{6.45}$$

$$w^* = \sqrt{\frac{\tau_0}{\rho_w}} \tag{6.46}$$

where: w^* is the frictional velocity in m/s.

τ_0 is the shear stress at the surface in Pa (Equation 6.47).

The drag force or shear stress on the water surface is primarily affected by wind speed, but it is also influenced by the fetch, the development of waves and their dissipation at the water's edge, and by wind speed variability and meteorological boundary layer stability over the water surface (Fischer *et al.*, 1979). In the pond model the shear stress was formulated as a function of wind speed, air density and a drag coefficient, C_{10}, which accounted for the other shear stress variables (Equation 6.47). Although the value of the drag coefficient is partially dependent on wave development, long waves are unable to fully develop in shallow ponds, hence a constant value of 1.0×10^{-3} (Culberson and Piedrahita, 1996) was assumed for the drag coefficient.

$$\tau_0 = C_{10}\,\rho_a\,(W_{10A})^2 \tag{6.47}$$

where: C_{10} is the drag coefficient ($C_{10} = 1.0 \times 10^{-3}$, Culberson and Piedrahita (1996));

ρ_a is the density of air in kg/m^3 (1.1988 kg/m^3); and

W_{10A} is the adjusted wind speed at 10 m in m/s.

It is widely accepted that turbulence induced by wind shear on the water surface governs the thermal structure of lakes but its relative importance in small ponds is less clear. Wind mixing is inhibited in small ponds due to the restricted fetch of the wind, which effectively lessens the turbulent diffusion. A fetch adjustment parameter (Equation 6.49) that was originally formulated by Henderson-Sellers (1977) has been used in the pond model to modify the wind speed (Equation 6.48) and hence allow for the reduced shear stress at the surface.

$$W_{10A} = f(A)\,W_{10} \tag{6.48}$$

$$f(A) = 1 - \exp(-k\,A) \tag{6.49}$$

where: W_{10} is the wind speed at 10m in m/s;

f(A) is the fetch adjustment parameter (fraction);

A is the pond surface area in m^2; and

k is an empirical constant.

The empirical constant, k, in Equation 6.49 was given a value of $1 \times 10^{-6} m^{-2}$ by Henderson-Sellers (1977). In model simulations however, this value was found to over-estimate the reduction in wind speed. A value of $1 \times 10^{-6} m^{-2}$ was found to provide a more realistic reduction in the wind speed.

6.2.2.3 Convective Mixing

Unlike diffusion, which involves the transfer of heat or salt without a net transfer of water, convection involves a net transfer of water that carries the heat and salt with it, which is a more rapid means of transfer. Convective mixing involves large-scale turbulent effects much larger than the small-scale turbulence induced by the wind above the water surface, hence wind speed is irrelevant in the simulation of convective processes.

Convective mixing occurs when there is a density instability in the water column. It frequently occurs during the night when the pond is cooling. Since heat loss from the pond occurs primarily at the surface, the surface water loses heat first and the greater buoyancy of the underlying water, which is still warmer and therefore less dense, causes vertical mixing. Density is also affected by the salt concentration of the water, therefore convective mixing may also be caused by water of a different salinity. A layer of salty water overlying freshwater for example, can lead to buoyant instability in the water column.

Knowledge of the mean velocity field is required to calculate convection precisely. However in lake temperature models convective mixing is generally simulated more simply, either by numerically averaging the temperature of the adjoining unstable layers or by allowing the effective diffusion coefficient to assume some maximum value when there is a negative downward heat gradient (Losordo and Piedrahita, 1991). In this pond model, the latter technique has been applied, an approach developed by Sundaram and Rehm (1973) and applied successfully in the shallow pond modelling of Losordo and Piedrahita (1991) and Culberson and Piedrahita (1996). Since convective mixing involves a mass transfer of water, the maximum effective diffusion coefficient value was assumed to apply equally to the transfer of salt. The convective transfer of heat and salt are shown by Equations 6.51 and 6.50

$$\frac{dH}{dt} = A\,\phi_{conv,z} = A\,\rho_w\,c_{pw}\,K_{max}\,\frac{dT}{dz} \tag{6.50}$$

$$\frac{dM}{dt} = A\,\Theta_{conv,z} = A\,K_{max}\,\frac{dS}{dz} \tag{6.51}$$

where: S is the concentration of salt in kg/m^3;

M is the mass of salt in kg;

A is the cross-sectional area in m^2;

K_{max} is the maximum value of the effective diffusion coefficient in m^2/h;

H is the heat in J;

ρ_w is the density of water in kg/m^3;

c_{pw} is the heat capacity of water in J/kg/°C; and

T is the water temperature in °C.

The value of K_{max} had to be carefully selected to ensure that the unstable water column was neither over-mixed or under-mixed. Of most importance was the relationship between the value of K_{max}, the depth interval (Δz) and the time step (Δt), which had to be such that the model was not numerically unstable and did not fail to converge. To ensure stability and convergence, the value of λ in Equation 6.52 was best set to a value less than or equal to ½ (Chapra and Canale, 1990). Setting $\lambda > ½$ led to oscillating errors.

$$\lambda = K_{max} \frac{\Delta t}{(\Delta z)^2} \tag{6.52}$$

Values of K_{max} for lakes and reservoirs have ranged from 0.02 to $21.0 m^2/h$ (Losordo and Piedrahita, 1991). In the shallow aquaculture pond modelling of Losordo and Piedrahita (1991) and Culberson and Piedrahita (1996) a value of $0.6 m^2/h$ was found to generate the appropriate degree of mixing of the ponds, and this value was applied in the pond model.

With a K_{max} value of $0.6 m^2/h$ and a depth interval of 0.05m, the maximum time step, in accordance with Equation 6.52 was 0.002 hours. A slightly smaller time step of 0.0014 hours was used in running the model, to ensure numerical stability.

6.2.3 Concrete Heat Transfer

Sedimentation ponds are typically constructed of concrete, which may act as either a source or sink for heat energy in the overlying water. The heat flux between the water at the bottom of the pond and the concrete base of the pond was simulated in the pond model using Equation 6.53. A positive flux value indicated a loss of heat from the water to the concrete, while a negative flux value indicated a transfer of heat from the concrete to the overlying water.

$$\phi_{conc} = k_{conc} \frac{dT}{dz} \tag{6.53}$$

where: ϕ_{conc} is the heat loss to the concrete in $kJ/m^2/h$;

k_{conc} is the thermal conductivity of the concrete in $kJ/m^2/h/m/°C$;

T is the temperature in °C; and

z is the depth in m.

Concrete is a relatively good conductor of heat. Its precise thermal conductivity depends on the mineralogical composition of the aggregate, its density and moisture content (Neville, 1981). In general, the greater the crystallinity of the aggregate, the better the heat conductivity. An aggregate with a high quartz content for example, will have a relatively high conductivity since quartz is highly crystalline. Air is a poor conductor, therefore lightweight or aerated concrete has a lower conductivity than high density concrete. Water however has a higher conductivity than air, so if a lightweight or aerated concrete is saturated its conductivity will increase.

In the pond model a value of $6.85 kJm^{-2}h^{-1}m^{-1}°C^{-1}$ was selected for the thermal conductivity constant, which is the value given by Neville (1981) for a typical normal weight aggregate concrete of density $2240 kgm^{-3}$, which is exposed to moisture. The concrete base of the pond was assumed to have an average thickness of 0.2m and an average temperature of 20°C.

6.3 Model Execution

6.3.1 Construction of the Model in STELLA

The model was constructed using the dynamic simulation software STELLA Research Version 5.0 (High Performance Systems, Inc.). STELLA has a graphical and multi-layered approach to modelling, which simplifies the construction of complex numerical integration problems such as the dynamics of one-dimensional density stratification in a sedimentation pond. It was originally developed for Macintosh computers, but more recent versions have been made available for running in a Windows '95 or Windows NT environment.

The multi-layered framework of STELLA facilitated a top-down approach to modelling – from concept level down to the fine detail. The highest level was the High-level Mapping layer that provided an overview of the whole model. This layer included tools that were used to develop a user-friendly interface that facilitated user interaction with the pond model, although this was not incorporated into the final model due to file size limitations. (The basic overview of the

pond model, illustrating the inter-dependence of the model sectors is contained in Appendix J.)

Below the High-level Mapping later was the Model Construction layer, which consisted of a detailed view of all the processes and variable relationships in the pond model. Another set of tools was provided in the Model Construction layer for construction of the model, and the majority of time was spent in this layer.

The model could also be viewed in the Equations View, which listed all the underlying model equations in the STELLA language. Output from the Equations View showing all the equations of the sedimentation pond model is shown in Appendix K.

The in-built tools and objects in STELLA enabled the sedimentation pond model to be constructed graphically. Tools such as stocks, flows and converters were used to represent the separate entities of the pond system and the relationships that existed between them. In this way, the model structure of the pond system could be conceptualised in its entirety without the distraction of trying to define underlying equations.

Once the model was conceptualised, a mixture of empirical, semi-empirical and analytical equations was then coded into the model in the STELLA language to define the relationships between the variables, and constant values were defined. Figure 6-8 illustrates a part of the pond model as constructed using the tools in STELLA.

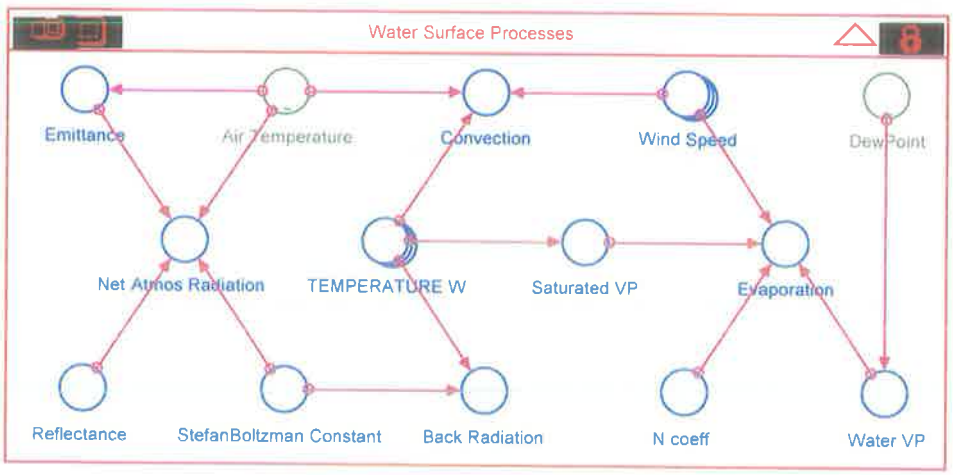

Figure 6-8: One sector of the sedimentation pond model in STELLA

Other model structuring techniques, such as arrays and sub-models that are commonly used in programming with the more traditional languages such as FORTRAN or C were also available in STELLA. Full use was made of these tools to avoid over-complexity of the pond model diagram.

6.3.2 Running the Model in STELLA

The numerical integration was carried out using Euler's method. Although the STELLA software has the capacity to employ more sophisticated 2^{nd} and 4^{th} order Runge-Kutta numerical integration techniques these methods were inappropriate when using the built-in logic functions. Logic functions, such as IF-THEN-ELSE generate integer values (i.e. 0 or 1), which are incompatible with the incremental solving technique of the Runge-Kutta methods. Implementation of the model with a small time step reduces the integration error of the simpler Euler's method.

Like all models, decreasing the magnitude of the time step and depth interval increased the accuracy of the model results, but extended the simulation run time. It could not, however be extended infinitely since STELLA Research 5.0 was limited in the number of iterations that it would perform (a maximum of approximately 30 000).

For simulation of stratification in the Morphett Road Sedimentation Pond, the model was structured to have a depth interval of 0.05m. A time step of 0.0014 hours was selected to ensure convergence and numerical stability in accordance with the convective mixing requirements outlined in Section 6.2.2.3. Hence the length of simulations was limited to approximately 24 hours, which was adequate for analysis of diurnal temperature and salinity fluctuations.

6.3.3 STELLA Output

STELLA incorporates two data output devices – graphs and tables. Any variable can be graphed or tabulated, although too many graphs and table slowed the running of the model. For the analysis of the model output for Morphett Road Sedimentation Pond, the data were plotted in EXCEL from data either directly pasted or linked to STELLA tables. This is illustrated in Figure 6-9, Figure 6-10 and Figure 6-11 for temperature, salinity and density predictions on 11 February 2000.

6.4 Input Data

The time series data were imported into the pond model using STELLA's graphical data input feature, and pond input data were entered directly into the model. The STELLA software had the capacity for linking the model to data input and output files, however the computer's memory (i.e. RAM) constraints and instability of the software limited the model's linking capacity.

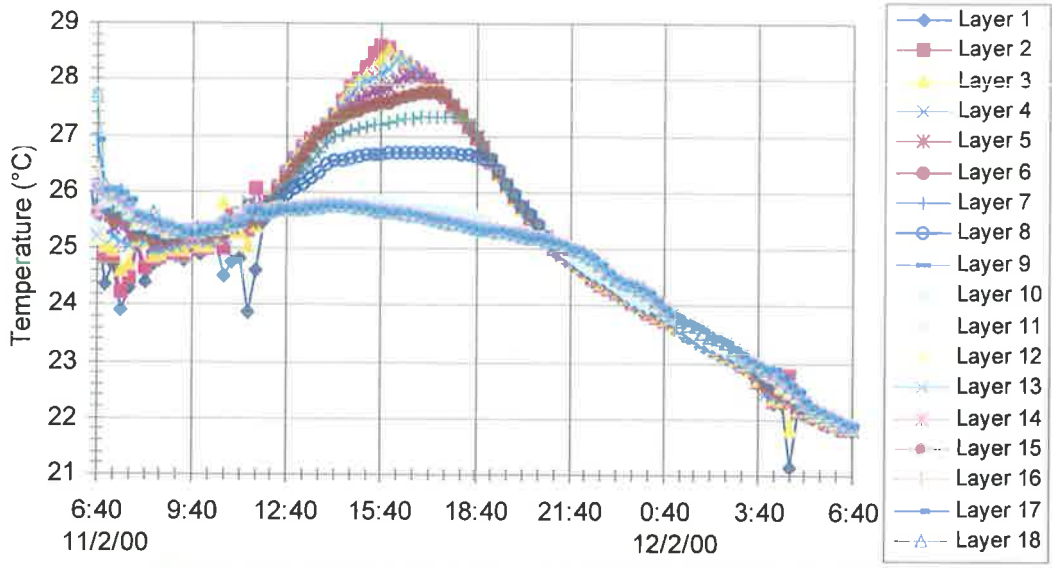

Figure 6-9: Model output of temperature on 11 February 2000

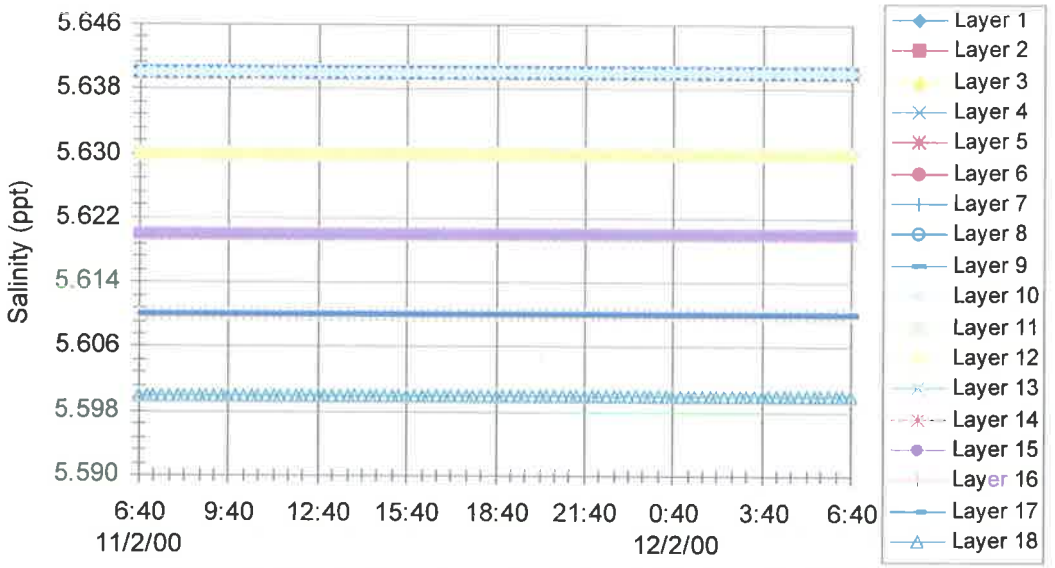

Figure 6-10: Model output of salinity on 11 February 2000

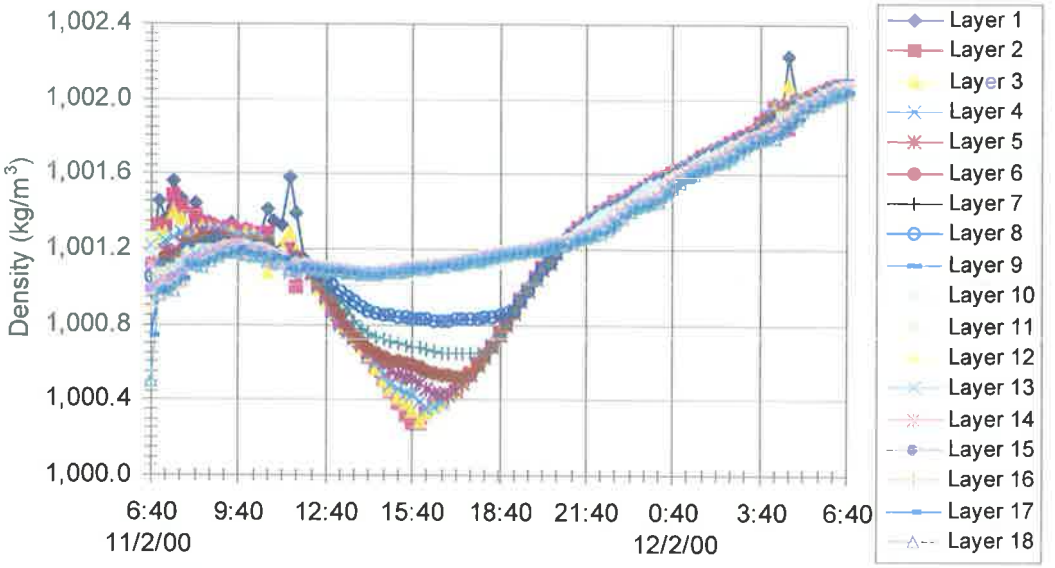

Figure 6-11: Model output of density on 11 February 2000

6.4.1 Time Series Data

The time series input data for the sedimentation pond model consisted of METAR Data (Meteorological Aerodrome Reports) and Solar Exposure Data from the Adelaide Airport Station of the Bureau of Meteorology. The Morphett Road Sedimentation Pond was situated between the Adelaide Airport and the Adelaide Airport Bureau of Meteorology Station.

General Bureau of Meteorology weather observations are made every 3 hours, but METAR weather observations are made half-hourly, specifically for the aviation industry. Although there is less quality control of the METAR data, the greater frequency of the observations was very important for the short-term (e.g. 24 hour) simulations of the sedimentation pond model. Linear interpolation was used to infill any missing data points.

The METAR data used in the sedimentation pond model consisted of wind speed and direction, air temperature and dew point temperature. The observations were reported using Universal Time (UT), which is a sidereal time and hence a measure of the rotation of the earth with respect to the motion of the stars rather than the earth. Equations 6.54 and 6.55 show the timezone and day light savings adjustments that were required for conversion of UT to Central Standard Time (CST) and South Australian Summer Time (SAST).

$$CST = UT + 9.5 \tag{6.54}$$

$$SAST = CST + 1 \tag{6.55}$$

where: UT, CST and SAST are in hours.

6.4.1.1 Air Temperature and Dew Point

Air temperature and dew point temperature were recorded by the Bureau of Meteorology in degrees Celsius and rounded to the nearest degree. Before being input to the sedimentation pond model, the records were converted to Kelvin using Equation 6.56.

$$T_{wK} = T_{wC} + 273 \tag{6.56}$$

where: T_{wK} is the temperature in Kelvin; and

T_{wC} is the temperature in °C.

6.4.1.2 Wind Speed and Direction

Each half-hour observation of wind direction and speed recorded by the Bureau of Meteorology was a mean of all the wind values recorded in the preceding 10 minute period. The mean wind direction was the angle from which the wind was blowing. It was recorded in degrees true and was rounded off to the nearest 10°. The mean wind speed was recorded in knots, and was converted to m/s using Equation 6.57.

$$W_{10k} = W_{10} \times \frac{1}{0.54} \times \frac{1}{3.6} \tag{6.57}$$

where: W_{10k} is the wind speed in knots; and

W_{10} is the wind speed in m/s.

The wind speed was recorded 10m above the ground. However, some of the empirical equations in the sedimentation pond model (e.g. for evaporative heat transfer) required wind speed data from closer to the water surface. A profile of wind speed up to 10m above the surface was determined using Equation 6.58 from Panofsky and Dutton (1984). Figure 6-3 shows the typical decline in wind speed close to the surface of the Morphett Road Sedimentation Pond for different wind speed conditions.

$$\frac{W_{10}}{W_z} = \frac{\ln\left[\frac{10}{z_0}\right]}{\ln\left[\frac{z}{z_0}\right]} \tag{6.58}$$

where: W_{10} is the wind speed at 10m above the surface in m/s;

W_z is the wind speed at zm above the surface in m/s;

z is the height above the surface in m; and

z_0 is the roughness length of the surface.

The wind speed data were corrected for the difference in surface roughness between the flat grassland where the wind was measured and the water surface of the pond. The wind speed is dependent on the roughness of the ground over which the wind is blowing. On a rough surface, such as grassland, there is a transfer of momentum to the ground due to the difference in pressure across the roughness elements, hence the speed of the wind is reduced in comparison to its speed over a smoother surface such as calm water.

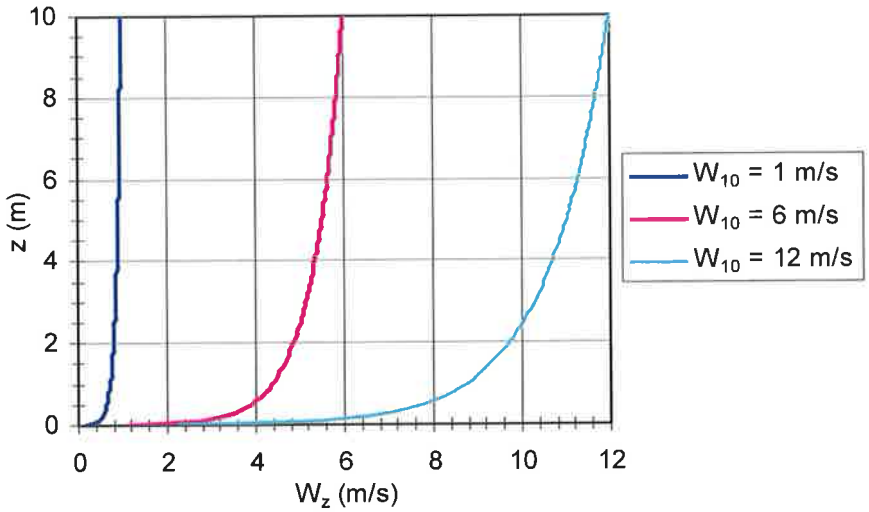

Figure 6-12: Wind speed profiles above the surface of the Morphett Road Sedimentation Pond

The roughness length represents the size of eddies generated at the surface and is an approximate measure of surface roughness. The roughness length has been estimated to be approximately 20cm for the type of grassland terrain where the wind data were recorded, and to vary between 0.01cm and 0.1cm for water, depending on the wind speed, which influences wave action (Panofsky and Dutton, 1984). The wind speeds up as it crosses from the grassland onto the smoother surface of the pond, and continues to increase in speed as it travels further across the water. The wind speed is also therefore dependent on fetch, which was taken to be the upwind distance to the edge of the pond (see Figure 6-13).

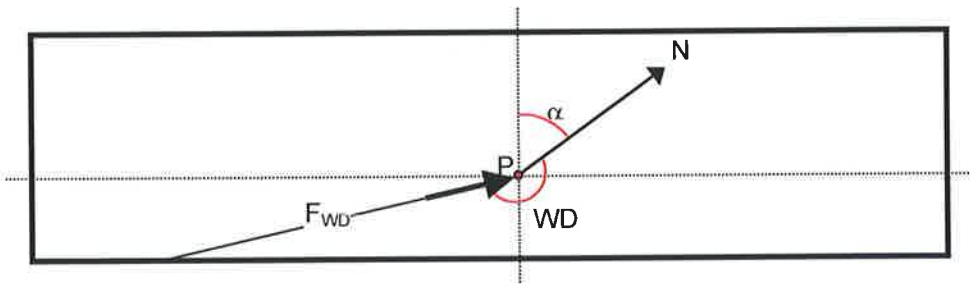

Figure 6-13: The fetch, F_{WD}, for wind of direction WD, measured at a point P in a pond (α is the angle of orientation of the pond)

An EXCEL spreadsheet was used to calculate the increase or decrease in wind speed using Equations 6.59 and 6.60, the formulae recommended by Walmsley (1996). Equation 6.60 was solved iteratively using the Goal Seek function in EXCEL to determine the height of the internal boundary layer, δ.

$$\Delta W_R = \frac{\ln\left(\frac{\Delta z}{z_0}\right)\ln\left(\frac{\delta}{z_{0u}}\right)}{\ln\left(\frac{\Delta z}{z_{0u}}\right)\ln\left(\frac{\delta}{z_0}\right)} - 1 \qquad \text{for } \Delta z < \delta \tag{6.59}$$

$$\Delta W_R = 0 \qquad \text{for } \Delta z \geq \delta$$

$$\frac{r}{z_0} = a\left[\frac{\delta}{z_0}\left(\ln\frac{\delta}{z_0} - 1\right) + 1\right] \tag{6.60}$$

where: ΔW_R is the change in wind speed due to roughness (fraction);

Δz is the height of the wind anemometer in m;

z_0 is the roughness length in m; and

δ is the height of the internal boundary layer in m;

a is a constant (a = 2); and

r is the distance downwind of the roughness change in m.

For simulations of the Morphett Road Sedimentation Pond, the height of the wind anemometer was 10 m (Szkup, 2000).

An adjustment to the wind speed data was also required to correct for the change in terrain between the location of the wind measurement and the Morphett Road Sedimentation Pond as shown in Figure 6-14. The terrain elevation adjustment of the wind speed was calculated using Equation 6.61 from Walmsley (1996).

$$\Delta W_S = B\left(\frac{h}{L}\right)\exp\left(\frac{-A\,\Delta z}{L}\right) \tag{6.61}$$

where: ΔW_S is the change in wind speed due to terrain (fraction);

h and L are in m (see Figure 6-14); and

A and B are terrain dependent parameters.

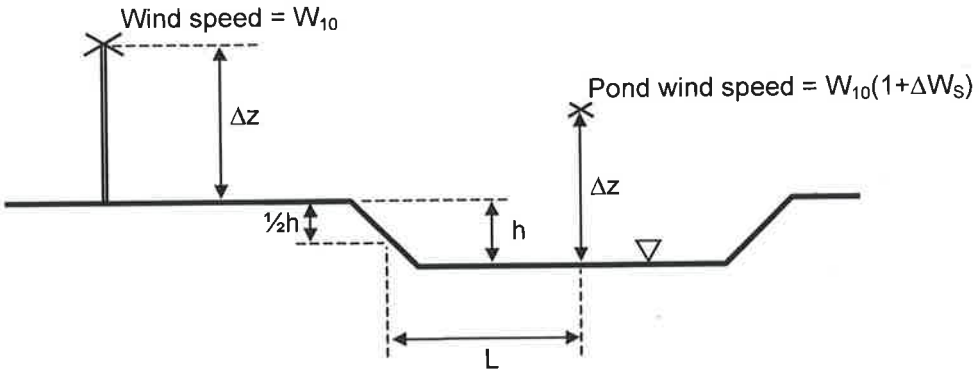

Figure 6-14: Cross-sectional view of the terrain surrounding the pond (not to scale)

The parameters A and B are dependent on the type of terrain (e.g. hill, ridge, escarpment, rolling terrain in two or three dimensions or flat terrain). For the Morphett Road Sedimentation Pond, there was a steep slope on either side of the pond (as shown in Figure 6-14), but the upstream and downstream ends of the pond were not bounded. Each slope was therefore classified as a ridge, which is defined by Linacre (1992) to be high land where the length is at least 10 times the height. The parameters A and B were therefore given the values A = 3.0 and B = 2.0, as defined for two-dimensional hills (ridges) by Walmsley (1996).

Correction of the Bureau of Meteorology Adelaide Airport Station wind speed data for conditions above the surface of the Morphett Road Sedimentation Pond, resulted in wind speed increases of between 0% and 32% due to the change in surface roughness, and wind speed decreases of between 0% and 37% due to terrain effects. The wind speed corrections became less significant with increasing distance (i.e. Δz) above the surface of the pond.

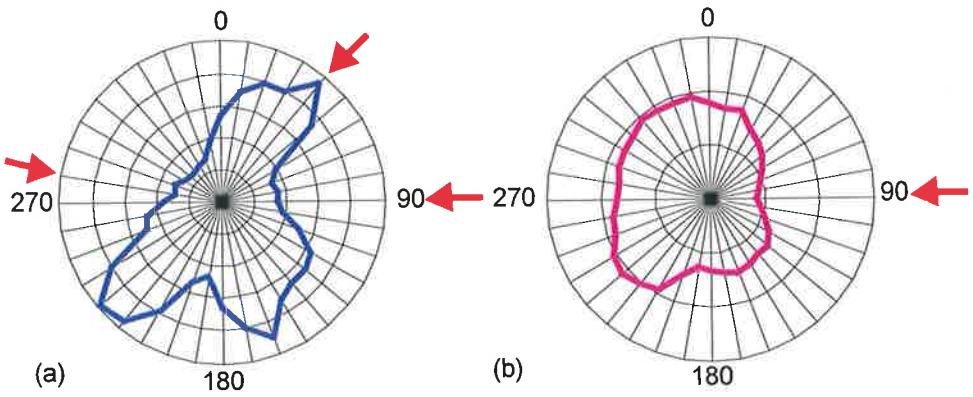

Figure 6-15: For the Morphett Road Sedimentation Pond from March 1999 to April 2000, (a) wind direction frequency, and (b) wind speed (directions are in degrees)

Overall, due to the orientation of the Morphett Road Sedimentation Pond, the greatest decrease in wind speed (37%) occurred when the wind was coming from either 40° or 280°. As can be seen from Figure 6-15, which shows the wind direction frequency and speed for the Morphett Road Sedimentation Pond during the monitoring period, wind from 280° was

relatively rare, but wind was frequently from 40°. The greatest overall increase in wind speed (25%) occurred when the wind was coming from 90° however, as can be seen from Figure 6-15, wind came from 90° infrequently and the average speed of the wind when it did come from 90° was relatively low.

6.4.1.3 Solar Exposure

Solar radiation is generally expressed as either 'irradiance' or 'radiant exposure'. Irradiance is the rate of energy received per unit area and is normally given in units of $J/s/m^2$. Radiant exposure is the time integral of irradiance and is normally given the units of J/m^2. Daily global solar exposure is an example of radiant exposure, and is the total amount of solar energy falling on a horizontal surface in one day. It can be determined from global solar irradiance data that are measured using a pyranometer at the ground or from satellite data.

Ground-based daily global exposure was recorded at the Adelaide Airport Bureau of Meteorology Station from 1983 to 1992 and from 1995 to January 1998. Since December 1990, daily global exposure has been estimated from hourly visible radiation images from Japan's Geostationary Meteorological Satellite, GMS-5. The light intensity of the pixels of the satellite image are analysed to determine irradiance at the top of the atmosphere, which is then modified by the cloud albedo, surface albedo and atmospheric absorption to estimate irradiance at the ground. Figure 6-16 shows a typical comparison of the satellite data with ground-based data for daily global exposure.

The greatest inaccuracies in the satellite-derived data are due to the irregular shape of cloud tops, which leads to variability in reflected irradiance depending on the relative position of the sun and the satellite. There are also inaccuracies in the estimation of atmospheric absorption due to water vapour in the atmosphere. Overall, the Bureau of Meteorology estimates that the satellite-derived daily global solar exposure data are up to 7% inaccurate in clear sky conditions, and up to 20% inaccurate when there is cloud (BOM, 1999a). However the magnitude of the error in cloudy conditions is reduced since less solar radiation actually reaches the ground.

The sedimentation pond model required hourly solar radiation data. Since only daily global solar exposure data were available, a radiation distribution equation from Duffie and Beckman (1980) was applied in the model (Equations 6.62 and 6.64). The equations, which were derived from statistical analysis of the time distribution of total radiation over the day, determines the ratio of total hourly to total daily radiation as a function of the hour in the day and the overall day length. The length of the day, which depended on the pond latitude and sun's declination (see Figure 6-3), was determined from the hour angle at sunset (Equation 6.63), and was assumed to be symmetrical about solar noon.

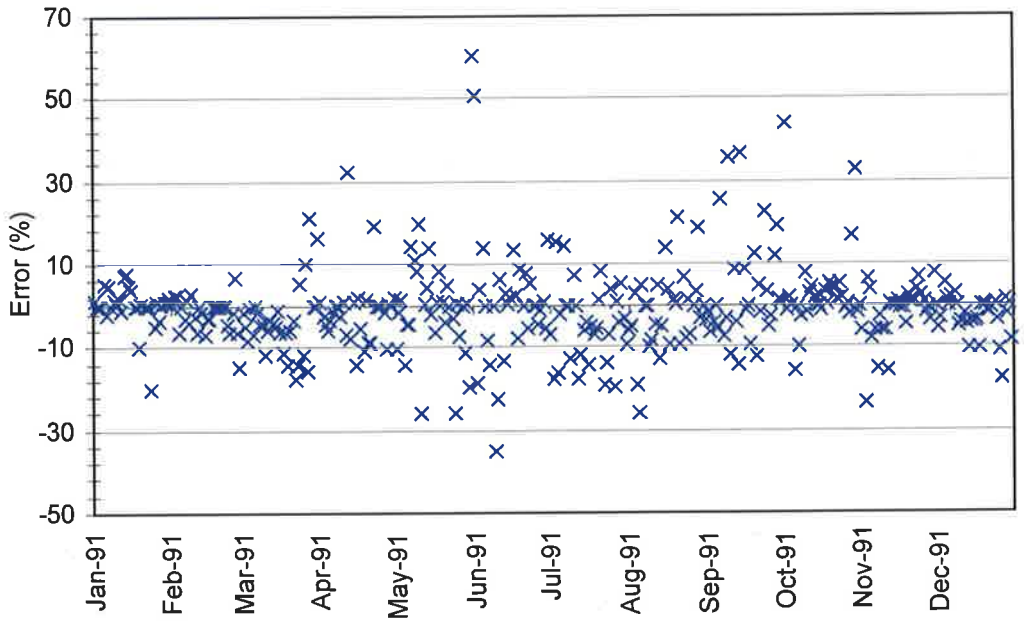

Figure 6-16: An example of the error in satellite-derived daily global exposure records (when compared to ground-based records) for the Adelaide Airport Bureau of Meteorology Station

$$r_t = \frac{\pi}{24}(a + b\cos\omega_s)\frac{\cos\omega - \cos\omega_s}{\sin\omega_s - \frac{\pi}{180}\omega_s\cos\omega_s} \tag{6.62}$$

$$\cos\omega_s = -\tan L\tan\delta \tag{6.63}$$

$$\begin{aligned} a &= 0.409 + 0.5016\sin(\omega_s - 60) \\ b &= 0.6609 - 0.4767\sin(\omega_s - 60) \end{aligned} \tag{6.64}$$

where: ω_s is the hour angle at sunset in °;

δ is the declination of the sun in °;

L is the latitude of the pond in ° (negative in the southern hemisphere); and

a and b are coefficients

$$R_h = r_t \times R_d \tag{6.65}$$

where: R_h is the total global exposure in an hour in kJ/m^2;

R_d is the total global exposure in a day in kJ/m^2; and

r_t is the radiation ratio at time t.

6.4.1.4 Cloud Cover

Direct solar radiation from the sun was the primary source of heat in the sedimentation pond model, with atmospheric radiation contributing a lesser amount, hence, quality solar exposure data were vital for accurate simulation of pond temperature. It is of particular importance for short-term simulations such as those performed in this study (Henderson-Sellers, 1989).

Inaccuracies in solar radiation data are mostly due to differences between the amount of solar radiation emitted by the sun and the amount of solar radiation striking the ground or water surface. The greatest difficulty in estimating ground level solar radiation is in accounting for the atmospheric attenuation due to cloud. Clouds tend to be highly random in atmospheric transmittance, distribution and albedo (Porto, 1993).

Unfortunately, cloud cover observations were unavailable for validation of the model in the Morphett Road Sedimentation Pond. The cloud parameters A and B (see Table 6-1) were defined in the pond model for scattered cloud conditions (10% to 50% cover), which was estimated to be an average for conditions at the site. Sensitivity analysis that was performed to assess the pond model's sensitivity to the cloud conditions that were selected showed that the model was not highly sensitive to alterations in the cloud conditions (see Section 6.6.2.1 for further details).

6.4.2 Pond Characteristics Data

The pond characteristics input data required in the sedimentation pond model included the length, width, depth and orientation of the pond as well as the depth of the concrete base. The sides of the pond although slightly sloping (approximately 45°) were assumed to be vertical for the purposes of one-dimensional prediction of vertical temperature and salinity flux.

The characteristics of the Morphett Road Sedimentation Pond are shown in Figure 6-17. Cross-sectional area and volume were calculated in the pond model using Equations 6.66 and 6.67.

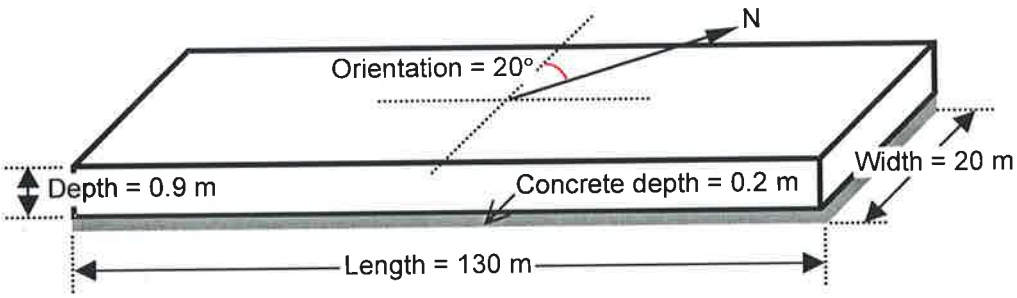

Figure 6-17: The characteristics of Morphett Road Sedimentation Pond

$$A_z = L \times W \tag{6.66}$$

$$V = L \times W \times d \tag{6.67}$$

where: A_z is the cross-sectional area at depth zm in m^2;

L is the length of the pond in m;

W is the width of the pond in m;

V is the volume of the pond in m^3; and

d is the total depth of the pond in m.

Table 6-2: Characteristic information about the Morphett Road Sedimentation Pond

Latitude	34.96°S
Longitude	138.53°E
Time Zone Longitude	142.5°E
Time Zone (CST)*	-9.5 hours
Time Zone (SAST)**	-10.5 hours

* CST – Central Standard Time

** SAST – South Australian Summer Time

Information about the global location of the pond was also required in the pond model. This included the latitude and longitude of the pond as well as the time zone and longitude of the time zone in which it was located. Table 6-2 shows the information that was used in the pond model simulations of the Morphett Road Sedimentation Pond.

6.4.3 Initial Conditions

The initial conditions required to run the pond model included initial temperature and conductivity profiles of the water column, concrete temperature and the SDD percentage. All initial data were incorporated into the STELLA model as one- or two-dimensional arrays.

For the Morphett Road Sedimentation Pond, the initial temperature profile was determined from continuously recorded temperature sensor data. Conductivity profiles and SDD readings were determined from the depth profiling described in Chapter 5. The SDD percentage was the proportion of the pond above the SDD reading (e.g. in a 1m pond with a SDD reading of 0.75, the SDD percentage was 75%).

Since the temperature sensors were positioned at only eight depths in the pond and conductivity readings were taken at just three depths, values at intermediate depths were linearly interpolated to develop full initial temperature and initial conductivity profiles.

SDD readings in the Morphett Road Sedimentation Pond were not significantly variable during each day of depth profiling, hence the mean daily SDD was used to determine the SDD percentage in the pond.

6.5 Model Testing and Validation

The pond model predictions were compared with temperature data recorded in the Morphett Road Sedimentation Pond in January, February and March of the year 2000. Conductivity and SDD data recorded during the depth profiling were used to determine the initial conditions. The temperature monitoring and depth profiling have already been described in Chapter 5.

Figure 6-18, Figure 6-19 and Figure 6-20 provide comparisons between the temperature data with the results of the 24 hour model simulations for 10 of the days of depth profiling. (The logger failed to record temperatures in the pond from 18 January 2000 to 20 January 2000, so these days were omitted from the comparisons despite the availability of conductivity and SDD data from the depth profiling.) Figure 6-18 illustrates the temperature stratification and Figure 6-19 illustrates the mean temperature. (Although not directly relevant to the analysis of pond stratification, the mean pond temperature is still of importance in assessing the accuracy of the model.) Figure 6-20 illustrates the surface and bottom temperatures in the pond.

The maximum stratification and maximum mean pond temperature predicted by the model on these days and the actual values that were observed in the pond, as well as the times at which the maximum values occurred are summarised in Table 6-3.

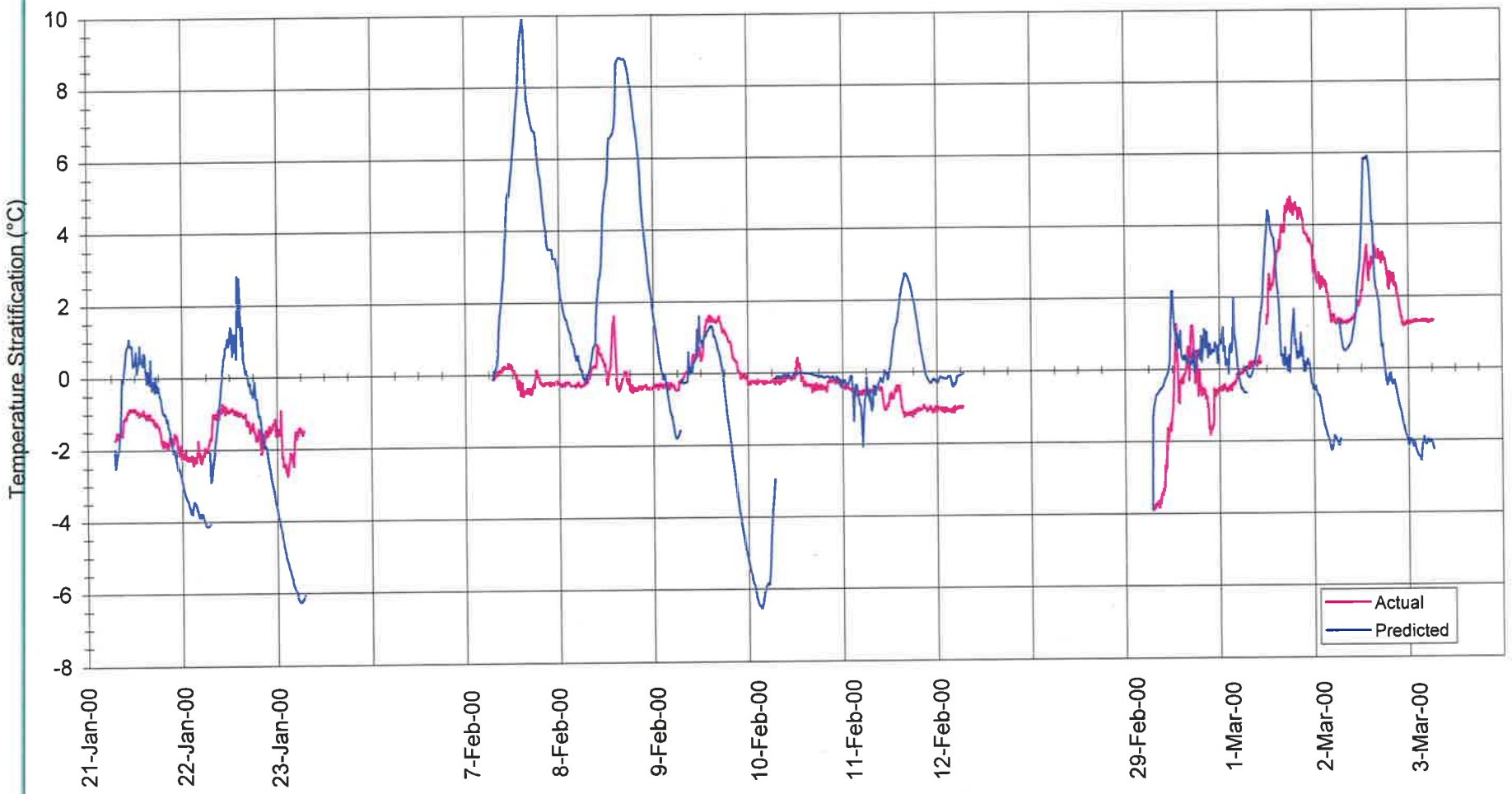

Figure 6-18: A comparison of actual temperature stratification recorded in the Morphett Road Sedimentation Pond with the values predicted by the model on 10 of the days of depth profiling

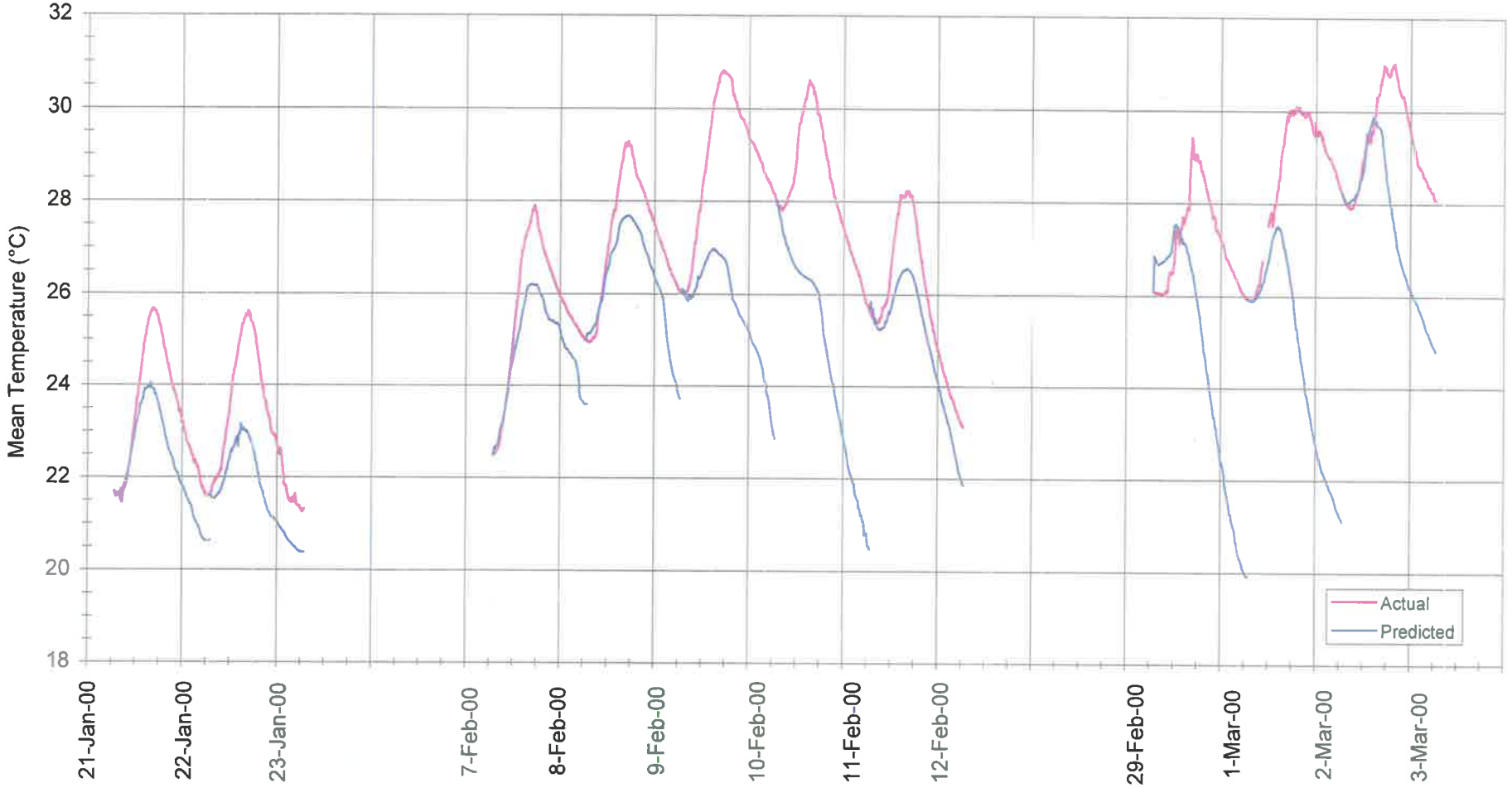

Figure 6-19: A comparison of actual mean temperature recorded in the Morphett Road Sedimentation Pond with the values predicted by the model on 10 of the days of depth profiling

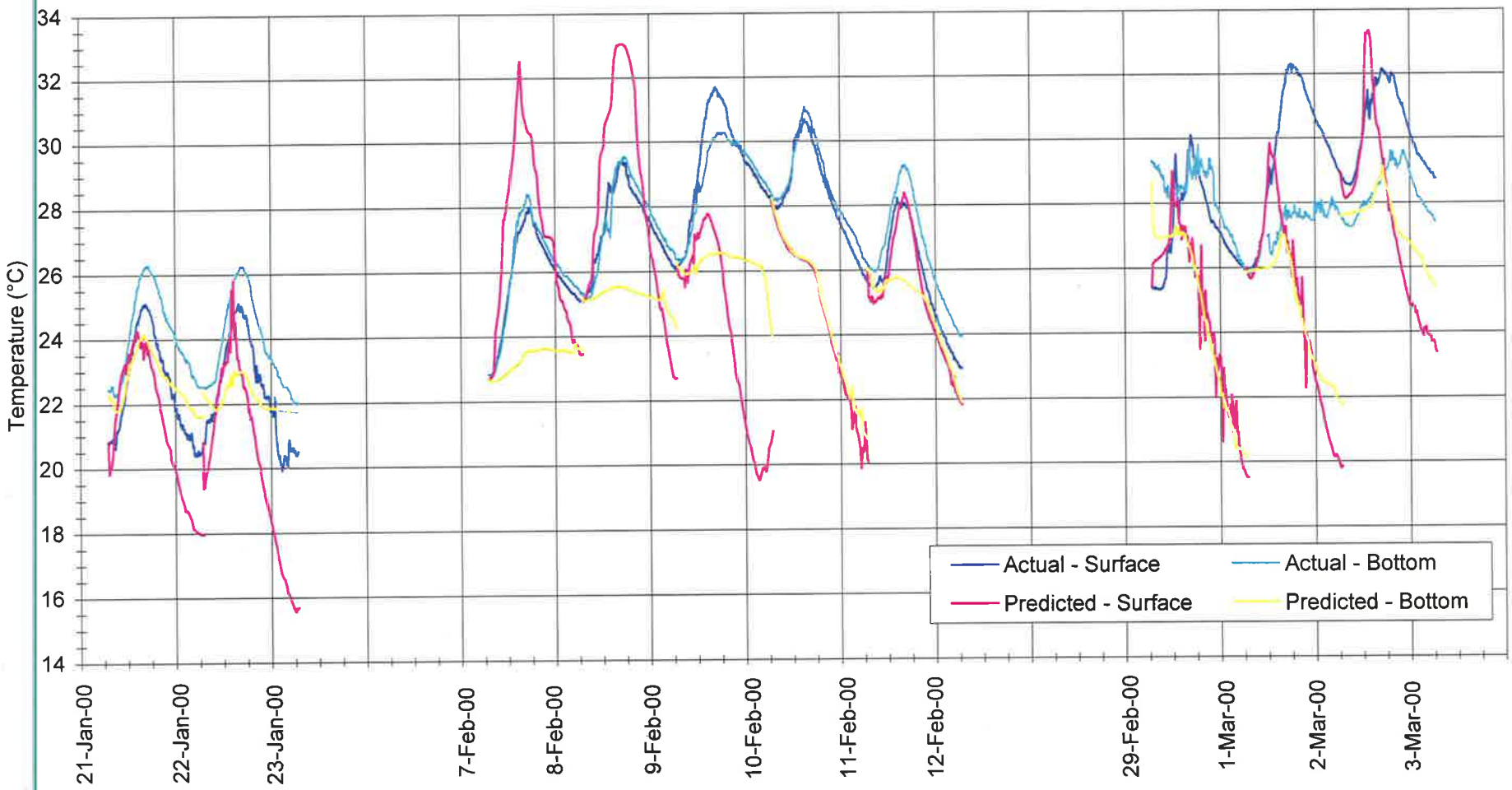

Figure 6-20: A comparison of surface and bottom temperatures recorded in the Morphett Road Sedimentation Pond with the values predicted by the model on 10 of the days of depth profiling

Table 6-3: Comparison of the maximum stratification and mean pond temperature predicted by the sedimentation pond model with actual values observed in the Morphett Road Sedimentation Pond (figures in brackets are the time of day at which the maximum value was predicted or occurred)

DATE	MAXIMUM STRATIFICATION		MAXIMUM MEAN POND TEMPERATURE	
	ACTUAL	PREDICTED	ACTUAL	PREDICTED
21 January 2000	-0.87°C (10:45)	1.07°C (10:30)	25.66°C (16:20)	24.04°C (16:00)
22 January 2000	-0.75°C (10:10)	2.81°C (14:04)	25.61°C (16:40)	23.15°C (14.49)
7 February 2000	0.31°C (11:10)	9.88°C (15:00)	27.89°C (17:20)	26.19°C (16:45)
8 February 2000	1.60°C (14:00)	8.78°C (15:48)	29.27°C (17:10)	27.67°C (17:10)
9 February 2000	1.60°C (14:10)	1.59°C (11:34)	30.80°C (17:20)	26.97°C (14:57)
10 February 2000	0.40°C (12:40)	0.00°C (13:19)	30.60°C (15:10)	28.01°C (7:04)
11 February 2000	-0.39°C (14:10)	2.74°C (16:10)	28.23°C (16:20)	26.55°C (16:03)
29 February 2000	1.25°C (13:00)	2.17°C (12:04)	29.41°C (16:40)	27.54°C (12:34)
1 March 2000	4.77°C (18:10)	4.40°C (12:25)	30.09°C (19:00)	27.50°C (14:18)
2 March 2000	3.41°C (15:30)	5.89°C (13:45)	31.01°C (19:50)	29.87°C (14:30)

The sedimentation pond model predicted minimal stratification (less than 2°C) on 3 of the 10 days, which concurred with the pond temperature observations. Stratification of more than 2°C was predicted by the model on the other 7 days although it was observed on only 3 of these days. The error in prediction was primarily due to under-estimation of the amount of heating of the bottom layer, although on 2 days there was also a significant over-estimation of heating of the surface layer.

The magnitude of the diel peak temperature stratification of the pond was generally over-estimated, with a mean difference of 2.8°C. Under-estimation of diel peak pond stratification was only ever slight, ranging from -0.40°C to -0.01°C. Over-estimation of diel peak pond stratification was between 0.92°C and 3.56°C on 5 days but was extremely high on 7 February 2000 (9.57°C) and 8 February 2000 (7.18°C). On these days, there was a significant over-estimation of the amount of heating of the surface water as well as an under-estimation of the heating of the bottom layer.

There was a mean difference of 54 minutes between the time at which peak diel stratification was predicted and the time at which it occurred. On 5 days the sedimentation pond model predicted the peak in stratification would be earlier than when it actually occurred in the pond (Range: 56 minutes – 5 hours and 45 minutes). On the other 5 days the prediction of peak stratification was later than its actual occurrence in the pond (range: 39 minutes – 3 hours and 54 minutes).

The predicted peak in mean pond temperature was consistently below the actual peak in the mean temperature of the pond on each day. The mean displacement between the maximum mean temperature predicted by the model and the maximum mean temperature that was observed was 2.1°C (range: 1.14 – 3.83°C).

The time of day at which the mean pond temperature was predicted to reach a peak was consistently earlier than when it actually occurred in the pond. On average the sedimentation pond model predicted the mean pond temperature would peak 2 hours and 46 minutes before it was observed to occur in the pond (range: 0 – 8 hours and 6 minutes).

The peak in pond stratification always preceded the peak in mean pond temperature by an average of 3 hours and 49 minutes (Range: 50 minutes – 6 hours and 30 minutes). Peak diel stratification occurred between 10:10AM and 6:10PM while the time of day at which the mean temperature peaked ranged from 3:10PM to 7:50PM.

Overall, for the 10 days of depth profiling in the Morphett Road Sedimentation Pond, the accuracy of the model was somewhat variable – sometimes under-estimating and sometimes over-estimating the mean pond temperature and degree of temperature stratification, and the times at which they occurred. In general, the sedimentation pond model over-estimated the

degree of stratification, but under-estimated the mean pond temperature and predicted that it would reach a peak earlier than when it actually did reach a peak in the pond.

The extremely high pond salinity during the 10 days of depth profiling may have led to inaccuracies in the model predictions. (The salinity of the Morphett Road Sedimentation Pond is described in Chapter 5.) Salinity was not expected to be an important factor in modelling concrete based sedimentation ponds inland from the sea. Modelling the density stratification behaviour of a pond affected by temperature and salt dynamics is much more complex than modelling the behaviour of a freshwater pond where density is a function of temperature alone. As explained in Section 6.2.2, temperature and salt can have opposing effects on the density leading to convective diffusion, which alters the vertical mixing that occurs in the pond. Although the model was extended to simulate mass transfer of salt through the depth of the pond, convective mixing was assumed to be negligible, no allowance was made for evaporation and the rate of diffusion was assumed to be identical to the rate of diffusion of heat (see Section 6.2.2.2). Incorporating these factors into the model might lead to improvements in the accuracy of simulations.

The discrepancy in timing and the under-estimation of mean pond temperature might also have been caused by the high banks on either side of the pond and the bridge at one end, all of which provided significant shading of the water, particularly early and late in the day. This was not taken into account in the model calculations.

Also incorporated into the pond model were a number of empirical and semi-empirical constants. The relevant literature was reviewed to determine the value to assign to each constant based on existing research, but many had never before been tested for Adelaide's Mediterranean climate or latitude or had not been applied in modelling shallow or small sedimentation ponds. The following section describes the model's sensitivity to the values that were assumed for these constants.

6.5.1 Model Sensitivity

Sensitivity analysis was performed to test the sensitivity of the pond model to the convective mixing, molecular diffusion and eddy diffusion coefficient constants and the fetch adjustment factor, which all influenced the rate of inter-layer heat and salt transfer, and the solar radiation absorption constant, which affected the amount of heat input to each layer.

The sensitivity analysis of each constant has been illustrated by the results for 11 February 2000. Figure 6-21 shows the comparison between the temperature predicted by the model and the actual temperature recorded by the temperature sensors on 11 February 2000. (11

February 2000 was chosen since the accuracy of model predictions for that day were close to the average accuracy of the model predictions over all the days of depth profiling.)

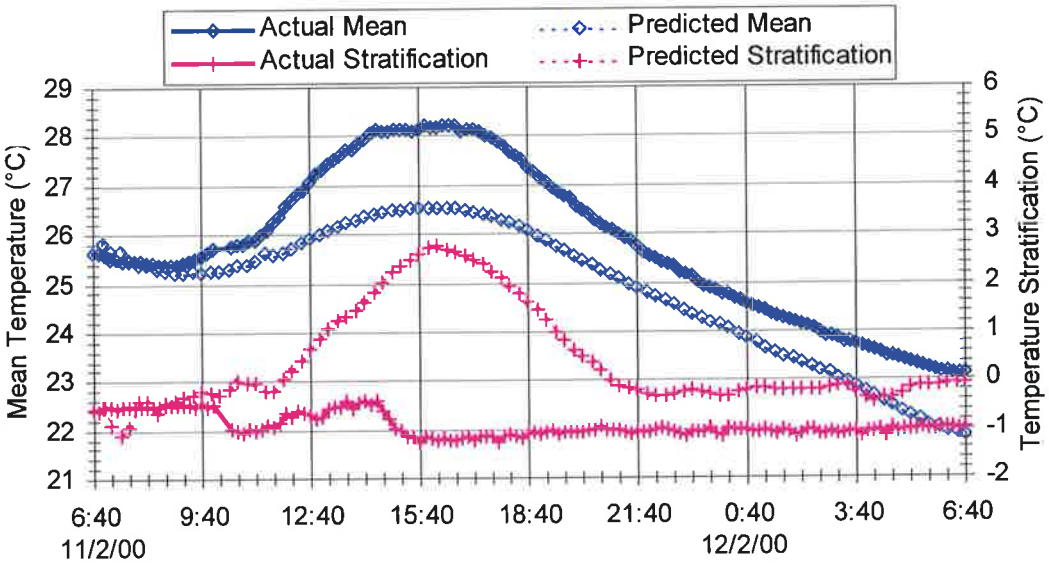

Figure 6-21: A comparison of the predicted and actual mean pond temperature and temperature stratification in the Morphett Road Sedimentation Pond on 11 February 2000

An outline of the process by which a value for each variable was selected has already been given in previous sections that describe the design of the model (see Section 6.2). In the sensitivity analysis, each variable was generally adjusted by ±10% and/or to the minimum or maximum values that have been applied in other studies that were reviewed (the specific basis for the change of each variable is described below). A summary of the sensitivity results is shown in Table 6-4. (Graphs illustrating the sensitivity of each variable are contained in Appendix L.)

The value of the molecular diffusion coefficient had relatively little impact on the sedimentation pond model's performance. Increasing the value of the molecular diffusion coefficient to $1.4 \times 10^{-7} m^2/s$, the maximum value generally used in diffusion simulations led to a decrease in mean stratification predictions of less than 0.01°C. Even a massive ten-fold increase in the value of the molecular diffusion coefficient (to $1.2 \times 10^{-6} m^2/s$) only led to a 0.12°C decrease in mean stratification, and the resulting prediction was still in excess of the actual mean temperature stratification observed in the pond. Ignoring the molecular diffusion coefficient altogether (i.e. setting it to $0 m^2/s$) led to an increase in the mean temperature stratification over the 24 hours of only 0.05°C.

The sensitivity of the pond model to the eddy diffusion coefficient parameters σ and n (see Equation 6.36) had a slightly bigger impact on the accuracy of the model. Increasing the value of σ and n to the values used by Munk and Anderson (1948) increased the magnitude of the error in prediction. However, when the value of σ was instead reduced to 0.05, which was one

of the modifications made by Culberson and Piedrahita (1996) on the Losordo and Piedrahita (1991) model, there was an improvement in model predictions. The prediction of mean pond temperature was increased by 0.07°C and the prediction of mean temperature stratification was decreased by 0.3°C.

Table 6-4: Sensitivity of the pond model simulations for 11 February 2000 to changes in the model constants (the changes in mean pond temperature and temperature stratification represent the mean change over the 24 hours of simulation)

VARIABLE	VARIABLE ADJUSTMENT	MEAN POND TEMPERATURE	TEMPERATURE STRATIFICATION
Convective Mixing Coefficient	0.02m^2/h (min.)	+0.38°C	-0.97°C
	0.54m^2/h (-10%)	-0.02°C	+0.02°C
	0.66m^2/h (+10%)	+0.04°C	+0.02°C
	21.0m^2/h (max.)	–	–
Molecular Diffusion Coefficient	0m^2/s (min.)	-0.01°C	+0.05°C
	$1.4 \times 10^{-7}$$m^2$/s (max.)	+0.003°C	-0.002°C
	$1.2 \times 10^{-6}$$m^2$/s (×100)	-0.01°C	-0.12°C
Eddy Diffusion Coefficient Constants	σ=0.05, n=1*	+0.07°C	-0.30°C
	σ=3.33, n=1.5**	-0.39°C	+0.10°C
Fetch Adjustment Factor	5×10^{-5} (-50%)	-0.10°C	+0.29°C
	9×10^{-5} (-10%)	-0.01°C	+0.09°C
	1.1×10^{-4} (+10%)	+0.03°C	-0.07°C
	1.5×10^{-4} (+50%)	+0.15°C	-0.47°C
Solar Radiation Absorption Constant	1.16 (min.)	-0.23°C	-0.23°C
	2.30 (max.)	+0.11°C	+0.20°C

*values used by Culberson and Piedrahita (1996)

** values used by Munk and Anderson (1948)

Unfortunately however, although the reduction in σ improved the mean predictions of mean pond temperature and stratification by producing a higher rate of diffusion, it enhanced the occasional oscillations in predicted stratification. The oscillations occurred when there was a switch between diffusion and convective mixing from one layer to the next and/or one time step to the next, and were due to differences between the rates of diffusion and convective

mixing. Manipulation of the time and depth interval and value of K_{max} (the value given to the eddy diffusion coefficient during convective mixing) within the appropriate limits (see Equation 6.52 in Section 6.2.2.3) may have eliminated the numerical instability. However the complex structure of the model in STELLA made alteration of the depth interval too time consuming to undertake further analysis in this study.

The sedimentation pond model was very sensitive to the value of the convective mixing coefficient. Values of K_{max} have ranged from 0.02 to 21.0m^2/h for lakes and reservoirs (Losordo and Piedrahita, 1991). When K_{max} was reduced to the minimum value of 0.02m^2/h in the pond model, the model predictions improved. The mean bottom temperature increased by 0.86°C and the mean surface temperature decreased marginally by 0.11°C leading to a decrease of 0.97°C in the mean magnitude of stratification over 24 hours. Overall the mean pond temperature increased by 0.38°C. Increasing K_{max} by 10% reduced the error in prediction of the mean pond temperature but increased the error in prediction of temperature stratification. Increasing K_{max} to the maximum value of 21.0m^2/h led to numerical instability.

The sedimentation pond model was also very sensitive to the value of the fetch adjustment factor that was used. The fetch adjustment factor was included in the pond model to account for the small surface area of ponds in comparison to lakes, reservoir and oceans (see Equation 6.49)

Reducing the value of the fetch adjustment factor increased the error in the model predictions. However increasing the value of the fetch adjustment factor improved the model predictions. When the value was raised by 10% to 1.1×10^{-4} there was a decrease of 0.07°C in the predicted mean temperature stratification and raising the value by 50% to 1.5×10^{-4} led to a 0.47°C decrease in the prediction of mean temperature stratification over the 24 hours. Mean pond temperature predicted by the pond model rose by 0.15°C. However, although increasing the value of the fetch adjustment factor reduced the error in stratification prediction, it led to the same sort of oscillatory behaviour that occurred when the eddy diffusion coefficient parameter σ was reduced, as described earlier.

The pond model was only moderately sensitive to the value of the solar radiation absorption constant (see Equation 6.30). In the pond model the constant was assigned a value of 1.7, although in the past it has been given values ranging from 1.16 to 2.3 (Davies-Colley and Vant, 1988). When the value of the constant was reduced, the error in prediction of mean temperature stratification improved, but the error in mean pond temperature increased. Conversely, when the value of the constant was increased, the error in prediction of mean pond temperature improved, but the error in prediction of mean temperature stratification increased.

6.5.2 Accuracy of the Sedimentation Pond Model

The results of the test simulations and sensitivity analysis clearly show that further work is needed to refine the sedimentation pond model if it is to be used to predict the specific magnitude and precise timing of stratification in the Morphett Road Sedimentation Pond. The inconsistencies were believed to be due to the powerful density effects of high summer salinity levels in the Morphett Road Sedimentation Pond.

Salinity gradients were not expected to be an important issue in modelling stratification in sedimentation ponds, because they are usually assumed to be freshwater environments. Hence the sedimentation pond model was initially expected to be primarily a temperature stratification model. Although due to increasing salinisation of many inland waterways the additional salinity sector was developed. However the salinity sector was intended to account for minor salinity increases that affected the whole water column equally, extreme water column gradients in the salinity were not anticipated. It was not until unusual temperature fluctuations were observed in the temperature monitoring results from the Morphett Road Sedimentation Pond, that it was suspected that salinity was influencing the density structure of the pond. This was confirmed by the results of the depth profiling of conductivity in the Morphett Road Sedimentation Pond, which showed salinity gradients of up to 7980μS/cm and surface salinity fluctuations of as much as 4295μS/cm in less than half a day.

It is only speculated that salinity gradients were responsible for the imprecision of the model in predicting the specific magnitude and timing of stratification in the Morphett Road Sedimentation Pond. It is a reasonable assumption given the satisfactory performance of the basic temperature stratification model of Losordo and Piedrahita (1991) and Culberson and Piedrahita (1996) in numerous ponds around the world (see Section 2.3.5). Nonetheless, the theory can only be verified by further testing of the sedimentation pond model in freshwater pond environments.

Fortunately, prediction of the precise magnitude and timing of stratification was not the primary goal in developing the model. Rather, the model was intended to be used as a tool to investigate the underlying causes of stratification in sedimentation ponds and the impact of meteorological and pond conditions and pond design factors on stratification behaviour. Hence experimentation with the model was still of relevance, and has been described for the Morphett Road Sedimentation Pond in the remainder of this chapter.

6.6 Evaluation of Stratification in the Morphett Road Sedimentation Pond

The model output was first analysed to determine the primary components of the heat energy flux in the pond. Simulations were then performed to assess the sensitivity of stratification to input variables, including meteorological conditions (e.g. solar radiation, cloud cover, air and dew point temperatures, and wind speed and direction), pond clarity and pond characteristics (e.g. pond base characteristics, and pond size and shape).

6.6.1 Heat Energy Flux

Fluctuations in energy flux were generally greatest at the air-water interface (i.e. surface layer) of the pond. Figure 6-22 shows the total heat energy flux over 24 hours predicted by the pond model at the surface, middle and bottom of the pond on 11 February 2000. (The energy flux components that are shown for each layer in Figure 6-22 are illustrated in Figure 6-23.)

Energy input to the pond was highest at the surface and decreased with depth due to the attenuation of light by the water. Loss of heat energy from the pond was also highest at the water surface. On 11 February 2000, heat loss from the water surface was relatively constant over 24 hours. The amount of heat lost from the water to the concrete base of the pond was less significant than the heat lost at the water surface, being equivalent to about 10% of the surface heat loss on average (range: 4 – 14%).

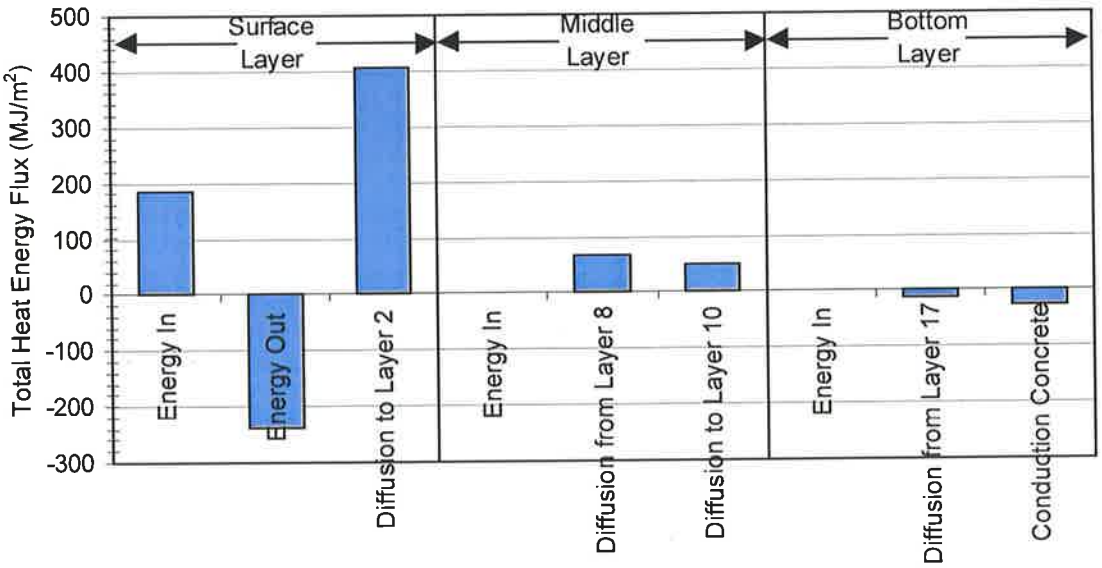

Figure 6-22: The total heat energy flux over 24 hours for the surface (layer 1), middle (layer 9) and bottom (layer 18) on 11 February 2000

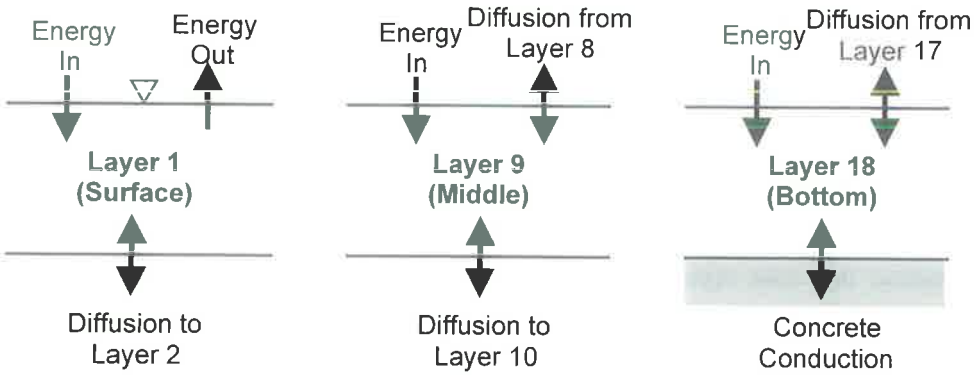

Figure 6-23: Energy flux components of the surface, middle and bottom layers of the pond

The total flux of energy within the pond (i.e. the inter-layer energy flux) was much greater than the loss or gain of heat to the atmosphere or the concrete bottom of the pond. The inter-layer energy flux also fluctuated much more significantly during the 24 hours. This is illustrated for the middle layer (layer 9) of the pond in Figure 6-24.

The internal energy exchange was due to diffusion or convective mixing of heat between the layers of the pond, and was a function of the temperature gradient and the eddy diffusion coefficient. When the pond temperature was increasing, the eddy diffusion coefficient was primarily dependent on wind conditions and the density gradient. However, when the pond temperature was decreasing and convective mixing was presumed to dominate a constant value was assumed for the eddy diffusion coefficient. The use of an appropriate constant value for the eddy diffusion coefficient inhibited generation of large energy diffusion fluxes during pond cooling. Therefore the largest fluctuations in diffusion occurred from shortly before sunrise to around noon, when the pond temperature was increasing. Diffusion was more stable when the pond was cooling.

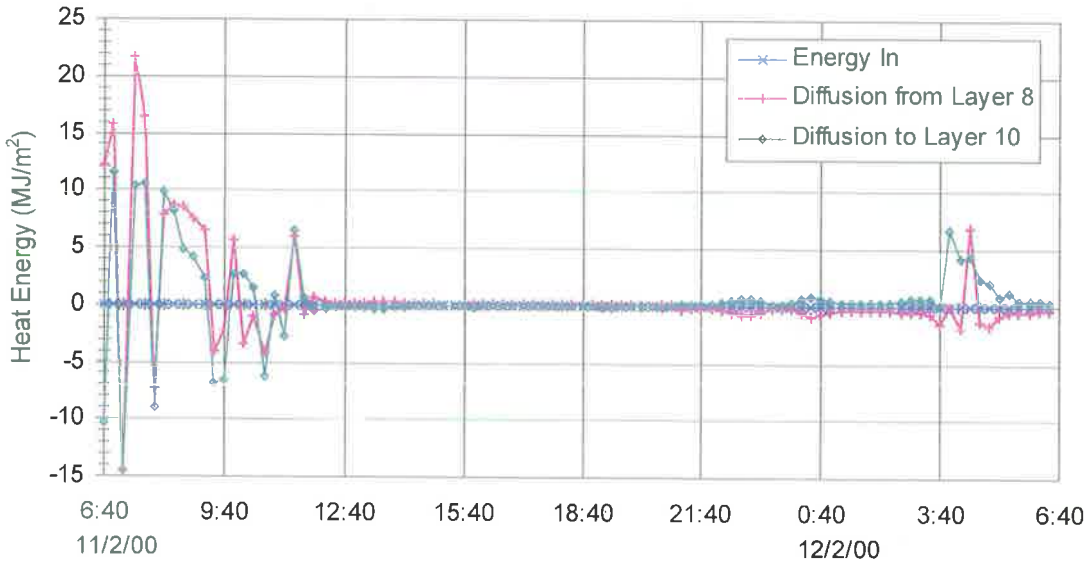

Figure 6-24: Middle layer (layer 9) energy flux on 11 February 2000

6.6.1.1 Surface Energy Flux Components

The major heat inputs and outputs to the pond occurred at the air-water interface. The surface flux components included penetrating solar radiation, net atmospheric radiation, back radiation, evaporation and convection. Figure 6-25 illustrates the relative magnitude of the surface energy flux components on 11 February 2000, and Figure 6-26 illustrates the variability in each flux component over the 24 hours.

Penetrating solar radiation (incoming shortwave solar radiation minus the reflected portion) was the biggest source of heat energy input to the pond. It was also the most variable over 24 hours, increasing from 0 at sunrise to a maximum at solar noon then decreasing to 0 again by sunset. Total pond energy input due to net atmospheric radiation over the 24 hours was almost equal to the total energy from the penetrating solar radiation, but was relatively stable over the 24 hours. Net atmospheric radiation was the only source of heat energy during the night.

Back radiation of heat from the pond was also relatively stable over the 24 hours. The amount of heat lost from the pond through back radiation was always slightly greater than the amount of heat contributed to the pond through net atmospheric radiation. Evaporative energy losses were quite variable, primarily due to changes in wind speed, although fluctuations in air and dew point temperature also influenced the evaporation. Loss of heat from the pond due to convection was relatively minor.

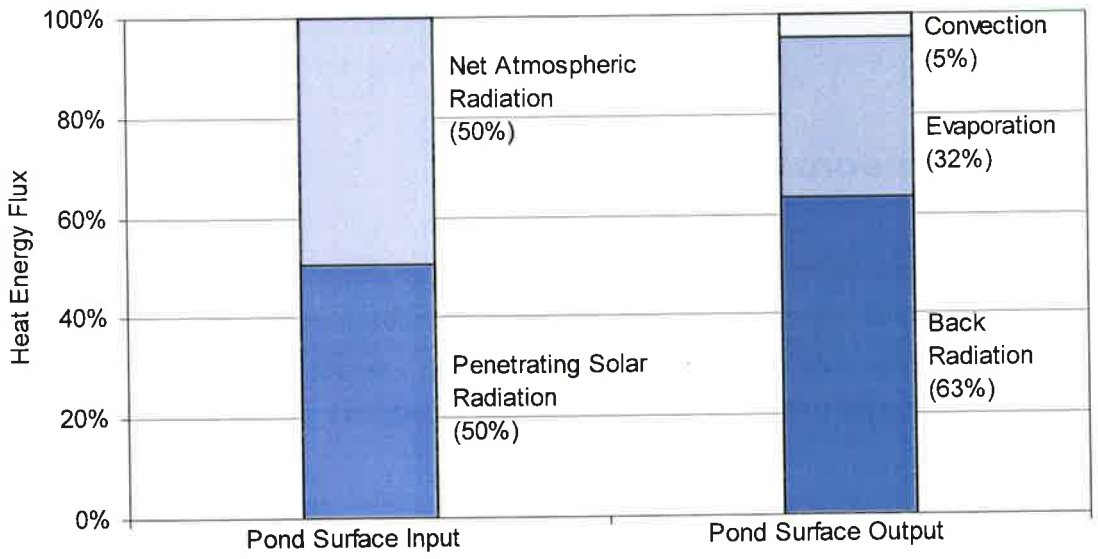

Figure 6-25: The relative magnitude of the surface energy flux components on 11 February 2000

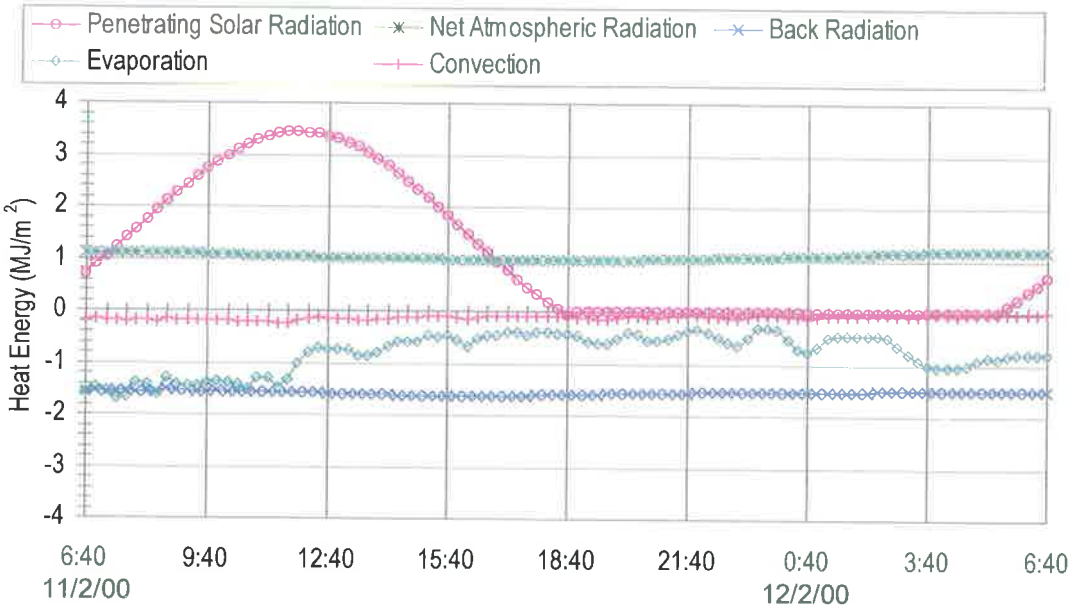

Figure 6-26: Components of surface layer (layer 1) energy flux on 11 February 2000

6.6.2 Stratification Sensitivity

Simulations were performed to assess the pond's sensitivity to input variables including meteorological conditions (solar radiation, cloud cover, air temperature, dew point temperature, wind speed and direction), water clarity (SDD) and pond characteristics (concrete thickness, pond dimensions). The results of the sensitivity analysis are summarised in Table 6-5.

6.6.2.1 Meteorological Data

The quality of the meteorological input data has been said to have a more profound impact on the accuracy of one-dimensional thermal stratification models than the model algorithm itself (Porto, 1993). The sensitivity analysis confirmed that accurate meteorological data was essential for accurate simulation of the mean pond temperature and degree of temperature stratification.

Air temperature and dew point temperature had the biggest impact on the 24 hour mean values of mean pond temperature and temperature stratification (see Figure 6-27 and Figure 6-28). The temperature affects were most noticeable at the surface of the pond, where atmospheric radiation, evaporation and convection took place.

Table 6-5: Sensitivity of the pond model simulations for 11 February 2000 to changes in the input variables

VARIABLE	VARIABLE ADJUSTMENT	MEAN POND TEMPERATURE*	TEMPERATURE STRATIFICATION*
Solar Radiation	-20 %	-0.74°C	-0.41°C
	-10 %	-0.38°C	-0.16°C
	+10 %	+0.37°C	+0.19°C
	+20 %	0.75°C	+0.41°C
Cloud Cover	Clear	-0.07°C	-0.04°C
	Broken Clouds	+0.01°C	+0.02°C
	Overcast	+0.16°C	+0.09°C
Air Temperature	-10 %	-2.31°C	-0.66°C
	+10 %	+3.11°C	+2.03°C
Dew Point Temperature	-10 %	-0.67°C	-0.17°C
	+10 %	+4.02°C	+0.98°C
Wind Speed	-10 %	+0.23°C	+0.27°C
	+10 %	-0.19°C	-0.26°C
Wind Direction	Reversal	+0.05°C	-0.10°C
SDD	0.81 m	+0.05°C	+0.07°C
	0.45 m	+0.17°C	+0.37°C
	0.09 m	+0.18°C	+0.40°C
Concrete Thickness	0.1 m	-0.41°C	+0.19°C
	0.3 m	+0.21°C	-0.08°C
	0.4 m	+0.33°C	-0.13°C
Pond Dimensions	65 × 20 × 2	+1.31°C	+0.09°C
	(130 × 20 × 2)	(+1.57°C)	(-0.13°C)

*Mean change over 24 hours

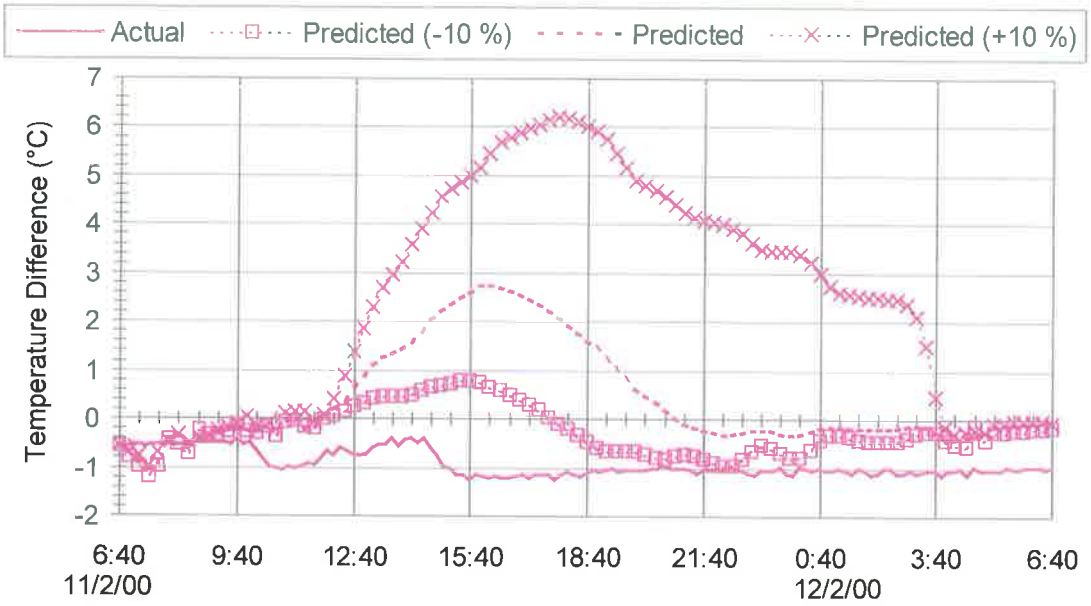

Figure 6-27: Sensitivity of the mean temperature stratification to changes in air temperature for 11 February 2000

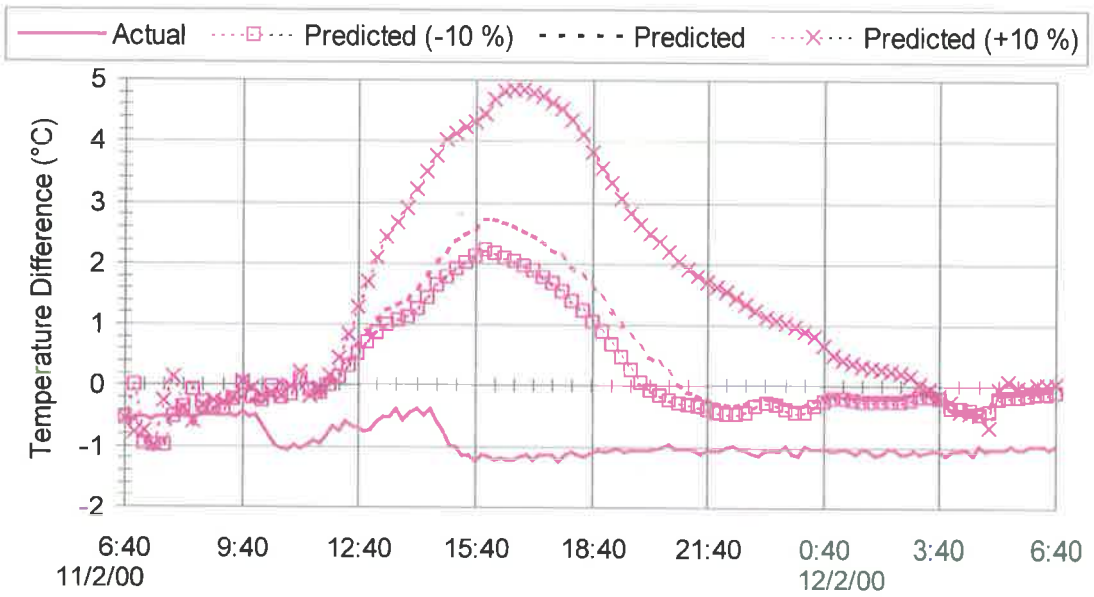

Figure 6-28: Sensitivity of the mean temperature stratification to changes in dew point temperature for 11 February 2000

The pond temperature stratification was most sensitive to the air temperature. A hypothetical 10% rise in air temperature produced a 2.03°C increase in temperature stratification over 24 hours and a dramatic increase in the duration of stratification. The change in air temperature affected the atmospheric radiative heat input at the surface of the pond, which was a major source of heat for the pond. While it also influenced the convective heat exchange at the surface, the overall magnitude of the convective flux was relatively insignificant. Air temperature also had a significant effect on the mean pond temperature over 24 hours.

The mean pond temperature over 24 hours was most sensitive to the dew point temperature. A hypothetical 10% rise in dew point temperature produced a 4.02°C increase in mean pond temperature over 24 hours. The change in dew point temperature influenced the vapour pressure above the water surface. The relationship between the vapour pressure above the surface and the saturated vapour pressure of the water surface affected evaporation, which was a significant source of heat loss from the pond. Dew point temperature also had a significant impact on the magnitude and duration of temperature stratification in the pond.

The wind speed primarily affected the amount of internal mixing due to diffusion and evaporative heat loss at the surface of the pond. It was influenced by the roughness of the surface over which it was blowing as well as the surrounding terrain. Since the wind speed anemometer was located some distance from the pond, numerous adjustments were made to the wind speed data to account for the difference in terrain and altitude between the anemometer and the water surface. It is possible that the data manipulations introduced inaccuracies into the wind speed data. The model's sensitivity to the wind speed is illustrated in Figure 6-29.

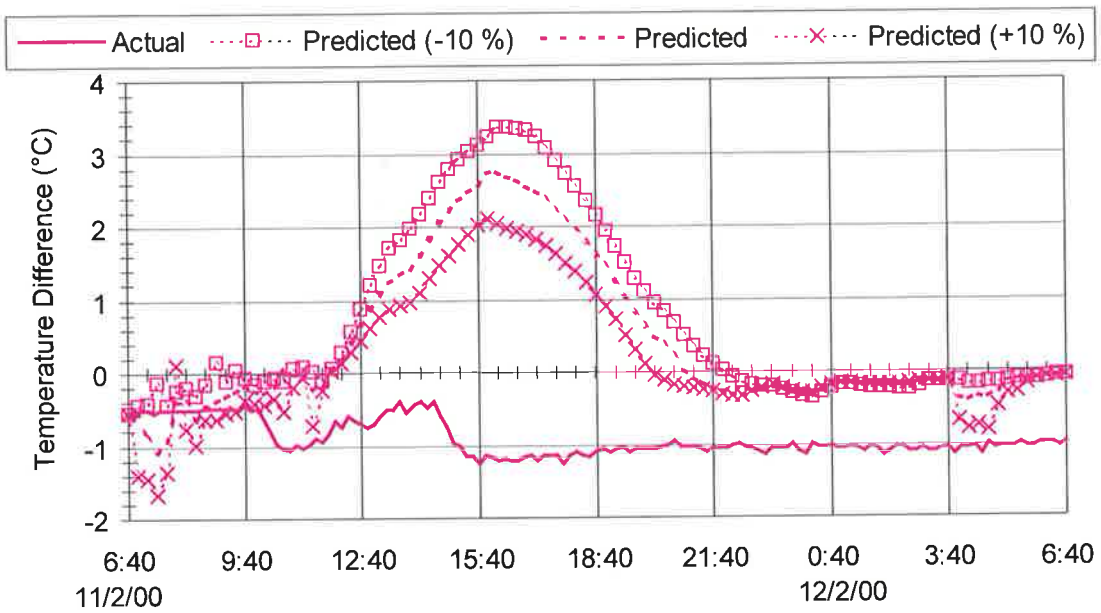

Figure 6-29: Sensitivity of the mean temperature stratification to changes in wind speed for 11 February 2000

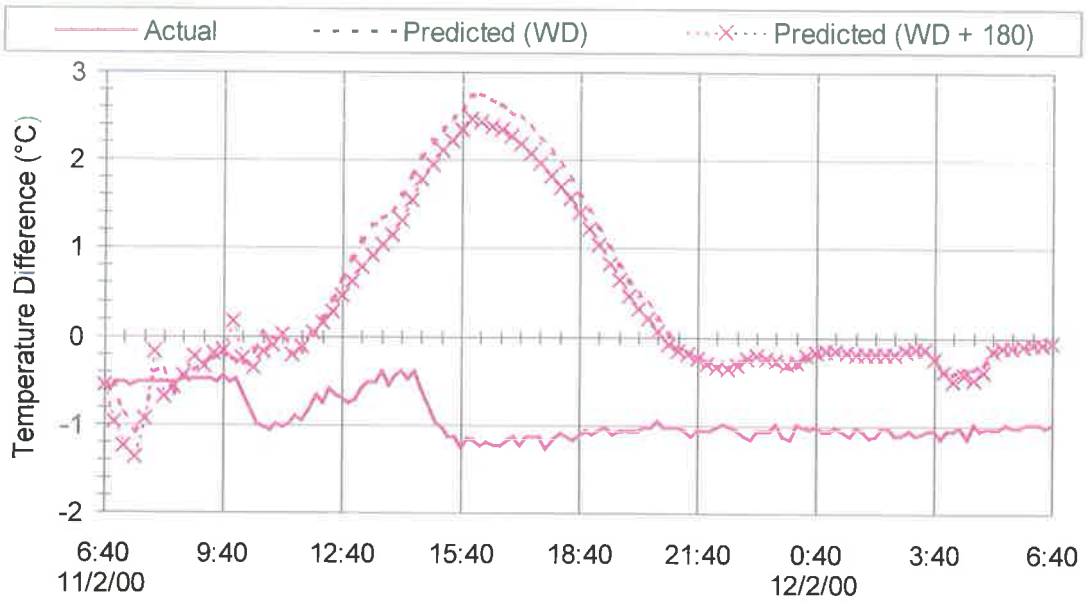

Figure 6-30: Sensitivity of the mean temperature stratification to a reversal in the wind direction (WD) for 11 February 2000

A 10 % over-estimation in the wind speed input data would have produced a 0.23°C increase in mean pond temperature and a 0.27°C increase in the mean temperature stratification over the 24 hours. A 10% under-estimation in the wind speed data would have led to a fall of 0.19°C in mean pond temperature and a fall of 0.26°C in the mean temperature stratification.

The sensitivity of the pond temperature to the wind speed decreased with increasing pond depth – the change in mean surface temperature due to the ±10% change in wind speed was 4 to 5 times greater than the change in temperature at the bottom of the pond.

Since the Morphett Road Sedimentation Pond was of a long thin design, with relatively high banks on either side, the direction of the wind was thought to be important. Winds blowing in a longitudinal direction for example travelled the furthest distance over water and may have been funelled by the high banks, while cross-winds travelled the shortest distance over water and were moderated at the water surface due to sheltering by the high banks. However, a reversal in wind direction had only minor effects on the mean pond temperature and temperature stratification, as shown in Figure 6-30.

Both the mean pond temperature and temperature stratification of the pond were relatively sensitive to errors in the solar radiation data. Solar radiation data from the Bureau of Meteorology is calculated from satellite data, which can be up to 20% inaccurate under cloud, when compared to ground-based records (BOM, 1999a). The pond model's sensitivity to the solar radiation data is illustrated in Figure 6-31.

An error of ±20% in the solar radiation data would have produced a change of approximately ±0.75°C in the mean pond temperature and a change of ±0.41°C in the mean temperature

stratification over 24 hours. The duration of the stratification was also dependent on the accuracy of the solar radiation data – an over-estimation of the magnitude of daily solar radiation led to an over-estimation of the duration of stratification, and vice versa.

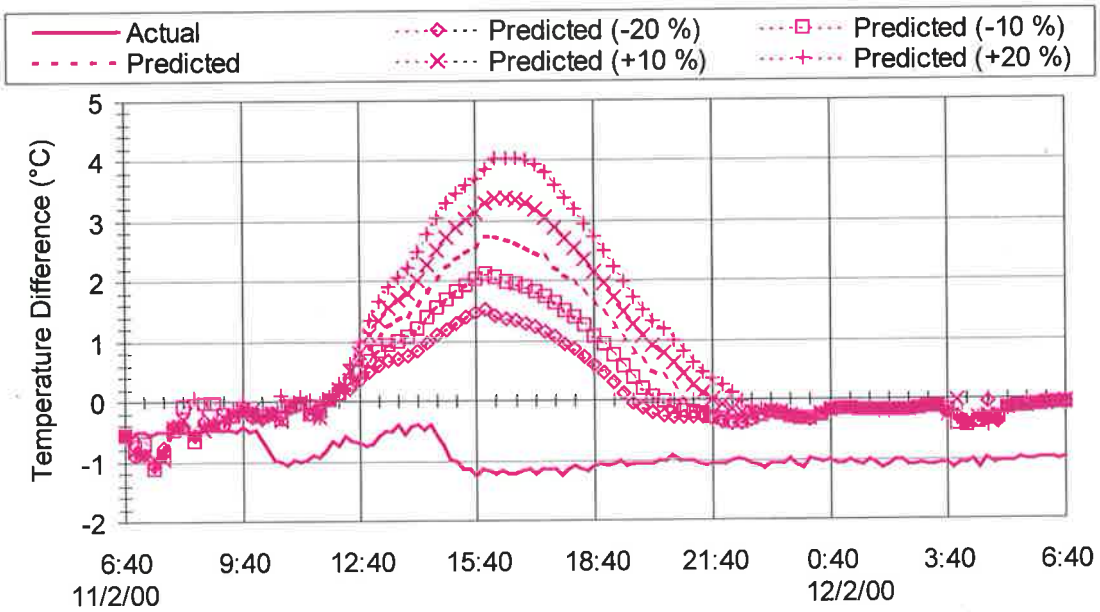

Figure 6-31: Sensitivity of the mean temperature stratification to changes in solar radiation for 11 February 2000

However, although the accuracy of solar radiation data was important, a change in cloud cover had relatively little impact on either mean pond temperature or mean temperature stratification over the 24 hours, as can be seen in Figure 6-32.

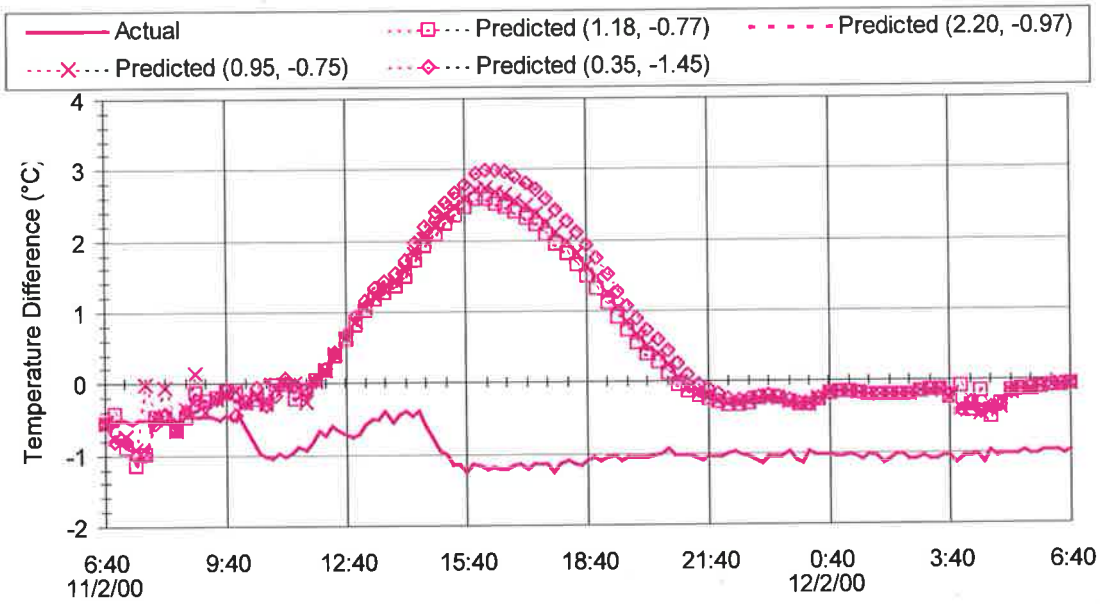

Figure 6-32: Sensitivity of the mean temperature stratification to changes in the cloud cover parameters (A, B) for 11 February 2000

6.6.2.2 Pond Clarity (SDD)

SDD is a measure of water clarity and was fundamental in determining the attenuation of light (and therefore heat) with increasing depth in the pond. Contrary to expectation however, the pond model was not highly sensitive to the SDD, as can be seen in Figure 6-33.

Only substantial reductions in pond clarity produced significant increases in the mean pond temperature and mean temperature stratification in the Morphett Road Sedimentation Pond. A reduction in SDD from 100% of the pond depth to 90% of the pond depth (i.e. from 0.9m to 0.81m) led to only minor changes in the mean pond temperature and mean temperature stratification over 24 hours. A large reduction in SDD from 100% of the pond depth to 10% of the pond depth (i.e. from 0.9m to 0.09m) led to a 0.18°C increase in mean pond temperature and a more significant 0.40°C increase in mean temperature stratification.

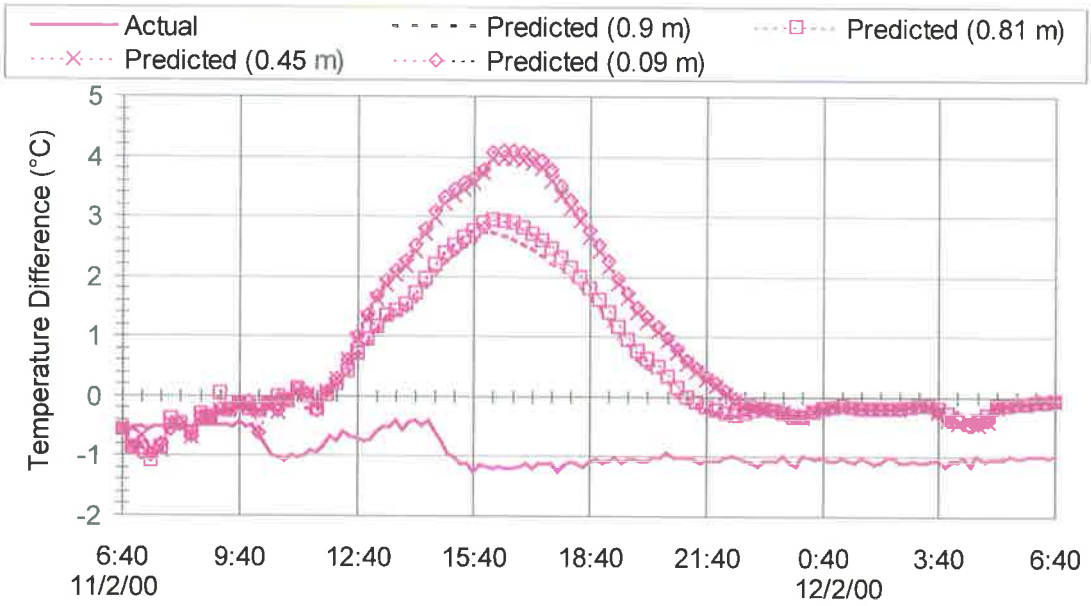

Figure 6-33: Sensitivity of the mean temperature stratification to changes in SDD for 11 February 2000

6.6.2.3 Pond Characteristics

The mean pond temperature and mean temperature stratification were moderately sensitive to the thickness of the concrete base, which conducted heat into and out of the water at the bottom of the pond. The magnitude of the heat energy flux was dependent on the thickness of the concrete base. The sensitivity of the pond model to changes in the concrete thickness is shown in Figure 6-34.

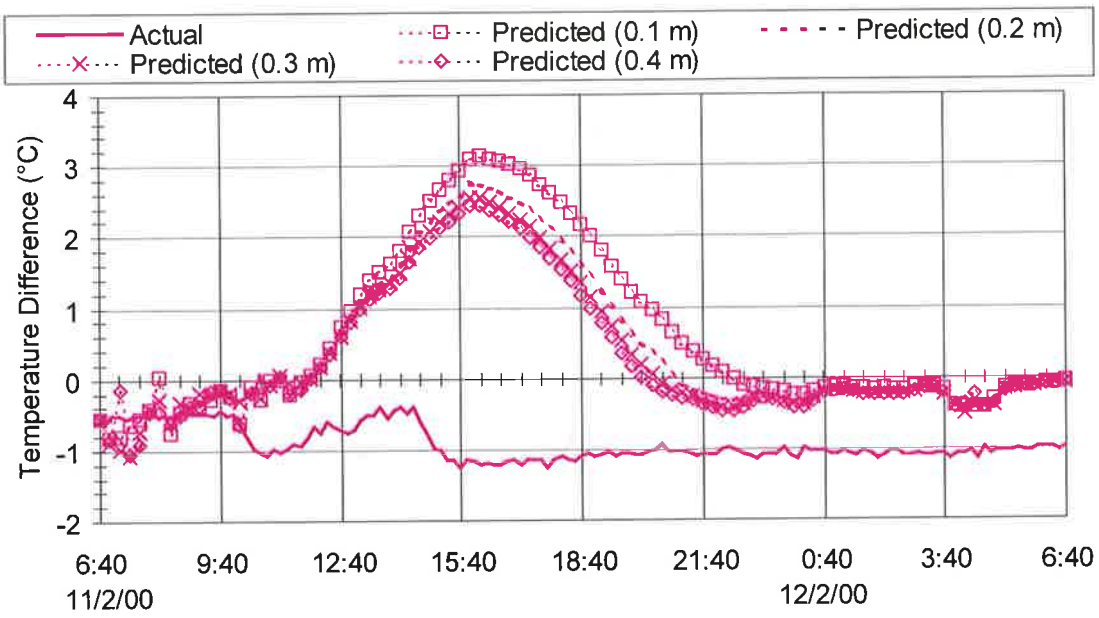

Figure 6-34: Sensitivity of the mean temperature stratification to changes in concrete thickness for 11 February 2000

When the depth of the concrete base was halved, there was a decrease in mean pond temperature of 0.41°C and an increase in mean temperature stratification of 0.19°C. A four fold increase in the depth of concrete led to a 0.33°C rise in mean pond temperature of 0.33°C and a slight fall in mean temperature stratification of 0.13°C over the 24 hours.

The dimensions of the pond were expected to have an important effect on the overall mean temperature of the pond and the distribution of heat through its depth. In a large shallow pond (i.e. with a high ratio of surface area to depth) the internal mixing (e.g. diffusion) is relatively less important in comparison to the surface and bottom heat flux. Whereas in a smaller and deeper pond (i.e. with a low surface area to depth ratio) the internal diffusive and convective heat fluxes become relatively more important.

The sensitivity of the pond model predictions of stratification to variations in pond design is illustrated in Figure 6-35. Figure 6-36 shows the specific sensitivity of the temperature predictions at the surface and bottom of the pond.

The pond model was initially run for a 1m deep pond with a surface area of 2600m^2 (130m × 20m). When the dimensions of the pond were altered to a smaller deeper pond of equivalent volume, which was twice the depth (2m) and half the surface area (1300m^2 or 65m × 20m), there was significantly less variation in mean pond temperature over the 24 hours. Overall, the mean temperature increased by 1.31°C.

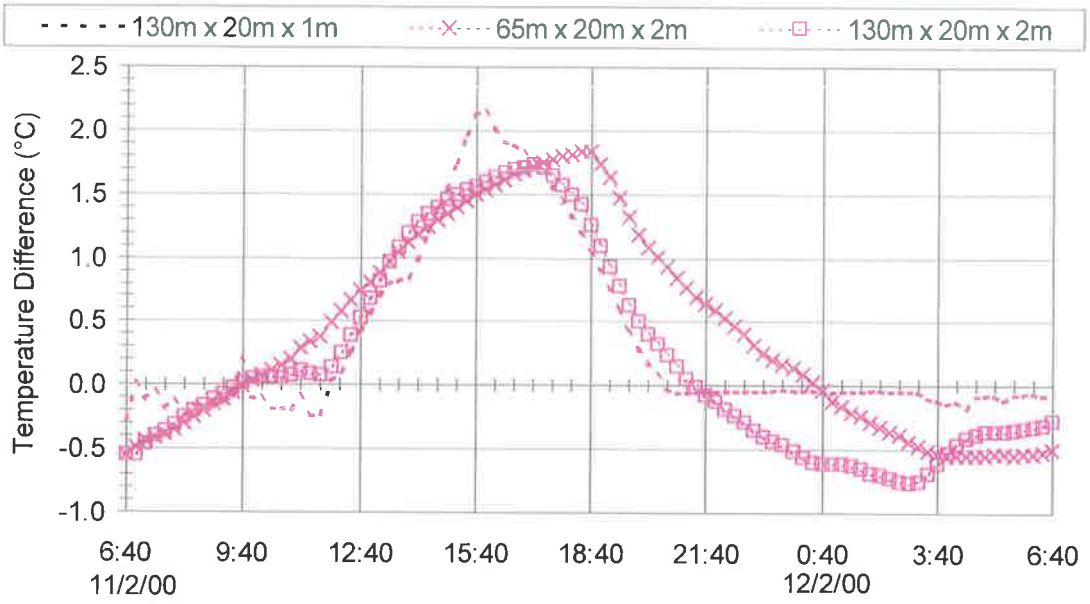

Figure 6-35: Sensitivity of the mean temperature stratification to changes in pond dimensions for 11 February 2000

The mean temperature stratification over the 24 hours differed only slightly from the mean temperature stratification predicted in the original pond, increasing by 0.09°C, but maximum temperature stratification was 0.3°C cooler and occurred 2¾ hours later in the day. There was also more significant negative stratification of temperature (temperature inversion) during the night primarily due to the greater storage of heat at the bottom of the pond. In general, although stratification was slightly higher when the pond was larger and shallower, pond temperatures were more dynamic because stratification and re-mixing occurred more rapidly.

When the pond volume was doubled by increasing the depth of the pond to 2m while maintaining a surface area of 2600m^2 (130m × 20m), the mean pond temperature over 24 hours increased by 1.57°C. The increase in depth allowed for greater heat input during daylight hours from penetrating solar radiation, and a larger storage capacity for heat. The temperature of water at the bottom of the 2m pond was much more stable over the 24 hours than the temperature of water at the bottom of the 1m pond. Heat loss from water at a depth of 1m occurred more quickly than from water at a depth of 2m, hence the water at the bottom of the 2m pond was generally warmer as well as being more stable.

Due to the storage of heat at the bottom of the 2m deep pond, temperature stratification became negative during the night. Maximum temperature stratification during the day was also 0.4°C lower than in the 1m pond and occurred 1¼ hours later. Over the 24 hours mean temperature stratification was 0.13°C lower in the 2m deep pond of the same surface area.

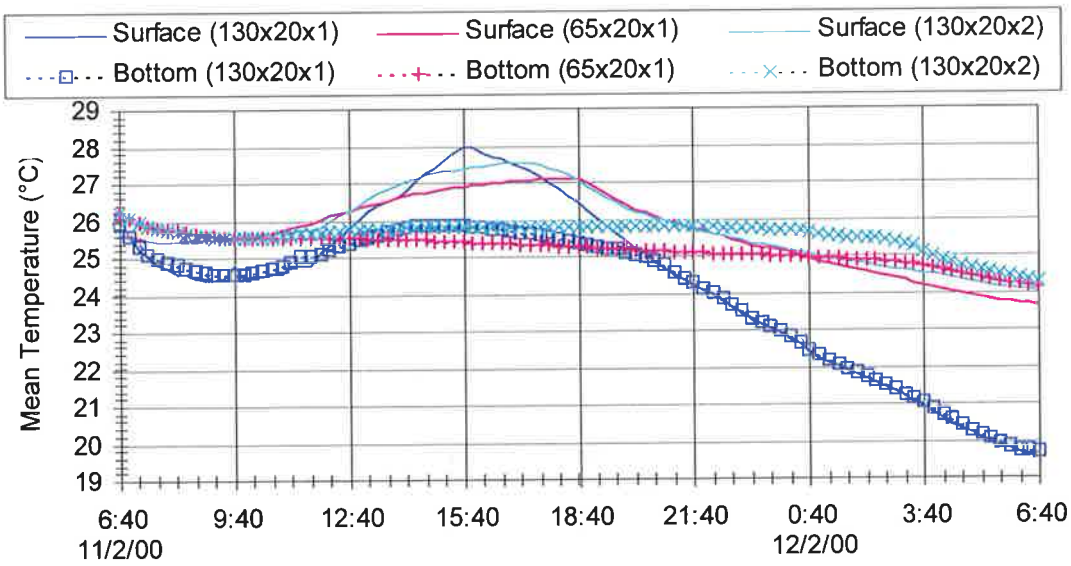

Figure 6-36: Sensitivity of the surface and bottom temperatures to changes in pond dimensions for 11 February 2000

6.7 Conclusions

Simulations with the sedimentation pond model demonstrated that stratification is caused by a complex combination of climate, water characteristics and pond design factors. The stratification was particularly sensitive to the meteorological conditions and pond dimensions, but relatively less sensitive to the orientation of the pond, thickness of the concrete base and clarity of the water.

Meteorological conditions primarily affect surface heat transfer processes rather than the internal fluxes or heat inputs. Since sedimentation ponds tend to have a high surface area to depth ratio (i.e. they are large and shallow rather than small and deep) sedimentation pond temperature stratification is highly dependent on the meteorological conditions.

Due to the high dependency of stratification on site specific conditions (e.g. climate, salinity, etc.) and pond design factors, it is recommended that stratification modelling be carried out using local data as part of the sedimentation pond design process. The accuracy of the meteorological data is paramount in successfully modelling sedimentation pond stratification. Hence it is recommended that where possible the meteorological parameters be measured at the surface of the pond, since the environment surrounding the instrumentation influences the meteorological parameters.

Using local input data, the model can be used to evaluate potential stratification outcomes of different design scenarios. Even if a full complement of data is unavailable, it is still possible

to experiment with a variety of pond designs and develop best and worst case scenarios in order to evaluate risks associated with the chosen design.

Experimentation with alternate designs of the Morphett Road Sedimentation Pond illustrated how the design of the sedimentation pond could influence the temperature stratification behaviour. Heating and cooling were found to be more extreme in a pond of large shallow design than in a smaller deeper pond of the same volume, which maintained a more stable temperature in the lower layers of water. The degree of temperature stratification was found to be higher in the smaller deeper pond. The design thickness of the concrete base of the pond also influenced the degree of stratification – the thicker the concrete, the smaller the magnitude and duration of stratification. However, pond orientation had only a minor impact on stratification in the pond.

CHAPTER 7

SUMMARY, CONCLUSIONS AND RECOMMENDATIONS

7.1 Summary

In this research, the efficacy of sedimentation ponds as a means of sediment and heavy metal remediation was investigated, with particular regard to the physical and chemical conditions that may lead to remobilisation of metals from the sediments (e.g. temperature stratification).

The research involved a combination of field sampling and data collection, laboratory analysis of samples, and numerical modelling of sedimentation pond processes. The field work and data collection for verification of the model was focused on the Patawalonga and Torrens catchments in Adelaide, South Australia.

In order to determine the characteristic nature and behaviour of sediments and their heavy metal content in the Patawalonga and Torrens catchments, a series of sediment sampling stations was set up around the two catchments. The sites included Weir 2 and Lockleys in the Torrens catchment and Burbridge Road Sedimentation Pond, Morphett Road Sedimentation Pond and the Patawalonga Basin in the Patawalonga catchment. The two sedimentation ponds were included in the study in order to evaluate the treatment performance of existing sedimentation ponds.

Equipment was also installed in the Morphett Road Sedimentation Pond to monitor the temperature stratification of the pond, and intensive sessions of monitoring were undertaken to measure conditions of DO, redox potential, pH, salinity and pond clarity, which can be conducive to remobilisation of pollutants from the sediments.

In addition a numerical model of sedimentation pond stratification was developed using STELLA™, and was verified using the temperature data collected in the Morphett Road

Sedimentation Pond. Multiple sedimentation pond stratification scenarios were simulated using the model in order to analyse the effects of meteorology, pond conditions and pond design on the development of stratification in sedimentation ponds.

7.2 Conclusions

The research has shown that remobilising conditions do occur at numerous locations in the Patawalonga and Torrens catchments, including the Patawalonga Basin, Burbridge Road Sedimentation Pond, Morphett Road Sedimentation Pond and in the River Torrens at Lockleys. It has further indicated that the occurrence of these remobilising conditions in the sedimentation ponds, as well as stratification of these ponds, has a number of implications for their efficiency in capturing and retaining sediments and heavy metal pollutants.

7.2.1 Sedimentation Pond Performance

With regard to the capture of sediments and heavy metals, this research showed that overall, the existing sedimentation ponds (Burbridge Road Sedimentation Pond and Morphett Road Sedimentation Pond) were effective. 66% to 69% of the material that was captured in the ponds was of the coarser (>63μm) particle size and this contributed 81% to 84% of the heavy metal load, the majority of which was captured in autumn. However the efficiency of the Morphett Road Sedimentation Pond in capturing sediments and heavy metals may have been affected by short-circuiting of flow due to persistent long-term stratification in late summer and early autumn, when salinity levels were high. (Differences in the capture efficiency of the two ponds was believed to be partly due to dissimilarities in opportunity for treatment of water and sediments upstream of the ponds.)

With regard to the retention of heavy metal pollutants in the sedimentation ponds, it was found that remobilising conditions were occurring in both Burbridge Road Sedimentation Pond and Morphett Road Sedimentation Pond, and that the sedimentation ponds may thus have been less effective at retaining heavy metals at these times.

The remobilising conditions commonly occurred when a period of warm air temperatures, relatively calm winds and low flow followed a flow event through the pond, which increased the organic loading in the pond. In the Burbridge Road Sedimentation Pond, where the organic proportion of the captured material was highest, the remobilising conditions led to multiple algal blooms and persistent and unpleasant pond odours. The remobilising conditions in the Morphett Road Sedimentation Pond were exacerbated by the onset of thermal stratification. Furthermore, conditions of salinity, pH and DO in the Morphett Road

Sedimentation Pond did not always comply with ANZECC (1999) guidelines for the protection of freshwater aquatic ecosystems.

With regard to stratification, simulations with the sedimentation pond model established that the development of stratification in sedimentation ponds is highly site specific and dependent on a combination of climatic, water characteristic and pond design factors. In particular, the modelling showed that stratification is highly dependent on local meteorological conditions, particularly air and dew point temperatures, due to the high ratio of surface area to depth of sedimentation ponds. Hence the dimensions of the sedimentation pond were also important in the development of stratification. However pond orientation and water clarity were relatively less influential. The modelling also highlighted the fact that salinity gradients and fluctuations in the water column may have a very powerful influence on the temperature stratification of the water column.

7.2.2 Sediments and Heavy Metals in the Patawalonga and Torrens Catchments

Heavy metals analysis of sediments trapped at a number of locations in the Patawalonga and Torrens catchments indicated that considerable quantities of metal contaminated sediments are being transported through both catchments throughout the year. The need for treatment in both catchments was clear, particularly for the metals lead and zinc. Table 7-1 gives a summary of heavy metal concentration results from each site in relation to the ANZECC (1999) guidelines. (The majority of metals were most concentrated in sediments from the Burbridge Road Sedimentation Pond.)

There was no significant difference between the concentration of metals on the fine (<63μm) and coarse (>63μm) particle sizes with the exception of boron and tin, which were consistently more concentrated on the finer (<63μm) particles. At all sites there was significant variability in transport of the fine (<63μm) and coarse (>63μm) sediment fractions and heavy metal contamination of the sediments from season to season, but no seasonal trends were apparent. (Catchment activities, such as the construction of Breakout Creek Wetland in the River Torrens, which led to large increases in sedimentation of the downstream environment, almost certainly masked any seasonal behaviour that might otherwise have been observed.)

Table 7-1: A summary of compliance (✓) or non-compliance (×) of average heavy metal sediment contamination with ANZECC (1999) guidelines for the protection of freshwater aquatic ecosystems

	Weir 2	Lockleys	Burbridge Road Sedimentation Pond	Morphett Road Sedimentation Pond	Patawalonga Basin
Lead	×	×	×	×	×
Zinc	×	×	×	×	✓
Copper	×	✓	×	✓	✓
Cadmium	✓	✓	×	✓	✓
Chromium	✓	✓	✓	✓	✓
Nickel	✓	✓	✓	✓	✓
Arsenic	✓	✓	✓	✓	✓
Antimony	✓	✓	✓	✓	✓
Barium			Metals detected, but no guideline levels have been determined		
Boron					
Vanadium					
Cobalt					
Beryllium					
Molybdenum					
Selenium					
Tin					

7.2.3 Final Conclusions and Recommendations

It is concluded that overall, sedimentation ponds can be effective at capturing sediments and heavy metals although there may be inefficiencies in capture and retention. They can potentially play a valuable role in catchment management, provided care is taken to tailor their management and design to local conditions.

High organic loadings are instrumental in the development of remobilising conditions and are present in both the Patawalonga and Torrens catchments, hence the need for more effective research, development and implementation of strategies is stressed to prevent organic material from entering stormwater. This applies equally to the problem of high salinity levels, which can trigger persistent long-term stratification that inhibits water quality treatment in sedimentation ponds (and can affect freshwater ecosystems).

With regard to sedimentation pond management, it is recommended that sedimentation ponds be cleaned more frequently, particularly after flow events in spring, summer and autumn. This would reduce the supply of organic material in the pond and could circumvent the problem of heavy metal remobilisation by removing their sediment source.

With regard to sedimentation pond design, it is recommended that ponds be individually designed to minimise the potential for stratification to develop, since pond stratification behaviour is highly dependent on local meteorological conditions and flow regime characteristics such as salinity. Hence it is recommended that stratification modelling be performed using local data to evaluate a variety of pond design stratification scenarios as part of the design process.

While sedimentation ponds are still considered to be a useful catchment management tool, it should be acknowledged that maximum efficiency may sometimes not be achieved. Hence it is recommended that sedimentation ponds be implemented as part of a treatment train (i.e. in combination with other treatment facilities such as grassed swales, wetlands, etc.).

Since many of these facilities (including sedimentation ponds) are in-stream devices, their construction may increase sedimentation of downstream environments. While acknowledging that some short-term increases in sediment pollution may be acceptable in order to achieve greater pollutant reduction in the long-term, it is recommended that more attention be given to methods of improving sediment control during construction, and that where possible construction be scheduled to avoid peak flow times.

7.3 Recommendations for Further Research

There are a number of areas in which further research could be undertaken to complement the work that has been done in this study.

The sedimentation pond model of stratification that has been developed as part of this research enables simulation of stratification for a multitude of design scenarios, to assist pond designers in deriving a pond design that minimises the potential for stratification to occur. There is potential for the stratification model developed here to be integrated with other

models, so that in effect it constitutes just one module of a much larger and more powerful sedimentation pond design model.

Another postgraduate student in the Department of Civil and Environmental Engineering is currently using the sedimentation pond model with the intention of integrating it with a model of phosphorus removal in a pond. Ultimately however, there is potential for developing a model that incorporates all the relevant factors of sedimentation pond design, including biological, physical, chemical, economic and social variables (e.g. algal growth, sedimentation, stratification, pollutant remobilisation, construction expenses, public liability constraints, etc.). Such a comprehensive model would be an excellent tool to assist decision-makers in deriving the most appropriate sedimentation pond design.

The spreadsheet model of Lawrence and Breen (1998) that was described in Chapter 2 is to date the most comprehensive of this type of model to be developed. It is recommended that more research be done to assess the integrative potential of these models and to continue developing models that simulate other pond design variables that have not so far been addressed (e.g. social and economic constraints).

There are also a number of ways in which the sedimentation pond stratification model could be improved. Inconsistencies in prediction of the precise magnitude and timing of stratification when the sedimentation pond model was applied to the Morphett Road Sedimentation Pond are believed to be due to the effects of salinity on the density gradient in the pond. Further testing of the model in a freshwater pond environment is recommended to confirm this theory.

Although adaptions were made to the model to incorporate the salinity effects, further work is required to refine this aspect of the modelling. This could include incorporating the effects of evaporation on salinity concentrations at the surface, and improving the simulation of inter-layer salt transfer by distinguishing between the rates of salt and heat transfer, and incorporating the effects of convective diffusion on the density behaviour.

Other work that might also enhance the scope and performance of the model, includes:

- undertaking further research to determine appropriate values for empirical parameters including the convective mixing coefficient and the fetch adjustment factor, both of which affect the inter-layer transfer of heat and salt in sedimentation ponds;
- incorporating the effects of sedimentary material at the bottom on the temperature of the pond (sedimentary material has a lower thermal conductivity than concrete hence it may have had an insulating effect on the water column temperature); and
- incorporating the shading effects of high pond banks, trees or other shade features that may surround sedimentation ponds.

Further research is also recommended to improve the management of the existing sedimentation ponds. It was found in this research that there was no time correlation between sedimentation and metal contamination of the sediment (e.g. in Burbridge Road Sedimentation Pond, sediment accumulation was highest in spring, but spring sediment loads had the lowest concentration of heavy metals). Although no general catchment trends were identified in the rate of sedimentation or degree of metal contamination of the sediment by comparison of the different sites, continued testing of sediments might reveal trends characteristic of each individual site that could not be identified from just a single year (approximately) of data. This is primarily recommended for the sedimentation ponds, where this knowledge could be used to develop optimum cleaning strategies.

CHAPTER 8

REFERENCES

Alloway, B. and Ayres, D. (1997). *Chemical principles of environmental pollution*. London, Chapman & Hall.

ANZECC (1992). *Australian Water Quality Guidelines for Fresh and Marine Waters*. Canberra, Australia and New Zealand Environment and Conservation Council.

ANZECC (1999). *Draft Australian and New Zealand Guidelines for Fresh and Marine Water Quality*. Canberra, Australia and New Zealand Environment and Conservation Council & Agriculture and Resource Management Council of Australia and New Zealand.

APHA (1995). *Standard Methods for the Examination of Water and Wastewater*. Washington DC, APHA - AWWA - WEF.

APHA (1998). *Standard Methods for the Examination of Water and Wastewater*. Washington DC, APHA - AWWA - WEF.

Athayde, D., Shelley, P., Driscol, E., Gabourry, D. and Boyd, G. (1984). *Results of the National Urban Runoff Program (NURP) Volume 1: Final Report*. Washington DC, USEPA.

ATSDR (1999). *HazDat*. Agency for Toxic Substances and Disease Registry, Division of Toxicology, US Department of Health and Human Services.

Australian Water Quality Centre (2000). *Torrens Lake: Monitoring, Research and Mangement of Cyanobacterial Growth*. Australian Water Quality Centre. T2/97/1.

Baas Becking, L., Kaplan, I. and Moore, D. (1960). Limits of the natural environment in terms of pH and oxidation-reduction potentials. *Journal of Geology* **68**: 243-284.

Baldwin, D., Mitchell, A. and Rees, G. (1997). Chemistry and microbial ecology: processes at the microscale. *Frontiers in Ecology: Building the Links*, Charles Sturt University, Albury, Ecological Society of Australia.

Ball, J. and Abustan, I. (1995). An investigation of particle size distribution during storm events from an urban catchment. *2nd International Symposium on Urban Stormwater Management*, Melbourne, Australia.

Bartone, D. and Uchrin, C. (1999). Comparison of pollutant removal efficiency for two residential storm water basins. *Journal of Environmental Engineering* **125**: 674-677.

Berner, R. (1981). A new geochemical classification of sedimentary environments. *Journal of Sedimentary Petrology* **51**: 359-365.

Bloesch, J. (1996). Towards a new generation of sediment traps and a better measurement/understanding of settling particle flux in lakes and oceans: A hydrodynamical protocol. *Aquatic Sciences* **58**: 283-296.

Bloesch, J. and Burns, N. (1980). A critical review of sedimentation trap technique. *Schweiz. Z. Hydrobiol.* **42**: 15-55.

Blomqvist, S. and Håkanson, L. (1981). A review on sediment traps in aquatic environments. *Archiv für Hydrobiologie* **91**: 101-132.

BOM (1999a). Daily Solar Radiation Model Description. http://www.bom.gov.au/sat/solradinfo.shtml.

BOM (1999b). *Solar and Terrestrial Radiation - glossary.* http://www.bom.gov.au/sat/glossary.shtml#gobalexposure.

Bourg, A. and Loch, J. (1995). Mobilization of heavy metals as affected by pH and redox conditions. *Biogeodynamics of Pollutants in Soils and Sediments*. W. Salomons and W. Stigliani, Eds. . Berlin Heidelberg, Springer-Verlag: 87-102.

Bourque, C. and Gullison, J. (1998). A technique to predict hourly potential solar radiation and temperature for a mostly unmonitored area in the Cape Breton Highlands. *Canadian Journal of Soil Science* **78**: 409-420.

Brookes, J., Burch, M. and Tarrant, P. (2000). Artificial destratification: evidence for improved water quality. *Water* July/August 2000.

Butcher, J. and Covington, S. (1996). Dissolved-oxygen analysis with temperature dependence. *Journal of Environmental Engineering* **121**(10): 756-759.

Butler, E. and Smith, J. (1985). Iodine and arsenic redox species in oxygen-deficient estuarine waters. *Australian Journal of Marine and Freshwater Research* **36**: 301-309.

CCREM (1996). *Canadian Water Quality Guidelines*. Ottawa, Canadian Council for Resource and Environment Ministers.

Chapra, S. and Canale, R. (1990). *Numerical Methods for Engineers*. Singapore, McGraw-Hill.

Characklis, G. and Wiesner, M. (1997). Particles, metals and water quality in runoff from a large urban watershed. *Journal of Environmental Engineering* **123**: 753-759.

Cole, G. (1983). *Textbook of Limnology*. St Louis, The C.V. Mosby Company.

Comings, K., Booth, D. and Horner, R. (2000). Storm water pollutant removal by two wet ponds in Bellevue, Washington. *Journal of Environmental Engineering* **126**: 321-330.

Connell, D. and Miller, G. (1984). *Chemistry and Ecotoxicology of Pollution*. New York, John Wiley & Sons.

Culberson, S. and Piedrahita, R. (1996). Aquaculture pond ecosystem model: temperature and dissolved oxygen prediction - mechanism and application. *Ecological Modelling* **89**: 231-258.

Davidson, M. and Abramowitz, M. (2000). *Molecular Expressions Microscopy Primer: Light and Color - Refraction of Light*.
http://micro.magnet.fsu.edu/primer/light and color/refraction.html.

Davies-Colley, R. and Vant, W. (1988). Estimation of optical properties of water from secchi disk depths. *Water Resources Bulletin* **24**(6): 1329-1335.

de Groot, A. (1995). Metals and sediment: a global perspective. *Metal Contaminated Aquatic Sediments*. H. Allen, Ed. . Chelsea, Ann Arbor Press.

Dempsey, B., Tai, Y. and Harrison, S. (1993). Mobilization and removal of contaminants associated with urban dust and dirt. *Water Science Technology* **28**: 225-230.

Dong, D., Nelson, Y., Lion, L., Schuler, M. and Ghiorse, W. (2000). Adsorption of Pb and Cd onto metal oxides and organic material in natural surface coatings as determined by selective extractions: new evidence for the importance of Mn and Fe oxides. *Water Research* **34**: 427-436.

Drapper, D., Tomlinson, R. and Williams, P. (2000). Pollutant concentrations in road runoff: Southeast Queensland case study. *Journal of Environmental Engineering* **126**: 313-320.

Duffie, J. and Beckman, W. (1980). *Solar Engineering of Thermal Processes*. New York, John Wiley & Sons.

Duncan, H. (1995). *A Review of Urban Stormwater Quality Processes*, Cooperative Research Centre for Catchment Hydrology.

Effler, S. (1988). Secchi disc transparency and turbidity. *Journal of Environmental Engineering* **114**(6): 1436-1447.

Eisma, D. (1992). *Suspended Matter in the Aquatic Environment*. Berlin Heidelberg, Springer Verlag.

Evans, R. and Håkanson , L. (1992). Measurement and prediction of sedimentation in small Swedish lakes. *Hydrobiologia* **235/236**: 143-152.

Farrow, D. and Patterson, J. (1994). The daytime circulation and temperature structure in a reservoir sidearm. *International Journal of Heat and Mass Transfer* **37**(13): 1957-1968.

Fennessy, S., Brueske, C. and Mitsch, W. (1994). Sediment deposition patterns in restored freshwater wetlands using sediment traps. *Ecological Engineering* **3**: 409-428.

Ferrara, R. and Witkowski, P. (1983). Stormwater quality characteristics in detention basins. *Journal of Environmental Engineering* **109**: 428-447.

Fischer, H., Imberger, J., List, E., Koh, R. and Brooks, N. (1979). *Mixing in Inland and Coastal Waters*. New York, Academic Press.

Fontaine, T., Moore, T. and Burgoa, B. (2000). Distributions of contaminant concentration and particle size in fluvial sediment. *Water Resources* **34**: 3473-3477.

Förstner, U. (1977). Forms and sediment associations of nutrients (C, N and P), pesticides and metals: trace metals. *The Fluvial Transport of Sediment Associated Nutrients and Contaminants*. H. Shear and A. Watson, Eds. . Ontario, International Joint Commission: 219-233.

Förstner, U. (1981). Metal transfer between solid and aqueous phases. *Metal pollution in the aquatic environment*. U. Förstner and G. Wittmann, Eds. . Berlin Heidelberg, Springer-Verlag.

Förstner, U. (1990). Inorganic sediment chemistry and elemental speciation. *Sediments: chemistry and toxicity of in-place pollutants*. R. Baudo, J. Giesy and H. Muntau, Eds. . Ann Arbor, Lewis Publishers.

Fritz, J., Meredith, D. and Middleton, A. (1980). Non-steady state bulk temperature determination for stabilization ponds. *Water Research* **14**: 413-420.

Frouin, R., Linger, D., Gautier, C., Baker, K. and Smith, R. (1989). A simple analytical formula to compute clear sky total and photosynthetically available solar irradiance at the ocean surface. *Journal of Geophysical Research* **94**(C7): 9731-9742.

Gardner, W. (1980a). Field assessment of sediment traps. *Journal of Marine Research* **38**: 41-52.

Gardner, W. (1980b). Sediment trap dynamics and calibration: a laboratory evaluation. *Journal of Marine Research* **38**: 17-39.

Gargett, A. (2000). *Differential diffusion: an oceanographic primer*, prepared for SCOR Working Group 108.

Gee, G. and Bauder, J. (1986). Particle size analysis. *Methods of Soil Analysis: Part I - Physical and Mineralogical Methods*. A. Klute, Ed. . Madison, Wisconsin, American Society of Agronomy and Soil Science Society of America**:** 383-411.

Gibbs, R. (1977). Transport phases of transition metals in the Amazon and Yukon Rivers. *Geological Society of America Bulletin* **88**: 829-843.

Ginot, V. and Hervé, J. (1994). Estimating the parameters of dissolved oxygen dynamics in shallow ponds. *Ecological Modelling* **73**: 169-187.

Goldman, C. and Horne, A. (1983). *Limnology*. New York, McGraw-Hill Book Company.

Grizzard, T., Randall, C., Weand, B. and Ellis, K. (1986). Effectiveness of extended detention ponds. *Urban Runoff Quality - Impact and Quality Enhancement Technology*, New Hampshire, ASCE.

Grundl, T. (1995). Determination of redox status in sediments. *Metal Contaminated Aquatic Sediments*. H. Allen, Ed. . Chelsea, Ann Arbor Press.

Hach (1996). *Combination ORP Electrode Model 50230 Instuction Manual*, Hach Company.

Hach (1997). *DO175 Dissolved Oxygen Meter Model 50175 Instruction Manual*, Hach Company.

Håkanson, L., Floderus, S. and Wallin, M. (1989). Sediment trap assemblages - a methodological description. *Hydrobiologia* **176/177**: 481-490.

Hannoun, I. and List, E. (1988). Turbulent mixing at a shear-free density interface. *Journal of Fluid Mechanics* **189**: 211-234.

Hansell, D. and Newton, J. (1994). Design and evaluation of a 'swimmer'-segregating particle interceptor trap. *Limnology and Oceanography* **39**: 1487-1495.

Henderson-Sellers, B. (1977). The thermal structure of small lakes: the influence of a modified wind speed. *Water Resources Research* **13**(4): 791-793.

Henderson-Sellers, B. (1984). *Engineering Limnology*. London, Pitman Publishing.

Henderson-Sellers, B. (1989). The sensitivity of thermocline models ot parametrisations of the surface energy budget and of wind mixing. *Ergebnisse der Limnologie* **33**: 113-122.

Henderson-Sellers, B., McCormick, M. and Scavia, D. (1983). A comparison of the formulation for eddy diffusion in two one-dimensional stratification models. *Applied Mathematical Modelling* **7**: 212-215.

Hicks, B. (1972). Some evaluations of drag and bulk transfer coefficients over water bodies of different sizes. *Boundary Layer Meteorology* **3**: 201-213.

Hondzo, M. and Stefan, H. (1993). Lake water temperature simulation model. *Journal of Hydraulic Engineering* **119**(11): 1251-1273.

Honeyman, B. and Santschi, P. (1988). Metals in aquatic systems. *Environmental Science and Technology* **22**(8): 862-871.

Horner, R., Skupien, J., Livingston, E. and Shaver, H. (1994). *Fundamentals of Urban Runoff Management: Technical and Institutional Issues*. Washington D.C., Terrene Institute.

Hostettler, J. (1984). Electrode electrons, aqueous electrons, and redox potentials in natural waters. *American Journal of Science* **284**: 737-759.

Hsieh, J. (1986). *Solar Energy Engineering*. Englewood Cliffs, NJ, Prentice-Hall.

Hughes, G., Dalziel, S., Linden, P. and Sutherland, B. (1998). Measurements of internal gravity waves. *GFD Annual Report*, Geophysical Fluid Dynamics Group, Research School of Earth Sciences, Australian National University.

Hurl, S. (2000). *Sediment Deposition Patterns and Concentrations of Heavy Metals Associated with Sediments in a Stormwater Treatment Wetland*. Adelaide University,

Hutchinson, G. (1957). *A Treatise on Limnology*. New York, Wiley.

HYDROLAB (1997). *DataSonde 4 and MiniSonde Water Quality Multiprobes: User's Manual*. HYDROLAB. HL#003078.

Imberger, J. and Patterson, J. (1981). Dynamic Reservoir Simulation Model - DYRESM: 5. *Transport Models for Inland and Coastal Waters*, Berkeley, California, Academic Press New York.

Imberger, J. and Patterson, J. (1990). Physical Limnology. *Advances in Applied Mechanics* **27**: 303-475.

Jassby, A. and Powell, T. (1975). Vertical patterns of eddy diffusion during stratification in Castle Lake, California. *Limnology and Oceanography* **20**: 530-543.

Johnson, D. (1977). Seston and sedimentation in Farmoor Reservoir, Great Britain. *Interactions Between Sediments and Fresh Water*, Amsterdam, the Netherlands, Dr W. Junk B. V. Publishers.

Kennish, M. (1992). *Ecology of Estuaries*. Boca Raton, CRC Press.

Kim, K. and Chapra, S. (1997). Temperature model for highly transient shallow streams. *Journal of Hydraulic Engineering* **123**(1): 30-40.

Kirchner, W. (1975). An evaluation of sediment trap methodology. *Limnology and Oceanography* **20**: 657-660.

Kraus, E. and Turner, J. (1967). A one-dimensional model of the seasonal thermocline. *Tellus* **19**: 292-309.

Lawrence, I. and Breen, P. (1998). *Design Guidelines: Stormwater Pollution Control Ponds and Wetlands*, Cooperative Research Centre for Freshwater Ecology.

Lee, C., Hedges, J., Wakeham, S. and Zhu, N. (1992). Effectiveness of various treatments in retarding microbial activity in sediment trap material and their effects on the collection of swimmers. *Limnology and Oceanography* **37**: 117-130.

Linacre, E. (1992). *Climate Data and Resources*. London, Routledge.

Loganathan, G., Watkins, E. and Kibler, D. (1994). Sizing storm-water detention basins for pollutant removal. *Journal of Environmental Engineering* **120**: 1380-1399.

Losordo, T. and Piedrahita, R. (1991). Modelling temperature variation and thermal stratification in shallow aquaculture ponds. *Ecological Modelling* **54**: 189-226.

Lower, S. (1998). *Redox Equilibria in Natural Waters*, Simon Fraser University.

Masscheleyn, P., DeLaune, R. and Patrick Jr., W. (1990). Transformation of selenium as affected by sediment oxidation-reduction potential and pH. *Environmental Science and Technology* **24**: 91-96.

Masscheleyn, P., DeLaune, R. and Patrick Jr., W. (1991). Effect of redox potential and pH on arsenic speciation and solubility in a contaminated soil. *Environmental Science and Technology* **25**: 1414-1419.

Masscheleyn, P., Pardue, J., DeLaune, R. and Patrick Jr., W. (1992). Chromium redox chemistry in a lower Mississippi Valley bottomland hardwood wetland. *Environmental Science and Technology* **26**: 1217-1226.

McCave, N., Bryant, R., Cook, H. and Coughanowr, C. (1986). Evaluation of a laser-diffraction analyzer for use with natural sediments. *Journal of Sedimentary Petrology* **56**: 4-6.

McCormick, M. and Scavia, D. (1981). Calculation of vertical profiles of lake-averaged temperature and diffusivity in Lakes Ontario and Washington. *Water Resources Research* **17**(2): 305-310.

McManus, J. (1988). Grain size determination and interpretation. *Techniques in Sedimentology*. M. Tucker, Ed. . Oxford, Blackwell Scientific Publications.

Mercier, P., Robert, M., Penven, M., Elsass, F., Jaunet, A., Muxart, T. and Lagadec, E. (1995). A methodology to study particulate matter. *Suspended Particulate Matter in Rivers and Estuaries*, Reinbek, Germany, E. Schweitzerbart'sche Verlagsbuchhandlung.

Metcalf, H. and Eddy, T. (1991). *Wastewater Engineering: Treatment, Disposal and Reuse*. New York, McGraw Hill.

Meybeck, M. (1984). *Les Fleuves at le Cycle Geochimique des Éléments*. Université Pierre et Marie Curie, Paris.

Munk, W. and Anderson, E. (1948). Notes on a theory of the thermocline. *Journal of Marine Research* **7**: 276-295.

Neville, A. (1981). *Properties of Concrete*. Essex, Longman Scientific & Technical.

Nix, S., Heaney, J. and Huber, W. (1989). Suspended solids removal in detention basins. *Journal of Environmental Engineering* **114**: 1331-1343.

Nõges, P., Tuvikene, L. and Kisand, A. (1999). Primary production, sedimentation and resuspension in large shallow Lake Võrtsjärv. *Aquatic Sciences* **61**: 168-182.

Octavio, K., Jirka, G. and Harleman, D. (1977). *Vertical Heat Transport Mechanisms in Lakes and Reservoirs*, Ralph M Parsons Laboratory, Massachusetts Institute of Technology.

Okubo, A. (1971). Horizontal and vertical mixing in the sea. *Impingement of Man on the Oceans*. D. Hood, Ed. . New York, Wiley: 89-168.

Ongley, E., Bynoe, M. and Percival, J. (1981). Physical and geochemical characteristics of suspended solids, Wilton Creek, Ontario. *Canadian Journal of Earth Science* **18**: 1365-1379.

Panofsky, H. and Dutton, J. (1984). *Atmospheric Turbulence: Models and Methods for Engineering Applications*. New York, John Wiley & Sons.

Pardue, J. and Patrick Jr., W. (1995). Changes in metal speciation following alteration of sediment redox status. *Metal Contaminated Aquatic Sediments*. H. Allen, Ed. . Chelsea, Ann Arbor Press.

Passfield, G. and Phillips, S. (1996). *Suspended Sediment Characteristics, Dry Creek Catchment, South Australia.* Department of Civil and Environmental Engineering, The University of Adelaide, Adelaide.

Patawalonga and Torrens Catchment Water Management Board (2000). *Trash Racks/Gross Pollutant Traps*.
http://www.cwmb.sa.gov.au/trashracks/index.htm.

Patawalonga Catchment Water Management Board (1996). *Patawalonga Catchment Water Management Plan: Appendices.* BC Tonkin & Associates.

Patawalonga Catchment Water Management Board (1997a). *Patawalonga Catchment Water Management Plan*. BC Tonkin & Associates.

Patawalonga Catchment Water Management Board (1997b). *Patawalonga Catchment Water Management Plan: Accompanying Report.* BC Tonkin & Associates. Ref. No. 95.0836.

Patawalonga Catchment Water Management Board (1997c). *Patawalonga Catchment Water Management Plan: Community Consultation Report.* BC Tonkin & Associates.

Peterson, W. and Dam, H. (1990). The influence of copepod 'swimmers' on pigment fluxes in brine-filled vs. ambient seawater-filled sedient traps. *Limnology and Oceanography* **35**: 448-455.

pH environment (1995). *Patawalonga Catchment Sediment Quality*. pH environment.

Porto, M. (1993). Stratification models sensitivity to solar radiation data. *Hydraulic Engineering '93*.

Pye, K. (1994). Properties of sediment particles. *Sediment Transport and Depositional Processes*. K. Pye, Ed. . Oxford, Blackwell Scientific: 1-24.

Rabl, A. and Nielsen, C. (1975). Solar ponds for space heating. *Solar Energy* **17**: 1-12.

Rafferty, K. (1986). Pond Heat Loss. *Geo-Heat Center Bulletin* Fall Issue.

Randall, W., Ellis, K., Grizzard, T. and Knocke, W. (1982). Urban runoff pollutant removal by sedimentation. *Stormwater Retention Facilities - Planning, Designing, Operation and Maintenance*. W. DeGroot, Ed. . New Hampshire, ASCE: 205-219.

Rawson, D. and Moore, J. (1944). The saline lakes of Saskatchewan. *Canadian Journal of Research (Section D, Zoological Sciences)* **22**: 141-201.

Reddy, K. and D'Angelo, E. (1994). Soil processes regulating water quality in wetlands. *Global Wetlands: Old World and New*. W. Mitsch, Ed. . Amsterdam, Elsevier Science: 309-324.

Reysenbach, A. (1999). *Yellowstone Microbes*. http://caddis.esr.pdx.edu/coursesalr/fieldnotes.htm.

Richardson, L. (1926). Atmospheric diffusion shown on a distance-neighbour graph. *Proceedings of the Royal Society: Series A* **110**: 709-737.

Rossby, C. and Montgomery, G. (1935). The layer of frictional influence in wind and ocean currents. *Pap. phys. Oceanogr. Meteorol.* **3**(3): 1-101.

Rudnick, D. and Ferrari, R. (1999). Compensation of horizontal temperature and salinity gradients in the ocean mixed layer. *Science* **283**: 526-529.

Salhotra, A., Adams, E. and Harleman, D. (1985). Effect of salinity and ionic composition on evaporation: analysis of Dead Sea Evaporation Pans. *Water Resources Research* **21**: 1336-1344.

Scanlon, P., O'Neill, I., Hughes, R. and McMahon, T. (1998). Stratification and pollution control pond efficiency. *Hydra Storm '98*, Adelaide, The Institution of Engineers.

Seki, H. (1982). *Organic Materials in Aquatic Ecosystems*. Boca Raton, CRC Press.

Sinnot, R. (1995). Sunrise/Sunset Challenge: the Winners. *Sky and Telescope* **89**: 84-86.

Slotton, D. and Reuter, J. (1995). Heavy metals in intact and resuspended sediments of a California reservoir, with emphasis on potential bioavailability of copper and zinc. *Marine and Freshwater Research* **46**: 257-265.

Smith, D., Davies-Colley, R., Knoef, J. and Slot, G. (1997). Optical characteristics of New Zealand rivers in relation to flow. *Journal of the American Water Resources Association* **33**(2): 301-312.

Smith, D. and Hoover, C. (1999). Use of a viewer box in secchi disk measurements. *Journal of the American Water Resources Association* **35**(5): 1183-1189.

Smith, I. (1979). Hydraulic conditions in isothermal lakes. *Freshwater Biology* **9**: 119-145.

Spencer, J. (1971). Fourier Series Representation of the Position of the Sun. *Search* **2**: 172.

Spigel, R., Imberger, J. and Raynor, K. (1986). Modelling the diurnal mixed layer. *Limnology and Oceanography* **31**(3): 533-556.

Spiro, T. and Stigliani, W. (1996). *Chemistry of the Environment*. London, Prentice-Hall.

Stefan, H. and Ford, D. (1975). Temperature dynamics in dimictic lakes. *Journal of the Hydraulics Division* **101**: 97-114.

Stewart, R. (1998). *Introduction to Physical Oceanography*, Department of Oceanography, Texas A & M University.

Stuart, R. (1995). *Sunrise/set*. Computer program, In: Sinnot (1995).

Sundaram, T. and Rehm, R. (1973). The seasonal thermal structure of deep temperate lakes. *Tellus* **25**(2): 157-167.

Szkup, R. (2000). Bureau of Meteorology, *Personal communication*.

Tamminga, G. (1992). Interpretation of sedimentation data measured in a former tidal channel Lake Volkerak. *Hydrobiologia* **235/236**: 107-117.

The Astronomical Almanac (1999). *The Astronomical Almanac for the Year 1999*. The Astronomical Almanac.

Torrens Catchment Water Management Board (1996). *Torrens Comprehensive Catchment Water Management Plan: Technical Reviews*. Hassell.

Torrens Catchment Water Management Board (1997a). *Torrens Catchment Water Quality Data: Appendix to the Torrens Comprehensive Catchment Water Management Plan*. Hassell.

Torrens Catchment Water Management Board (1997b). *Torrens Comprehensive Catchment Water Management Plan*. Hassell.

Torrens Catchment Water Management Board (1997c). *Torrens Comprehensive Catchment Water Management Plan: Consultation Supplement*. Hassell.

Turner, J. (1985). Multicomponent Convection. *Annual Review of Fluid Mechanics* **17**: 11-44.

Tyler, J. (1968). The secchi disc. *Limnology and Oceanography* **13**(1): 1-6.

USEPA (1996). *Ecological Restoration: A Tool to Manage Stream Quality*.

http://www.epa.gov/OWOW/NPS/Ecology/.

Vaithiyanathan, P., Ramanathan, A. and Subramanian, V. (1992). Sediment transport in the Cauvery River basin: sediment characteristics and controlling factors. *Journal of Hydrology* **139**: 197-210.

Van Buren, M., Watt, W., Marsalek, J. and Anderson, B. (2000). Thermal balance of on-stream storm-water management pond. *Journal of Environmental Engineering* **126**: 509-517.

Van Rijn, L. (1994). *Principles of Sediment Transport in Rivers, Estuaries and Coastal Seas*. The Netherlands, Aqua Publications.

Wakeham, S., Hedges, J., Lee, C. and Pease, T. (1993). Effects of poisons and preservatives on the composition of organic matter in a sediment trap experiment. *Journal of Marine Research* **51**: 669-696.

Walker, D., Passfield, G., Phillips, S., Botting, J. and Pitrans, H. (1997). Stormwater sediment properties and land use in Tea Tree Gully, South Australia. *Water in the Balance: AWWA 17th Federal Convention*, Melbourne.

Walling, D. (1996). Suspended sediment transport by rivers: a geomorphological and hydrological perspective. *Suspended Particulate Matter in Rivers and Estuaries*. H. Kausch and W. Michaelis, Eds. . Reinbek, Germany, E. Schweitzerbart'sche Verlagsbuchhandlung**:** 1-27.

Walling, D., He, Q. and Nicholas, A. (1996). Floodplains as sediment sinks. *Floodplain Processes*. M. Anderson, D. Walling and P. Bates, Eds. . Chichester, John Wiley & Sons.

Walling, D. and Kane, P. (1984). Suspended sediment properties and their geomorphological significance. *Catchment Experiments in Fluvial Geomorphology*. T. Burt and D. Walling, Eds. . Norich, Geo Books.

Walmsley, J. (1996). Guidelines for estimating wind speed and turbulence in complex terrain. *Modelling of Atmospheric Flow Fields*. D. Lalas and C. Ratto, Eds. . Singapore, World Scientific**:** 719-737.

Wang, F. and Chen, J. (2000). Relation of sediment characteristics to trace metal concentrations: a statistical study. *Water Research* **34**: 694-698.

Wangersky, P. (1994). Sampling and Analysis of Particulate and Dissolved Matter. *The Biology of Particles in Aquatic Systems*. R. Wotton, Ed. . Boca Raton, Lewis Publishers.

Ward, P. (1984). Measurement of sediment yield. *Erosion and Sediment Yield: some methods of measurement and modelling*. R. Hadley and D. Walling, Eds. . Norwich, England, Geo Books.

Warren, L. and Zimmermann, A. (1994). Suspended particulate grain size dynamics and their implications for trace metal sorption in the Don River. *Aquatic Sciences* **56**(4): 348-362.

Waters, M. and Luketina, D. (1998). The development of temperature stratification in freshwater wetlands. *13th Australasian Fluid Mechanics Conference*, Monash University, Melbourne, Australia.

Webb, E. (1960). *Evaporation from Lake Eucumbene*, CSIRO, Australia.

Welch, E. (1980). *Ecological Effects of Waste Water*. Cambridge, Cambridge University Press.

Western, A., O'Neill, I., Hughes, R. and Nolan, J. (1996). The behaviour of stratified pools in the Wimmera River, Australia. *Water Resources Research* **32**(10): 3197-3206.

Wetzel, R. (1975). *Limnology*. Philadelphia, W B Saunders Company.

Wetzel, R. and Likens, G. (1991). *Limnological Analyses*. New York, Springer-Verlag.

Weyhenmeyer, G. (1996). The influence of stratification on the amount and distribution of different settling particles in Lake Erken. *Canadian Journal of Fisheries and Aquatic Sciences* **53**: 1254-1262.

Weyhenmeyer, G., Meili, M. and Pierson, D. (1995). A simple method to quantify sources of settling particles in lakes: resuspension versus new sedimentation of material from planktonic production. *Marine and Freshwater Resources* **46**: 223-231.

Whytcross, G., Johnston, T., Nagy, L. and Farrant, A. (1998). Design guidelines for gross pollutant traps. *Waterfall*(9): 15-18.

Willing and Partners (1996). *Review of the Glenelg Foreshore and Environs EIS and Implications for the Board's Catchment Management Plan*. Willing and Partners and Cooperative Research Centre for Freshwater Ecology. Project no. 3691.

Willing and Partners (1997). *Supplementary Review of the Glenelg Foreshore and Environs EIS and its Implications for the Patawalonga Catchment Management Plan*. Willing and Partners and Cooperative Research Centre for Freshwater Ecology. Project no. 3691.

Wotton, R. (1994). The classification of particulate and dissolved matter. *The Biology of Particles in Aquatic Systems*. R. Wotton, Ed. . Boca Raton, Lewis Publishers.

Wrigley, T., Farrell, P. and Griffiths, D. (1991). Ecologically sustainable water clarification at the Clear Water Lagoon, Mt Isa. *Water* **18**: 32-34.

Wu, J., Holman, B. and Dorney, J. (1989). Water quality study on urban wet detention ponds. *Design of Urban Runoff Quality Controls*. L. Roesner, B. Urbonas and M. Sonnen, Eds. . New York, ASCE.

Yechieli, Y., Gavrieli, I., Berkowitz, B. and Ronen, D. (1998). Will the Dead Sea die? *Geology* **26**: 755-758.

Zhang, H., Davison, W. and Ottley, C. (1999). Remobilisation of major ions in freshly deposited lacustrine sediment at overturn. *Aquatic Sciences* **61**: 354-361.

Appendix A

Site Logbook

WEIR 2 SAMPLING

Date	Action	Comments
6/05/1998	Trap 1 installed	Location 1
13/05/1998	Trap 1 removed	
13/08/1998	Trap 2 installed	
10/09/1998	Trap 2 gone	
23/09/1998	Trap 3 installed	
1/10/1998	Trap 3 gone	
16/10/1998	Trap 4 installed	Location 2
22/10/1998		
5/11/1998		
18/11/1998		
2/12/1998		
18/12/1998	Trap 4 gone	
6/01/1999	Trap 5 installed	Temporary trap
21/01/1999	Trap 5 removed	Left post in
18/02/1999	Trap 6 installed	
3/03/1999		
18/03/1999		
1/04/1999		
15/04/1999		
29/04/1999		Re-secured trap
13/05/1999		
27/05/1999		Trap survived storm
10/06/1999		
24/06/1999		
15/07/1999		
29/07/1999		
12/08/1999		
2/09/1999		Mysterious attachment of buoy
16/09/1999		
30/09/1999	Trap 6 removed	Trap had been moved

LOCKLEYS SAMPLING

Date	Action	Comments
13/08/1998	Trap 1 installed	
10/09/1998		
23/09/1998		Too deep to replace bottles
1/10/1998		2 bottles gone, trap re-secured
9/10/1998		Replaced with longer post, added rubber bands
22/10/1998		
5/11/1998		Very shallow
18/11/1998		Black muds, very odorous
2/12/1998		
18/12/1998		
6/01/1999		Still shallow, black muds, less odorous
21/01/1999		Even shallower, upstream wetlands under-way
4/02/1999		Heavy earth works upstream
18/02/1999		1 bottle gone, river blocked upstream
3/03/1999		Even shallower again, 1 or 2 cm over bottles, found lost bottle
18/03/1999		Deeper again, wetland over-flowing
1/04/1999		
15/04/1999		
29/04/1999		
13/05/1999		
27/05/1999		2 bottles gone, very deep
10/06/1999		
24/06/1999		
15/07/1999	Trap 1 removed	2 bottles gone, (only sampler removed)
29/07/1999	Trap 2 installed	
12/08/1999		
2/09/1999		
16/09/1999	Trap 2 removed	(Only sampler removed)

BURBRIDGE ROAD SEDIMENTATION POND SAMPLING

Date	Action	Comments
20/08/1998	Trap 1 installed	
10/09/1998		
23/09/1998		Dead cat
9/10/1998		
22/10/1998		
5/11/1998		
18/11/1998		
2/12/1998		
18/12/1998		
6/01/1999		
21/01/1999		
4/02/1999		Very odorous
18/02/1999		1 bottle gone
3/03/1999		Very very odorous
18/03/1999		Putrid
1/04/1999		
15/04/1999		
29/04/1999		
13/05/1999		
27/05/1999		Less odorous, recent event, GPTs emptied
10/06/1999		
24/06/1999		
15/07/1999		Very odorous
29/07/1999		Very odorous, milky, photo taken
12/08/1999		Not milky, recent flow event
2/09/1999		Milky again
16/09/1999		
30/09/1999	Trap 1 removed	

MORPHETT ROAD SEDIMENTATION POND SAMPLING

Date	Action	Comments
27/08/1998	Trap 1 installed	
10/09/1998		
23/09/1998		Too deep
1/10/1998		Pushed over
9/10/1998	Trap 1 removed	Pushed over again
30/11/1998	Trap 2 installed	
18/12/1998		
6/01/1999		Upgraded with bigger bottles, no flow, shallow, very clear
21/01/1999		Downgraded to normal bottles
4/02/1999		
18/02/1999		No flow
3/03/1999		Very shallow
18/03/1999		Very deep, recent flow event, 2 yabbies
1/04/1999		
15/04/1999		
29/04/1999		
13/05/1999		
27/05/1999		Very deep, recent flow event, GPTs emptied?
10/06/1999		
24/06/1999		
15/07/1999		
29/07/1999		
12/08/1999		
2/09/1999		
16/09/1999		Deep, during flow event (hail)
30/09/1999		
19/10/1999		
3/11/1999		
18/11/1999		
2/12/1999	Trap 2 removed	

MORPHETT ROAD SEDIMENTATION POND MONITORING

Date	Action	Comments
21/01/1999	Platform installed	
25/01/1999		Trialled pump sampler
3/03/1999	Sensors installed	
18/03/1999	Downloaded data, changed batteries	
1/04/1999	Downloaded data, changed batteries	
15/04/1999	Downloaded data, changed batteries	
19/04/1999	Downloaded data, changed batteries	Adjusted logger
29/04/1999	Downloaded data, changed batteries	
13/05/1999	Downloaded data, changed batteries	Trialled pump sampler
27/05/1999	Downloaded data, changed batteries	Changed clock on logger
10/06/1999	Downloaded data, changed batteries	
24/06/1999	Downloaded data, changed batteries	
13/07/1999	Downloaded data, changed batteries	Trialled pump sampler
15/07/1999	Downloaded data, changed batteries	
29/07/1999	Downloaded data, changed batteries	
4/08/1999	Downloaded data, changed batteries	Trialled pump sampler
12/08/1999	Downloaded data, changed batteries	
2/09/1999	Downloaded data, changed batteries	
16/09/1999	Downloaded data, changed batteries	
30/09/1999	Downloaded data, changed batteries	
19/10/1999	Downloaded data, changed batteries	

3/11/1999	Downloaded data, changed batteries	
18/11/1999	Downloaded data, changed batteries	
1/12/1999	Downloaded data, changed batteries	Trialled Hydrolab
2/12/1999	Downloaded data, changed batteries	
21/12/1999		Computer dead
6/01/2000		Computer dead
18/01/2000	Downloaded data, changed batteries	Profiling, logger failed
19/01/2000		Profiling
20/01/2000		Profiling, logger restarted
21/01/2000		Profiling
22/01/2000		Profiling
31/01/2000	Downloaded data, changed batteries	
7/02/2000		Profiling
8/02/2000		Profiling
9/02/2000		Profiling
10/02/2000		Profiling
11/02/2000	Downloaded data, changed batteries	Profiling
29/02/2000		Profiling
1/03/2000	Downloaded data, changed batteries	Profiling
2/03/2000		Profiling
14/03/2000	Downloaded data, changed batteries	
3/05/2000	Downloaded data, Sensors removed	

PATAWALONGA BASIN SAMPLING

Date	Action	Comments
27/08/1998	Trap 1 installed	1.5 m deep approx.
10/09/1998		
23/09/1998		
9/10/1998		Too windy
14/10/1998		Shallow
22/10/1998		Even shallower
5/11/1998		Black muds, 1 bottle carrier broken
18/11/1998		Very shallow, 1 bottle carrier still broken
2/12/1998		Too windy
18/12/1998	Trap 2 installed	New location
6/01/1999		
21/01/1999		Dead calm
4/02/1999	Trap 2 re-installed	Post had been removed
18/02/1999		
3/03/1999	Trap 2 removed	Barnacle encrustation
15/04/1999	Trap 3 installed	
29/04/1999	Trap 3 removed	Came loose, too windy to re-secure it
13/05/1999	Trap 3 re-installed	Longer post
27/05/1999		Dead calm
10/06/1999		
24/06/1999		
15/07/1999		Very shallow, bottles out of water, waded out
29/07/1999		Deep again, post loose
12/08/1999		Re-secured post
2/09/1999		Too deep to collect
16/09/1999		Too windy
30/09/1999	Trap 3 removed	

Appendix B

Sample Preparation for XRF/XRD Analysis

Two days should be allowed to prepare between 10 and 15 samples for XRF and XRD analysis. Steps 1 to 4 can be completed in one day and Steps 5 to 7 on the second day.

1. Washing and Drying

- Assemble 1 vial (with lip), 2 vials with lids (no lip) and 1 small crucible for each sample. (The vials with lips should be washed and placed in the oven first, so they will be ready for Step 2.)
- Fill bucket in sink with hot water and detergent, and use bottle brush and cloth to scrub the vials, crucibles and lids clean (emery paper may be required for crucibles).
- Rinse once in tap water to remove detergent, then three times in de-ionised water to remove tap water.
- Place up-right in glassware oven to dry.

2. Preparation for LOI

- Place 1 flat spoon of sample in each vial (with lip), wiping the spoon clean between each sample.
- Label vials.
- Place in oven to dry.

3. Slide Preparation

- Place 1 micro-spatula of sample in mortar (be careful not to take too much).
- Add approximately 4 drops of de-ionised water and mix to a slurry, grinding any lumps or gritty particles if required.
- Wipe a microscope slide with acetone to clean.
- Pour slurry onto slide, leaving one end clean.
- Label clean end and rest on paper towel on bench to dry.
- Wipe spatula clean, and rinse mortar and pestle well in bucket of water before drying.
- Return to the beginning of Step 3 to prepare remaining samples.

4. Pellet Preparation

- Place 3 spoons (approximately 15g) of sample in small zip-lock bag. (Use 1.5 spoons if sample is small.)
- Add approximately 8mL of polymer binding solution using a syringe. (Use 4mL for smaller sample.)
- Seal bag and rub contents together until completely mixed.
- Clean all parts of the pellet press (see Figure B–1) with ethanol before assembling. (If using small sample, the additional cylinder will be required.)

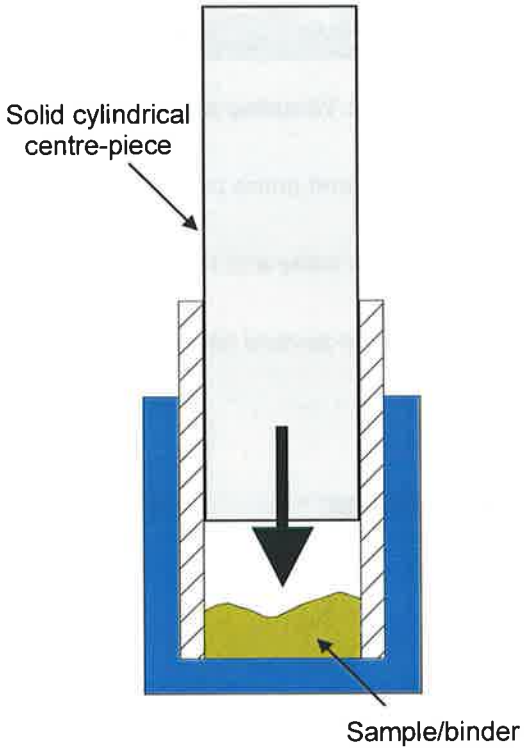

Figure B–1: Pellet press.

- Pour sample-binder mix into the central chamber.
- If the sample is small and the additional cylinder is used, gently tamp down the sample using the plastic tamp (shown in Figure B–2), and carefully remove the additional cylinder so that the sample remains in the centre. Fill around the edges with backing powder and add another 2 spoonfuls to form a base for the pellet.
- Insert solid cylindrical centre-piece and allow it to sink slowly down to the sample.
- Place pellet press in press.

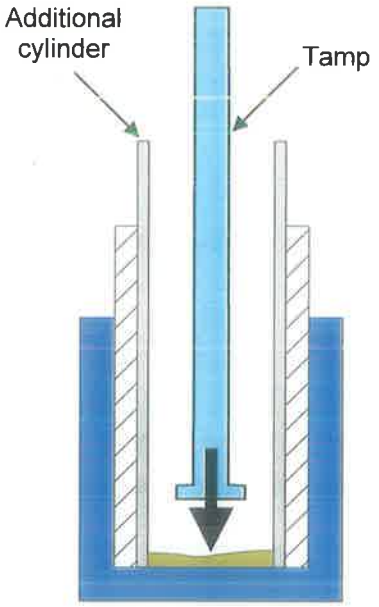

Figure B–2: Tamping a small sample

- Turn screw clockwise to lock valve and pump pressure to approximately level 5.
- Turn screw anti-clockwise to unlock valve and remove pellet press.
- Remove centre-piece, invert and tap several times to release pellet (see Figure B–3).

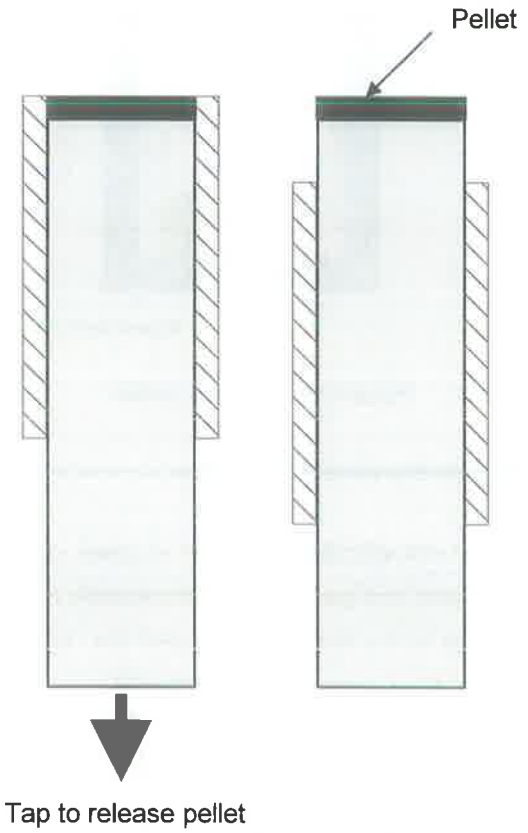

Figure B–3: Removing the pellet

- Remove pellet (carefully since it will still be soft) and place on paper to dry (label the paper to identify each sample).
- When dry, write label on pellet.

5. LOI

- Remove samples in crucibles from furnace and place in desiccator to cool for an hour.
- Enter sample name/number in computer program and press <Rtn>.
- Zero the scale by pressing the Tare button.
- Press the print button and record the crucible + sample weight and the LOI weight.
- Break up sample in the crucible then tip it into a vial.
- Cap the vial and label it with the sample name/number and "ig" to identify it as the ignited sample.

6. Preparation of Samples for Fusing

- Label empty vial and place on scale.
- Enter sample name/number in computer program and press <Rtn>. Scale will automatically zero.
- Crush the sample to a powder in the vial or with the mortar and pestle. (Mortar and pestle should be cleaned with ethanol between each sample.)
- Use the vibrating spatula to add 1 – 1.1g of sample to the vial on the scale. Brush any spillages from the scale using the brush.
- Wipe spatula clean and remove lithium flux powder from desiccator. (The flux powder is poisonous so it is a good idea not to inhale it.)
- Press the Print button on the scale and record the exact mass of the sample.
- Use the vibrating spatula to add 4 – 4.1g of flux powder. Brush any spillages from the scale using the brush.
- Replace flux powder in desiccator. (It is very hygroscopic and should be kept out of the desiccator for a minimum amount of time.)

- Press the Print button on scale and record the exact mass of flux powder in the vial and the weight ratio.
- Remove the vial from the scale and put the lid on.
- Use the test tube shaker to homogenise the sample/flux mixture.

7. Fusing

Fusing involves heating the sample/flux mixture prepared in Step 6 over an oxygen/propane flame to fuse it into a disk for XRD analysis. The fusing of samples takes co-ordination and efficiency, as it is done in one continuous procedure – one sample is being heated and mixed, while the previous sample is being cooled and stored, equipment is being cleaned and the next sample is being prepared. Despite the need for accurate timing, it is important not to rush – fusing involves using open flames and handling equipment that is extremely hot – a mistake could result in a serious injury.

- Ask someone else to switch on the gas bottles, taps, etc. and light the burners.
- Ensure the bucket in the sink is filled with water and the tap is turned on to create a continual flow of water through the bucket.
- Pour the well-mixed sample/flux mixture into 1 of the 2 platinum/aluminium crucibles, tapping both the vial and lid with the glass stirring rod to ensure no sample is lost.
- Using the big tongs, place the crucible on the left burner and start the stopwatch. (Once the crucible is red-hot, it will need to be picked up using the big tongs and swirled every few minutes during the fusing process.)
- While the crucible is heating, prepare the second crucible with the next sample/flux mixture to be fused.
- After approximately 4 minutes, add a small spatula (the size of a match-head) of ammonium iodide to the crucible to encourage the mixture to coalesce.
- At approximately 6 – 7 minutes, using the needle-nosed tongs place the mould on the right burner, ensuring it is level, and light the burner.
- When the sample/flux is fully fused (around 8.5 – 10 minutes) and the mould is hot, use the big tongs to give the mixture a final swirl before pouring it into the mould and putting the empty crucible on the asbestos tripod to cool.
- Switch off the right burner and turn on the air blowers to cool the mould.

- Stop, re-set and re-start the stopwatch.
- Using the big tongs place the second crucible onto the left burner, beginning again with fusing of the second sample, while continuing with the steps below to store the first sample and prepare for the next.
- Record the time taken for the first sample to fuse.
- After approximately 2 minutes, use the enormous tongs to drop the cooling (but still VERY HOT) crucible in the bucket of running water.
- Also at approximately 2 minutes, the mould will be cool enough to be removed from the burner and placed on the asbestos mat using the needle-nosed tongs. The air blowers can then be turned off.
- Using the plastic-tipped tongs, remove the crucible from the running bucket of water. It will now be cool enough to handle. Check the inside and lip of the crucible for hardened mixture adhered to the metal. (Be very careful doing this – it is now glass and it is sharp.) If there are any lumps that cannot be removed with a finger-nail, the crucible will need to be cleaned following the crucible cleaning procedure.

Crucible Cleaning Procedure

- Sprinkle sodium carbonate over the adhered lumps of sample.
- Open the oxygen valve on the large single burner (to the right of the fusing equipment) so that the blue cones appear.
- Using the enormous tongs move the crucible in the flame until the sodium carbonate and sample has liquidised in the bottom of the crucible.
- Drop the hot crucible into the bucket of running water.
- Adjust the oxygen valve to return the burner to the visible orange flame.
- Use the plastic-tipped tongs to remove the crucible from the water and place it in a beaker of hydrochloric acid – it will immediately fizz. (Do not put the hot crucible straight into the hydrochloric acid.)
- When the fizzing has stopped, use the plastic-tipped tongs to remove the crucible from the acid and put it back into the running water bucket.
- Use the plastic-tipped tongs to remove the crucible form the running water bucket. It should now be cool enough to handle.

- When the crucible is clean, rinse in de-ionised water and dry with paper towel. It is then ready to be loaded with the next sample.

- At about 4 minutes, the mould will be cool enough to handle. Stick a label on the top side of the disk, then de-mould it onto a sheet of paper, label side down. Without touching the upper-most surface (the side without label), store the disk in a zip-lock bag.

Appendix C

Sediment Flux Data

Sedimentation Rate ($g/m^2/day$)

	Date	> 63 ug	< 63 ug	Total
WEIR 2	Summer	3.40	1.18	4.58
	Autumn	41.91	0.52	42.43
	Winter	1.32	0.08	1.30
	Spring	1.95	0.34	2.30
LOCK	Summer	2.94	1.54	4.49
	Autumn	7.53	0.92	8.45
	Winter	9.23	0.24	9.47
	Spring	42.07	1.07	43.13
BURB	Summer	0.91	0.46	1.37
	Autumn	0.85	0.16	1.01
	Winter	0.85	0.22	1.07
	Spring	1.72	1.10	2.82
PAT	Summer	8.38	7.42	15.80
	Autumn	22.42	5.20	27.62
	Winter	7.66	2.22	9.88
	Spring	1.06	5.03	6.08
MORPH	Summer	0.25	0.85	1.10
	Autumn	1.25	0.27	1.53
	Winter	0.69	0.14	0.84
	Spring	0.61	0.16	0.77

Appendix D

Major and Trace Element Data

Major Elements

% (expressed as oxides)

	Si	Al	Fe	Mn	Mg	Ca	Na	K	Ti	P	S	LOI %	Total %	LOI % **
Weir 2 (> 63μm)														
Summer	54.43	11.40	5.24	0.16	2.53	3.64	0.82	2.27	0.65	0.30	0.37	17.73	99.55	
Autumn	85.11	3.87	1.45	0.03	0.80	2.26	0.67	1.27	0.17	0.06	0.07	4.08	99.83	
Winter	61.74	11.62	4.97	0.09	2.44	1.37	0.71	2.40	0.67	0.23	0.20	12.96	99.41	
Spring	61.16	11.29	4.95	0.11	2.38	1.77	0.76	2.33	0.65	0.23	0.37	13.47	99.47	
Mean	**65.61**	**9.55**	**4.15**	**0.10**	**2.04**	**2.26**	**0.74**	**2.07**	**0.54**	**0.21**	**0.25**	**12.06**		
Range	**30.68**	**7.75**	**3.80**	**0.13**	**1.73**	**2.27**	**0.15**	**1.14**	**0.50**	**0.24**	**0.30**	**13.65**		
Lockleys (> 63μm)														
Summer	57.13	11.92	5.46	0.05	2.73	3.07	0.90	2.26	0.73	0.21	0.62	14.40	99.49	
Autumn	66.78	11.02	4.21	0.04	2.04	1.78	1.74	2.19	0.78	0.11	0.12	8.66	99.48	
Winter	81.25	6.77	2.21	0.03	0.99	0.79	0.90	1.72	0.43	0.07	0.08	4.64	99.86	
Spring	84.34	4.37	1.61	0.02	0.92	2.34	0.51	1.16	0.25	0.06	0.15	4.40	100.12	
Mean	**72.38**	**8.52**	**3.37**	**0.04**	**1.67**	**2.00**	**1.01**	**1.83**	**0.55**	**0.11**	**0.24**	**8.03**		
Range	**17.56**	**6.65**	**2.61**	**0.02**	**1.12**	**1.55**	**1.23**	**1.04**	**0.53**	**0.06**	**0.16**	**4.26**		
Burbridge Rd (> 63μm)														
Summer	35.51	6.44	2.91	0.03	2.81	5.40	0.94	1.26	0.43	0.32	0.44	42.99	99.48	
Autumn	39.05	7.54	3.42	0.03	2.75	3.88	0.74	1.64	0.49	0.35	0.69	38.57	99.16	
Winter	41.05	8.14	3.53	0.03	3.24	3.22	0.75	1.81	0.53	0.26	0.83	35.76	99.15	

Spring	41.70	7.14	3.08	0.03	3.11	3.80	0.89	1.65	0.47	0.26	0.89	36.22	99.24
Mean	**39.33**	**7.32**	**3.24**	**0.03**	**2.98**	**4.08**	**0.83**	**1.59**	**0.48**	**0.30**	**0.71**	**38.39**	
Range	**2.65**	**1.00**	**0.45**	**0.00**	**0.49**	**0.86**	**0.15**	**0.22**	**0.06**	**0.09**	**0.20**	**2.81**	
Morphett Rd (> 63μm)													
Summer	-	-	-	-	-	-	-	-	-	-	-	-	-
Autumn	58.46	9.42	4.57	0.06	2.37	3.27	0.84	2.11	0.64	0.30	0.50	16.83	99.39
Winter	54.89	11.89	5.42	0.06	2.78	2.22	0.70	2.40	0.75	0.23	0.41	17.31	99.05
Spring	48.90	10.20	5.15	0.17	2.40	4.84	0.67	2.03	0.66	0.42	0.84	23.13	99.41
Mean	**54.08**	**10.50**	**5.05**	**0.10**	**2.52**	**3.44**	**0.74**	**2.18**	**0.68**	**0.32**	**0.58**	**19.09**	
Range	**9.56**	**2.47**	**0.85**	**0.11**	**0.41**	**2.62**	**0.17**	**0.36**	**0.11**	**0.19**	**0.43**	**6.30**	
Pat Basin (> 63μm)													
Summer	84.93	2.94	1.32	0.01	0.52	2.52	1.02	0.68	0.26	0.08	0.19	5.26	99.73
Autumn	87.38	2.71	1.16	0.02	0.39	1.44	0.66	0.63	0.32	0.06	0.08	4.63	99.47
Winter	82.06	4.29	1.84	0.02	0.72	2.12	0.37	0.98	0.31	0.10	0.34	6.97	100.12
Spring	56.96	7.82	3.82	0.02	1.71	2.44	1.72	1.61	0.53	0.23	0.28	22.34	99.49
Mean	**77.83**	**4.44**	**2.03**	**0.02**	**0.84**	**2.13**	**0.94**	**0.98**	**0.36**	**0.12**	**0.22**	**9.80**	
Range	**30.42**	**5.11**	**2.66**	**0.01**	**1.32**	**1.08**	**1.35**	**0.98**	**0.27**	**0.17**	**0.26**	**17.71**	

	Si	**Al**	**Fe**	**Mn**	**Mg**	**Ca**	**Na**	**K**	**Ti**	**P**	**S**	**LOI %**	**Total %**	**LOI % ****
Pat Basin (< 63μm)														
Summer*	0.95	0.21	0.05	0.00	5.40	0.93	31.67	0.60	0.00	0.07	5.49	0.00	45.37	81.01

Autumn*	2.07	0.55	0.16	0.00	5.31	0.94	33.20	0.64	0.00	0.07	5.71	0.00	48.65	60.80
Winter***	5.53	1.40	0.36	0.00	5.39	1.01	52.54	0.80	0.01	0.09	5.03	27.85	100.00	
Spring***	3.23	0.77	0.19	0.00	5.59	0.86	64.07	0.70	0.00	0.09	4.75	32.24	112.50	
Lockleys (< 63μm)														
Summer	44.11	13.60	6.20	0.10	4.31	3.80	4.40	2.42	0.84	0.22	0.87	19.00	99.86	
Morphett Rd (< 63μm)														
Summer*	8.36	1.89	0.65	0.03	4.73	2.05	27.98	0.71	0.05	0.21	0.66	0.00	47.32	34.05

* Analyses on dried but unignited samples. There will be loss of weight at the time of fusion.

** LOI measured but not included in total. The LOI for two of the three samples which fused into the crucible at the time of ignition seems to be excessive, even allowing for considerable NaCl and perhaps organic material. The samples may have started to volatilise. Other samples with high LOI contain organic material.

*** These samples are essentially halite (sodium chloride). The Na is expressed in the form Na2O, but is probably in the form NaCl. The presence of Cl was not checked.

Trace Elements

	Zr ppm	Nb ppm	Y ppm	Sr ppm	Rb ppm	U ppm	Th ppm	Pb ppm	Ga ppm	Cu ppm	Zn ppm	Ni ppm	Ba ppm	Sc ppm	Co ppm	V ppm	Ce ppm	Nd ppm	La ppm	Cr ppm	As ppm
Pat Basin (> 63mm)																					
Summer	262.7	4.8	9.9	99.8	28.5	1.5	5.1	40.3	2.1	11	109	6	137	3.3	45	28	22	8	11	25	5
Autumn	396.1	7.4	11.0	55.9	26.0	2.3	6.3	61.4	3.3	16	191	6	145	3.6	60	26	26	11	9	22	5
Winter	171.9	5.1	10.7	89.0	39.2	1.5	4.4	87.2	5.7	25	274	11	206	6.7	38	46	29	9	12	40	
Spring	196.2	8.1	16.2	114.0	68.0	2.1	7.6	219.3	10.6	104	736	21	245	8.7	42	63	37	14	16	78	
Burbridge Rd (> 63mm)																					
Summer	128.0	5.7	12.8	201.8	58.8	5.7	7.2	696.0	9.7	163	2075	47	306	6.9	31	55	35	12	11	189	23
Autumn	141.3	7.1	14.5	128.8	68.4	2.9	8.7	772.4	10.9	184	2525	85	370	8.3	31	62	40	17	17	302	28
Winter	146.7	8.4	15.4	118.9	75.9	3.2	8.0	789.3	12.6	166	2254	32	385	8.8	33	66	42	18	17	141	
Spring	143.1	7.5	13.8	181.0	67.2	5.1	6.3	746.5	11.7	195	2066	31	337	8.2	27	58	40	15	16	99	
Lockleys (> 63mm)																					
Summer	151.4	10.9	23.2	115.0	120.7	3.4	11.7	136.8	16.1	53	565	24	459	14.3	29	99	62	27	29	90	11
Autumn	263.2	12.6	24.9	91.3	99.7	3.9	11.5	118.3	12.4	45	338	96	417	12.0	31	81	59	25	27	362	12
Winter	203.0	7.7	17.8	52.2	62.5	2.2	6.1	72.7	8.6	24	242	11	340	7.4	45	46	42	17	18	43	
Spring	97.7	4.5	11.6	70.4	43.9	2.4	2.8	43.5	5.9	17	165	7	234	5.9	53	33	27	13	15	27	
Weir 2 (> 63mm)																					
Summer	177.5	9.6	22.0	113.8	108.8	3.8	10.7	300.8	14.9	87	766	155	579	12.3	55	89	57	23	26	574	17

Autumn	83.6	3.5	8.7	75.4	45.2	1.2	4.6	44.3	4.2	11	105	5	218	3.1	55	24	20	8	7	17	7
Winter	201.5	11.3	21.5	66.2	112.4	2.0	10.2	255.8	14.9	96	783	20	425	12.8	49	84	58	24	26	80	
Spring	198.3	10.9	21.9	74.1	109.3	2.7	10.7	266.9	13.8	103	796	22	438	12.3	38	83	56	24	25	84	
Morphett Rd (> 63mm)																					
Summer																					
Autumn	203.8	7.8	19.1	123.3	88.2	1.9	10.0	199.5	12.5	77	1229	250	352	11.3	42	79	47	17	19	941	19
Winter	182.7	11.5	21.4	84.1	111.9	3.2	9.9	252.8	15.7	76	1209	38	396	13.1	51	94	51	22	20	90	
Spring	169.7	9.2	18.9	127.9	90.2	1.7	8.6	238.2	13.7	83	1379	28	412	12.4	44	86	50	22	20	81	

	Zr ppm	Nb ppm	Y ppm	Sr ppm	Rb ppm	U ppm	Th ppm	Pb ppm	Ga ppm	Cu ppm	Zn ppm	Ni ppm	Ba ppm	Sc ppm	Co ppm	V ppm	Ce ppm	Nd ppm	La ppm	Cr ppm	As ppm
Pat Basin (< 63μm)																					
Summer	11.1	1.0		199.3	9.5	1.6	4.3	4.5	0.0	4	16	0	3	1.6	3	2	7	0	0	1	18
Autumn	15.9			184.7	11.5	0.5	2.5	13.5	0.0	3	46	0			3	3					18
Winter	27.2	1.4	1.6	186.6	17.1	0.3	4.3	30.8	0.7	20	124	2	55	2.7	68	18	8	1	2	13	
Spring	14.0	-0.5	0.2	186.8	10.9	0.4	2.0	18.0	-0.6	20	79	0	31	2.7	77	12	6	-2	5	7	
Lockleys (< 63μm)																					
Summer	157.6	10.3	25.1	159.3	140.4	3.4	13.0	139.8	17.4	62	501	22	348	11.8	12	80	51	17	21	76	16
Morphett Rd (< 63μm)																					
Summer	43.4	2.5	1.4	270.7	23.8	2.5	3.5	81.3	2.1	43	642	4	125	3.3	2	11	13	1	5	17	22

Appendix E

Particle Size Distributions

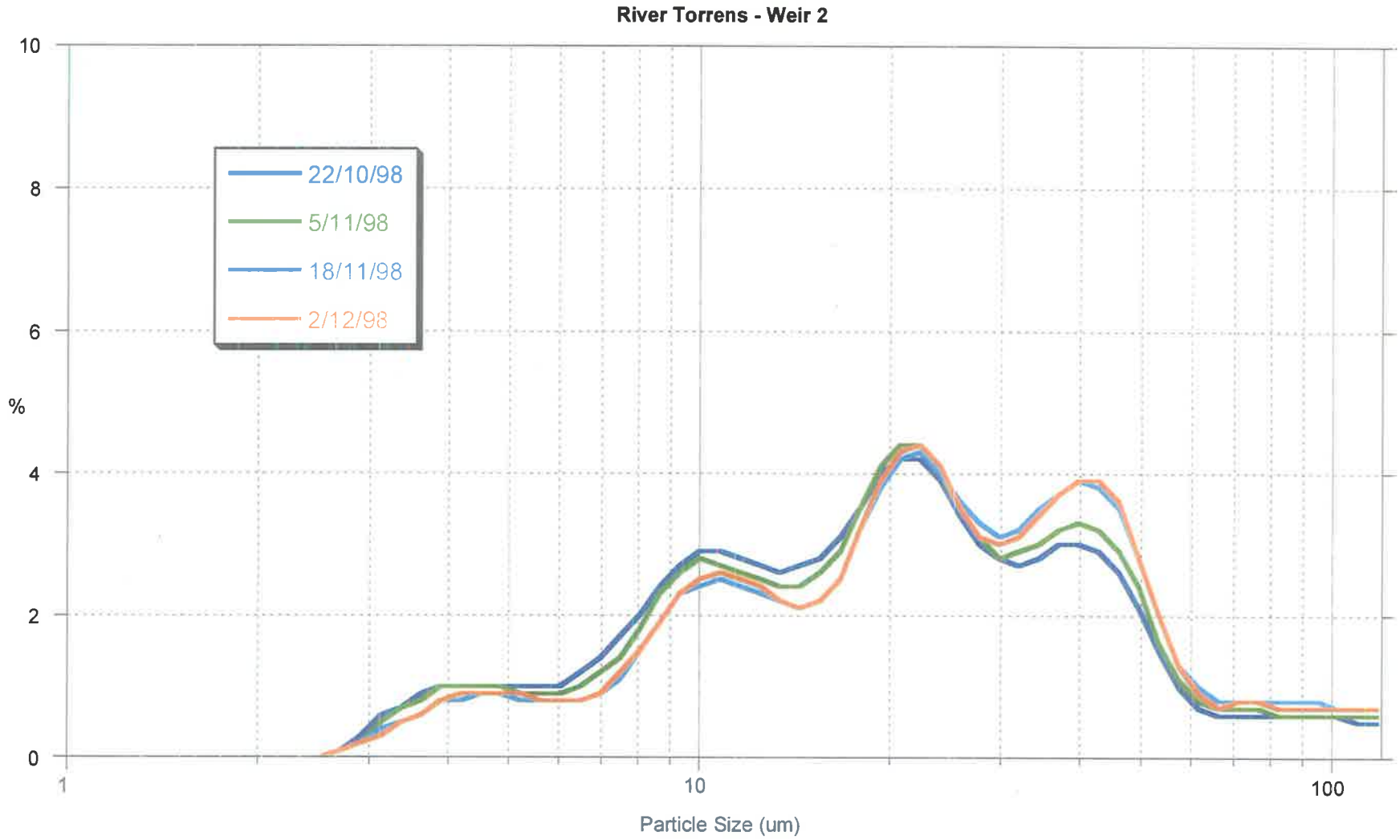
River Torrens - Weir 2
22/10/98
5/11/98
18/11/98
2/12/98
%
10
8
6
4
2
0
1
10
100
Particle Size (um)

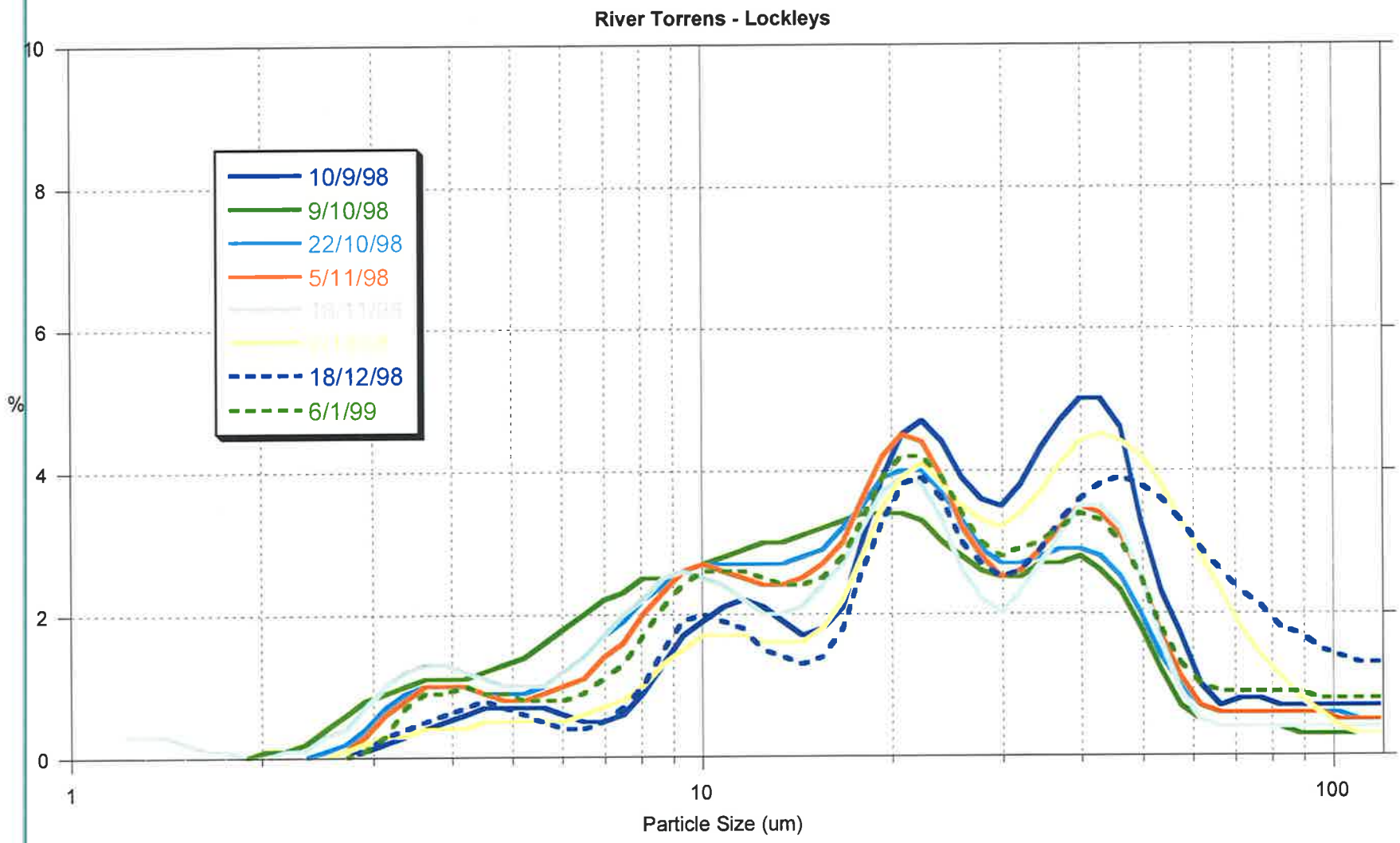
River Torrens - Lockleys
10
8
6
4
2
0
%
10/9/98
9/10/98
22/10/98
5/11/98
18/12/98
6/1/99
1
10
100
Particle Size (um)

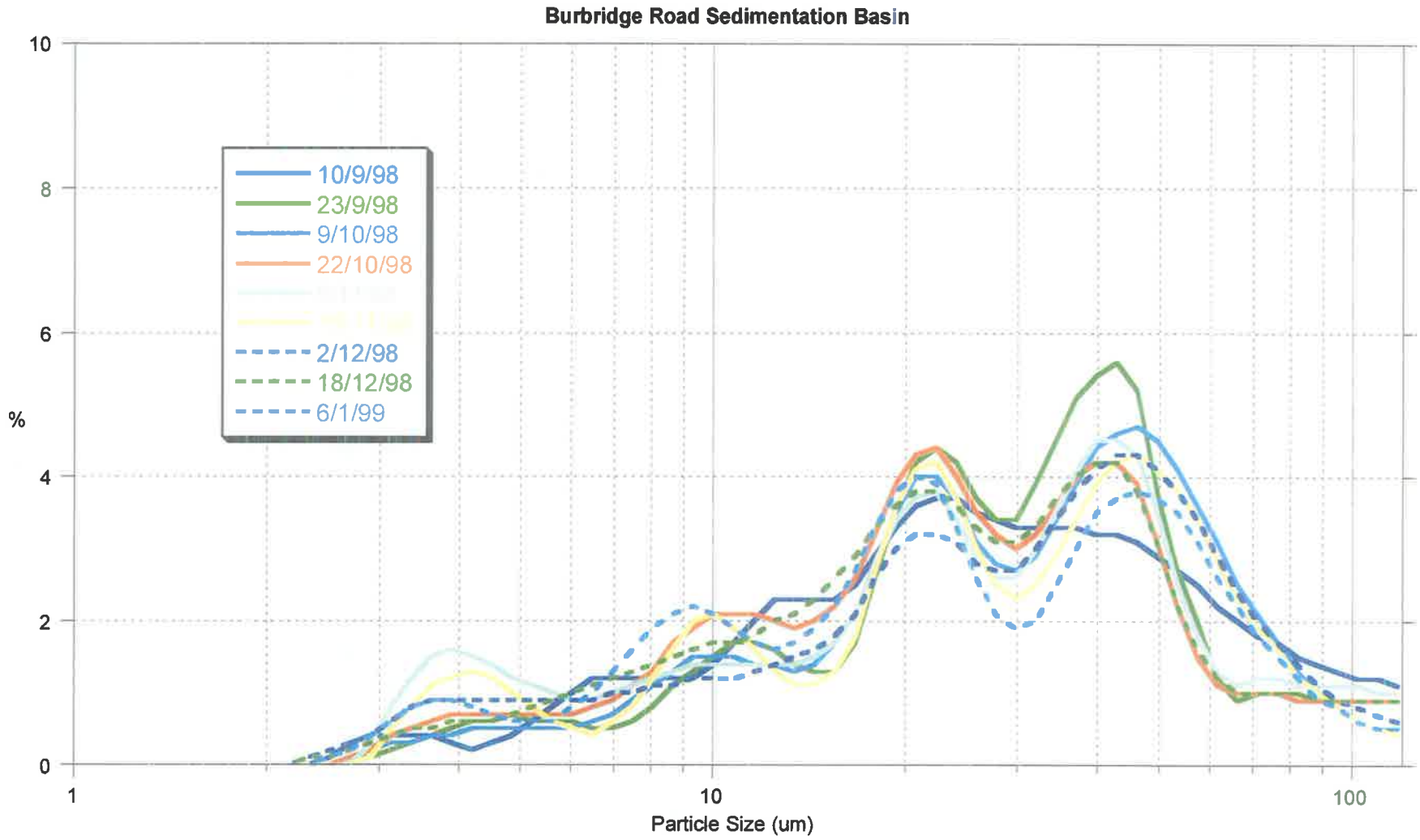
Burbridge Road Sedimentation Basin
10
8
6
4
2
0
%
10/9/98
23/9/98
9/10/98
22/10/98
2/12/98
18/12/98
6/1/99
1
10
100
Particle Size (um)

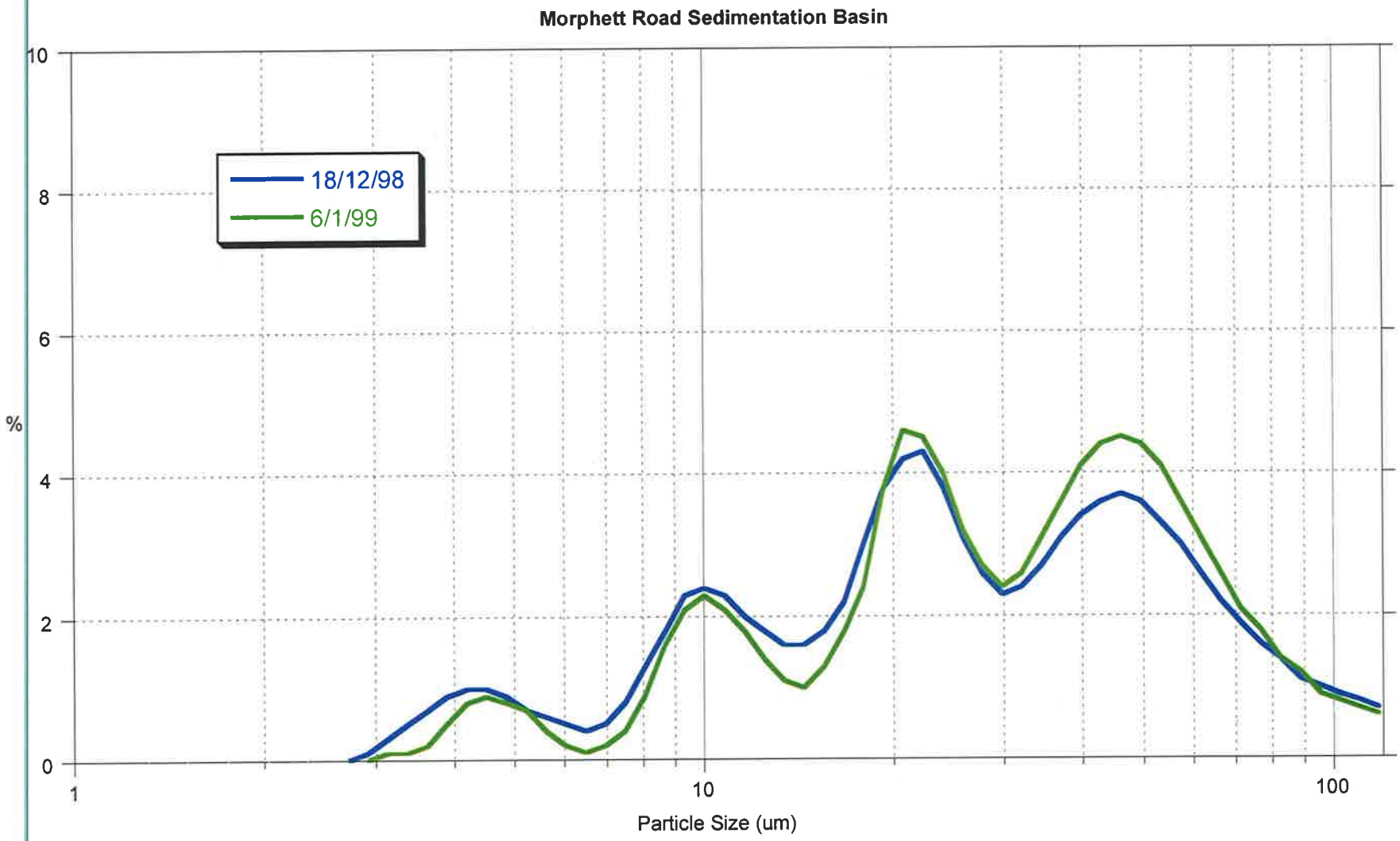
Morphett Road Sedimentation Basin
18/12/98
6/1/99
%
10
8
6
4
2
0
1
10
100
Particle Size (um)

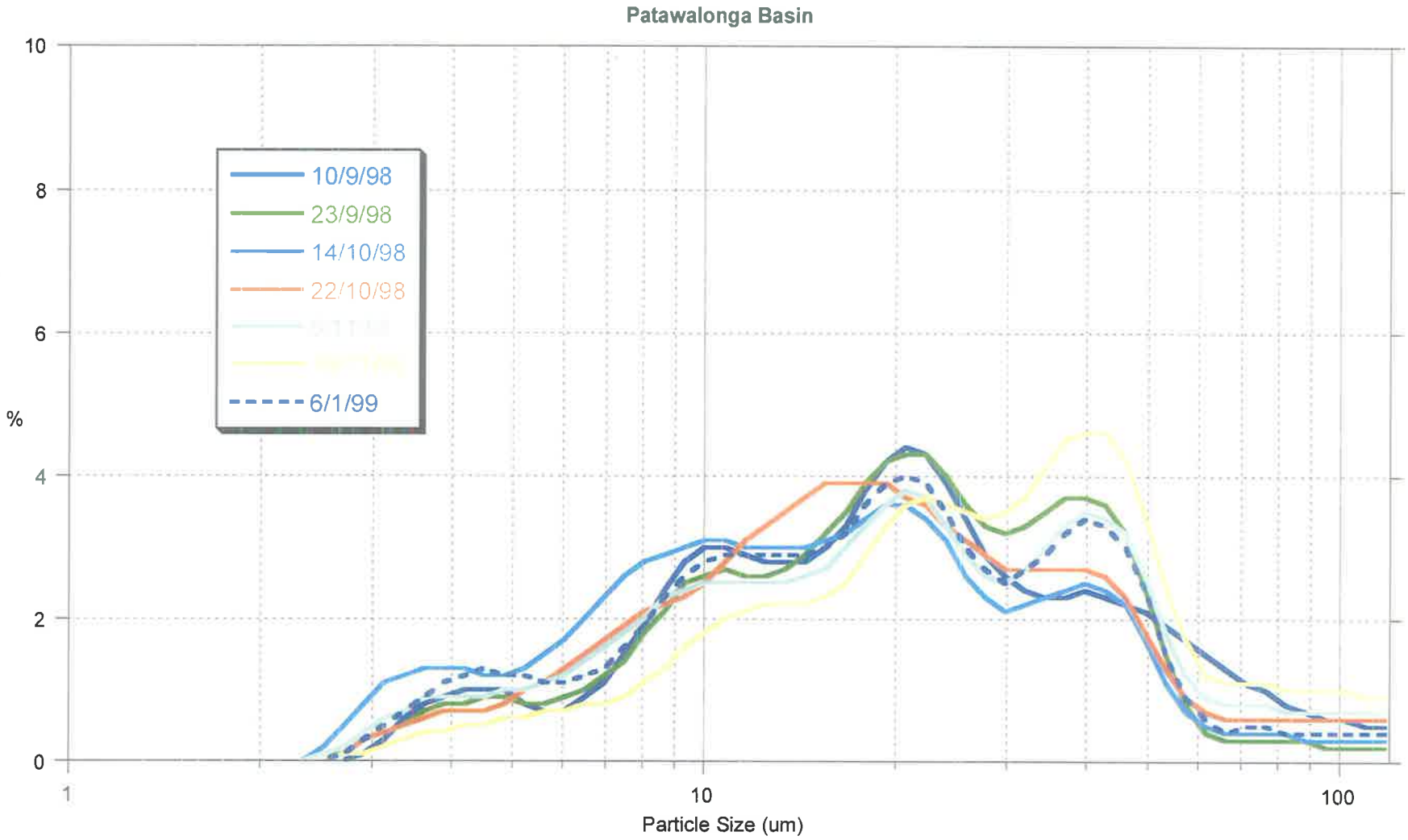
Patawalonga Basin
10
8
6
4
2
0
%
10/9/98
23/9/98
14/10/98
22/10/98
6/1/99
1
10
100
Particle Size (um)

Appendix F

Heavy Metal Concentration Data

WEIR 2

		Antimony	Arsenic	Barium	Beryllium	Boron	Cadmium	Chromium	Cobalt	Copper	Lead	Molybdenum	Nickel	Selenium	Tin	Vanadium	Zinc
Summer	< 63 μm	1.1	8	270	<0.5	-	0.5	24	6.6	80	210	<0.5	12	0.9	5.5	22	360
Summer	> 63 μm	0.8	8.5	280	0.5	-	0.7	31	8.7	72	300	<0.5	13	<0.5	1.1	28	540
Autumn	< 63 μm	1.9	7.4	190	<0.5	-	0.7	28	7.5	73	260	<0.5	12	0.6	5.3	24	490
Autumn	> 63 μm	2.2	2.5	46	<0.5	-	<0.5	9.7	3.1	21	68	<0.5	5.3	<0.5	<0.5	9	180
Winter	< 63 μm	<2.0	9.7	160	<1.0	66	<1.0	31	8.3	94	250	<5.0	12	4.5	4.9	25	680
Winter	> 63 μm	<2.0	9.2	150	<1.0	2.6	<1.0	31	10	95	330	<5.0	14	3.1	<2.0	27	840
Spring	< 63 μm	<2.0	20	170	<1.0	74	<1.0	45	9	160	210	<5.0	19	3.5	6.1	23	660
Spring	> 63 μm	<2.0	8.6	140	<1.0	5.6	<1.0	25	8.6	80	300	<5.0	11	<3.0	<2.0	24	720

LOCKLEYS

		Antimony	Arsenic	Barium	Beryllium	Boron	Cadmium	Chromium	Cobalt	Copper	Lead	Molybdenum	Nickel	Selenium	Tin	Vanadium	Zinc
Summer	< 63 µm	<0.5	6.3	210	0.8	-	<0.5	37	10	46	140	<0.5	18	1.4	3.3	28	330
Summer	> 63 µm	<0.5	5.5	180	0.6	-	<0.5	32	9.5	42	130	<0.5	14	<0.5	<0.5	28	390
Autumn	< 63 µm	1	6.8	180	0.6	-	<0.5	36	9.9	42	130	<0.5	15	<0.5	3.1	28	290
Autumn	> 63 µm	1.1	5.2	120	<0.5	-	<0.5	29	8	37	120	<0.5	12	<0.5	<0.5	23	260
Winter	< 63 µm	<2.0	12	140	<1.0	34	<1.0	39	10	57	150	<5.0	15	<3.0	3.4	26	400
Winter	> 63 µm	<2.0	5.9	72	<1.0	2.2	<1.0	19	6	32	120	<5.0	8.2	<3.0	<2.0	17	300
Spring	< 63 µm	<2.0	8.7	160	<1.0	29	<1.0	29	13	44	130	<5.0	15	<3.0	<2.0	21	370
Spring	> 63 µm	<2.0	2.5	35	<1.0	<2.0	<1.0	9	3.5	13	52	<5.0	3.5	<3.0	<2.0	9	140

BURBRIDGE ROAD SEDIMENTATION POND

		Antimony	Arsenic	Barium	Beryllium	Boron	Cadmium	Chromium	Cobalt	Copper	Lead	Molybdenum	Nickel	Selenium	Tin	Vanadium	Zinc
Summer	< 63 μm	2.6	7.7	100	<0.5	-	0.8	20	3.7	89	320	2.1	18	1.2	4.2	11	680
Summer	> 63 μm	1.2	14	150	<0.5	-	1.7	46	7.6	160	740	4.6	30	1.6	1.4	23	1600
Autumn	< 63 μm	1.9	15	200	<0.5	-	1.5	51	7.4	150	610	2.6	22	<0.5	3.8	22	1300
Autumn	> 63 μm	2.1	17	180	<0.5	-	1.9	66	8.3	170	840	3.7	28	<0.5	1	25	1900
Winter	< 63 μm	<2.0	9	86	<1.0	180	<1.0	48	3.6	63	260	7.5	11	3.1	3.9	10	780
Winter	> 63 μm	<2.0	21	140	<1.0	35	2.1	77	8.4	170	750	5.1	24	<3.0	<2.0	24	2100
Spring	< 63 μm	2.7	4.9	51	<1.0	260	<1.0	12	2	43	140	9.9	4.8	3.1	<2.0	4.9	290
Spring	> 63 μm	<2.0	18	110	<1.0	56	2	37	7.8	160	730	7	22	4	<2.0	22	1900

MORPHETT ROAD SEDIMENTATION POND

		Antimony	Arsenic	Barium	Beryllium	Boron	Cadmium	Chromium	Cobalt	Copper	Lead	Molybdenum	Nickel	Selenium	Tin	Vanadium	Zinc
Summer	< 63 µm	1.3	7.3	72	<0.5	-	<0.5	9.2	4.3	36	75	2.4	5.2	1.1	1.7	7.6	400
Summer	> 63 µm	0.6	22	160	<0.5	-	1.4	32	14	110	280	1.3	17	<0.5	1	24	1600
Autumn	< 63 µm	0.8	10	120	<0.5	-	0.8	30	8.5	53	170	1.4	16	<0.5	4.8	27	620
Autumn	> 63 µm	<0.5	11	130	<0.5	-	0.8	24	11	62	200	<0.5	14	<0.5	<0.5	22	910
Winter	< 63 µm	<2.0	9.6	110	<1.0	110	<1.0	29	7.2	75	130	<5.0	13	<3.0	4.3	19	450
Winter	> 63 µm	<2.0	12	130	<1.0	7.9	1	29	11	73	280	<5.0	17	<3.0	<2.0	26	1200
Spring	< 63 µm	<2.0	9.9	81	<1.0	81	<1.0	23	10	180	54	<5.0	7.4	4.9	<2.0	9.5	400
Spring	> 63 µm	<2.0	16	160	<1.0	14	<1.0	27	13	73	240	<5.0	16	<3.0	<2.0	25	1300

PATAWALONGA BASIN

		Antimony	Arsenic	Barium	Beryllium	Boron	Cadmium	Chromium	Cobalt	Copper	Lead	Molybdenum	Nickel	Selenium	Tin	Vanadium	Zinc
Summer	< 63 μm (6/1)	<0.5	<0.5	2	<0.5	-	<0.5	1.3	<0.5	2.9	5	<0.5	1.4	<0.5	<0.5	1	20
Summer	< 63 μm (21/1)	16	0.6	2.7	<0.5	-	<0.5	1.5	<0.5	4	6.2	<0.5	1.6	0.9	0.5	1.6	21
Summer	< 63 μm (18/2)	4.4	<0.5	1.4	<0.5	-	<0.5	0.8	<0.5	2.3	<0.5	<0.5	0.8	<0.5	<0.5	<0.5	5.5
Summer	> 63 μm	<0.5	3.1	15	<0.5	-	<0.5	8	1.5	11	37	0.7	4.7	<0.5	1.3	11	98
Autumn	< 63 μm (29/4)	<0.5	<0.5	4.2	<0.5	-	<0.5	2.7	<0.5	4.7	13	<0.5	1.9	<0.5	4.4	2.4	42
Autumn	< 63 μm (27/5)	<0.5	7.5	150	<0.5	-	<0.5	28	8.7	45	160	<0.5	14	<0.5	3.4	25	420
Autumn	> 63 μm	<0.5	2	31	<0.5	-	<0.5	9.2	1.6	14	52	<0.5	4.5	<0.5	0.5	8.6	150
Winter	< 63 μm	<2.0	2.3	16	<1.0	100	<1.0	5.3	<2.0	12	37	<5.0	2.5	<3.0	<2.0	5.5	80
Winter	> 63 μm	<2.0	5.5	37	<1.0	6.6	<1.0	8.8	2	16	75	<5.0	4.5	<3.0	<2.0	12	160
Spring	< 63 μm	<2.0	<2.0	8.4	<1.0	100	<1.0	3	<2.0	7.2	21	<5.0	<2.0	<3.0	<2.0	2.2	45
Spring	> 63 μm	<2.0	11	71	<1.0	46	1.2	26	6.2	130	300	<5.0	15	<3.0	4.5	26	780

Appendix G

Heavy Metal Concentration Graphs


Zinc
Concentration (mg/kg)
3000
2500
2000
1500
1000
500
0
< 63 um
> 63 um
Weir 2
Lockleys
Burb Rd
Morph Rd
Pat Basin


Lead
Concentration (mg/kg)
1200
1000
800
600
400
200
0
< 63 um
> 63 um
Weir 2
Lockleys
Burb Rd
Morph Rd
Pat Basin

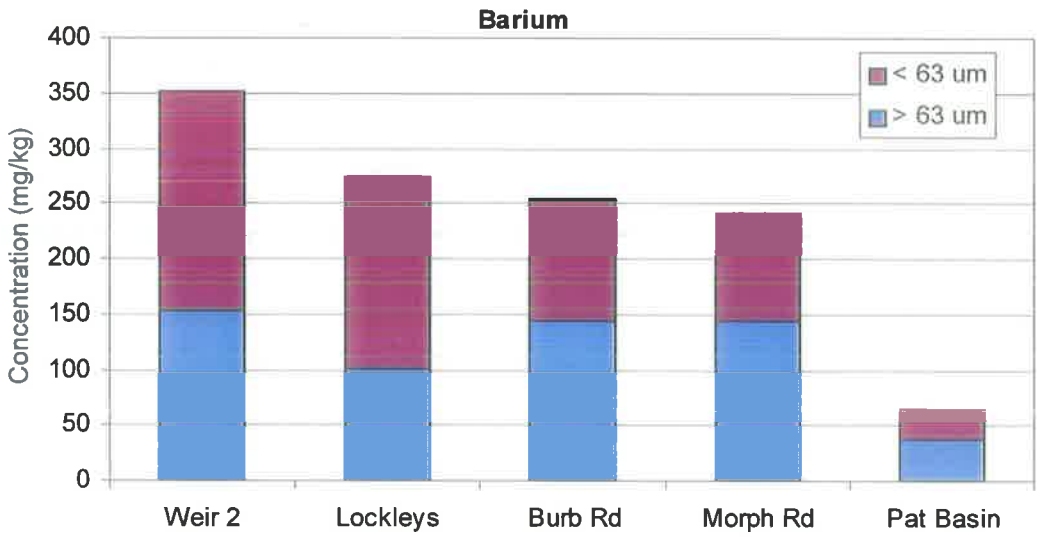
Barium
Concentration (mg/kg)
400
350
300
250
200
150
100
50
0
< 63 um
> 63 um
Weir 2
Lockleys
Burb Rd
Morph Rd
Pat Basin

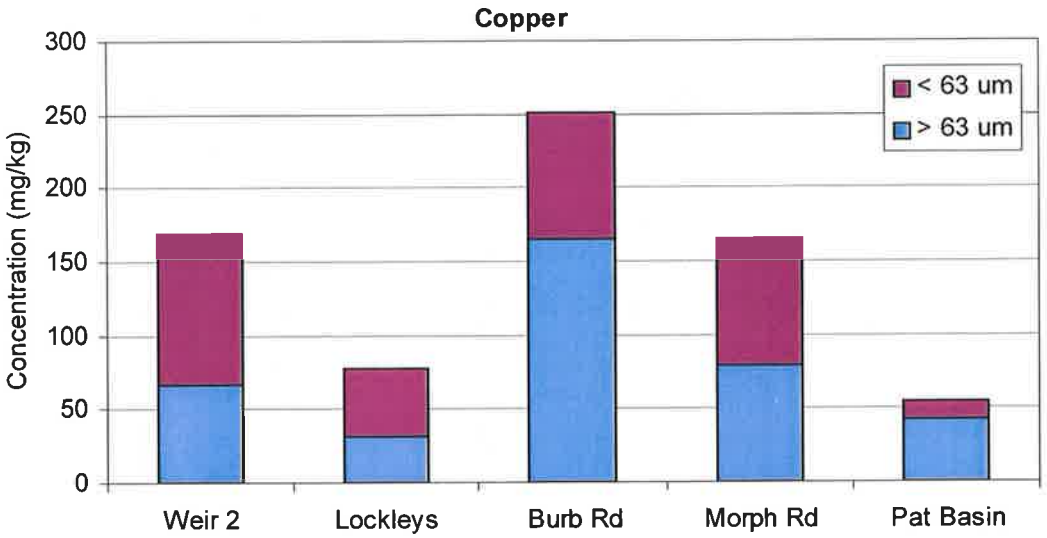
Copper
Concentration (mg/kg)
300
250
200
150
100
50
0
< 63 um
> 63 um
Weir 2
Lockleys
Burb Rd
Morph Rd
Pat Basin

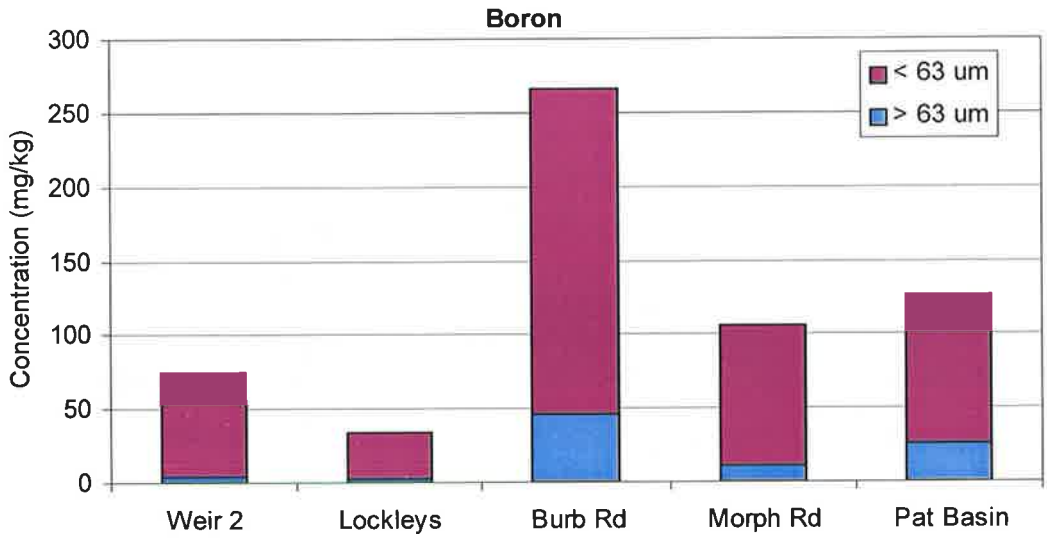
Boron
Concentration (mg/kg)
300
250
200
150
100
50
0
< 63 um
> 63 um
Weir 2
Lockleys
Burb Rd
Morph Rd
Pat Basin

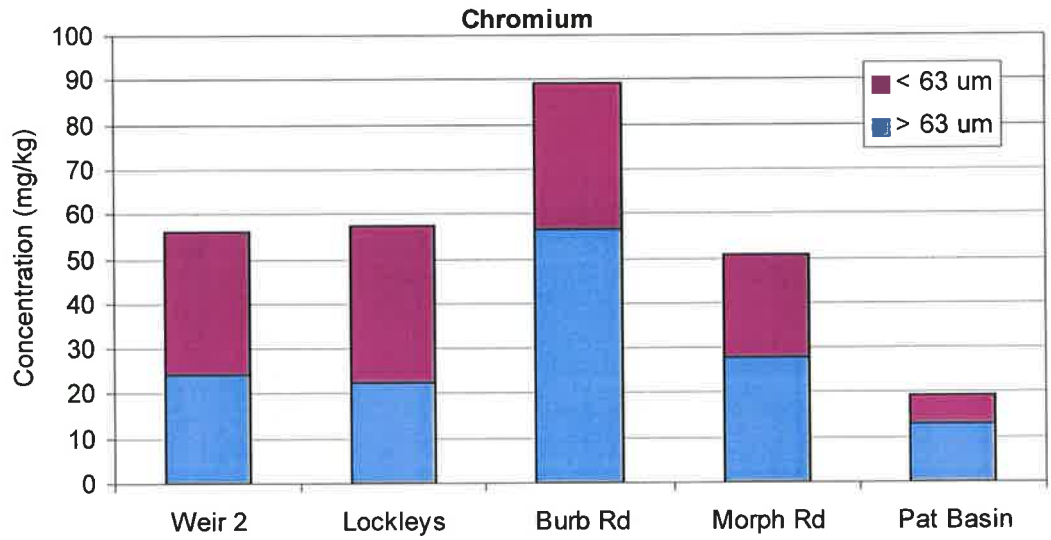
Chromium
Concentration (mg/kg)
100
90
80
70
60
50
40
30
20
10
0
< 63 um
> 63 um
Weir 2
Lockleys
Burb Rd
Morph Rd
Pat Basin

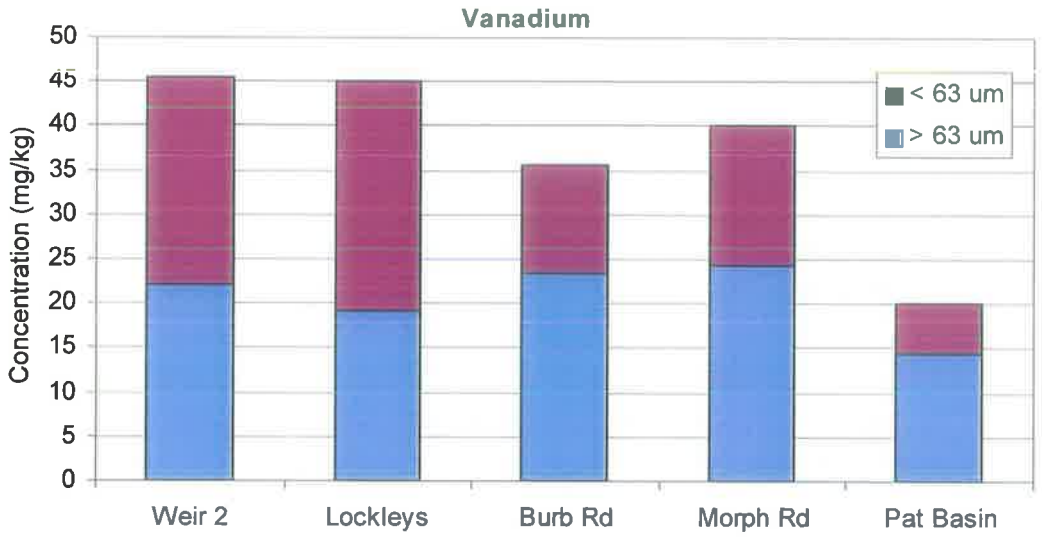
Vanadium
Concentration (mg/kg)
50
45
40
35
30
25
20
15
10
5
0
< 63 um
> 63 um
Weir 2
Lockleys
Burb Rd
Morph Rd
Pat Basin

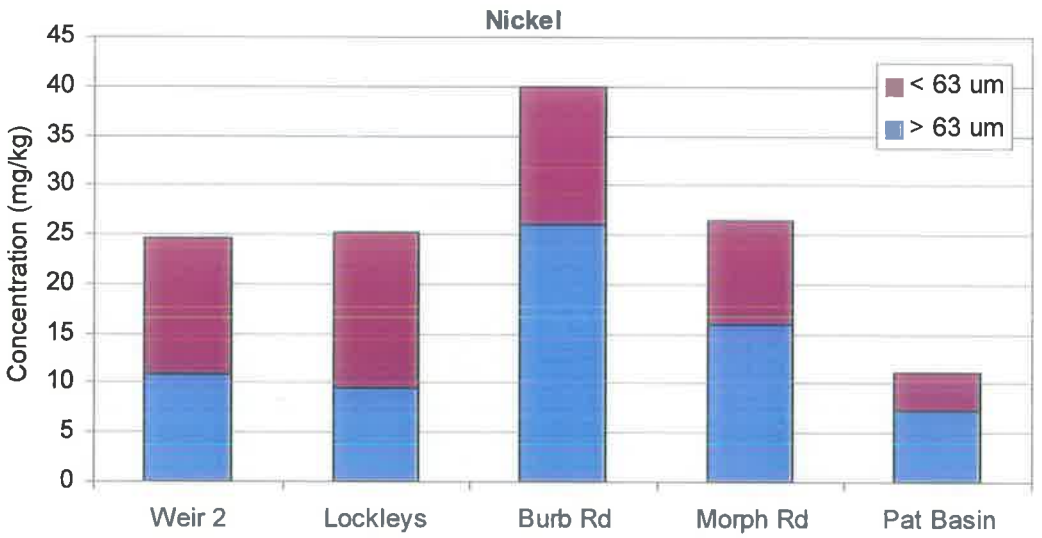
Nickel
Concentration (mg/kg)
45
40
35
30
25
20
15
10
5
0
< 63 um
> 63 um
Weir 2
Lockleys
Burb Rd
Morph Rd
Pat Basin

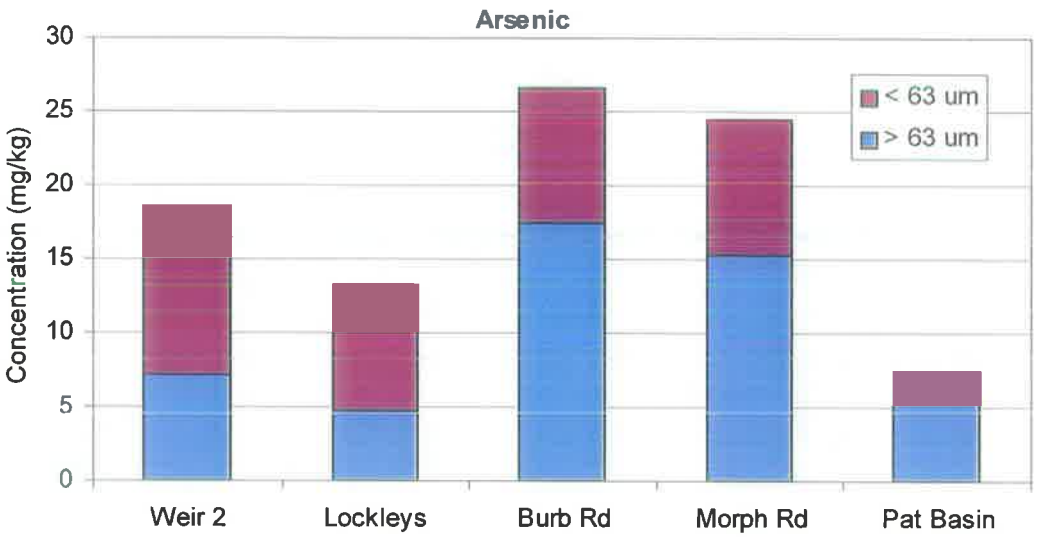
Arsenic
Concentration (mg/kg)
30
25
20
15
10
5
0
< 63 um
> 63 um
Weir 2
Lockleys
Burb Rd
Morph Rd
Pat Basin

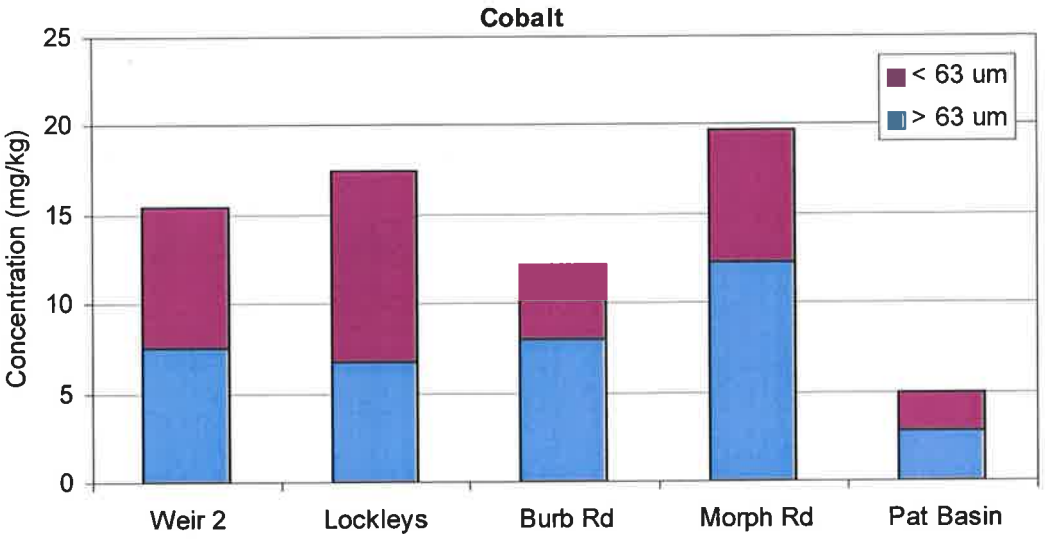
Cobalt
Concentration (mg/kg)
25
20
15
10
5
0
< 63 um
> 63 um
Weir 2
Lockleys
Burb Rd
Morph Rd
Pat Basin

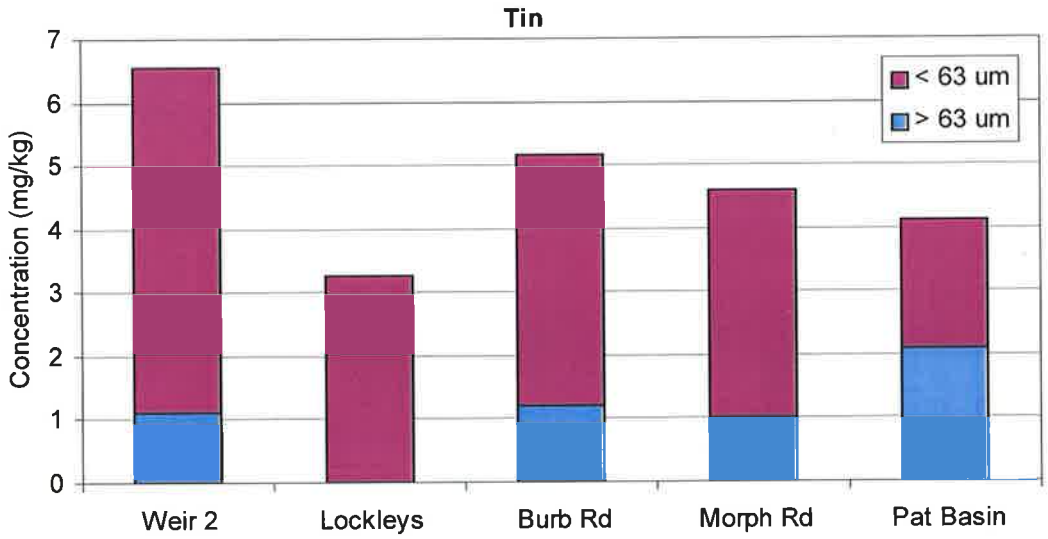
Tin
Concentration (mg/kg)
7
6
5
4
3
2
1
0
< 63 um
> 63 um
Weir 2
Lockleys
Burb Rd
Morph Rd
Pat Basin

Appendix H

Temperature Sensor Calibration

To calibrate temperature sensors, the specific temperature-voltage relationship had to be determined for each sensor.

Calibration equipment included:

- temperature sensors
- power source
- voltmeter
- Hannah temperature probe
- 1L esky
- tap water
- ice
- hot water

A 1L esky was filled with tap water and allowed to stabilise at room temperature for 2 days prior to the temperature sensor calibration.

Sensors were wired together in a bunch, around a Hannah temperature probe, then the sensors and probe were passed through a hole in the top of the esky so that they were completely immersed in the water. When the reading from the temperature probe had stabilised, the temperature was recorded, and the corresponding voltage of each sensor was determined, using a voltmeter. (Voltage readings were repeated for all sensors for confirmation.)

An ice bath was then prepared by completely filling the esky with crushed ice and water. The temperature and voltage of each sensor were again recorded at the lower temperature.

The esky was then filled with hot (approximately 40°C) water and the recording procedure repeated. Voltage readings had to be taken rapidly to ensure all sensors were at a uniform temperature. (All sensors did not need not to be at the same temperature, as long as the exact temperature of the sensor was recorded at the time the voltage reading was taken.)

The temperature-voltage relationship for each sensor was assumed to be perfectly linear, thus a minimum of 2 temperature-voltage readings were required to calibrate each sensor. Greater accuracy could be achieved, however, by increasing the number of data points that could be used to determine the temperature-voltage relationship, thus the third reading was taken at the hotter temperature. Furthermore, the sensors were allowed to soak in the cooling water for a further 3 days, before the temperature and voltages were again recorded, which acted as a check on the linear relationship that had been calculated. (A consistent voltage reading could not be obtained for sensor 10 on that occasion.)

A linear trend line was fitted to the 3 data points for each sensor. Plots of the temperature-voltage relationship are shown in Figure H–1 through Figure H–10. Table H–1 shows the temperature-voltage readings that were taken and slopes that were calculated.

Table H–1: Voltage readings for the 10 sensors at 4 different temperatures in V

	Temperature Sensor									
Temp (°C)	**1**	**2**	**3**	**4**	**5**	**6**	**7**	**8**	**9**	**10**
0.8	2.74	2.741	2.73	2.731	2.722	2.734	2.723	2.741	2.729	2.728
22.5	2.964	2.965	2.955	2.957	2.946	2.957	2.947	2.965	2.953	2.955
44	3.183	3.167	3.175	3.167	3.177	3.176	3.184	3.186	3.174	3.176
26.2*	3.001	3.002	2.993	3.004	2.985	2.995	2.985	3.033	2.991	-
Slope	**0.01**	**0.01**	**0.01**	**0.01**	**0.011**	**0.01**	**0.011**	**0.01**	**0.01**	**0.01**
R^2	1.000	0.999	1.000	1.000	1.000	1.000	1.000	1.000	1.000	1.000

*Voltage readings for the fourth temperature were recorded, but not used in the analysis

Following calibration, sensors 1 to 8 were wired to a data logger, which was set to take readings at 5 minute intervals. The sensors were placed in a vessel of hot water and allowed to sit for 45 hours and 45 minutes while the water cooled to room temperature, which fluctuated with the daily air temperature changes in the laboratory. A new battery was installed and the logger re-set to run a further 46 hours and 40 minutes.

Analysis of the temperatures recorded for the 8 sensors showed a difference of 0.27°C to 0.43°C between the highest and lowest temperature sensor. This is illustrated in Figure H–11. Further calibration of the sensors by setting the datum level using the program STERM was able to reduce the temperature range between the highest and lowest sensor to between 0.08°C and 0.21°C when the sensors were run for a further 68 hours and 5 minutes.

The temperature behaviour of the sensors during the testing and calibration is illustrated in Figure H–12. Figure H–13 gives a magnification of the temperature sensor behaviour shown in Figure H–12 at two different times on Day 1. The mean temperature of the 8 sensors is in the low to mid-thirties in the first graph in Figure H–13 and in the low to mid-twenties in the second graph in Figure H–13. The temperature of each sensor relative to the mean temperature of all 8 sensors clearly changes with temperature, illustrating the non-linearity of the temperature-voltage relationship.

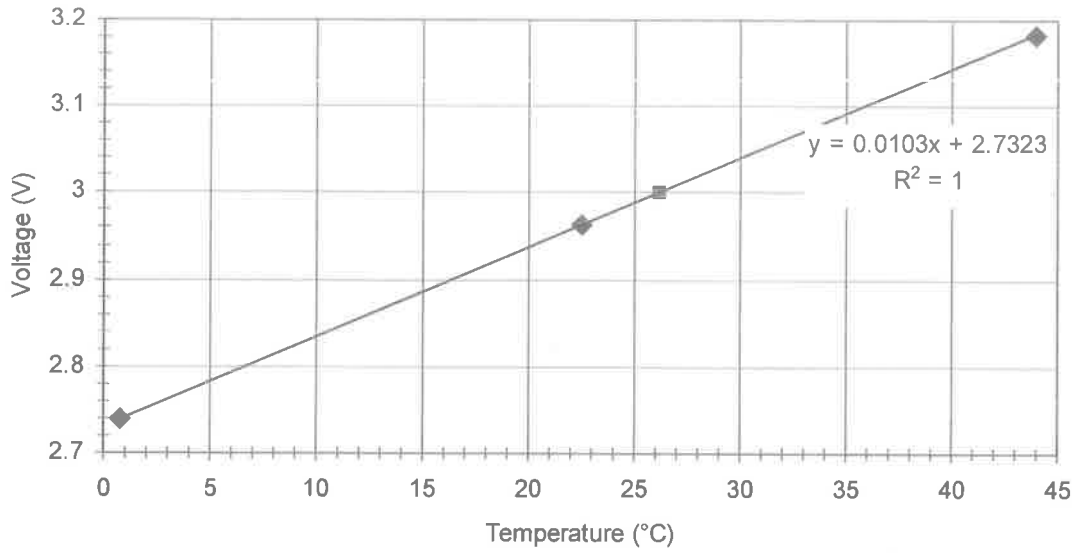

Figure H–1: The temperature-voltage relationship for sensor 1

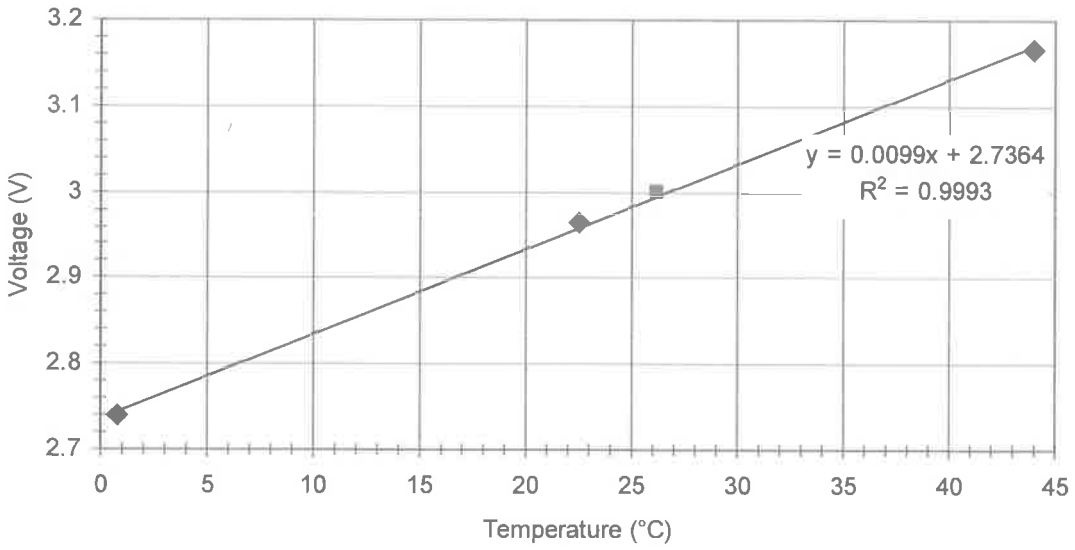

Figure H–2: The temperature-voltage relationship for sensor 2

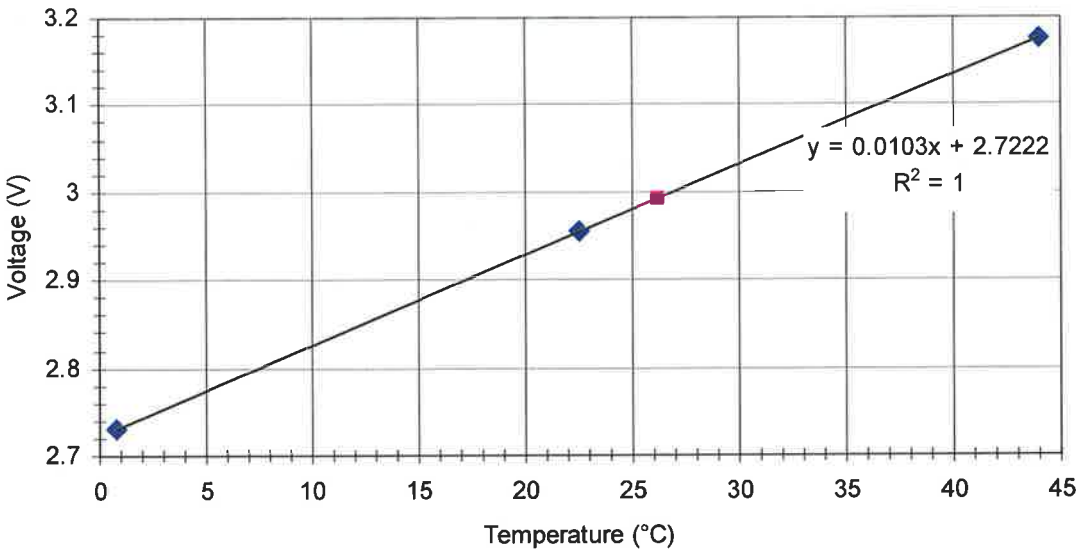

Figure H–3: The temperature-voltage relationship for sensor 3

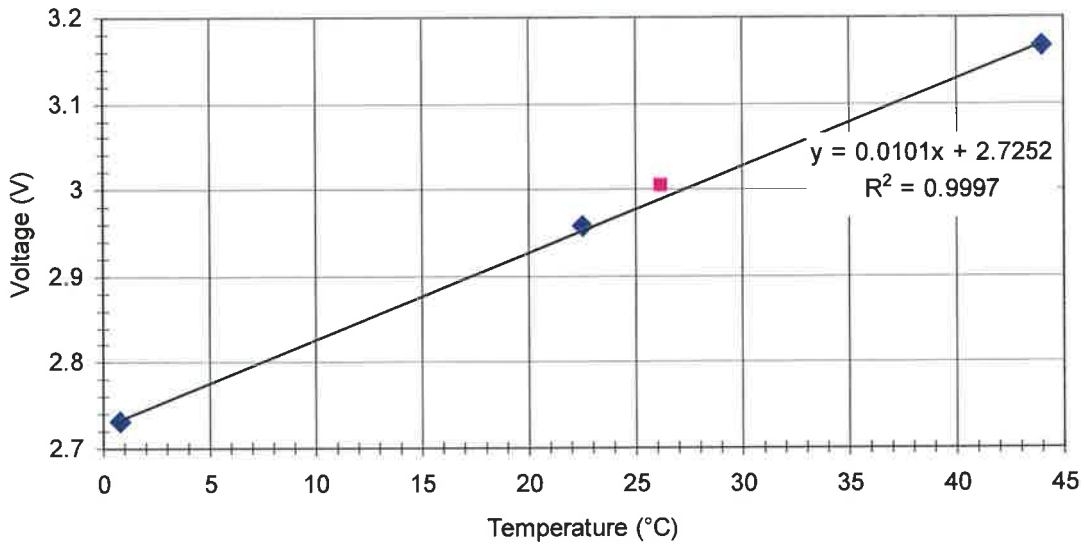

Figure H–4: The temperature-voltage relationship for sensor 4

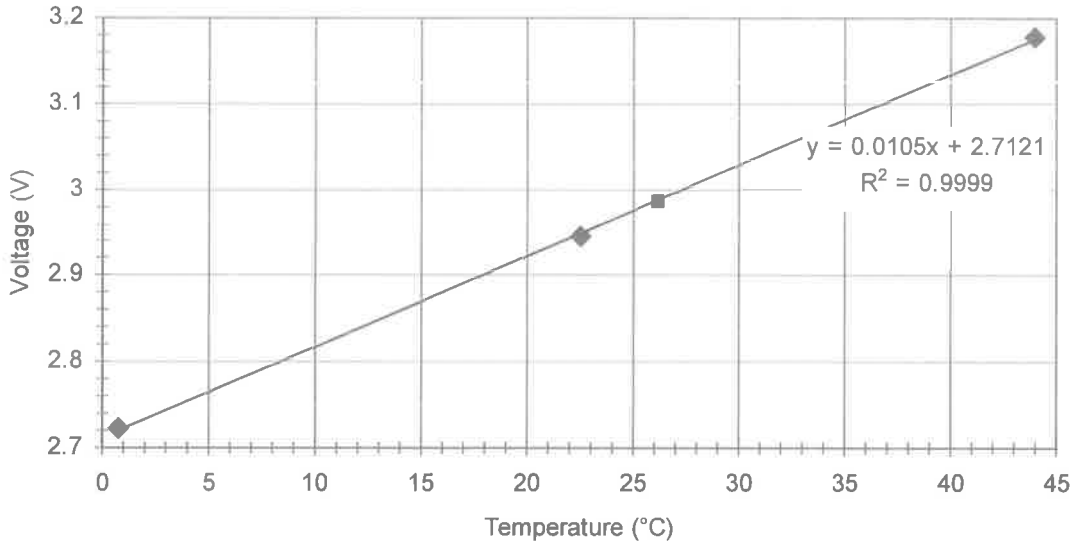

Figure H–5: The temperature-voltage relationship for sensor 5

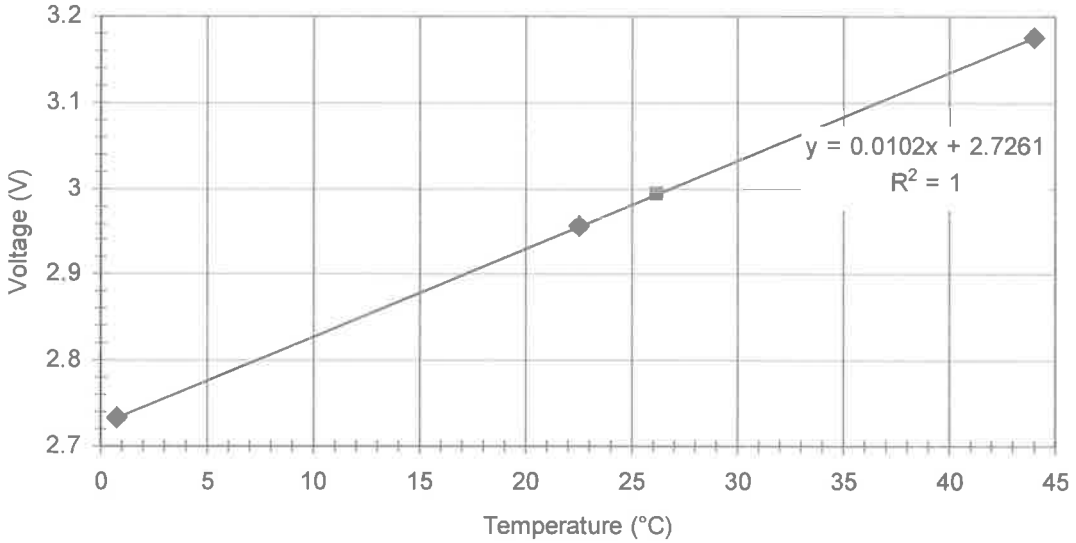

Figure H–6: The temperature-voltage relationship for sensor 6

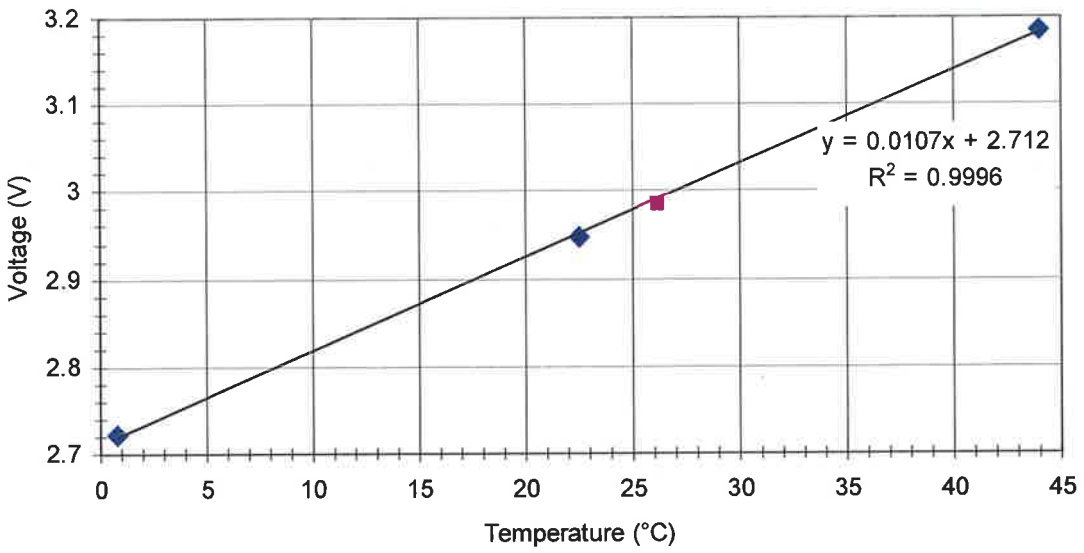

Figure H–7: The temperature-voltage relationship for sensor 7

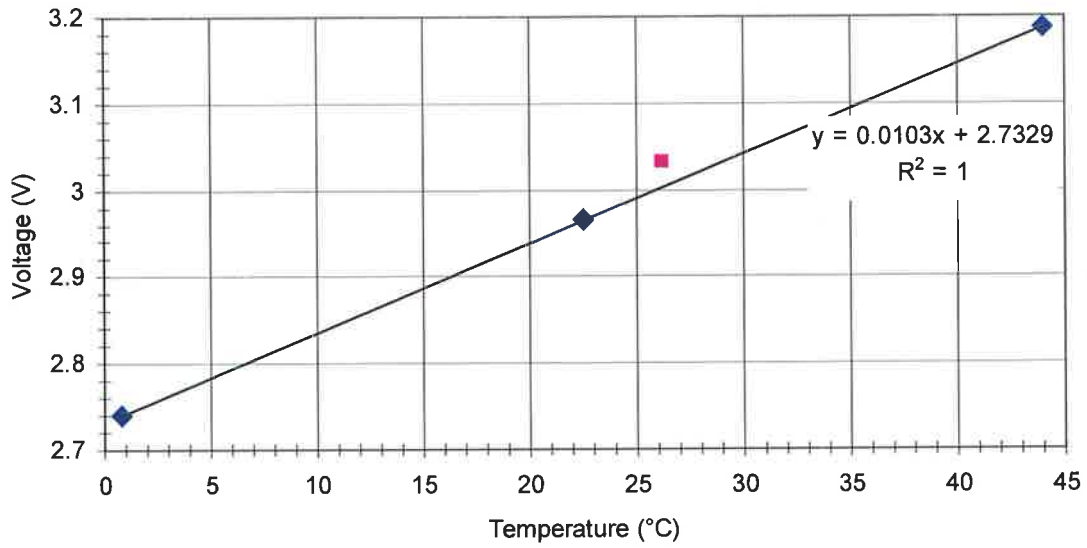

Figure H–8: The temperature-voltage relationship for sensor 8

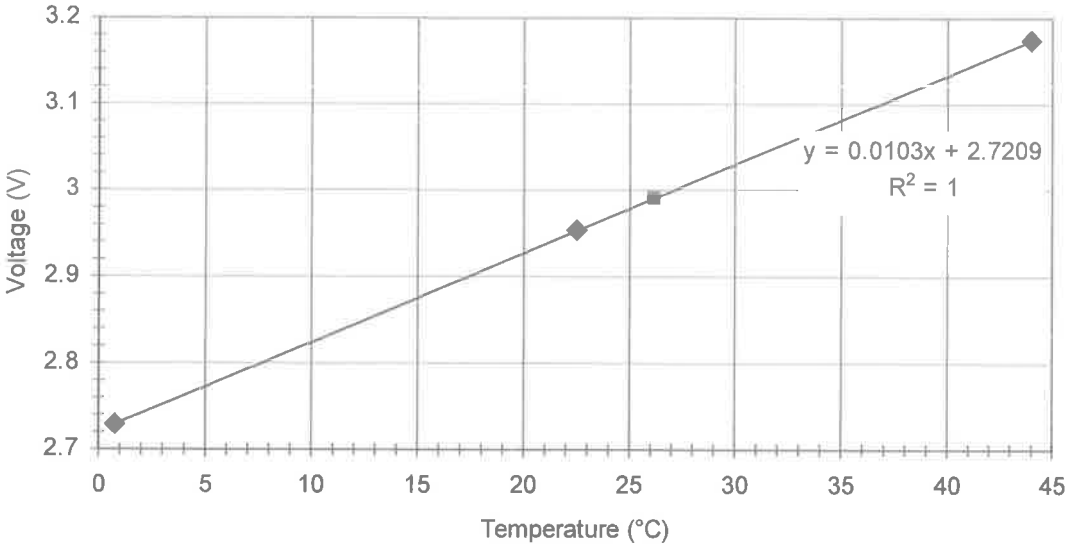

Figure H–9: The temperature-voltage relationship for sensor 9

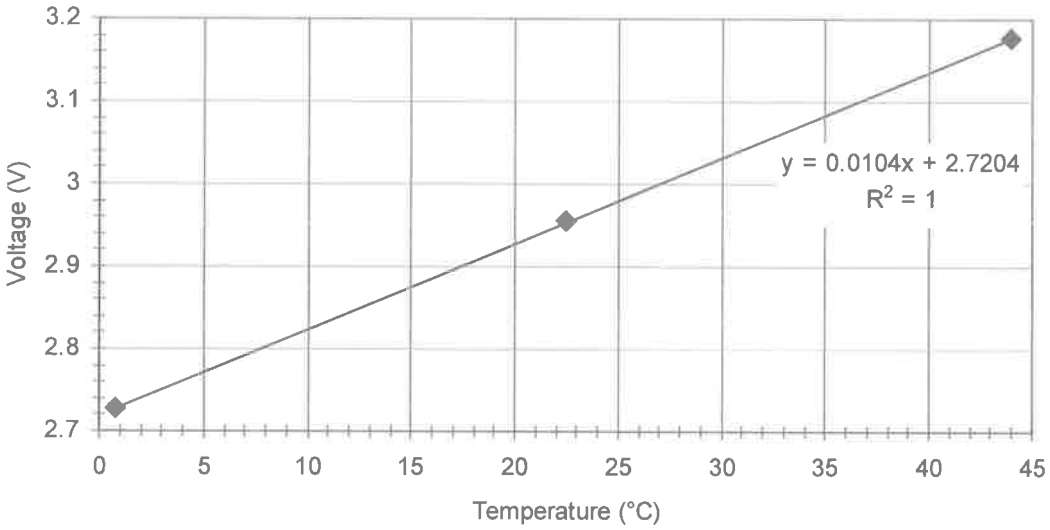

Figure H–10: The temperature-voltage relationship for sensor 10

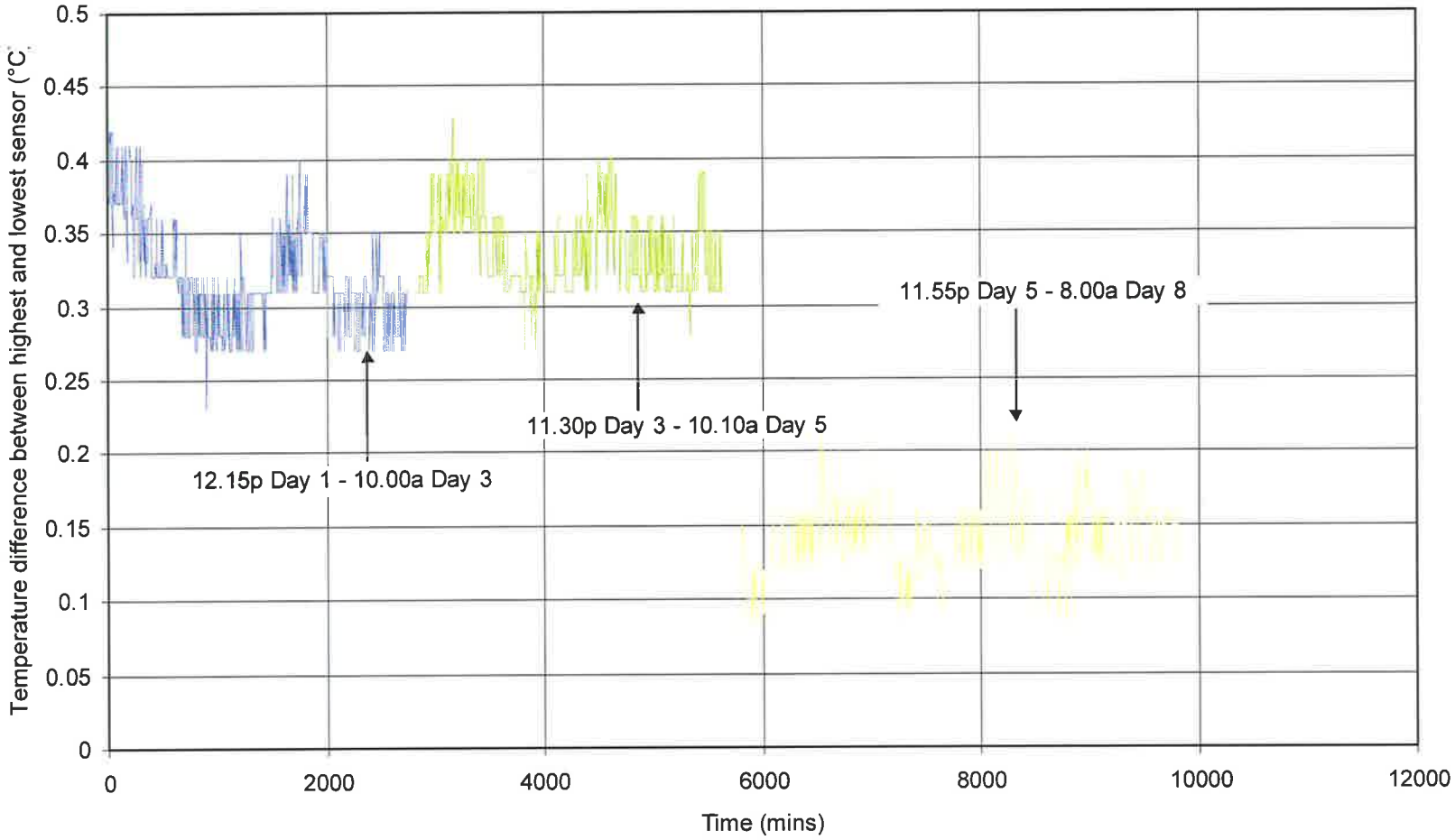

Figure H–11: The maximum temperature difference between the sensors (note the improvement following calibration in STERM on Day 5)

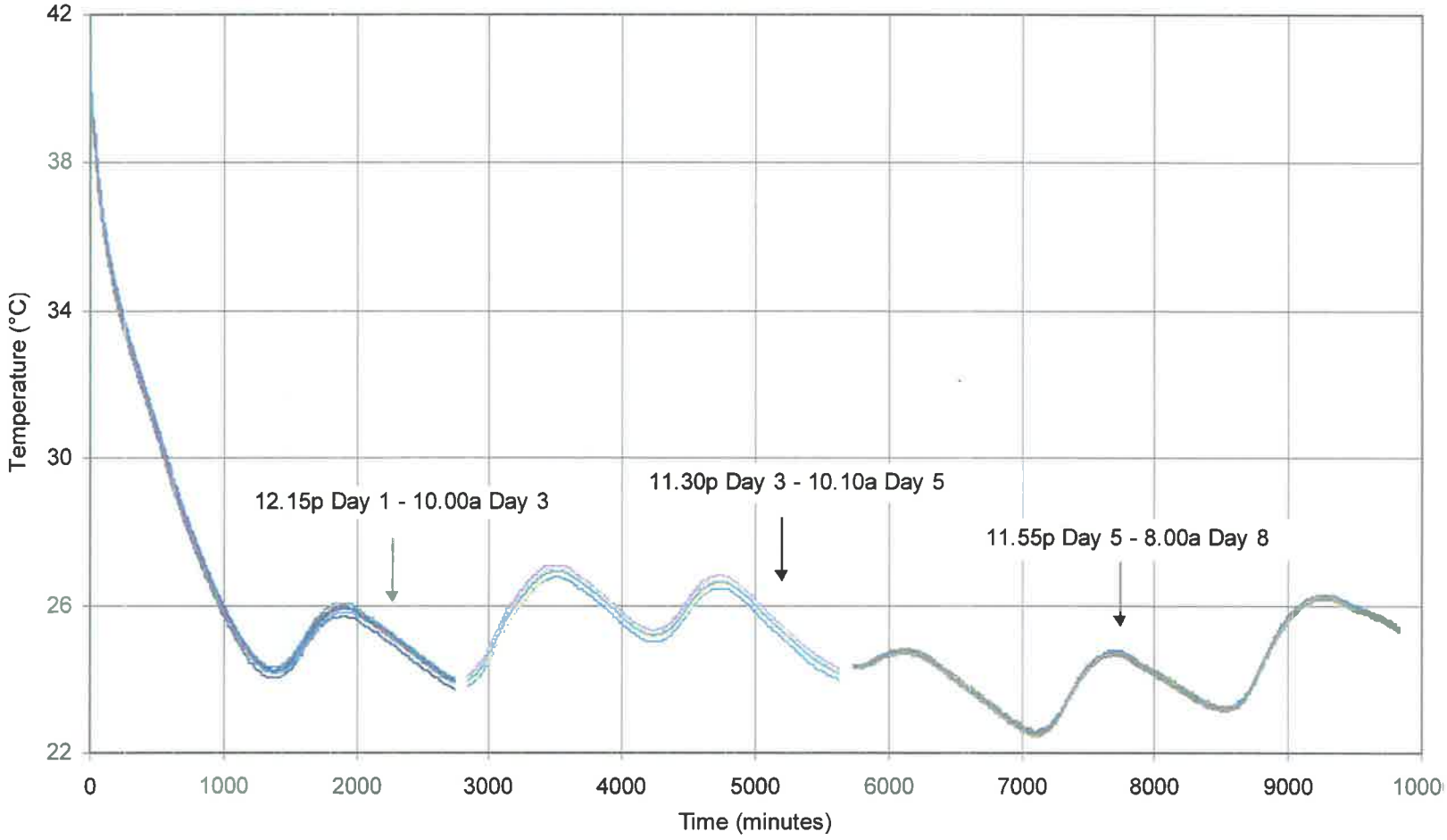

Figure H–12: The behaviour of the temperature sensors following immersion in hot water (Day 1 – Day 3), changing of the battery (Day 3 – Day 5) and further calibration in STERM (Day 5 – Day 8)

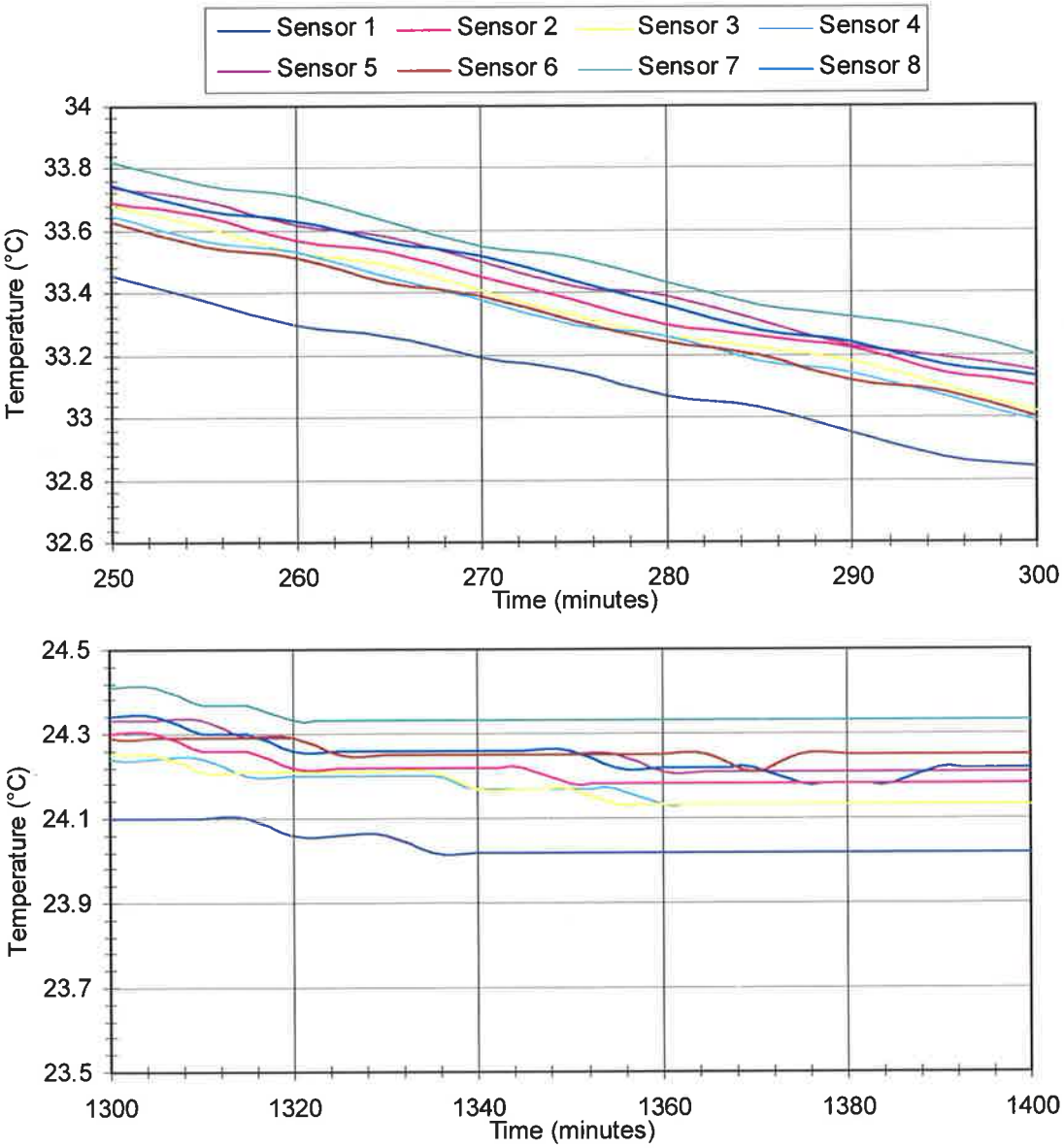

Figure H–13: The difference in temperature of the 8 sensors at two different times on Day 1

Appendix I

Morphett Road Sedimentation Pond Temperature Profiles

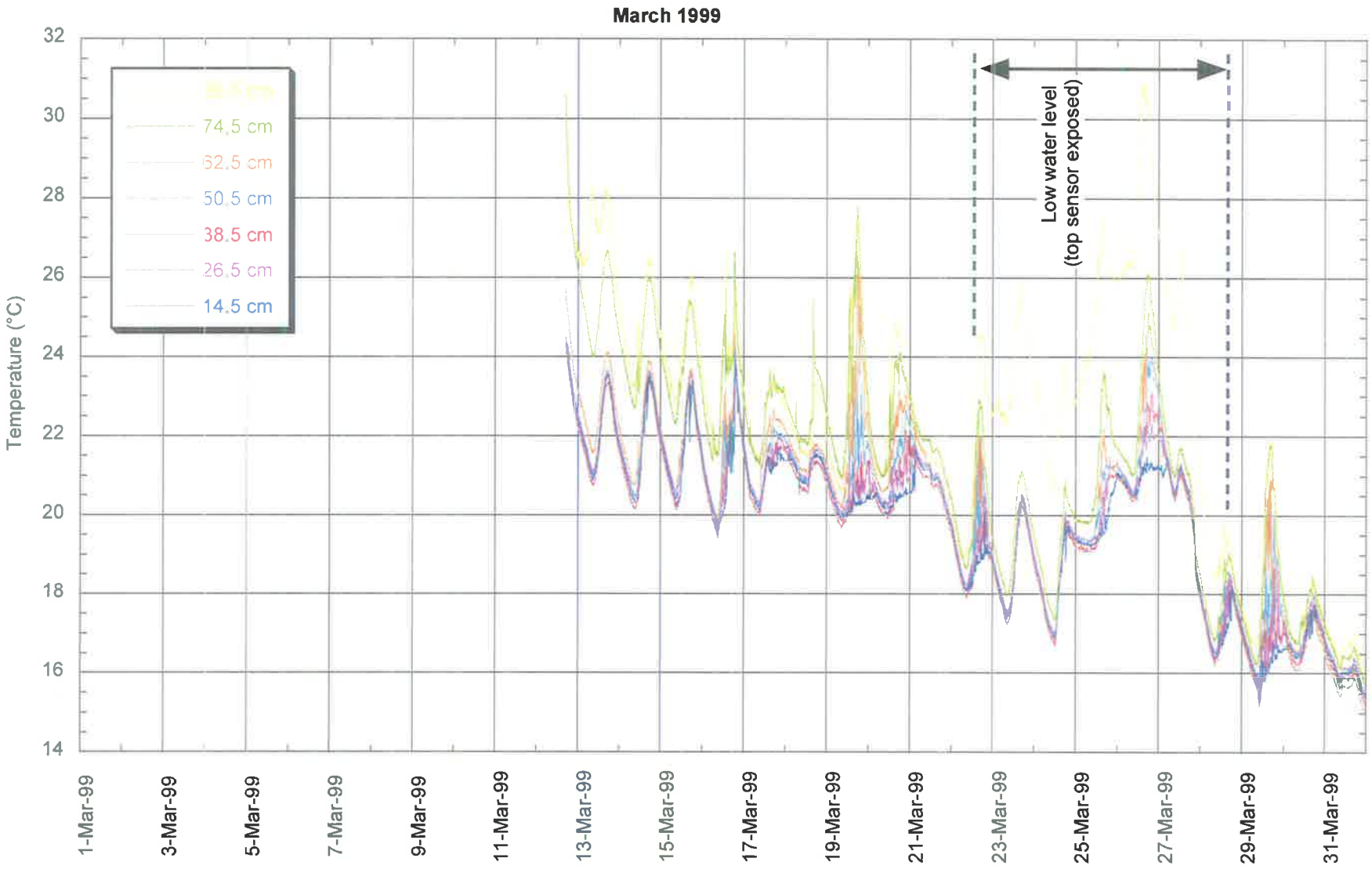
March 1999
Temperature (°C)
32
30
28
26
24
22
20
18
16
14
74.5 cm
62.5 cm
50.5 cm
38.5 cm
26.5 cm
14.5 cm
Low water level
(top sensor exposed)
1-Mar-99
3-Mar-99
5-Mar-99
7-Mar-99
9-Mar-99
11-Mar-99
13-Mar-99
15-Mar-99
17-Mar-99
19-Mar-99
21-Mar-99
23-Mar-99
25-Mar-99
27-Mar-99
29-Mar-99
31-Mar-99

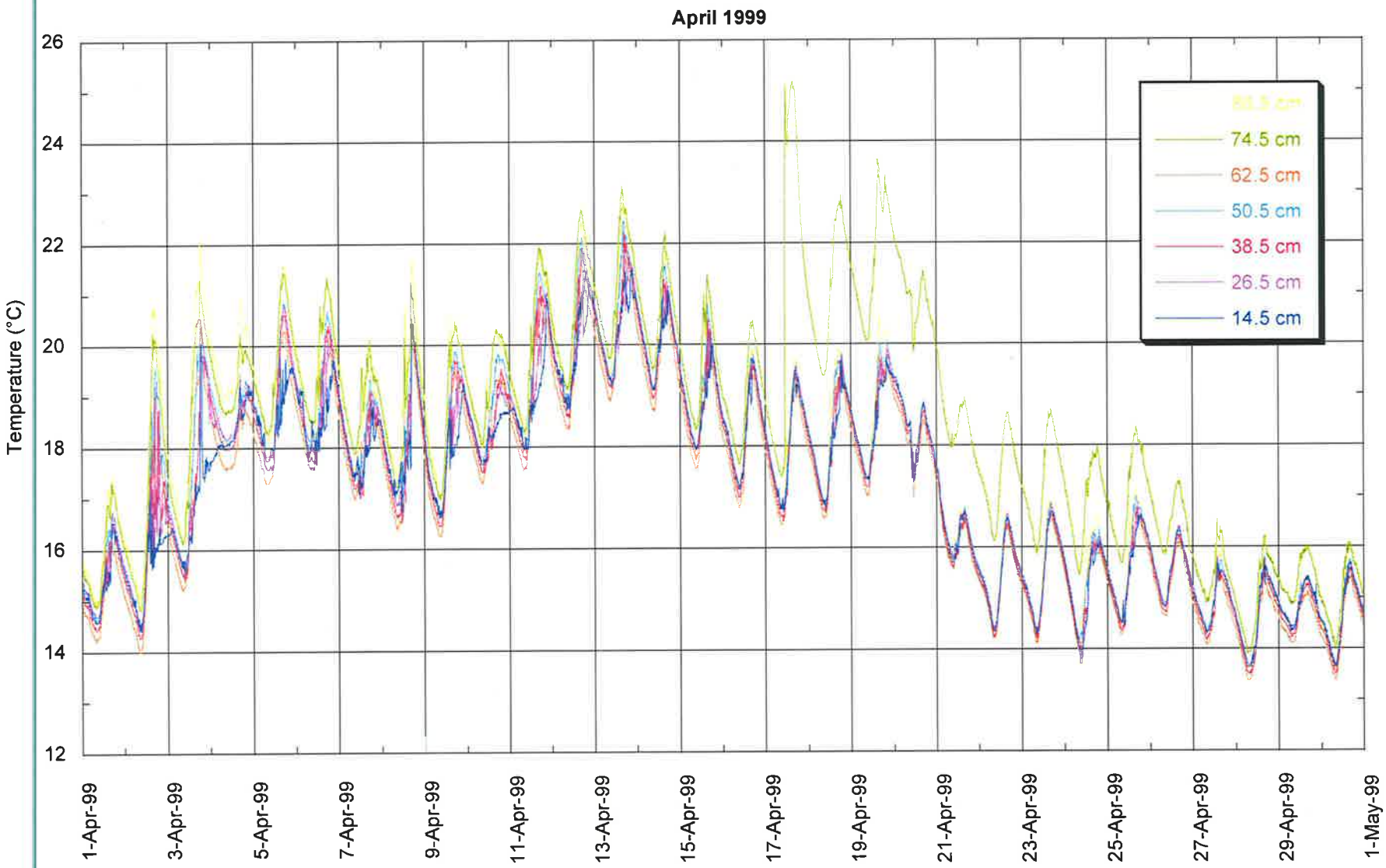
April 1999
Temperature (°C)
26
24
22
20
18
16
14
12
84.5 cm
74.5 cm
62.5 cm
50.5 cm
38.5 cm
26.5 cm
14.5 cm
1-Apr-99
3-Apr-99
5-Apr-99
7-Apr-99
9-Apr-99
11-Apr-99
13-Apr-99
15-Apr-99
17-Apr-99
19-Apr-99
21-Apr-99
23-Apr-99
25-Apr-99
27-Apr-99
29-Apr-99
1-May-99

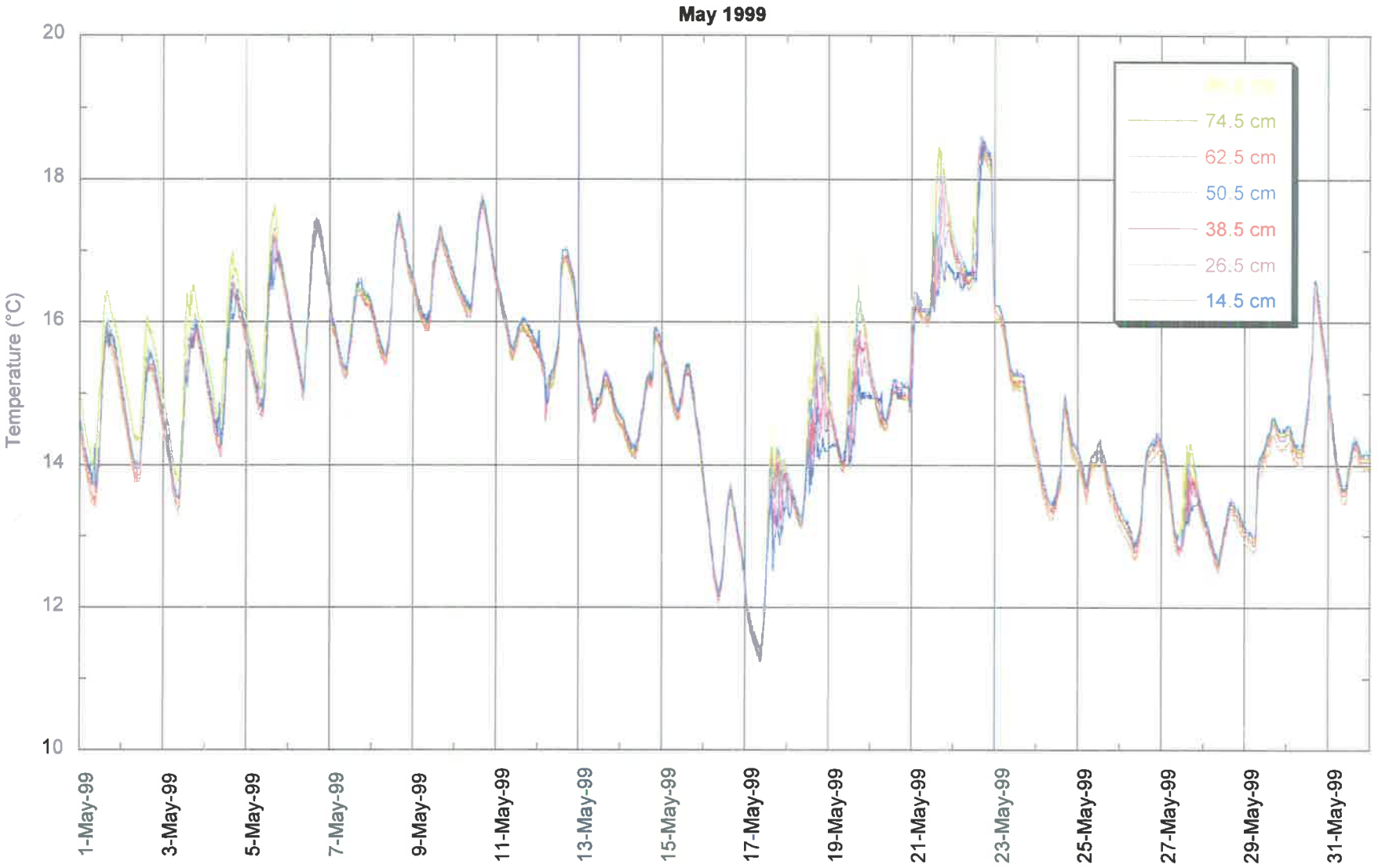
May 1999
Temperature (°C)
20
18
16
14
12
10
74.5 cm
62.5 cm
50.5 cm
38.5 cm
26.5 cm
14.5 cm
1-May-99
3-May-99
5-May-99
7-May-99
9-May-99
11-May-99
13-May-99
15-May-99
17-May-99
19-May-99
21-May-99
23-May-99
25-May-99
27-May-99
29-May-99
31-May-99

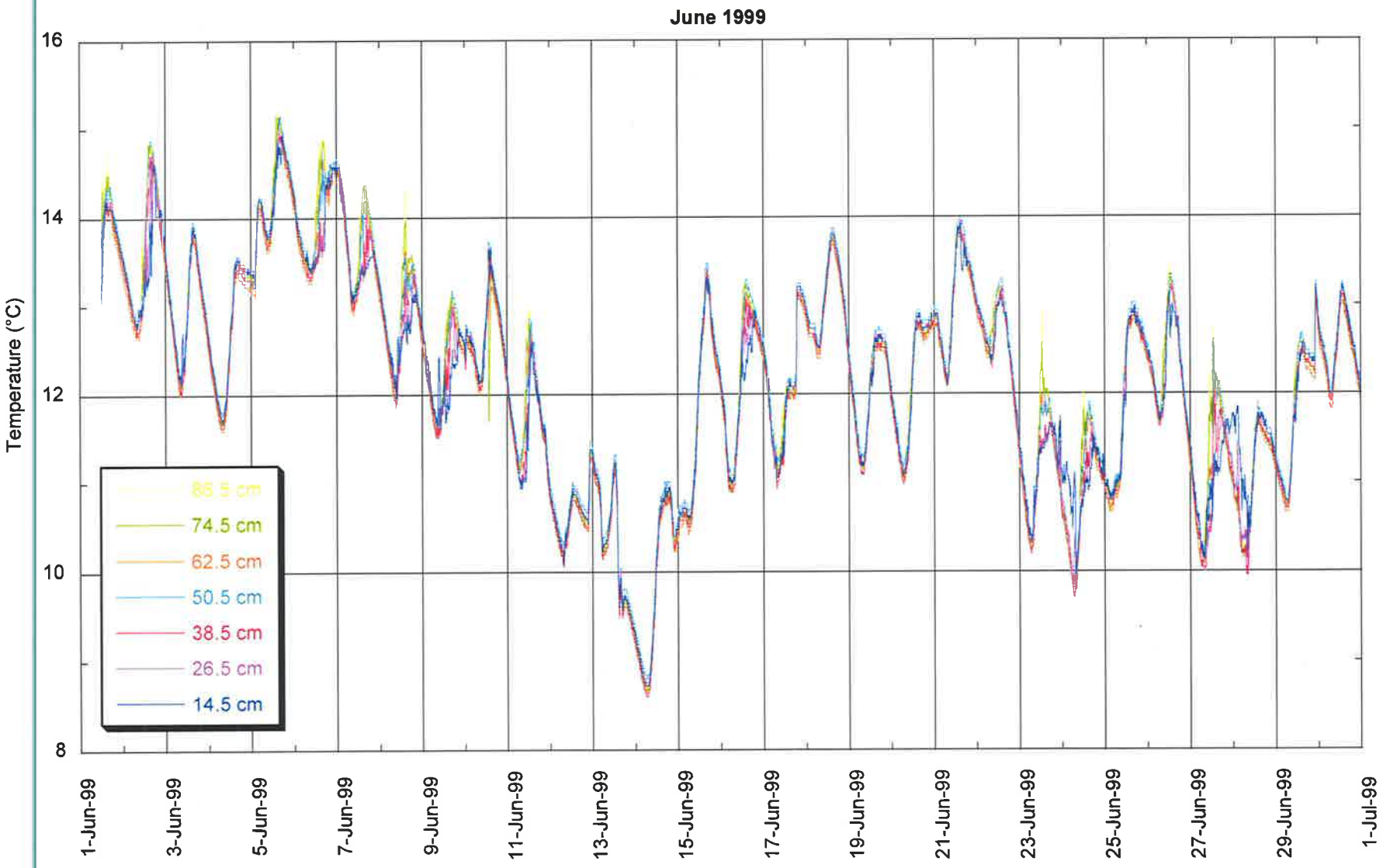
June 1999
Temperature (°C)
16
14
12
10
8
86.5 cm
74.5 cm
62.5 cm
50.5 cm
38.5 cm
26.5 cm
14.5 cm
1-Jun-99
3-Jun-99
5-Jun-99
7-Jun-99
9-Jun-99
11-Jun-99
13-Jun-99
15-Jun-99
17-Jun-99
19-Jun-99
21-Jun-99
23-Jun-99
25-Jun-99
27-Jun-99
29-Jun-99
1-Jul-99

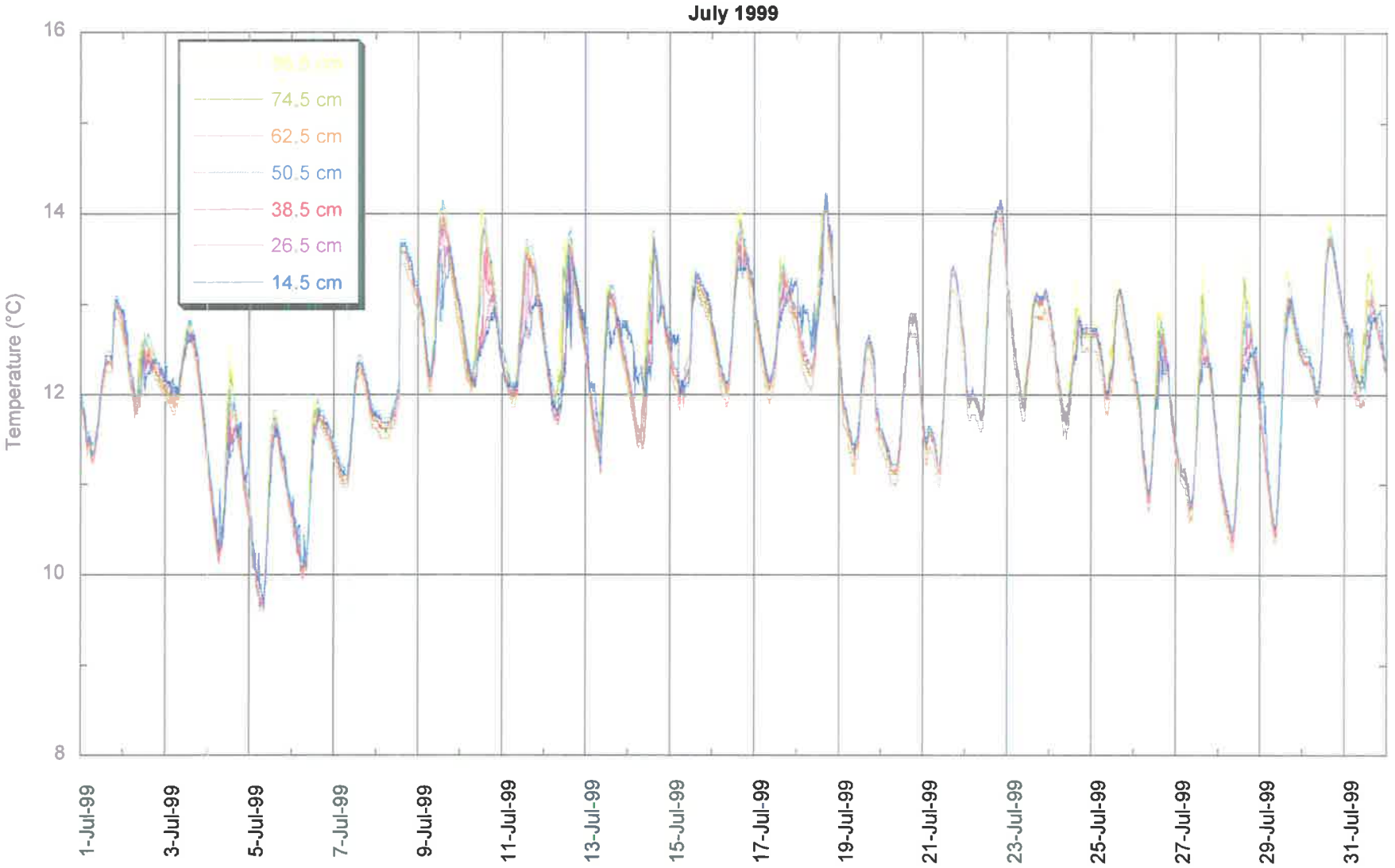
July 1999
Temperature (°C)
16
14
12
10
8
74.5 cm
62.5 cm
50.5 cm
38.5 cm
26.5 cm
14.5 cm
1-Jul-99
3-Jul-99
5-Jul-99
7-Jul-99
9-Jul-99
11-Jul-99
13-Jul-99
15-Jul-99
17-Jul-99
19-Jul-99
21-Jul-99
23-Jul-99
25-Jul-99
27-Jul-99
29-Jul-99
31-Jul-99

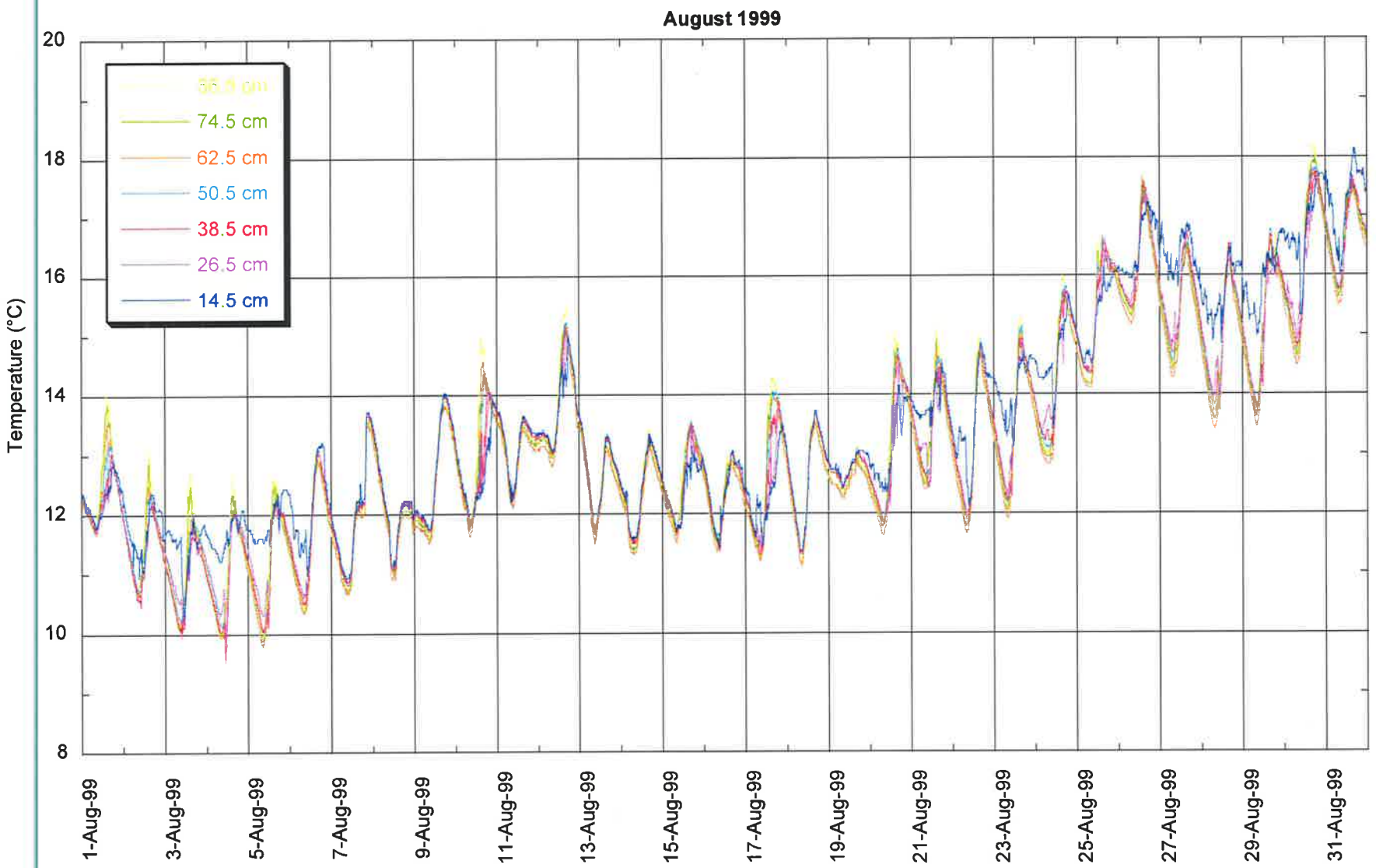
August 1999
Temperature (°C)
20
18
16
14
12
10
8
74.5 cm
62.5 cm
50.5 cm
38.5 cm
26.5 cm
14.5 cm
1-Aug-99
3-Aug-99
5-Aug-99
7-Aug-99
9-Aug-99
11-Aug-99
13-Aug-99
15-Aug-99
17-Aug-99
19-Aug-99
21-Aug-99
23-Aug-99
25-Aug-99
27-Aug-99
29-Aug-99
31-Aug-99

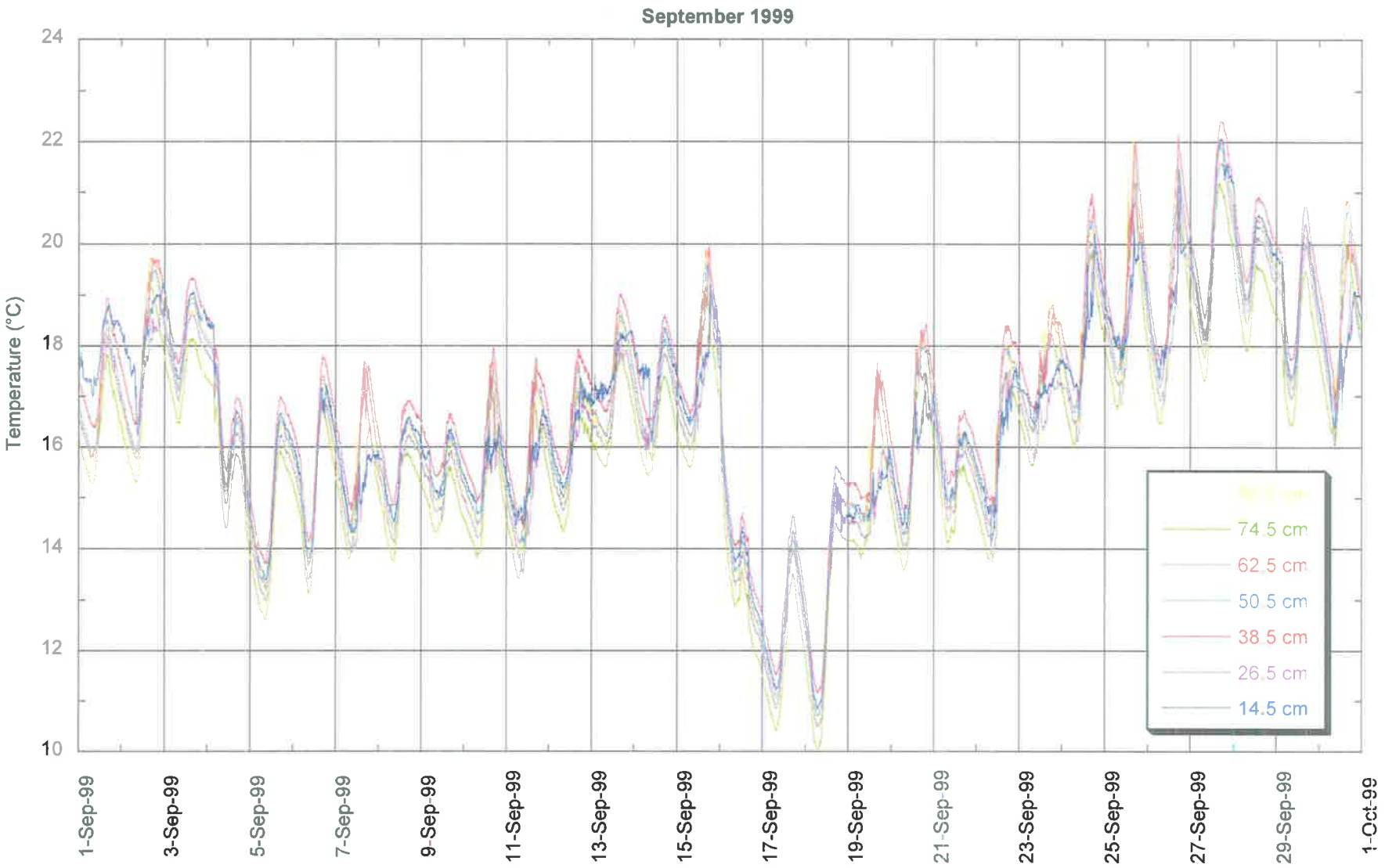
September 1999
Temperature (°C)
24
22
20
18
16
14
12
10
74.5 cm
62.5 cm
50.5 cm
38.5 cm
26.5 cm
14.5 cm
1-Sep-99
3-Sep-99
5-Sep-99
7-Sep-99
9-Sep-99
11-Sep-99
13-Sep-99
15-Sep-99
17-Sep-99
19-Sep-99
21-Sep-99
23-Sep-99
25-Sep-99
27-Sep-99
29-Sep-99
1-Oct-99

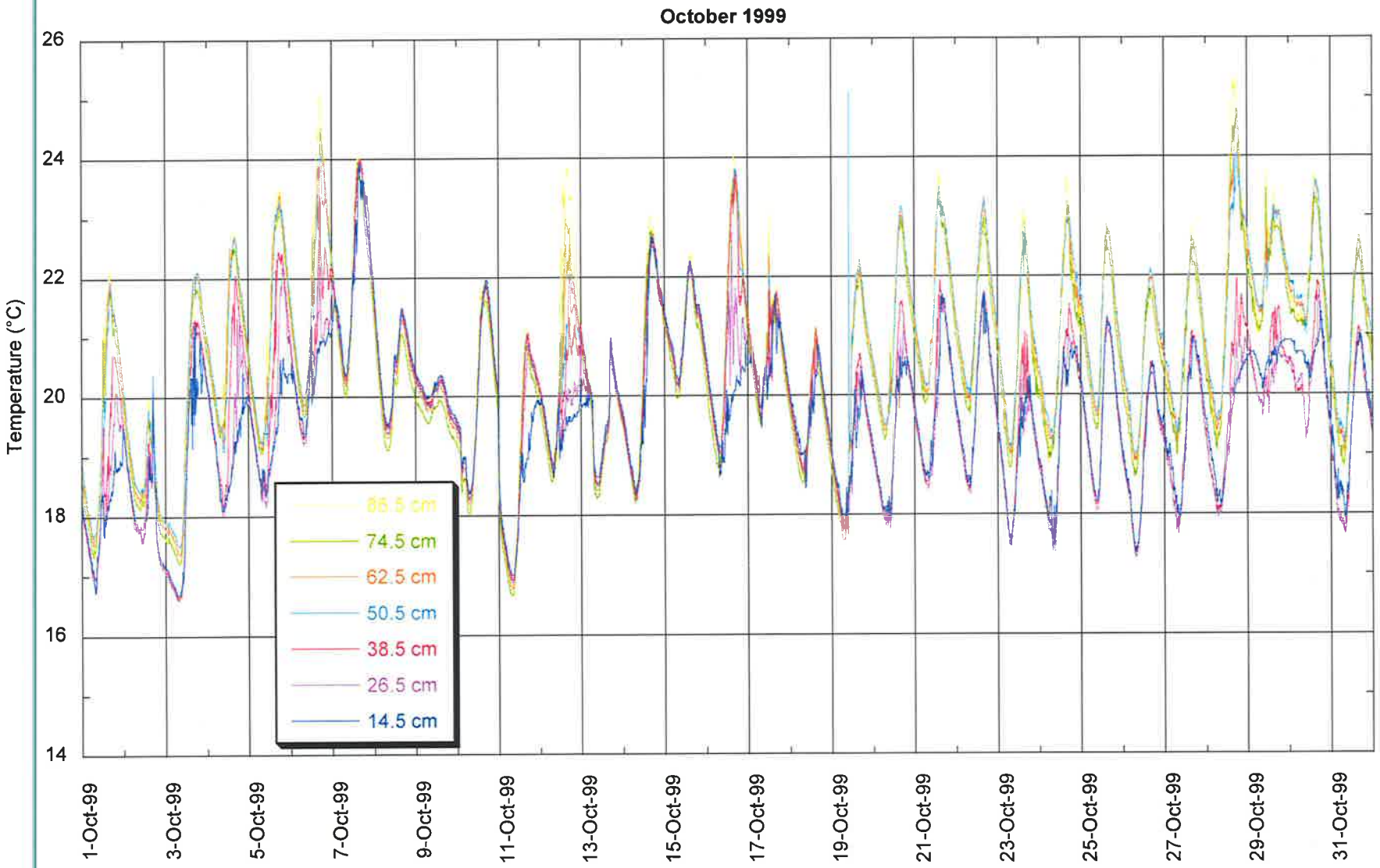
October 1999
Temperature (°C)
26
24
22
20
18
16
14
86.5 cm
74.5 cm
62.5 cm
50.5 cm
38.5 cm
26.5 cm
14.5 cm
1-Oct-99
3-Oct-99
5-Oct-99
7-Oct-99
9-Oct-99
11-Oct-99
13-Oct-99
15-Oct-99
17-Oct-99
19-Oct-99
21-Oct-99
23-Oct-99
25-Oct-99
27-Oct-99
29-Oct-99
31-Oct-99

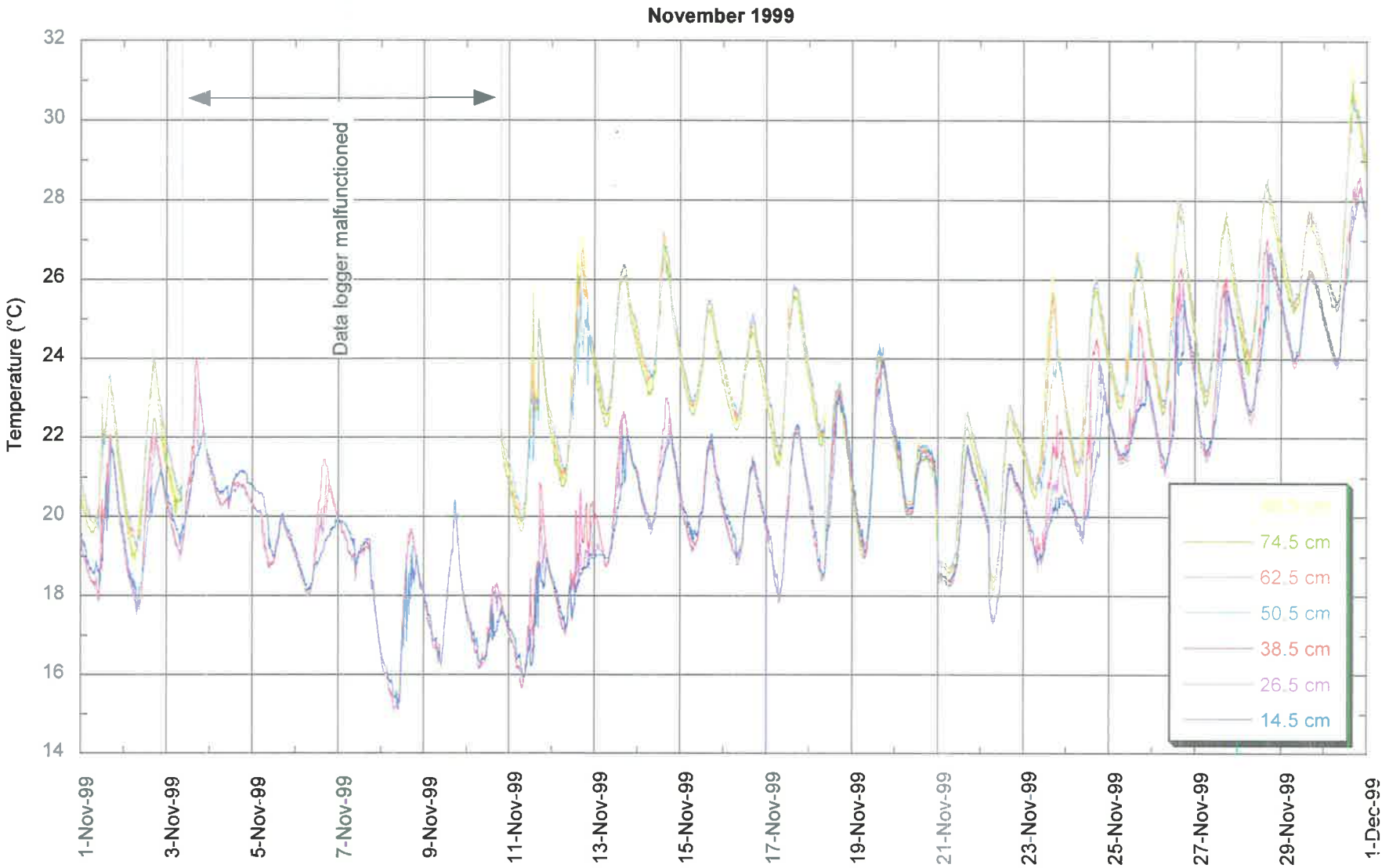
November 1999
Temperature (°C)
32
30
28
26
24
22
20
18
16
14
Data logger malfunctioned
74.5 cm
62.5 cm
50.5 cm
38.5 cm
26.5 cm
14.5 cm
1-Nov-99
3-Nov-99
5-Nov-99
7-Nov-99
9-Nov-99
11-Nov-99
13-Nov-99
15-Nov-99
17-Nov-99
19-Nov-99
21-Nov-99
23-Nov-99
25-Nov-99
27-Nov-99
29-Nov-99
1-Dec-99

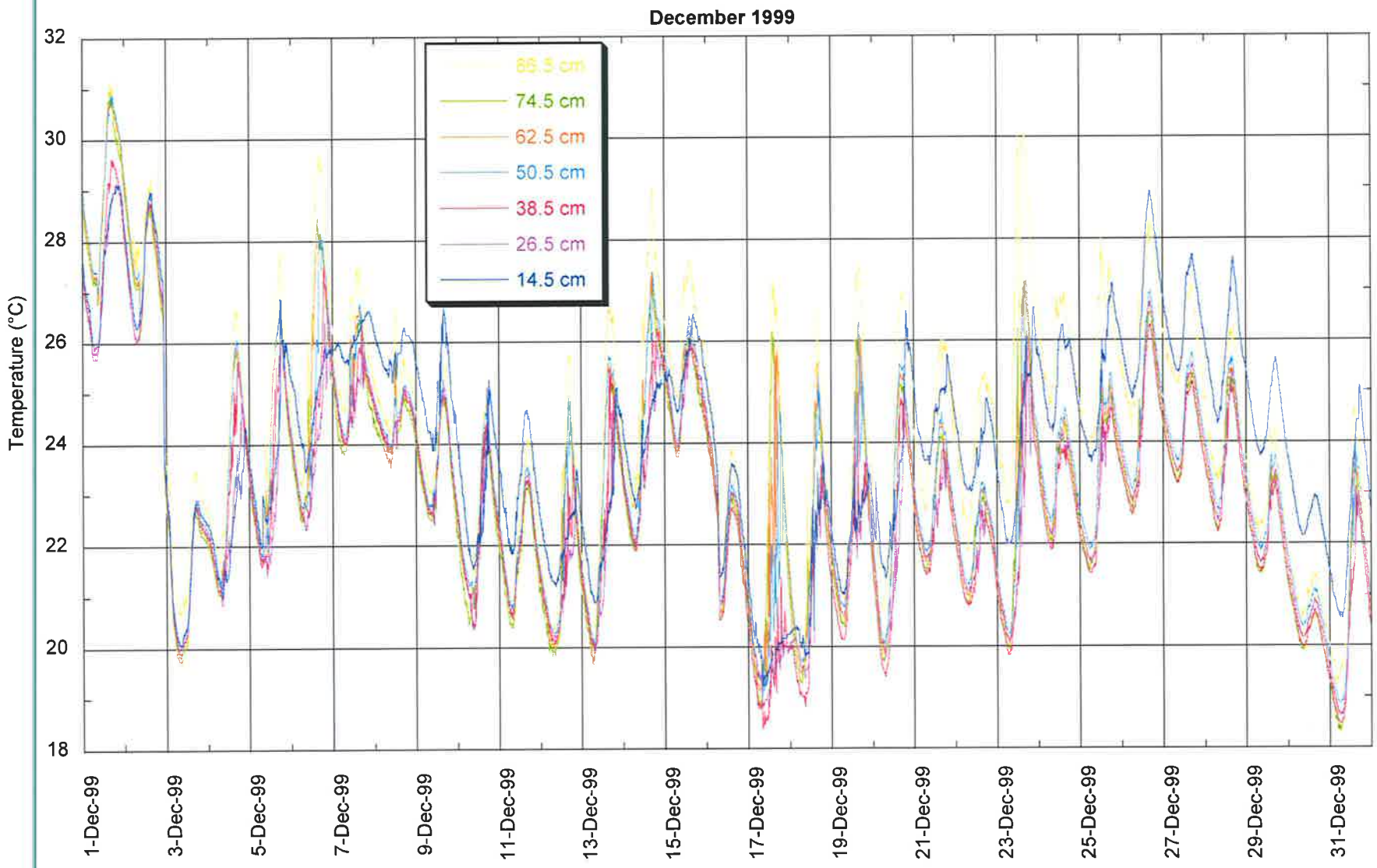
December 1999
Temperature (°C)
32
30
28
26
24
22
20
18
86.5 cm
74.5 cm
62.5 cm
50.5 cm
38.5 cm
26.5 cm
14.5 cm
1-Dec-99
3-Dec-99
5-Dec-99
7-Dec-99
9-Dec-99
11-Dec-99
13-Dec-99
15-Dec-99
17-Dec-99
19-Dec-99
21-Dec-99
23-Dec-99
25-Dec-99
27-Dec-99
29-Dec-99
31-Dec-99

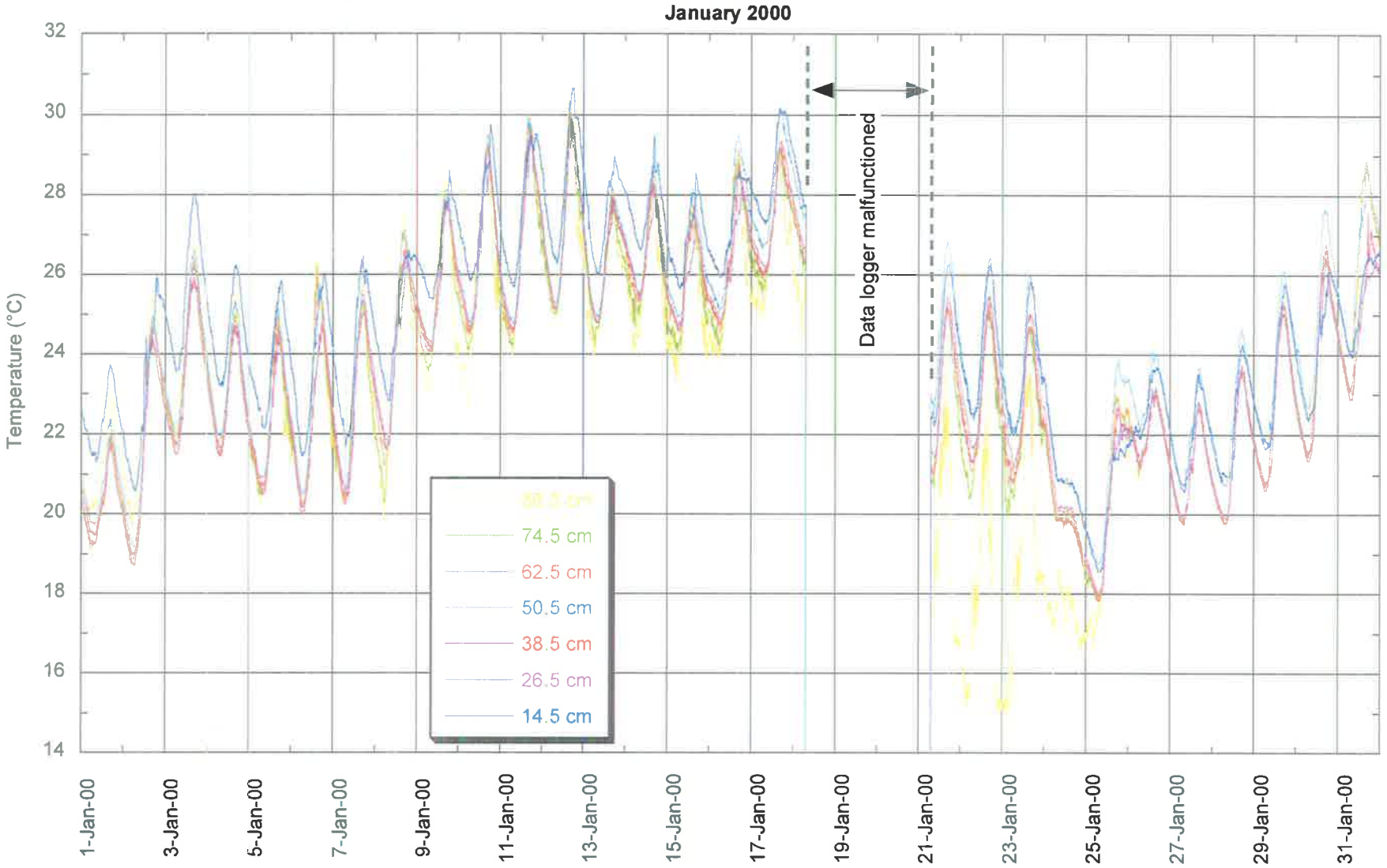
January 2000
Temperature (°C)
32
30
28
26
24
22
20
18
16
14
Data logger malfunctioned
74.5 cm
62.5 cm
50.5 cm
38.5 cm
26.5 cm
14.5 cm
1-Jan-00
3-Jan-00
5-Jan-00
7-Jan-00
9-Jan-00
11-Jan-00
13-Jan-00
15-Jan-00
17-Jan-00
19-Jan-00
21-Jan-00
23-Jan-00
25-Jan-00
27-Jan-00
29-Jan-00
31-Jan-00

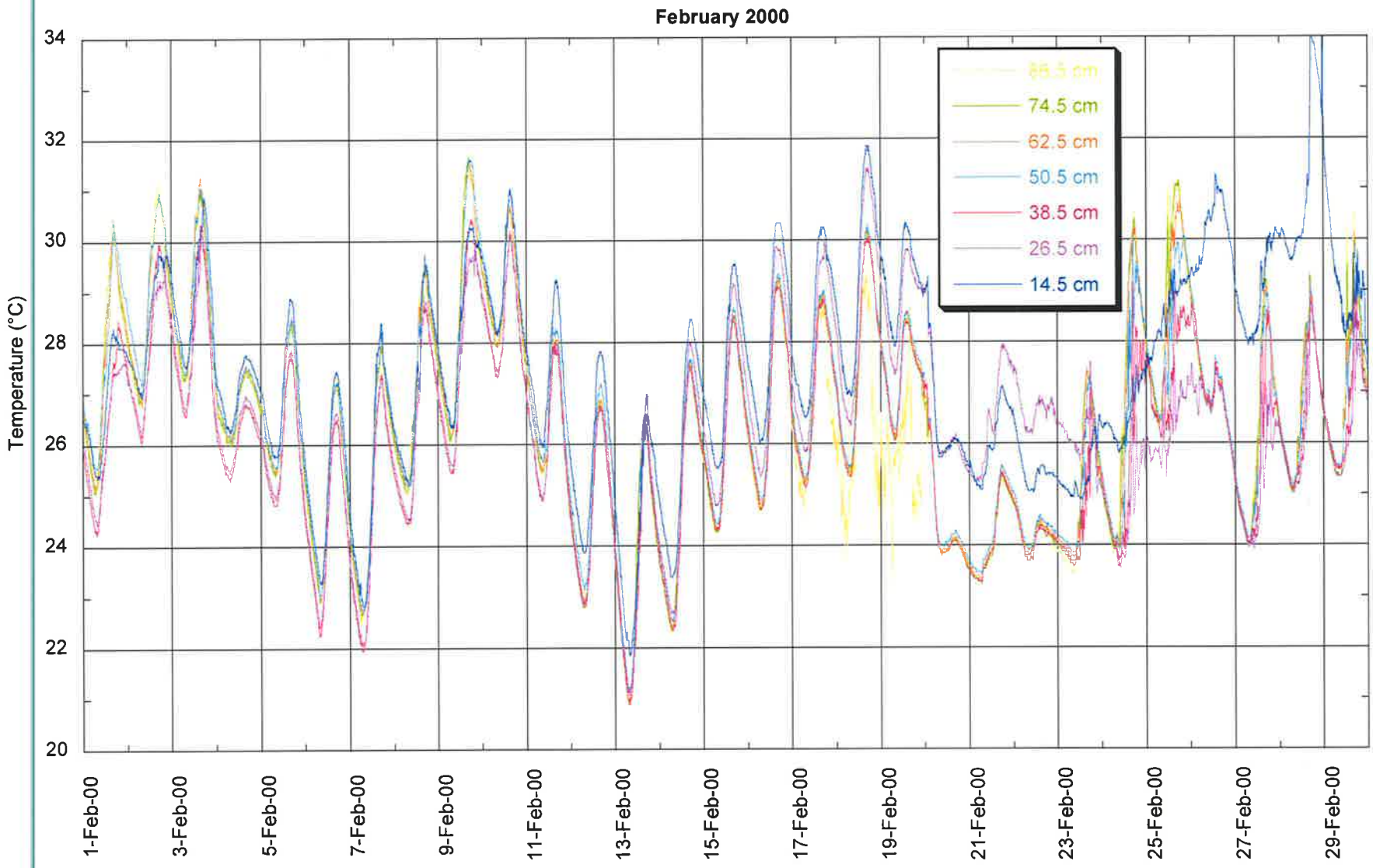
February 2000
Temperature (°C)
34
32
30
28
26
24
22
20
85.5 cm
74.5 cm
62.5 cm
50.5 cm
38.5 cm
26.5 cm
14.5 cm
1-Feb-00
3-Feb-00
5-Feb-00
7-Feb-00
9-Feb-00
11-Feb-00
13-Feb-00
15-Feb-00
17-Feb-00
19-Feb-00
21-Feb-00
23-Feb-00
25-Feb-00
27-Feb-00
29-Feb-00

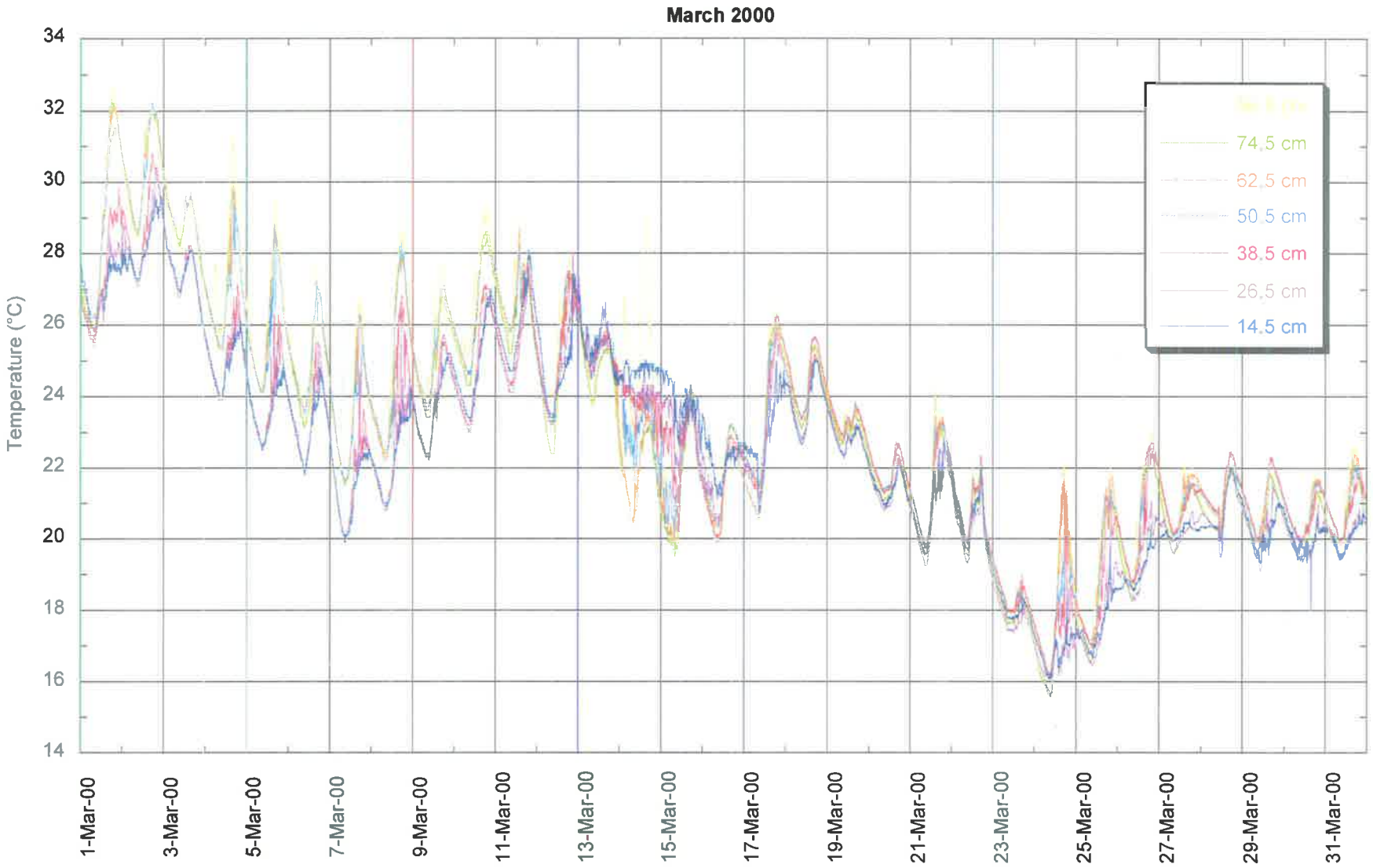
March 2000
Temperature (°C)
34
32
30
28
26
24
22
20
18
16
14
74.5 cm
62.5 cm
50.5 cm
38.5 cm
26.5 cm
14.5 cm
1-Mar-00
3-Mar-00
5-Mar-00
7-Mar-00
9-Mar-00
11-Mar-00
13-Mar-00
15-Mar-00
17-Mar-00
19-Mar-00
21-Mar-00
23-Mar-00
25-Mar-00
27-Mar-00
29-Mar-00
31-Mar-00

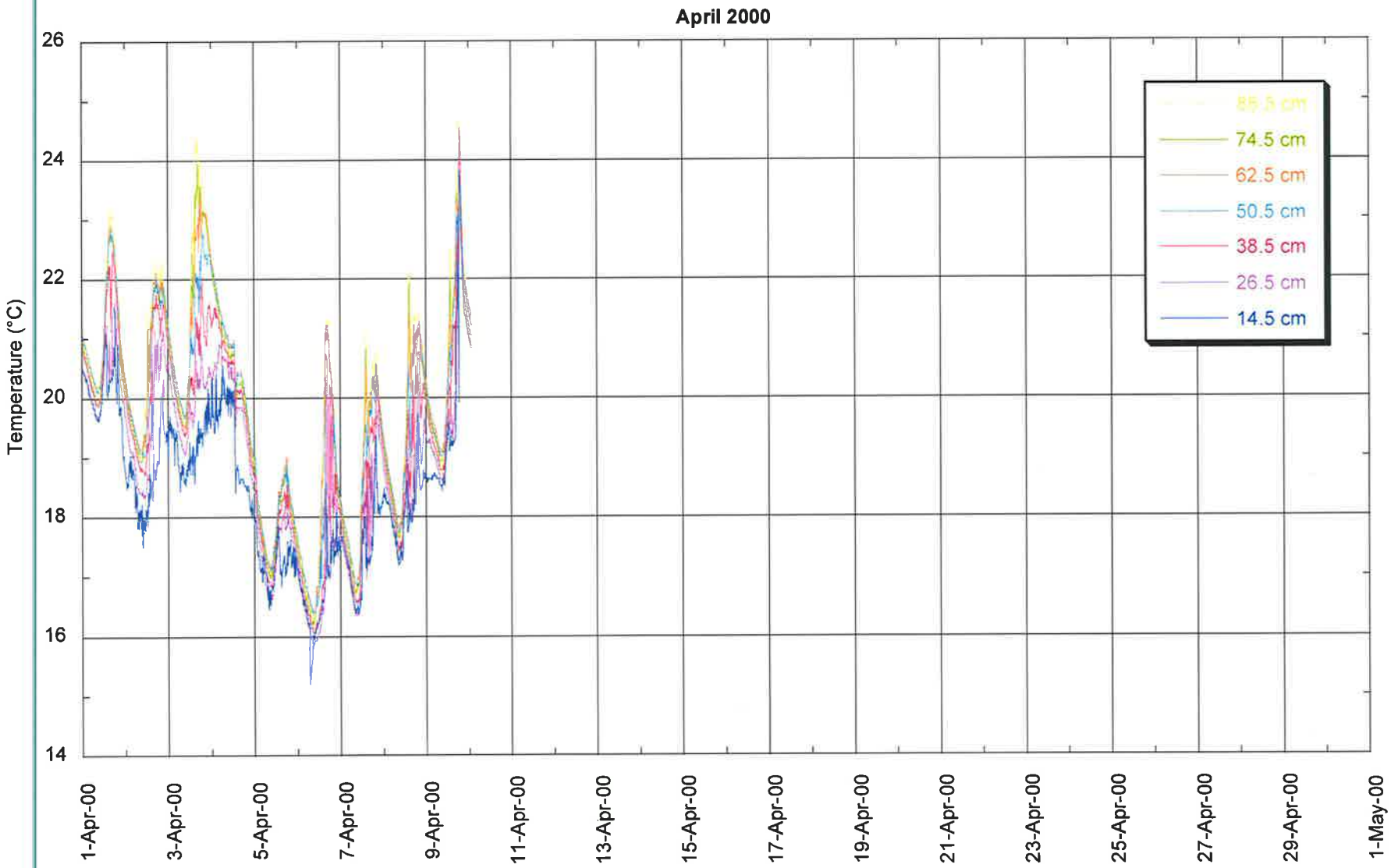
April 2000
Temperature (°C)
26
24
22
20
18
16
14
1-Apr-00
3-Apr-00
5-Apr-00
7-Apr-00
9-Apr-00
11-Apr-00
13-Apr-00
15-Apr-00
17-Apr-00
19-Apr-00
21-Apr-00
23-Apr-00
25-Apr-00
27-Apr-00
29-Apr-00
1-May-00
74.5 cm
62.5 cm
50.5 cm
38.5 cm
26.5 cm
14.5 cm

Appendix J

Sector Diagram in STELLA

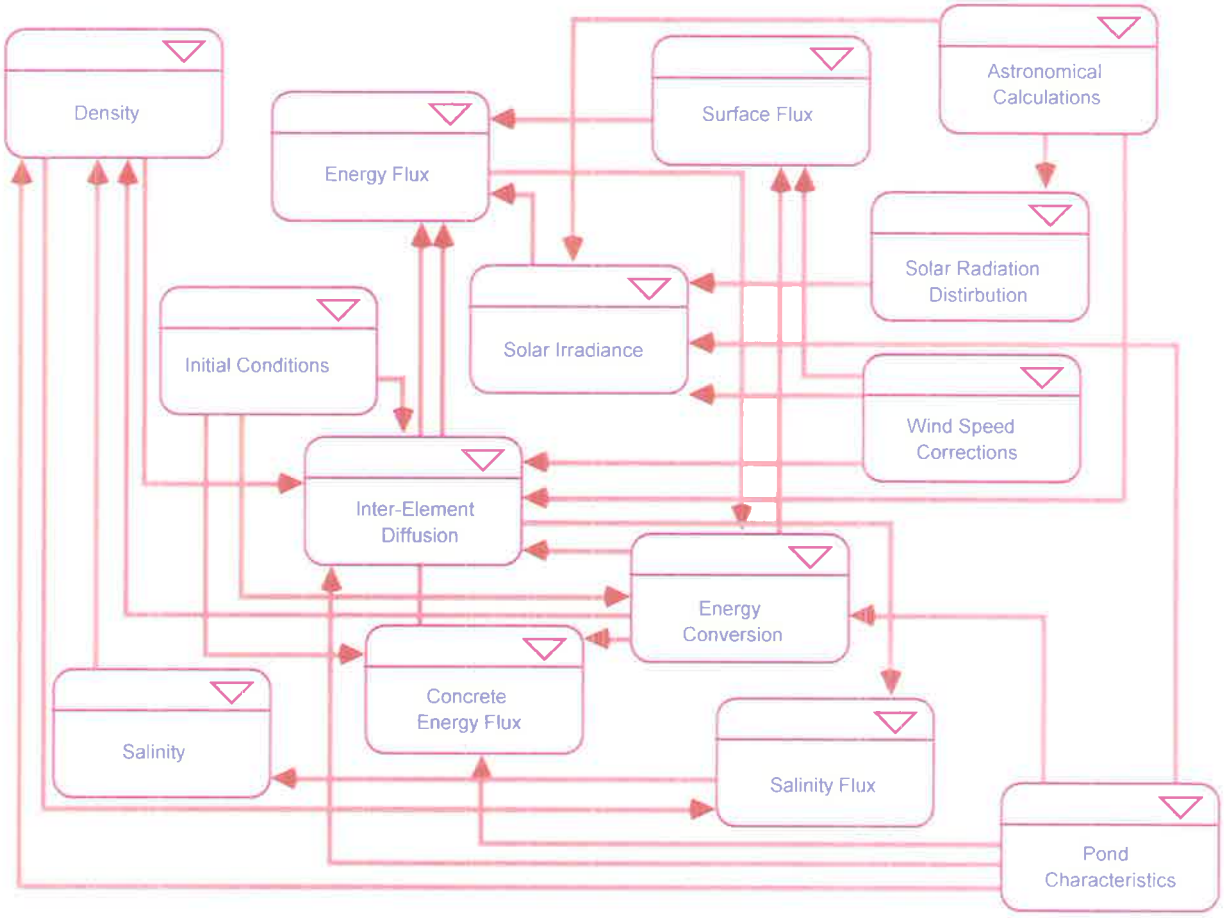
Density
Energy Flux
Surface Flux
Astronomical Calculations
Solar Radiation Distirbution
Initial Conditions
Solar Irradiance
Wind Speed Corrections
Inter-Element Diffusion
Energy Conversion
Concrete Energy Flux
Salinity
Salinity Flux
Pond Characteristics

Appendix K

Model Equations in STELLA

Salinity_Layer_1(t) = Salinity_Layer_1(t - dt) + (- S_Diffusion_1_to_2) * dt

INIT Salinity_Layer_1 = Salinity_Initial[Layer_1]
S_Diffusion_1_to_2 = K_diff[Layer_1]*Salinity_Gradient[Layer_1]
Salinity_Layer_10(t) = Salinity_Layer_10(t - dt) + (S_Diffusion_9_to_10 - S_Diffusion_10_to_11) * dt
INIT Salinity_Layer_10 = Salinity_Initial[Layer_10]
S_Diffusion_9_to_10 = K_diff[Layer_9]*Salinity_Gradient[Layer_9]
S_Diffusion_10_to_11 = K_diff[Layer_10]*Salinity_Gradient[Layer_10]
Salinity_Layer_11(t) = Salinity_Layer_11(t - dt) + (S_Diffusion_10_to_11 - S_Diffusion_11_to_12) * dt
INIT Salinity_Layer_11 = Salinity_Initial[Layer_11]
S_Diffusion_10_to_11 = K_diff[Layer_10]*Salinity_Gradient[Layer_10]
S_Diffusion_11_to_12 = K_diff[Layer_11]*Salinity_Gradient[Layer_11]
Salinity_Layer_12(t) = Salinity_Layer_12(t - dt) + (S_Diffusion_11_to_12 - S_Diffusion_12_to_13) * dt
INIT Salinity_Layer_12 = Salinity_Initial[Layer_12]
S_Diffusion_11_to_12 = K_diff[Layer_11]*Salinity_Gradient[Layer_11]
S_Diffusion_12_to_13 = K_diff[Layer_12]*Salinity_Gradient[Layer_12]
Salinity_Layer_13(t) = Salinity_Layer_13(t - dt) + (S_Diffusion_12_to_13 - S_Diffusion_13_to_14) * dt
INIT Salinity_Layer_13 = Salinity_Initial[Layer_13]
S_Diffusion_12_to_13 = K_diff[Layer_12]*Salinity_Gradient[Layer_12]
S_Diffusion_13_to_14 = K_diff[Layer_13]*Salinity_Gradient[Layer_13]
Salinity_Layer_14(t) = Salinity_Layer_14(t - dt) + (S_Diffusion_13_to_14 - S_Diffusion_14_to_15) * dt
INIT Salinity_Layer_14 = Salinity_Initial[Layer_14]
S_Diffusion_13_to_14 = K_diff[Layer_13]*Salinity_Gradient[Layer_13]
S_Diffusion_14_to_15 = K_diff[Layer_14]*Salinity_Gradient[Layer_14]
Salinity_Layer_15(t) = Salinity_Layer_15(t - dt) + (S_Diffusion_14_to_15 - S_Diffusion_15_to_16) * dt
INIT Salinity_Layer_15 = Salinity_Initial[Layer_15]
S_Diffusion_14_to_15 = K_diff[Layer_14]*Salinity_Gradient[Layer_14]
S_Diffusion_15_to_16 = K_diff[Layer_15]*Salinity_Gradient[Layer_15]
Salinity_Layer_16(t) = Salinity_Layer_16(t - dt) + (S_Diffusion_15_to_16 - S_Diffusion_16_to_17) * dt
INIT Salinity_Layer_16 = Salinity_Initial[Layer_16]
S_Diffusion_15_to_16 = K_diff[Layer_15]*Salinity_Gradient[Layer_15]
S_Diffusion_16_to_17 = K_diff[Layer_16]*Salinity_Gradient[Layer_16]
Salinity_Layer_17(t) = Salinity_Layer_17(t - dt) + (S_Diffusion_16_to_17 - S_Diffusion_17_to_18) * dt
INIT Salinity_Layer_17 = Salinity_Initial[Layer_17]
S_Diffusion_16_to_17 = K_diff[Layer_16]*Salinity_Gradient[Layer_16]
S_Diffusion_17_to_18 = K_diff[Layer_17]*Salinity_Gradient[Layer_17]
Salinity_Layer_18(t) = Salinity_Layer_18(t - dt) + (S_Diffusion_17_to_18) * dt
INIT Salinity_Layer_18 = Salinity_Initial[Layer_18]
S_Diffusion_17_to_18 = K_diff[Layer_17]*Salinity_Gradient[Layer_17]
Salinity_Layer_2(t) = Salinity_Layer_2(t - dt) + (S_Diffusion_1_to_2 - S_Diffusion_2_to_3) * dt
INIT Salinity_Layer_2 = Salinity_Initial[Layer_2]
S_Diffusion_1_to_2 = K_diff[Layer_1]*Salinity_Gradient[Layer_1]
S_Diffusion_2_to_3 = K_diff[Layer_2]*Salinity_Gradient[Layer_2]
Salinity_Layer_3(t) = Salinity_Layer_3(t - dt) + (S_Diffusion_2_to_3 - S_Diffusion_3_to_4) * dt
INIT Salinity_Layer_3 = Salinity_Initial[Layer_3]
S_Diffusion_2_to_3 = K_diff[Layer_2]*Salinity_Gradient[Layer_2]
S_Diffusion_3_to_4 = K_diff[Layer_3]*Salinity_Gradient[Layer_3]
Salinity_Layer_4(t) = Salinity_Layer_4(t - dt) + (S_Diffusion_3_to_4 - S_Diffusion_4_to_5) * dt
INIT Salinity_Layer_4 = Salinity_Initial[Layer_4]
S_Diffusion_3_to_4 = K_diff[Layer_3]*Salinity_Gradient[Layer_3]
S_Diffusion_4_to_5 = K_diff[Layer_4]*Salinity_Gradient[Layer_4]
Salinity_Layer_5(t) = Salinity_Layer_5(t - dt) + (S_Diffusion_4_to_5 - S_Diffusion_5_to_6) * dt
INIT Salinity_Layer_5 = Salinity_Initial[Layer_5]
S_Diffusion_4_to_5 = K_diff[Layer_4]*Salinity_Gradient[Layer_4]
S_Diffusion_5_to_6 = K_diff[Layer_5]*Salinity_Gradient[Layer_5]
Salinity_Layer_6(t) = Salinity_Layer_6(t - dt) + (S_Diffusion_5_to_6 - S_Diffusion_6_to_7) * dt
INIT Salinity_Layer_6 = Salinity_Initial[Layer_6]
S_Diffusion_5_to_6 = K_diff[Layer_5]*Salinity_Gradient[Layer_5]
S_Diffusion_6_to_7 = K_diff[Layer_6]*Salinity_Gradient[Layer_6]
Salinity_Layer_7(t) = Salinity_Layer_7(t - dt) + (S_Diffusion_6_to_7 - S_Diffusion_7_to_8) * dt
INIT Salinity_Layer_7 = Salinity_Initial[Layer_7]
S_Diffusion_6_to_7 = K_diff[Layer_6]*Salinity_Gradient[Layer_6]
S_Diffusion_7_to_8 = K_diff[Layer_7]*Salinity_Gradient[Layer_7]
Salinity_Layer_8(t) = Salinity_Layer_8(t - dt) + (S_Diffusion_7_to_8 - s_Diffusion_8_to_9) * dt
INIT Salinity_Layer_8 = Salinity_Initial[Layer_8]
S_Diffusion_7_to_8 = K_diff[Layer_7]*Salinity_Gradient[Layer_7]

```
s_Diffusion_8_to_9 = K_diff[Layer_8]*Salinity_Gradient[Layer_8]
Salinity_Layer_9(t) = Salinity_Layer_9(t - dt) + (s_Diffusion_8_to_9 - S_Diffusion_9_to_10) * dt
INIT Salinity_Layer_9 = Salinity_Initial[Layer_9]
s_Diffusion_8_to_9 = K_diff[Layer_8]*Salinity_Gradient[Layer_8]
S_Diffusion_9_to_10 = K_diff[Layer_9]*Salinity_Gradient[Layer_9]
Angle_of_Incidence = 90-Solar_Altitude_Angle
Angle_of_Refraction =
ARCTAN((Refractivity_Index_Air/Refractivity_Index_Water*SIN(Angle_of_Incidence))/SQRT(1-
(Refractivity_Index_Air/Refractivity_Index_Water*SIN(Angle_of_Incidence))^2))
Light_Extinction_Coeff = 1.7/SDD
Light_Extinction_Coeff_E = Light_Extinction_Coeff/COS(Angle_of_Refraction*PI/180)
Net_Solar_Irrad[Volume_Elements] = (Solar_Irradiance-Reflected_Solar_Irrad)*(1-
Surface_Absorbtion)*EXP(-Light_Extinction_Coeff_E*(Depth[Volume_Elements]))
Pen_Solar_Irrad = Solar_Irradiance-Reflected_Solar_Irrad
Reflected_Solar_Irrad = Reflectivity*Solar_Irradiance
Reflectivity = Reflectivity_S*(1-(0.08*Wind_Speed[Two_metres]))
Reflectivity_S = IF(Solar_Altitude_Angle<0.5) THEN 2 ELSE (2.2*(Solar_Altitude_Angle)^-0.97)
Refractivity_Index_Air = 1.0003
Refractivity_Index_Water = 1.33
SDD = Depth_total*SDD_percentage[Feb_11]
SDD_percentage[Jan_18] = 1
SDD_percentage[Jan_19] = 1
SDD_percentage[Jan_20] = 1
SDD_percentage[Jan_21] = 1
SDD_percentage[Jan_22] = 1
SDD_percentage[Feb_7] = 1
SDD_percentage[Feb_8] = 1
SDD_percentage[Feb_9] = 1
SDD_percentage[Feb_10] = 1
SDD_percentage[Feb_11] = 1
SDD_percentage[Feb_29] = 0.79
SDD_percentage[Mar_1] = 0.85
SDD_percentage[Mar_2] = 0.79
Surface_Absorbtion = IF(0.265*LOGN(Light_Extinction_Coeff_E)+0.614)>1 THEN 1 ELSE
(0.265*LOGN(Light_Extinction_Coeff_E)+0.614)
Conversion[Volume_Elements] =
Surface_Area/(Volume*Heat_Capacity_Initial[Volume_Elements]*Density_Initial[Volume_Elements])
ENERGY_W[Layer_1] =
(Energy_Layer_1+Energy_Layer_2+Energy_Layer_3+Energy_Layer_4+Energy_Layer_5+Energy_Layer
_6+Energy_Layer_7+Energy_Layer_8+Energy_Layer_9+Energy_Layer_10+Energy_Layer_11+Energy_
Layer_12+Energy_Layer_13+Energy_Layer_14+Energy_Layer_15+Energy_Layer_16+Energy_Layer_1
7+Energy_Layer_18)-
(Energy_Layer_2+Energy_Layer_3+Energy_Layer_4+Energy_Layer_5+Energy_Layer_6+Energy_Layer
_7+Energy_Layer_8+Energy_Layer_9+Energy_Layer_10+Energy_Layer_11+Energy_Layer_12+Energy
_Layer_13+Energy_Layer_14+Energy_Layer_15+Energy_Layer_16+Energy_Layer_17+Energy_Layer_
18)
ENERGY_W[Layer_2] =
(Energy_Layer_1+Energy_Layer_2+Energy_Layer_3+Energy_Layer_4+Energy_Layer_5+Energy_Layer
_6+Energy_Layer_7+Energy_Layer_8+Energy_Layer_9+Energy_Layer_10+Energy_Layer_11+Energy_
Layer_12+Energy_Layer_13+Energy_Layer_14+Energy_Layer_15+Energy_Layer_16+Energy_Layer_1
7+Energy_Layer_18)-
(Energy_Layer_1+Energy_Layer_3+Energy_Layer_4+Energy_Layer_5+Energy_Layer_6+Energy_Layer
_7+Energy_Layer_8+Energy_Layer_9+Energy_Layer_10+Energy_Layer_11+Energy_Layer_12+Energy
_Layer_13+Energy_Layer_14+Energy_Layer_15+Energy_Layer_16+Energy_Layer_17+Energy_Layer_
18)
ENERGY_W[Layer_3] =
(Energy_Layer_1+Energy_Layer_2+Energy_Layer_3+Energy_Layer_4+Energy_Layer_5+Energy_Layer
_6+Energy_Layer_7+Energy_Layer_8+Energy_Layer_9+Energy_Layer_10+Energy_Layer_11+Energy_
Layer_12+Energy_Layer_13+Energy_Layer_14+Energy_Layer_15+Energy_Layer_16+Energy_Layer_1
7+Energy_Layer_18)-
(Energy_Layer_1+Energy_Layer_2+Energy_Layer_4+Energy_Layer_5+Energy_Layer_6+Energy_Layer
_7+Energy_Layer_8+Energy_Layer_9+Energy_Layer_10+Energy_Layer_11+Energy_Layer_12+Energy
_Layer_13+Energy_Layer_14+Energy_Layer_15+Energy_Layer_16+Energy_Layer_17+Energy_Layer_
18)
ENERGY_W[Layer_4] =
(Energy_Layer_1+Energy_Layer_2+Energy_Layer_3+Energy_Layer_4+Energy_Layer_5+Energy_Layer
_6+Energy_Layer_7+Energy_Layer_8+Energy_Layer_9+Energy_Layer_10+Energy_Layer_11+Energy_
```

Layer_12+Energy_Layer_13+Energy_Layer_14+Energy_Layer_15+Energy_Layer_16+Energy_Layer_17+Energy_Layer_18)-
(Energy_Layer_1+Energy_Layer_2+Energy_Layer_3+Energy_Layer_5+Energy_Layer_6+Energy_Layer_7+Energy_Layer_8+Energy_Layer_9+Energy_Layer_10+Energy_Layer_11+Energy_Layer_12+Energy_Layer_13+Energy_Layer_14+Energy_Layer_15+Energy_Layer_16+Energy_Layer_17+Energy_Layer_18)
ENERGY_W[Layer_5] =
(Energy_Layer_1+Energy_Layer_2+Energy_Layer_3+Energy_Layer_4+Energy_Layer_5+Energy_Layer_6+Energy_Layer_7+Energy_Layer_8+Energy_Layer_9+Energy_Layer_10+Energy_Layer_11+Energy_Layer_12+Energy_Layer_13+Energy_Layer_14+Energy_Layer_15+Energy_Layer_16+Energy_Layer_17+Energy_Layer_18)-
(Energy_Layer_1+Energy_Layer_2+Energy_Layer_3+Energy_Layer_4+Energy_Layer_6+Energy_Layer_7+Energy_Layer_8+Energy_Layer_9+Energy_Layer_10+Energy_Layer_11+Energy_Layer_12+Energy_Layer_13+Energy_Layer_14+Energy_Layer_15+Energy_Layer_16+Energy_Layer_17+Energy_Layer_18)
ENERGY_W[Layer_6] =
(Energy_Layer_1+Energy_Layer_2+Energy_Layer_3+Energy_Layer_4+Energy_Layer_5+Energy_Layer_6+Energy_Layer_7+Energy_Layer_8+Energy_Layer_9+Energy_Layer_10+Energy_Layer_11+Energy_Layer_12+Energy_Layer_13+Energy_Layer_14+Energy_Layer_15+Energy_Layer_16+Energy_Layer_17+Energy_Layer_18)-
(Energy_Layer_1+Energy_Layer_2+Energy_Layer_3+Energy_Layer_4+Energy_Layer_5+Energy_Layer_7+Energy_Layer_8+Energy_Layer_9+Energy_Layer_10+Energy_Layer_11+Energy_Layer_12+Energy_Layer_13+Energy_Layer_14+Energy_Layer_15+Energy_Layer_16+Energy_Layer_17+Energy_Layer_18)
ENERGY_W[Layer_7] =
(Energy_Layer_1+Energy_Layer_2+Energy_Layer_3+Energy_Layer_4+Energy_Layer_5+Energy_Layer_6+Energy_Layer_7+Energy_Layer_8+Energy_Layer_9+Energy_Layer_10+Energy_Layer_11+Energy_Layer_12+Energy_Layer_13+Energy_Layer_14+Energy_Layer_15+Energy_Layer_16+Energy_Layer_17+Energy_Layer_18)-
(Energy_Layer_1+Energy_Layer_2+Energy_Layer_3+Energy_Layer_4+Energy_Layer_5+Energy_Layer_6+Energy_Layer_8+Energy_Layer_9+Energy_Layer_10+Energy_Layer_11+Energy_Layer_12+Energy_Layer_13+Energy_Layer_14+Energy_Layer_15+Energy_Layer_16+Energy_Layer_17+Energy_Layer_18)
ENERGY_W[Layer_8] =
(Energy_Layer_1+Energy_Layer_2+Energy_Layer_3+Energy_Layer_4+Energy_Layer_5+Energy_Layer_6+Energy_Layer_7+Energy_Layer_8+Energy_Layer_9+Energy_Layer_10+Energy_Layer_11+Energy_Layer_12+Energy_Layer_13+Energy_Layer_14+Energy_Layer_15+Energy_Layer_16+Energy_Layer_17+Energy_Layer_18)-
(Energy_Layer_1+Energy_Layer_2+Energy_Layer_3+Energy_Layer_4+Energy_Layer_5+Energy_Layer_6+Energy_Layer_7+Energy_Layer_9+Energy_Layer_10+Energy_Layer_11+Energy_Layer_12+Energy_Layer_13+Energy_Layer_14+Energy_Layer_15+Energy_Layer_16+Energy_Layer_17+Energy_Layer_18)
ENERGY_W[Layer_9] =
(Energy_Layer_1+Energy_Layer_2+Energy_Layer_3+Energy_Layer_4+Energy_Layer_5+Energy_Layer_6+Energy_Layer_7+Energy_Layer_8+Energy_Layer_9+Energy_Layer_10+Energy_Layer_11+Energy_Layer_12+Energy_Layer_13+Energy_Layer_14+Energy_Layer_15+Energy_Layer_16+Energy_Layer_17+Energy_Layer_18)-
(Energy_Layer_1+Energy_Layer_2+Energy_Layer_3+Energy_Layer_4+Energy_Layer_5+Energy_Layer_6+Energy_Layer_7+Energy_Layer_8+Energy_Layer_10+Energy_Layer_11+Energy_Layer_12+Energy_Layer_13+Energy_Layer_14+Energy_Layer_15+Energy_Layer_16+Energy_Layer_17+Energy_Layer_18)
ENERGY_W[Layer_10] =
(Energy_Layer_1+Energy_Layer_2+Energy_Layer_3+Energy_Layer_4+Energy_Layer_5+Energy_Layer_6+Energy_Layer_7+Energy_Layer_8+Energy_Layer_9+Energy_Layer_10+Energy_Layer_11+Energy_Layer_12+Energy_Layer_13+Energy_Layer_14+Energy_Layer_15+Energy_Layer_16+Energy_Layer_17+Energy_Layer_18)-
(Energy_Layer_1+Energy_Layer_2+Energy_Layer_3+Energy_Layer_4+Energy_Layer_5+Energy_Layer_6+Energy_Layer_7+Energy_Layer_8+Energy_Layer_9+Energy_Layer_11+Energy_Layer_12+Energy_Layer_13+Energy_Layer_14+Energy_Layer_15+Energy_Layer_16+Energy_Layer_17+Energy_Layer_18)
ENERGY_W[Layer_11] =
(Energy_Layer_1+Energy_Layer_2+Energy_Layer_3+Energy_Layer_4+Energy_Layer_5+Energy_Layer_6+Energy_Layer_7+Energy_Layer_8+Energy_Layer_9+Energy_Layer_10+Energy_Layer_11+Energy_Layer_12+Energy_Layer_13+Energy_Layer_14+Energy_Layer_15+Energy_Layer_16+Energy_Layer_17+Energy_Layer_18)-
(Energy_Layer_1+Energy_Layer_2+Energy_Layer_3+Energy_Layer_4+Energy_Layer_5+Energy_Layer_6+Energy_Layer_7+Energy_Layer_8+Energy_Layer_9+Energy_Layer_10+Energy_Layer_12+Energy_

Layer_13+Energy_Layer_14+Energy_Layer_15+Energy_Layer_16+Energy_Layer_17+Energy_Layer_1
8)
ENERGY_W[Layer_12] =
(Energy_Layer_1+Energy_Layer_2+Energy_Layer_3+Energy_Layer_4+Energy_Layer_5+Energy_Layer
_6+Energy_Layer_7+Energy_Layer_8+Energy_Layer_9+Energy_Layer_10+Energy_Layer_11+Energy_
Layer_12+Energy_Layer_13+Energy_Layer_14+Energy_Layer_15+Energy_Layer_16+Energy_Layer_1
7+Energy_Layer_18)-
(Energy_Layer_1+Energy_Layer_2+Energy_Layer_3+Energy_Layer_4+Energy_Layer_5+Energy_Layer
_6+Energy_Layer_7+Energy_Layer_8+Energy_Layer_9+Energy_Layer_10+Energy_Layer_11+Energy_
Layer_13+Energy_Layer_14+Energy_Layer_15+Energy_Layer_16+Energy_Layer_17+Energy_Layer_1
8)
ENERGY_W[Layer_13] =
(Energy_Layer_1+Energy_Layer_2+Energy_Layer_3+Energy_Layer_4+Energy_Layer_5+Energy_Layer
_6+Energy_Layer_7+Energy_Layer_8+Energy_Layer_9+Energy_Layer_10+Energy_Layer_11+Energy_
Layer_12+Energy_Layer_13+Energy_Layer_14+Energy_Layer_15+Energy_Layer_16+Energy_Layer_1
7+Energy_Layer_18)-
(Energy_Layer_1+Energy_Layer_2+Energy_Layer_3+Energy_Layer_4+Energy_Layer_5+Energy_Layer
_6+Energy_Layer_7+Energy_Layer_8+Energy_Layer_9+Energy_Layer_10+Energy_Layer_11+Energy_
Layer_12+Energy_Layer_14+Energy_Layer_15+Energy_Layer_16+Energy_Layer_17+Energy_Layer_1
8)
ENERGY_W[Layer_14] =
(Energy_Layer_1+Energy_Layer_2+Energy_Layer_3+Energy_Layer_4+Energy_Layer_5+Energy_Layer
_6+Energy_Layer_7+Energy_Layer_8+Energy_Layer_9+Energy_Layer_10+Energy_Layer_11+Energy_
Layer_12+Energy_Layer_13+Energy_Layer_14+Energy_Layer_15+Energy_Layer_16+Energy_Layer_1
7+Energy_Layer_18)-
(Energy_Layer_1+Energy_Layer_2+Energy_Layer_3+Energy_Layer_4+Energy_Layer_5+Energy_Layer
_6+Energy_Layer_7+Energy_Layer_8+Energy_Layer_9+Energy_Layer_10+Energy_Layer_11+Energy_
Layer_12+Energy_Layer_13+Energy_Layer_15+Energy_Layer_16+Energy_Layer_17+Energy_Layer_1
8)
ENERGY_W[Layer_15] =
(Energy_Layer_1+Energy_Layer_2+Energy_Layer_3+Energy_Layer_4+Energy_Layer_5+Energy_Layer
_6+Energy_Layer_7+Energy_Layer_8+Energy_Layer_9+Energy_Layer_10+Energy_Layer_11+Energy_
Layer_12+Energy_Layer_13+Energy_Layer_14+Energy_Layer_15+Energy_Layer_16+Energy_Layer_1
7+Energy_Layer_18)-
(Energy_Layer_1+Energy_Layer_2+Energy_Layer_3+Energy_Layer_4+Energy_Layer_5+Energy_Layer
_6+Energy_Layer_7+Energy_Layer_8+Energy_Layer_9+Energy_Layer_10+Energy_Layer_11+Energy_
Layer_12+Energy_Layer_13+Energy_Layer_14+Energy_Layer_16+Energy_Layer_17+Energy_Layer_1
8)
ENERGY_W[Layer_16] =
(Energy_Layer_1+Energy_Layer_2+Energy_Layer_3+Energy_Layer_4+Energy_Layer_5+Energy_Layer
_6+Energy_Layer_7+Energy_Layer_8+Energy_Layer_9+Energy_Layer_10+Energy_Layer_11+Energy_
Layer_12+Energy_Layer_13+Energy_Layer_14+Energy_Layer_15+Energy_Layer_16+Energy_Layer_1
7+Energy_Layer_18)-
(Energy_Layer_1+Energy_Layer_2+Energy_Layer_3+Energy_Layer_4+Energy_Layer_5+Energy_Layer
_6+Energy_Layer_7+Energy_Layer_8+Energy_Layer_9+Energy_Layer_10+Energy_Layer_11+Energy_
Layer_12+Energy_Layer_13+Energy_Layer_14+Energy_Layer_15+Energy_Layer_17+Energy_Layer_1
8)
ENERGY_W[Layer_17] =
(Energy_Layer_1+Energy_Layer_2+Energy_Layer_3+Energy_Layer_4+Energy_Layer_5+Energy_Layer
_6+Energy_Layer_7+Energy_Layer_8+Energy_Layer_9+Energy_Layer_10+Energy_Layer_11+Energy_
Layer_12+Energy_Layer_13+Energy_Layer_14+Energy_Layer_15+Energy_Layer_16+Energy_Layer_1
7+Energy_Layer_18)-
(Energy_Layer_1+Energy_Layer_2+Energy_Layer_3+Energy_Layer_4+Energy_Layer_5+Energy_Layer
_6+Energy_Layer_7+Energy_Layer_8+Energy_Layer_9+Energy_Layer_10+Energy_Layer_11+Energy_
Layer_12+Energy_Layer_13+Energy_Layer_14+Energy_Layer_15+Energy_Layer_16+Energy_Layer_1
8)
ENERGY_W[Layer_18] =
(Energy_Layer_1+Energy_Layer_2+Energy_Layer_3+Energy_Layer_4+Energy_Layer_5+Energy_Layer
_6+Energy_Layer_7+Energy_Layer_8+Energy_Layer_9+Energy_Layer_10+Energy_Layer_11+Energy_
Layer_12+Energy_Layer_13+Energy_Layer_14+Energy_Layer_15+Energy_Layer_16+Energy_Layer_1
7+Energy_Layer_18)-
(Energy_Layer_1+Energy_Layer_2+Energy_Layer_3+Energy_Layer_4+Energy_Layer_5+Energy_Layer
_6+Energy_Layer_7+Energy_Layer_8+Energy_Layer_9+Energy_Layer_10+Energy_Layer_11+Energy_
Layer_12+Energy_Layer_13+Energy_Layer_14+Energy_Layer_15+Energy_Layer_16+Energy_Layer_1
7)
~~TEMPERATURE_W[Volume_Elements] =~~
ENERGY_W[Volume_Elements]*Conversion[Volume_Elements]

Back_Radiation = 0.97*StefanBoltzman_Constant*(TEMPERATURE_W[Layer_1]+273)^4
Convection = 1.5701*(Wind_Speed[Two_metres]*60*60/1000)*(TEMPERATURE_W[Layer_1]-(Air_Temperature-273))
Emittance = 0.398E-5*Air_Temperature^2.148
Evaporation = N_coeff*(Wind_Speed[Two_metres]*60*60/1000)*(Saturated_VP-Water_VP)
Net_Atmos_Radiation = (1-Reflectance)*Emittance*StefanBoltzman_Constant*Air_Temperature^4
N_coeff = 5.0593
Reflectance = 0.03
Saturated_VP = 25.374*EXP(17.62-5271/(TEMPERATURE_W[Layer_1]+273))
StefanBoltzman_Constant = 2.04E-7
Water_VP = 610.78*EXP(17.2694*(DewPoint-273.16)/(DewPoint-35.86))*760/101.325/1000
Air_Temperature = GRAPH(TIME)
(888, 294), (888, 292), (889, 292), (889, 293), (890, 292), (890, 290), (891, 290), (891, 292), (892, 293), (892, 291), (893, 291), (893, 295), (893, 296), (894, 297), (894, 296), (895, 296), (895, 298), (896, 301), (896, 304), (897, 306), (897, 302), (898, 304), (898, 304), (899, 305), (899, 301), (899, 301), (900, 304), (900, 304), (901, 303), (901, 304), (902, 305), (902, 304), (903, 304), (903, 299), (904, 300), (904, 301), (904, 300), (905, 299), (905, 300), (906, 300), (906, 300), (907, 300), (907, 299), (908, 297), (908, 297), (909, 298), (909, 298), (910, 297), (910, 296), (910, 295), (911, 295), (911, 295), (912, 296), (912, 297), (913, 298), (913, 298), (914, 297), (914, 297), (915, 297), (915, 297), (915, 296), (916, 296), (916, 296), (917, 296), (917, 295), (918, 294), (918, 294), (919, 293), (919, 293), (920, 294), (920, 295), (920, 296), (921, 297), (921, 297), (922, 296), (922, 297), (923, 296), (923, 295), (924, 294), (924, 294), (925, 295), (925, 296), (926, 297), (926, 297), (926, 297), (927, 296), (927, 296), (928, 295), (928, 295), (929, 294), (929, 294), (930, 293), (930, 293), (931, 293), (931, 293), (931, 292), (932, 293), (932, 293), (933, 292), (933, 291), (934, 291), (934, 291), (935, 291), (935, 291), (936, 291), (936, 291), (936, 291), (937, 290), (937, 290), (938, 290), (938, 290), (939, 290), (939, 290), (940, 290), (940, 290), (941, 290), (941, 291), (942, 292), (942, 291), (942, 292), (943, 291), (943, 292), (944, 293), (944, 293), (945, 293), (945, 293), (946, 293), (946, 292), (947, 292), (947, 293), (947, 292), (948, 291), (948, 291), (949, 291), (949, 290), (950, 290), (950, 289), (951, 289), (951, 288), (952, 288), (952, 288), (953, 288), (953, 287), (953, 287), (954, 287), (954, 287), (955, 287), (955, 287), (956, 287), (956, 287), (957, 287), (957, 287), (958, 287), (958, 286), (958, 286), (959, 287), (959, 287), (960, 287), (960, 287), (961, 287), (961, 288), (962, 288), (962, 289), (963, 289), (963, 289), (963, 290), (964, 290), (964, 290), (965, 291), (965, 291), (966, 291), (966, 291), (967, 291), (967, 291), (968, 291), (968, 291), (969, 291), (969, 291), (969, 291), (970, 291), (970, 291), (971, 291), (971, 291), (972, 290), (972, 290), (973, 290), (973, 290), (974, 289), (974, 289), (974, 288), (975, 288), (975, 287), (976, 287), (976, 287), (977, 287), (977, 287), (978, 287), (978, 288), (979, 288), (979, 288), (979, 288), (980, 289), (980, 288), (981, 289), (981, 289), (982, 289), (982, 289), (983, 289), (983, 289), (984, 289), (984, 290), (985, 289), (985, 291), (985, 290), (986, 291), (986, 291), (987, 290), (987, 290), (988, 291), (988, 291), (989, 291), (989, 291), (990, 291), (990, 291), (990, 292), (991, 292), (991, 291), (992, 291), (992, 290), (993, 290), (993, 291), (994, 290), (994, 290), (995, 289), (995, 289), (996, 288), (996, 288), (996, 288), (997, 287), (997, 287), (998, 287), (998, 287), (999, 287), (999, 287), (1000, 286), (1000, 286), (1001, 286), (1001, 286), (1001, 285), (1002, 286), (1002, 286), (1003, 285), (1003, 285), (1004, 285), (1004, 285), (1005, 286), (1005, 287), (1006, 287), (1006, 287), (1006, 288), (1007, 288), (1007, 288), (1008, 289), (1008, 290), (1009, 290), (1009, 290), (1010, 291), (1010, 292), (1011, 293), (1011, 293), (1012, 293), (1012, 294), (1012, 294), (1013, 294), (1013, 294), (1014, 294), (1014, 294), (1015, 294), (1015, 294), (1016, 293), (1016, 292), (1017, 291), (1017, 290), (1017, 289), (1018, 289), (1018, 288), (1019, 288), (1019, 288), (1020, 288), (1020, 288), (1021, 288), (1021, 288), (1022, 288), (1022, 288), (1022, 288), (1023, 288), (1023, 288), (1024, 288), (1024, 288), (1025, 288), (1025, 288), (1026, 288), (1026, 287), (1027, 286), (1027, 287), (1028, 288), (1028, 289), (1028, 290), (1029, 291), (1029, 292), (1030, 292), (1030, 292), (1031, 293), (1031, 294), (1032, 295), (1032, 295), (1033, 295), (1033, 295), (1033, 295), (1034, 296), (1034, 296), (1035, 296), (1035, 296), (1036, 296), (1036, 296), (1037, 296), (1037, 296), (1038, 295), (1038, 296), (1039, 297), (1039, 296), (1039, 295), (1040, 294), (1040, 294), (1041, 293), (1041, 293), (1042, 293), (1042, 293), (1043, 293), (1043, 294), (1044, 294), (1044, 294), (1044, 294), (1045, 292), (1045, 289), (1046, 290), (1046, 289), (1047, 288), (1047, 287), (1048, 288), (1048, 288), (1049, 289), (1049, 290), (1049, 292), (1050, 296), (1050, 297), (1051, 298), (1051, 298), (1052, 298), (1052, 302), (1053, 302), (1053, 303), (1054, 304), (1054, 301), (1055, 299), (1055, 299), (1055, 300), (1056, 301), (1056, 301), (1057, 301), (1057, 301), (1058, 302), (1058, 304), (1059, 304), (1059, 303), (1060, 302), (1060, 302), (1060, 301), (1061, 301), (1061, 300), (1062, 301), (1062, 300), (1063, 300), (1063, 300), (1064, 298), (1064, 298), (1065, 297), (1065, 296), (1065, 296), (1066, 296), (1066, 295), (1067, 295), (1067, 295), (1068, 295), (1068, 292), (1069, 292), (1069, 293), (1070, 294), (1070, 294), (1071, 295), (1071, 298), (1071, 300), (1072, 301), (1072, 303), (1073, 304), (1073, 305), (1074, 307), (1074, 307), (1075, 307), (1075, 308), (1076, 308), (1076, 308), (1076, 308), (1077, 307), (1077, 307), (1078, 307), (1078, 307), (1079, 307), (1079, 307), (1080, 306), (1080, 305), (1081, 305), (1081, 304), (1082, 304), (1082, 305), (1082, 305), (1083, 303), (1083, 302), (1084, 299), (1084, 298), (1085, 298), (1085, 297), (1086, 295), (1086, 294), (1087, 294), (1087, 294), (1087, 293), (1088, 292), (1088, 291), (1089, 291), (1089, 291), (1090, 290), (1090, 290), (1091, 290), (1091, 290), (1092, 290), (1092, 291), (1092, 291), (1093, 290), (1093, 291), (1094, 290), (1094, 291), (1095, 291), (1095, 292), (1096, 292), (1096, 290), (1097, 291), (1097, 291), (1098, 292), (1098, 292), (1098, 292), (1099, 292), (1099, 293), (1100, 292), (1100, 292), (1101, 292), (1101, 292),

(1102, 292), (1102, 291), (1103, 291), (1103, 291), (1103, 291), (1104, 291), (1104, 291), (1105, 291), (1105, 290), (1106, 290), (1106, 289), (1107, 289), (1107, 288), (1108, 288), (1108, 288), (1108, 288), (1109, 288), (1109, 288), (1110, 288), (1110, 287), (1111, 287), (1111, 287), (1112, 287), (1112, 286), (1113, 286), (1113, 286), (1114, 285), (1114, 286), (1114, 286), (1115, 285), (1115, 286), (1116, 287), (1116, 287), (1117, 288), (1117, 289), (1118, 289), (1118, 290), (1119, 290), (1119, 290), (1119, 292), (1120, 292), (1120, 292), (1121, 292), (1121, 293), (1122, 293), (1122, 293), (1123, 293), (1123, 293), (1124, 293), (1124, 294), (1125, 293), (1125, 293), (1125, 292), (1126, 292), (1126, 292), (1127, 291), (1127, 291), (1128, 290), (1128, 289), (1129, 288), (1129, 288), (1130, 288), (1130, 287), (1130, 287), (1131, 287), (1131, 286), (1132, 286), (1132, 286), (1133, 286), (1133, 286), (1134, 285), (1134, 285), (1135, 285), (1135, 285), (1135, 285), (1136, 284), (1136, 283), (1137, 283), (1137, 284), (1138, 284), (1138, 285), (1139, 286), (1139, 288), (1140, 289), (1140, 289), (1141, 291), (1141, 291), (1141, 292), (1142, 292), (1142, 292), (1143, 292), (1143, 293), (1144, 293), (1144, 294), (1145, 294), (1145, 296), (1146, 295), (1146, 295), (1146, 295), (1147, 295), (1147, 294), (1148, 294), (1148, 294), (1149, 293), (1149, 293), (1150, 292), (1150, 291), (1151, 290), (1151, 290), (1151, 289), (1152, 289), (1152, 288), (1153, 288), (1153, 288), (1154, 288), (1154, 288), (1155, 287), (1155, 287), (1156, 287), (1156, 287), (1157, 287), (1157, 286), (1157, 287), (1158, 286), (1158, 286), (1159, 286), (1159, 286), (1160, 286), (1160, 287), (1161, 288), (1161, 289), (1162, 289), (1162, 289), (1162, 290), (1163, 291), (1163, 291), (1164, 291), (1164, 291), (1165, 291), (1165, 292), (1166, 293), (1166, 293), (1167, 293), (1167, 294), (1168, 295), (1168, 295), (1168, 295), (1169, 295), (1169, 295), (1170, 294), (1170, 293), (1171, 292), (1171, 292), (1172, 291), (1172, 290), (1173, 289), (1173, 288), (1173, 288), (1174, 288), (1174, 288), (1175, 288), (1175, 288), (1176, 288), (1176, 289), (1177, 289), (1177, 289), (1178, 288), (1178, 289), (1178, 288), (1179, 288), (1179, 288), (1180, 288), (1180, 287), (1181, 287), (1181, 287), (1182, 287), (1182, 289), (1183, 290), (1183, 291), (1184, 291), (1184, 291), (1184, 292), (1185, 293), (1185, 293), (1186, 294), (1186, 294), (1187, 295), (1187, 295), (1188, 295), (1188, 296), (1189, 296), (1189, 295), (1189, 296), (1190, 296), (1190, 296), (1191, 296), (1191, 296), (1192, 296), (1192, 298), (1193, 298), (1193, 296), (1194, 295), (1194, 294), (1194, 293), (1195, 293), (1195, 292), (1196, 292), (1196, 292), (1197, 292), (1197, 292), (1198, 292), (1198, 292), (1199, 293), (1199, 293), (1200, 293), (1200, 293), (1200, 293), (1201, 293), (1201, 291), (1202, 292), (1202, 292), (1203, 293), (1203, 292), (1204, 292), (1204, 292), (1205, 292), (1205, 295), (1205, 296), (1206, 297), (1206, 298), (1207, 299), (1207, 299), (1208, 300), (1208, 300), (1209, 300), (1209, 300), (1210, 298), (1210, 299), (1211, 299), (1211, 300), (1211, 300), (1212, 300), (1212, 299), (1213, 299), (1213, 298), (1214, 299), (1214, 298), (1215, 298), (1215, 299), (1216, 297), (1216, 297), (1216, 296), (1217, 296), (1217, 296), (1218, 296), (1218, 295), (1219, 295), (1219, 295), (1220, 295), (1220, 295), (1221, 295), (1221, 295), (1221, 295), (1222, 295), (1222, 295), (1223, 294), (1223, 294), (1224, 294), (1224, 294), (1225, 294), (1225, 294), (1226, 294), (1226, 294), (1227, 294), (1227, 295), (1227, 295), (1228, 296), (1228, 297), (1229, 296), (1229, 297), (1230, 297), (1230, 298), (1231, 299), (1231, 299), (1232, 299), (1232, 299), (1232, 300), (1233, 299), (1233, 298), (1234, 298), (1234, 298), (1235, 298), (1235, 298), (1236, 298), (1236, 297), (1237, 296), (1237, 296), (1237, 296), (1238, 296), (1238, 295), (1239, 295), (1239, 295), (1240, 294), (1240, 295), (1241, 295), (1241, 295), (1242, 294), (1242, 294), (1243, 294), (1243, 294), (1243, 294), (1244, 294), (1244, 294), (1245, 294), (1245, 293), (1246, 293), (1246, 293), (1247, 293), (1247, 292), (1248, 291), (1248, 291), (1248, 291), (1249, 291), (1249, 291), (1250, 291), (1250, 293), (1251, 295), (1251, 295), (1252, 296), (1252, 297), (1253, 298), (1253, 299), (1254, 299), (1254, 300), (1254, 300), (1255, 300), (1255, 299), (1256, 300), (1256, 302), (1257, 301), (1257, 301), (1258, 301), (1258, 302), (1259, 301), (1259, 300), (1259, 299), (1260, 298), (1260, 296), (1261, 296), (1261, 295), (1262, 294), (1262, 293), (1263, 293), (1263, 293), (1264, 293), (1264, 294), (1264, 293), (1265, 293), (1265, 293), (1266, 293), (1266, 293), (1267, 292), (1267, 292), (1268, 291), (1268, 291), (1269, 291), (1269, 291), (1270, 291), (1270, 291), (1270, 291), (1271, 291), (1271, 292), (1272, 292), (1272, 293), (1273, 295), (1273, 295), (1274, 296), (1274, 298), (1275, 299), (1275, 299), (1275, 299), (1276, 299), (1276, 299), (1277, 300), (1277, 300), (1278, 300), (1278, 300), (1279, 300), (1279, 300), (1280, 300), (1280, 299), (1280, 299), (1281, 298), (1281, 297), (1282, 296), (1282, 296), (1283, 296), (1283, 295), (1284, 295), (1284, 295), (1285, 294), (1285, 294), (1286, 293), (1286, 293), (1286, 293), (1287, 294), (1287, 294), (1288, 293), (1288, 294), (1289, 294), (1289, 293), (1290, 293), (1290, 293), (1291, 292), (1291, 292), (1291, 292), (1292, 291), (1292, 291), (1293, 294), (1293, 295), (1294, 296), (1294, 296), (1295, 298), (1295, 298), (1296, 299), (1296, 300), (1297, 300), (1297, 300), (1297, 300), (1298, 300), (1298, 301), (1299, 298), (1299, 298), (1300, 296), (1300, 296), (1301, 297), (1301, 297), (1302, 294), (1302, 295), (1302, 297), (1303, 298), (1303, 297), (1304, 298), (1304, 297), (1305, 297), (1305, 296), (1306, 296), (1306, 295), (1307, 295), (1307, 294), (1307, 294), (1308, 293), (1308, 293), (1309, 293), (1309, 293), (1310, 292), (1310, 292), (1311, 292), (1311, 293), (1312, 292), (1312, 292), (1313, 292), (1313, 292), (1313, 292), (1314, 292), (1314, 291), (1315, 292), (1315, 293), (1316, 294), (1316, 294), (1317, 294), (1317, 294), (1318, 295), (1318, 296), (1318, 297), (1319, 295), (1319, 295), (1320, 296), (1320, 296), (1321, 295), (1321, 295), (1322, 295), (1322, 296), (1323, 295), (1323, 296), (1323, 296), (1324, 296), (1324, 295), (1325, 294), (1325, 294), (1326, 293), (1326, 293), (1327, 293), (1327, 292), (1328, 292), (1328, 292), (1329, 291), (1329, 291), (1329, 291), (1330, 291), (1330, 291), (1331, 291), (1331, 290), (1332, 291), (1332, 291), (1333, 291), (1333, 291), (1334, 291), (1334, 291), (1334, 291), (1335, 291), (1335, 291), (1336, 291), (1336, 291), (1337, 291), (1337, 291), (1338, 291), (1338, 291), (1339, 291), (1339, 291), (1340, 292), (1340, 292), (1340, 292), (1341, 293), (1341, 293), (1342, 293), (1342, 293), (1343, 293), (1343, 294), (1344, 294), (1344, 294), (1345, 293), (1345, 293), (1345, 293), (1346, 294), (1346, 294),

(1347, 293), (1347, 293), (1348, 292), (1348, 292), (1349, 292), (1349, 291), (1350, 291), (1350, 290), (1350, 290), (1351, 290), (1351, 290), (1352, 290), (1352, 290), (1353, 290), (1353, 290), (1354, 290), (1354, 290), (1355, 290), (1355, 290), (1356, 290), (1356, 289), (1356, 289), (1357, 290), (1357, 290), (1358, 289), (1358, 289), (1359, 289), (1359, 289), (1360, 290), (1360, 290), (1361, 290), (1361, 290), (1361, 291), (1362, 293), (1362, 293), (1363, 293), (1363, 293), (1364, 294), (1364, 294), (1365, 294), (1365, 295), (1366, 295), (1366, 294), (1366, 294), (1367, 294), (1367, 294), (1368, 294), (1368, 293), (1369, 293), (1369, 293), (1370, 292), (1370, 292), (1371, 292), (1371, 292), (1372, 292), (1372, 291), (1372, 291), (1373, 290), (1373, 290), (1374, 290), (1374, 290), (1375, 290), (1375, 290), (1376, 290), (1376, 290), (1377, 290), (1377, 290), (1377, 290), (1378, 290), (1378, 289), (1379, 289), (1379, 289), (1380, 289), (1380, 289), (1381, 288), (1381, 288), (1382, 288), (1382, 288), (1383, 288), (1383, 288), (1383, 288), (1384, 289), (1384, 289), (1385, 288), (1385, 289), (1386, 289), (1386, 289), (1387, 291), (1387, 291), (1388, 291), (1388, 291), (1388, 291), (1389, 291), (1389, 293), (1390, 292), (1390, 292), (1391, 292), (1391, 291), (1392, 291), (1392, 291), (1393, 291), (1393, 290), (1393, 290), (1394, 290), (1394, 289), (1395, 289), (1395, 289), (1396, 289), (1396, 288), (1397, 288), (1397, 287), (1398, 287), (1398, 287), (1399, 287), (1399, 288), (1399, 288), (1400, 288), (1400, 288), (1401, 288), (1401, 288), (1402, 288), (1402, 288), (1403, 288), (1403, 288), (1404, 288), (1404, 288), (1404, 288), (1405, 288), (1405, 288), (1406, 288), (1406, 288), (1407, 288), (1407, 289), (1408, 289), (1408, 289), (1409, 289), (1409, 289), (1409, 291), (1410, 290), (1410, 291), (1411, 290), (1411, 290), (1412, 290), (1412, 290), (1413, 291), (1413, 291), (1414, 291), (1414, 290), (1415, 291), (1415, 289), (1415, 289), (1416, 289), (1416, 289), (1417, 289), (1417, 288), (1418, 288), (1418, 288), (1419, 288), (1419, 288), (1420, 288), (1420, 288), (1420, 288), (1421, 288), (1421, 288), (1422, 288), (1422, 287), (1423, 287), (1423, 287), (1424, 287), (1424, 286), (1425, 286), (1425, 284), (1426, 284), (1426, 285), (1426, 286), (1427, 287), (1427, 287), (1428, 288), (1428, 289), (1429, 289), (1429, 290), (1430, 290), (1430, 291), (1431, 292), (1431, 292), (1431, 292), (1432, 292), (1432, 293), (1433, 293), (1433, 292), (1434, 293), (1434, 293), (1435, 293), (1435, 293), (1436, 292), (1436, 292), (1436, 292), (1437, 291), (1437, 291), (1438, 291), (1438, 291), (1439, 291), (1439, 291), (1440, 290), (1440, 290), (1441, 289), (1441, 288), (1442, 288), (1442, 288), (1442, 288), (1443, 287), (1443, 287), (1444, 287), (1444, 287), (1445, 287), (1445, 287), (1446, 287), (1446, 287), (1447, 287), (1447, 286), (1447, 287), (1448, 286), (1448, 286), (1449, 286), (1449, 286), (1450, 285), (1450, 286), (1451, 286), (1451, 286), (1452, 287), (1452, 287), (1452, 287), (1453, 288), (1453, 288), (1454, 289), (1454, 289), (1455, 290), (1455, 290), (1456, 290), (1456, 290), (1457, 291), (1457, 290), (1458, 291), (1458, 291), (1458, 291), (1459, 291), (1459, 293), (1460, 292), (1460, 292), (1461, 291), (1461, 291), (1462, 291), (1462, 291), (1463, 290), (1463, 289), (1463, 289), (1464, 288), (1464, 288), (1465, 287), (1465, 287), (1466, 287), (1466, 287), (1467, 287), (1467, 287), (1468, 287), (1468, 288), (1469, 287), (1469, 287), (1469, 287), (1470, 287), (1470, 287), (1471, 287), (1471, 287), (1472, 287), (1472, 287), (1473, 287), (1473, 286), (1474, 287), (1474, 289), (1474, 290), (1475, 291), (1475, 291), (1476, 292), (1476, 293), (1477, 293), (1477, 293), (1478, 293), (1478, 294), (1479, 294), (1479, 294), (1479, 296), (1480, 297), (1480, 297), (1481, 297), (1481, 296), (1482, 297), (1482, 297), (1483, 297), (1483, 296), (1484, 297), (1484, 296), (1485, 296), (1485, 295), (1485, 294), (1486, 294), (1486, 294), (1487, 294), (1487, 293), (1488, 292), (1488, 291), (1489, 290), (1489, 289), (1490, 289), (1490, 290), (1490, 290), (1491, 290), (1491, 290), (1492, 289), (1492, 288), (1493, 287), (1493, 287), (1494, 287), (1494, 287), (1495, 286), (1495, 289), (1495, 290), (1496, 292), (1496, 293), (1497, 294), (1497, 294), (1498, 294), (1498, 296), (1499, 296), (1499, 296), (1500, 295), (1500, 295), (1501, 295), (1501, 295), (1501, 295), (1502, 295), (1502, 295), (1503, 295), (1503, 296), (1504, 294), (1504, 294), (1505, 294), (1505, 293), (1506, 293), (1506, 292), (1506, 292), (1507, 292), (1507, 291), (1508, 291), (1508, 291), (1509, 291), (1509, 291), (1510, 291), (1510, 291), (1511, 291), (1511, 291), (1512, 291)

DewPoint = GRAPH(TIME)

(888, 282), (888, 283), (889, 283), (889, 283), (890, 283), (890, 285), (891, 285), (891, 283), (892, 285), (892, 287), (893, 287), (893, 279), (893, 281), (894, 282), (894, 288), (895, 288), (895, 287), (896, 285), (896, 280), (897, 278), (897, 288), (898, 282), (898, 283), (899, 282), (899, 283), (899, 281), (900, 279), (900, 279), (901, 280), (901, 278), (902, 279), (902, 278), (903, 278), (903, 285), (904, 281), (904, 281), (904, 282), (905, 284), (905, 282), (906, 281), (906, 281), (907, 281), (907, 283), (908, 287), (908, 287), (909, 285), (909, 283), (910, 284), (910, 286), (910, 287), (911, 287), (911, 287), (912, 285), (912, 284), (913, 282), (913, 283), (914, 286), (914, 283), (915, 283), (915, 284), (915, 286), (916, 286), (916, 289), (917, 288), (917, 290), (918, 291), (918, 291), (919, 291), (919, 291), (920, 291), (920, 292), (920, 290), (921, 289), (921, 288), (922, 289), (922, 289), (923, 290), (923, 290), (924, 291), (924, 292), (925, 292), (925, 290), (926, 290), (926, 290), (926, 290), (927, 290), (927, 290), (928, 291), (928, 291), (929, 291), (929, 291), (930, 291), (930, 292), (931, 291), (931, 291), (931, 290), (932, 290), (932, 290), (933, 288), (933, 288), (934, 288), (934, 288), (935, 287), (935, 287), (936, 287), (936, 287), (936, 287), (937, 287), (937, 286), (938, 286), (938, 286), (939, 287), (939, 285), (940, 285), (940, 285), (941, 284), (941, 284), (942, 283), (942, 284), (942, 283), (943, 284), (943, 283), (944, 283), (944, 282), (945, 282), (945, 282), (946, 280), (946, 280), (947, 279), (947, 280), (947, 278), (948, 278), (948, 278), (949, 277), (949, 279), (950, 279), (950, 278), (951, 276), (951, 276), (952, 276), (952, 277), (953, 278), (953, 277), (953, 277), (954, 278), (954, 278), (955, 277), (955, 277), (956, 276), (956, 277), (957, 277), (957, 278), (958, 277), (958, 278), (958, 279), (959, 278), (959, 278), (960, 278), (960, 277), (961, 277), (961, 277), (962, 277), (962, 278), (963, 278), (963, 278), (963, 278), (964, 277), (964, 278), (965, 279), (965, 278), (966, 279), (966, 280), (967, 280), (967, 280), (968, 280), (968, 280), (969, 280), (969, 281), (969, 281), (970, 281),

(970, 281), (971, 281), (971, 281), (972, 281), (972, 281), (973, 281), (973, 282), (974, 282), (974, 281), (974, 281), (975, 281), (975, 281), (976, 281), (976, 281), (977, 281), (977, 282), (978, 282), (978, 281), (979, 280), (979, 280), (979, 280), (980, 281), (980, 282), (981, 281), (981, 280), (982, 281), (982, 281), (983, 281), (983, 282), (984, 282), (984, 282), (985, 284), (985, 283), (985, 283), (986, 283), (986, 283), (987, 284), (987, 285), (988, 283), (988, 281), (989, 281), (989, 279), (990, 278), (990, 277), (990, 277), (991, 278), (991, 277), (992, 278), (992, 278), (993, 277), (993, 277), (994, 275), (994, 275), (995, 275), (995, 276), (996, 277), (996, 278), (996, 278), (997, 278), (997, 278), (998, 279), (998, 279), (999, 279), (999, 279), (1000, 279), (1000, 279), (1001, 278), (1001, 278), (1001, 278), (1002, 277), (1002, 278), (1003, 278), (1003, 278), (1004, 278), (1004, 278), (1005, 278), (1005, 278), (1006, 279), (1006, 279), (1006, 280), (1007, 280), (1007, 280), (1008, 281), (1008, 278), (1009, 280), (1009, 280), (1010, 280), (1010, 280), (1011, 279), (1011, 280), (1012, 281), (1012, 281), (1012, 281), (1013, 280), (1013, 280), (1014, 280), (1014, 280), (1015, 280), (1015, 280), (1016, 280), (1016, 280), (1017, 280), (1017, 280), (1017, 281), (1018, 281), (1018, 281), (1019, 281), (1019, 282), (1020, 281), (1020, 282), (1021, 282), (1021, 282), (1022, 282), (1022, 282), (1022, 282), (1023, 282), (1023, 282), (1024, 282), (1024, 282), (1025, 282), (1025, 281), (1026, 281), (1026, 282), (1027, 282), (1027, 283), (1028, 282), (1028, 282), (1028, 282), (1029, 282), (1029, 283), (1030, 283), (1030, 283), (1031, 283), (1031, 283), (1032, 284), (1032, 284), (1033, 283), (1033, 285), (1033, 283), (1034, 282), (1034, 283), (1035, 281), (1035, 282), (1036, 281), (1036, 281), (1037, 282), (1037, 282), (1038, 285), (1038, 286), (1039, 282), (1039, 281), (1039, 281), (1040, 282), (1040, 281), (1041, 281), (1041, 280), (1042, 279), (1042, 279), (1043, 280), (1043, 281), (1044, 281), (1044, 281), (1044, 281), (1045, 282), (1045, 283), (1046, 282), (1046, 283), (1047, 283), (1047, 283), (1048, 283), (1048, 283), (1049, 284), (1049, 285), (1049, 285), (1050, 283), (1050, 281), (1051, 281), (1051, 286), (1052, 286), (1052, 278), (1053, 277), (1053, 278), (1054, 277), (1054, 284), (1055, 287), (1055, 288), (1055, 284), (1056, 283), (1056, 283), (1057, 282), (1057, 280), (1058, 277), (1058, 279), (1059, 278), (1059, 279), (1060, 279), (1060, 278), (1060, 278), (1061, 280), (1061, 281), (1062, 280), (1062, 282), (1063, 282), (1063, 280), (1064, 282), (1064, 282), (1065, 283), (1065, 284), (1065, 286), (1066, 285), (1066, 280), (1067, 282), (1067, 279), (1068, 279), (1068, 282), (1069, 281), (1069, 279), (1070, 278), (1070, 278), (1071, 278), (1071, 275), (1071, 276), (1072, 276), (1072, 273), (1073, 272), (1073, 272), (1074, 273), (1074, 270), (1075, 271), (1075, 274), (1076, 273), (1076, 271), (1076, 271), (1077, 273), (1077, 272), (1078, 272), (1078, 274), (1079, 271), (1079, 271), (1080, 272), (1080, 273), (1081, 275), (1081, 275), (1082, 275), (1082, 270), (1082, 275), (1083, 279), (1083, 281), (1084, 286), (1084, 286), (1085, 287), (1085, 287), (1086, 289), (1086, 290), (1087, 290), (1087, 290), (1087, 291), (1088, 291), (1088, 289), (1089, 289), (1089, 289), (1090, 289), (1090, 289), (1091, 288), (1091, 288), (1092, 288), (1092, 287), (1092, 285), (1093, 286), (1093, 286), (1094, 284), (1094, 285), (1095, 284), (1095, 285), (1096, 286), (1096, 286), (1097, 285), (1097, 283), (1098, 283), (1098, 283), (1098, 281), (1099, 282), (1099, 281), (1100, 280), (1100, 281), (1101, 281), (1101, 282), (1102, 280), (1102, 281), (1103, 279), (1103, 279), (1103, 279), (1104, 278), (1104, 278), (1105, 279), (1105, 279), (1106, 278), (1106, 277), (1107, 275), (1107, 276), (1108, 277), (1108, 278), (1108, 278), (1109, 278), (1109, 276), (1110, 276), (1110, 275), (1111, 276), (1111, 276), (1112, 276), (1112, 275), (1113, 275), (1113, 273), (1114, 274), (1114, 275), (1114, 275), (1115, 275), (1115, 276), (1116, 276), (1116, 276), (1117, 276), (1117, 277), (1118, 276), (1118, 275), (1119, 277), (1119, 277), (1119, 277), (1120, 276), (1120, 276), (1121, 275), (1121, 276), (1122, 276), (1122, 277), (1123, 276), (1123, 277), (1124, 277), (1124, 277), (1125, 276), (1125, 277), (1125, 276), (1126, 276), (1126, 278), (1127, 278), (1127, 278), (1128, 278), (1128, 278), (1129, 279), (1129, 279), (1130, 279), (1130, 279), (1130, 279), (1131, 279), (1131, 279), (1132, 279), (1132, 279), (1133, 279), (1133, 279), (1134, 279), (1134, 279), (1135, 280), (1135, 279), (1135, 280), (1136, 280), (1136, 280), (1137, 280), (1137, 280), (1138, 280), (1138, 281), (1139, 280), (1139, 280), (1140, 280), (1140, 279), (1141, 279), (1141, 279), (1141, 279), (1142, 279), (1142, 279), (1143, 279), (1143, 279), (1144, 280), (1144, 278), (1145, 280), (1145, 278), (1146, 277), (1146, 277), (1146, 278), (1147, 278), (1147, 278), (1148, 279), (1148, 280), (1149, 279), (1149, 280), (1150, 280), (1150, 280), (1151, 280), (1151, 281), (1151, 281), (1152, 282), (1152, 282), (1153, 282), (1153, 282), (1154, 282), (1154, 282), (1155, 282), (1155, 282), (1156, 282), (1156, 282), (1157, 282), (1157, 282), (1157, 282), (1158, 282), (1158, 282), (1159, 282), (1159, 283), (1160, 283), (1160, 283), (1161, 283), (1161, 283), (1162, 283), (1162, 283), (1162, 282), (1163, 282), (1163, 282), (1164, 282), (1164, 282), (1165, 282), (1165, 282), (1166, 282), (1166, 281), (1167, 281), (1167, 281), (1168, 281), (1168, 280), (1168, 279), (1169, 277), (1169, 277), (1170, 280), (1170, 280), (1171, 280), (1171, 280), (1172, 281), (1172, 281), (1173, 281), (1173, 281), (1173, 281), (1174, 282), (1174, 282), (1175, 282), (1175, 282), (1176, 282), (1176, 281), (1177, 281), (1177, 279), (1178, 278), (1178, 276), (1178, 275), (1179, 275), (1179, 275), (1180, 276), (1180, 275), (1181, 276), (1181, 278), (1182, 277), (1182, 278), (1183, 276), (1183, 277), (1184, 277), (1184, 278), (1184, 278), (1185, 279), (1185, 279), (1186, 279), (1186, 280), (1187, 280), (1187, 280), (1188, 281), (1188, 281), (1189, 280), (1189, 282), (1189, 281), (1190, 280), (1190, 280), (1191, 282), (1191, 283), (1192, 284), (1192, 279), (1193, 276), (1193, 278), (1194, 278), (1194, 278), (1194, 277), (1195, 278), (1195, 278), (1196, 278), (1196, 277), (1197, 277), (1197, 276), (1198, 275), (1198, 276), (1199, 276), (1199, 277), (1200, 277), (1200, 276), (1200, 276), (1201, 277), (1201, 279), (1202, 278), (1202, 277), (1203, 273), (1203, 279), (1204, 278), (1204, 280), (1205, 281), (1205, 279), (1205, 279), (1206, 275), (1206, 274), (1207, 275), (1207, 274), (1208, 275), (1208, 275), (1209, 275), (1209, 275), (1210, 279), (1210, 281), (1211, 280), (1211, 276), (1211, 274), (1212, 276), (1212, 276), (1213, 280), (1213, 282), (1214, 276), (1214, 277), (1215, 284), (1215, 277), (1216, 279), (1216, 278), (1216, 278), (1217, 277), (1217, 277), (1218, 277), (1218, 278),

(1219, 278), (1219, 280), (1220, 281), (1220, 281), (1221, 282), (1221, 282), (1221, 281), (1222, 280), (1222, 281), (1223, 281), (1223, 281), (1224, 281), (1224, 281), (1225, 281), (1225, 280), (1226, 280), (1226, 281), (1227, 279), (1227, 279), (1227, 280), (1228, 280), (1228, 281), (1229, 281), (1229, 281), (1230, 281), (1230, 281), (1231, 281), (1231, 281), (1232, 284), (1232, 282), (1232, 281), (1233, 280), (1233, 282), (1234, 281), (1234, 283), (1235, 281), (1235, 282), (1236, 282), (1236, 282), (1237, 281), (1237, 282), (1237, 283), (1238, 282), (1238, 282), (1239, 282), (1239, 282), (1240, 281), (1240, 280), (1241, 279), (1241, 279), (1242, 280), (1242, 280), (1243, 280), (1243, 281), (1243, 281), (1244, 281), (1244, 282), (1245, 282), (1245, 283), (1246, 283), (1246, 283), (1247, 284), (1247, 284), (1248, 285), (1248, 285), (1248, 285), (1249, 285), (1249, 285), (1250, 285), (1250, 285), (1251, 285), (1251, 285), (1252, 285), (1252, 285), (1253, 285), (1253, 284), (1254, 284), (1254, 284), (1254, 283), (1255, 287), (1255, 287), (1256, 286), (1256, 284), (1257, 284), (1257, 284), (1258, 284), (1258, 283), (1259, 283), (1259, 284), (1259, 284), (1260, 284), (1260, 284), (1261, 283), (1261, 283), (1262, 283), (1262, 284), (1263, 284), (1263, 284), (1264, 284), (1264, 284), (1264, 284), (1265, 284), (1265, 284), (1266, 284), (1266, 283), (1267, 283), (1267, 284), (1268, 284), (1268, 284), (1269, 284), (1269, 283), (1270, 283), (1270, 283), (1270, 283), (1271, 282), (1271, 283), (1272, 283), (1272, 283), (1273, 283), (1273, 284), (1274, 284), (1274, 285), (1275, 284), (1275, 284), (1275, 284), (1276, 284), (1276, 284), (1277, 283), (1277, 283), (1278, 283), (1278, 283), (1279, 283), (1279, 284), (1280, 283), (1280, 283), (1280, 284), (1281, 285), (1281, 284), (1282, 284), (1282, 284), (1283, 283), (1283, 283), (1284, 282), (1284, 282), (1285, 282), (1285, 280), (1286, 279), (1286, 281), (1286, 280), (1287, 280), (1287, 281), (1288, 284), (1288, 284), (1289, 285), (1289, 286), (1290, 286), (1290, 286), (1291, 286), (1291, 286), (1291, 286), (1292, 286), (1292, 287), (1293, 286), (1293, 286), (1294, 286), (1294, 287), (1295, 286), (1295, 286), (1296, 286), (1296, 286), (1297, 286), (1297, 287), (1297, 286), (1298, 287), (1298, 286), (1299, 290), (1299, 290), (1300, 289), (1300, 289), (1301, 289), (1301, 289), (1302, 291), (1302, 290), (1302, 290), (1303, 288), (1303, 287), (1304, 287), (1304, 288), (1305, 287), (1305, 287), (1306, 287), (1306, 287), (1307, 288), (1307, 288), (1307, 288), (1308, 288), (1308, 288), (1309, 288), (1309, 288), (1310, 289), (1310, 288), (1311, 288), (1311, 288), (1312, 288), (1312, 288), (1313, 288), (1313, 288), (1313, 288), (1314, 288), (1314, 288), (1315, 289), (1315, 289), (1316, 289), (1316, 289), (1317, 289), (1317, 289), (1318, 288), (1318, 288), (1318, 287), (1319, 289), (1319, 290), (1320, 290), (1320, 290), (1321, 290), (1321, 290), (1322, 290), (1322, 290), (1323, 289), (1323, 289), (1323, 289), (1324, 288), (1324, 288), (1325, 289), (1325, 289), (1326, 288), (1326, 288), (1327, 287), (1327, 287), (1328, 287), (1328, 287), (1329, 287), (1329, 287), (1329, 287), (1330, 286), (1330, 287), (1331, 287), (1331, 287), (1332, 287), (1332, 287), (1333, 287), (1333, 287), (1334, 287), (1334, 287), (1334, 287), (1335, 287), (1335, 287), (1336, 287), (1336, 287), (1337, 287), (1337, 287), (1338, 287), (1338, 287), (1339, 287), (1339, 286), (1340, 286), (1340, 287), (1340, 287), (1341, 286), (1341, 287), (1342, 286), (1342, 287), (1343, 286), (1343, 287), (1344, 287), (1344, 286), (1345, 286), (1345, 286), (1345, 286), (1346, 286), (1346, 286), (1347, 286), (1347, 286), (1348, 285), (1348, 286), (1349, 286), (1349, 287), (1350, 287), (1350, 287), (1350, 287), (1351, 287), (1351, 287), (1352, 287), (1352, 287), (1353, 287), (1353, 287), (1354, 286), (1354, 286), (1355, 287), (1355, 286), (1356, 286), (1356, 286), (1356, 286), (1357, 285), (1357, 285), (1358, 284), (1358, 283), (1359, 283), (1359, 284), (1360, 283), (1360, 283), (1361, 282), (1361, 283), (1361, 283), (1362, 282), (1362, 281), (1363, 281), (1363, 280), (1364, 279), (1364, 279), (1365, 279), (1365, 280), (1366, 280), (1366, 280), (1366, 280), (1367, 280), (1367, 281), (1368, 281), (1368, 281), (1369, 282), (1369, 281), (1370, 281), (1370, 282), (1371, 281), (1371, 282), (1372, 281), (1372, 282), (1372, 282), (1373, 282), (1373, 282), (1374, 282), (1374, 282), (1375, 283), (1375, 283), (1376, 284), (1376, 284), (1377, 284), (1377, 284), (1377, 282), (1378, 282), (1378, 282), (1379, 281), (1379, 281), (1380, 282), (1380, 281), (1381, 282), (1381, 281), (1382, 280), (1382, 279), (1383, 279), (1383, 279), (1383, 279), (1384, 280), (1384, 280), (1385, 281), (1385, 281), (1386, 280), (1386, 280), (1387, 278), (1387, 279), (1388, 279), (1388, 279), (1388, 278), (1389, 277), (1389, 276), (1390, 277), (1390, 277), (1391, 278), (1391, 279), (1392, 278), (1392, 278), (1393, 278), (1393, 278), (1393, 279), (1394, 278), (1394, 279), (1395, 279), (1395, 279), (1396, 280), (1396, 280), (1397, 280), (1397, 280), (1398, 280), (1398, 280), (1399, 279), (1399, 280), (1399, 280), (1400, 279), (1400, 279), (1401, 279), (1401, 279), (1402, 279), (1402, 279), (1403, 279), (1403, 279), (1404, 278), (1404, 278), (1404, 279), (1405, 280), (1405, 280), (1406, 279), (1406, 280), (1407, 280), (1407, 279), (1408, 279), (1408, 279), (1409, 280), (1409, 281), (1409, 280), (1410, 280), (1410, 280), (1411, 280), (1411, 280), (1412, 281), (1412, 280), (1413, 281), (1413, 280), (1414, 280), (1414, 281), (1415, 280), (1415, 281), (1415, 281), (1416, 281), (1416, 280), (1417, 280), (1417, 282), (1418, 281), (1418, 281), (1419, 280), (1419, 280), (1420, 280), (1420, 280), (1420, 280), (1421, 280), (1421, 280), (1422, 281), (1422, 280), (1423, 280), (1423, 280), (1424, 281), (1424, 281), (1425, 282), (1425, 282), (1426, 281), (1426, 283), (1426, 283), (1427, 283), (1427, 284), (1428, 284), (1428, 282), (1429, 281), (1429, 279), (1430, 278), (1430, 278), (1431, 277), (1431, 277), (1431, 277), (1432, 276), (1432, 276), (1433, 277), (1433, 277), (1434, 276), (1434, 276), (1435, 275), (1435, 275), (1436, 276), (1436, 276), (1436, 276), (1437, 277), (1437, 277), (1438, 277), (1438, 277), (1439, 278), (1439, 278), (1440, 278), (1440, 278), (1441, 278), (1441, 279), (1442, 279), (1442, 279), (1442, 279), (1443, 279), (1443, 279), (1444, 279), (1444, 278), (1445, 278), (1445, 279), (1446, 279), (1446, 279), (1447, 279), (1447, 280), (1447, 280), (1448, 280), (1448, 278), (1449, 277), (1449, 277), (1450, 277), (1450, 277), (1451, 277), (1451, 277), (1452, 277), (1452, 277), (1452, 277), (1453, 277), (1453, 277), (1454, 277), (1454, 277), (1455, 277), (1455, 277), (1456, 278), (1456, 278), (1457, 278), (1457, 279), (1458, 279), (1458, 278), (1458, 278), (1459, 278), (1459, 278), (1460, 278), (1460, 279), (1461, 278), (1461, 279), (1462, 279), (1462, 280), (1463, 280), (1463, 280), (1463, 281),

(1464, 280), (1464, 281), (1465, 281), (1465, 281), (1466, 281), (1466, 281), (1467, 282), (1467, 281), (1468, 282), (1468, 282), (1469, 282), (1469, 282), (1469, 281), (1470, 281), (1470, 280), (1471, 280), (1471, 280), (1472, 280), (1472, 280), (1473, 280), (1473, 281), (1474, 281), (1474, 281), (1474, 282), (1475, 282), (1475, 283), (1476, 283), (1476, 283), (1477, 283), (1477, 282), (1478, 283), (1478, 283), (1479, 284), (1479, 283), (1479, 284), (1480, 281), (1480, 283), (1481, 279), (1481, 282), (1482, 280), (1482, 281), (1483, 281), (1483, 280), (1484, 279), (1484, 280), (1485, 279), (1485, 281), (1485, 282), (1486, 285), (1486, 283), (1487, 282), (1487, 282), (1488, 282), (1488, 283), (1489, 283), (1489, 283), (1490, 283), (1490, 282), (1490, 281), (1491, 280), (1491, 280), (1492, 283), (1492, 282), (1493, 282), (1493, 282), (1494, 281), (1494, 282), (1495, 282), (1495, 282), (1495, 282), (1496, 280), (1496, 281), (1497, 283), (1497, 284), (1498, 284), (1498, 282), (1499, 281), (1499, 283), (1500, 283), (1500, 285), (1501, 285), (1501, 286), (1501, 286), (1502, 286), (1502, 286), (1503, 285), (1503, 287), (1504, 287), (1504, 287), (1505, 286), (1505, 286), (1506, 286), (1506, 286), (1506, 286), (1507, 285), (1507, 285), (1508, 284), (1508, 283), (1509, 283), (1509, 283), (1510, 283), (1510, 283), (1511, 283), (1511, 283), (1512, 284)

Energy_Layer_1(t) = Energy_Layer_1(t - dt) + (In_Layer_1 - Out_Layer_1 - Diffusion_1_to_2) * dt
INIT Energy_Layer_1 = Temperature_Initial[Layer_1]/Conversion[Layer_1]
In_Layer_1 = Net_Atmos_Radiation+Pen_Solar_Irrad-Net_Solar_Irrad[Layer_1]+Q_Energy_In[Layer_1]
Out_Layer_1 = Back_Radiation+Convection+Evaporation
Diffusion_1_to_2 = Diffusion[Layer_1]
Energy_Layer_10(t) = Energy_Layer_10(t - dt) + (Diffusion_9_to_10 + In_Layer_10 - Diffusion_10_to_11) * dt
INIT Energy_Layer_10 = Temperature_Initial[Layer_10]/Conversion[Layer_10]
Diffusion_9_to_10 = Diffusion[Layer_9]
In_Layer_10 = Net_Solar_Irrad[Layer_9]-Net_Solar_Irrad[Layer_10]+Q_Energy_In[Layer_10]
Diffusion_10_to_11 = Diffusion[Layer_10]
Energy_Layer_11(t) = Energy_Layer_11(t - dt) + (Diffusion_10_to_11 + In_Layer_11 - Diffusion_11_to_12) * dt
INIT Energy_Layer_11 = Temperature_Initial[Layer_11]/Conversion[Layer_11]
Diffusion_10_to_11 = Diffusion[Layer_10]
In_Layer_11 = Net_Solar_Irrad[Layer_10]-Net_Solar_Irrad[Layer_11]+Q_Energy_In[Layer_11]
Diffusion_11_to_12 = Diffusion[Layer_11]
Energy_Layer_12(t) = Energy_Layer_12(t - dt) + (In_Layer_12 + Diffusion_11_to_12 - Diffusion_12_to_13) * dt
INIT Energy_Layer_12 = Temperature_Initial[Layer_12]/Conversion[Layer_12]
In_Layer_12 = Net_Solar_Irrad[Layer_11]-Net_Solar_Irrad[Layer_12]+Q_Energy_In[Layer_12]
Diffusion_11_to_12 = Diffusion[Layer_11]
Diffusion_12_to_13 = Diffusion[Layer_12]
Energy_Layer_13(t) = Energy_Layer_13(t - dt) + (In_Layer_13 + Diffusion_12_to_13 - Diffusion_13_to_14) * dt
INIT Energy_Layer_13 = Temperature_Initial[Layer_13]/Conversion[Layer_13]
In_Layer_13 = Net_Solar_Irrad[Layer_12]-Net_Solar_Irrad[Layer_13]+Q_Energy_In[Layer_13]
Diffusion_12_to_13 = Diffusion[Layer_12]
Diffusion_13_to_14 = Diffusion[Layer_13]
Energy_Layer_14(t) = Energy_Layer_14(t - dt) + (In_Layer_14 + Diffusion_13_to_14 - Diffusion_14_to_15) * dt
INIT Energy_Layer_14 = Temperature_Initial[Layer_14]/Conversion[Layer_14]
In_Layer_14 = Net_Solar_Irrad[Layer_13]-Net_Solar_Irrad[Layer_14]+Q_Energy_In[Layer_14]
Diffusion_13_to_14 = Diffusion[Layer_13]
Diffusion_14_to_15 = Diffusion[Layer_14]
Energy_Layer_15(t) = Energy_Layer_15(t - dt) + (Diffusion_14_to_15 + In_Layer_15 - Diffusion_15_to_16) * dt
INIT Energy_Layer_15 = Temperature_Initial[Layer_15]/Conversion[Layer_15]
Diffusion_14_to_15 = Diffusion[Layer_14]
In_Layer_15 = Net_Solar_Irrad[Layer_14]-Net_Solar_Irrad[Layer_15]+Q_Energy_In[Layer_15]
Diffusion_15_to_16 = Diffusion[Layer_15]
Energy_Layer_16(t) = Energy_Layer_16(t - dt) + (Diffusion_15_to_16 + In_Layer_16 - Diffusion_16_to_17) * dt
INIT Energy_Layer_16 = Temperature_Initial[Layer_16]/Conversion[Layer_16]
Diffusion_15_to_16 = Diffusion[Layer_15]
In_Layer_16 = Net_Solar_Irrad[Layer_15]-Net_Solar_Irrad[Layer_16]+Q_Energy_In[Layer_16]
Diffusion_16_to_17 = Diffusion[Layer_16]
Energy_Layer_17(t) = Energy_Layer_17(t - dt) + (In_Layer_17 + Diffusion_16_to_17 - Diffusion_17_to_18) * dt
INIT Energy_Layer_17 = Temperature_Initial[Layer_17]/Conversion[Layer_17]
In_Layer_17 = Net_Solar_Irrad[Layer_16]-Net_Solar_Irrad[Layer_17]+Q_Energy_In[Layer_17]
Diffusion_16_to_17 = Diffusion[Layer_16]
Diffusion_17_to_18 = Diffusion[Layer_17]

Energy_Layer_18(t) = Energy_Layer_18(t - dt) + (In_Layer_18 + Diffusion_17_to_18 - Conduction) * dt
INIT Energy_Layer_18 = Temperature_Initial[Layer_18]/Conversion[Layer_18]
In_Layer_18 = Net_Solar_Irrad[Layer_17]-Net_Solar_Irrad[Layer_18]+Q_Energy_In[Layer_18]
Diffusion_17_to_18 = Diffusion[Layer_17]
Conduction = Conduction_C
Energy_Layer_2(t) = Energy_Layer_2(t - dt) + (Diffusion_1_to_2 + In_Layer_2 - Diffusion_2_to_3) * dt
INIT Energy_Layer_2 = Temperature_Initial[Layer_2]/Conversion[Layer_2]
Diffusion_1_to_2 = Diffusion[Layer_1]
In_Layer_2 = Net_Solar_Irrad[Layer_1]-Net_Solar_Irrad[Layer_2]+Q_Energy_In[Layer_2]
Diffusion_2_to_3 = Diffusion[Layer_2]
Energy_Layer_3(t) = Energy_Layer_3(t - dt) + (Diffusion_2_to_3 + In_Layer_3 - Diffusion_3_to_4) * dt
INIT Energy_Layer_3 = Temperature_Initial[Layer_3]/Conversion[Layer_3]
Diffusion_2_to_3 = Diffusion[Layer_2]
In_Layer_3 = Net_Solar_Irrad[Layer_2]-Net_Solar_Irrad[Layer_3]+Q_Energy_In[Layer_3]
Diffusion_3_to_4 = Diffusion[Layer_3]
Energy_Layer_4(t) = Energy_Layer_4(t - dt) + (Diffusion_3_to_4 + In_Layer_4 - Diffusion_4_to_5) * dt
INIT Energy_Layer_4 = Temperature_Initial[Layer_4]/Conversion[Layer_4]
Diffusion_3_to_4 = Diffusion[Layer_3]
In_Layer_4 = Net_Solar_Irrad[Layer_3]-Net_Solar_Irrad[Layer_4]+Q_Energy_In[Layer_4]
Diffusion_4_to_5 = Diffusion[Layer_4]
Energy_Layer_5(t) = Energy_Layer_5(t - dt) + (In_Layer_5 + Diffusion_4_to_5 - Diffusion_5_to_6) * dt
INIT Energy_Layer_5 = Temperature_Initial[Layer_5]/Conversion[Layer_5]
In_Layer_5 = Net_Solar_Irrad[Layer_4]-Net_Solar_Irrad[Layer_5]+Q_Energy_In[Layer_5]
Diffusion_4_to_5 = Diffusion[Layer_4]
Diffusion_5_to_6 = Diffusion[Layer_5]
Energy_Layer_6(t) = Energy_Layer_6(t - dt) + (In_Layer_6 + Diffusion_5_to_6 - Diffusion_6_to_7) * dt
INIT Energy_Layer_6 = Temperature_Initial[Layer_6]/Conversion[Layer_6]
In_Layer_6 = Net_Solar_Irrad[Layer_5]-Net_Solar_Irrad[Layer_6]+Q_Energy_In[Layer_6]
Diffusion_5_to_6 = Diffusion[Layer_5]
Diffusion_6_to_7 = Diffusion[Layer_6]
Energy_Layer_7(t) = Energy_Layer_7(t - dt) + (In_Layer_7 + Diffusion_6_to_7 - Diffusion_7_to_8) * dt
INIT Energy_Layer_7 = Temperature_Initial[Layer_7]/Conversion[Layer_7]
In_Layer_7 = Net_Solar_Irrad[Layer_6]-Net_Solar_Irrad[Layer_7]+Q_Energy_In[Layer_7]
Diffusion_6_to_7 = Diffusion[Layer_6]
Diffusion_7_to_8 = Diffusion[Layer_7]
Energy_Layer_8(t) = Energy_Layer_8(t - dt) + (In_Layer_8 + Diffusion_7_to_8 - Diffusion_8_to_9) * dt
INIT Energy_Layer_8 = Temperature_Initial[Layer_8]/Conversion[Layer_8]
In_Layer_8 = Net_Solar_Irrad[Layer_7]-Net_Solar_Irrad[Layer_8]+Q_Energy_In[Layer_8]
Diffusion_7_to_8 = Diffusion[Layer_7]
Diffusion_8_to_9 = Diffusion[Layer_8]
Energy_Layer_9(t) = Energy_Layer_9(t - dt) + (In_Layer_9 + Diffusion_8_to_9 - Diffusion_9_to_10) * dt
INIT Energy_Layer_9 = Temperature_Initial[Layer_9]/Conversion[Layer_9]
In_Layer_9 = Net_Solar_Irrad[Layer_8]-Net_Solar_Irrad[Layer_9]+Q_Energy_In[Layer_9]
Diffusion_8_to_9 = Diffusion[Layer_8]
Diffusion_9_to_10 = Diffusion[Layer_9]
AA[Volume_Elements] = 8.24493e-1-4.0899e-3*TEMPERATURE_W[Volume_Elements]+7.6438e-5*TEMPERATURE_W[Volume_Elements]^2-8.2467e-7*TEMPERATURE_W[Volume_Elements]^3+5.3875e-9*TEMPERATURE_W[Volume_Elements]^4
BB[Volume_Elements] = -5.72466e-3+1.0227e-4*TEMPERATURE_W[Volume_Elements]-1.6546e-6*TEMPERATURE_W[Volume_Elements]^2
CC = 4.8314e-4
Density[Volume_Elements] = Density_Water[Volume_Elements]+AA[Volume_Elements]*Salinity[Volume_Elements]+BB[Volume_Elements]*Salinity[Volume_Elements]^1.5+CC*Salinity[Volume_Elements]^2
Density_Water[Volume_Elements] = 999.842594+6.793952e-2*TEMPERATURE_W[Volume_Elements]-9.095290e-3*TEMPERATURE_W[Volume_Elements]^2+1.001685e-4*TEMPERATURE_W[Volume_Elements]^3-1.120083e-6*TEMPERATURE_W[Volume_Elements]^4+6.536332e-9*TEMPERATURE_W[Volume_Elements]^5
Salinity_Gradient[Layer_1] = (Salinity[Layer_1]-Salinity[Layer_2])/Element_Height
Salinity_Gradient[Layer_2] = (Salinity[Layer_2]-Salinity[Layer_3])/Element_Height
Salinity_Gradient[Layer_3] = (Salinity[Layer_3]-Salinity[Layer_4])/Element_Height
Salinity_Gradient[Layer_4] = (Salinity[Layer_4]-Salinity[Layer_5])/Element_Height
Salinity_Gradient[Layer_5] = (Salinity[Layer_5]-Salinity[Layer_6])/Element_Height
Salinity_Gradient[Layer_6] = (Salinity[Layer_6]-Salinity[Layer_7])/Element_Height
Salinity_Gradient[Layer_7] = (Salinity[Layer_7]-Salinity[Layer_8])/Element_Height
Salinity_Gradient[Layer_8] = (Salinity[Layer_8]-Salinity[Layer_9])/Element_Height

```
Salinity_Gradient[Layer_9] = (Salinity[Layer_9]-Salinity[Layer_10])/Element_Height
Salinity_Gradient[Layer_10] = (Salinity[Layer_10]-Salinity[Layer_11])/Element_Height
Salinity_Gradient[Layer_11] = (Salinity[Layer_11]-Salinity[Layer_12])/Element_Height
Salinity_Gradient[Layer_12] = (Salinity[Layer_12]-Salinity[Layer_13])/Element_Height
Salinity_Gradient[Layer_13] = (Salinity[Layer_13]-Salinity[Layer_14])/Element_Height
Salinity_Gradient[Layer_14] = (Salinity[Layer_14]-Salinity[Layer_15])/Element_Height
Salinity_Gradient[Layer_15] = (Salinity[Layer_15]-Salinity[Layer_16])/Element_Height
Salinity_Gradient[Layer_16] = (Salinity[Layer_16]-Salinity[Layer_17])/Element_Height
Salinity_Gradient[Layer_17] = (Salinity[Layer_17]-Salinity[Layer_18])/Element_Height
Salinity_Gradient[Layer_18] = (Salinity[Layer_18]-Salinity[Layer_18])/Element_Height
Air_Density = 1.1988
Area_function = 1-EXP(-k_constant*Surface_Area)
Density_Gradient[Layer_1] = (Density[Layer_1]-Density[Layer_2])/Element_Height
Density_Gradient[Layer_2] = (Density[Layer_2]-Density[Layer_3])/Element_Height
Density_Gradient[Layer_3] = (Density[Layer_3]-Density[Layer_4])/Element_Height
Density_Gradient[Layer_4] = (Density[Layer_4]-Density[Layer_5])/Element_Height
Density_Gradient[Layer_5] = (Density[Layer_5]-Density[Layer_6])/Element_Height
Density_Gradient[Layer_6] = (Density[Layer_6]-Density[Layer_7])/Element_Height
Density_Gradient[Layer_7] = (Density[Layer_7]-Density[Layer_8])/Element_Height
Density_Gradient[Layer_8] = (Density[Layer_8]-Density[Layer_9])/Element_Height
Density_Gradient[Layer_9] = (Density[Layer_9]-Density[Layer_10])/Element_Height
Density_Gradient[Layer_10] = (Density[Layer_10]-Density[Layer_9])/Element_Height
Density_Gradient[Layer_11] = (Density[Layer_11]-Density[Layer_12])/Element_Height
Density_Gradient[Layer_12] = (Density[Layer_12]-Density[Layer_13])/Element_Height
Density_Gradient[Layer_13] = (Density[Layer_13]-Density[Layer_14])/Element_Height
Density_Gradient[Layer_14] = (Density[Layer_14]-Density[Layer_15])/Element_Height
Density_Gradient[Layer_15] = (Density[Layer_15]-Density[Layer_16])/Element_Height
Density_Gradient[Layer_16] = (Density[Layer_16]-Density[Layer_17])/Element_Height
Density_Gradient[Layer_17] = (Density[Layer_17]-Density[Layer_18])/Element_Height
Density_Gradient[Layer_18] = (Density[Layer_18]-Density[Layer_18])/Element_Height
Diffusion[Volume_Elements] =
(Density[Volume_Elements]*Heat_Capacity[Volume_Elements]*Idealised_SA*K_diff[Volume_Elements]
*Temp_Gradient[Volume_Elements])*60*60
Drift_v[Volume_Elements] = 30*Frictional_v[Volume_Elements]
Frictional_v[Volume_Elements] = SQRT(Shear_Stress[Volume_Elements]/Density[Volume_Elements])
g = 9.81
Idealised_SA = 1
k = if(Wind_Speed[Ten_metres]<1) then 100000000 else
6.6*sqrt(sin(Latitude)*pi/180)/(Wind_Speed[Ten_metres]^1.84)
k_constant = 1E-4
K_diff[Volume_Elements] = IF(Density_Gradient[Volume_Elements]>0) THEN K_max ELSE
(K_neutral[Volume_Elements]*(1+sigma*Richardson_No[Volume_Elements])^-1)+Molecular_Diff_Coeff
K_max = 0.6/60/60
K_neutral[Volume_Elements] = IF(Wind_Speed[Ten_metres]<1) THEN 0 ELSE
frictional_v[Volume_Elements]^2/(Drift_v[Volume_Elements]*k)*EXP(-k*Depth[Volume_Elements])
Molecular_Diff_Coeff = 1.2e-7
Resistance_Coeff = 1.0E-3
Richardson_No[Volume_Elements] = IF(Frictional_v[Volume_Elements]=0) THEN 0 ELSE (-
1/Density[Volume_Elements]*Density_Gradient[Volume_Elements]*g*Depth[Volume_Elements]^2/Fricti
onal_v[Volume_Elements]^2)
Shear_Stress[Volume_Elements] =
Air_Density*Resistance_Coeff*(Wind_Speed[Ten_metres]*Area_function)^2
sigma = 0.1
Temp_Gradient[Layer_1] = ((TEMPERATURE_W[Layer_1]+273)-
(TEMPERATURE_W[Layer_2]+273))/Element_Height+Temperature_C-Temperature_C
Temp_Gradient[Layer_2] = ((TEMPERATURE_W[Layer_2]+273)-
(TEMPERATURE_W[Layer_3]+273))/Element_Height+Temperature_C-Temperature_C
Temp_Gradient[Layer_3] = ((TEMPERATURE_W[Layer_3]+273)-
(TEMPERATURE_W[Layer_4]+273))/Element_Height+Temperature_C-Temperature_C
Temp_Gradient[Layer_4] = ((TEMPERATURE_W[Layer_4]+273)-
(TEMPERATURE_W[Layer_5]+273))/Element_Height+Temperature_C-Temperature_C
Temp_Gradient[Layer_5] = ((TEMPERATURE_W[Layer_5]+273)-
(TEMPERATURE_W[Layer_6]+273))/Element_Height+Temperature_C-Temperature_C
Temp_Gradient[Layer_6] = ((TEMPERATURE_W[Layer_6]+273)-
(TEMPERATURE_W[Layer_7]+273))/Element_Height+Temperature_C-Temperature_C
Temp_Gradient[Layer_7] = ((TEMPERATURE_W[Layer_7]+273)-
(TEMPERATURE_W[Layer_8]+273))/Element_Height+Temperature_C-Temperature_C
```

```
Temp_Gradient[Layer_8] = (TEMPERATURE_W[Layer_8]-
TEMPERATURE_W[Layer_9])/Element_Height+Temperature_C-Temperature_C
Temp_Gradient[Layer_9] = (TEMPERATURE_W[Layer_9]-
TEMPERATURE_W[Layer_10])/Element_Height+Temperature_C-Temperature_C
Temp_Gradient[Layer_10] = (TEMPERATURE_W[Layer_10]-
TEMPERATURE_W[Layer_11])/Element_Height+Temperature_C-Temperature_C
Temp_Gradient[Layer_11] = (TEMPERATURE_W[Layer_11]-
TEMPERATURE_W[Layer_12])/Element_Height+Temperature_C-Temperature_C
Temp_Gradient[Layer_12] = (TEMPERATURE_W[Layer_12]-
TEMPERATURE_W[Layer_13])/Element_Height+Temperature_C-Temperature_C
Temp_Gradient[Layer_13] = (TEMPERATURE_W[Layer_13]-
TEMPERATURE_W[Layer_14])/Element_Height+Temperature_C-Temperature_C
Temp_Gradient[Layer_14] = (TEMPERATURE_W[Layer_14]-
TEMPERATURE_W[Layer_15])/Element_Height+Temperature_C-Temperature_C
Temp_Gradient[Layer_15] = (TEMPERATURE_W[Layer_15]-
TEMPERATURE_W[Layer_16])/Element_Height+Temperature_C-Temperature_C
Temp_Gradient[Layer_16] = (TEMPERATURE_W[Layer_16]-
TEMPERATURE_W[Layer_17])/Element_Height+Temperature_C-Temperature_C
Temp_Gradient[Layer_17] = (TEMPERATURE_W[Layer_17]-
TEMPERATURE_W[Layer_18])/Element_Height+Temperature_C-Temperature_C
Temp_Gradient[Layer_18] = (TEMPERATURE_W[Layer_18]-Temperature_C)/Element_Height
Conduction_C = k_C*Temp_Gradient_C
delta_z_C = Element_Height/2+Thickness_C/2
k_C = 6.85
Temp_Gradient_C = (TEMPERATURE_W[Layer_18]-Temperature_C)/delta_z_C
Thickness_C = 0.2
a_coeff = 0.409+0.5016*SIN((h_sunset-60)*PI/180)
b_coeff = 0.6609-0.4767*SIN((h_sunset-60)*PI/180)
Hourly_Global_Exposure = if (Radiation_Ratio>0) then Radiation_Ratio*Daily_Global_Exposure else 0
Radiation_Ratio = PI/24*(a_coeff+b_coeff*COS(h*PI/180))*(COS(h*PI/180)-
COS(h_sunset*PI/180))/(SIN(h_sunset*PI/180)-(2*PI*h_sunset/360)*COS(h_sunset*PI/180))
Solar_Irradiance = Hourly_Global_Exposure*1000
Daily_Global_Exposure = GRAPH(TIME)
(888, 31.2), (912, 28.0), (936, 30.4), (960, 12.7), (984, 27.5), (1008, 27.1), (1032, 30.2), (1056, 30.1),
(1080, 29.9), (1104, 29.7), (1128, 27.3), (1152, 28.2), (1176, 11.2), (1200, 7.04), (1224, 7.13), (1248,
19.3), (1272, 25.4), (1296, 28.4), (1320, 27.7), (1344, 21.2), (1368, 25.6), (1392, 16.6), (1416, 21.6),
(1440, 26.6), (1464, 26.9), (1488, 10.3), (1512, 10.3)
C =
180/PI*ARCTAN(((0.3978*SIN(Sun's_mean_longitude+(0.03342*SIN(Sun's_mean_longitude+1.345)))*
SIN(Latitude*PI/180)+0.0145)/(COS(Latitude*PI/180)*SQRT(1-
(0.3978*SIN(Sun's_mean_longitude+(0.03342*SIN(Sun's_mean_longitude+1.345))))^2)))/SQRT(1-
((0.3978*SIN(Sun's_mean_longitude+(0.03342*SIN(Sun's_mean_longitude+1.345)))*SIN(Latitude*PI/18
0)+0.0145)/(COS(Latitude*PI/180)*SQRT(1-
(0.3978*SIN(Sun's_mean_longitude+(0.03342*SIN(Sun's_mean_longitude+1.345))))^2)))^2))
Declination = 23.45*SIN(360/365*(284+n)*PI/180)
Declination' = 23.45*SIN(360/365*(284+n-1)*PI/180)
Equn_of_time =
180/PI*(ARCTAN(TAN(Sun's_mean_longitude+(0.03342*SIN(Sun's_mean_longitude+1.345))))-
ARCTAN(0.9175*TAN(Sun's_mean_longitude+(0.03342*SIN(Sun's_mean_longitude+1.345))))-
(0.03342*SIN(Sun's_mean_longitude+1.345)))
h = -1/4*(12-Solar_Time)*60
h_sunset = IF(ARCTAN(SQRT(1-(-TAN(Latitude*PI/180)*TAN(Declination*PI/180))^2)/(-
TAN(Latitude*PI/180)*TAN(Declination*PI/180)))*180/PI>0) THEN (ARCTAN(SQRT(1-(-
TAN(Latitude*PI/180)*TAN(Declination*PI/180))^2)/(-
TAN(Latitude*PI/180)*TAN(Declination*PI/180)))*180/PI) ELSE (ARCTAN(SQRT(1-(-
TAN(Latitude*PI/180)*TAN(Declination*PI/180))^2)/(-
TAN(Latitude*PI/180)*TAN(Declination*PI/180)))*180/PI+180)
Latitude = -34.96
Longitude = 138.53
n = INT(TIME/24)
RA_1 = ARCTAN((TAN(Declination*PI/180)/TAN(23.45*PI/180))/SQRT(1-
(TAN(Declination*PI/180)/TAN(23.45*PI/180))^2))*180/PI/15
RA_2 = 180/15-RA_1
Right_Ascension = IF((Declination-Declination')>0) THEN (IF(Declination>0) THEN RA_1 ELSE
(RA_1+24)) ELSE RA_2
Solar_Altitude_Angle =
IF(ARCTAN((SIN(Latitude*PI/180)*SIN(Declination*PI/180)+COS(Latitude*PI/180)*COS(Declination*PI/
```

180)*COS(h*PI/180))/SQRT(1-
(SIN(Latitude*PI/180)*SIN(Declination*PI/180)+COS(Latitude*PI/180)*COS(Declination*PI/180)*COS(h*
PI/180))^2))*180/PI)>0 THEN
(ARCTAN((SIN(Latitude*PI/180)*SIN(Declination*PI/180)+COS(Latitude*PI/180)*COS(Declination*PI/18
0)*COS(h*PI/180))/SQRT(1-
(SIN(Latitude*PI/180)*SIN(Declination*PI/180)+COS(Latitude*PI/180)*COS(Declination*PI/180)*COS(h*
PI/180))^2))*180/PI) ELSE 0
Solar_Time = TIME-24*INT(TIME/24)+((4*(((180-Time_zone_Longitude)+180)-((180-
Longitude)+180)))+4*Equn_of_time)/60
Sun's_mean_longitude = 4.8771+0.0172*(n+0.5-Longitude/360)
Sunrise = 6-Time_zone-(Longitude+Equn_of_time+C)/15
Sunset = 18-Time_zone-(Longitude+Equn_of_time-C)/15
Time_zone = -9.5
Time_zone_Longitude = 142.5
Adj_Wind_Speed_@_h_from_150[Two_metres] = IF(Wind_Direction=360)THEN
Wind_Speed_@_h[Two_metres]*(1+dW[360,Two_metres])ELSE IF(Wind_Direction=350)THEN
Wind_Speed_@_h[Two_metres]*(1+dW[350,Two_metres])ELSE IF(Wind_Direction=340)THEN
Wind_Speed_@_h[Two_metres]*(1+dW[340,Two_metres])ELSE IF(Wind_Direction=330)THEN
Wind_Speed_@_h[Two_metres]*(1+dW[330,Two_metres])ELSE IF(Wind_Direction=320)THEN
Wind_Speed_@_h[Two_metres]*(1+dW[320,Two_metres])ELSE IF(Wind_Direction=310)THEN
Wind_Speed_@_h[Two_metres]*(1+dW[310,Two_metres])ELSE IF(Wind_Direction=300)THEN
Wind_Speed_@_h[Two_metres]*(1+dW[300,Two_metres])ELSE IF(Wind_Direction=290)THEN
Wind_Speed_@_h[Two_metres]*(1+dW[290,Two_metres])ELSE IF(Wind_Direction=280)THEN
Wind_Speed_@_h[Two_metres]*(1+dW[280,Two_metres])ELSE IF(Wind_Direction=270)THEN
Wind_Speed_@_h[Two_metres]*(1+dW[270,Two_metres])ELSE IF(Wind_Direction=260)THEN
Wind_Speed_@_h[Two_metres]*(1+dW[260,Two_metres])ELSE IF(Wind_Direction=250)THEN
Wind_Speed_@_h[Two_metres]*(1+dW[250,Two_metres])ELSE IF(Wind_Direction=240)THEN
Wind_Speed_@_h[Two_metres]*(1+dW[240,Two_metres])ELSE IF(Wind_Direction=230)THEN
Wind_Speed_@_h[Two_metres]*(1+dW[230,Two_metres])ELSE IF(Wind_Direction=220)THEN
Wind_Speed_@_h[Two_metres]*(1+dW[220,Two_metres])ELSE IF(Wind_Direction=210)THEN
Wind_Speed_@_h[Two_metres]*(1+dW[210,Two_metres])ELSE IF(Wind_Direction=200)THEN
Wind_Speed_@_h[Two_metres]*(1+dW[200,Two_metres])ELSE IF(Wind_Direction=190)THEN
Wind_Speed_@_h[Two_metres]*(1+dW[190,Two_metres])ELSE IF(Wind_Direction=180)THEN
Wind_Speed_@_h[Two_metres]*(1+dW[180,Two_metres])ELSE IF(Wind_Direction=170)THEN
Wind_Speed_@_h[Two_metres]*(1+dW[170,Two_metres])ELSE IF(Wind_Direction=160)THEN
Wind_Speed_@_h[Two_metres]*(1+dW[160,Two_metres])ELSE IF(Wind_Direction=150)THEN
Wind_Speed_@_h[Two_metres]*(1+dW[150,Two_metres])ELSE
Adj_Wind_Speed_@_h_to_150[Two_metres]
Adj_Wind_Speed_@_h_from_150[Ten_metres] = IF(Wind_Direction=360)THEN
Wind_Speed_@_h[Ten_metres]*(1+dW[360,Ten_metres])ELSE IF(Wind_Direction=350)THEN
Wind_Speed_@_h[Ten_metres]*(1+dW[350,Ten_metres])ELSE IF(Wind_Direction=340)THEN
Wind_Speed_@_h[Ten_metres]*(1+dW[340,Ten_metres])ELSE IF(Wind_Direction=330)THEN
Wind_Speed_@_h[Ten_metres]*(1+dW[330,Ten_metres])ELSE IF(Wind_Direction=320)THEN
Wind_Speed_@_h[Ten_metres]*(1+dW[320,Ten_metres])ELSE IF(Wind_Direction=310)THEN
Wind_Speed_@_h[Ten_metres]*(1+dW[310,Ten_metres])ELSE IF(Wind_Direction=300)THEN
Wind_Speed_@_h[Ten_metres]*(1+dW[300,Ten_metres])ELSE IF(Wind_Direction=290)THEN
Wind_Speed_@_h[Ten_metres]*(1+dW[290,Ten_metres])ELSE IF(Wind_Direction=280)THEN
Wind_Speed_@_h[Ten_metres]*(1+dW[280,Ten_metres])ELSE IF(Wind_Direction=270)THEN
Wind_Speed_@_h[Ten_metres]*(1+dW[270,Ten_metres])ELSE IF(Wind_Direction=260)THEN
Wind_Speed_@_h[Ten_metres]*(1+dW[260,Ten_metres])ELSE IF(Wind_Direction=250)THEN
Wind_Speed_@_h[Ten_metres]*(1+dW[250,Ten_metres])ELSE IF(Wind_Direction=240)THEN
Wind_Speed_@_h[Ten_metres]*(1+dW[240,Ten_metres])ELSE IF(Wind_Direction=230)THEN
Wind_Speed_@_h[Ten_metres]*(1+dW[230,Ten_metres])ELSE IF(Wind_Direction=220)THEN
Wind_Speed_@_h[Ten_metres]*(1+dW[220,Ten_metres])ELSE IF(Wind_Direction=210)THEN
Wind_Speed_@_h[Ten_metres]*(1+dW[210,Ten_metres])ELSE IF(Wind_Direction=200)THEN
Wind_Speed_@_h[Ten_metres]*(1+dW[200,Ten_metres])ELSE IF(Wind_Direction=190)THEN
Wind_Speed_@_h[Ten_metres]*(1+dW[190,Ten_metres])ELSE IF(Wind_Direction=180)THEN
Wind_Speed_@_h[Ten_metres]*(1+dW[180,Ten_metres])ELSE IF(Wind_Direction=170)THEN
Wind_Speed_@_h[Ten_metres]*(1+dW[170,Ten_metres])ELSE IF(Wind_Direction=160)THEN
Wind_Speed_@_h[Ten_metres]*(1+dW[160,Ten_metres])ELSE IF(Wind_Direction=150)THEN
Wind_Speed_@_h[Ten_metres]*(1+dW[150,Ten_metres])ELSE
Adj_Wind_Speed_@_h_to_150[Ten_metres]
Adj_Wind_Speed_@_h_to_150[Two_metres] = IF(Wind_Direction=140)THEN
Wind_Speed_@_h[Two_metres]*(1+dW[140,Two_metres])ELSE IF(Wind_Direction=130)THEN
Wind_Speed_@_h[Two_metres]*(1+dW[130,Two_metres])ELSE IF(Wind_Direction=120)THEN
Wind_Speed_@_h[Two_metres]*(1+dW[120,Two_metres])ELSE IF(Wind_Direction=110)THEN
Wind_Speed_@_h[Two_metres]*(1+dW[110,Two_metres])ELSE IF(Wind_Direction=100)THEN

Wind_Speed_@_h[Two_metres]*(1+dW[100,Two_metres])ELSE IF(Wind_Direction=90)THEN
Wind_Speed_@_h[Two_metres]*(1+dW[90,Two_metres])ELSE IF(Wind_Direction=80)THEN
Wind_Speed_@_h[Two_metres]*(1+dW[80,Two_metres])ELSE IF(Wind_Direction=70)THEN
Wind_Speed_@_h[Two_metres]*(1+dW[70,Two_metres])ELSE IF(Wind_Direction=60)THEN
Wind_Speed_@_h[Two_metres]*(1+dW[60,Two_metres])ELSE IF(Wind_Direction=50)THEN
Wind_Speed_@_h[Two_metres]*(1+dW[50,Two_metres])ELSE IF(Wind_Direction=40)THEN
Wind_Speed_@_h[Two_metres]*(1+dW[40,Two_metres])ELSE IF(Wind_Direction=30)THEN
Wind_Speed_@_h[Two_metres]*(1+dW[30,Two_metres])ELSE IF(Wind_Direction=20)THEN
Wind_Speed_@_h[Two_metres]*(1+dW[20,Two_metres])ELSE IF(Wind_Direction=10)THEN
Wind_Speed_@_h[Two_metres]*(1+dW[10,Two_metres])ELSE Wind_Speed_@_h[Two_metres]
Adj_Wind_Speed_@_h_to_150[Ten_metres] = IF(Wind_Direction=140)THEN
Wind_Speed_@_h[Ten_metres]*(1+dW[140,Ten_metres])ELSE IF(Wind_Direction=130)THEN
Wind_Speed_@_h[Ten_metres]*(1+dW[130,Ten_metres])ELSE IF(Wind_Direction=120)THEN
Wind_Speed_@_h[Ten_metres]*(1+dW[120,Ten_metres])ELSE IF(Wind_Direction=110)THEN
Wind_Speed_@_h[Ten_metres]*(1+dW[110,Ten_metres])ELSE IF(Wind_Direction=100)THEN
Wind_Speed_@_h[Ten_metres]*(1+dW[100,Ten_metres])ELSE IF(Wind_Direction=90)THEN
Wind_Speed_@_h[Ten_metres]*(1+dW[90,Ten_metres])ELSE IF(Wind_Direction=80)THEN
Wind_Speed_@_h[Ten_metres]*(1+dW[80,Ten_metres])ELSE IF(Wind_Direction=70)THEN
Wind_Speed_@_h[Ten_metres]*(1+dW[70,Ten_metres])ELSE IF(Wind_Direction=60)THEN
Wind_Speed_@_h[Ten_metres]*(1+dW[60,Ten_metres])ELSE IF(Wind_Direction=50)THEN
Wind_Speed_@_h[Ten_metres]*(1+dW[50,Ten_metres])ELSE IF(Wind_Direction=40)THEN
Wind_Speed_@_h[Ten_metres]*(1+dW[40,Ten_metres])ELSE IF(Wind_Direction=30)THEN
Wind_Speed_@_h[Ten_metres]*(1+dW[30,Ten_metres])ELSE IF(Wind_Direction=20)THEN
Wind_Speed_@_h[Ten_metres]*(1+dW[20,Ten_metres])ELSE IF(Wind_Direction=10)THEN
Wind_Speed_@_h[Ten_metres]*(1+dW[10,Ten_metres])ELSE Wind_Speed_@_h[Ten_metres]
Anemometer_height = 10
dW[360,Two_metres] = -0.26387
dW[360,Ten_metres] = -0.00007
dW[10,Two_metres] = -0.28559
dW[10,Ten_metres] = -0.00015
dW[20,Two_metres] = -0.31420
dW[20,Ten_metres] = -0.00039
dW[30,Two_metres] = -0.34499
dW[30,Ten_metres] = -0.00126
dW[40,Two_metres] = -0.36645
dW[40,Ten_metres] = -0.00467
dW[50,Two_metres] = -0.35382
dW[50,Ten_metres] = -0.01788
dW[60,Two_metres] = -0.25939
dW[60,Ten_metres] = -0.05699
dW[70,Two_metres] = -0.00540
dW[70,Ten_metres] = -0.00528
dW[80,Two_metres] = -0.05124
dW[80,Ten_metres] = -0.04127
dW[90,Two_metres] = 0.24896
dW[90,Ten_metres] = -0.04995
dW[100,Two_metres] = 0.22417
dW[100,Ten_metres] = -0.06193
dW[110,Two_metres] = 0.15208
dW[110,Ten_metres] = -0.06859
dW[120,Two_metres] = .05824
dW[120,Ten_metres] = -0.07188
dW[130,Two_metres] = -.00929
dW[130,Ten_metres] = -.07321
dW[140,Two_metres] = -.05831
dW[140,Ten_metres] = -.07356
dW[150,Two_metres] = -.09242
dW[150,Ten_metres] = -.07355
dW[160,Two_metres] = -.11348
dW[160,Ten_metres] = -.07351
dW[170,Two_metres] = -.12252
dW[170,Ten_metres] = -.07355
dW[180,Two_metres] = -.12001
dW[180,Ten_metres] = -.07356
dW[190,Two_metres] = -.11523
dW[190,Ten_metres] = -.07355
dW[200,Two_metres] = -.13690

dW[200,Ten_metres] = -.07185
dW[210,Two_metres] = -.15906
dW[210,Ten_metres] = -.06811
dW[220,Two_metres] = -.23177
dW[220,Ten_metres] = -.06475
dW[230,Two_metres] = -.23747
dW[230,Ten_metres] = -.06332
dW[240,Two_metres] = -.22579
dW[240,Ten_metres] = -.06616
dW[250,Two_metres] = -.00588
dW[250,Ten_metres] = -.00574
dW[260,Two_metres] = -.25939
dW[260,Ten_metres] = -.05699
dW[270,Two_metres] = -.35382
dW[270,Ten_metres] = -.01788
dW[280,Two_metres] = -.36645
dW[280,Ten_metres] = -.00467
dW[290,Two_metres] = -.34499
dW[290,Ten_metres] = -.00126
dW[300,Two_metres] = -.31420
dW[300,Ten_metres] = -.00039
dW[310,Two_metres] = -.28559
dW[310,Ten_metres] = -.00015
dW[320,Two_metres] = -.26387
dW[320,Ten_metres] = -.00007
dW[330,Two_metres] = -.25780
dW[330,Ten_metres] = -.05749
dW[340,Two_metres] = -.26027
dW[340,Ten_metres] = -.05671
dW[350,Two_metres] = -.25062
dW[350,Ten_metres] = -.00005
Wind_Speed[Two_metres] = IF(Wind_Direction<150) THEN
Adj_Wind_Speed_@_h_to_150[Two_metres] ELSE Adj_Wind_Speed_@_h_from_150[Two_metres]
Wind_Speed[Ten_metres] = IF(Wind_Direction<150) THEN
Adj_Wind_Speed_@_h_to_150[Ten_metres] ELSE Adj_Wind_Speed_@_h_from_150[Ten_metres]
Wind_Speed_@_h[Two_metres] = Wind_Speed_Data*LOGN(2/z0)/LOGN(Anemometer_height/z0)
Wind_Speed_@_h[Ten_metres] = Wind_Speed_Data*LOGN(10/z0)/LOGN(Anemometer_height/z0)
z0 = 0.2
Wind_Direction = GRAPH(TIME)
(888, 360), (888, 20.0), (889, 330), (889, 340), (890, 340), (890, 250), (891, 0.00), (891, 350), (892, 100), (892, 20.0), (893, 40.0), (893, 30.0), (893, 30.0), (894, 240), (894, 230), (895, 210), (895, 170), (896, 80.0), (896, 20.0), (897, 10.0), (897, 310), (898, 310), (898, 320), (899, 320), (899, 220), (899, 190), (900, 180), (900, 200), (901, 180), (901, 190), (902, 170), (902, 150), (903, 120), (903, 230), (904, 190), (904, 170), (904, 210), (905, 220), (905, 170), (906, 170), (906, 180), (907, 240), (907, 200), (908, 180), (908, 240), (909, 190), (909, 130), (910, 110), (910, 200), (910, 320), (911, 0.00), (911, 360), (912, 40.0), (912, 30.0), (913, 20.0), (913, 40.0), (914, 20.0), (914, 20.0), (915, 30.0), (915, 30.0), (915, 20.0), (916, 300), (916, 280), (917, 290), (917, 290), (918, 320), (918, 350), (919, 360), (919, 30.0), (920, 20.0), (920, 20.0), (920, 360), (921, 100), (921, 230), (922, 270), (922, 250), (923, 280), (923, 280), (924, 290), (924, 80.0), (925, 50.0), (925, 160), (926, 50.0), (926, 270), (926, 260), (927, 250), (927, 240), (928, 250), (928, 270), (929, 230), (929, 210), (930, 210), (930, 200), (931, 200), (931, 220), (931, 220), (932, 220), (932, 210), (933, 170), (933, 160), (934, 190), (934, 190), (935, 170), (935, 190), (936, 190), (936, 180), (936, 180), (937, 180), (937, 180), (938, 190), (938, 190), (939, 200), (939, 180), (940, 170), (940, 180), (941, 180), (941, 180), (942, 180), (942, 160), (942, 180), (943, 190), (943, 180), (944, 200), (944, 220), (945, 210), (945, 220), (946, 220), (946, 220), (947, 210), (947, 200), (947, 210), (948, 210), (948, 200), (949, 170), (949, 160), (950, 160), (950, 180), (951, 180), (951, 180), (952, 180), (952, 170), (953, 180), (953, 180), (953, 180), (954, 180), (954, 170), (955, 180), (955, 190), (956, 160), (956, 170), (957, 190), (957, 170), (958, 180), (958, 160), (958, 180), (959, 150), (959, 140), (960, 190), (960, 180), (961, 180), (961, 140), (962, 170), (962, 180), (963, 170), (963, 200), (963, 210), (964, 220), (964, 220), (965, 240), (965, 240), (966, 240), (966, 240), (967, 230), (967, 230), (968, 230), (968, 230), (969, 220), (969, 220), (969, 220), (970, 220), (970, 220), (971, 210), (971, 210), (972, 210), (972, 210), (973, 210), (973, 210), (974, 210), (974, 170), (974, 150), (975, 160), (975, 150), (976, 150), (976, 140), (977, 140), (977, 120), (978, 180), (978, 230), (979, 230), (979, 220), (979, 230), (980, 230), (980, 230), (981, 220), (981, 230), (982, 230), (982, 220), (983, 220), (983, 220), (984, 230), (984, 230), (985, 220), (985, 230), (985, 220), (986, 220), (986, 220), (987, 210), (987, 200), (988, 210), (988, 180), (989, 210), (989, 220), (990, 210), (990, 210), (990, 210), (991, 210), (991, 210), (992, 200), (992, 200), (993, 190), (993, 170), (994, 190), (994, 180), (995, 180), (995, 160), (996, 190), (996, 180), (996, 180), (997, 180), (997, 180), (998, 190), (998, 170), (999, 170), (999, 190), (1000, 180), (1000, 180), (1001, 170), (1001, 180),

(1001, 180), (1002, 170), (1002, 170), (1003, 180), (1003, 170), (1004, 160), (1004, 150), (1005, 150), (1005, 160), (1006, 150), (1006, 180), (1006, 150), (1007, 160), (1007, 140), (1008, 140), (1008, 140), (1009, 130), (1009, 110), (1010, 130), (1010, 80.0), (1011, 200), (1011, 250), (1012, 170), (1012, 160), (1012, 170), (1013, 160), (1013, 160), (1014, 150), (1014, 160), (1015, 150), (1015, 160), (1016, 150), (1016, 150), (1017, 160), (1017, 160), (1017, 150), (1018, 150), (1018, 150), (1019, 150), (1019, 150), (1020, 140), (1020, 130), (1021, 130), (1021, 120), (1022, 120), (1022, 120), (1022, 110), (1023, 100), (1023, 100), (1024, 100), (1024, 110), (1025, 110), (1025, 110), (1026, 110), (1026, 360), (1027, 300), (1027, 300), (1028, 300), (1028, 280), (1028, 290), (1029, 320), (1029, 260), (1030, 250), (1030, 240), (1031, 240), (1031, 240), (1032, 230), (1032, 230), (1033, 220), (1033, 220), (1033, 230), (1034, 210), (1034, 220), (1035, 220), (1035, 220), (1036, 220), (1036, 220), (1037, 220), (1037, 210), (1038, 210), (1038, 210), (1039, 160), (1039, 140), (1039, 130), (1040, 130), (1040, 140), (1041, 120), (1041, 110), (1042, 110), (1042, 110), (1043, 110), (1043, 110), (1044, 110), (1044, 120), (1044, 110), (1045, 30.0), (1045, 340), (1046, 90.0), (1046, 90.0), (1047, 0.00), (1047, 0.00), (1048, 300), (1048, 300), (1049, 300), (1049, 270), (1049, 80.0), (1050, 50.0), (1050, 30.0), (1051, 40.0), (1051, 350), (1052, 320), (1052, 20.0), (1053, 40.0), (1053, 20.0), (1054, 10.0), (1054, 260), (1055, 240), (1055, 240), (1055, 230), (1056, 240), (1056, 240), (1057, 220), (1057, 210), (1058, 230), (1058, 220), (1059, 150), (1059, 220), (1060, 220), (1060, 210), (1060, 190), (1061, 200), (1061, 170), (1062, 140), (1062, 100), (1063, 120), (1063, 100), (1064, 50.0), (1064, 30.0), (1065, 40.0), (1065, 40.0), (1065, 40.0), (1066, 40.0), (1066, 40.0), (1067, 30.0), (1067, 30.0), (1068, 40.0), (1068, 30.0), (1069, 30.0), (1069, 30.0), (1070, 40.0), (1070, 40.0), (1071, 40.0), (1071, 50.0), (1071, 40.0), (1072, 40.0), (1072, 30.0), (1073, 20.0), (1073, 10.0), (1074, 360), (1074, 350), (1075, 340), (1075, 350), (1076, 330), (1076, 330), (1076, 320), (1077, 320), (1077, 330), (1078, 330), (1078, 330), (1079, 330), (1079, 340), (1080, 340), (1080, 340), (1081, 350), (1081, 350), (1082, 340), (1082, 350), (1082, 310), (1083, 340), (1083, 330), (1084, 250), (1084, 200), (1085, 200), (1085, 280), (1086, 210), (1086, 200), (1087, 190), (1087, 200), (1087, 210), (1088, 230), (1088, 240), (1089, 240), (1089, 240), (1090, 230), (1090, 240), (1091, 230), (1091, 230), (1092, 240), (1092, 240), (1092, 240), (1093, 240), (1093, 240), (1094, 240), (1094, 240), (1095, 240), (1095, 260), (1096, 280), (1096, 260), (1097, 240), (1097, 230), (1098, 240), (1098, 240), (1098, 230), (1099, 220), (1099, 230), (1100, 230), (1100, 230), (1101, 230), (1101, 230), (1102, 220), (1102, 220), (1103, 220), (1103, 210), (1103, 220), (1104, 200), (1104, 210), (1105, 200), (1105, 200), (1106, 200), (1106, 200), (1107, 200), (1107, 180), (1108, 170), (1108, 160), (1108, 170), (1109, 170), (1109, 180), (1110, 170), (1110, 170), (1111, 180), (1111, 190), (1112, 180), (1112, 180), (1113, 180), (1113, 180), (1114, 170), (1114, 180), (1114, 190), (1115, 190), (1115, 170), (1116, 160), (1116, 170), (1117, 170), (1117, 170), (1118, 170), (1118, 150), (1119, 160), (1119, 170), (1119, 160), (1120, 180), (1120, 180), (1121, 160), (1121, 170), (1122, 160), (1122, 140), (1123, 160), (1123, 150), (1124, 170), (1124, 160), (1125, 210), (1125, 220), (1125, 170), (1126, 150), (1126, 160), (1127, 160), (1127, 170), (1128, 140), (1128, 160), (1129, 160), (1129, 160), (1130, 150), (1130, 140), (1130, 160), (1131, 160), (1131, 170), (1132, 170), (1132, 180), (1133, 180), (1133, 170), (1134, 180), (1134, 170), (1135, 170), (1135, 170), (1135, 170), (1136, 200), (1136, 180), (1137, 170), (1137, 150), (1138, 130), (1138, 100), (1139, 170), (1139, 150), (1140, 200), (1140, 170), (1141, 150), (1141, 150), (1141, 140), (1142, 200), (1142, 230), (1143, 240), (1143, 240), (1144, 230), (1144, 230), (1145, 230), (1145, 220), (1146, 180), (1146, 160), (1146, 170), (1147, 160), (1147, 180), (1148, 170), (1148, 160), (1149, 160), (1149, 170), (1150, 170), (1150, 160), (1151, 160), (1151, 150), (1151, 160), (1152, 160), (1152, 160), (1153, 170), (1153, 160), (1154, 180), (1154, 170), (1155, 170), (1155, 180), (1156, 190), (1156, 180), (1157, 180), (1157, 180), (1157, 170), (1158, 170), (1158, 170), (1159, 180), (1159, 180), (1160, 190), (1160, 200), (1161, 180), (1161, 160), (1162, 140), (1162, 130), (1162, 130), (1163, 130), (1163, 120), (1164, 100), (1164, 130), (1165, 130), (1165, 120), (1166, 110), (1166, 140), (1167, 140), (1167, 130), (1168, 150), (1168, 140), (1168, 150), (1169, 150), (1169, 160), (1170, 150), (1170, 160), (1171, 150), (1171, 160), (1172, 150), (1172, 140), (1173, 140), (1173, 150), (1173, 150), (1174, 140), (1174, 140), (1175, 130), (1175, 110), (1176, 120), (1176, 120), (1177, 130), (1177, 120), (1178, 110), (1178, 110), (1178, 100), (1179, 100), (1179, 100), (1180, 100), (1180, 80.0), (1181, 70.0), (1181, 80.0), (1182, 70.0), (1182, 70.0), (1183, 70.0), (1183, 70.0), (1184, 240), (1184, 220), (1184, 250), (1185, 240), (1185, 230), (1186, 250), (1186, 240), (1187, 240), (1187, 230), (1188, 240), (1188, 240), (1189, 230), (1189, 230), (1189, 230), (1190, 220), (1190, 210), (1191, 220), (1191, 220), (1192, 220), (1192, 220), (1193, 160), (1193, 140), (1194, 120), (1194, 120), (1194, 120), (1195, 120), (1195, 110), (1196, 110), (1196, 120), (1197, 120), (1197, 120), (1198, 110), (1198, 120), (1199, 110), (1199, 110), (1200, 120), (1200, 120), (1200, 80.0), (1201, 70.0), (1201, 120), (1202, 110), (1202, 100), (1203, 60.0), (1203, 310), (1204, 20.0), (1204, 20.0), (1205, 200), (1205, 280), (1205, 230), (1206, 360), (1206, 50.0), (1207, 30.0), (1207, 20.0), (1208, 40.0), (1208, 30.0), (1209, 30.0), (1209, 270), (1210, 270), (1210, 220), (1211, 230), (1211, 230), (1211, 240), (1212, 230), (1212, 220), (1213, 210), (1213, 210), (1214, 210), (1214, 210), (1215, 210), (1215, 160), (1216, 140), (1216, 140), (1216, 140), (1217, 150), (1217, 140), (1218, 140), (1218, 140), (1219, 130), (1219, 140), (1220, 130), (1220, 130), (1221, 120), (1221, 120), (1221, 100), (1222, 110), (1222, 130), (1223, 130), (1223, 130), (1224, 130), (1224, 140), (1225, 130), (1225, 130), (1226, 140), (1226, 140), (1227, 140), (1227, 120), (1227, 120), (1228, 110), (1228, 360), (1229, 290), (1229, 10.0), (1230, 250), (1230, 250), (1231, 220), (1231, 250), (1232, 240), (1232, 250), (1232, 270), (1233, 110), (1233, 120), (1234, 160), (1234, 170), (1235, 170), (1235, 140), (1236, 130), (1236, 120), (1237, 130), (1237, 170), (1237, 210), (1238, 210), (1238, 240), (1239, 230), (1239, 230), (1240, 210), (1240, 190), (1241, 140), (1241, 140), (1242, 140), (1242, 130), (1243, 130), (1243, 130), (1243, 130), (1244, 120), (1244,

130), (1245, 120), (1245, 120), (1246, 50.0), (1246, 100), (1247, 130), (1247, 150), (1248, 130), (1248, 140), (1248, 150), (1249, 140), (1249, 140), (1250, 130), (1250, 130), (1251, 140), (1251, 160), (1252, 110), (1252, 170), (1253, 130), (1253, 250), (1254, 20.0), (1254, 110), (1254, 130), (1255, 230), (1255, 230), (1256, 230), (1256, 160), (1257, 140), (1257, 160), (1258, 170), (1258, 160), (1259, 140), (1259, 140), (1259, 130), (1260, 140), (1260, 140), (1261, 140), (1261, 150), (1262, 140), (1262, 130), (1263, 140), (1263, 150), (1264, 170), (1264, 180), (1264, 170), (1265, 180), (1265, 160), (1266, 120), (1266, 120), (1267, 160), (1267, 140), (1268, 140), (1268, 140), (1269, 130), (1269, 120), (1270, 110), (1270, 100), (1270, 100), (1271, 100), (1271, 120), (1272, 130), (1272, 120), (1273, 110), (1273, 130), (1274, 100), (1274, 120), (1275, 100), (1275, 100), (1275, 80.0), (1276, 90.0), (1276, 110), (1277, 120), (1277, 100), (1278, 110), (1278, 150), (1279, 150), (1279, 160), (1280, 160), (1280, 140), (1280, 150), (1281, 150), (1281, 160), (1282, 160), (1282, 160), (1283, 160), (1283, 160), (1284, 150), (1284, 150), (1285, 140), (1285, 150), (1286, 160), (1286, 160), (1286, 150), (1287, 140), (1287, 130), (1288, 160), (1288, 110), (1289, 140), (1289, 130), (1290, 160), (1290, 140), (1291, 130), (1291, 110), (1291, 100), (1292, 130), (1292, 130), (1293, 100), (1293, 90.0), (1294, 140), (1294, 210), (1295, 300), (1295, 150), (1296, 90.0), (1296, 120), (1297, 130), (1297, 140), (1297, 90.0), (1298, 120), (1298, 120), (1299, 230), (1299, 220), (1300, 220), (1300, 220), (1301, 200), (1301, 80.0), (1302, 10.0), (1302, 130), (1302, 140), (1303, 130), (1303, 150), (1304, 130), (1304, 130), (1305, 140), (1305, 130), (1306, 150), (1306, 130), (1307, 140), (1307, 160), (1307, 130), (1308, 180), (1308, 190), (1309, 180), (1309, 170), (1310, 190), (1310, 170), (1311, 170), (1311, 140), (1312, 190), (1312, 190), (1313, 180), (1313, 170), (1313, 110), (1314, 160), (1314, 220), (1315, 200), (1315, 180), (1316, 170), (1316, 150), (1317, 140), (1317, 160), (1318, 170), (1318, 150), (1318, 170), (1319, 220), (1319, 220), (1320, 220), (1320, 220), (1321, 220), (1321, 220), (1322, 210), (1322, 210), (1323, 220), (1323, 220), (1323, 220), (1324, 210), (1324, 210), (1325, 210), (1325, 210), (1326, 210), (1326, 200), (1327, 190), (1327, 190), (1328, 190), (1328, 180), (1329, 160), (1329, 160), (1329, 170), (1330, 200), (1330, 200), (1331, 190), (1331, 200), (1332, 180), (1332, 180), (1333, 190), (1333, 190), (1334, 190), (1334, 190), (1334, 170), (1335, 180), (1335, 200), (1336, 190), (1336, 190), (1337, 190), (1337, 190), (1338, 180), (1338, 180), (1339, 180), (1339, 190), (1340, 200), (1340, 210), (1340, 210), (1341, 210), (1341, 210), (1342, 210), (1342, 210), (1343, 230), (1343, 210), (1344, 220), (1344, 210), (1345, 210), (1345, 220), (1345, 220), (1346, 210), (1346, 210), (1347, 210), (1347, 210), (1348, 180), (1348, 210), (1349, 180), (1349, 190), (1350, 180), (1350, 180), (1350, 200), (1351, 200), (1351, 180), (1352, 190), (1352, 200), (1353, 190), (1353, 180), (1354, 170), (1354, 170), (1355, 190), (1355, 180), (1356, 180), (1356, 190), (1356, 190), (1357, 180), (1357, 190), (1358, 170), (1358, 170), (1359, 180), (1359, 180), (1360, 160), (1360, 160), (1361, 170), (1361, 180), (1361, 160), (1362, 170), (1362, 180), (1363, 160), (1363, 150), (1364, 160), (1364, 160), (1365, 170), (1365, 160), (1366, 170), (1366, 170), (1366, 170), (1367, 160), (1367, 150), (1368, 170), (1368, 170), (1369, 160), (1369, 170), (1370, 160), (1370, 170), (1371, 150), (1371, 170), (1372, 170), (1372, 160), (1372, 170), (1373, 160), (1373, 160), (1374, 160), (1374, 170), (1375, 170), (1375, 170), (1376, 160), (1376, 160), (1377, 150), (1377, 170), (1377, 180), (1378, 180), (1378, 170), (1379, 160), (1379, 170), (1380, 180), (1380, 180), (1381, 160), (1381, 160), (1382, 170), (1382, 180), (1383, 180), (1383, 160), (1383, 170), (1384, 130), (1384, 130), (1385, 160), (1385, 140), (1386, 150), (1386, 130), (1387, 140), (1387, 170), (1388, 170), (1388, 150), (1388, 160), (1389, 150), (1389, 170), (1390, 160), (1390, 150), (1391, 150), (1391, 150), (1392, 160), (1392, 170), (1393, 160), (1393, 180), (1393, 170), (1394, 160), (1394, 160), (1395, 170), (1395, 170), (1396, 160), (1396, 160), (1397, 170), (1397, 180), (1398, 180), (1398, 160), (1399, 160), (1399, 160), (1399, 170), (1400, 160), (1400, 160), (1401, 170), (1401, 180), (1402, 150), (1402, 150), (1403, 160), (1403, 170), (1404, 180), (1404, 170), (1404, 170), (1405, 180), (1405, 180), (1406, 170), (1406, 170), (1407, 160), (1407, 180), (1408, 180), (1408, 160), (1409, 150), (1409, 150), (1409, 150), (1410, 150), (1410, 170), (1411, 190), (1411, 190), (1412, 150), (1412, 180), (1413, 170), (1413, 170), (1414, 150), (1414, 160), (1415, 160), (1415, 170), (1415, 160), (1416, 170), (1416, 170), (1417, 180), (1417, 180), (1418, 170), (1418, 180), (1419, 170), (1419, 170), (1420, 170), (1420, 170), (1420, 160), (1421, 160), (1421, 160), (1422, 160), (1422, 160), (1423, 160), (1423, 160), (1424, 150), (1424, 170), (1425, 200), (1425, 170), (1426, 160), (1426, 210), (1426, 200), (1427, 150), (1427, 150), (1428, 140), (1428, 140), (1429, 150), (1429, 150), (1430, 150), (1430, 140), (1431, 160), (1431, 160), (1431, 150), (1432, 150), (1432, 160), (1433, 160), (1433, 170), (1434, 160), (1434, 160), (1435, 160), (1435, 150), (1436, 170), (1436, 180), (1436, 160), (1437, 180), (1437, 160), (1438, 160), (1438, 160), (1439, 170), (1439, 160), (1440, 160), (1440, 160), (1441, 170), (1441, 160), (1442, 150), (1442, 170), (1442, 170), (1443, 160), (1443, 160), (1444, 150), (1444, 150), (1445, 160), (1445, 170), (1446, 160), (1446, 160), (1447, 150), (1447, 150), (1447, 170), (1448, 150), (1448, 150), (1449, 150), (1449, 140), (1450, 200), (1450, 150), (1451, 150), (1451, 120), (1452, 130), (1452, 140), (1452, 140), (1453, 130), (1453, 160), (1454, 140), (1454, 150), (1455, 160), (1455, 160), (1456, 170), (1456, 140), (1457, 150), (1457, 140), (1458, 150), (1458, 150), (1458, 170), (1459, 150), (1459, 160), (1460, 160), (1460, 170), (1461, 160), (1461, 150), (1462, 160), (1462, 160), (1463, 170), (1463, 160), (1463, 160), (1464, 160), (1464, 170), (1465, 160), (1465, 170), (1466, 210), (1466, 170), (1467, 170), (1467, 160), (1468, 140), (1468, 130), (1469, 120), (1469, 110), (1469, 120), (1470, 100), (1470, 100), (1471, 110), (1471, 120), (1472, 110), (1472, 90.0), (1473, 90.0), (1473, 0.00), (1474, 330), (1474, 320), (1474, 320), (1475, 270), (1475, 240), (1476, 240), (1476, 220), (1477, 260), (1477, 250), (1478, 230), (1478, 240), (1479, 240), (1479, 230), (1479, 220), (1480, 220), (1480, 220), (1481, 230), (1481, 220), (1482, 210), (1482, 220), (1483, 210), (1483, 210), (1484, 220), (1484, 220), (1485, 210), (1485, 210), (1485, 210), (1486, 190), (1486, 160), (1487, 140), (1487, 130), (1488, 150), (1488, 120), (1489, 110), (1489, 210), (1490,

290), (1490, 200), (1490, 160), (1491, 140), (1491, 120), (1492, 100), (1492, 100), (1493, 170), (1493, 150), (1494, 0.00), (1494, 50.0), (1495, 40.0), (1495, 70.0), (1495, 190), (1496, 160), (1496, 180), (1497, 250), (1497, 260), (1498, 220), (1498, 230), (1499, 260), (1499, 250), (1500, 240), (1500, 220), (1501, 220), (1501, 210), (1501, 220), (1502, 220), (1502, 220), (1503, 220), (1503, 170), (1504, 160), (1504, 160), (1505, 160), (1505, 150), (1506, 160), (1506, 170), (1506, 160), (1507, 170), (1507, 160), (1508, 170), (1508, 170), (1509, 170), (1509, 170), (1510, 160), (1510, 160), (1511, 160), (1511, 180), (1512, 170)

Wind_Speed_Data = GRAPH(TIME)

(888, 1.00), (888, 1.00), (889, 2.00), (889, 1.00), (890, 1.00), (890, 1.00), (891, 0.00), (891, 1.00), (892, 3.00), (892, 1.00), (893, 3.00), (893, 5.00), (893, 3.00), (894, 3.00), (894, 3.00), (895, 3.00), (895, 1.00), (896, 2.00), (896, 3.00), (897, 5.00), (897, 4.00), (898, 3.00), (898, 4.00), (899, 3.00), (899, 6.00), (899, 4.00), (900, 3.00), (900, 3.00), (901, 3.00), (901, 3.00), (902, 3.00), (902, 4.00), (903, 3.00), (903, 5.00), (904, 6.00), (904, 5.00), (904, 4.00), (905, 4.00), (905, 3.00), (906, 2.00), (906, 3.00), (907, 4.00), (907, 2.00), (908, 4.00), (908, 5.00), (909, 3.00), (909, 4.00), (910, 1.00), (910, 1.00), (910, 1.00), (911, 0.00), (911, 1.00), (912, 2.00), (912, 4.00), (913, 3.00), (913, 4.00), (914, 2.00), (914, 3.00), (915, 2.00), (915, 3.00), (915, 2.00), (916, 3.00), (916, 4.00), (917, 7.00), (917, 7.00), (918, 3.00), (918, 5.00), (919, 3.00), (919, 4.00), (920, 4.00), (920, 4.00), (920, 3.00), (921, 1.00), (921, 4.00), (922, 4.00), (922, 2.00), (923, 3.00), (923, 5.00), (924, 3.00), (924, 2.00), (925, 4.00), (925, 1.00), (926, 1.00), (926, 2.00), (926, 3.00), (927, 4.00), (927, 3.00), (928, 3.00), (928, 1.00), (929, 2.00), (929, 2.00), (930, 2.00), (930, 2.00), (931, 2.00), (931, 2.00), (931, 2.00), (932, 2.00), (932, 2.00), (933, 4.00), (933, 4.00), (934, 3.00), (934, 3.00), (935, 4.00), (935, 3.00), (936, 3.00), (936, 4.00), (936, 3.00), (937, 3.00), (937, 3.00), (938, 3.00), (938, 4.00), (939, 7.00), (939, 7.00), (940, 6.00), (940, 6.00), (941, 7.00), (941, 5.00), (942, 5.00), (942, 6.00), (942, 6.00), (943, 7.00), (943, 6.00), (944, 7.00), (944, 9.00), (945, 9.00), (945, 9.00), (946, 10.0), (946, 8.00), (947, 8.00), (947, 9.00), (947, 10.0), (948, 9.00), (948, 8.00), (949, 7.00), (949, 7.00), (950, 7.00), (950, 6.00), (951, 7.00), (951, 7.00), (952, 6.00), (952, 5.00), (953, 4.00), (953, 4.00), (953, 3.00), (954, 3.00), (954, 3.00), (955, 5.00), (955, 5.00), (956, 5.00), (956, 2.00), (957, 2.00), (957, 2.00), (958, 3.00), (958, 2.00), (958, 1.00), (959, 2.00), (959, 2.00), (960, 2.00), (960, 3.00), (961, 3.00), (961, 2.00), (962, 2.00), (962, 2.00), (963, 3.00), (963, 3.00), (963, 4.00), (964, 5.00), (964, 5.00), (965, 4.00), (965, 6.00), (966, 7.00), (966, 6.00), (967, 7.00), (967, 7.00), (968, 7.00), (968, 7.00), (969, 7.00), (969, 7.00), (969, 7.00), (970, 7.00), (970, 7.00), (971, 7.00), (971, 7.00), (972, 6.00), (972, 6.00), (973, 6.00), (973, 5.00), (974, 5.00), (974, 4.00), (974, 3.00), (975, 3.00), (975, 2.00), (976, 2.00), (976, 2.00), (977, 2.00), (977, 1.00), (978, 2.00), (978, 5.00), (979, 7.00), (979, 7.00), (979, 5.00), (980, 7.00), (980, 6.00), (981, 6.00), (981, 6.00), (982, 7.00), (982, 7.00), (983, 7.00), (983, 8.00), (984, 8.00), (984, 8.00), (985, 7.00), (985, 8.00), (985, 8.00), (986, 7.00), (986, 7.00), (987, 10.0), (987, 8.00), (988, 8.00), (988, 9.00), (989, 9.00), (989, 11.0), (990, 9.00), (990, 10.0), (990, 9.00), (991, 10.0), (991, 10.0), (992, 9.00), (992, 9.00), (993, 8.00), (993, 8.00), (994, 7.00), (994, 8.00), (995, 8.00), (995, 6.00), (996, 8.00), (996, 5.00), (996, 4.00), (997, 4.00), (997, 4.00), (998, 4.00), (998, 3.00), (999, 3.00), (999, 2.00), (1000, 2.00), (1000, 3.00), (1001, 2.00), (1001, 2.00), (1001, 2.00), (1002, 2.00), (1002, 2.00), (1003, 2.00), (1003, 3.00), (1004, 3.00), (1004, 2.00), (1005, 3.00), (1005, 3.00), (1006, 2.00), (1006, 2.00), (1006, 3.00), (1007, 4.00), (1007, 2.00), (1008, 2.00), (1008, 4.00), (1009, 5.00), (1009, 3.00), (1010, 3.00), (1010, 3.00), (1011, 3.00), (1011, 5.00), (1012, 7.00), (1012, 8.00), (1012, 8.00), (1013, 8.00), (1013, 7.00), (1014, 6.00), (1014, 6.00), (1015, 6.00), (1015, 5.00), (1016, 6.00), (1016, 7.00), (1017, 7.00), (1017, 8.00), (1017, 7.00), (1018, 8.00), (1018, 8.00), (1019, 7.00), (1019, 7.00), (1020, 6.00), (1020, 6.00), (1021, 4.00), (1021, 4.00), (1022, 4.00), (1022, 4.00), (1022, 3.00), (1023, 4.00), (1023, 4.00), (1024, 2.00), (1024, 4.00), (1025, 3.00), (1025, 3.00), (1026, 3.00), (1026, 1.00), (1027, 2.00), (1027, 2.00), (1028, 1.00), (1028, 2.00), (1028, 1.00), (1029, 1.00), (1029, 3.00), (1030, 4.00), (1030, 4.00), (1031, 4.00), (1031, 4.00), (1032, 4.00), (1032, 5.00), (1033, 5.00), (1033, 6.00), (1033, 6.00), (1034, 6.00), (1034, 5.00), (1035, 6.00), (1035, 6.00), (1036, 7.00), (1036, 7.00), (1037, 7.00), (1037, 8.00), (1038, 8.00), (1038, 6.00), (1039, 8.00), (1039, 6.00), (1039, 5.00), (1040, 3.00), (1040, 3.00), (1041, 3.00), (1041, 3.00), (1042, 4.00), (1042, 4.00), (1043, 4.00), (1043, 4.00), (1044, 5.00), (1044, 3.00), (1044, 3.00), (1045, 1.00), (1045, 2.00), (1046, 1.00), (1046, 1.00), (1047, 0.00), (1047, 0.00), (1048, 2.00), (1048, 1.00), (1049, 1.00), (1049, 1.00), (1049, 1.00), (1050, 4.00), (1050, 4.00), (1051, 3.00), (1051, 4.00), (1052, 2.00), (1052, 6.00), (1053, 5.00), (1053, 4.00), (1054, 4.00), (1054, 5.00), (1055, 5.00), (1055, 5.00), (1055, 5.00), (1056, 5.00), (1056, 5.00), (1057, 4.00), (1057, 3.00), (1058, 4.00), (1058, 4.00), (1059, 1.00), (1059, 4.00), (1060, 4.00), (1060, 4.00), (1060, 4.00), (1061, 3.00), (1061, 3.00), (1062, 3.00), (1062, 2.00), (1063, 2.00), (1063, 2.00), (1064, 2.00), (1064, 2.00), (1065, 2.00), (1065, 2.00), (1065, 3.00), (1066, 3.00), (1066, 4.00), (1067, 4.00), (1067, 4.00), (1068, 4.00), (1068, 4.00), (1069, 4.00), (1069, 4.00), (1070, 5.00), (1070, 5.00), (1071, 5.00), (1071, 4.00), (1071, 5.00), (1072, 5.00), (1072, 7.00), (1073, 6.00), (1073, 7.00), (1074, 6.00), (1074, 7.00), (1075, 8.00), (1075, 8.00), (1076, 8.00), (1076, 9.00), (1076, 10.0), (1077, 10.0), (1077, 10.0), (1078, 10.0), (1078, 10.0), (1079, 10.0), (1079, 9.00), (1080, 8.00), (1080, 8.00), (1081, 7.00), (1081, 7.00), (1082, 6.00), (1082, 8.00), (1082, 7.00), (1083, 5.00), (1083, 7.00), (1084, 7.00), (1084, 2.00), (1085, 2.00), (1085, 1.00), (1086, 5.00), (1086, 5.00), (1087, 3.00), (1087, 3.00), (1087, 4.00), (1088, 6.00), (1088, 9.00), (1089, 9.00), (1089, 9.00), (1090, 8.00), (1090, 8.00), (1091, 6.00), (1091, 6.00), (1092, 8.00), (1092, 9.00), (1092, 9.00), (1093, 8.00), (1093, 8.00), (1094, 8.00), (1094, 7.00), (1095, 8.00), (1095, 6.00), (1096, 8.00), (1096, 10.0), (1097, 11.0), (1097, 10.0), (1098, 10.0), (1098, 10.0), (1098, 10.0), (1099, 9.00), (1099, 9.00), (1100, 10.0), (1100, 9.00), (1101, 10.0), (1101, 9.00), (1102, 10.0), (1102, 8.00), (1103, 7.00), (1103, 7.00),

(1103, 8.00), (1104, 7.00), (1104, 8.00), (1105, 8.00), (1105, 8.00), (1106, 8.00), (1106, 7.00), (1107, 7.00), (1107, 6.00), (1108, 4.00), (1108, 4.00), (1108, 4.00), (1109, 5.00), (1109, 7.00), (1110, 6.00), (1110, 4.00), (1111, 5.00), (1111, 3.00), (1112, 5.00), (1112, 6.00), (1113, 6.00), (1113, 4.00), (1114, 3.00), (1114, 3.00), (1114, 4.00), (1115, 4.00), (1115, 4.00), (1116, 4.00), (1116, 4.00), (1117, 4.00), (1117, 6.00), (1118, 7.00), (1118, 7.00), (1119, 7.00), (1119, 6.00), (1119, 5.00), (1120, 5.00), (1120, 5.00), (1121, 6.00), (1121, 6.00), (1122, 5.00), (1122, 6.00), (1123, 6.00), (1123, 7.00), (1124, 7.00), (1124, 6.00), (1125, 8.00), (1125, 9.00), (1125, 6.00), (1126, 7.00), (1126, 7.00), (1127, 7.00), (1127, 7.00), (1128, 7.00), (1128, 7.00), (1129, 5.00), (1129, 6.00), (1130, 5.00), (1130, 4.00), (1130, 4.00), (1131, 3.00), (1131, 3.00), (1132, 3.00), (1132, 3.00), (1133, 3.00), (1133, 3.00), (1134, 2.00), (1134, 3.00), (1135, 2.00), (1135, 2.00), (1135, 2.00), (1136, 2.00), (1136, 2.00), (1137, 2.00), (1137, 2.00), (1138, 2.00), (1138, 1.00), (1139, 1.00), (1139, 2.00), (1140, 3.00), (1140, 3.00), (1141, 4.00), (1141, 4.00), (1141, 4.00), (1142, 4.00), (1142, 7.00), (1143, 6.00), (1143, 7.00), (1144, 8.00), (1144, 9.00), (1145, 10.0), (1145, 8.00), (1146, 5.00), (1146, 7.00), (1146, 8.00), (1147, 7.00), (1147, 7.00), (1148, 7.00), (1148, 6.00), (1149, 7.00), (1149, 8.00), (1150, 8.00), (1150, 8.00), (1151, 7.00), (1151, 7.00), (1151, 6.00), (1152, 7.00), (1152, 5.00), (1153, 5.00), (1153, 4.00), (1154, 5.00), (1154, 3.00), (1155, 3.00), (1155, 4.00), (1156, 3.00), (1156, 3.00), (1157, 2.00), (1157, 3.00), (1157, 3.00), (1158, 3.00), (1158, 2.00), (1159, 2.00), (1159, 2.00), (1160, 2.00), (1160, 2.00), (1161, 2.00), (1161, 3.00), (1162, 3.00), (1162, 5.00), (1162, 6.00), (1163, 6.00), (1163, 6.00), (1164, 6.00), (1164, 7.00), (1165, 5.00), (1165, 6.00), (1166, 5.00), (1166, 5.00), (1167, 6.00), (1167, 4.00), (1168, 5.00), (1168, 6.00), (1168, 5.00), (1169, 6.00), (1169, 7.00), (1170, 6.00), (1170, 7.00), (1171, 7.00), (1171, 6.00), (1172, 7.00), (1172, 6.00), (1173, 8.00), (1173, 8.00), (1173, 5.00), (1174, 5.00), (1174, 5.00), (1175, 5.00), (1175, 4.00), (1176, 7.00), (1176, 8.00), (1177, 8.00), (1177, 8.00), (1178, 7.00), (1178, 7.00), (1178, 7.00), (1179, 6.00), (1179, 4.00), (1180, 2.00), (1180, 4.00), (1181, 2.00), (1181, 2.00), (1182, 2.00), (1182, 4.00), (1183, 3.00), (1183, 2.00), (1184, 2.00), (1184, 3.00), (1184, 3.00), (1185, 4.00), (1185, 4.00), (1186, 4.00), (1186, 5.00), (1187, 5.00), (1187, 6.00), (1188, 6.00), (1188, 6.00), (1189, 6.00), (1189, 7.00), (1189, 7.00), (1190, 7.00), (1190, 7.00), (1191, 7.00), (1191, 7.00), (1192, 6.00), (1192, 3.00), (1193, 3.00), (1193, 6.00), (1194, 4.00), (1194, 5.00), (1194, 3.00), (1195, 5.00), (1195, 4.00), (1196, 3.00), (1196, 4.00), (1197, 4.00), (1197, 5.00), (1198, 4.00), (1198, 4.00), (1199, 4.00), (1199, 4.00), (1200, 3.00), (1200, 4.00), (1200, 2.00), (1201, 1.00), (1201, 2.00), (1202, 3.00), (1202, 2.00), (1203, 4.00), (1203, 2.00), (1204, 2.00), (1204, 2.00), (1205, 1.00), (1205, 1.00), (1205, 2.00), (1206, 3.00), (1206, 4.00), (1207, 4.00), (1207, 4.00), (1208, 3.00), (1208, 3.00), (1209, 3.00), (1209, 3.00), (1210, 1.00), (1210, 1.00), (1211, 1.00), (1211, 2.00), (1211, 4.00), (1212, 5.00), (1212, 6.00), (1213, 5.00), (1213, 6.00), (1214, 5.00), (1214, 6.00), (1215, 4.00), (1215, 6.00), (1216, 6.00), (1216, 6.00), (1216, 6.00), (1217, 6.00), (1217, 6.00), (1218, 7.00), (1218, 7.00), (1219, 7.00), (1219, 7.00), (1220, 7.00), (1220, 7.00), (1221, 6.00), (1221, 6.00), (1221, 5.00), (1222, 5.00), (1222, 7.00), (1223, 7.00), (1223, 7.00), (1224, 6.00), (1224, 5.00), (1225, 5.00), (1225, 3.00), (1226, 3.00), (1226, 4.00), (1227, 3.00), (1227, 5.00), (1227, 6.00), (1228, 3.00), (1228, 2.00), (1229, 2.00), (1229, 2.00), (1230, 3.00), (1230, 2.00), (1231, 2.00), (1231, 3.00), (1232, 4.00), (1232, 2.00), (1232, 2.00), (1233, 4.00), (1233, 5.00), (1234, 7.00), (1234, 6.00), (1235, 5.00), (1235, 4.00), (1236, 6.00), (1236, 5.00), (1237, 5.00), (1237, 3.00), (1237, 3.00), (1238, 2.00), (1238, 3.00), (1239, 5.00), (1239, 4.00), (1240, 4.00), (1240, 3.00), (1241, 8.00), (1241, 8.00), (1242, 9.00), (1242, 8.00), (1243, 8.00), (1243, 9.00), (1243, 9.00), (1244, 8.00), (1244, 9.00), (1245, 7.00), (1245, 5.00), (1246, 5.00), (1246, 5.00), (1247, 5.00), (1247, 4.00), (1248, 6.00), (1248, 6.00), (1248, 5.00), (1249, 6.00), (1249, 6.00), (1250, 6.00), (1250, 5.00), (1251, 4.00), (1251, 3.00), (1252, 2.00), (1252, 4.00), (1253, 2.00), (1253, 2.00), (1254, 3.00), (1254, 4.00), (1254, 4.00), (1255, 7.00), (1255, 8.00), (1256, 8.00), (1256, 6.00), (1257, 7.00), (1257, 7.00), (1258, 7.00), (1258, 7.00), (1259, 8.00), (1259, 8.00), (1259, 8.00), (1260, 8.00), (1260, 8.00), (1261, 6.00), (1261, 8.00), (1262, 7.00), (1262, 9.00), (1263, 9.00), (1263, 8.00), (1264, 4.00), (1264, 2.00), (1264, 3.00), (1265, 4.00), (1265, 5.00), (1266, 7.00), (1266, 6.00), (1267, 3.00), (1267, 6.00), (1268, 4.00), (1268, 5.00), (1269, 5.00), (1269, 3.00), (1270, 5.00), (1270, 5.00), (1270, 4.00), (1271, 5.00), (1271, 4.00), (1272, 3.00), (1272, 3.00), (1273, 3.00), (1273, 3.00), (1274, 3.00), (1274, 3.00), (1275, 5.00), (1275, 5.00), (1275, 5.00), (1276, 6.00), (1276, 6.00), (1277, 6.00), (1277, 6.00), (1278, 6.00), (1278, 5.00), (1279, 4.00), (1279, 6.00), (1280, 7.00), (1280, 7.00), (1280, 7.00), (1281, 7.00), (1281, 7.00), (1282, 8.00), (1282, 6.00), (1283, 7.00), (1283, 7.00), (1284, 7.00), (1284, 5.00), (1285, 5.00), (1285, 8.00), (1286, 6.00), (1286, 5.00), (1286, 5.00), (1287, 7.00), (1287, 6.00), (1288, 2.00), (1288, 3.00), (1289, 2.00), (1289, 3.00), (1290, 3.00), (1290, 3.00), (1291, 3.00), (1291, 4.00), (1291, 4.00), (1292, 2.00), (1292, 1.00), (1293, 1.00), (1293, 2.00), (1294, 3.00), (1294, 3.00), (1295, 2.00), (1295, 3.00), (1296, 4.00), (1296, 4.00), (1297, 5.00), (1297, 4.00), (1297, 3.00), (1298, 6.00), (1298, 3.00), (1299, 8.00), (1299, 7.00), (1300, 8.00), (1300, 7.00), (1301, 6.00), (1301, 6.00), (1302, 3.00), (1302, 5.00), (1302, 3.00), (1303, 4.00), (1303, 5.00), (1304, 4.00), (1304, 4.00), (1305, 4.00), (1305, 7.00), (1306, 5.00), (1306, 4.00), (1307, 4.00), (1307, 4.00), (1307, 4.00), (1308, 4.00), (1308, 3.00), (1309, 4.00), (1309, 3.00), (1310, 3.00), (1310, 3.00), (1311, 3.00), (1311, 2.00), (1312, 2.00), (1312, 3.00), (1313, 2.00), (1313, 2.00), (1313, 1.00), (1314, 1.00), (1314, 2.00), (1315, 1.00), (1315, 4.00), (1316, 5.00), (1316, 6.00), (1317, 6.00), (1317, 6.00), (1318, 4.00), (1318, 6.00), (1318, 7.00), (1319, 7.00), (1319, 9.00), (1320, 9.00), (1320, 10.0), (1321, 10.0), (1321, 11.0), (1322, 10.0), (1322, 10.0), (1323, 11.0), (1323, 10.0), (1323, 9.00), (1324, 8.00), (1324, 10.0), (1325, 9.00), (1325, 10.0), (1326, 11.0), (1326, 9.00), (1327, 7.00), (1327, 6.00), (1328, 6.00), (1328, 5.00), (1329, 5.00), (1329, 5.00), (1329, 4.00), (1330, 3.00), (1330, 3.00), (1331, 3.00), (1331, 4.00), (1332, 6.00), (1332, 5.00), (1333, 4.00), (1333,

4.00), (1334, 3.00), (1334, 4.00), (1334, 4.00), (1335, 5.00), (1335, 4.00), (1336, 4.00), (1336, 3.00), (1337, 3.00), (1337, 3.00), (1338, 3.00), (1338, 4.00), (1339, 4.00), (1339, 5.00), (1340, 4.00), (1340, 5.00), (1340, 7.00), (1341, 6.00), (1341, 7.00), (1342, 7.00), (1342, 7.00), (1343, 8.00), (1343, 8.00), (1344, 8.00), (1344, 9.00), (1345, 9.00), (1345, 9.00), (1345, 8.00), (1346, 8.00), (1346, 9.00), (1347, 9.00), (1347, 8.00), (1348, 7.00), (1348, 7.00), (1349, 7.00), (1349, 6.00), (1350, 6.00), (1350, 6.00), (1350, 5.00), (1351, 6.00), (1351, 5.00), (1352, 5.00), (1352, 5.00), (1353, 5.00), (1353, 6.00), (1354, 5.00), (1354, 6.00), (1355, 5.00), (1355, 5.00), (1356, 6.00), (1356, 4.00), (1356, 5.00), (1357, 5.00), (1357, 5.00), (1358, 5.00), (1358, 4.00), (1359, 5.00), (1359, 6.00), (1360, 6.00), (1360, 7.00), (1361, 6.00), (1361, 7.00), (1361, 8.00), (1362, 7.00), (1362, 7.00), (1363, 8.00), (1363, 9.00), (1364, 9.00), (1364, 8.00), (1365, 8.00), (1365, 9.00), (1366, 8.00), (1366, 9.00), (1366, 10.0), (1367, 9.00), (1367, 9.00), (1368, 8.00), (1368, 9.00), (1369, 9.00), (1369, 8.00), (1370, 10.0), (1370, 9.00), (1371, 9.00), (1371, 9.00), (1372, 9.00), (1372, 8.00), (1372, 9.00), (1373, 8.00), (1373, 5.00), (1374, 8.00), (1374, 8.00), (1375, 7.00), (1375, 5.00), (1376, 6.00), (1376, 6.00), (1377, 5.00), (1377, 5.00), (1377, 5.00), (1378, 4.00), (1378, 5.00), (1379, 5.00), (1379, 4.00), (1380, 3.00), (1380, 4.00), (1381, 5.00), (1381, 5.00), (1382, 4.00), (1382, 3.00), (1383, 3.00), (1383, 5.00), (1383, 4.00), (1384, 4.00), (1384, 3.00), (1385, 5.00), (1385, 4.00), (1386, 6.00), (1386, 5.00), (1387, 5.00), (1387, 7.00), (1388, 7.00), (1388, 8.00), (1388, 7.00), (1389, 6.00), (1389, 7.00), (1390, 7.00), (1390, 8.00), (1391, 7.00), (1391, 6.00), (1392, 6.00), (1392, 7.00), (1393, 8.00), (1393, 9.00), (1393, 7.00), (1394, 8.00), (1394, 7.00), (1395, 8.00), (1395, 6.00), (1396, 8.00), (1396, 5.00), (1397, 5.00), (1397, 4.00), (1398, 3.00), (1398, 5.00), (1399, 4.00), (1399, 3.00), (1399, 3.00), (1400, 4.00), (1400, 3.00), (1401, 3.00), (1401, 3.00), (1402, 5.00), (1402, 5.00), (1403, 4.00), (1403, 5.00), (1404, 5.00), (1404, 4.00), (1404, 5.00), (1405, 5.00), (1405, 5.00), (1406, 5.00), (1406, 4.00), (1407, 5.00), (1407, 5.00), (1408, 6.00), (1408, 6.00), (1409, 6.00), (1409, 6.00), (1409, 5.00), (1410, 6.00), (1410, 6.00), (1411, 6.00), (1411, 7.00), (1412, 7.00), (1412, 7.00), (1413, 6.00), (1413, 7.00), (1414, 7.00), (1414, 7.00), (1415, 7.00), (1415, 8.00), (1415, 8.00), (1416, 8.00), (1416, 8.00), (1417, 6.00), (1417, 5.00), (1418, 5.00), (1418, 6.00), (1419, 5.00), (1419, 5.00), (1420, 6.00), (1420, 5.00), (1420, 4.00), (1421, 5.00), (1421, 5.00), (1422, 4.00), (1422, 5.00), (1423, 4.00), (1423, 3.00), (1424, 4.00), (1424, 3.00), (1425, 2.00), (1425, 1.00), (1426, 1.00), (1426, 2.00), (1426, 1.00), (1427, 1.00), (1427, 3.00), (1428, 4.00), (1428, 7.00), (1429, 7.00), (1429, 8.00), (1430, 8.00), (1430, 8.00), (1431, 7.00), (1431, 7.00), (1431, 7.00), (1432, 7.00), (1432, 7.00), (1433, 7.00), (1433, 8.00), (1434, 6.00), (1434, 8.00), (1435, 8.00), (1435, 8.00), (1436, 8.00), (1436, 8.00), (1436, 8.00), (1437, 8.00), (1437, 8.00), (1438, 8.00), (1438, 8.00), (1439, 8.00), (1439, 8.00), (1440, 9.00), (1440, 9.00), (1441, 10.0), (1441, 9.00), (1442, 6.00), (1442, 7.00), (1442, 7.00), (1443, 8.00), (1443, 9.00), (1444, 9.00), (1444, 8.00), (1445, 5.00), (1445, 4.00), (1446, 5.00), (1446, 4.00), (1447, 4.00), (1447, 3.00), (1447, 3.00), (1448, 3.00), (1448, 3.00), (1449, 4.00), (1449, 4.00), (1450, 2.00), (1450, 3.00), (1451, 2.00), (1451, 3.00), (1452, 3.00), (1452, 3.00), (1452, 5.00), (1453, 5.00), (1453, 5.00), (1454, 5.00), (1454, 7.00), (1455, 6.00), (1455, 8.00), (1456, 8.00), (1456, 6.00), (1457, 8.00), (1457, 8.00), (1458, 8.00), (1458, 7.00), (1458, 9.00), (1459, 9.00), (1459, 8.00), (1460, 8.00), (1460, 8.00), (1461, 8.00), (1461, 8.00), (1462, 7.00), (1462, 7.00), (1463, 7.00), (1463, 7.00), (1463, 6.00), (1464, 6.00), (1464, 6.00), (1465, 5.00), (1465, 5.00), (1466, 3.00), (1466, 3.00), (1467, 3.00), (1467, 3.00), (1468, 3.00), (1468, 2.00), (1469, 3.00), (1469, 4.00), (1469, 3.00), (1470, 3.00), (1470, 3.00), (1471, 4.00), (1471, 4.00), (1472, 3.00), (1472, 1.00), (1473, 1.00), (1473, 0.00), (1474, 2.00), (1474, 2.00), (1474, 2.00), (1475, 3.00), (1475, 2.00), (1476, 3.00), (1476, 3.00), (1477, 5.00), (1477, 4.00), (1478, 4.00), (1478, 5.00), (1479, 7.00), (1479, 7.00), (1479, 7.00), (1480, 5.00), (1480, 6.00), (1481, 7.00), (1481, 7.00), (1482, 7.00), (1482, 6.00), (1483, 6.00), (1483, 7.00), (1484, 6.00), (1484, 6.00), (1485, 6.00), (1485, 5.00), (1485, 4.00), (1486, 4.00), (1486, 3.00), (1487, 3.00), (1487, 3.00), (1488, 2.00), (1488, 1.00), (1489, 1.00), (1489, 1.00), (1490, 1.00), (1490, 2.00), (1490, 2.00), (1491, 2.00), (1491, 1.00), (1492, 1.00), (1492, 1.00), (1493, 1.00), (1493, 1.00), (1494, 0.00), (1494, 2.00), (1495, 1.00), (1495, 1.00), (1495, 1.00), (1496, 1.00), (1496, 1.00), (1497, 3.00), (1497, 3.00), (1498, 3.00), (1498, 2.00), (1499, 4.00), (1499, 4.00), (1500, 6.00), (1500, 7.00), (1501, 7.00), (1501, 9.00), (1501, 9.00), (1502, 9.00), (1502, 10.0), (1503, 10.0), (1503, 8.00), (1504, 7.00), (1504, 7.00), (1505, 7.00), (1505, 7.00), (1506, 7.00), (1506, 7.00), (1506, 7.00), (1507, 6.00), (1507, 6.00), (1508, 7.00), (1508, 5.00), (1509, 5.00), (1509, 4.00), (1510, 4.00), (1510, 3.00), (1511, 3.00), (1511, 3.00), (1512, 3.00)

AA_Initial[Volume_Elements] = 8.24493e-1-4.0899e-3*Temperature_Initial[Volume_Elements]+7.6438e-5*Temperature_Initial[Volume_Elements]^2-8.2467e-7*Temperature_Initial[Volume_Elements]^3+5.3875e-9*Temperature_Initial[Volume_Elements]^4

BB_Initial[Volume_Elements] = -5.72466e-3+1.0227e-4*Temperature_Initial[Volume_Elements]-1.6546e-6*Temperature_Initial[Volume_Elements]^2

CC_Initial = 4.8314e-4

Concentration_Initial[Volume_Elements] = 0.68*Conductivity_Initial[Volume_Elements]

Conductivity_Initial[Volume_Elements] = Initial_Conductivity[Volume_Elements,Feb_11]

Density_Initial[Volume_Elements] = Density_Water_Initial[Volume_Elements]+AA_Initial[Volume_Elements]*Salinity_Initial[Volume_Elements]+BB_Initial[Volume_Elements]*Salinity_Initial[Volume_Elements]^1.5+CC_Initial*Salinity_Initial[Volume_Elements]^2

Density_Water_Initial[Volume_Elements] = 999.842594+6.793952e-2*Temperature_Initial[Volume_Elements]-9.095290e-

3*Temperature_Initial[Volume_Elements]^2+1.001685e-4*Temperature_Initial[Volume_Elements]^3-1.120083e-6*Temperature_Initial[Volume_Elements]^4+6.536332e-9*Temperature_Initial[Volume_Elements]^5
Heat_Capacity[Volume_Elements] = IF(Temperature_Initial[Volume_Elements]<34.5) THEN 4.184*(0.99716+3.979E-4*(EXP((34.5-Temperature_Initial[Volume_Elements])/10.6)+EXP(-(34.5-Temperature_Initial[Volume_Elements])/10.6))) ELSE 4.184*(0.99716+3.979E-4*(EXP((2.08*(Temperature_Initial[Volume_Elements]-34.5)^0.67)/10.6)+EXP(-(2.08*(Temperature_Initial[Volume_Elements]-34.5)^0.67)/10.6)))
Heat_Capacity_Initial[Volume_Elements] = IF(Temperature_Initial[Volume_Elements]<34.5) THEN 4.184*(0.99716+3.979E-4*(EXP((34.5-Temperature_Initial[Volume_Elements])/10.6)+EXP(-(34.5-Temperature_Initial[Volume_Elements])/10.6))) ELSE 4.184*(0.99716+3.979E-4*(EXP((2.08*(Temperature_Initial[Volume_Elements]-34.5)^0.67)/10.6)+EXP(-(2.08*(Temperature_Initial[Volume_Elements]-34.5)^0.67)/10.6)))
Initial_Conductivity[Layer_1,Jan_18] = 6046
Initial_Conductivity[Layer_1,Jan_19] = 6292
Initial_Conductivity[Layer_1,Jan_20] = 6468
Initial_Conductivity[Layer_1,Jan_21] = 0
Initial_Conductivity[Layer_1,Jan_22] = 0
Initial_Conductivity[Layer_1,Feb_7] = 1783
Initial_Conductivity[Layer_1,Feb_8] = 0
Initial_Conductivity[Layer_1,Feb_9] = 0
Initial_Conductivity[Layer_1,Feb_10] = 8124
Initial_Conductivity[Layer_1,Feb_11] = 8283
Initial_Conductivity[Layer_1,Feb_29] = 328
Initial_Conductivity[Layer_1,Mar_1] = 0
Initial_Conductivity[Layer_1,Mar_2] = 0
Initial_Conductivity[Layer_2,Jan_18] = 6041
Initial_Conductivity[Layer_2,Jan_19] = 6291
Initial_Conductivity[Layer_2,Jan_20] = 6468
Initial_Conductivity[Layer_2,Jan_21] = 0
Initial_Conductivity[Layer_2,Jan_22] = 0
Initial_Conductivity[Layer_2,Feb_7] = 2473
Initial_Conductivity[Layer_2,Feb_8] = 0
Initial_Conductivity[Layer_2,Feb_9] = 0
Initial_Conductivity[Layer_2,Feb_10] = 8123
Initial_Conductivity[Layer_2,Feb_11] = 8285
Initial_Conductivity[Layer_2,Feb_29] = 443
Initial_Conductivity[Layer_2,Mar_1] = 0
Initial_Conductivity[Layer_2,Mar_2] = 0
Initial_Conductivity[Layer_3,Jan_18] = 6035
Initial_Conductivity[Layer_3,Jan_19] = 6290
Initial_Conductivity[Layer_3,Jan_20] = 6468
Initial_Conductivity[Layer_3,Jan_21] = 0
Initial_Conductivity[Layer_3,Jan_22] = 0
Initial_Conductivity[Layer_3,Feb_7] = 3163
Initial_Conductivity[Layer_3,Feb_8] = 259
Initial_Conductivity[Layer_3,Feb_9] = 0
Initial_Conductivity[Layer_3,Feb_10] = 8121
Initial_Conductivity[Layer_3,Feb_11] = 8287
Initial_Conductivity[Layer_3,Feb_29] = 557
Initial_Conductivity[Layer_3,Mar_1] = 19
Initial_Conductivity[Layer_3,Mar_2] = 67
Initial_Conductivity[Layer_4,Jan_18] = 6030
Initial_Conductivity[Layer_4,Jan_19] = 6289
Initial_Conductivity[Layer_4,Jan_20] = 6469
Initial_Conductivity[Layer_4,Jan_21] = 1480
Initial_Conductivity[Layer_4,Jan_22] = 171
Initial_Conductivity[Layer_4,Feb_7] = 3853
Initial_Conductivity[Layer_4,Feb_8] = 1455
Initial_Conductivity[Layer_4,Feb_9] = 397
Initial_Conductivity[Layer_4,Feb_10] = 8120
Initial_Conductivity[Layer_4,Feb_11] = 8289
Initial_Conductivity[Layer_4,Feb_29] = 672
Initial_Conductivity[Layer_4,Mar_1] = 241
Initial_Conductivity[Layer_4,Mar_2] = 291
Initial_Conductivity[Layer_5,Jan_18] = 6024
Initial_Conductivity[Layer_5,Jan_19] = 6288

Initial_Conductivity[Layer_5,Jan_20] = 6469
Initial_Conductivity[Layer_5,Jan_21] = 2960
Initial_Conductivity[Layer_5,Jan_22] = 1883
Initial_Conductivity[Layer_5,Feb_7] = 4543
Initial_Conductivity[Layer_5,Feb_8] = 2651
Initial_Conductivity[Layer_5,Feb_9] = 1721
Initial_Conductivity[Layer_5,Feb_10] = 8118
Initial_Conductivity[Layer_5,Feb_11] = 8291
Initial_Conductivity[Layer_5,Feb_29] = 786
Initial_Conductivity[Layer_5,Mar_1] = 463
Initial_Conductivity[Layer_5,Mar_2] = 515
Initial_Conductivity[Layer_6,Jan_18] = 6019
Initial_Conductivity[Layer_6,Jan_19] = 6287
Initial_Conductivity[Layer_6,Jan_20] = 6469
Initial_Conductivity[Layer_6,Jan_21] = 4441
Initial_Conductivity[Layer_6,Jan_22] = 3595
Initial_Conductivity[Layer_6,Feb_7] = 5233
Initial_Conductivity[Layer_6,Feb_8] = 3846
Initial_Conductivity[Layer_6,Feb_9] = 3045
Initial_Conductivity[Layer_6,Feb_10] = 8117
Initial_Conductivity[Layer_6,Feb_11] = 8293
Initial_Conductivity[Layer_6,Feb_29] = 900
Initial_Conductivity[Layer_6,Mar_1] = 686
Initial_Conductivity[Layer_6,Mar_2] = 739
Initial_Conductivity[Layer_7,Jan_18] = 6014
Initial_Conductivity[Layer_7,Jan_19] = 6286
Initial_Conductivity[Layer_7,Jan_20] = 6470
Initial_Conductivity[Layer_7,Jan_21] = 5921
Initial_Conductivity[Layer_7,Jan_22] = 5307
Initial_Conductivity[Layer_7,Feb_7] = 5923
Initial_Conductivity[Layer_7,Feb_8] = 5042
Initial_Conductivity[Layer_7,Feb_9] = 4369
Initial_Conductivity[Layer_7,Feb_10] = 8115
Initial_Conductivity[Layer_7,Feb_11] = 8295
Initial_Conductivity[Layer_7,Feb_29] = 1015
Initial_Conductivity[Layer_7,Mar_1] = 908
Initial_Conductivity[Layer_7,Mar_2] = 962
Initial_Conductivity[Layer_8,Jan_18] = 6013
Initial_Conductivity[Layer_8,Jan_19] = 6287
Initial_Conductivity[Layer_8,Jan_20] = 6470
Initial_Conductivity[Layer_8,Jan_21] = 6663
Initial_Conductivity[Layer_8,Jan_22] = 6848
Initial_Conductivity[Layer_8,Feb_7] = 6613
Initial_Conductivity[Layer_8,Feb_8] = 6238
Initial_Conductivity[Layer_8,Feb_9] = 5693
Initial_Conductivity[Layer_8,Feb_10] = 8114
Initial_Conductivity[Layer_8,Feb_11] = 8297
Initial_Conductivity[Layer_8,Feb_29] = 1129
Initial_Conductivity[Layer_8,Mar_1] = 1130
Initial_Conductivity[Layer_8,Mar_2] = 1186
Initial_Conductivity[Layer_9,Jan_18] = 6016
Initial_Conductivity[Layer_9,Jan_19] = 6290
Initial_Conductivity[Layer_9,Jan_20] = 6470
Initial_Conductivity[Layer_9,Jan_21] = 6668
Initial_Conductivity[Layer_9,Jan_22] = 6850
Initial_Conductivity[Layer_9,Feb_7] = 7303
Initial_Conductivity[Layer_9,Feb_8] = 7434
Initial_Conductivity[Layer_9,Feb_9] = 7017
Initial_Conductivity[Layer_9,Feb_10] = 8112
Initial_Conductivity[Layer_9,Feb_11] = 8298
Initial_Conductivity[Layer_9,Feb_29] = 1244
Initial_Conductivity[Layer_9,Mar_1] = 1352
Initial_Conductivity[Layer_9,Mar_2] = 1410
Initial_Conductivity[Layer_10,Jan_18] = 6019
Initial_Conductivity[Layer_10,Jan_19] = 6294
Initial_Conductivity[Layer_10,Jan_20] = 6470
Initial_Conductivity[Layer_10,Jan_21] = 6672

Initial_Conductivity[Layer_10,Jan_22] = 6852
Initial_Conductivity[Layer_10,Feb_7] = 7649
Initial_Conductivity[Layer_10,Feb_8] = 7793
Initial_Conductivity[Layer_10,Feb_9] = 7944
Initial_Conductivity[Layer_10,Feb_10] = 8114
Initial_Conductivity[Layer_10,Feb_11] = 8292
Initial_Conductivity[Layer_10,Feb_29] = 1303
Initial_Conductivity[Layer_10,Mar_1] = 1419
Initial_Conductivity[Layer_10,Mar_2] = 1478
Initial_Conductivity[Layer_11,Jan_18] = 6023
Initial_Conductivity[Layer_11,Jan_19] = 6297
Initial_Conductivity[Layer_11,Jan_20] = 6470
Initial_Conductivity[Layer_11,Jan_21] = 6677
Initial_Conductivity[Layer_11,Jan_22] = 6853
Initial_Conductivity[Layer_11,Feb_7] = 7650
Initial_Conductivity[Layer_11,Feb_8] = 7794
Initial_Conductivity[Layer_11,Feb_9] = 7944
Initial_Conductivity[Layer_11,Feb_10] = 8115
Initial_Conductivity[Layer_11,Feb_11] = 8285
Initial_Conductivity[Layer_11,Feb_29] = 1306
Initial_Conductivity[Layer_11,Mar_1] = 1418
Initial_Conductivity[Layer_11,Mar_2] = 1479
Initial_Conductivity[Layer_12,Jan_18] = 6026
Initial_Conductivity[Layer_12,Jan_19] = 6301
Initial_Conductivity[Layer_12,Jan_20] = 6469
Initial_Conductivity[Layer_12,Jan_21] = 6681
Initial_Conductivity[Layer_12,Jan_22] = 6855
Initial_Conductivity[Layer_12,Feb_7] = 7652
Initial_Conductivity[Layer_12,Feb_8] = 7795
Initial_Conductivity[Layer_12,Feb_9] = 7944
Initial_Conductivity[Layer_12,Feb_10] = 8117
Initial_Conductivity[Layer_12,Feb_11] = 8278
Initial_Conductivity[Layer_12,Feb_29] = 1310
Initial_Conductivity[Layer_12,Mar_1] = 1418
Initial_Conductivity[Layer_12,Mar_2] = 1480
Initial_Conductivity[Layer_13,Jan_18] = 6029
Initial_Conductivity[Layer_13,Jan_19] = 6304
Initial_Conductivity[Layer_13,Jan_20] = 6469
Initial_Conductivity[Layer_13,Jan_21] = 6686
Initial_Conductivity[Layer_13,Jan_22] = 6857
Initial_Conductivity[Layer_13,Feb_7] = 7654
Initial_Conductivity[Layer_13,Feb_8] = 7795
Initial_Conductivity[Layer_13,Feb_9] = 7944
Initial_Conductivity[Layer_13,Feb_10] = 8118
Initial_Conductivity[Layer_13,Feb_11] = 8271
Initial_Conductivity[Layer_13,Feb_29] = 1313
Initial_Conductivity[Layer_13,Mar_1] = 1418
Initial_Conductivity[Layer_13,Mar_2] = 1481
Initial_Conductivity[Layer_14,Jan_18] = 6032
Initial_Conductivity[Layer_14,Jan_19] = 6308
Initial_Conductivity[Layer_14,Jan_20] = 6469
Initial_Conductivity[Layer_14,Jan_21] = 6690
Initial_Conductivity[Layer_14,Jan_22] = 6859
Initial_Conductivity[Layer_14,Feb_7] = 7655
Initial_Conductivity[Layer_14,Feb_8] = 7796
Initial_Conductivity[Layer_14,Feb_9] = 7945
Initial_Conductivity[Layer_14,Feb_10] = 8120
Initial_Conductivity[Layer_14,Feb_11] = 8265
Initial_Conductivity[Layer_14,Feb_29] = 1317
Initial_Conductivity[Layer_14,Mar_1] = 1417
Initial_Conductivity[Layer_14,Mar_2] = 1482
Initial_Conductivity[Layer_15,Jan_18] = 6036
Initial_Conductivity[Layer_15,Jan_19] = 6311
Initial_Conductivity[Layer_15,Jan_20] = 6469
Initial_Conductivity[Layer_15,Jan_21] = 6695
Initial_Conductivity[Layer_15,Jan_22] = 6860
Initial_Conductivity[Layer_15,Feb_7] = 7657

Initial_Conductivity[Layer_15,Feb_8] = 7797
Initial_Conductivity[Layer_15,Feb_9] = 7945
Initial_Conductivity[Layer_15,Feb_10] = 8121
Initial_Conductivity[Layer_15,Feb_11] = 8258
Initial_Conductivity[Layer_15,Feb_29] = 1320
Initial_Conductivity[Layer_15,Mar_1] = 1417
Initial_Conductivity[Layer_15,Mar_2] = 1483
Initial_Conductivity[Layer_16,Jan_18] = 6039
Initial_Conductivity[Layer_16,Jan_19] = 6315
Initial_Conductivity[Layer_16,Jan_20] = 6469
Initial_Conductivity[Layer_16,Jan_21] = 6700
Initial_Conductivity[Layer_16,Jan_22] = 6862
Initial_Conductivity[Layer_16,Feb_7] = 7658
Initial_Conductivity[Layer_16,Feb_8] = 7797
Initial_Conductivity[Layer_16,Feb_9] = 7945
Initial_Conductivity[Layer_16,Feb_10] = 8123
Initial_Conductivity[Layer_16,Feb_11] = 8251
Initial_Conductivity[Layer_16,Feb_29] = 1324
Initial_Conductivity[Layer_16,Mar_1] = 1417
Initial_Conductivity[Layer_16,Mar_2] = 1484
Initial_Conductivity[Layer_17,Jan_18] = 6042
Initial_Conductivity[Layer_17,Jan_19] = 6318
Initial_Conductivity[Layer_17,Jan_20] = 6469
Initial_Conductivity[Layer_17,Jan_21] = 6704
Initial_Conductivity[Layer_17,Jan_22] = 6864
Initial_Conductivity[Layer_17,Feb_7] = 7660
Initial_Conductivity[Layer_17,Feb_8] = 7798
Initial_Conductivity[Layer_17,Feb_9] = 7945
Initial_Conductivity[Layer_17,Feb_10] = 8124
Initial_Conductivity[Layer_17,Feb_11] = 8244
Initial_Conductivity[Layer_17,Feb_29] = 1327
Initial_Conductivity[Layer_17,Mar_1] = 1416
Initial_Conductivity[Layer_17,Mar_2] = 1485
Initial_Conductivity[Layer_18,Jan_18] = 6045
Initial_Conductivity[Layer_18,Jan_19] = 6322
Initial_Conductivity[Layer_18,Jan_20] = 6469
Initial_Conductivity[Layer_18,Jan_21] = 6709
Initial_Conductivity[Layer_18,Jan_22] = 6866
Initial_Conductivity[Layer_18,Feb_7] = 7662
Initial_Conductivity[Layer_18,Feb_8] = 7798
Initial_Conductivity[Layer_18,Feb_9] = 7945
Initial_Conductivity[Layer_18,Feb_10] = 8126
Initial_Conductivity[Layer_18,Feb_11] = 8238
Initial_Conductivity[Layer_18,Feb_29] = 1331
Initial_Conductivity[Layer_18,Mar_1] = 1416
Initial_Conductivity[Layer_18,Mar_2] = 1486
Initial_Temperature[Layer_1,Jan_18] = 25.32
Initial_Temperature[Layer_1,Jan_19] = 0
Initial_Temperature[Layer_1,Jan_20] = 0
Initial_Temperature[Layer_1,Jan_21] = 16.93
Initial_Temperature[Layer_1,Jan_22] = 17.17
Initial_Temperature[Layer_1,Feb_7] = 22.67
Initial_Temperature[Layer_1,Feb_8] = 25.04
Initial_Temperature[Layer_1,Feb_9] = 26.14
Initial_Temperature[Layer_1,Feb_10] = 28.05
Initial_Temperature[Layer_1,Feb_11] = 25.59
Initial_Temperature[Layer_1,Feb_29] = 25.32
Initial_Temperature[Layer_1,Mar_1] = 25.86
Initial_Temperature[Layer_1,Mar_2] = 28.67
Initial_Temperature[Layer_2,Jan_18] = 25.76
Initial_Temperature[Layer_2,Jan_19] = 0
Initial_Temperature[Layer_2,Jan_20] = 0
Initial_Temperature[Layer_2,Jan_21] = 18.50
Initial_Temperature[Layer_2,Jan_22] = 18.64
Initial_Temperature[Layer_2,Feb_7] = 22.68
Initial_Temperature[Layer_2,Feb_8] = 25.06
Initial_Temperature[Layer_2,Feb_9] = 26.12

Initial_Temperature[Layer_2,Feb_10] = 28.05
Initial_Temperature[Layer_2,Feb_11] = 25.62
Initial_Temperature[Layer_2,Feb_29] = 25.35
Initial_Temperature[Layer_2,Mar_1] = 25.89
Initial_Temperature[Layer_2,Mar_2] = 28.76
Initial_Temperature[Layer_3,Jan_18] = 26.19
Initial_Temperature[Layer_3,Jan_19] = 0
Initial_Temperature[Layer_3,Jan_20] = 0
Initial_Temperature[Layer_3,Jan_21] = 20.07
Initial_Temperature[Layer_3,Jan_22] = 20.11
Initial_Temperature[Layer_3,Feb_7] = 22.69
Initial_Temperature[Layer_3,Feb_8] = 25.07
Initial_Temperature[Layer_3,Feb_9] = 26.11
Initial_Temperature[Layer_3,Feb_10] = 28.05
Initial_Temperature[Layer_3,Feb_11] = 25.66
Initial_Temperature[Layer_3,Feb_29] = 25.38
Initial_Temperature[Layer_3,Mar_1] = 25.93
Initial_Temperature[Layer_3,Mar_2] = 28.84
Initial_Temperature[Layer_4,Jan_18] = 26.41
Initial_Temperature[Layer_4,Jan_19] = 0
Initial_Temperature[Layer_4,Jan_20] = 0
Initial_Temperature[Layer_4,Jan_21] = 20.82
Initial_Temperature[Layer_4,Jan_22] = 20.79
Initial_Temperature[Layer_4,Feb_7] = 22.68
Initial_Temperature[Layer_4,Feb_8] = 25.11
Initial_Temperature[Layer_4,Feb_9] = 26.12
Initial_Temperature[Layer_4,Feb_10] = 28.06
Initial_Temperature[Layer_4,Feb_11] = 25.68
Initial_Temperature[Layer_4,Feb_29] = 25.41
Initial_Temperature[Layer_4,Mar_1] = 25.99
Initial_Temperature[Layer_4,Mar_2] = 28.90
Initial_Temperature[Layer_5,Jan_18] = 26.49
Initial_Temperature[Layer_5,Jan_19] = 0
Initial_Temperature[Layer_5,Jan_20] = 0
Initial_Temperature[Layer_5,Jan_21] = 21.07
Initial_Temperature[Layer_5,Jan_22] = 20.97
Initial_Temperature[Layer_5,Feb_7] = 22.66
Initial_Temperature[Layer_5,Feb_8] = 25.16
Initial_Temperature[Layer_5,Feb_9] = 26.15
Initial_Temperature[Layer_5,Feb_10] = 28.07
Initial_Temperature[Layer_5,Feb_11] = 25.70
Initial_Temperature[Layer_5,Feb_29] = 25.45
Initial_Temperature[Layer_5,Mar_1] = 26.09
Initial_Temperature[Layer_5,Mar_2] = 28.94
Initial_Temperature[Layer_6,Jan_18] = 26.60
Initial_Temperature[Layer_6,Jan_19] = 0
Initial_Temperature[Layer_6,Jan_20] = 0
Initial_Temperature[Layer_6,Jan_21] = 21.36
Initial_Temperature[Layer_6,Jan_22] = 21.19
Initial_Temperature[Layer_6,Feb_7] = 22.65
Initial_Temperature[Layer_6,Feb_8] = 25.22
Initial_Temperature[Layer_6,Feb_9] = 26.19
Initial_Temperature[Layer_6,Feb_10] = 28.10
Initial_Temperature[Layer_6,Feb_11] = 25.72
Initial_Temperature[Layer_6,Feb_29] = 25.49
Initial_Temperature[Layer_6,Mar_1] = 26.19
Initial_Temperature[Layer_6,Mar_2] = 28.98
Initial_Temperature[Layer_7,Jan_18] = 26.99
Initial_Temperature[Layer_7,Jan_19] = 0
Initial_Temperature[Layer_7,Jan_20] = 0
Initial_Temperature[Layer_7,Jan_21] = 22.07
Initial_Temperature[Layer_7,Jan_22] = 21.70
Initial_Temperature[Layer_7,Feb_7] = 22.66
Initial_Temperature[Layer_7,Feb_8] = 25.21
Initial_Temperature[Layer_7,Feb_9] = 26.25
Initial_Temperature[Layer_7,Feb_10] = 28.22
Initial_Temperature[Layer_7,Feb_11] = 25.82

Initial_Temperature[Layer_7,Feb_29] = 25.52
Initial_Temperature[Layer_7,Mar_1] = 26.21
Initial_Temperature[Layer_7,Mar_2] = 28.99
Initial_Temperature[Layer_8,Jan_18] = 27.37
Initial_Temperature[Layer_8,Jan_19] = 0
Initial_Temperature[Layer_8,Jan_20] = 0
Initial_Temperature[Layer_8,Jan_21] = 22.78
Initial_Temperature[Layer_8,Jan_22] = 22.22
Initial_Temperature[Layer_8,Feb_7] = 22.68
Initial_Temperature[Layer_8,Feb_8] = 25.21
Initial_Temperature[Layer_8,Feb_9] = 26.31
Initial_Temperature[Layer_8,Feb_10] = 28.34
Initial_Temperature[Layer_8,Feb_11] = 25.91
Initial_Temperature[Layer_8,Feb_29] = 25.55
Initial_Temperature[Layer_8,Mar_1] = 26.24
Initial_Temperature[Layer_8,Mar_2] = 28.99
Initial_Temperature[Layer_9,Jan_18] = 27.17
Initial_Temperature[Layer_9,Jan_19] = 0
Initial_Temperature[Layer_9,Jan_20] = 0
Initial_Temperature[Layer_9,Jan_21] = 22.48
Initial_Temperature[Layer_9,Jan_22] = 22.07
Initial_Temperature[Layer_9,Feb_7] = 22.48
Initial_Temperature[Layer_9,Feb_8] = 24.99
Initial_Temperature[Layer_9,Feb_9] = 26.07
Initial_Temperature[Layer_9,Feb_10] = 28.12
Initial_Temperature[Layer_9,Feb_11] = 25.70
Initial_Temperature[Layer_9,Feb_29] = 25.54
Initial_Temperature[Layer_9,Mar_1] = 26.08
Initial_Temperature[Layer_9,Mar_2] = 28.59
Initial_Temperature[Layer_10,Jan_18] = 26.72
Initial_Temperature[Layer_10,Jan_19] = 0
Initial_Temperature[Layer_10,Jan_20] = 0
Initial_Temperature[Layer_10,Jan_21] = 21.75
Initial_Temperature[Layer_10,Jan_22] = 21.62
Initial_Temperature[Layer_10,Feb_7] = 22.18
Initial_Temperature[Layer_10,Feb_8] = 24.68
Initial_Temperature[Layer_10,Feb_9] = 25.69
Initial_Temperature[Layer_10,Feb_10] = 27.75
Initial_Temperature[Layer_10,Feb_11] = 25.36
Initial_Temperature[Layer_10,Feb_29] = 25.53
Initial_Temperature[Layer_10,Mar_1] = 25.84
Initial_Temperature[Layer_10,Mar_2] = 28.02
Initial_Temperature[Layer_11,Jan_18] = 26.44
Initial_Temperature[Layer_11,Jan_19] = 0
Initial_Temperature[Layer_11,Jan_20] = 0
Initial_Temperature[Layer_11,Jan_21] = 21.28
Initial_Temperature[Layer_11,Jan_22] = 21.36
Initial_Temperature[Layer_11,Feb_7] = 21.98
Initial_Temperature[Layer_11,Feb_8] = 24.48
Initial_Temperature[Layer_11,Feb_9] = 25.45
Initial_Temperature[Layer_11,Feb_10] = 27.51
Initial_Temperature[Layer_11,Feb_11] = 25.13
Initial_Temperature[Layer_11,Feb_29] = 25.49
Initial_Temperature[Layer_11,Mar_1] = 25.66
Initial_Temperature[Layer_11,Mar_2] = 27.60
Initial_Temperature[Layer_12,Jan_18] = 26.58
Initial_Temperature[Layer_12,Jan_19] = 0
Initial_Temperature[Layer_12,Jan_20] = 0
Initial_Temperature[Layer_12,Jan_21] = 21.41
Initial_Temperature[Layer_12,Jan_22] = 21.52
Initial_Temperature[Layer_12,Feb_7] = 22.01
Initial_Temperature[Layer_12,Feb_8] = 24.55
Initial_Temperature[Layer_12,Feb_9] = 25.52
Initial_Temperature[Layer_12,Feb_10] = 27.57
Initial_Temperature[Layer_12,Feb_11] = 25.16
Initial_Temperature[Layer_12,Feb_29] = 25.43
Initial_Temperature[Layer_12,Mar_1] = 25.61

Initial_Temperature[Layer_12,Mar_2] = 27.56
Initial_Temperature[Layer_13,Jan_18] = 26.73
Initial_Temperature[Layer_13,Jan_19] = 0
Initial_Temperature[Layer_13,Jan_20] = 0
Initial_Temperature[Layer_13,Jan_21] = 21.57
Initial_Temperature[Layer_13,Jan_22] = 21.69
Initial_Temperature[Layer_13,Feb_7] = 22.04
Initial_Temperature[Layer_13,Feb_8] = 24.62
Initial_Temperature[Layer_13,Feb_9] = 25.60
Initial_Temperature[Layer_13,Feb_10] = 27.63
Initial_Temperature[Layer_13,Feb_11] = 25.20
Initial_Temperature[Layer_13,Feb_29] = 25.36
Initial_Temperature[Layer_13,Mar_1] = 25.56
Initial_Temperature[Layer_13,Mar_2] = 27.51
Initial_Temperature[Layer_14,Jan_18] = 27.15
Initial_Temperature[Layer_14,Jan_19] = 0
Initial_Temperature[Layer_14,Jan_20] = 0
Initial_Temperature[Layer_14,Jan_21] = 21.93
Initial_Temperature[Layer_14,Jan_22] = 22.03
Initial_Temperature[Layer_14,Feb_7] = 22.37
Initial_Temperature[Layer_14,Feb_8] = 24.91
Initial_Temperature[Layer_14,Feb_9] = 25.92
Initial_Temperature[Layer_14,Feb_10] = 27.92
Initial_Temperature[Layer_14,Feb_11] = 25.63
Initial_Temperature[Layer_14,Feb_29] = 27.00
Initial_Temperature[Layer_14,Mar_1] = 25.70
Initial_Temperature[Layer_14,Mar_2] = 27.53
Initial_Temperature[Layer_15,Jan_18] = 27.57
Initial_Temperature[Layer_15,Jan_19] = 0
Initial_Temperature[Layer_15,Jan_20] = 0
Initial_Temperature[Layer_15,Jan_21] = 22.29
Initial_Temperature[Layer_15,Jan_22] = 22.38
Initial_Temperature[Layer_15,Feb_7] = 22.69
Initial_Temperature[Layer_15,Feb_8] = 25.21
Initial_Temperature[Layer_15,Feb_9] = 26.24
Initial_Temperature[Layer_15,Feb_10] = 28.22
Initial_Temperature[Layer_15,Feb_11] = 26.05
Initial_Temperature[Layer_15,Feb_29] = 28.65
Initial_Temperature[Layer_15,Mar_1] = 25.85
Initial_Temperature[Layer_15,Mar_2] = 27.55
Initial_Temperature[Layer_16,Jan_18] = 27.91
Initial_Temperature[Layer_16,Jan_19] = 0
Initial_Temperature[Layer_16,Jan_20] = 0
Initial_Temperature[Layer_16,Jan_21] = 22.58
Initial_Temperature[Layer_16,Jan_22] = 22.65
Initial_Temperature[Layer_16,Feb_7] = 22.95
Initial_Temperature[Layer_16,Feb_8] = 25.44
Initial_Temperature[Layer_16,Feb_9] = 26.50
Initial_Temperature[Layer_16,Feb_10] = 28.45
Initial_Temperature[Layer_16,Feb_11] = 26.39
Initial_Temperature[Layer_16,Feb_29] = 29.96
Initial_Temperature[Layer_16,Mar_1] = 25.96
Initial_Temperature[Layer_16,Mar_2] = 27.56
Initial_Temperature[Layer_17,Jan_18] = 28.42
Initial_Temperature[Layer_17,Jan_19] = 0
Initial_Temperature[Layer_17,Jan_20] = 0
Initial_Temperature[Layer_17,Jan_21] = 23.01
Initial_Temperature[Layer_17,Jan_22] = 23.06
Initial_Temperature[Layer_17,Feb_7] = 23.35
Initial_Temperature[Layer_17,Feb_8] = 25.79
Initial_Temperature[Layer_17,Feb_9] = 26.89
Initial_Temperature[Layer_17,Feb_10] = 28.80
Initial_Temperature[Layer_17,Feb_11] = 26.91
Initial_Temperature[Layer_17,Feb_29] = 31.93
Initial_Temperature[Layer_17,Mar_1] = 26.13
Initial_Temperature[Layer_17,Mar_2] = 27.58
Initial_Temperature[Layer_18,Jan_18] = 29.27

Initial_Temperature[Layer_18,Jan_19] = 0
Initial_Temperature[Layer_18,Jan_20] = 0
Initial_Temperature[Layer_18,Jan_21] = 23.73
Initial_Temperature[Layer_18,Jan_22] = 23.75
Initial_Temperature[Layer_18,Feb_7] = 24.00
Initial_Temperature[Layer_18,Feb_8] = 26.38
Initial_Temperature[Layer_18,Feb_9] = 27.54
Initial_Temperature[Layer_18,Feb_10] = 29.39
Initial_Temperature[Layer_18,Feb_11] = 27.76
Initial_Temperature[Layer_18,Feb_29] = 35.22
Initial_Temperature[Layer_18,Mar_1] = 26.42
Initial_Temperature[Layer_18,Mar_2] = 27.62
Salinity_Initial[Volume_Elements] = Concentration_Initial[Volume_Elements]/1000
Temperature_C = 20
Temperature_Initial[Volume_Elements] = Initial_Temperature[Volume_Elements,Feb_11]
Salinity[Layer_1] =
(2*Salinity_Layer_1+Salinity_Layer_2+Salinity_Layer_3+Salinity_Layer_4+Salinity_Layer_5+Salinity_La
yer_6+Salinity_Layer_7+Salinity_Layer_8+Salinity_Layer_9+Salinity_Layer_10+Salinity_Layer_11+Sali
nity_Layer_12+Salinity_Layer_13+Salinity_Layer_14+Salinity_Layer_15+Salinity_Layer_16+Salinity_La
yer_17+Salinity_Layer_18)-
(Salinity_Layer_1+Salinity_Layer_2+Salinity_Layer_3+Salinity_Layer_4+Salinity_Layer_5+Salinity_Laye
r_6+Salinity_Layer_7+Salinity_Layer_8+Salinity_Layer_9+Salinity_Layer_10+Salinity_Layer_11+Salinit
y_Layer_12+Salinity_Layer_13+Salinity_Layer_14+Salinity_Layer_15+Salinity_Layer_16+Salinity_Laye
r_17+Salinity_Layer_18)
Salinity[Layer_2] =
(Salinity_Layer_1+2*Salinity_Layer_2+Salinity_Layer_3+Salinity_Layer_4+Salinity_Layer_5+Salinity_La
yer_6+Salinity_Layer_7+Salinity_Layer_8+Salinity_Layer_9+Salinity_Layer_10+Salinity_Layer_11+Sali
nity_Layer_12+Salinity_Layer_13+Salinity_Layer_14+Salinity_Layer_15+Salinity_Layer_16+Salinity_La
yer_17+Salinity_Layer_18)-
(Salinity_Layer_1+Salinity_Layer_2+Salinity_Layer_3+Salinity_Layer_4+Salinity_Layer_5+Salinity_Laye
r_6+Salinity_Layer_7+Salinity_Layer_8+Salinity_Layer_9+Salinity_Layer_10+Salinity_Layer_11+Salinit
y_Layer_12+Salinity_Layer_13+Salinity_Layer_14+Salinity_Layer_15+Salinity_Layer_16+Salinity_Laye
r_17+Salinity_Layer_18)
Salinity[Layer_3] =
(Salinity_Layer_1+Salinity_Layer_2+2*Salinity_Layer_3+Salinity_Layer_4+Salinity_Layer_5+Salinity_La
yer_6+Salinity_Layer_7+Salinity_Layer_8+Salinity_Layer_9+Salinity_Layer_10+Salinity_Layer_11+Sali
nity_Layer_12+Salinity_Layer_13+Salinity_Layer_14+Salinity_Layer_15+Salinity_Layer_16+Salinity_La
yer_17+Salinity_Layer_18)-
(Salinity_Layer_1+Salinity_Layer_2+Salinity_Layer_3+Salinity_Layer_4+Salinity_Layer_5+Salinity_Laye
r_6+Salinity_Layer_7+Salinity_Layer_8+Salinity_Layer_9+Salinity_Layer_10+Salinity_Layer_11+Salinit
y_Layer_12+Salinity_Layer_13+Salinity_Layer_14+Salinity_Layer_15+Salinity_Layer_16+Salinity_Laye
r_17+Salinity_Layer_18)
Salinity[Layer_4] =
(Salinity_Layer_1+Salinity_Layer_2+Salinity_Layer_3+2*Salinity_Layer_4+Salinity_Layer_5+Salinity_La
yer_6+Salinity_Layer_7+Salinity_Layer_8+Salinity_Layer_9+Salinity_Layer_10+Salinity_Layer_11+Sali
nity_Layer_12+Salinity_Layer_13+Salinity_Layer_14+Salinity_Layer_15+Salinity_Layer_16+Salinity_La
yer_17+Salinity_Layer_18)-
(Salinity_Layer_1+Salinity_Layer_2+Salinity_Layer_3+Salinity_Layer_4+Salinity_Layer_5+Salinity_Laye
r_6+Salinity_Layer_7+Salinity_Layer_8+Salinity_Layer_9+Salinity_Layer_10+Salinity_Layer_11+Salinit
y_Layer_12+Salinity_Layer_13+Salinity_Layer_14+Salinity_Layer_15+Salinity_Layer_16+Salinity_Laye
r_17+Salinity_Layer_18)
Salinity[Layer_5] =
(Salinity_Layer_1+Salinity_Layer_2+Salinity_Layer_3+Salinity_Layer_4+2*Salinity_Layer_5+Salinity_La
yer_6+Salinity_Layer_7+Salinity_Layer_8+Salinity_Layer_9+Salinity_Layer_10+Salinity_Layer_11+Sali
nity_Layer_12+Salinity_Layer_13+Salinity_Layer_14+Salinity_Layer_15+Salinity_Layer_16+Salinity_La
yer_17+Salinity_Layer_18)-
(Salinity_Layer_1+Salinity_Layer_2+Salinity_Layer_3+Salinity_Layer_4+Salinity_Layer_5+Salinity_Laye
r_6+Salinity_Layer_7+Salinity_Layer_8+Salinity_Layer_9+Salinity_Layer_10+Salinity_Layer_11+Salinit
y_Layer_12+Salinity_Layer_13+Salinity_Layer_14+Salinity_Layer_15+Salinity_Layer_16+Salinity_Laye
r_17+Salinity_Layer_18)
Salinity[Layer_6] =
(Salinity_Layer_1+Salinity_Layer_2+Salinity_Layer_3+Salinity_Layer_4+Salinity_Layer_5+2*Salinity_La
yer_6+Salinity_Layer_7+Salinity_Layer_8+Salinity_Layer_9+Salinity_Layer_10+Salinity_Layer_11+Sali
nity_Layer_12+Salinity_Layer_13+Salinity_Layer_14+Salinity_Layer_15+Salinity_Layer_16+Salinity_La
yer_17+Salinity_Layer_18)-
(Salinity_Layer_1+Salinity_Layer_2+Salinity_Layer_3+Salinity_Layer_4+Salinity_Layer_5+Salinity_Laye
r_6+Salinity_Layer_7+Salinity_Layer_8+Salinity_Layer_9+Salinity_Layer_10+Salinity_Layer_11+Salinit

y_Layer_12+Salinity_Layer_13+Salinity_Layer_14+Salinity_Layer_15+Salinity_Layer_16+Salinity_Laye
r_17+Salinity_Layer_18)
Salinity[Layer_7] =
(Salinity_Layer_1+Salinity_Layer_2+Salinity_Layer_3+Salinity_Layer_4+Salinity_Layer_5+Salinity_Laye
r_6+2*Salinity_Layer_7+Salinity_Layer_8+Salinity_Layer_9+Salinity_Layer_10+Salinity_Layer_11+Sali
nity_Layer_12+Salinity_Layer_13+Salinity_Layer_14+Salinity_Layer_15+Salinity_Layer_16+Salinity_La
yer_17+Salinity_Layer_18)-
(Salinity_Layer_1+Salinity_Layer_2+Salinity_Layer_3+Salinity_Layer_4+Salinity_Layer_5+Salinity_Laye
r_6+Salinity_Layer_7+Salinity_Layer_8+Salinity_Layer_9+Salinity_Layer_10+Salinity_Layer_11+Salinit
y_Layer_12+Salinity_Layer_13+Salinity_Layer_14+Salinity_Layer_15+Salinity_Layer_16+Salinity_Laye
r_17+Salinity_Layer_18)
Salinity[Layer_8] =
(Salinity_Layer_1+Salinity_Layer_2+Salinity_Layer_3+Salinity_Layer_4+Salinity_Layer_5+Salinity_Laye
r_6+Salinity_Layer_7+2*Salinity_Layer_8+Salinity_Layer_9+Salinity_Layer_10+Salinity_Layer_11+Sali
nity_Layer_12+Salinity_Layer_13+Salinity_Layer_14+Salinity_Layer_15+Salinity_Layer_16+Salinity_La
yer_17+Salinity_Layer_18)-
(Salinity_Layer_1+Salinity_Layer_2+Salinity_Layer_3+Salinity_Layer_4+Salinity_Layer_5+Salinity_Laye
r_6+Salinity_Layer_7+Salinity_Layer_8+Salinity_Layer_9+Salinity_Layer_10+Salinity_Layer_11+Salinit
y_Layer_12+Salinity_Layer_13+Salinity_Layer_14+Salinity_Layer_15+Salinity_Layer_16+Salinity_Laye
r_17+Salinity_Layer_18)
Salinity[Layer_9] =
(Salinity_Layer_1+Salinity_Layer_2+Salinity_Layer_3+Salinity_Layer_4+Salinity_Layer_5+Salinity_Laye
r_6+Salinity_Layer_7+Salinity_Layer_8+2*Salinity_Layer_9+Salinity_Layer_10+Salinity_Layer_11+Sali
nity_Layer_12+Salinity_Layer_13+Salinity_Layer_14+Salinity_Layer_15+Salinity_Layer_16+Salinity_La
yer_17+Salinity_Layer_18)-
(Salinity_Layer_1+Salinity_Layer_2+Salinity_Layer_3+Salinity_Layer_4+Salinity_Layer_5+Salinity_Laye
r_6+Salinity_Layer_7+Salinity_Layer_8+Salinity_Layer_9+Salinity_Layer_10+Salinity_Layer_11+Salinit
y_Layer_12+Salinity_Layer_13+Salinity_Layer_14+Salinity_Layer_15+Salinity_Layer_16+Salinity_Laye
r_17+Salinity_Layer_18)
Salinity[Layer_10] =
(Salinity_Layer_1+Salinity_Layer_2+Salinity_Layer_3+Salinity_Layer_4+Salinity_Layer_5+Salinity_Laye
r_6+Salinity_Layer_7+Salinity_Layer_8+Salinity_Layer_9+2*Salinity_Layer_10+Salinity_Layer_11+Sali
nity_Layer_12+Salinity_Layer_13+Salinity_Layer_14+Salinity_Layer_15+Salinity_Layer_16+Salinity_La
yer_17+Salinity_Layer_18)-
(Salinity_Layer_1+Salinity_Layer_2+Salinity_Layer_3+Salinity_Layer_4+Salinity_Layer_5+Salinity_Laye
r_6+Salinity_Layer_7+Salinity_Layer_8+Salinity_Layer_9+Salinity_Layer_10+Salinity_Layer_11+Salinit
y_Layer_12+Salinity_Layer_13+Salinity_Layer_14+Salinity_Layer_15+Salinity_Layer_16+Salinity_Laye
r_17+Salinity_Layer_18)
Salinity[Layer_11] =
(Salinity_Layer_1+Salinity_Layer_2+Salinity_Layer_3+Salinity_Layer_4+Salinity_Layer_5+Salinity_Laye
r_6+Salinity_Layer_7+Salinity_Layer_8+Salinity_Layer_9+Salinity_Layer_10+2*Salinity_Layer_11+Sali
nity_Layer_12+Salinity_Layer_13+Salinity_Layer_14+Salinity_Layer_15+Salinity_Layer_16+Salinity_La
yer_17+Salinity_Layer_18)-
(Salinity_Layer_1+Salinity_Layer_2+Salinity_Layer_3+Salinity_Layer_4+Salinity_Layer_5+Salinity_Laye
r_6+Salinity_Layer_7+Salinity_Layer_8+Salinity_Layer_9+Salinity_Layer_10+Salinity_Layer_11+Salinit
y_Layer_12+Salinity_Layer_13+Salinity_Layer_14+Salinity_Layer_15+Salinity_Layer_16+Salinity_Laye
r_17+Salinity_Layer_18)
Salinity[Layer_12] =
(Salinity_Layer_1+Salinity_Layer_2+Salinity_Layer_3+Salinity_Layer_4+Salinity_Layer_5+Salinity_Laye
r_6+Salinity_Layer_7+Salinity_Layer_8+Salinity_Layer_9+Salinity_Layer_10+Salinity_Layer_11+2*Sali
nity_Layer_12+Salinity_Layer_13+Salinity_Layer_14+Salinity_Layer_15+Salinity_Layer_16+Salinity_La
yer_17+Salinity_Layer_18)-
(Salinity_Layer_1+Salinity_Layer_2+Salinity_Layer_3+Salinity_Layer_4+Salinity_Layer_5+Salinity_Laye
r_6+Salinity_Layer_7+Salinity_Layer_8+Salinity_Layer_9+Salinity_Layer_10+Salinity_Layer_11+Salinit
y_Layer_12+Salinity_Layer_13+Salinity_Layer_14+Salinity_Layer_15+Salinity_Layer_16+Salinity_Laye
r_17+Salinity_Layer_18)
Salinity[Layer_13] =
(Salinity_Layer_1+Salinity_Layer_2+Salinity_Layer_3+Salinity_Layer_4+Salinity_Layer_5+Salinity_Laye
r_6+Salinity_Layer_7+Salinity_Layer_8+Salinity_Layer_9+Salinity_Layer_10+Salinity_Layer_11+Salinit
y_Layer_12+2*Salinity_Layer_13+Salinity_Layer_14+Salinity_Layer_15+Salinity_Layer_16+Salinity_La
yer_17+Salinity_Layer_18)-
(Salinity_Layer_1+Salinity_Layer_2+Salinity_Layer_3+Salinity_Layer_4+Salinity_Layer_5+Salinity_Laye
r_6+Salinity_Layer_7+Salinity_Layer_8+Salinity_Layer_9+Salinity_Layer_10+Salinity_Layer_11+Salinit
y_Layer_12+Salinity_Layer_13+Salinity_Layer_14+Salinity_Layer_15+Salinity_Layer_16+Salinity_Laye
r_17+Salinity_Layer_18)
Salinity[Layer_14] =
(Salinity_Layer_1+Salinity_Layer_2+Salinity_Layer_3+Salinity_Layer_4+Salinity_Layer_5+Salinity_Laye

r_6+Salinity_Layer_7+Salinity_Layer_8+Salinity_Layer_9+Salinity_Layer_10+Salinity_Layer_11+Salinit
y_Layer_12+Salinity_Layer_13+2*Salinity_Layer_14+Salinity_Layer_15+Salinity_Layer_16+Salinity_La
yer_17+Salinity_Layer_18)-
(Salinity_Layer_1+Salinity_Layer_2+Salinity_Layer_3+Salinity_Layer_4+Salinity_Layer_5+Salinity_Laye
r_6+Salinity_Layer_7+Salinity_Layer_8+Salinity_Layer_9+Salinity_Layer_10+Salinity_Layer_11+Salinit
y_Layer_12+Salinity_Layer_13+Salinity_Layer_14+Salinity_Layer_15+Salinity_Layer_16+Salinity_Laye
r_17+Salinity_Layer_18)
Salinity[Layer_15] =
(Salinity_Layer_1+Salinity_Layer_2+Salinity_Layer_3+Salinity_Layer_4+Salinity_Layer_5+Salinity_Laye
r_6+Salinity_Layer_7+Salinity_Layer_8+Salinity_Layer_9+Salinity_Layer_10+Salinity_Layer_11+Salinit
y_Layer_12+Salinity_Layer_13+Salinity_Layer_14+2*Salinity_Layer_15+Salinity_Layer_16+Salinity_La
yer_17+Salinity_Layer_18)-
(Salinity_Layer_1+Salinity_Layer_2+Salinity_Layer_3+Salinity_Layer_4+Salinity_Layer_5+Salinity_Laye
r_6+Salinity_Layer_7+Salinity_Layer_8+Salinity_Layer_9+Salinity_Layer_10+Salinity_Layer_11+Salinit
y_Layer_12+Salinity_Layer_13+Salinity_Layer_14+Salinity_Layer_15+Salinity_Layer_16+Salinity_Laye
r_17+Salinity_Layer_18)
Salinity[Layer_16] =
(Salinity_Layer_1+Salinity_Layer_2+Salinity_Layer_3+Salinity_Layer_4+Salinity_Layer_5+Salinity_Laye
r_6+Salinity_Layer_7+Salinity_Layer_8+Salinity_Layer_9+Salinity_Layer_10+Salinity_Layer_11+Salinit
y_Layer_12+Salinity_Layer_13+Salinity_Layer_14+Salinity_Layer_15+2*Salinity_Layer_16+Salinity_La
yer_17+Salinity_Layer_18)-
(Salinity_Layer_1+Salinity_Layer_2+Salinity_Layer_3+Salinity_Layer_4+Salinity_Layer_5+Salinity_Laye
r_6+Salinity_Layer_7+Salinity_Layer_8+Salinity_Layer_9+Salinity_Layer_10+Salinity_Layer_11+Salinit
y_Layer_12+Salinity_Layer_13+Salinity_Layer_14+Salinity_Layer_15+Salinity_Layer_16+Salinity_Laye
r_17+Salinity_Layer_18)
Salinity[Layer_17] =
(Salinity_Layer_1+Salinity_Layer_2+Salinity_Layer_3+Salinity_Layer_4+Salinity_Layer_5+Salinity_Laye
r_6+Salinity_Layer_7+Salinity_Layer_8+Salinity_Layer_9+Salinity_Layer_10+Salinity_Layer_11+Salinit
y_Layer_12+Salinity_Layer_13+Salinity_Layer_14+Salinity_Layer_15+Salinity_Layer_16+2*Salinity_La
yer_17+Salinity_Layer_18)-
(Salinity_Layer_1+Salinity_Layer_2+Salinity_Layer_3+Salinity_Layer_4+Salinity_Layer_5+Salinity_Laye
r_6+Salinity_Layer_7+Salinity_Layer_8+Salinity_Layer_9+Salinity_Layer_10+Salinity_Layer_11+Salinit
y_Layer_12+Salinity_Layer_13+Salinity_Layer_14+Salinity_Layer_15+Salinity_Layer_16+Salinity_Laye
r_17+Salinity_Layer_18)
Salinity[Layer_18] =
(Salinity_Layer_1+Salinity_Layer_2+Salinity_Layer_3+Salinity_Layer_4+Salinity_Layer_5+Salinity_Laye
r_6+Salinity_Layer_7+Salinity_Layer_8+Salinity_Layer_9+Salinity_Layer_10+Salinity_Layer_11+Salinit
y_Layer_12+Salinity_Layer_13+Salinity_Layer_14+Salinity_Layer_15+Salinity_Layer_16+Salinity_Laye
r_17+2*Salinity_Layer_18)-
(Salinity_Layer_1+Salinity_Layer_2+Salinity_Layer_3+Salinity_Layer_4+Salinity_Layer_5+Salinity_Laye
r_6+Salinity_Layer_7+Salinity_Layer_8+Salinity_Layer_9+Salinity_Layer_10+Salinity_Layer_11+Salinit
y_Layer_12+Salinity_Layer_13+Salinity_Layer_14+Salinity_Layer_15+Salinity_Layer_16+Salinity_Laye
r_17+Salinity_Layer_18)
Depth[Layer_1] = Element_Height*1
Depth[Layer_2] = Element_Height*2
Depth[Layer_3] = Element_Height*3
Depth[Layer_4] = Element_Height*4
Depth[Layer_5] = Element_Height*5
Depth[Layer_6] = Element_Height*6
Depth[Layer_7] = Element_Height*7
Depth[Layer_8] = Element_Height*8
Depth[Layer_9] = Element_Height*9
Depth[Layer_10] = Element_Height*10
Depth[Layer_11] = Element_Height*11
Depth[Layer_12] = Element_Height*12
Depth[Layer_13] = Element_Height*13
Depth[Layer_14] = Element_Height*14
Depth[Layer_15] = Element_Height*15
Depth[Layer_16] = Element_Height*16
Depth[Layer_17] = Element_Height*17
Depth[Layer_18] = Element_Height*18
Depth_total = 0.9
Element_Height = Depth_total/No_of_layers
No_of_layers = 18
Pond_Length = 130
Pond_Width = 20
Surface_Area = Pond_Length*Pond_Width

Volume = Surface_Area*Element_Height

Appendix L

Graphs of Pond Model Sensitivity

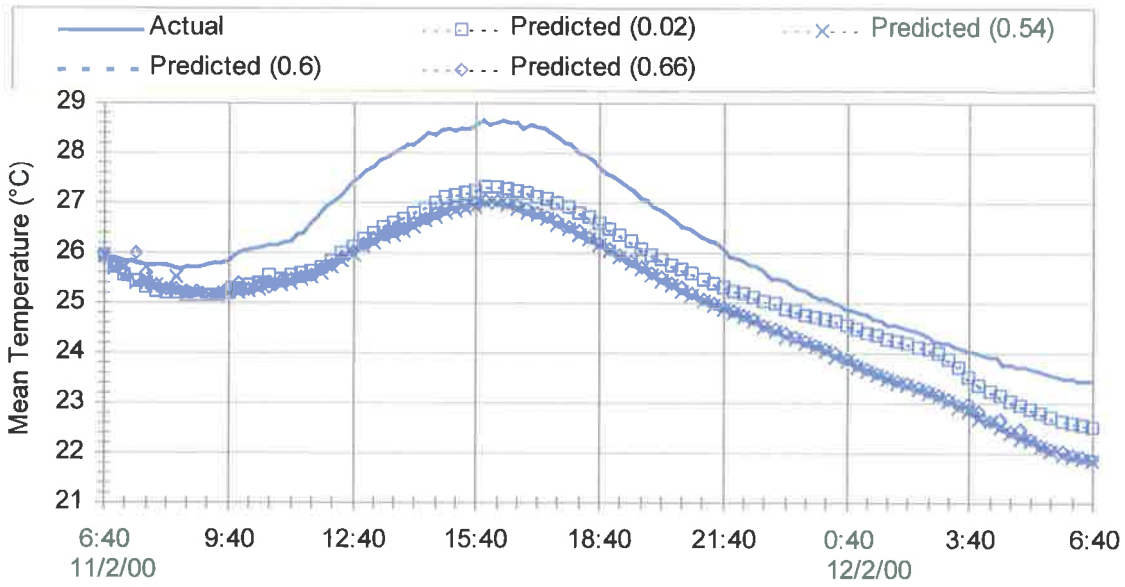

Figure L-1: Sensitivity of the mean pond temperature to changes in the value of K_{max} (in m^2/h), for 11 February 2000

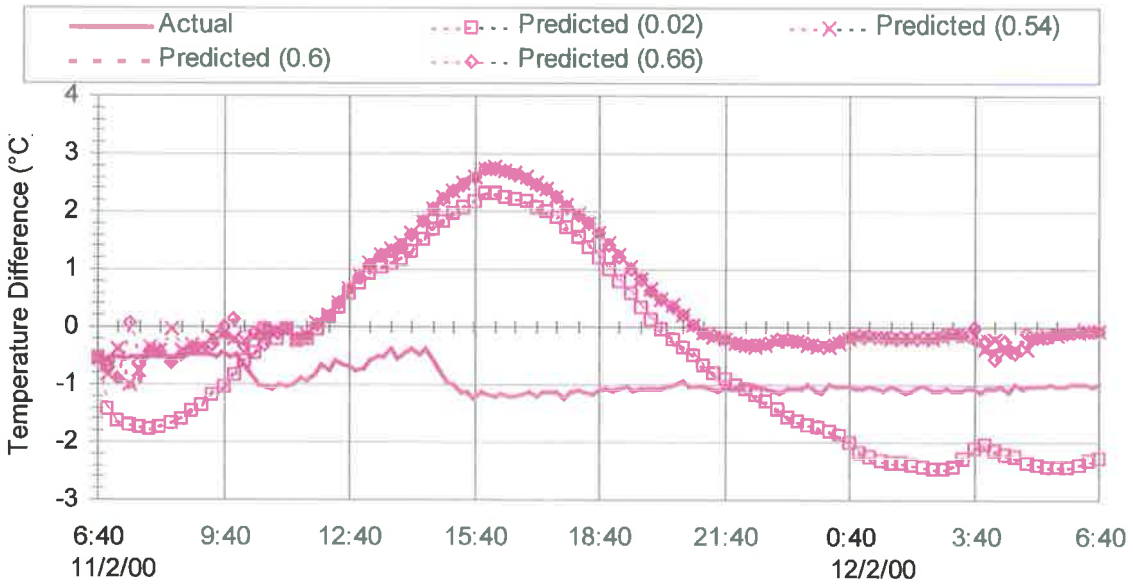

Figure L-2: Sensitivity of the mean temperature stratification to changes in the value of K_{max} (in m^2/h), for 11 February 2000

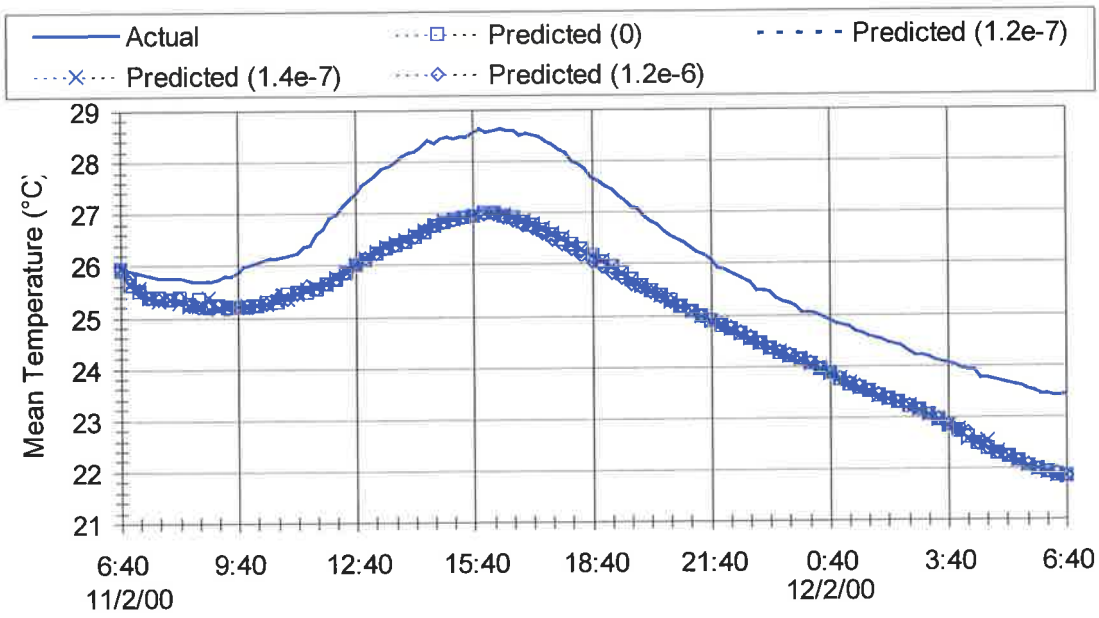

Figure L-3: Sensitivity of the mean pond temperature to changes in the value of α (in m^2/s) for 11 February 2000

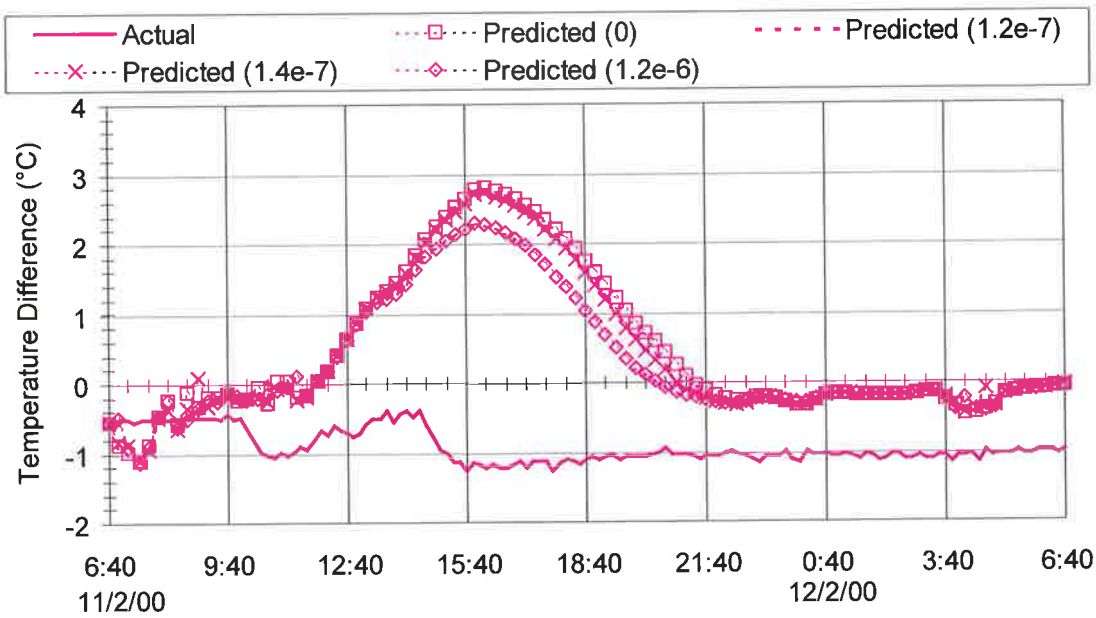

Figure L-4: Sensitivity of the mean temperature stratification to changes in the value of α (in m^2/s) for 11 February 2000

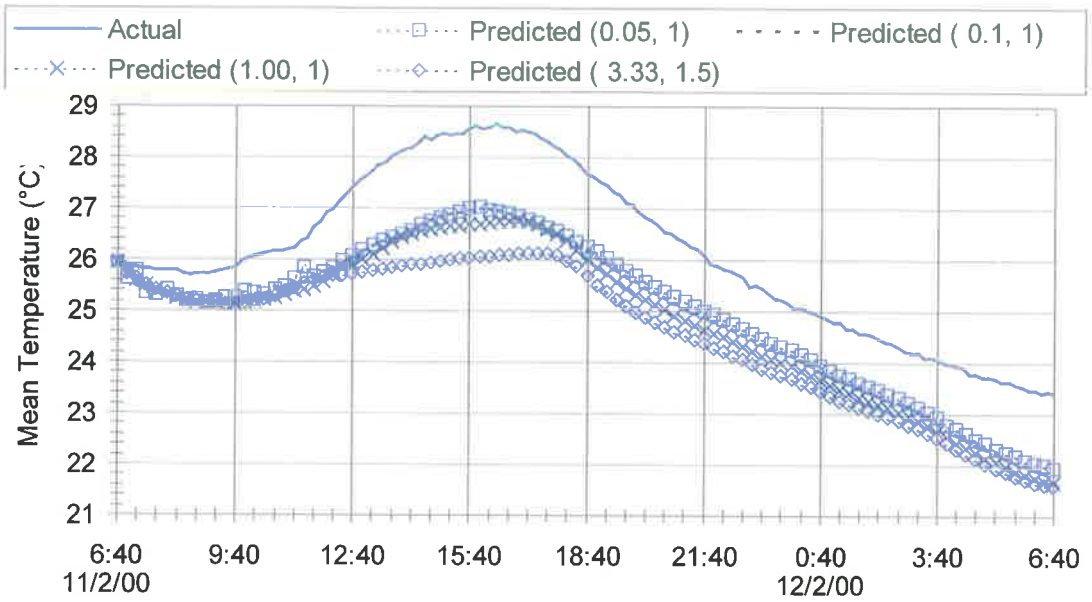

Figure L-5: Sensitivity of the mean pond temperature to changes in the values of σ and n for 11 February 2000

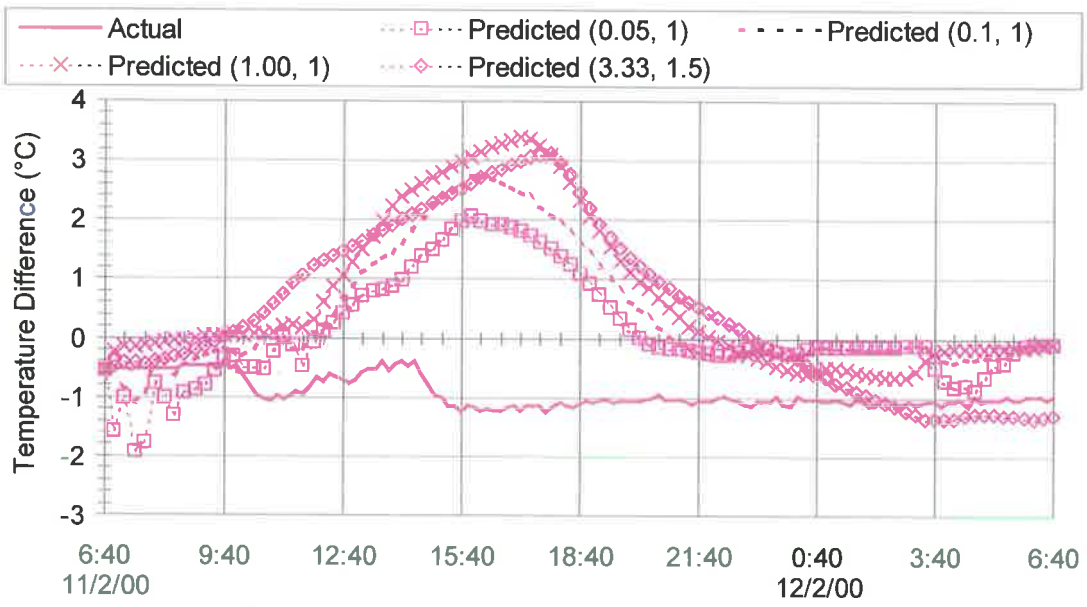

Figure L-6: Sensitivity of the mean temperature stratification to changes in the values of σ and n for 11 February 2000

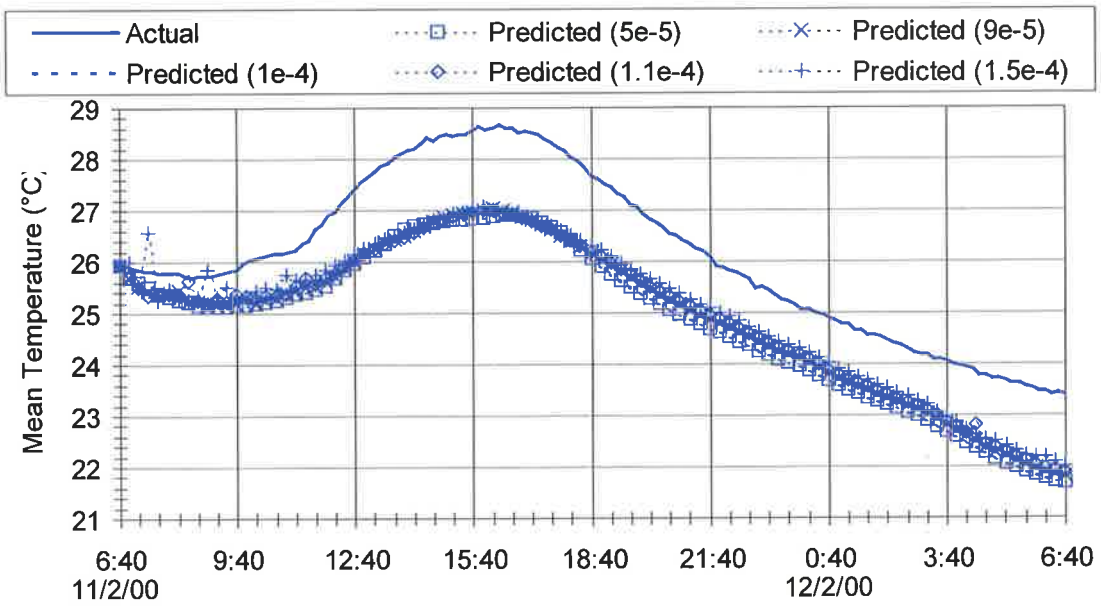

Figure L-7: Sensitivity of the mean pond temperature to changes in the value of k for 11 February 2000

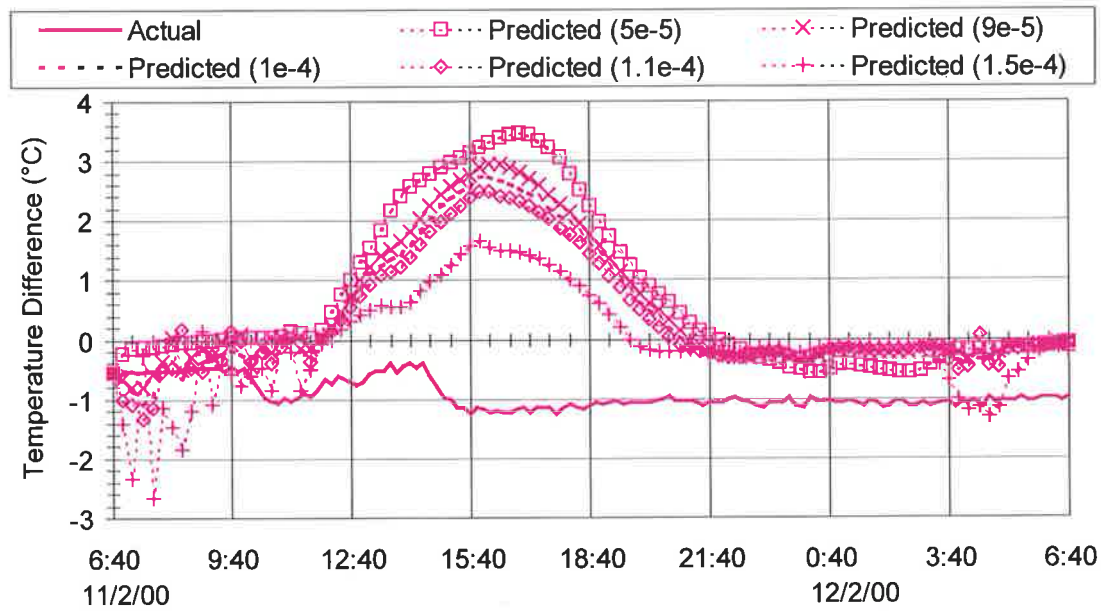

Figure L-8: Sensitivity of the mean temperature stratification to changes in the value of k for 11 February 2000

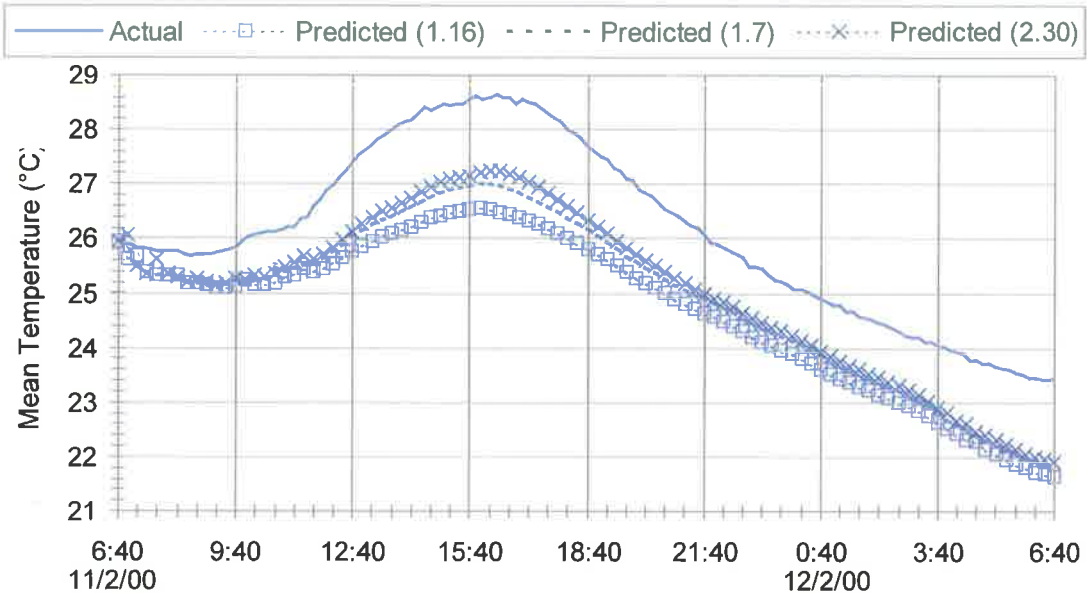

Figure L-9: Sensitivity of the mean pond temperature to changes in the value of κ for 11 February 2000

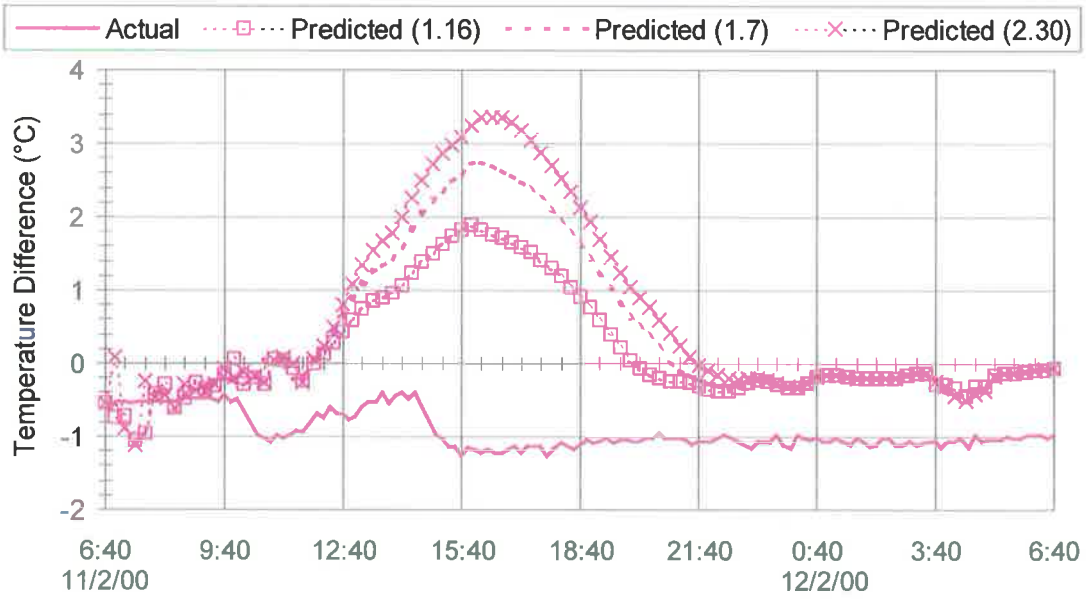

Figure L-10: Sensitivity of the mean temperature stratification to changes in the value of κ for 11 February 2000

Addendum - A Note on Model Timesteps

The results reported in this thesis are for simulations run with a timestep of 0.0014 hours (5 seconds). The value was chosen with consideration given to the accuracy and stability of the solution. A number of runs have been undertaken where the timestep has been varied and the results are as follows.

- For timesteps greater than 0.002 hours (7.5 seconds) the model was unstable and rarely converged (i.e. the model stopped running when infinite values for the diffusion coefficient were generated).

- For timesteps between 0.0014 and 0.002 hours (5 and 7.5 seconds) oscillations sometimes occurred indicating numerical instability but the model almost always converged. When temperature oscillations occurred they were generally confined to the upper layers of the pond where the heat flux was highest.

- For timesteps below 0.0014 hours (5 seconds) the model was nearly always stable and always produced a solution. In general, the smaller the timestep the closer the simulated temperature curves mimicked the actual pond temperature curves.

Although reducing the timestep below 0.0014 hours (5 seconds) had a smoothing effect on the temperature curves it had a negligible effect on the overall error in mean pond temperature and temperature stratification. Losordo and Piedrahita (1991) using a similar modeling technique found that a timestep of 0.025 hours (1.5 minutes) was sufficiently small to achieve satisfactory results for pond temperature behaviour in aquaculture ponds. It is probable that differences between the actual and predicted values for the sedimentation pond model are primarily due to deficiencies in the model algorithm itself rather than the solving technique that has been employed.